THE UNIVERSITY OF
SYDNEY

COPYRIGHT AND USE OF THIS THESIS

This thesis must be used in accordance with the provisions of the Copyright Act 1968.

Reproduction of material protected by copyright may be an infringement of copyright and copyright owners may be entitled to take legal action against persons who infringe their copyright.

Section 51 (2) of the Copyright Act permits an authorized officer of a university library or archives to provide a copy (by communication or otherwise) of an unpublished thesis kept in the library or archives, to a person who satisfies the authorized officer that he or she requires the reproduction for the purposes of research or study.

The Copyright Act grants the creator of a work a number of moral rights, specifically the right of attribution, the right against false attribution and the right of integrity.

You may infringe the author's moral rights if you:

- fail to acknowledge the author of this thesis if you quote sections from the work
- attribute this thesis to another author
- subject this thesis to derogatory treatment which may prejudice the author's reputation

For further information contact the University's Director of Copyright Services

sydney.edu.au/copyright

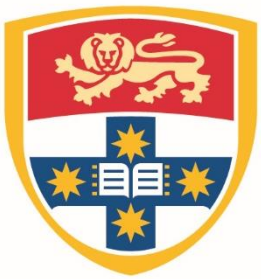

THE UNIVERSITY OF SYDNEY

BLOOD PROTEIN AND PLATELET INTERACTIONS ON SURFACE ENGINEERED BIOMATERIALS

A thesis submitted in fulfilment of the requirements for the degree of Doctor of Philosophy in Engineering

Deepika Nandakumar

SUPERVISOR: PROFESSOR ANDREW J. RUYS

ASSOCIATE SUPERVISORS: DR. MEGAN S. LORD &

DR. PHILLIP J. MARTIN

School of Aerospace, Mechanical and Mechatronic Engineering

University of Sydney
Sydney, Australia

April, 2015

STATEMENT OF CONTRIBUTION

'I hereby declare that the work embodied in this thesis is the result of my own work and to the best of my knowledge it contains no materials previously published or written by another person, or substantial proportions of material which have been accepted for the award of any other degree or diploma at University of Sydney or any other educational institution, except where due acknowledgement is made in the thesis. Any contribution made to the research by others, with whom I have worked with is explicitly acknowledged in the thesis. I also declare that the intellectual content of this thesis is the product of my own work, except to the extent that assistance from others in the project's design and conception or in style, presentation and linguistic expression is acknowledged.'

....

SIGNATURE (Deepika Nandakumar, Student) DATE

The above represents an accurate account of the student's contribution.

....

SIGNATURE (Prof. Andrew J. Ruys) DATE

ACKNOWLEDGEMENTS

These pages are a culmination of many, many, many hours of hard work to which would not have been accomplished without the help, support and guidance of many people.

Firstly, I owe my deepest gratitude to my supervisors Megan Lord and Andrew Ruys, who have both been there with their support, advice, guidance, and encouragement right up until the very end. I would especially like to thank Megan for granting access to Level 4 (GSBME). Your direction, discussions and knowledge of all things proteins, platelets and QCM related were instrumental to my completion of this study. I could not have done without them.

I would like to thank Avi Bendavid and Phillip J Martin, from CSIRO, for the fabrication of DLC and titania thin films and for their knowledge and technical support.

I would also like to thank Dr. Ken Shorts from ANSTO for his guidance in using the AFM and for allowing me to use the fish bowl as I needed. I would like to thank Dr. Kenneth Harris, of University of Alberta, for the fabrication of nano-structured silicon wafers using block co-polymer technology. Staff from the UNSW BMIF, Renee Whan and Warren, for all their technical support and assistance with the AFM. And, I would like to thank the ACMM staff Matthew Foley, Steve Moody, Ellie Kable and Naveena Gokoolparsadh for all their technical support with sample preparation and SEM use.

I would like to thank the School of Engineering at Sydney University, PRSS, Professor Andrew Ruys and Dr. Megan Lord and Australasian Society of Biomaterials and Tissue Engineering (ASBTE) for their financial support that allowed me to complete this project and travel to national and international conferences.

To my awesome friends and colleagues at Sydney University and UNSW, past and present, Howard, Edwin, Dorji, Romzies, Stevee, Adry, James, Pascal and Sal-Sal for all the coffee-breaks, lunch-breaks, hospital visits and catch-up sessions. When I think back all my fondest memories during my PhD involve us in some way. I could not have done without your laughter, humour and distractions. Stevee and Romana thank you for your support and for being there, whether it was 5am in the morning or 12 at night, and Romana, especially, for all things blood related.

To my dearest friends; Jacqui and Viju, thank you for listening and knowing just what to say. Thanks for being there and for all the little distractions, but mostly for your friendship. I cannot wait to start painting our futures in shades of yellow!

Most importantly, my family, Mummy, Daddy and Amamma, thank you for your encouragement, love and support. You are my inspiration.

To,

My Parents...

ABSTRACT

Modulation of blood-surface interactions to increase the thrombo-resistance of a synthetic biomaterial is a vital aspect in the design of haemocompatible surfaces. Recent work suggests that chemical and physical properties of a surface fundamentally influence the biological responses of adsorbed proteins and platelets. A non-haemocompatible material surface may ubiquitously adsorb specific plasma proteins that form a proteinacious layer which mediates the adhesion and activation of platelets and the clotting cascade, and consequently the formation of blood clots. This will ultimately lead to the rejection of the material and subsequently, the implanted medical device.

Currently the preferential adsorption of specific proteins, their exact interaction and the effect of physical and spatial cues from the nano-environment in platelet adhesion, spreading and its subsequent activation still remain unclear. Apart from surface chemistry and wetability of the surface, variation in the nano-structure of biomaterials, structural differences between different proteins, the various forces involved and their combinatorial effect, and the dynamic nature of each protein (their ability to exist and co-exist in various conformations depending on the surrounding nano-environment) prevents us from acknowledging a general description of the interplay between proteins and biomaterials. Thus the purpose of this study is to investigate the effect of plasma protein adsorption and subsequent platelet interactions on the smooth and nano-patterned commercially used biomaterials such as: hydrogenated amorphous carbon (a-C:H), tetrahedral amorphous carbon (ta-C) and titania (TiO_2) surfaces. Protein interactions were investigated using a combination of atomic force microscopy (AFM), quartz crystal microbalance with dissipation (QCM-D), enzyme-linked immunosorbant assay (ELISA) and fluorescence microscopy, while platelet interactions were examined using scanning electron microscopy (SEM), AFM, QCM, ELISA, fluorescence microscopy and flow cytometry, *in-vitro*.

Results have shown a-C:H and ta-C surfaces exhibited increased affinity to fibrinogen than TiO_2 surfaces, while facilitating similar levels of platelet attachment. Differences in platelet attachment between protein pre-coated surfaces showed the necessary role of fibrinogen in platelet adhesion. The a-C:H coated surfaces resulted in decreased cellular spreading when compared with ta-C and TiO_2 coated surfaces, while same level of platelet activation was detected indicating that platelets could exist in their activated state without spreading. When platelet interactions on nano-patterned surfaces were compared against smooth surfaces, nano-rough a-C:H and ta-C surfaces presented with increased levels of platelet attachment as well as its spreading when compared with TiO_2, while similar levels of platelet activation was detected amongst the smooth and the rough substrates. Furthermore, excessive platelet adhesion and spreading were noted on fibrinogen pre-coated nano-patterned and flat surfaces when compared to albumin and plasma pre-coated surfaces, with minimal changes in activation levels on each platelet. Increased levels of platelet adhesion and spreading were positively correlated with increased fibrinogen adsorption, reinforcing the crucial role of fibrinogen in platelet binding but also its possible role in platelet spreading.

TABLE OF CONTENTS

STATEMENT OF CONTRIBUTION I

ACKNOWLEDGEMENTS II

ABSTRACT V

TABLE OF CONTENTS VII

LIST OF FIGURES XIII

LIST OF TABLES XVIII

LIST OF PUBLICATIONS XIX

ABBREVIATIONS XX

1 INTRODUCTION 1

Aims 3

2 LITERATURE REVIEW 4

2.1 The Cardiovascular System 4

2.1.1 Blood Vasculature 4

2.1.2 Blood and Its Composition 7

2.1.3 White Blood Cells 10

2.1.4 Blood Platelets 12

2.1.4.1 Platelet Biology 14

2.1.4.2 Platelet receptors 16

2.1.4.2.1 GP Ib 19

2.1.4.2.2 GP IIb/IIIa 19

2.1.4.2.3 GP Ia/IIa 21

2.1.4.2.4 P-selectin 21

2.1.5 Platelet Interactions 22

2.1.5.1 Platelet adhesion and activation 23

Structural changes during platelet activation 27

2.3 Coagulation Cascade 28

2.1.6.1 The Extrinsic Pathway 30

2.1.6.2 Intrinsic Pathway 31

2.1.6.3 The Common Pathway 32
2.1.7 Plasma proteins *33*
2.1.7.1 Fibrinogen 35
2.1.7.2 Albumin 37
2.2 Blood-compatible Surfaces 38
2.2.1 Surface Modification *39*
2.2.1.1 Diamond-Like Carbon (DLC) surface coatings 43
2.2.1.1.1 Chemical and mechanical properties 44
2.2.1.1.2 Biocompatibility 48
2.2.1.2 Titania (TiO_2) surface coatings 50
2.2.1.2.1 Chemical and mechanical properties 51
2.2.1.2.2 Biocompatibility 54
2.2.1.3 Haemocompatibility 56
2.2.1.3.1 DLC 56
2.2.1.3.2 TiO_2 61
2.2.1.4 Surface nano-patterning 63
2.2.1.4.1 Surface nano-patterning techniques 64
2.2.1.4.2 Influence of nano-topography on blood compatibility 67

3 MATERIALS AND METHODS 71

3.1 Material Processing and Surface Characterisation 72
3.1.1 Surface Preparation *72*
3.1.1.1 Initial preparation 72
3.1.1.2 Surface nano-patterning 73
3.1.1.3 Surface coating 74
3.1.1.3.1 Hydrogenated-Amorphous Carbon (a-C:H) deposition 74
3.1.1.3.2 Tetrahedral Amorphous Carbon (ta-C) deposition 74
3.1.1.3.3 Titania (TiO_2) deposition 75
3.1.1.4 Surface cleaning 75
3.1.1.4.1 Flat discs 76
3.1.1.4.2 Flat QCM-sensors 76
3.1.1.4.3 Nano-patterned discs 77
3.1.2 Surface Characterisation *77*

3.1.2.1 X-ray Photoelectron Spectroscopy (XPS) 77
3.1.2.2 Scanning Electron Microscopy (SEM) 77
Focused Ion Beam (FIB) microscopy 78
3.1.2.3 Atomic Force Microscopy (AFM) 78
3.2 Protein Studies 79
3.2.1 Protein Preparation and Characterisation *80*
3.2.1.1 Sodium Dodecyl Sulphate Polyacrelamide Gel Electrophoresis (SDS-PAGE) 80
3.2.1.2 Western blotting 81
3.2.1.3 Biotin labelling of fibrinogen and albumin 82
3.2.1.4 Coomassie blue protein assay 83
3.2.2 Protein Adsorption *83*
3.2.2.1 Enzyme Linked Immuno-Sorbent Assay (ELISA) 84
3.2.2.1.1 Simple and complex studies 84
3.2.2.1.2 Conformation of adsorbed fibrinogen measured using ELISA 85
3.2.2.2 Fluorescence Microscopy 86
3.2.2.3 AFM 87
3.2.2.4 Quartz Crystal Microbalance with Dissipation monitoring (QCM-D) 88
3.2.3 Clotting Cascade Experiments *89*
3.2.3.1 Plasma Purification for Clotting Cascade Experiments 89
3.2.3.2 Prothrombin Time (PT) 90
3.2.3.3 Activated Partial Thromboplastin Time (aPTT) 90
3.2.3.4 Thrombin Time (TT) 91
3.2.4 Platelet Studies *91*
3.2.4.1 Platelet and surface preparation for platelet studies 92
3.2.4.1.1 Platelet isolation from human blood 92
3.2.4.1.2 Pre-incubating platelet solutions with integrin $\alpha_{IIb}\beta_3$ antibody 93
3.2.4.1.3 Pre-coating surfaces with protein solutions 93
3.2.4.2 Platelet adhesion studies 94
3.2.4.2.1 Fluorescence Microscopy 94
3.2.4.2.2 SEM 95
3.2.4.2.3 AFM 96

3.2.4.2.4 QCM-D 96
3.2.4.3 Platelet activation studies 97
3.2.4.3.1 ELISA 97
3.2.4.3.2 Fluorescence microscopy 98
3.2.4.3.3 Flow-cytometry 100

4 MATERIAL CHARACTERISATION AND PROTEIN ADSORPTION 102

4.1 Introduction 102
4.2 Material characterisation 102
4.2.1 XPS 102
4.2.2 SEM and FIB 107
4.2.3 AFM 116
4.3 Protein adsorption studies on flat surfaces 126
4.3.1 ELISA 127
4.3.1.1 Adsorption studies 128
4.3.1.2 Conformation studies 133
4.3.2 Fluorescence microscopy 137
4.3.3 AFM 143
4.3.4 QCM-D 161
4.4 Summary 175

5 PLATELET ADHESION 177

5.1 Introduction 177
5.2 Results and Discussion 178
5.2.1 Morphology and concentration of surface-adhered platelets 178
5.2.1.1 Flat Surfaces 179
5.2.1.2 Role of $\alpha_{IIb}\beta_3$ integrins in platelet adhesion 198
5.2.1.3 Nano-patterned surfaces 210
5.2.2 QCM-D studies 226
5.3 Summary 238

6 CLOTTING CASCADE AND PLATELET ACTIVATION 241

6.1 Introduction 241
6.2 Results and Discussion 242

6.2.1 Coagulation of Plasma Proteins *242*
6.2.1.1 Prothrombin (PT) clotting assay 242
6.2.1.2 Activated partial thromboplastin (aPTT) clotting assay 245
6.2.1.3 Thrombin time (TT) clotting assay 247
6.2.2 Platelet Activation Studies *248*
6.2.2.1 ELISA 249
6.2.2.2 Fluorescence Microscopy 253
6.2.2.2.1 $\alpha_{IIb}\beta_3$ Activation and Actin staining on Nano-patterned Surfaces 253
6.2.2.2.2 P-selectin and $\alpha_{IIb}\beta_3$ Activation on Flat Surfaces 263
6.2.2.2.3 P-selectin and $\alpha_{IIb}\beta_3$ Activation on Nano-patterned Surfaces 273
6.2.2.3 Flow Cytometry 282
6.3 Summary 287

7 OVERALL DISCUSSION 289

7.1 Influence of Surface Chemistry on Plasma Protein Adsorption and Coagulation Cascade Activation 290
7.2 Influence of Plasma Proteins on Platelet Interactions 295
7.3 Influence of Surface Nano-topography on Protein Adsorption and Platelet Interactions 300

8 CONCLUSIONS 306

Recommendations 309

9 REFERENCES 310

10 APPENDIX A 342

10.1 Experimental Techniques 342
10.1.1 X-ray Photoelectron Spectroscopy (XPS) *342*
10.1.2 Scanning Electron Microscopy (SEM) *345*
10.1.3 Focused Ion Beam (FIB) Microscopy *346*
10.1.4 Atomic Force Microscopy (AFM) *347*
10.1.5 Enzyme-Linked Immunosorbant Assay (ELISA) *348*
10.1.6 Fluorescence Microscopy *349*
10.1.7 Quartz Crystal Microbalance with Dissipation monitoring (QCM-D) *350*

10.1.8 Flow-cytometry 354

LIST OF FIGURES

Figure 2.1 Schematic diagram of the circulatory system 5
Figure 2.2 Schematic diagram of the structural layers of arteries and veins 7
Figure 2.3 Differentiation of haematopoietic stem cells 8
Figure 2.4 Overview of blood biomaterial interactions 9
Figure 2.5 Blood to biomaterial interactions 10
Figure 2.6 Platelet plug formation during haemostasis 13
Figure 2.7 Platelet receptors involved in platelet biomaterial interactions 17
Figure 2.8 Inside-out and outside-in platelet integrin signalling 18
Figure 2.9 Platelet adhesion and aggregation on biomaterial surfaces 25
Figure 2.10 Morphological changes in platelets during platelet activation 26
Figure 2.11 Simplified version of the coagulation cascade 29
Figure 2.12 Comprehensive diagram of the coagulation cascade 31
Figure 2.13 Ternary phase diagram showing the various forms of DLC 45
Figure 2.14 Mechanical properties of various DLC films 46
Figure 2.15 Bulk crystal structures of rutile and anastase TiO_2 52
Figure 4.1 Full spectrum and high resolution XPS of TiO_2 surfaces. 103
Figure 4.2 Full spectrum and high resolution XPS of a-C:H films. 105
Figure 4.3 Full spectrum and high resolution XPS of ta-C films 106
Figure 4.4 SEM image of flat substrates. 108
Figure 4.5 SEM image of flat substrates 109
Figure 4.6 SEM image of nano-patterned surfaces. 111
Figure 4.7 High resolution SEM image of nano-patterns on a-C:H surfaces 112
Figure 4.8 FIB image showing cross-section of a-C:H films 113
Figure 4.9 FIB image showing thickness of TiO_2, a-C:H and ta-C coatings on nano-patterned surfaces 115
Figure 4.10 AFM topographical image of flat substrates. 119
Figure 4.11 AFM topographical image of QCM crystals. 122
Figure 4.12 AFM topographical image of nano-patterned surfaces 124
Figure 4.13 Roughness profile of nano-patterned surfaces determined by AFM 126
Figure 4.14 Absorbance of SA-HRP binding to biotinylated fibrinogen and albumin on flat substrates from simple and complex solutions 129

Figure 4.15 Percentage decrease in the amount of albumin and fibrinogen adsorbed from complex solution, relative to their adsorption from their single solution, as determined using flat substrates 131

Figure 4.16 Albumin to fibrinogen binding ratio on flat substrates as determined using single and complex solutions..... 132

Figure 4.17 Absorbance detected for 2C2-G7, Fg-α, and fg-γ binding to adsorbed fibrinogen on flat substrates from simple, complex and plasma; as determined by ELISA. 135

Figure 4.18 Fluorescence microscope images showing distribution of alexa fluorophore 488 tagged 2C2-G7mAB antibodies bound to adsorbed fibrinogen on flat subsutrates from simple and plasma solutions..... 140

Figure 4.19 Amount of alexa fluorophore 488 tagged 2C2-G7mAB binding to adsorbed fibrinogen from simple and plasma solution on flat substrates as determined using fluorescence microscopy 141

Figure 4.20 Amount of alexa fluorophore 488 tagged 2C2-G7mAB detected on flat and nano-patterned surfaces pre-coated with fibrinogen. 142

Figure 4.21 2D AFM images of adsorbed fibrinogen on flat surfaces..... 147

Figure 4.22 2D AFM images of adsorbed fibrinogen on nano-patterned surfaces. 149

Figure 4.23 Roughness profiles of adsorbed fibrinogen on flat and nano-patterned surfaces as determined using AFM. 151

Figure 4.24 Roughness values (RMS) of flat and nano-patterned surfaces in the presence and absence of fibrinogen as determined by AFM. 152

Figure 4.25 2D AFM images of adsorbed plasma proteins on flat surfaces 155

Figure 4.26 2D AFM images of adsorbed plasma proteins on nano-patterned surfaces..... 158

Figure 4.27 Roughness profiles of adsorbed plasma proteins on flat and nano-patterned surfaces as determined using AFM 160

Figure 4.28 Roughness values (RMS) of flat and nano-patterned surfaces in the presence and absence of plasma proteins as determined by AFM..... 161

Figure 4.29 QCM-D f and D response to albumin, fibrinogen and plasma proteins adsorption on flat silica, TiO2 and a-C:H flat surfaces..... 164

Figure 4.30 Comparison of albumin, fibrinogen and plasma protein mass attached to flat silica, TiO2 and a-C:H surfaces 168

Figure 4.31 Comparison of adsorbed fibrinogen and albumin concentrations on flat silica, TiO2 and a-C:H surfaces as determined using QCM-D 170

Figure 4.32 Df plots and final D vs.f ratio of fibrinogen and plasma adsorption on flat silica, TiO2 and a-C:H surfaces 172

Figure 4.33 Rate of fibrinogen and plasma adsorption as a function of mass on silica, TiO2 and a-C:H surfaces as determined using QCM-D 174

Figure 5.1 Fluorescence microscope images of platelets (actin) on bare or protein pre-coated (albumin, fibrinogen or plasma) TCPS and flat surfaces 185

Figure 5.2 SEM images of platelets on albumin pre-coated flat surfaces..... 186

Figure 5.3 SEM images of platelets on bare flat surfaces..... 187

Figure 5.4 SEM images of platelets on fibrinogen pre-coated flat surfaces. 187

Figure 5.5 SEM images of platelets on plasma pre-coated flat surfaces 188

Figure 5.6 Platelet aggregation on fibrinogen pre-coated ta-C, and plasma pre-coated silicon surfaces as visualised using SEM..... 189

Figure 5.7 2D and 3D AFM topographical images of platelets on fibrinogen pre-coated a-C:H flat surfaces 191

Figure 5.8 Amount of adhered platelets and mean percent platelet coverage on bare and protein pre-coated flat surfaces 194

Figure 5.9 Number of round and spread platelets on bare and protein-precoated flat surfaces..... 196

Figure 5.10 Ratios of round and spread platelets on bare and protein-precoated flat surfaces..... 197

Figure 5.11 Fluorescence microscope images of platelets (actin), pre-incubated with ReoPro, on bare or protein pre-coated (albumin, fibrinogen or plasma) flat surfaces..... 205

Figure 5.12 Amount of adhered ReoPro-bound platelets and mean percent platelet coverage on bare and protein pre-coated flat surfaces 206

Figure 5.13 2D and 3D AFM topographical images of ReoPro-bound platelets on fibrinogen pre-coated a-C:H flat surfaces 208

Figure 5.14 Number of round and spread ReoPro-bound platelets on bare and protein-precoated flat surfaces 209

Figure 5.15 Fluorescence microscope images of platelets (actin) on bare or protein pre-coated (albumin, fibrinogen or plasma) nano-patterned surfaces..... 216

Figure 5.16 SEM of platelets on albumin pre-coated nano-patterned surfaces 217

Figure 5.17 SEM of platelets on bare nano-patterned surfaces 217

Figure 5.18 SEM of platelets on fibrinogen pre-coated nano-patterned surfaces.... 218

Figure 5.19 SEM of platelets on plasma pre-coated nano-patterned surfaces. 218

Figure 5.20 2D and 3D AFM topographical images of platelets on fibrinogen pre-coated a-C:H nano-patterned surfaces 220

Figure 5.21 2D and 3D AFM topographical images showing platelet-platelet interaction on fibrinogen pre-coated a-C:H nano-patterned surfaces. 221

Figure 5.22 Amount of adhered platelets and mean percent platelet coverage on bare and protein pre-coated nano-patterned surfaces..... 223

Figure 5.23 Number of round and spread platelets on bare and protein-precoated nano-patterned surfaces..... 225

Figure 5.24 Df plots of normal and ReoPro-bound platelets on albumin pre-coated flat silica, TiO2 and a-C:H surfaces 229

Figure 5.25 D*f* plots of normal and ReoPro-bound platelets on bare silica, TiO2 and a-C:H surfaces. 232

Figure 5.26 D*f* plots of normal and ReoPro-bound platelets on fibrinogen pre-coated flat silica, TiO2 and a-C:H surfaces 234

Figure 5.27 D*f* plots of normal and Reopro-bound platelets on plasma pre-coated flat silica, TiO2 and a-C:H surfaces 237

Figure 6.1 PT clotting times on flat surfaces 243

Figure 6.2 Change in PT clotting times on flat surfaces at increasing heparin concentations 244

Figure 6.3 APTT clotting times on flat surfaces 245

Figure 6.4 Change in APTT clotting times on flat surfaces at increasing heparin concentations 246

Figure 6.5 TT clotting times on flat surfaces 248

Figure 6.6 Absorbance detected for ReoPro binding to activated αIIbβ3 receptors on platelets exposed to bare and protein pre-coated flat surfaces as determined by ELISA 251

Figure 6.7 Absorbance detected for anti-α2β1 antibody binding to activated α2β1 receptors on platelets exposed to bare and protein pre-coated flat surfaces as determined by ELISA 252

Figure 6.8 Fluorescence microscope images of platelets (FITC-ReoPro + actin) on albumin pre-coated nano-patterned surfaces 255

Figure 6.9 Fluorescence microscope images of platelets (FITC-ReoPro + actin) on bare nano-patterned surfaces. 257

Figure 6.10 Fluorescence microscope images of platelets (FITC-ReoPro + actin) on fibrinogen pre-coated nano-patterned surfaces 259

Figure 6.11 Fluorescence microscope images of platelets (FITC-ReoPro + actin) on plasma pre-coated nano-patterned surfaces 261

Figure 6.12 Fluorescence microscope images of platelets (RPE-CD62P + FITC-ReoPro) on albumin pre-coated flat surfaces 265

Figure 6.13 Fluorescence microscope images of platelets (RPE-CD62P + FITC-ReoPro) on bare flat surfaces. 267

Figure 6.14 Fluorescence microscope images of platelets (RPE-CD62P + FITC-ReoPro) on fibrinogen pre-coated flat surfaces.. 269

Figure 6.15 Fluorescence microscope images of platelets (RPE-CD62P + FITC-ReoPro) on plasma pre-coated flat surfaces. 271

Figure 6.16 Fluorescence microscope images of platelets (RPE-CD62P + FITC-ReoPro) on albumin pre-coated nano-patterned surfaces 275

Figure 6.17 Fluorescence microscope images of platelets (RPE-CD62P + FITC-ReoPro) on bare nano-patterned surfaces. 277

Figure 6.18 Fluorescence microscope images of platelets (RPE-CD62P + FITC-ReoPro) on fibrinogen pre-coated nano-patterned surfaces 279

Figure 6.19 Fluorescence microscope images of platelets (RPE-CD62P + FITC-ReoPro) on plasma pre-coated nano-patterned surfaces 281

Figure 6.20 Flow cytometric analysis of αIIbβ3 activation on suspended platelets exposed to bare and protein pre-coated, flat and nano-patterned surfaces 285

Figure 6.21 Flow cytometric analysis of CD62 P-selectin expression on suspended platelets exposed to bare and protein pre-coated, flat and nano-patterned surfaces..... 287

Figure 10.1 Schematic diagram of the X-ray photoelectron spectroscopy 344

Figure 10.2 Schematic diagram of SEM 345

Figure 10.3 Schematic diagram of the FIB column 346

Figure 10.4 Focused ion beam induced milling 347

Figure 10.5 Principles behind AFM operation..... 348

Figure 10.6 Basic principles behind flow cytometry 355

LIST OF TABLES

Table 4.1 Thickness of a-C:H, ta-C and TiO2 thin film coatings as determined using FIB. 114

Table 4.2 Surface roughness (RMS) of bare QCM and flat surfaces as determined using AFM 119

Table 4.3 Surface roughness (RMS) of nano-patterned surfaces as determined using AFM. 125

Table 4.4 Nano-topography induced increase ((as a percentage) in 2C2-G7 binding to adsorbed fibrinogen on silicon, TiO2, a-C:H and ta-C 143

LIST OF PUBLICATIONS

In Preparation:

Surface analysis and blood-compatibility of novel nanostructured Diamond-like Carbon & Titania films
Deepika Nandakumar, Avi Bendavid, Phillip Martin, Kenneth Harris, Andrew Ruys, Megan Lord

Biophysical analysis of albumin and fibrinogen adsorption on biomaterial surfaces
Deepika Nandakumar, Avi Bendavid, Kenneth Harris, Andrew Ruys, Megan Lord

Protein, platelet and clotting factor interactions on surface engineered Diamond-like Carbon & Titania surfaces with varying nano-topographies
Deepika Nandakumar, Avi Bendavid, Phillip Martin, Kenneth Harris, Andrew Ruys, Megan Lord

Blood compatibility of Diamond-like Carbon surfaces
Deepika Nandakumar, Avi Bendavid, Phillip Martin, Kenneth Harris, Andrew Ruys, Megan Lord

ABBREVIATIONS

a-C:H	amorphous hydrogenated carbon
ADP	adenosine diphosphate
AFM	atomic force microscopy
AMP	adenosine monophosphate
ATP	adenosine triphosphate
BSA	bovine serum albumin
c-AMP	cyclic adenosine mono-phosphate
c-GMP	cyclic guanosine mono-phosphate
D	dissipation
D*f* plot	dissipation versus frequency plot
DLC	diamond like carbon
DPBS	Dulbecco's phosphate buffered saline
ELISA	enzyme-linked immunosorbent assay
ESAM	endothelial cell specific adhesion molecule
f	frequency
Fg	human fibrinogen
FIB	focused ion beam (SEM)
hz	hertz
IgG	immunoglobulin
mAb	monoclonal antibody
PECVD	plasma enhanced chemical vapour deposition
QCM	quartz crystal microbalance
QCM-D	quartz crystal microbalance with dissipation
RMS	root mean square
SEM	scanning electron microscopy
Si	silicon
ta-C	tetrahedral amorphous carbon

TCPS	tissue culture polystyrene
TEM	transmission electron microscopy
TiO_2	titania (also known as; titanium dioxide)
TxA_2	thromboxane-2
XPS	X-ray photoelectron spectroscopy

1 INTRODUCTION

Cardiovascular disease (CVD) has become the leading killer of men and women with mortality and morbidity rates of approximately 17 million people each year [1]. Apart from an ageing popular, with average life expectancy of 80+ years and increasing [2], increases in the prevalence of cigarette smoking, stress, obesity and decreases in participation in physical activity have been shown to exacerbate this epidemic over the last few decades [3]. Almost 3.5 million Australians have been reported to suffer from long-term cardiovascular diseases, with over 500,000 deaths attributed to this cause each year [3]. Invasive treatments for cardiovascular diseases have been shown to reduce the quality of life for many and are a significant socioeconomic burden on our economy [4].

Almost all cardiovascular devices and cardiovascular disease related procedures, either short-term or long-term, require significant anticoagulation, at high cost and with considerable risk to the patient [5]. In Australia, approximately $5.9 billion dollars are spent each year in health care expenditure, of which, approximately $3 billion dollars been spent on hospitalisation, $1.6 billion on prescriptions and over $1.1 billion on medical services such as implants, and post-operative care [3]. In terms of the world market for medical devices, cardiovascular devices were forecasted to grow in single digit percentage each year and likely to exceed USD $27 billion dollars by 2017 [6]. Despite the millions of dollars spent on the research and development of cardiovascular implants and blood-compatible materials, the formation of blood clots (thrombosis) remains a major problem with blood-contacting devices. Even after six decades, a truly blood compatible (haemocompatibile) biomaterial is yet to be identified [5].

The design of haemocompatible biomaterials is complicated by our poor understanding of not only the individual blood–material interactions that contribute to platelet adhesion and contact activation, but also the consequences of their interplay to coagulation as a whole. From what is understood, blood contacting

devices such as catheters, blood vessel grafts, vascular stents, artificial heart valves, circulatory support devices, various extracorporeal tubings, hemodialysis, hemapheresis and oxygenator membranes perform in a corrosive bio-environment due to the metabolic activity of the cells and fluids in our body, which, for biomaterials with a low wear resistance, causes the release of metal ions and wear debris. Platelets play a crucial role by recognizing and adhering to the surface of the foreign implant and its wear debris, signalling additional platelets and forming a haemostatic plug as part of the coagulation cascade. This response is initiated by the rapid adsorption of plasma proteins, such as the fibrinogen, followed by its adhesion and activation. Therefore studying the interplay between platelets and the biomaterial surface is necessary to overcome thrombogensis-related device failure - especially when considering the potential of surface modifications such as diamond like carbon (DLC) or titania (TiO_2) coatings, which can greatly influence these interactions.

Inorganic coatings such as diamond-like carbon (DLC) and titania (TiO_2), because of their excellent mechanical properties and smooth surface finishing have gained popularity for their use as an effective surface modification on implantable devices. Both materials' have been shown to improve haemocompatibility without affecting the mechanical and physical properties of the underlying bulk material. Despite the excellent response to blood proteins and cells *in vitro* and *in vivo*, unexpected negative results from various clinical studies significantly affect their potential as a passivating coating for cardiovascular applications. A better understanding of the material science in relation to their interaction with blood proteins and cellular components is needed. At present, no consistent relationship has been established between the materials' physical and chemical structure, and its haemocompatibility. The exact mechanism behind the preferential adsorption of fibrinogen and albumin during blood interaction, or the complex and synergistic interactions between platelets and plasma proteins on such surfaces are still not fully understood.

Aims

The overall purpose of this study was to investigate the role of plasma proteins, surface chemistry and nano-patterned surface on the haemocompatibility of biomaterial surfaces, and to enhance the overall understanding of haemostatic responses on biomaterial surfaces.

The specific aim of this study was investigated by:

1. Characterising TiO_2, a-C:H, ta-C surface coatings with varying nano-topographies;
2. Investigating the adsorption of serum protein and, platelet adhesion and aggregation on surfaces pre-coated with serum proteins; and,
3. Analysing the activation of platelets and clot formation on protein pre-coated surfaces

2 LITERATURE REVIEW

2.1 The Cardiovascular System

The cardiovascular system, also known as the circulatory system, is mainly composed of the heart, blood and blood vessels, and, plays an important role in sustaining life by maintaining homeostasis. The cardiovascular system aids behaves as a transport system by circulating O_2 (oxygenated), CO_2 (deoxygenated), heat, metabolic wastes, nutrients, electrolytes and regulatory hormones within the body. These materials are carried by blood in its dissolved as well as its suspended state. The flow of blood is continually directed by the vasculature as well as chemical and topographical cues released within the vascular walls [7]. A schematic of the human circulatory system is shown in Figure 2.1.

2.1.1 Blood Vasculature

Blood vessels are conduits forming two vascular loops called the systemic and pulmonary circulation. Each loop forms a closed-system with a continuum of different blood vessels that begin and end with the heart. Pulmonary circulation carries blood between the heart and the lungs and the systemic circulation carries blood between the heart and other body tissues.

Arteries rapidly distribute blood from the heart to various organs by expanding the arterial wall elastically. When the heart relaxes, the elastin fibres tighten causing the wall passively recoil and consequently forcing excess blood within the arteries downstream. The collagen fibres in the arterial connective tissue provide strength against high inter-luminal pressure caused by pumping of the heart. Arteries sequentially diverge into smaller arteries and once reaching an organ the smaller

arteries branch into numerous arterioles to supply oxygenated blood within the organ tissues. Arterioles provide high resistance against blood flow. Due to their significantly smaller radius, a major drop in mean arterial pressure occurs when blood flows from small arteries to arterioles. Arterioles branch further to form the smallest vessels, called capillaries, where all exchanges are made with surrounding cells via diffusion.

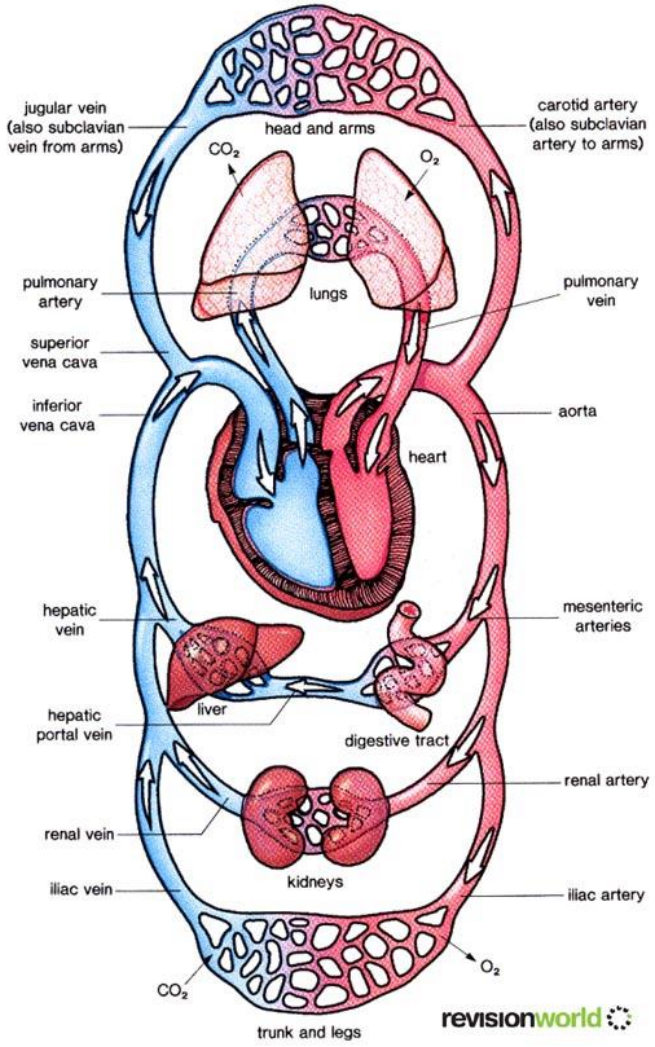

Figure 2.1 Schematic diagram of the circulatory system [8]

Capillaries have 1µm thin walls with a lumen which is approximately 7µm thick, enough to facilitate one red blood cell to pass through at a time. Extensive capillary branching reduces blood flow rate and increases the available surface area for heat, metabolite and nutrient exchange with the nearest cell. Pores on capillary walls are

filled with water to permit water soluble material exchange. Branched capillaries reconverge to form venules and eventually merge into small veins. Smaller veins reunite to form large veins which carry deoxygenated blood from the organs back to the heart. Venules and veins have little tone (thin smooth muscle layer) and resistance. Veins especially, have large luminal diameter with little luminal elastin and hence are often called capacitance vessels. They act as storage reservoirs, constantly distending to accommodate higher blood volume without recoil. Sequentially located, one-way venous valves counteract gravitational effects by preventing back flow of blood. Movement from skeletal muscles greatly facilitates passage of blood through the veins back to the heart. A schematic cross-section of arteries and veins is shown in Figure 2.2.

Typically, the blood vessel wall is composed of three layers: intima, media and adventitia, except for the capillaries, which consist of a single layer of endothelial cells. The outermost layer of arteries and veins are called the tunica adventitia. It is made up of collagen and elastic fibres which form the connective tissue of the vessel wall. The intermediate layer, called the tunica media, is composed of smooth muscle and elastic fibres, and inner layer of the arteries and veins are called the tunica intima. In arteries, the intima layer is made up of smooth endothelium lined with an elastic membrane that is covered by elastic tissues. Veins, on the other hand, do not contain this elastic membrane lining. The innermost layer of tunica intima is composed of endothelial cells. Endothelial cells are simple squamous epithelial cells that act as a semi permeable membrane between and tissue and blood in the lumen.

These cells are regulated by hormones and growth factors which circulate in blood and are involved in vascular regulation by releasing vasoconstrictors and vasodilators, secretion of immune-regulatory and neuro-regulatory factors to sustain haemostasis, differentiation and proliferation of cell mediated and humoral response immune cells, as well as induction of inflammatory response by activating leukocytes at site of tissue injury or infection, and, blood clot formation by angiogenesis, coagulation and vasculogenesis [9].

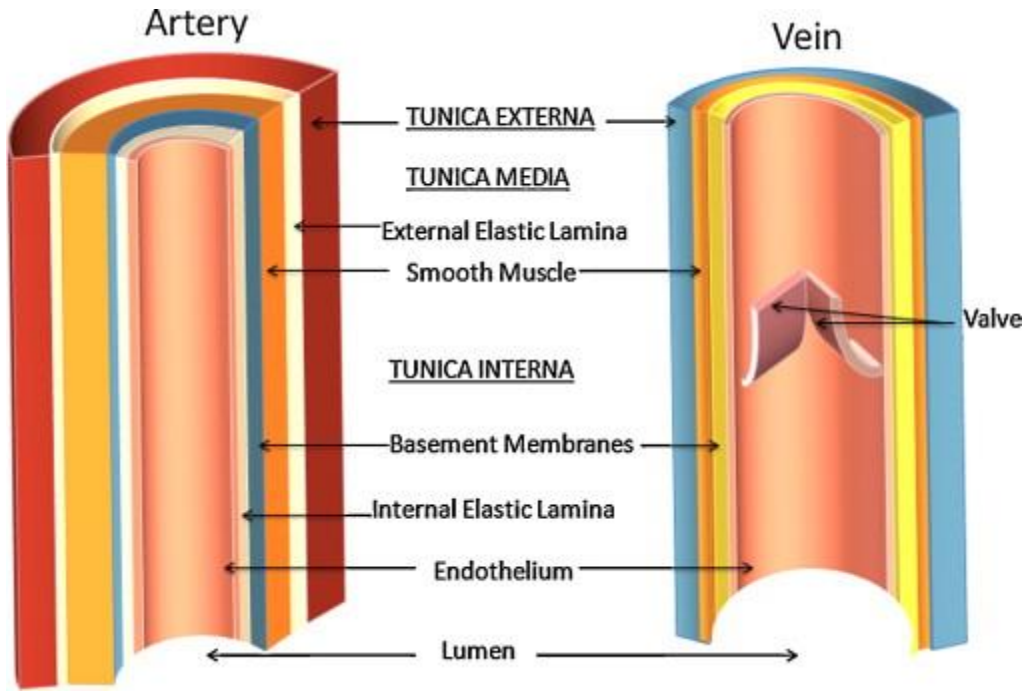

Figure 2.2 Schematic cross-sectional diagram showing the structural layers of arteries and veins [10]

2.1.2 Blood and Its Composition

Almost 8% of our total body weight is represented by blood. Women approximately carry 5 litres of blood while men carry over 5.5 litres. Blood is composed of three types of specialised cells; erythrocytes (red blood cells), leukocytes (white blood cells) and platelets (thrombocytes), all differentiated from haemocytoblast cells, as shown in Figure 2.3. These blood cells are suspended in a pool of complex liquid, called plasma. In fact over 99% of the cells in plasma are erythrocytes. The average packed cell volume, also known as 'haemocrit' of blood, consists of 45% erythrocytes (5 billion red blood cells per 1mm blood volume), 55% blood plasma and less than 1% of platelets and leukocytes.

The major role of blood is to maintain homeostasis. This is done by transporting materials to and from cells, distributing oxygen to cells for energy synthesis, pH balance, removing excess heat from the body, defending the body against pathogens

and foreign material by providing immunity, initiating haemostatic response and consequently surface induced-thrombosis during vascular damage.

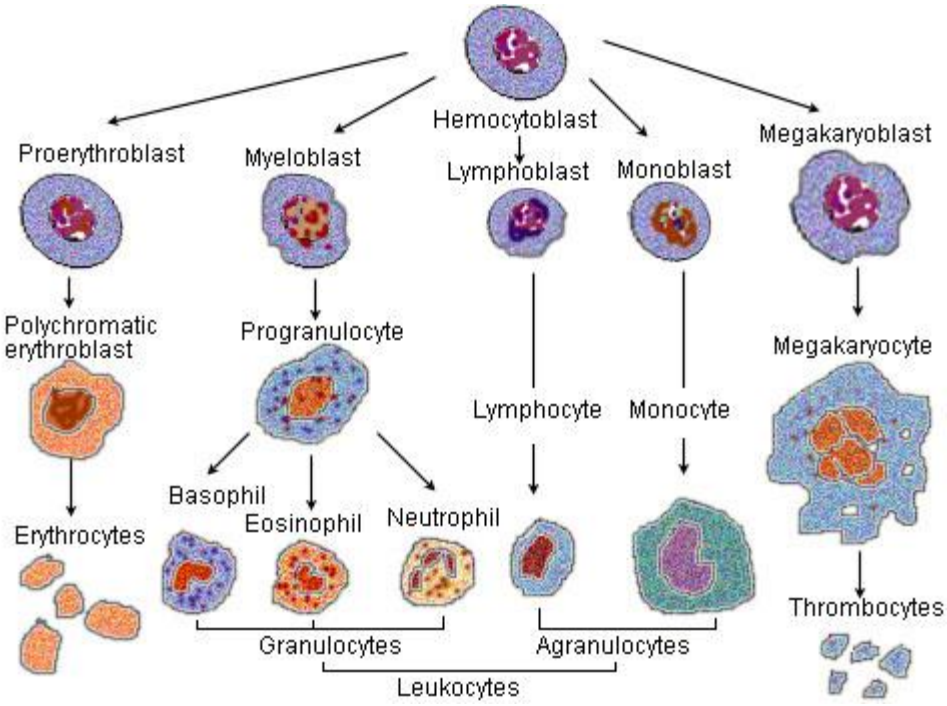

Figure 2.3 Differentiation of haematopoietic stem cells showing the three types of blood cells: red blood cells, white blood cells and platelets [11]

Haemostasis is a process that involves the minimisation of blood loss and the control of haemorrhage to avoid total exanguination [12, 13]. Under normal physiological conditions, the endothelial layer of the vessel wall behaves as a thrombo-resistant surface, promoting anti-thrombotic activities which allow the blood remain in its fluidic state [14, 15]. However, when the walls of the vasculature are damaged, blood circulating within the vessel walls becomes exposed to cells and sub-endothelial extra cellular matrix (ECM) within the wall causing an immediate and rapid haemostatic response as well as an inflammatory response. The haemostatic response involves two simultaneously occurring, yet distinctive, stages;

- The contraction of smooth muscle cells with the blood vessels, known as, primary haemostasis
- The adhesion and activation of blood platelets as well as the coagulation of plasma proteins, known as the secondary haemostasis

Implantation of a cardiovascular device represents the introduction of a foreign material, with properties different to that of the endothelium. Even after vascular healing, the interaction between blood and the blood-contacting surface of the biomaterial triggers a series of complex and interlinked events (Figure 2.4).

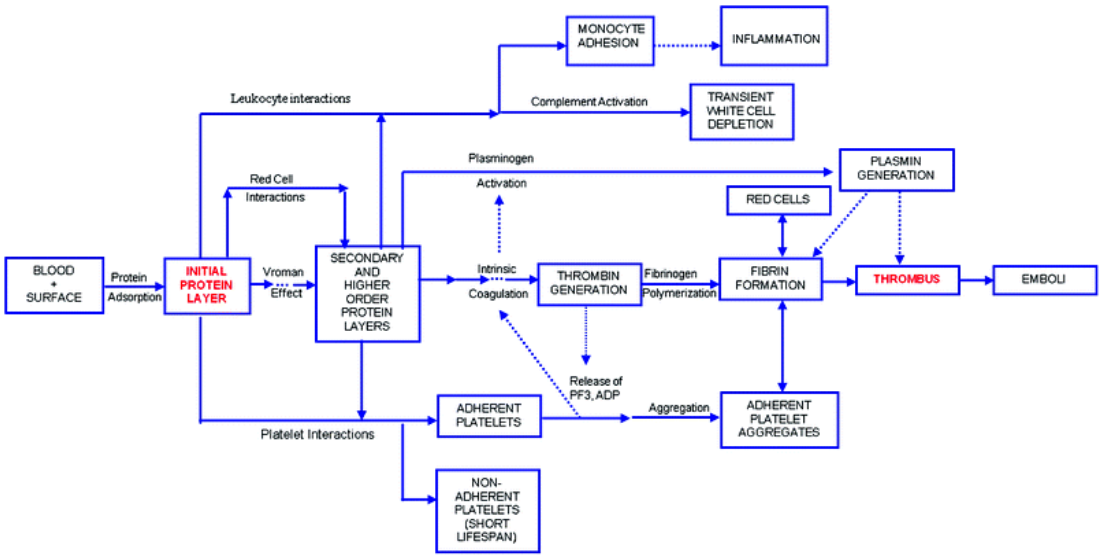

Figure 2.4 Overview of blood biomaterial interactions [16]

This includes: protein adsorption, platelet and leukocyte activation/adhesion, and the activation of complement and coagulation system (Figure 2.5); all of which are mechanisms of a thrombotic response to the biomaterial.

The following subsections explain the interaction between plasma proteins, blood platelets and white blood cells to produce the observed thrombosis during vascular injury as well as during blood-biomaterial interactions.

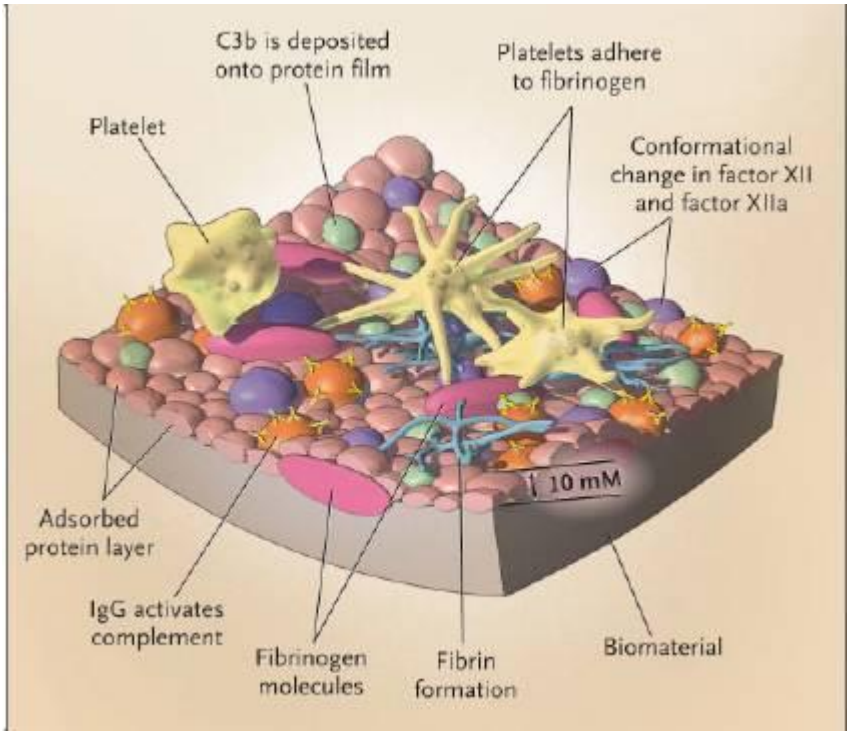

Figure 2.5 Typical response of blood to biomaterial surfaces [17]

2.1.3 White Blood Cells

White blood cells, or leukocytes primarily function to defend the human body by providing an immune barrier against pathogens and other foreign materials [18]. The inflammatory response is initiated almost immediately after platelet activation and also aids in the removal of damaged cells [19, 20].

The five main types of leukocytes include; neutrophils, eosinophils, basophils, monocytes, and, B- and T- lymphocytes. Lymphocytes provide targeted defence against pathogens. B-lymphocytes produce antibodies against a specific pathogen causing antibody-mediated destruction while T-lymphocytes produce destructive chemicals and chemotaxis against infected or aberrant cell, inducing a cell mediated immune response. Eosinophils respond during allergic reactions and attack parasitic worms. Basophils release two chemicals, heparin and histamine. Heparin dissolves fat content in blood and prevents blood coagulation. Histamine is involved in increasing blood flow by causing vasodilatation and smooth muscle contraction in

response to allergic reactions. Neutrophils are the most leukocytes and they represent 40–60% (3–5 x 10^6 neutrophils/ml) of the total leukocyte count in blood, while, monocytes represent 5% with a concentration of 0.2–1 x 10^6 monocytes/ml. Neutrophils have a half-life between 8-20hours and behave as phagocytes by engulfing bacteria and debris. On the other hand, monocytes, with half lives of 2-4 days, migrate into tissues where they maturate and differentiate into macrophages before ingest foreign material and debris, in a similar manner to neutrophils [21]. Together, leukocytes and their derivates with the help of certain plasma proteins make up the immune system.

The two main cell types involved with inflammatory response with cardiovascular devices are neutrophils and monocytes. These cells are known to further contribute to localised thrombogenesis [22]. When an inflammatory response triggered by stimulants such as cytokines, neutrophils take on a more active role and increase their lifespan by three-fold [23], while, monocytes increase their life span and deposit onto the damaged blood vessel for a short time before differentiating into macrophages. Both, monocytes and neutrophils, have been shown to activate by pro-inflammatory mediators such as platelet activating factors and cytokines, complement proteins, adhesion, spreading and activation of blood platelets as well as β-thromboglobulin and platelet derived growth factors (PDGF) release by platelets, adhesion of other cells, as well as bacteria and their products [24-26].

Several studies looking at inflammatory response from angioplasty [27], haemodialysis [28], and cardiopulmonary bypass [29] have shown that leukocyte activation causes a change in the expression of membrane receptors such as CD11b, synthesis and expression of tissue factor, release of inflammatory mediators such as tissue necrotic factor (TNF), release of granular contents (degranulation) and cytokines, production of arachidonic acid metabolites, such as leukotriene B4 and platelet activating factor on neutrophils and/or monocytes [30]. Large biomaterial surfaces cannot be engulfed by leukocytes as such adherent neutrophils and monocytes undergo a frustrated phagocytosis whereby they release oxidants such as O_2^- and H_2O_2 and increase their adhesive capacity on endothelial cells and other

surfaces by interacting more favourably with adhesive molecules such as L-selectins, immunoglobulins and integrins [21, 27, 31]. When adhering on endothelial cells, leukocytes roll onto endothelial cells by latching onto the cell's L-selectin molecules. This inevitably reduces their speed and the leukocytes become activated due to local stimulation and additional interaction between leukocyte receptors and cellular ligands. Over-expression and functional changes of leukocytes CD11 receptors occur, further increasing the leukocytes adhesive properties to not only endothelial cells but also blood platelets. Platelets adhered on biomaterial surfaces have been known to mediate leukocyte adhesion via the interaction between platelet receptors P-selectin and $\alpha_{IIb}\beta_3$ with leukocyte receptors PSGL-1 and CD11b, respectively [32, 33]. Surface chemistry, surface topography as well as surface adsorbed proteins such as fibrinogen on the blood-contacting biomaterial have been shown to modulate the level of leukocyte adhesion and their activation [34, 35]. Several *in vivo* studies have shown neutrophil and monocyte adhesion on vascular grafts, stents, oxygenators, and haemodialysis membranes [34, 36-38].

2.1.4 Blood Platelets

Platelets are involved in blood clot formation to minimise blood loss and are known to be the primary cells involved in haemostasis. Under normal physiological conditions, circulating platelets remain in their 'rested' or 'inactivated' state while interacting with the thrombo-resistant endothelial lining of the vessel wall [39]. The endothelial cells release anti-coagulants such as prostacyclin and nitric oxide, as well as convert activation inducers such as adenosine diphosphate (ADP) into adenosine monophosphate (AMP) to maintain platelets in their inactive state [14, 15, 40].

In non-haemostatic conditions, platelets preserve the integrity of the vasculature by responding to minimal stimulation. They become activated upon contact with thrombogenic surfaces like: injured endothelium, sub-endothelium and artificial surfaces forming a haemostatic plug. The signalling pathway of circulating platelets

allows for their rapid capture at site of thrombogenic surface followed by a thrombotic response to arrest uncontrollable blood loss.

During vascular injury, damage to blood vessels exposes agonisits such as: sub-endothelial collagen, microfibrils and von Willebrand factor, to platelets and other blood elements, as shown in Figure 2.6. In addition to these agonists, thrombin, produced downstream of the coagulation cascade, also effectively activates platelet response.

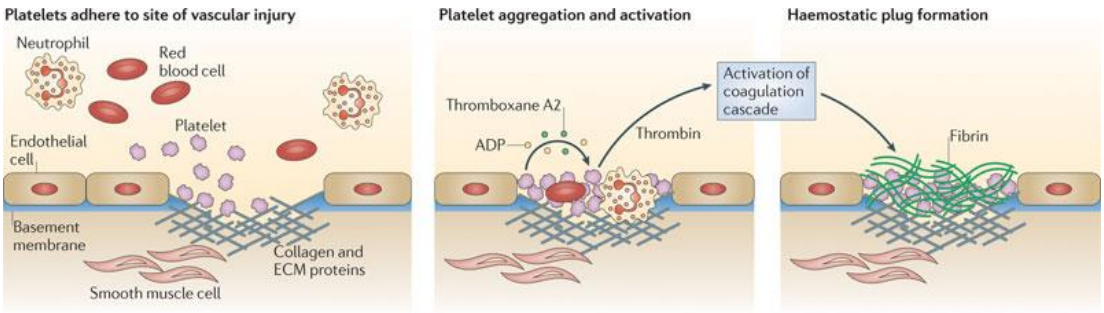

Figure 2.6 Platelet plug formation during haemostasis [41]

However, in the presence of blood-contacting artificial surfaces, platelet response is initiated by the interaction of extracellular stimulus such as: plasma proteins that rapidly adsorb on the platelet surface; exposed collagen from injury to surrounding tissues; molecules derived from: consequent inflammatory response, such as leukocytes, or, circulating activated platelets, such as platelet activating factor. This blood-biomaterial interaction also involves the coupling of the agonist to specific receptors on the platelet plasma membrane for platelet activation [22, 42].

Activated platelets adhere to sub-endothelial components, biomaterial surface and to each other, forming “white” thrombus. As such, the activation of platelets can be described in three steps: adhesion of platelets to collagen fibrils of the sub-endothelium or artificial surfaces; spreading and aggregation of platelets via autocatalytic signalling; activation of platelets and formation of a thrombus clot, although platelet spreading, aggregation and activation has been shown to occur simultaneously [43]. The three steps occur through interactions between extracellular

proteins and receptors on the platelet surface membrane [15]. The thrombus aims to effectively seal the haemorrhaging vessel. In depth review of platelet adhesion and their subsequent activation is detailed in the following sub-sections.

2.1.4.1 Platelet Biology

Platelets are colourless, outer-edge cell fragments shed from megakaryocytes (bone marrow cells, precursor to erythrocytic and leukocytic cell lines) and have a life span of 8-12 days before being removed and phagocytosed by macrophages. Platelets are vesicles containing megakaryotic cytoplasm surrounded by plasma membrane. Typically one thousand platelets are secreted from each megakaryocyte under the stimuli of thrombopoietin hormone. Spleen stores approximately 1/3rd of circulating platelets in blood filled pockets and releases during splenic contraction during sympathetic neuronal stimuli.

Resting platelets follow a discoid a-nuclear structure. They are 2-4µm in diameter and 1µm thick. Platelets are considered the smaller blood cells and they circulate the blood in concentrations of 2-3 x 10^8 cells per millilitre of blood. Platelets lack nuclei and thus do not store DNA. However, platelets contain RNA which gets transcribed during platelet activation, and, cytosolic enzymes and organelles for energy generation and, to synthesise and secrete chemicals from its secretory granules [44]. Actin and myosin proteins exist in high concentration within platelets to facilitate platelet contraction.

The bi-lamellar plasma membrane of the platelet is a multiple-channel, surface-connected canalicular system, which not only increases the surface area of the platelet but also tunnels granular secretory contents outside of platelets [42]. The plasma membrane skeleton, comprised of crosslinked short-actin filaments connected to plasma membrane via actin binding molecules, preserve the structural integrity of the plasma membrane by stabilising the lipid bilayer. Sodium and calcium ATPase pumps on the plasma membrane regulate ionic homeostasis by facilitating the

exchange of molecules to and from the ECM. Platelet receptors are located on the glycocalyx, an outer coating on the exterior surface plasma membrane [39, 45]. They serve as activating and inhibitory agents and are composed of glycoproteins (GP) such as: GPIaIIa, GP Ib, GP IIbIIIa and GP IV. The receptors are connected to the membrane's phospholipid bilayer made up of negatively charged phosphatidylinositol and phosphatidylserine residues. The negatively charged outer surface of the platelets have been suspected to minimise attachment between circulating platelets [45].

The intra-cytoplasmic tail of each receptor is in close contact with the actin and actin-binding contractile systems within the platelet cytoplasmic skeleton (also known as: platelet cytoskeleton). The platelet cytoskeleton not only maintains the rounded shape of the resting platelets, but also facilitates morphological changes within platelets during activation [46]. Actin exists in two forms: in its monomeric state (G-actin) and its polymerised state (F-actin) and constitutes to 15-20% of platelets total protein content. These actin filaments with association to proteins such as tropomysin, α-actinin and actin binding protein, make up a platelet's cytoskeleton. During platelet activation G-actin molecules polymerise causing an increase in the total F-actin concentrations from 30-40% to 60-70% [47, 48]. This causes platelets to change their morphology from a discoid shape to its spread form, with extended filopodia [47, 48]. Microtubular network in conjunction with the canal system forms the membrane complex that are involved in localising enzymes involved in the synthesis of prostaglandins and sequestering calcium ions [42]. The microtubular coil beneath platelet membrane, formed by tubulin proteins and short actin filaments (microfilaments), also sustain the discoid shape of an unstimulated platelet [49, 50]. During platelet activation, the microtubules disassemble then reassemble. The actin binding, myosin, molecules cross-link with actin filaments creating sufficient tension to centralise the granules within platelets [51].

The platelet's cytoplasm consists of numerous organelles such as: mitochondriae, glycogen, and peroxisomes; and granules such as: α- and dense granules and lysosomes. The α and dense granules are the two main types of granular components

in promoting immediate haemostatic response and they play an important role in storing growth factors, enzymes, receptors and mediators necessary for platelet function and their activity. During platelet stimulation these granules release all of their secretory contents. The more predominant α- granule is involved in the storage of platelet membrane receptors such as GPIb and GPIIb/IIIa. Apart from this, proteins such as platelet factor 4, β-thrombomodulin, platelet derived growth factors (PDGF), fibrinogen, fibronectin, thrombospondin, plasminogen activator inhibitor 1, von Willebrand factor, and other cytokines are also stored in α-granules [52, 53]. These proteins behave as pro-inflammatory mediators, receptor-ligand signalling and exert chemotactic responses during vascular injury [54]. On the other hand, dense bodies contain serotonin, adenosine diphosphate (ADP), adenosine triphosphate (ATP), magnesium and calcium, all of whom behave as pro-aggregation factors involved in the activation of platelets [42]. Lysosomes are primarily involved in the lysis of thrombus clots [55]. They contain enzymes such as: elastase [56], collagenase [57] and heparanase [58]; and are released upon stimulation from stronger agonists such as: collagen from ECM and thrombin from the blood plasma [54, 59].

2.1.4.2 Platelet receptors

The activity of platelets during haemostasis is dictated by platelet-membrane adhesive receptors. There are several different types of adhesive receptors on the membrane surface, of which most of them belong to the immunoglobulin (IgG) superfamily, integrins, cadherins and selectins. However, the most predominant family of receptors are known as the integrins [60]. Integrins have a primary role of mediating interactions between platelets; and between platelets and ECM and/or plasma proteins during the adhesion and activation process. This is carried out via inside-out integrin signalling from inside of platelets to the ECM and plasma protein ligands, as well as outside-in signalling [60]. The most important receptors involved during biomaterial related haemostasis and their respective ligands for binding are shown Figure 2.7.

Resting platelets have been found to express integrins: $\alpha_2\beta_1$ (GPIa/IIa), $\alpha_5\beta_1$ (GPIc/IIa), $\alpha_6\beta_1$ (GPIc'/IIa), $\alpha_v\beta_3$ (vitronectin receptor), and $\alpha_{IIb}\beta_3$ (GPIIb/IIIa) on its surface, where each integrin can bind to more than one ligand [61-64]. Of all the platelet receptors, GP Ib and $\alpha_{IIb}\beta_3$ integrins are predominantly and constitutively expressed with the highest densities on platelets.

Receptor	Ligand/agonist
(a) Receptors leading to platelet activation	
Thrombin receptor	Thrombin
Thromboxane A_2 receptor	TxA_2, PGH_2, PGG_2
V_1A receptor	Vasopressin
PAF receptor	Platelet activating factor
$5HT_2$ receptor	Serotonin or 5-OH tryptamine
α_2 receptor	Epinephrine
ADP receptor	ADP, ATP
PGE_2 receptor	PGE_2
C1q receptor	C1q
(b) Receptors leading to platelet inhibition	
A_2 receptor	Adenosine
PGI_2 receptor	PGI_2, PGE_1
PGD_2 receptor	PGD_2
(c) Platelet adhesion receptors (binding may also result in platelet activation)	
GPIa/IIa or VLA-2	Collagen
GPIb/IX or GPIb	Von Willebrand factor (vWF), thrombin
GPIc/IIa or VLA-5	Fibronectin
GPIc'/IIa or VLA-6	Laminin
GPIIb/IIIa	Collagen, fibrinogen, fibronectin, vitronectin, vWF
GPIV or GPIIIb	Collagen, thrombospondin,
GPVI	Collagen
Vitronectin receptor	Vitronectin, thrombospondin
PECAM-1	Heparin
Fcγ-RII	Immune complexes
ICAM-2	LFA-1
P-selectin	Sialyl-Le^x
Leukosialin, sialophorin	ICAM-1

GP: glycoprotein; VLA: very late antigen.

Figure 2.7 Platelet receptors involved in platelet biomaterial interactions [22]

During platelet activation, such as with blood vessel injury or due to biomaterial surfaces; the conformation of the resting integrin changes from its inactive state to its activated state. The control of change in conformational state from a low to high affinity state occurs within a short time frame, depending on their ligand-binding properties [64, 65] and can be characterised into inside-out and outside-in signalling [66, 67]. This is shown in Figure 2.8.

Inside-out signalling increases the binding affinity of integrins located outside the platelet membrane to bind to extracellular ligands. It involves the transfer of signal from an activator from the inside of an activated platelet, to the outside to ultimately control the adhesion strength and binding affinity between the integrins and, ECM proteins for the adhesion and aggregation of platelets. However, outside-in signalling is applicable for integrins that behave like traditional signalling receptors, where binding between integrins to their extracellular ligands causes a conformational change within the integrin leading to integrin clustering [68]. Often, inside-out signalling leads to outside-in signalling and vice versa.

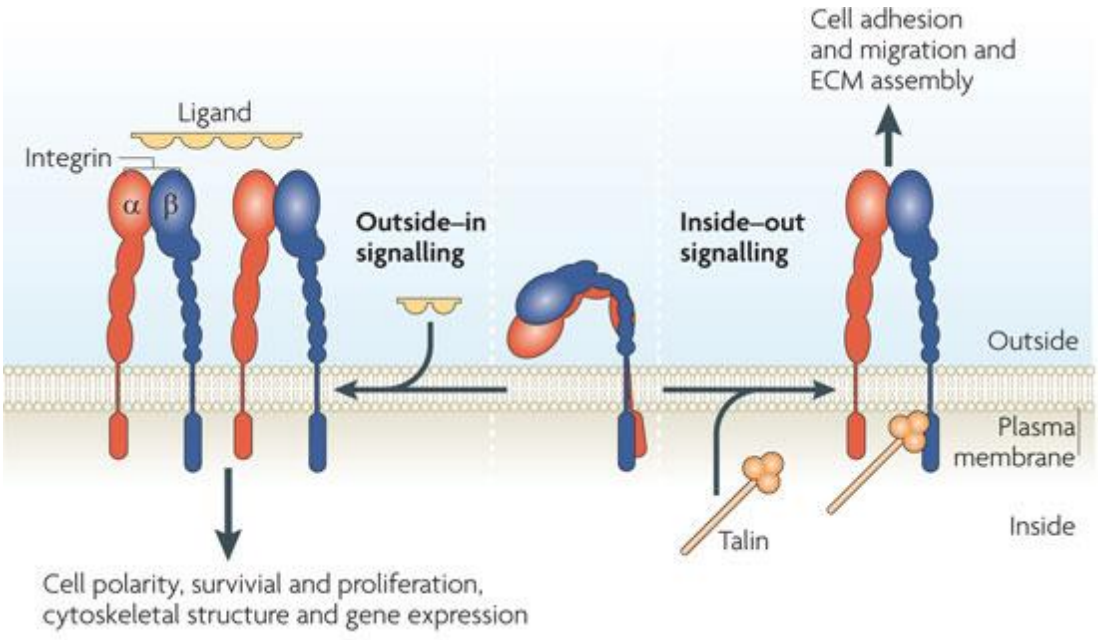

Figure 2.8 Inside-out and outside-in platelet integrin signalling [69]

For example: activation of platelet integrins may increase ligand binding, may generate outside-in signalling of other integrins; while, ligand binding caused by outside-in signalling may induce inside-out signalling of integrins [68].

2.1.4.2.1 GP Ib

GP Ib, also known as CD42, are leucine-rich glycoprotein receptors from the immunoglobulin super family. These receptors are generally complexed with GP IX. There are approximately 25,000 receptors present on the surface of circulating platelets [70, 71] and they appear as long molecules that are easily susceptible to conformational change upon shear stress caused by flowing blood. GP Ib indirectly mediates platelet interaction to collagen by binding to von Willebrand factor [72]. Under static conditions, GP Ib will not bind plasma von Willebrand factor without the presence of antibiotics such as: ristocetin; or, toxins such as: botrocetin snake venom is present. Shear stress induces the required conformational change within von Willebrand factor to increase it affinity to GP Ib receptors for receptor-ligand binding [22]. However, in the presence of biomaterial surfaces, GP Ib has been shown to bind to von Willebrand factor proteins adsorbed onto biomaterial surfaces both: under static and shear flow.

2.1.4.2.2 GP IIb/IIIa

GPIIbIIIa (CD41/CD61) is a symmetrical, heterodimeric, transmembrane molecule primarily known to bind to fibrinogen, although not exclusively, to enhance platelet activation. GPIIbIIIa have also been known to bind to von Willebrand factor and fibronectin to induce platelet spreading; and mediate platelet adhesion on biomaterial surfaces by preferentially binding to immobilised fibrinogen [73], in a similar manner to von Willebrand factor binding to GPIb. These receptors belong to the integrin family, where it is known as $\alpha_{IIb}\beta_3$. There are over 40,000-80,000 $\alpha_{IIb}\beta_3$ complexes on the surface of each platelet, and an additional 20,000-40,000 integrins

positioned in the α-granules and the canal system of the plasma membrane [70]. During activation, inside-out signalling triggers the release of stored integrins, where they get translocated to the platelet membrane to enhance the adhesiveness of platelets. Agonists such as thrombin, ADP and TxA_2 are potent activators of $\alpha_{IIb}\beta_3$ integrins [74, 75].

The $\alpha_{IIb}\beta_3$ receptors are made of two components; an α (GPIIb) subunit and β (GPIIIa) subunit, each produced from different genes [76]. The extracellular α-subunit is composed of a 125kDa extracellular heavy chain molecule and a 22kDa light chain molecule that protrudes into the cell membrane. The β-subunit consists of one single 95kDa chain that also traverses the cell membrane, similar to the α-light chain [75]. The NH_2 extracellular terminal on α- and β- subunits form a 3-D binding pocket for fibrinogen, and other ligands such as; von Willebrand factor, fibronectin and viteronectin [75]. The stability of the integrin structure is sustained by the pairing of their cystine rich residues via disulfide bonds [76]. During activation the Ca^{2+}, Mg^{2+}, and Mn^{2+} divalent cations on the extracellular α-domain behave as co-factors for integrin binding [77]. Fibrinogen uses the calcium dependent pathway when binding to the α_{IIb} subunit of $\alpha_{IIb}\beta_3$ complex via its RGD sequence located in fibrinogen's Aα and a 12 amino acid sequence located at the carboxyl terminus of its γ chain [42]. While, von Willebrand factor, thrombospondin, fibronectin and vitronectin adhesive glycoproteins bind to activated $\alpha_{IIb}\beta_3$ receptors via their RGD tract [78].

Resting platelets express $\alpha_{IIb}\beta_3$ receptors in their inactive form. The conformation of the inactive receptors present their low-affinity binding site to tightly regulate their adhesion to fibrinogen, however, upon platelet activation, a rapid conformational change occurs within the receptor exposing the receptor's high affinity binding site for soluble-fibrinogen [79]. Activation of the integrins increases their adhesive capacity, and thus facilitates aggregation of platelets by cross-linking with $\alpha_{IIb}\beta_3$ receptors on adjacent platelets, as well as, Mac-1 receptors on leukocytes by fibrinogen.

2.1.4.2.3 GP Ia/IIa

GPIa/IIa (also known as $\alpha_2\beta_1$, VLA2, CD49b/CD29) expressed on platelet membrane directly mediates the first contact of platelets to collagen and is a major receptor for collagen exposed from the subendothelial basement membrane [80-85]. Like $\alpha_{IIb}\beta_3$, $\alpha_2\beta_1$ is also a heterodimeric molecule, part of the integrin family. While, $\alpha_2\beta_1$ integrins have been implicated with primary interactions between collagen and platelets, they need to work in concert with GPIV (CD36) and GPVI receptors to sufficiently induce collagen dependent platelet activation [69, 86-93]. This is carried out by promoting a conformational change within $\alpha_{IIb}\beta_3$ receptors for platelet aggregation.

The $\alpha_2\beta_1$ complex is composed of an α_2 subunit of molecular weight 150 kDa and a β_1 subunit of molecular weight 130 kDa [94]. The I domain within the α_2 subunit (amino acids 140-349) is homologous to the A domain of von Willebrand factor, and it plays an important role in binding to collagen [94, 95]. Collagen is a long, insoluble, fibrillar-protein [82], that bind to the α_2-I domain via divalent cations located in the metal ion-dependent adhesion site (MIDAS) [94, 95]. The $\alpha_2\beta_1$ integrin, even at its low affinity state have been shown to mediate platelet adhesion to collagen, by binding to collagen's Gly-Phe-Hyp-Gly-Glu-Arg (GFOGER) peptide sequence. Binding of GFOGER site on collagen to the α_2-I domain in collagen have led to the activation of $\alpha_2\beta_1$ complex to its high affinity state[96]. This enhances the receptors adhesive properties to collagen proteins, resulting in platelet activation [80].

2.1.4.2.4 P-selectin

P-selectin (also known as CD62P, and previously known as PADGEM and GMP-140) is a member of the selectin family, along with L-selectin, E-selectin adhesive proteins [97, 98]. P-selectin is a single-chain transmembrane glycoprotein, rich in cystine residues with many N-linked oligosaccharide chains. It has a mass of

approximately 140kDa and shares common structural features with the selectin family: an N-terminal, extracellular calcium-dependent lectin domain (approximately 120 amino acid residues), a transmembrane domain, discrete complement regulatory-like repeated units (2 repeats for for L-selectins, 6 repeats for E-selectins and 9 repeats for P-selectins), epidermal growth factor (EGF) like domain and an intracellular cytoplasmic tail [99]. However, they are distributed differently on different cells.

P-selectin is located on the membrane of the α-granules of platelets. On activation, P-selectin is translocated and expressed on the membrane surface of activated platelets for a period of up to 1-4 hours (depending on the level of stimulus) before they are shed into blood plasma [100]. P-selectin receptors bind to mucin-like glycoprotein ligand for P-selectin (PSGL-1), commonly found on neutrophils, natural killer cells, monocytes and T-lymplocytes [101]. As such P-selectin is known for playing an important role in mediating the adhesion between activated platelets and neutrophils, monocytes and some lymphocytes. Furthermore, thrombin behaves as a potent agonist for increased surface expression of P-selectin on stimulated platelets [100]. As P-selectin expression on membrane surface only occurs on stimulated and activated platelets, the detection of P-selectin (CD62P) on the membranes of adsorbed platelets is considered as an indication of end stage activation. Furthermore, P-selectin is also found on the membrane of Weibel-Palade body of endotheial cells [102]. Upon endotheial stimulation, the endothelial P-selectins mobilise to the cell surface to facilitate possible interactions between activated platelets and endothelial cells.

2.1.5 Platelet Interactions

Platelet adhesion on implanted biomaterial surface or an injured vessel wall is known to be the primary and most important step in the sequence of events leading to the spreading and activation of platelets to form a haemostatic plug (thrombosis). The adhesion of platelets is a complex process involving platelet surface integrins and

exposed ECM proteins, as well as intracellular signalling processes which lead to activation and aggregation of platelets [103]. Furthermore, haemostatic interactions are further exacerbated by hydrodynamic conditions such as: shear rates and stress [104]. Platelets are susceptible to integrin activation when they are circulating at high shear rates, or velocity, however, there is time limited contact between the adhering surface and platelet integrins, decreasing the efficiency of platelet adhesion [105, 106]. This causes the detachment of adhered platelets increasing the likelihood of embolisation of platelet clots [105, 106].

2.1.5.1 Platelet adhesion and activation

During a thrombotic event, platelets adhere to and consequently spread when exposed to sub-endothelial collagen microfilaments of the vascular endothelial cell lining or adsorbed plasma proteins on biomaterial surfaces. In the event of a blood vessel injury, collagen directly binds to platelets via collagen receptors, $\alpha_2\beta_1$ and GPVI. GPVI receptors especially have been shown to generate a strongest activating signal. However, during high shear conditions, platelet adhesion is initiated by: fibrinogen, fibronectin and the most commonly occurring, collagen bound multimeric- von Willebrand factor. This occurs via $\alpha_{IIb}\beta_3$, $\alpha_2\beta_1$, GPIcIIa and GPIb platelet receptors [72]. Once platelets adhere to collagen, the probability of GPVI signalling mediated by collagen becomes greater with increased GPVI clustering [107]. Clustering of GPVI glycoprotein causes the phosphorylation of Fc receptor γ chain in GPVI by tyrosine kinases of the Src family [108] . Spleen tyrosine kinases identifies and activates in response to phosphotyrosine residues (PLCγ2) inducing the activation of PLCγ2. Phosphotyrosine residues further converts phosphatidylinositol (PI)-4, 5 P2 to 1,4,5- IP3and diacyl glycerol complex, opening calcium (Ca^{2+}) channels [109]. This causes a rapid store operated calcium entry increasing Ca^{2+} concentrations in the cytoplasm.

When blood is in contact with artificial biomaterials, platelet receptors recognise and bind to plasma proteins such as: fibrinogen, fibronectin, vitronectin,

immunoglobulins and von Willebrand factor [110-115]. However, of these proteins, fibrinogen has been shown to play a fundamental role in the adhesion process, while, fibronectin, von Willebrand factor and immunoglobulins have been shown to provide only a supporting role leasing to the activation of platelets [116-119]. Adsorbed fibrinogen binds to and activates platelet receptor integrin $\alpha_{IIb}\beta_3$ by changing the conformation of the β-integrins. This change causes a shift in the integrin from their low affinity into their high affinity state by inside-out signalling [120]. However, $\alpha_{IIb}\beta_3$ receptors in their low-affinity state have also been shown to bind to surface adsorbed fibrinogen [121]. The adhesion of platelets and their subsequent aggregation on biomaterial surfaces is shown in a schematic diagram in Figure 2.9.

Platelet spreading and subsequent activation on the site of vascular injury or biomaterial surface occurs as a result of tight binding of platelets to the surface when multiple focal contacts form with fibrinogen and other surface adsorbed proteins [122]. Fibrinogen, von Willebrand factor and fibronectin binds to $\alpha_{IIb}\beta_3$ integrins [123]. Adhesive proteins contain a RGD sequence at their cell recognition site, which behave as a switch for spreading. However, in the absence of fibrinogen, when von Willebrand factor binds to $\alpha_{IIb}\beta_3$, the integrin recognises the RGD sequence in von Willebrand factor and platelet spreading is initiated [42]. During activation, when the α granular membrane fuses with the plasma membrane, $\alpha_{IIb}\beta_3$ receptors from the α-granules along with any remaining $\alpha_{IIb}\beta_3$ intra-platelet receptors from the canaliculli system present themselves to the cell surface. Platelet aggregation occurs when fibrinogen, due to its symmetrical structure, acts as a bridge to connect activated $\alpha_{IIb}\beta_3$ receptors of adjacent platelets.

Hillary et al [124] showed phosphorylation of the cytoplasmic domain of the GPIIIa subunit of the $\alpha_{IIb}\beta_3$ receptor complex was necessary to activate the receptor prior to fibrinogen binding. Protein kinase C [125], and increased intracellular calcium ion levels provokes $\alpha_{IIb}\beta_3$ activation. However, protein kinase C activation can cause other integrin activation, aggregation and secretion independently of calcium (Ca^{2+}) ions [126].

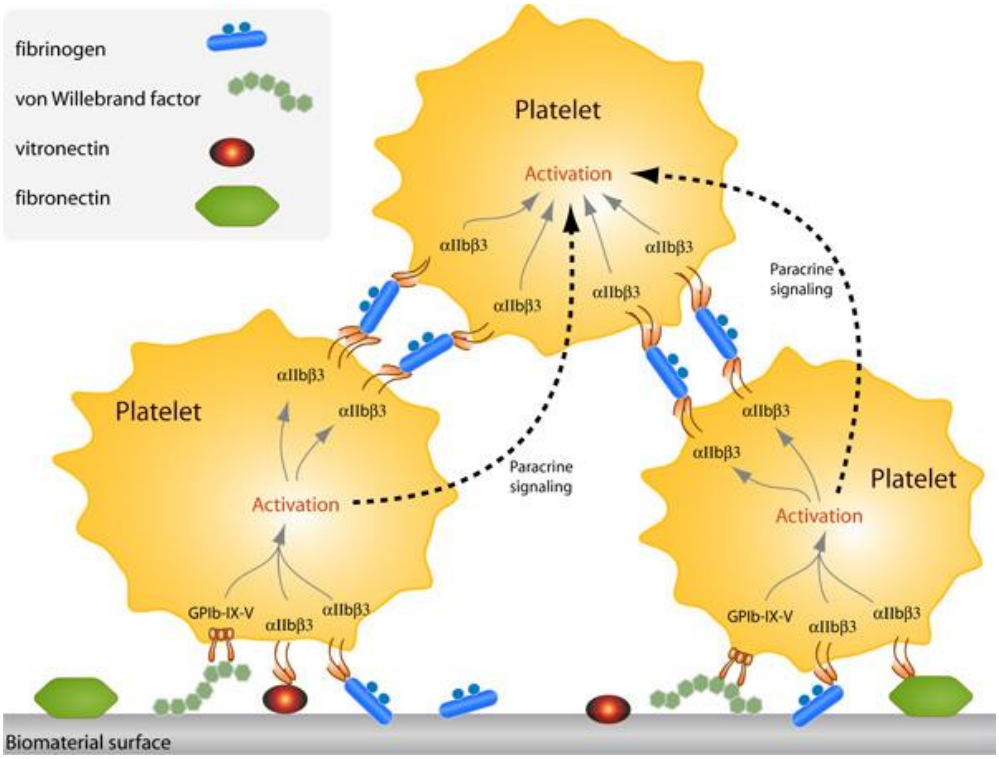

Figure 2.9 Platelet adhesion and aggregation on biomaterial surfaces [127]

Nitric oxide and prostacyclin (PGI_2) released from damaged endothelium elevates intracellular cyclic adenosine mono-phosphate (c-AMP) levels [128, 129]. C-AMP and cyclic guanosine mono-phosphate (c-GMP), governed by protein kinase C, down-regulates receptor exposure by phosphorylating threonine and serine residues of an intermediating regulatory protein. Following fibrinogen binding, a sequence of tyrosin phosphorylation of intracellular proteins, initiated by the β subunit [130] of the activated receptor, causes cytoskeletal rearrangements in platelets for filopodia development [92, 131, 132]. ADP released from the dense granules binds to P_2Y_1 and P_2Y_{12} receptors on platelets causing intracellular calcium ion mobilisation, which initiates a change in platelet morphology [133, 134] as shown in Figure 2.10. ADP also binds to P_2X_1, an ATP gated channel, opening the channel to facilitate the influx of extracellular calcium across the membrane [135]. Increase in calcium ion levels to 1μM activates Rap 1B (Ras family member) molecules [136], which further activates $\alpha_{IIb}\beta_3$ integrins [137]. Thrombospondin binds to GPIV inducing the stabilisation of fibrinogen bridges [138].

The aggregation reaction causes thromboxane-2 (TxA_2) synthesis. Furthermore, ADP released from dense granules, and thrombospondin released from α-granules of platelets enhances platelet aggregation. Agonists such as TxA_2 (by binding to TP receptors on platelets) and ADP (by binding to PAR1 and PAR4 receptors on platelets) along with the sequence of events following thrombin activation potentiate the growth of thrombus by forming a layered platelet plug. The above mentioned agonists signal via G-protein coupled receptors on the platelet surface facilitating the detachment of α and β subunits [139]. The dissociated subunits interact with platelet enzymes, adenyl cyclise, causing calcium ion release.

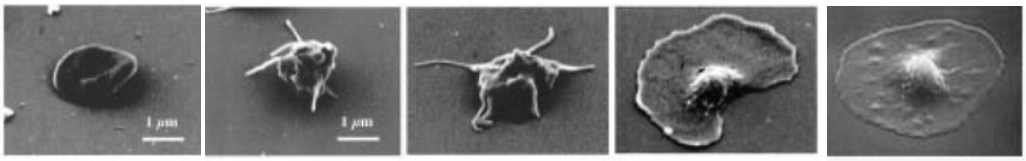

Figure 2.10 Morphological changes in platelets during activation. Image shows platelets in their rested state, various stages of shape change with filopodial extrusions and completely spread stage. [140]

During high shear stress conditions, such as during circulation through micro-vessels or stenoic arteries, aggregation is also mediated by von Willebrand factor and its interaction with GPIb. Following a series of events, upon binding, intracellular calcium ions increase causing conformational change in $\alpha_{IIb}\beta_3$ integrins activating the receptor for von Willebrand factor binding [141]. Downstream of fibrinogen bridge formation, extracellular to intracellular cell signalling occurs. Proteins such as talin, myosin, tyrosine kinases (spleen tyrosine kinase and Src) and C1B1 bind with the $\alpha_{IIb}\beta_3$ cytoplasmic domains causing the phosphorylation of the β_3 strand of the integrin [142]. Furthermore, binding of fibrinogen to this integrin causes an increase in Src activity causing an increase in integrin activation for thrombus. von Willebrand factor have been shown to bind to and activate GPIb, as well as, aggregate platelets by forming inter-platelet bridges by binding to adjacent $\alpha_{IIb}\beta_3$ integrins [138]. However, during low shear-shear stress conditions, fibrinogen, fibronectin and other platelet activators play an vital role in platelet aggregation [130, 143]. Clot stabilisation is controlled by adhesion molecules such as: junctional adhesion molecule A and C, which mediate the signalling process and attachment

between platelets and between platelets and leukocytes [144, 145]. Other adhesion molecules expressed on activated platelets include endothelial cell specific adhesion molecule (ESAM) [146], CD 226 [147], and, signalling lymphocyte activation molecule [148] and CD84 [149]. Receptor-ligand binding induces Rap1B integrin activation and signalling [142].

Structural changes during platelet activation

During platelet activation, platelets transition from their discoid shape to a spherical figure with extensive and pointed pseudopodia, by depolymerisation of microtubular bundles and polymerisation of actin monomers to actin filaments. The actin filaments cause surface of platelets to contract and form indents with bulky protrusions alongside. Actin monomers, in its resting state are bound to ADP. During activation, ATP becomes available for actin to assemble into ATP-bound monomers with two pointed ends, one low affinity actin binding end and one high affinity fast growing end [42]. Actin filaments form local adhesion sites with the plasma membrane by anchoring to transmembrane integrin molecules such as: $\alpha_{IIb}\beta_3$ [150] and one none non-integrin molecule GPIbIX. Stability of the focal adhesion point is regulated by a protein called RHO (member of the RAS family) [151]. Thrombin activation eventuates the activation RHO [152] and consequently, the activated RHO further activates kinases, which phosphorylate myosin light chain kinase, regulating actin dependent cytoskeletal shape [153-155]. Thrombin activates platelets in two way; first by signalling via PAR1 and followed by Par4 platelet receptors or by binding to GP1bα integrins [156-159]. In general, shape change can be either induced by many agonists such as: thrombin, TxA_2, vasopressin, platelet activating factor, U44069 and ADP via calcium independent pathways.

Microtubules and microfilaments within platelets re-assemble to form a central ring enclosing all the organelles. The granules are contracted towards the surface where its secretory contents are extruded. The membranes of granules fuse with the membrane complex releasing P-selectin (GMP-140, PADGEM – granular membrane

protein) into the plasma membrane. α-granules require high concentrations of an agonist, similar to lysosomal granule, which requires high concentrations of collagen or powerful activating agents like thrombin, to release their granular particles. Dense granule, on the other hand, can easily secrete its contents. Apart from these three granules, during activation and aggregation, when activated by agonists such as thrombin and collagen, platelets synthesise and release thromboxane (TX)A_2 and platelet activating factor to create a positive feedback loop. Immobilised calcium ion in platelets activates phospholipase A2 [160], which in turn modulates phospholipids in plasma membrane into arachidonate acid which in-turn forms TxA_2 by an enzyme called cyclooxygenase [161]. Due to its short half-life (30seconds), TxA_2 immediately crosses the membrane barrier activating surrounding platelets.

Di-acyl glycerol (a component of phospholipase C, which activates protein kinase C to release Ca^{2+} ions from dense tubular system) mediates the fusion of granular membrane to plasma membrane [109, 162]. Interaction of actin filaments with myosin heads facilitates contraction within platelets for granular centralization and secretion. ADP and collagen induces the phosphorylation of myosin molecule and the subsequent contractile movement between actin and myosin, while tropomyosin and caldesmon proteins in platelets regulate this process.

2.1.6 Coagulation Cascade

The coagulation of blood involves the transference of blood from its liquid state to a gel-like texture triggered by a chain reaction involving, platelets and coagulation factors. While platelets immediately establish a thrombus seal, called the primary hemostasis; soluble-coagulation factors (or clothing factors) from the blood plasma respond in a cascade of complex and sequential proteolytic (enzymatic) reactions, which results in formation of a fibrin-dependant blood clot. This is shown in Figure 2.11.

Initiation of fibrin-dependant clotting occurs either by endothelial surface-mediated reactions, or through tissue factor (TF) expression by cells, leading to the formation of Factor Xa. The tissue factor dependent clotting follows the extrinsic pathway, while the negatively charged surface-mediated clotting occurs via the intrinsic pathway. The common pathway refers to the series of events that follow downstream of thrombin formation to produce fibrin clot. Essentially thrombin cleaves fibrinogen to fibrin allowing fibrin monomers subsequent polymerisation which strengthens the platelet plug.

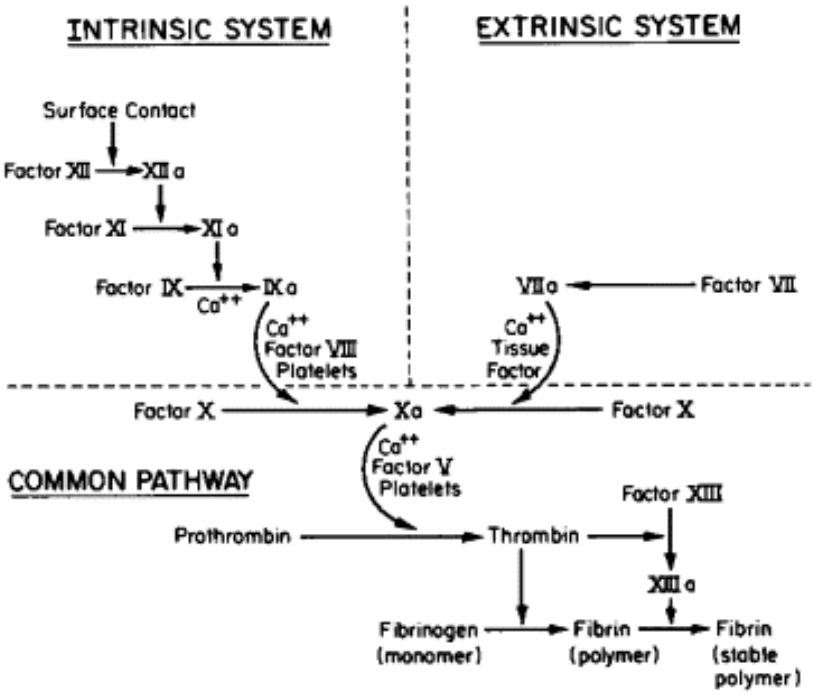

Figure 2.11 Simplified version of the coagulation cascade. [22, 163]

The activation of the clotting factor occurs as an inactive factor becomes enzymatically active upon contacting a surface or after being proteolytically cleaved by other enzymes. Once activated, the newly activate enzyme then activates another inactive precursor factor, until Factor XIII is activated by thrombin. Fibrinogen then crosslinks to form and stabilise the fibrin clot into an insoluble fibrin gel. The fibrin chain holds the loosely aggregated platelets, and can be degraded via fibrinolysis [164]. Occurring simultaneously, the fibrin clot reinforces and stabilises the initial platelet plug, inducing a more efficient secondary hemostasis.

With the exclusion of thrombin and fibrin, the newly formed enzymes have low activity until they bind to membrane receptors of the activated platelet or to enzyme-specific protein co-factors. This cascading reaction process is mediated by the presence of plasma inhibitors and active proteases.

2.1.6.1 The Extrinsic Pathway

Tissue factor, usually absent from blood-contacting cells but expressed on damaged non-vascular cells at the site of injury [165], binds to the inactive plasma Factor VII and activates this vitamin K-dependent factor. In specific, monocytes [166-168] and leukocytes (because of monocytes) [169], in the presence of a blood contacting biomaterial have been shown to express tissue factors. Under normal conditions, approximately 1% of available Factor VII circulates in plasma in their activated state (Factor VIIa) [170]. Upon exposure to tissue factor, Factor VII and VIIa form tissue factor:VII and tissue factor:VIIa extrinsic tenase complexes with tissue factor, respectively. Factor VII assembles on the phosphylipid surface of the cell membrane via calcium binding. Prothrombinase enzyme cleaves prothrombin to thrombin. Once bound, the tissue factor:VIIa complexes (aswell as Factors IXa, Xa, XIIa and thrombin [171, 172]) activate the inactive Factor VII in remaining tissue factor:VII complexes forming a self-amplifying, auto-catalytic feedback loop [173]. In addition, tissue factor:VIIa complexes either readily activates Factor X [174], or, activates Factor IX, by proteolysis, which then causes Factor IXa to convert Factor X to its activated state (Factor Xa) under the presence of cofactor Factor VIII. The extrinsic pathway is highlighted in red, in Figure 2.12.

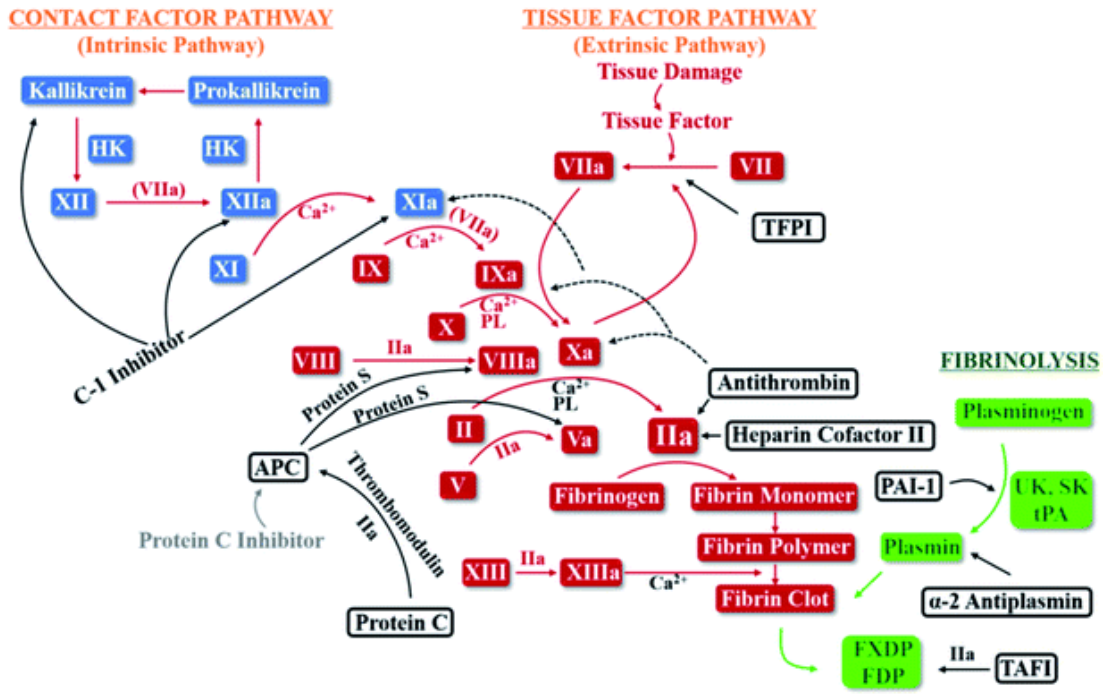

Figure 2.12 A comprehensive diagram of the coagulation cascade [16]

2.1.6.2 Intrinsic Pathway

The intrinsic pathway (highlighted in blue in Figure 2.12) is initiated by contact activation of Factor XII, by latching its heavy chain, to a negatively charged surface. Factor XIIa automatically activates circulating Factor XII and converts Factor XI into Factor XIa, dimeric serine protease. Factor XIIa also activates prekallikrein into kallikrein and cleaves the light chain of high molecular weight kininogen to carry out its pro-coagulant activity. This liberates Factor XIa from its activating surface. Kallikrein reciprocates by activating Factor XII and converts high molecular weight kinogen to bradykinin. The cleaved high molecular weight kinogen, or bradykinin, binds readily to prekallikrein to form kallikrein. This allows for a potent association between the inflammatory and coagulation pathways, facilitating the conversion of Factor X to Factor Xa by Factor XIa.

Collagen present in the sub-endothelium after vessel injury has been known to initiate the above mentioned sequence of intrinsic reactions [175]. However, the

significance of the intrinsic pathway to blood coagulation on artificial biomaterials remains speculative, as the occurrence of negatively charged surfaces *in vitro* and *in vivo* is limited. In fact previous studies have shown that that deficiencies in high molecular weight kinogen, prekallikrein and Factor XII, have not shown any abnormal bleeding in *in vivo* models [176-178].

2.1.6.3 The Common Pathway

The common pathway, as the name suggests, applies to both the intrinsic and extrinsic coagulation pathway. Activated Factor X converts vitamin K-dependent prothrombin to its activated state, thrombin by cleaving the Gla portion of the N-terminal of prothrombin. Thrombin, like Factor VII, requires calcium to bind to the platelet phospholipid membrane. Thrombin interacts with Factors V, VIII, XI, platelet receptors and proteins S and C to mediate the synthesis and breakdown of thrombin enzymes. Factor Xa along with calcium, Activated Factor V, released from platelets α-granule, along with phospholipids form a prothrombinase complex that increases the rate of thrombin production by 300,000 fold.

Thrombin binds to fibrinogen's central domain and cleaves fibrinopeptides A and B to form fibrin monomer. Fibrin monomers attach to one another side to side, half way along the length of the protein to form long, thin fibrin monomer strands. Heavy crosslinking of Factor XIIIa provides strength for mesh-like formation and against plasmin degradation. Platelet plug formed from primary haemostasis is fastened by the fibrin mesh, encapsulating and occluding the ruptured vessel wall. The fibrin strands bind to platelet receptor glycoproteins as well as adhesion protein such as thrombospondin, von Willebrand factor and fibronectin. Adhesive proteins act as bridges between fibrin mesh and platelets, platelets and sub-endothelial matrix, and, collagen and plasma proteins. Fibrinogen links to actin filaments in intracellular platelets via $\alpha_{IIb}\beta_3$ receptors reducing the retraction of blood clots and increases the available passageway for blood in the vessel lumen.

The size and extent of thrombus formation is limited by several factors such as; shear forces, activated protein C and other plasma inhibitors (namely C1 and AIII and tissue factor pathway inhibitor). Shear forces generated by the rapid flow of blood tear away weakly formed platelet clots, while, activated protein C, created by thrombin-thrombomodulin complex formed on endothelial surface, inhibits the function of Factors V and VII and plasma inhibitors. Both conditions work synergistically to limit the function of soluble pro-coagulant molecules such as Factor Xa and thrombin. Several inhibitors can interfere with these clotting reactions (shown in Figure 2.12). C1 (serpin protease) and AIII (anti-thrombin) and tissue factor pathway inhibitor inhibit the clotting cascade activity by limiting the function of Factors Xa, XIa, XIIa and IXa; and heparin, inhibits thrombin, and Factors Xa, IXa and Xia, by accelerating their interactions with AIII.

2.1.7 Plasma proteins

Proteins present in blood plasma, known as: serum proteins or, plasma proteins, are either involved with the maintenance of osmotic pressure of blood; aid in the transport of hormones, vitamins, metals and lipids in the circulatory system; and behave as enzymes, complement components, protease inhibitors and kinin precursors. Apart from this, the adhesion and activation of platelets, activation of the coagulation cascade and the regulation of immunological mechanisms are also mediated by plasma proteins. Over 100 different plasma proteins have been identified with their concentrations in plasma ranging between 35-50 mg/mL for serum albumin to only 0-5 pg/mL for interleukin 6 [179].

On blood contacting biomaterials, plasma proteins readily and rapidly adsorb onto the surface within seconds to generate a biologically active surface for haemostatic response [180, 181]. Blood cells arriving at the biomaterial surface primarily interact with the surface adsorbed plasma proteins rather than directly with the material itself, as such, understanding the initial adsorption of proteins onto a biomaterial surface is key in determining the biomcompatibility and haemocompatibility of the implanted

biomaterial. Fibrinogen, fibronectin, vitronectin, immunoglobulins and von Willebrand factor are naturally soluble plasma proteins found to be potential mediators of platelet adhesion and aggregation. And of these proteins, fibrinogen has been found to be the key protein in the adhesion process, while, fibronectin, von Willebrand factor and immunoglobulins merely play a supporting role. Apart from platelet activating proteins; other proteins such as: the highly adsorbing albumin, as well as Hageman factor, high molecular weight kinogen (HWMK), and factor VIII/ von Willebrand factor complex, which adsorb at less concentrations also readily adhere onto biomaterial surfaces [182].

The type of protein adsorbed and the dynamics behind protein adsorption is dictated by chemical and physical properties of the biomaterial surface. Thermodynamically, it has been shown that the adsorption of proteins may only occur if there is a decrease in Gibbs free energy (G):

$$\Delta_{ads}G=\Delta_{ads}H-T\Delta_{ads}S<0 \qquad \text{eq 1}$$

where

H=enthalpy

S=entropy

T=temperature

Δ_{ads} = overall change in the characteristic function of adsorption

This decrease is generally attributed from an increase in system entropy caused by the interactions between charged groups at the surface-blood interface and conformational changes in the structure of the adsorbed protein. Not all proteins are indefinitely bound to the surface after adsorption. Proteins have been shown to de-attach and re-attach changing the composition of proteins over time, known as the Vroman effect phenomena [183, 184]. The Vroman effect also states that the adsorbed proteins form a monolayer covering on the surface and the thickness of the adsorbed protein monolayer has been found to range between 2-10 nm, depending on

the size and shape of the protein [185]. Shear flow have not been shown to affect the adsorption process, even at high shear rates such as: 2700 s^{-1} [186]. The surface properties of the biomaterial determine the selectivity of the proteins adsorbed on the surface where the concentrations of the adsorbed proteins may be 1000- fold higher than normally found in blood [187, 188]. It has been found that maximum protein adsorption is achieved when surfaces and proteins possess opposite net charges with a pH between the isoelectric points (pI) of the surface and the protein [187]. The biological activity of plasma proteins has been shown to change upon adsorption due to tertiary and secondary conformational changes within the protein structure [188].

2.1.7.1 Fibrinogen

Fibrinogen (Fg) is an trinodal [189], elongated extracellular protein and makes up 2-3% of plasma proteins. It has a molecular weight of M_w = 340 kDa and appears as a rod like structure with dimensions 45 × 9 × 6 nm. Fibrinogen has 3 subdomains (E, D and α-C), with a central globular domain attached to two elongated domains positioned distal to one another [190]. Furthermore, firbinogen is a negatively charged protein at physiological pH (pI 5.5) because of its D and E domains. These two domains are the most surface active domains involved in surface and platelet binding. The α-C domain on the other hand, is positively charged and acts as a pioneer in the surface binding process, although, it does not bind to the surface [191, 192].

Fibrinogen is found in blood in concentrations of 3mg/ml and is known for its pivotal involvement in the adhesion of platelets. Stanford, Munoz and Vroman [193] in 1983 showed platelets adhere onto biomaterial surfaces pre-adsorbed with plasma proteins primarily via surface-bound fibrinogen. Fibrinogen is an adhesive protein that interacts strongly with biomaterial surfaces irrespective of the electrostatic charge on the surface [117, 194, 195]. Fibrinogen adsorbs onto biomaterials almost immediately upon contact, causing its spreading, denaturation, or, unfolding of its

tertiary structure. This conformational transformation causes tight binding of fibrinogen to the biomaterial surface allowing for increased platelet interaction [196].

Tsai et al [116] deduced that apart from fibrinogen, vitronectin, fibronectin and von Willebrand factor can also induce platelet adhesion, although, surface-bound fibrinogen was the major plasma protein involved in platelet adhesion. Even at small concentrations fibrinogen has been shown to elicit a full-scale platelet attachment [197], while, fibronectin, only at 10x its physiological concentration or greater can mediate the same response [198]. Fibrinogen proteins bind to platelets via activated their $\alpha_{IIb}\beta_3$ integrins on the platelet surface, although binding of fibrinogen to inactive $\alpha_{IIb}\beta_3$ integrins have also been reported [120, 199, 200]. Fibrinogen binding to agonist-stimulated platelets results in platelet aggregation, by cross-linking adjacent activated platelets. Unstimulated platelets do not allow for fibrinogen related aggregation because of tightly regulated constraints placed by actin or actin-associated proteins located within the platelet sub-membrane [201]. Turnover of actin filaments upon platelet stimulation have been shown to facilitate $\alpha_{IIb}\beta_3$ platelet receptor binding to fibrinogen.

The γ chain of the carboxyl (C)-terminal dodecapeptide sequences located at amino actid resides 400-411 in fibrinogen, known as the platelet binding domain, have been implicated as the major site of platelet attachment [202]. The γ-chain sequences are located at distal ends of the protein and either: bind to the overlapping sites in $\alpha_{IIb}\beta_3$ integrins, or, to two distinct sites, where the binding of one site causes a conformational change in the integrin, precluding the binding of the other peptide [203, 204]. The tri-peptide Arg-Gly-Asp (RGD) sequences in fibrinogen, also adheres to platelets, in a similar manner to vitronectin, fibronectin and von Willebrand factor, although, it does so at a much lesser extent [199, 200].

2.1.7.2 Albumin

Albumin is a relatively large, globular, extracellular protein with dimensions; 8 × 8.7 × 6 nm, and molecular weight of *M*w = 65 kD. It has an abundance of 60-70% in the plasma [205]. It is a main constituent of blood plasma serving the transport of metabolites and regulates osmotic pressure [206]. Albumin is a negatively charged protein (pI 4.9) and is composed of three homologous domains comprising a total of 585 amino acids. Each of its domains consists of two sub-domains stabilised by 17 disulfide bridges [207].

Albumin readily adsorbs on biomaterial surfaces, irrespective of electrostatic interactions because of its low conformational stability [208]. In 1969 Salzman and colleagues [209, 210] stumbled upon the role of human serum albumin in decreasing the affinity for platelet binding onto biocompatible surfaces by showing the preferential adhesion of albumin on heparinised surfaces, by competing with fibrinogen for surface binding-sites, reducing the total concentration of fibrinogen proteins adsorbed on the surfaces. Since it was known that platelets requires a protein co-factor (such as fibrinogen) to adsorb onto biomaterials to promote platelet activation, they proposed that albumin may play a possible role in minimising platelet attachment [209]. For this reason albumin has been utilised as a possible thrombo-resistant coating for several haemocompatible applications.

In fact, albumin is often used to coat vascular grafts to passivate surfaces from platelet and leukocyte attachment and activation, although, albumin has been implicated with mediating monocyte attachment on biomaterial surfaces [205, 211-213]. It has been shown that albumin proteins do not possess the adhesive sequences necessary to mediate the adhesion of platelets to biomaterial surfaces [214, 215]. Nimeri and colleagues [216] in 1998 analysed the degree of neutrophil activation on immunoglobulin (IgG) and albumin protein-coated surfaces. Results showed that when compared with IgG, albumin coated surfaces exhibited decreased neutrophil response showing decreased cell spreading and lack of reactive species production, necessary for neutrophil activation. Furthermore, it was found that neutrophil

attachment occurred more slowly on albumin-adsorbed surfaces. Another study by Renner and colleagues [217] looked at patterns of competitive protein adsorption between fibronectin and albumin. Albumin was shown to have a higher binding affinity to the surface than fibronectin, although, the binding affinity of albumin to the surface can be owed to the surface chemistry of the material. Similar results were found when Fibrinogen was displaced with albumin [218].

2.2 Blood-compatible Surfaces

Blood contacting implants perform in a corrosive bio-environment due to the metabolic activity of the cells and fluids in our body, which, for biomaterials with a low wear resistance, causes the release of metal ions and wear debris. This results in cellular and tissue damage, infections and thrombus generation, leading to adverse medical conditions and failure of the implant. The bio-surfaces of devices such as: catheters, blood vessel grafts, vascular stents, artificial heart valves, circulatory support devices, various extracorporeal tubings, hemodialysis, hemapheresis and oxygenator membranes; that are in direct contact with streaming blood are selected with biomaterials that exhibit good mechanical properties, stability, tribological properties, biocompatibility, and most importantly: haemocompatibility.

Despite over several decades of progress in understanding the interplay between blood and biomaterial surfaces [5, 219, 220], the development of a non-thrombogenic surface still remains an ongoing task. Insufficient hemocompatibility impacts patient mortality by impairing the functionality and the safety of the device [5]. Thrombotic occlusion of blood vessels, resulting in emboli and proliferative processes in the vessel wall has been attributed to the adhesion and activation of haemostatic (blood coagulation and platelets), and immune systems [221]. At present, thrombotic event has been suppressed by consuming prophylactic anti-coagulant medication (heparin, warfarin, etc). Though it is not ideal, such medications need to be chronically administered to prevent adverse conditions, or patient morbidity.

The interactions between blood and biomaterial surfaces are initiated by the physical and chemical properties of the foreign material. Efforts have therefore been directed towards modulating biomaterial surfaces by: altering the physiochemical and topographical characteristics; to control the composition of the layer of plasma proteins that is invariably adsorbed upon blood contact, and consequently, interactions with haemostatic (platelets and coagulation cascade and the complement system) blood components [5]. This has an added advantage of improving the biomaterial's haemocompatibility whilst retaining the advantageous mechanical and physical properties of the underlying bulk substrate. Therefore, surface modifications such as: the implementation of thin surface coatings, and nano-topographical changes to the bulk substrate, which can vastly influence these haemostatic responses will be discussed in the following subsections.

.

2.2.1 Surface Modification

Modification to an implant surface by the addition of thin film coatings can vastly influence a biomaterial surface's interaction with blood is an ideal means of improving the biomaterial's haemocompatibility without affecting the bulk material's mechanical and physical properties. Presently researched surface modifications can be categorised into 5 groups: inorganic and organic surface coatings; as well as, functionalisation of surfaces using: bioactive and passivating molecules, and the endothelialisation of biomaterial surfaces.

Organic coatings have already been employed in several commercially available blood-contacting devices. Polymers such as polyethersulfone and cellulose are the principle materials used in haemodialysis, while polysiloxane and polypropylene are used in oxygenator membranes [222-224]. Dacron^{TM}, knitted polyester, and expanded polytetrafluorethylene foils (GoreTex^{TM}) are widely used in vascular grafts; and polytetrafluorethylene, polyethylene, polyvinylchloride, polyurethanes and polysiloxane and PEBAX^{TM} (a polyether block amide) are used in catheters [222-224]. While, the surfaces of these polymers can be used to easily modify

biomaterial surfaces, they have been shown to undergo hydrolytic degradation, *in vivo*, adversely triggering the systemic immune response [225, 226].

Another approach used to minimise thrombotic events caused by biomaterial surfaces is by passivating the blood-contacting devices such as: dialysis membranes, stents and stent grafts with inert long-chained hydrophilic molecules such as: polyethylene oxide (PEO), polyethylene glycol (PEG) and tetraethylene glycol dimethyl ether (tetraglyme) [22, 227-231]. These functionalised molecules have been implanted on biomaterial surfaces by methods such as: physisorption, covalent bonding and block integration [232]. Results show that the above mentioned modified surfaces have been found to reduce coagulation activation, blood platelet adhesion and complement activation [229]. Apart from functionalised molecules, inert bio-molecules such as albumin have also been used to passivate bio-surfaces [233, 234]. Albumin is found in high concentrations in blood plasma. It can be used to mask the biomaterial surface from clot formation as it lacks the biological sequences necessary for platelet receptor adhesion. However, because of changed to the protein upon surface adsorption, and the physiological degradation of the protein from sterilisation or over time due to a limited shelf life, limits the potential of albumin [233, 234]. Furthermore, albumin is derived from humans and as such may pose a major risk of the transmission of infectious diseases to patients.

Opposite to surface passivation, bioactive coatings using immobilisation of functionalised molecules and biomolecules such as: sulfated mucopolysaccharide heparin (to mimic the anti-coagulant, heparin sulphate), have been used in tubing's and oxygenator membranes, dialysis membranes, vascular stents, stent grafts, bypass grafts, and ventricular assist devices [235-238]. Bioactive coatings aim to mimic active anticoagulant mechanisms performed by the anti-coagulant enzymes in blood and endothelial cells of the vascular lining. This method is still at its infancy, as targeting complex receptors using appropriate bioactive ligands that are immobilised, oriented and presented at high concentrations is a complex process that is still not completely understood. The immobilised bio-molecules like heparin-sulphate are highly susceptible to degradation caused by normal physiological processes of

proteolytic enzymes (inactivation by protamine sulphate) which can quickly deactivate the surface modification [239-242]. Apart from this, technological issues such as: limited shelf life and limited sterilisability are impending problems that haven't been addressed [239, 241]. Sulfated pentasaccharides have been recently studied as a replacement for the long-chain heparin [243]. While, these structures are more resistant against enzymatic degradation than the whole heparin molecule, the affinity of the immobilised molecule heparin-binding ligands did not lead to a heparin-like activity in complex blood [243]. Other molecules such as: hirudin covalently immobilised to Darcon^{TM} for vascular grafts) [244, 245] and benzamidine (immobilised on polyoctadecene alt maleic anhydride, PO-MA) [246] have been used as a direct inhibitor of thrombin. While, these surfaces have shown decreased fibrin formation and cell adhesion onto the surfaces when compared with compared with the non-coated surfaces, the modification has not come to clinical application because of the high expenses involved and a possible degradation of the molecule *in vivo* [221]. As an alternative to the inhibition of the coagulation cascade, the active inhibition of platelet activation and aggregation through using drug eluting coatings have also been studied. Abciximab [247] and dipyridamol [248], an antagonist to platelet integrin $\alpha_{IIb}\beta_3$, and ADP, respectively, as well as the release of nitric oxide from surface coatings. While these surfaces have been shown to reduce platelet adhesion and aggregation; cytotoxic effects to the surrounding tissue and blood were also reported [249].

Endothelialisation of biomaterial surfaces is another form of surface modification to produce a permanently active haemocompatible coating [221]. Typically, autologous endothelial cells are harvested and cultivated, *in vitro*, on immobilised ECM on biomaterial surfaces, followed by their implantation [250]. The ECM provides the peptide sequences and framework for endothelial cell binding and growth, although, the matrix alone exhibit highly thrombogenic cues for platelet adhesion and activation [251]. As such, a complete coverage by cells is necessary prior to contact with blood [251]. As an alternative, surfaces were immobilised with antibodies specific for endothelial cells, to allow the favourable binding of the cells to the biomaterial surface upon implantation. An example of which is the sustained release of vascular endothelial growth factor VEGF [252]. While VEFG was employed to

stimulate endothelialisation from cells within the body, the rapid degradation of the factor, *in vivo*, as well as limitations associated with implant sterilisation were limiting causes for further investigation [253].

Commercially available vascular stents or mechanical heart valves already employ haemocompatible inorganic ceramic coatings such as: nitrides, metal oxides like titanium oxide, and carbon based inorganic coatings like hydrogenated amorphous carbon (a-C:H, diamond-like carbon DLC) [254]. Inorganic coatings behave as passive, corrosion resistant coatings and have been shown to exhibit high inertness, mechanical and chemical stability. DLC coatings are presently being used in artificial heart valves [255, 256] and on vascular stents [257]. DLC offers several advantages over other materials as they highly inert, very smooth, present low friction and minimal wear. DLC's hydrophobic nature allows for an increased adsorption of albumin proteins and enhanced adhesion of blood platelets. Apart from DLC; titanium oxides and titanium nitrides were also widely investigated. Titanium has a tendency to readily form a native oxide layer. This oxide layer is only a few nano-meters in thickness and has thus far exhibited low haemocompatibility [258]. Studies have shown, increasing the coating thickness to a few hundred nano-meters, using deposition techniques such as FAD [259], have greatly improved the surface's haemocompatibility [260-262]. Titanium oxide coatings have been demonstrated to adsorb lower concentrations of fibrinogen on the surface, suppress the activation of the coagulation cascade and reduce blood platelet adhesion when compared with non-coated titanium films [263]. Haemocompatibility of titanium oxide [264, 265], oxynitride [266] and nitinol [261] surfaces have also been demonstrated under shear flow *in vivo* [267]. Amorphous silicon carbide (a-SiC:H) with similar properties to titanium oxide has also been commercially used as a coating on vascular stents and heart valves [268, 269]. Whilst commercially used inorganic biomaterial coatings have shown to reduce the severity of haemostatic responses, they have not completely suppressed the activation of coagulation factors and platelet interactions.

Apart from the addition of a thin film coating, changing a material's nano-topography has also been shown to vastly influence blood proteins adsorption and

platelet interactions on biomaterial surfaces. The interaction between blood and topography involve different mechanisms depending on the typical feature size of the topography. As such, evaluating the interaction of blood with surface topography requires a strict control on the chemistry at the material's interface. Many surface modification techniques such as: chemical treatment, lithographic techniques, glancing angle deposition and self-directed assembly of nanoparticles using block co-polymer techniques; have been employed to improve biomaterial's haemocompatibility. Nano-topographical changes have resulted in the formation of particles, pores, pits, and grooves, though it is still unclear to what extent such surface nano-topographies influence blood interactions. A review of surface nano-patterning techniques and the influence of nano-patterns on platelet interaction is detailed in Section 2.2.1.4.

2.2.1.1 Diamond-Like Carbon (DLC) surface coatings

Carbon (C) is a fundamental element existent in all organic molecules and it can exist in three different hybridisation states sp^1 (carbon-based polymers), sp^2 (graphitic) and sp^3 (diamond-like) [270]. This allows carbon to co-exist in a variety of crystalline and disordered-amorphous phases [270, 271]. Diamond has 100% sp^3 carbon bond configuration with four valence electrons positioned in a symmetrical orbital structure. Each valence electron forms strong covalent σ bonds with adjacent atoms and it is these strong bonds that are responsible for diamond's excellent hardness, electrical resistivity, chemical inertness, and wear properties [270]. Graphite exhibits sp^2 hybridisation of its carbon atoms presenting strong anisotropic properties in one direction because of strong intra-layer covalent bonds (three of the four valence electrons exhibit strong σ bonding, similar to diamond), while, the perpendicular direction (between layers) only possesses weak van der Waals forces from weak π bonding between the fourth electron and adjacent atoms. The sp^2 hybridisation results in low hardness, electrical resistivity, and high wear rate, combined with low friction [272]

Diamond-like carbon (DLC) is a class of materials with diamond-like and graphite-like properties. It resembles a metastable form of amorphous carbon with varying atomic bond structures depending upon their: hydrogen content (up to 40%); the proportion of sp^3; and sp^2 hybridisation states [273]. The ratio of the three factors allows DLC to exhibit range of characteristics resembling a mix of graphite-like and diamond-like properties such as: high mechanical hardness, chemical inertness, low friction coefficient, low wear resistance, corrosion resistance, optical and infrared-transparency, semiconductor-like properties because of its wide band gap, and excellent smoothness because its amorphous nature (no grain boundaries) [273-282]. As such, DLC can be applied as a thin film coating and can adhere well to metallic and non-metallic biomaterials [270, 283, 284]. Over the past two decades DLC has emerged as a potential material because the above mentioned properties of DLC match the criteria required for a good biomaterial for its application in the cardiovascular field, as well as other fields such as: dentistry, orthopaedic and optometry [285].

In the cardiovascular field, the main causes of implant failure within the body has been due to a lack of compatibility between the surface of the biomaterial and blood, as well as, wear particle formation from constant delamination of the implant surface under shear stress [286]. Both adverse conditions ultimately lead to the formation of thrombus clots which can eventuate into patient death. A haemocompatible, low friction, smooth, biocompatible coating, with excellent tribological properties such as DLC, would reduce these problems.

2.2.1.1.1 Chemical and mechanical properties

DLC exists as amorphous carbon with a disordered network of sp^3 and sp^2 coordinated bonds, as well as hydrogenated alloys. Amorphous carbon (a-C) films have high sp^2, while, coatings with high concentrations of sp^3 bonds are referred to as tetrahedral amorphous carbon (ta-C) [274, 287]. Amorphous carbon coatings with high concentrations of hydrogen atoms are known as hydrogenated amourphous-

carbon (a-C:H) [274]. The surface characteristics of each coating vary considerably with varying compositions of hydrogen, sp^2 and sp^3 bonding [286]. An adaptation of Robertson's [270] ternary phase diagram, shown in Figure 2.13, illustrates the various forms of DLC and their respective deposition techniques. The sp^2 corner of the ternary diagram represents materials of graphitic nature while the materials of a diamond-like nature lie near the sp^3 corner. The limits of the triangle are defined by hydrocarbon polymers (H-C polymers). Any point beyond this line, deposition of carbon will not allow for interconnected networks, instead only the formation of carbon molecules is possible.

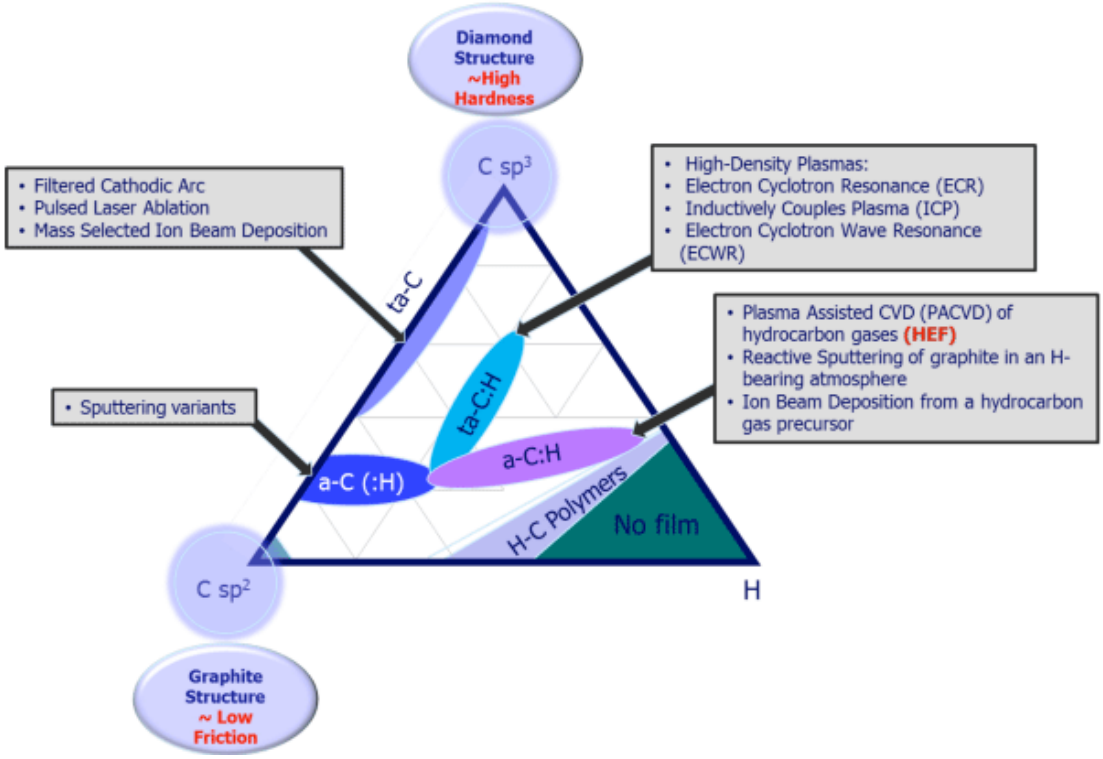

Figure 2.13 Ternary phase diagram showing the various forms of DLC and their respective deposition techniques [288].

The mechanical and physical properties of the various DLC films, as shown in Figure 2.14, can be produced by modulating the deposition parameters of various coating technologies [278, 286]. In general, DLC films are formed by bombarding high energy carbon or hydrocarbon radical species with impact energies ranging from 50 to several hundred electron volts. A number of techniques have been employed to synthesise DLC films namely: ion beam deposition (IBD), radio frequency plasma enhanced chemical vapour deposition (r.f.-PECVD), filtered

cathodic vacuum arc (FCVA), ion plating, plasma immersion ion implantation and deposition (PIIID), magnetron sputtering, ion beam sputtering, pulsed laser deposition, and mass selected ion beam deposition [289-297]. It has been shown that the coating technology and carbon substrates determine the hydrogen content of DLC, while, the impact energy dictates the propensity of the sp^3 fractions, and consequently the type of DLC film produced [298, 299]. Furthermore, when compared with diamond, these coatings can be fabricated in an economical manner for mass productions.

	sp^3 (%)	H (%)	Density (g cm^{-3})	Gap (eV)	Hardness (GPa)
Diamond	100	0	3.515	55	100
Graphite	0	0	2.267	0	
C_{60}	0	0		1.6	
Glassy C	0	0	1.3–1.55	0.01	3
Evaporated C	0	0	1.9	0.4–0.7	3
Sputtered C	5	0	2.2	0.5	
ta-C	80–88	0	3.1	2.5	80
a-C:H hard	40	30–40	1.6–2.2	1.1–1.7	10–20
a-C:H soft	60	40–50	1.2–1.6	1.7–4	<10
ta-C:H	70	30	2.4	2.0–2.5	50
Polyethylene	100	67	0.92	6	0.01

Figure 2.14 A comparison of the mechanical properties of various DLC films [270]

In comparison to the various forms of DLC, a-C:H and ta-C are the most commonly used coatings applications in biomedical field, and as such a-C:H and ta-C will be the primary focus in the following subsections. Unlike diamond, DLC coatings have superior smoothness and can be deposited at room temperature [300, 301], however they exhibit high intrinsic stresses and thermal stability (not application for ta-C), increasing their likelihood to delaminate off the underlying substrate. When compared with a-C:H; ta-C thin films, because of its inherently high sp^3 (diamond-like) fractions, exhibited higher density, increased elastic modulus (300 GPa for a-C:H and 757 GPa for ta-C) and hardness values [270]. Addition of hydrogen atoms, as found in a-C:H, reduces the ratio of sp^3/sp^2 bonds and consequently exhibits

reduced hardness values and co-efficient of friction. A-C:H surfaces have been reported to achieve a co-efficient of friction of 0.05 [302], while ta-C surfaces exhibit co-efficient of friction between 0.1-0.15 [303]. In terms of surface characteristics, DLC has an inherently low surface energy. Amorphous carbon coatings have surface energies close to 40-54 mNm^{-1} with contact angles between 55-70º in water [304, 305].

Wear rates determine the degree of spallation or delamination of the coating. Biomaterial coatings with high wear rates would be ideal for cardiovascular applications, as it enables the substrate to withstand high shear rates with minimal delamination within the vascular walls. Ta-C surface have been shown to exhibit wear rates close to 10^{-9} $mm^3N^{-1}m^-1$, while, a-C:H surfaces have shown wear rates between 10^{-6} and 10^{-7} $mm^3N^{-1}m^-1$ [306]. Further, wear rates are inversely proportional to stress, young's modulus and hardness; so a thicker layer of DLC coating should ideally increase the wear properties of DLC films. However, the adhesion strength between the coating and substrate have been reported to be higher with thin films suggesting that thin films are more wear resistant than thick films [270].

DLC coatings in blood and medical applications pose an attractive prospect because they possess excellent haemocompatibility, wear properties, low co-efficient of friction, smooth finish and they provide desirable surface modifications to commonly used biomaterials. DLC, as thin films, have been used as a protective layer for: optical windows, magnetic storage disks, machinery and car parts, cutting tools, cold extrusion dies, micro-electromechanical devices (MEMs), etc [270, 300, 301, 303, 307, 308]. Apart from this, in the biomedical field, DLC films are of particular interest as a protective coating for implants. The excellent wear resistance, non leaching properties and good sterilisation compatibility makes DLC ideal for several biomedical applications including: orthopaedic implants, surgical tools, contact lenses, dental implants, mechanical heart valves, ventricular assist devices, vascular stents, guidewires etc due to its excellent biocompatibility [254-256, 286, 308-311].

2.2.1.1.2 Biocompatibility

Ratner [312] defines biocompatibility as "the ability of a material to locally trigger and guide normal wound healing, reconstruction, and/or tissue integration with only low degrees of inflammatory reaction" and surface compatibility as "the chemical, biological and physical appropriateness of an implant surface to the host tissues" [312]. Therefore, by investigating the interaction between cells and biomaterial surfaces; or, proteins and biomaterial surfaces, the biocompatibility of an implant material could be estimated.

The biocompatibility and surface of DLC coatings were investigated extensively since the early 90's through several cell culture techniques and *in vivo* studies analysing the tissue-biomaterial interface and the bio-tolerance of DLC films after long term implantation [281, 313, 314]. Macrophage and monocytic cells play a dominant role the in inflammation and interaction with implanted materials and as such the activation of these cells has been used as an important determinant in evaluating the immunological response of a biomaterial. When compared with polyurethane-coated, and uncoated 316-L stainless steel; ta-C coated substrates presented decreased spreading of macrophages and decreased inflammatory activity [315].

To evaluate the integration of the implant with the biological environment, the contact and growth of tissue specific cells such as: osteoblasts, fibroblasts, endothelial cells; were monitored for their adhesion, spreading and proliferation on the implant surface. Human fibroblasts and osteoblast-like cells did not show any cytotoxic effects when exposed to DLC films [316-318]. In fact, DLC coatings also showed promising results as a haemocompatible material [319-321]. Thompson et al [281] and Evans et al [314] studied the influence of a-C:H surfaces in activating mouse macrophage and mouse fibroblast cells. The results showed that fibroblast cells grew the thin films with no inflammation or toxicological effects, *in vitro*. Similar results were obtained from other studies looking at fibroblast and

macrophage response on a-C:H and ta-C films produced using glow discharge and various PECVD methods [316, 317, 322-324].

A study looking at the incorporation of titanium (Ti) ions into a-C:H films, prepared by using a magnetron sputtering, on the activity of osteoblast, and osteoclast cells showed that the addition of Ti ions increased bone cell proliferation and minimised activity of osteoclast-like cell [323]. The incorporation of calcium oxide (CaO) in a-C:H coatings, prepared using plasma decomposition of gaseous carbon precursors, showed improved biological acceptance of mouse fibroblasts to the doped thin films [325]. The influence of inductively coupled PECVD a-C:H and ta-C in glial and fibroblast cells for neuro-prosthetic implants *in vitro* was also investigated [326].

Several *in vivo* studies were also carried out to analyse the influence of various conditions in the physiological environment on the biocompatibility of DLC surfaces. A study conducted by Mohanty et al [318] looked at the tissue response of a-C:H-coated titanium substrates after its implantation in skeletal muscles of rabbit for 1 year. The results showed no cytotoxic or adverse immunological response, and the surfaces did not present any delamination of the film. A 52 week study investigating fibrous tissue formation and phagocytic response on a-C:H-coated orthopaedic pins and screws in guinea pigs showed the formation of thin connective-tissue capsules by fibrocytes and collagen fibers in the subcutaneous layer [313]. Apart from this, bone and muscular apposition was also noticed, with no phagocytic reaction and corrosion products in the walls of the capsule. Another study looking at the implantation of a-C:H-coated CoCr cylinders in trans-cortical sites of sheep and intramuscular location of rats also showed no significant toxicological response because of the a-C:H coated implant [310]. All these studies indicate that DLC coatings are quite biocompatible and do not activate any inflammatory reaction *in vivo*. This provokes a growing interest in DLC as a protective coating for orthopaedics, cardiovascular, and dental application [327].

2.2.1.2 Titania (TiO_2) surface coatings

In the biomedical field, titanium and titanium based alloys have been widely utilised for their excellent corrosion-resistance and biocompatibility [328]. Although, titanium's remarkable corrosion resistance has been widely attributed to the naturally-forming, passive oxide film on the surface of titanium [329-331]. This oxide layer forms spontaneously in air, water or other electrolytic solutions, and reforms upon surface damage. The thin native oxide film has thickness of 5-6 nm [332] and primarily consists of amorphous titanium dioxide (TiO_2), while the presence of Ti_3O, Ti_2O, Ti_3O_2, TiO, Ti_2O_3, Ti_3O_5 also have been reported [333-337]. Titanium can exist in many different states because the solubility of oxygen is relatively high in titanium. As such the ratio of oxygen to titanium gradually changes, along with its physical properties, until the oxide layer reaches its stable form, TiO_2. This protective and highly stable, passive TiO_2 film is, in effect, the surface that will interact with the *in vivo* environment and is therefore of huge importance when considering cell-surface interactions. The bulk titanium will seldom play a role in blood-surface, or, tissue-surface interactions during the initial acceptance of the implant *in vivo*. As such there is a growing interest in TiO_2 for its use as a surface coating in biomedical applications.

The ratio of concentrations between oxygen and titanium ions at the interface between TiO2 and the bulk titanium, regresses from 2:1 (oxygen: titanium) to a much lower ratio in the bulk material. The most external layer of the interface has titanium ions bonded to chemisorbed water and weak, physisorbed hydroxide anions on the surface. Further, exposure time and environmental factors such as: humidity, pollutants/contaminants (especially hydrocarbons) and air quality influence the penetration of hydrocarbons and metal-organic compounds (alkoxides or carboxylates) into titanium [338]. While TiO_2 has gained much interest, protein studies from *in vivo* experimentation have shown that the harsh chemical environment within the human body tends to accelerate the corrosion process affecting the use of titanium in long term biomedical applications [339-341]. The titanium dioxide layer formed on titanium surfaces is soluble in pH 3-12 and as such

can readily dissolute *in vivo*. The Ti ion binds its four positive charges with negative charges found in physiology (e.g. oxygen), to form $Ti(OH)_4$ (aq). The reactive oxygen species interacts with cation $Ti(OH)_3^+$, found in normal physiological conditions to form an electro-neutral species. The neutral hydrolysis of Ti suppresses the affinity of Ti ions to organic molecules within the body, and as such does not cause a toxic chemical response *in vivo* [339]. While the corrosion product of Ti does not behave as a chemical burden, the wear particles have been shown to induce thrombotic events within the body [342].

Crystalline TiO_2 films, produced in a similar manner to DLC using titanium-based reactive species, have been shown to improve the stability of TiO_2 *in vivo* [343]. The thickness of the thin film can be increased from several nano-meters to 200nm, increasing its corrosion resistant properties [344]. As such the following sections will focus on crystalline TiO_2 in terms of its chemical, mechanical and tissue compatible properties.

2.2.1.2.1 Chemical and mechanical properties

Crystalline TiO_2 exists in three different phases: rutile and anatase, and brookite. The rutile and anastase phase follows a tetragonal structure (rutile: a = b = 4.584 Å, c = 2.953 Å; and, anatase: a = b = 3.782 Å, c = 9.502 Å), as shown in Figure 2.15, while the bookite phase follow an orthorhombic/rhombohedral structure (a = 5.436 Å, b = 9.166 Å, c = 5.135 Å) [345-347]. The rutile and anatase crystals are formed by one titanium atom surrounded by six oxygen atoms. The differences between the two crystal structures are the assembly pattern of the tetrahedral chains, also known as distortion pattern [347]. In the rutile structure, the cubic lattice is symmetrical and is stretched beyond a cubic shape, while, the tetrahedral shape in anastase is significantly distorted, making the structure more asymmetrical. In effect, the specific distortion pattern of each phase determine its electronic band structures, surface structure, bulk diffusion, surface transfer capability and redox potentials [347]. Because of its structure, the rutile phase has the highest refractive index and

behaves more thermodynamically stable than the others. This is because rutile and anastase crystal structure is denser and more closely packed than brookite and amorphous TiO_2, hence providing fewer paths for ion diffusion and release. Because of its low thermodynamic stability, brookite and amorphous phases of TiO_2 are less studied in experimental investigations.

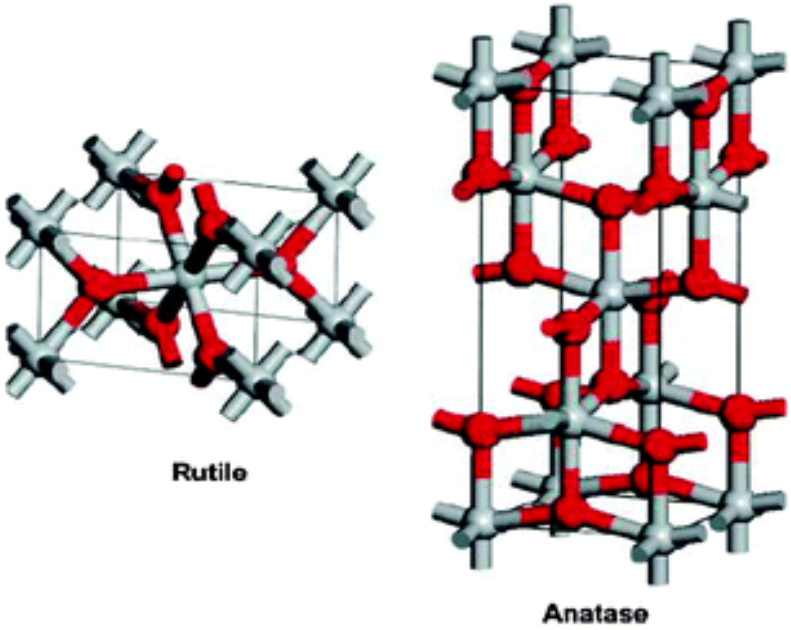

Figure 2.15 Bulk crystal structures of rutile and anastase forms of TiO_2 [348]

TiO_2 films have been synthesised from a variety of techniques, some include: the sol–gel process [349], chemical vapour deposition [350], evaporation [351], reactive sputtering techniques [352, 353], ion beam assisted process [354], atomic layer deposition [355], pulse laser deposition [356], cathodic arc deposition and filtered arc deposition (FAD) [259, 357]. Of the techniques mentioned, FACVD has recently been of interest and is used in this study, because this method allows for deposition of crystalline TiO_2 at room temperature and the technique can be modulated to produce higher propensities of the highly stable, rutile and anastase phase. The samples substrates used in this project were anastase TiO_2 coatings prepared with FACVD deposition technique.

Rutile and anastase TiO_2 thin films behave as good insulators and can prevent the influx of anion impurities such as: chlorine, phosphates and fluorine, from the

environment. TiO_2 can naturally bind with acids and bases (amphoteric) because of the intermediate hydroxyl group, $Ti(OH)_3^+$, formed by titanium ions after exposure to an aqueous environment [341]. The crystalline oxide layer has been shown to exhibit a hydroxylated layer similar to what is expected on naturally occurring, amorphous TiO_2 [358, 359]. TiO_2 has a near neutral pH of 6 and in physiological conditions have been shown to carry no charge [360, 361]. Because of their attraction to water and water-soluble molecules, these films are highly polar, and consequently display high surface energies and hydrophilic properties [362]. This enables TiO_2 surface to interact favourably with passivating proteins such as: albumin, and exhibit good biocompatibility for cell adhesion. The refractive index of rutile TiO_2 films is higher than anastase because the rutile structure has a higher density than anastase. TiO_2 films used in this study were produced by Bendavid et al [357] using FACVD method. The coatings were reported to exhibit refractive index values of 2.62, in between the values obtained for amorphous and rutile films (2.56 and 2.72, respectively). The hardness was shown to be between 11.6 and 18.5 GPa, with elastic modulus between 140 and 225 GPa, and compressive stress within 0.7 and 2.6 GPa [357]. An increase in the density of the deposited films (>3.85 g/cm^3) was strongly correlated with enhanced optical and mechanical properties. However, this is ultimately dependent on the energy of the titanium ions and the substrate bias [357].

TiO_2's chemical and physical properties make it pliable to many different commercial applications. As an n-type semiconducting material, semiconductor grade TiO_2, because of their photoswitchable surface wettability, high photocatalytic activity, bistable electrical resistance states, strong oxidising properties and high electron drift mobility properties have been commercially used as antifogging, self-cleaning and disinfecting coatings on medical devices, food preparation surfaces and building materials [363-365].

In its powder form, TiO_2 is the most widely used white pigment in products such as: paints, coatings, plastics, paper, inks, fibres, food and cosmetics. The degree of opacity necessary for a material to confer to the host matrix is determined by its refractive index and its brightness [363]. Because TiO_2 has a high refractive index

and high brightness, it can be used to produce the technical effect of a whitening agent, at very low concentrations. TiO_2 is considered non-toxic and as such is often used in the food and drug industry as an intense white pigment for confectionary, baked goods, cheeses, icings, toppings, toothpaste, food supplements and pharmaceuticals [366].

2.2.1.2.2 Biocompatibility

The biocompatibility and surface of TiO_2 coatings were investigated extensively through several cell culture techniques and *in vivo* studies analysing the tissue-biomaterial interface and the bio-tolerance of TiO_2 films for orthopaedic applications. The activation of macrophage and monocytic cell lines are determinants of the immunological response of a biomaterial. An *in vitro* investigation conducted by Valles et al [343] showed, TiO_2 surfaces exhibited suppressed macrophage response when compared with titanium. This indicates TiO_2 is tolerated by the body and does not induce any immunological response.

Crystalline TiO_2 were found to be less bio-reactive than commercially pure titanium. A study conducted by Li et al [367] investigated the bioactivity of TiO_2 films by measuring its ability to induce apatite deposition using stimulated body fluids (SBF), *in vitro*. Results showed that TiO_2 was able to grow apatite on its surface by exposing its negatively charged TiO^- groups to calcium ions in SBF via an ion exchange process. This property has been attributed to the biocompatibility of TiO_2 coatings. Wu et al [368] analysed the bioactive properties of TiO_2 *in vivo*. Results showed that when compared with amorphous TiO_2, crystalline TiO_2 showed greater bioactivity. This shows the potential of TiO_2 as a bioactive coating for inert bulk substrates for its application in the orthopaedic industry.

TiO_2 is a relatively hydrophilic surface and as such have been implicated with increased adsorption of serum proteins. As, glycoprotein and fibronectin mediate and promote the spreading and adhesion of cells on biomaterials; the adsorption of such

proteins were investigated. A study conducted by Ellingsen [369] in 1991 showed serum proteins, such as fibronectin, readily adsorb onto titania surfaces. In the orthopaedic industry, the adsorption of proteins onto an implant is essentially the first step to osseo-integrating a biomaterial surface with bone for long term implantation. TiO_2 surfaces synthesised at low concentrations, with increased thickness, have been shown to induce increased protein adsorption. Furthermore, this study was able to show proteins bind to TiO_2 in a similar manner to calcium binding from SBF. Similar to plasma protein adsorption on hydroxyapatite surfaces, calcium uptake on TiO_2 surfaces has been correlated with increased adsorption of albumin and glycosaminoglycans [332]. TiO_2 with increased surface thickness have also been shown to provide a haemocompatible response by adsorbing a higher ratio of albumin to fibrinogen. Sunny et al [344] showed a seven fold increase in albumin adsorption, when compared with fibrinogen, on TiO_2 coatings of thickness 200nm. This ratio was found to be significantly lower at lower coating thickness.

To evaluate the integration of the implant with the biological environment, the contact and growth of tissue specific cells such as: osteoblasts, fibroblasts, endothelial cells; were monitored for their adhesion, spreading and proliferation *in vitro* and *in vivo*. Apart from fibronectin, other cell adhesion molecules such as vitronectin, have also been shown to adsorb at high concentrations, along with the binding of osteoblast cells for bone apposition [370]. Several studies have shown that TiO_2 exhibits increased osseointegration properties, when compared with titanium surfaces by increasing the adhesion and proliferation of osteoblast cells [371, 372]. As a biomaterial, TiO_2 have also been shown to be beneficial for endothelial cells, encouraging more ECM secretion and functions, while inhibiting VSMC growth [373, 374]. Similar results have been found in other studies involving endothelial cells and vascular smooth muscle cells [375]. Apart from osteoblasts and VSMC, TiO_2 have also been shown to promote fibroblast adhesion and growth [376], reinforcing the biocompatible, non-cytotoxic properties of TiO_2 surfaces.

The above mentioned studies essentially show the biocompatibility and bioactive properties of TiO_2 films by promoting tissue specific cell growth without any toxicological or immunological effect. The influence of blood and blood cells on TiO_2 will be detailed in the following subsections.

2.2.1.3 Haemocompatibility

Haemocompatibility is defined as the tolerance of blood and its components to blood-contacting surfaces. Since, blood is the first bodily fluid that contacts artificial surfaces the haemocompatibility of a biomaterial is of great importance. It is important to fabricate biomaterial surfaces such that when a biomaterial comes in contact with blood, it does not activate blood platelets or the coagulation system to induce thrombosis. Upon blood contact, plasma proteins, especially: albumin and fibrinogen, from the blood rapidly adsorb onto the surface. The ratio of adsorbed albumin and fibrinogen determines the haemocompatibility of the biomaterial, as the adsorption of albumin reduced the adhesion, spreading and activation of platelets, while adsorption of fibrinogen promotes platelet adhesion and activation [327]. The haemolysis ratio characterised by the release of haemoglobin into the plasma from ruptured blood cell is also good indication of biocompatibility. A low haemolysis ratio is indicative of a more haemocompatible material. Furthermore, the effect of the coagulation cascade on a-C:H surfaces was measured using the clotting times. The activated partial pro-thrombin time (APTT) measures the ability of the biomaterial to retard blood coagulation via the intrinsic (tissue factor dependent) pathway, and as such governs the influence of synthetic biomaterials on coagulation time.

2.2.1.3.1 DLC

DLC surfaces have been reported as extremely haemocompatible surfaces, where their blood compatibility has attributed to low surface energy, effective work function and smooth surface finish. A study conducted by Yu et al [321] investigated anticoagulant properties of ta-C films deposited by FVAD method. It was shown when compared with isotropic pyrolytic carbon (LTI carbon), ta-C surfaces exhibited lower haemolysis ratio and platelet adhesion, while presenting similar levels of albumin and fibrinogen adsorption as LTI. Reduced platelet adhesion with similar levels of protein adsorption between the two surfaces was attributed to the varying Fermi energies between the two surfaces. Nurdin et al [319] found that it was not the

work function of the surfaces, but surface energies of a-C:H that was responsible for the drastically reduced activation of platelets and complement convertase.

Yang et al [320], by comparing PECVD a-C:H surfaces coated under low substrate bias with 316-L steel, proposed that the smoothness of the biomaterial coating and its inherent low co-efficient of friction was responsible for the increased haemocompatibility of a-C:H surfaces. Jones et al [263] reaffirmed the significance of surface energy in haemocompatibility by using scanning electron microscopy (SEM), to show low surface energy a-C:H films produced on titanium substrates via PECVD using an TiC-TiN interlayer did not present any platelet spreading or aggregation, when compared with high surface energy substrates coated with the interlayer only.

To analyse the influence of surface chemistry on haemocompatibility, several studies looked into doping various elements into DLC to improve its blood-compatibility *in vitro*. In 2005, Kwok et al [377] doped phosphorous (P) ions into a-C:H films deposited via PIIID. The introduction of P-ions reduced the contact angle of a-C:H films to 16.9° and increased the surface adsorption of albumin proteins. Incorporating Si ions into PECVD deposited a-C:H films reduced the overall platelet attachment on the surface [282, 378]. This positive response was implicated with the lowered surface energy of a-C:H surfaces from the addition of Si ions. The addition of F ions to a-C:H and ta-C surfaces presented similar results of reduced platelet adhesion and activation [379] reinforcing the role of surface energy in platelet adhesion.

Apart from surface chemistry, the influence of deposition methods on platelet interactions was also investigated. In 2003, Yang et al [320] showed that films deposited at a lower substrate bias (−75 V) than normal (−900 V) reduced platelet adhesion and its subsequent activation. Furthermore, it was shown that a reduced bias elongated the overall APTT clotting times when compared with stainless steel. Logothetidis et al [380] evaluated the influence of hydrogen content and substrate bias on the haemocompatibility of a-C:H and ta-C films using spectroscopic

ellipsometry. Results showed that the albumin/fibrinogen ratio for a-C:H surfaces with increased hydrogen content, lower refractive index and positive substrate bias was higher, suggesting that a-C:H films with surface chemistries more polymeric in nature exhibited better haemocompatibility. Contrastingly, a study conducted by Ma et al [271] showed that the albumin/fibrinogen ratio was found to be inversely proportional to the hydrogen content, where an increase in hydrogen content decreases the overall surface adsorption of albumin and fibrinogen proteins and decreases the overall albumin/fibrinogen ratio.

Changing the ratio of sp^3 and sp^2 hybridization fractions was also shown to modulate surface haemocompatibility of DLC films. Leng et al [381], using ta-C films deposited using pulse laser, showed an increase in sp^2 to sp^3 ratio correlated with reduced platelet attachment. Similarly, Chen et al [382] used PIIID coated a-C:H to show the same. However, Logothetidis et al [380] showed increasing the sp^3 fraction of a-C films decreased the overall platelet attachment.

An *in vitro* study conducted by Gutensohn et al [383] evaluated the expression of platelet activation factors, CD62-P and CD63, on DLC coated stainless steel arterial stents. The results, when compared with uncoated stainless steel stents, showed a decrease in antigen expression on DLC surfaces. This was attributed to the suppression of ion leaching from the stainless steel by DLC coating. DLC was also found to reduce platelet adhesion under shear flow [384, 385].

Haemocompatibility of DLC films were also evaluated in terms of the surface wettability and the surface energy. Reducing the surface energy of DLC films by doping with P-ions have shown a preferential adsorption of albumin proteins and weak adsorption of other plasma proteins [377]. Huang et al [267] showed that blood compatibility improved on hydrophilic surfaces, by increasing albumin uptake on DLC surfaces. However, Leech et al [386], while investigating the thrombogenic response of hydrophilic coated catheters in dogs, by measuring the amount of clot formation, observed that the hydrophilic coatings were as thrombogenic as the uncoated stainless steel catheters. Similarly, Jones et al [387] showed titanium-based

hydrophilic surfaces presented enhanced fibrinogen adsorption and platelet spreading, and related DLC's haemocompatibility to its low surface energy, hydrophobicity, and smooth surface finish. Another study, evaluating the influence of silicon, when doped with a-C:H, in promoting haemocompatibility found silicon ions lowered the surface energy, and increased the hydrophobicity, of a-C:H surfaces and consequently presented decreased platelet adhesion [378]. However, Saito et al [379] showed that increasing a-C:H's hydrophobicity by incorporating fluorine atoms, increased the number of platelets attached onto a biomaterial surface as well as their spreading.

Though, a-C:H and ta-C films did not show any cytotoxic effects *in vitro* and *in vivo*, its response to blood during clinical evaluation ultimately dictate its haemocompatibility. DLC films in recent years have been used to coat stents, guidewires, heart valves and left ventricular assist devices. The application of stents, to keep the vasculature open to prevent its occlusion, has been largely limited by restenosis, occlusion, and stent-associated thrombosis. Arterial stents have been shown to leach metal ions such as: Ni, Cr, Mo, and Mn; into the blood, increasing the overall thrombogenicity of the implant [388]. However, DLC coating also reduced platelet activation and thrombogenicity to a significant extent [389]. A study conducted by Bartorelli et al [389] demonstrated the effect of PVD-deposited DLC coating in Carbostent™ (Sorin, Saluggia, Italy) in reducing restenosis. 165 DLC-coated stents were implanted into 110 patients for 129 lesions, and clinical success was noted in all cases. There was no development of stent-related thrombosis after 30 days after implantation. Similarly, another study conducted by Antoniucci et al [390] evaluated the influence of Carbostent™ in a clinical study consisting of 112 patients for 6 months. Angiographic results showed less than 11% restenosis rate amongst 108 patients, showing that Carbostent™ significantly suppressed thrombus formation. Similarly, Schaefer et al [391] implanted a DLC-coated nitinol stent for endovascular treatment of superficial femoral artery occlusive disease. The results obtained 12 months after intervention showed 100% pretency rate, reinforcing the beneficial role of DLC. However, a clinical trial conducted in 2004 did not show any appreciable difference between DLC coated and uncoated stents. Haase et al [392] compared Carbostent™ with non-DLC coated bare metal stents to find that

Carbostent™ does not provide any clinical advantage (18% restenosis rate) when compared with uncoated stainless steel stents (and 21% restenosis rate) with similar design and structure.

Apart from Sorin (manufacturer of Carbostent™), other companies such: as Plasma Chem (BioDiamond™; Mainz, Germany), Phytis (Diamond Flex™; Dreieich, Germany) and Bekaert (Dylyn™; Kortrijk, Belgium) also have come forward to use DLC coatings in medical implants. Plasma chem's Biodiamond is nanocomposite multilayer-coated stent with a DLC intermediate layer coating the inside and outside of their stainless steel 316-L stent. Airoldi et al [393] investigated the influence of a-C:H coating on Biodiamond's and Diamond Flex's 316-L stainless steel vascular stents, for the treatment of coronary artery disease amongst 347 patients (502 lesions). The thrombotic effects of DLC were evaluated through angiographic tests against uncoated 316- stainless steel stents, after 6 months of implantation. Results showed that the binary restenosis for a-C:H stents were 31.8% and 35.9% for stainless steel stents, while the major adverse cardiac effect was 30.5% for a-C:H coated stainless steel stents and 32.7% for uncoated one. This again prooves no appreciable difference between DLC coated and uncoated stents.

Despite the excellent *in vitro* and *in vivo* biocompatibility and haemocompatibty results of DLC surfaces, the unexpected negative results from various clinical tests significantly affect the cardiovascular applications of DLC coatings [393]. The exact mechanism behind the preferential adsorption of fibrinogen and albumin during DLC-blood interaction, or the interactions between platelets and plasma proteins on DLC films is still not fully understood. A better understanding of the material science and the interaction of blood components with the biomaterial surface is therefore still needs to be addressed.

2.2.1.3.2 TiO_2

TiO_2 coatings, like DLC, have been studied as very haemocompatible materials, where the haemocompatibility of the coating has been correlated to its thickness and structure of the oxide layer. Sunny et al [344] highlighted the importance of the thickness of the coated layer by reporting a seven fold increase in ratio of albumin to fibrinogen adsorption to 200nm. Preferential adsorption of albumin over fibrinogen has been attributed to a reduction in the adhesion and activation of platelets. The thickness of the oxide layer has also been implicated with the suppression of the coagulation cascade. Huang et al [264] showed that when the thickness of the TiO_2 layer was increased from 10nm to 250nm, APTT clotting time was increased by a factor of 1.5. However, when the thickness of the oxide layer was increased by pre-treating the bulk substrate with hydrogen peroxide (H_2O_2) prior to oxide coating, an increased adsorption of fibrinogen and high molecular weight kininogen proteins was observed. Since these proteins activate platelet response, severe activation of platelets and the clotting cascade was noted on treated TiO_2 surfaces.

Along with surface thickness, the crystal structures of the coating also have shown to have an impact on the degree of plasma adsorption. TiO_2 surfaces with greater crystallinity, such as rutile surfaces, were found to induce less platelet adherence and activation in comparison to amorphous oxide surfaces; whilst, the opposite effect was observed on the clotting cascade, rutile surfaces exhibiting increased coagulation cascade activation [394]. McAlarney et al [395] showed complement C3 adsorption on crystalline TiO_2 surfaces increased with increasing thickness. Spontaneous activation of the C3 proteins on the TiO_2 may lead to the consequent activation of the coagulation cascade and as such can greatly aid in the formation of thrombus clots.

Several theories have been proposed to understand the mechanism by which changes in the thickness, structure and chemical composition of TiO_2 impact the surface's haemocompatibility. Surface charge of TiO_2 is proposed to be a significant contributor to reduced plasma protein adsorption and subsequent platelet activation. The hydroxide groups formed on TiO_2 surfaces upon contact with water is thought to

behave as positively charged species in the acidic biological condition caused by the implantation process. The positive surface charge has been proposed to inhibit the adsorption of positively charged plasma proteins like fibrinogen, and facilitate the adsorption of negatively charged proteins like the anti-thrombotic albumin, to promote the overall haemocompatibility of the surface.

Another hypothesis is that the low surface energy and the semiconductor nature of TiO_2 are the underlying factors behind TiO_2's haemocompatibility. Low surface energy, increased by the increased atomic density of the crystal structure; have been shown to decrease fibrinogen uptake on the surface [396], while, surfaces with high surface energies and hence low wettability (like LITC), cause plasma fibrinogen to irreversibly bind onto the solid surface to lower the overall surface-interfacial tension. Decreased fibrinogen adsorption on TiO_2 surfaces has been attributed to weak interactions between the surface and the protein. Crystalline TiO_2 has been reported to have a electronic band gap of 3.2eV, while fibrinogen's electronic band gap is 1.8 [397, 398]. Since the conduction and valence bands of fibrinogen lie within TiO_2's band gap, the inhibition of electrons transferred from fibrinogen to the crystalline oxide layer has been linked with decreased fibrinogen adsorption [399, 400]. A higher band gap on crystalline surfaces is correlated with the degree of crystallinity. As rutile and anastase TiO_2 surfaces exhibit increased crystallinity when compared with amorphous oxide, they have been attributed with an increased band gap.

In an effort to understand the influence of surface chemistry and surface charge on the adhesion of plasma proteins, numerous studies have analysed the effect of doping TiO_2 with either tantalum, chromium or phosphorus ions to produce n-type semiconductors. Doping the surface with cations such as tantalum, chromium and phosphorous; have shown to reduce fibrinogen adsorption, the activation of the clotting cascade, and platelet adhesion [394, 396]. This has been attributed to the positive charge of the surface formed by the influx of positive cations from the doping process. However this was only true for samples that had not undergone tempering. Samples that were tempered during phosphorous ion implantation showed

lower protein adsorption, platelet adhesion and activation, and lower clotting cascade activation; while, chromium ion-implanted surfaces exhibited low fibrinogen adsorption, and significantly increased levels of platelet adhesion and activation, and coagulation cascade activation. This suggests that the theory that n-type semiconductors prevent electron transfer from fibrinogen may not extend to proteins involved in the clotting cascade, and that clotting activation on ion-implanted oxide are reduced through other mechanisms such as lower interfacial energy or surface chemistry [394]. Furthermore, enhanced haemocompatibility from phosphorous ions have been attributed to platelet membranes enriched with phosphorous-based molecules which recognises the phosphorous ions on the oxide coating, reducing their overall adhesion and activation.

Whilst, the physical, chemical and biological properties of TiO_2 coatings render it a promising biomaterial for its use in the cardiovascular industry, the various studies into the interactions of the TiO_2 surface layer with blood proteins such as fibrinogen, platelets and the coagulation cascade have only highlighted the some aspects of its haemocompatibility. Further investigation of the material science and its dynamic and synergistic interaction with blood components is still necessary to better understand its haemocompatibility.

2.2.1.4 Surface nano-patterning

The various strategies described thus far are based on modifying surface chemistry to achieve favourable biological interactions. However, it is becoming increasingly evident that apart from the chemical composition of the surface, surface topography also influences biological response [401]. In specific, patterning the topography of a biomaterial surface with nanoscale features, to create a nano-topographical surface, is known to play a significant role in modulating interactions at the bio-interface. It has been hypothesised that the geometrical and chemical features of the nano-patterns may control the interactions between proteins and cells at the bio-interface. Nano-patterns may mimic the structure of natural extracellular matrix (ECM) in

which cells reside and function, and as such, tailoring the topographical cues can be influential in controlling cellular interactions on implant surface. Though it is still unclear just to what extent, several studies have shown topographical features such as nano-particles, nano-pores, nano-pits, or nano-grooves have modified the surface interactions of proteins such as: fibrinogen, fibronectin, viteronectin and lysozymes; and cells such as: osteoblast, osteoclast, fibroblast, endothelial, macrophage and stem cells [402-412]. Therefore, a detailed understanding of the dynamic physiochemical interactions between proteins, cells and nano-patterned surfaces at the bio-interface is fundamental for improvements in areas in such as cell culture technology, biosensing and medical device development [413]. As for the cardiovascular field, understanding the optimum nano-topography or range of nano-topographies which can greatly enhance surface haemocompatibility will aid in synthesis of non-thrombogenic biomaterials.

To investigate platelet adhesion and protein adsorption on nano-topographical surfaces, it is necessary to fabricate 2-dimensional surfaces with well-defined nano-topographies that are highly reproducible with uniform nanostructures and homogenous surface chemistry. The nano-patterned surfaces should be cheap to fabricate and that too within a short period of time, especially when considering certain studies that require numerous samples, with large surface areas [413]. Furthermore, the fabrication method needs to be translatable for high throughput volume and the fabricated nano-topographies should be transferable onto 3-dimensional biomaterials for future commercial and clinical applications [413]. At present, 2-D fabrication methods are at their infancy and the use of 2-D nano-structures on 3-D biomaterials still remains a challenging task.

2.2.1.4.1 Surface nano-patterning techniques

Several strategies have gained considerable interest in the recent years for the fabrication of 2-D structures. Some include electron beam lithography (e-beam), chemical etching, glancing angle deposition, self-assembly nano-patterning, polymer

de-mixing and block co-polymers. Apart from e-beam lithography, the above mentioned synthesis techniques have been used to produce surface nano-topographies that are to some degree parallel, but not periodic. E-beam lithography has been appointed as the preferred technique to produce regular arrays of nano-patterns.

Electron beam lithography has been used as a gold standard in producing high resolution, ordered arrays of nano-topographies, however, it is mainly used to fabricate masters for parallel replication processes such as photolithography and nano-imprint lithography (NIL) [414]. The resolution of nano-particles is limited by the wavelength of the light source used for exposure of the coated resist at the wafer [413, 414]. Wavelengths down to approximately 10 nm are currently being explored to produce nano-features with dimensions in the sub-20nm and sub-10nm range [415, 416]. E-beam lithography is a very expensive and a time consuming process that is limited to the fabrication of nano-topographies on small surface areas. As such, alternative fabrication processes are being developed as a means to produce low-cost, highly-reproducible nano-topographies.

Chemical modifications such as chemical etching and oxidation have been used to create nano-roughness with irregular topographies. Columnar structures can be produced using techniques like reactive-ion etching; whilst nano-patterns can be fabricated using controlled chemical oxidative patterning and alkaline modifications of metals [417-419]. By changing the solution or the concentration of the solution, as well as exposure time and substrate type, it is possible to modulate the roughness of the surface [420]. However, etching causes localised changes to surface chemistry, rendering it difficult to distinguish between changes in surface chemistry and topography as topographical changes for biological interactions [421, 422].

Glancing angle deposition technique is a physical vapour deposition (PVD) technique in which the particle flux is deposited on the surface from an oblique (or, glancing) incidence to create thin films that are anisotropic, porous and highly structured [423]. Growth of the thin film is dominated by atomic-shadowing,

wherein nucleation sites on the substrate evolve into a tilted columnar microstructure. By changing process parameters including substrate tilt angles, adatom diffusion, collimated vapour flux and the sample rotation speed, it is possible to fabricate thin coatings with a variety of exotic nano-structures [424]. It is also possible to create glancing angle deposition thin films composed of multiple materials and different hetero-structures [425].

Self-assembly nano-patterning involves the controlled assembly of colloidal nano-particles either by electrostatic interactions or by a simple close packing of the particles [426]. The assembly of colloidal particles have been optimised to produce hexagonally closed-packed arrays, covering domains up to 100 μm^2 [413]. Self-assembly of colloidal particles, through electrostatic assembly, has been optimised to produce large areas with uniform structures. These methods offer several advantages such as reproducibility, reliability, ease of production within a quick time-frame; however, aggregation of the colloidal particles with particle diameters less than 40 nm has been reported.

Polymer de-mixing involves the spontaneous phase separation of two immiscible thin spin-cast polymer blends to create nanotopographical morphologies [427, 428]. This technique is relatively simple means of producing nano-features onto polymer substrates in a controlled manner. The size, structure and pitch of the nano-features is dependent on the immiscibility of the two polymers chosen, their molecular weight, the specific solvent used and the thickness of the spin-coated film [429-431].

Block co-polymer is similar to polymer de-mixing in that it too is a phase separation technique used for the production of nano-patterned thin spin-cast surface coatings [432-434]. The polymer chains, or blocks, are selected to covalently attach to each other, and because of their immiscibility, phase separation will take place [434]. The polymers organise themselves into laterally ordered, periodic arrays of self assembled features, for the addition of metallic salts. The original block co-polymers are etched away after the films are exposed to metal salts, resulting in a pattern of metal nano-structures on the surface replicating the pattern of the phase-separated

block co-polymer features. The size and pitch between the nano-patterns can be varied in relation to to the size of the domains on the co-polymer chains [435, 436]. Block co-polymer allows for nano-patterning with features of dimensions below 10nm [437]. Whilst block co-polymer allows for pseudo-regular nano-patterns, the lack large-scale ordered and symmetrical array may influence biological response such as platelet adhesion and their spreading.

2.2.1.4.2 Influence of nano-topography on blood compatibility

While, DLC's haemocompatibility has been attributed to its smooth surface finish, in recent years, it has been shown that platelet adhesion and the adsorption of fibrinogen can in fact be minimised to levels lower than on the corresponding smooth surfaces by carefully optimising the surface nano-topography in the nanometer to sub-micrometer range [438]. Chen et al [439] proposed that roughness should be catagorised into three groups:

- Greater than 2 μm;
- Between 2 μm and 50 nm; and
- Less than 50 nm

It was hypothesised that creating a roughness greater than 2 μm will allow for nano-patterns with dimensions greater than the diameter of a resting platelet, and, consequently will result in an overall increase in surface contact area, which may promote platelet-surface adhesion, and hence thrombogenic response. Nano-pillars or nano-grooves fabricated to produce a roughness value between 2 μm and 50 nm will mimic the dimension of proteins; and will effectively reduce the contact area for platelet adhesion by only allowing platelets to interact on the apical side of the nano-topographic surface, suppressing their adhesion and consequently their activation. They prescribed that nano-patterns within this range will be optimum to create a thrombo-resistant surface, as surface structures that are less than 50 nm high might exhibit little influence on platelet interactions. It was suggested that nano-structures less than 50 nm will create nano-features that are smaller than the average size of filopods exhibited on activated platelets and may not recognisable by platelets.

Consequently, platelets may respond in a similar way as they would on smooth surfaces exhibiting their influence based on other dominating factors. Furthermore, it was proposed that a more propitious response can be created by optimising both: the surface roughness and surface chemistry; and using them in combination [16].

A study conducted Sun et al [438] investigated platelet interactions on fluorinated polycarbonate urethane (FPCU) nano-patterned with carbon nanotube arrays (ACNT) of diameter 39.7nm and length 20μm. The results showed that when compared to a flat FPCU surfaces, the nano-patterned surfaces suppressed platelet adhesion, when compared with the flat substrates. Platelet activation studies using fluorescence microscopy presented minimal platelet activation on the nano-patterned surfaces. Furthermore, it was found that ACNT nano-tubes decreased the overall surface wettability, and consequently lowered the surface free energy of FPCU. This was in corroboration with Chen's [439] hypothesis. Another study conducted by Milner et al [440] investigated the influence of polyether(urethane urea) (PUU) surfaces nano-patterned with 700 nm and 400 nm square pillars on platelet adhesion under low shear stress. Results showed that the nano-patterned surfaces reduced platelet adhesion from a pool of plasma proteins. Again, no significant changes in platelet activation was observed on the nano-patterned surfaces, suggesting that although the pillars lead to an increase of the total surface area, the actual contact area between platelets and surface was limited to the top of the nano-patterns. Since, increased hydrophobicity of a biomaterial has already been attributed with decreased platelet adhesion; it was unclear just to what level of influence the nano-patterned structure exhibited on lowering the adhesion and activation of platelets.

Minelli et al [441] nano-patterned polymethylmethacrylate (PMMA) surfaces using polymer de-mixing to produce nano features of size 27, 50, 60, 150 and 1240 nm and height 3, 4, 10, 50 and 120 nm, respectively. Von Willebrand factor, albumin and fibrinogen adsorption and platelet adhesion was investigated on these nano-patterned surfaces and the results were compared with the flat substrates. The findings showed that the adsorption of albumin and von Willebrand factor increased with increasing surface roughness, while, fibrinogen adsorption decreased. SEM images of platelet

adhesion showed that platelets (from a solution of plasma proteins) adhered more strongly, displaying spreading and platelet-platelet aggregation, as the size of the nano-features increased. These results contradict Chen's [439] hypothesis as the largest nano-feature was significantly less than 2μm, and surfaces with nano-patternes less than 50nm showed decreased platelet adhesion than surfaces with nano-patterns between the range 50nm and 2μm. Similar to Minelli's finding, Kubo et al [442] showed, using titanium surfaces with 100nm nano-pits, a two fold increase in albumin adsorption on nano-pattered surfaces.

Sutherland et al [408] found an increase in platelet adhesion on fibrinogen pre-adsorbed nano-pitted TiO_2 substrates (nano-pit dimension: 40nm wide and 10nm deep), when compared with fibrinogen pre-adsorbed flat surfaces. This suggested that nano-pits were responsible for increased adsorption of fibrinogen and conformational changes within the protein for platelet binding. Furthermore, when comparing platelet adhesion on the bare surfaces, it was noticed that nano-pits suppressed platelet adhesion, reinforcing the significant role of surface topography in protein adsorption and conformation, as well as the influence of fibrinogen in platelet adhesion. It was also interesting to note, while Minelli reported an increase in platelet adhesion with increasing roughness on PMMA surfaces, Sutherland was able to show a decrease in platelet adhesion on increasing roughness of TiO_2 surfaces.

Dolatshahi-Pirouz et al [423], reported atomic force microscopy (AFM) studies which revealed that fibrinogen conformation on nano-rough platinum surfaces (RMS of 9nm) exhibited an unfolding of the protein structure as compared to the fibrinogen conformation on platinum surfaces with a mean roughness of 1.5nm. It was found that nano-patterns with roughness in the same order as proteins were found to not exert any influence on the protein's conformation, while surfaces with dimensions greater than or less than the dimensions of proteins influence the conformation of the protein upon adsorption [413]. However, it is was specific to the protein adsorbed and the surface chemistry of the biomaterial [413].

Furthermore, apart from the size, the spatial arrangements of nano-features are also important factors that contribute in modulating biological response. Curtis et al [443] compared the effect of cell adhesion on the regularity of nano-structures. The study found that regular nano-structures (60-150nm, formed using electron beam lithography), promoted cellular adhesion when compared with irregular/pseudo-regular nano-patterns. Similarly, Koh et al [444] was able to show, using platelets, that platelet adhesion and activation on irregularly arranged multi-walled carbon nano-tube (MWNT)-polylactic-co-glycolic-acid (PLGA) was significantly reduced when compared with the flat substrates and regularly arranged carbon nano-tubes.

While a synergistic combination of surface topography and surface chemistry is necessary to better influence platelet interactions, a clear understanding of how surface chemistry and topography relate to interfacial properties and biological interactions and the degree of influence nano-patterns play on platelet adhesion and activation is still poorly understood.

3 MATERIALS AND METHODS

In physiological conditions, surface influenced platelet response to clot formation is the result of a complex biological system involving the adsorption of proteins, platelet receptor-ligand binding and signal transduction. Protein ad sorption mediates the platelet interactions and consequent responses on biomaterial surfaces, while, surface topography of the underlying substrate have been shown to influence the concentration and conformation of the adsorbed proteins.

A number of experimental investigations with increasing complexity were tested to relay the interplay between platelets, plasma proteins, such as albumin and fibrinogen, and haemocompatibile biomaterial coatings. Techniques employed for such an investigation include; x-ray spectroscopy (XPS), atomic force microscopy (AFM), scanning electron microscopy (SEM), focused ion beam (FIB), enzyme linked immuno-sorbant assay (ELISA), fluorescence microscopy, flow cytometry and quartz crystal microbalance with dissipation technology (QCM-D). A combination of techniques was employed to overcome the limitations of each method [445]. Further, the topography of the flat surfaces were modified, using the block co-polymer technique, to produce pseudo-regular nano-patterns, and their ability to influence protein adsorption and platelet attachment and activation was also analysed.

Surface coatings analysed in this project include; amorphous-hydrogenated diamond like carbon (a-C:H), tetrahedral amorphous carbon (ta-C) and titania (TiO_2) on ultra flat silicon wafers. Where necessary, the results derived from these experiments were compared with two types of control surfaces; flat and nano-patterned silicon (Si) wafers, as well as tissue culture polystyrene (TCPS).

3.1 Material Processing and Surface Characterisation

In this study hydrogenous amorphous carbon (a-C:H), hydrogen free-tetrahedral amorphous carbon (ta-C) and titania (TiO_2) were coated on either; nano-patterned or unpatterned semiconductor grade silicon (1 0 0) wafer disks and quartz crystal microbalance (QCM) sensors. These surfaces were characterised using X-ray photoelectron spectroscopy (XPS), atomic force microscopy (AFM), scanning electron microscopy (SEM), and focused ion beam (FIB) measurements. Smooth and patterned si-wafer discs were used as control. All buffers and solutions used were degassed and filtered using 0.2µm Millipore filter.

3.1.1 Surface Preparation

3.1.1.1 Initial preparation

Ultra-flat silicon wafers, purchased from Silicon Wafers Enterprises LLC, CA, USA, were coated with a-C:H and ta-C diamond like carbon, and TiO_2 at CSIRO Material Science and Engineering (NSW, Australia). 4" single crystal circular silicon wafers (1 0 0) with resistivity 0.008-0.020 ohms and thickness of 0.5-0.55 mm were cut into 15 mm diameter discs using a diamond coated hole-saw with a water based coolant. The samples were pre-cut into 15 mm diameter discs with 0.5 mm tolerance to comfortably fit into 12-well culture plates for *in-vitro* experiments.

The surfaces were pre-treated ultrasonically with acetone followed by ethanol for 5 mins each to clean the surfaces prior to coating. QCM sensor crystals (purchased from ATA scientific, NSW, Australia) were cleaned using de-ionised water, followed by; Hellmanex III (2% - Sigma Aldrich), de-ionised water and ethanol (80% v/v) for 5 minutes each. The samples were then dried using Nitrogen (N_2) gas and sterilised in an UV/Ozone chamber for 15mins to remove all organic and in-organic substances

prior to coating. A few discs QCM-D sensors were retained as controls with unaltered surface topography.

3.1.1.2 Surface nano-patterning

Present nano-fabrication techniques facilitate the production of nano-features within the size range required for nano-sized proteins and micro-sized platelets to recognise and interact with the surface. The exact nano-structure design and size of nano-particles employed was identified after carefully evaluating present literature on the range of nano-patterning techniques available to create specific roughness values and the beneficial effects of such nano-patterns on influencing biological interactions. The following describes the method employed to develop nano-patterned surfaces, through block co-polymer technique, used for this study.

Si wafer samples were kindly patterned with gold (Au) particles at NRC National Institute for Nanotechnology (AB, Canada) using a specific block co-polymer colloidal deposition technique with polystyrene (PS) and polyvinylpyridine (PVP).

Typically, silicon wafers were cleaned using the RCA method [446] before being spun coated with a solution of 1% polystyrene- polyvinylpyridine (PS-P_4VP, 12k-3.2k) block co-polymer in toluene for 20 seconds at 3800 rpm. The block co-polymer films were then soaked in a solution containing gold salts (1.2% HCl_{aq} v/v with 200mM $KAuCl_4$) for 3 hours. The films were etched with oxygen plasma for 30 seconds before drying with nitrogen gas. The metal ions bind to PVP exposing the PS and excess PVP to the reactive oxygen ions. The plasma removes the polymer film and reduces the Au ions to form a pseudo-regular Au nano-structure pattern on the silicon surface [435, 436].

3.1.1.3 Surface coating

Nano-patterned and flat (un-patterned) substrates were vapour coated with either hydrogenated amorphous diamond like carbon (a-C:H), tetrahedral amorphous carbon (ta-C) or titania (TiO_2) coating.

3.1.1.3.1 Hydrogenated-Amorphous Carbon (a-C:H) deposition

Commercially available a-C:H was coated onto the specimens using a chemical vapour deposition technique called RF Plasma Enhanced Chemical Vapour Deposition (RF-PECVD) to synthesise quality coatings at low temperatures. The deposition system consisted of a plasma reactor equipped with rotary and turbo molecular pumps with controlled gas supply and pumping system, in a manner described elsewhere [447]. A base pressure of $1x10^{-3}$ Pa was attained in the chamber prior to deposition. The diamond like carbon (DLC) films were deposited onto silicon wafers and QCM sensor chips, both flat and nano-patterned. Acetylene (C_2H_2), CF_4 and argon (Ar), were used as process gases. The gases were introduced into the system through a gas distributor using mass flow controllers. The total pressure was set independently of the gas flow by adjusting a throttle valve. Prior to deposition, the substrates was sputter cleaned in-situ for 15 seconds in argon plasma operated at 3.3 Pa with the argon flow rate set at 10 sccm at 200 W RF power. The flow rate of C_2H_2 was kept constant at 60 sccm. The deposition pressure was set at 6.6 Pa at an rf power of 200 W for 10 seconds.

3.1.1.3.2 Tetrahedral Amorphous Carbon (ta-C) deposition

Hydrogen-free tetrahedral amorphous carbon (ta-C) was deposited on silicon wafers and silica QCM-sensors using a physical vapour deposition technique called the Filtered Cathodic Vacuum Arc (FCVA). The system employed is described in detail

elsewhere [448]. The arc source was operated at DC arc current of 60 A, producing a positive carbon ion current of 200 mA, (measured at the exit of the arc source), with a shutter of 140 mm in diameter. The cathode used for producing the arc was high purity graphite (99.9%). A DC substrate bias voltage of −100 V was applied to the substrate. The deposition was performed at room temperature and the deposition rate was 50 nm/min.

3.1.1.3.3 Titania (TiO_2) deposition

Crystalline, anastase, titanium dioxide (titania, TiO_2) was deposited onto nano-patterned and flat, silicon and silica QCM substrates using a physical vapour deposition technique called the filtered arc cathodic vacuum arc deposition (FACVD) system, described in detail elsewhere [357]. The thin films were deposited from the plasma discharged from the titanium electrode (cathode) of the cathodic arc to the substrate. This occurs in vacuum at a low voltage, high current setting. The base pressure of the system was reduced to $2x10^{-4}$ Pa prior to coating. The sample substrates were subjected to the following deposition conditions: 120A dc arc current; 12sccm O_2 gas flow rate; 0.35Pa chamber pressure; 200mA measured titanium ion arc beam current with an area of 8 cm^2 biased at -100 V at the substrate position, -50V substrate bias and a deposition time of 15 sec. The deposition process was conducted at room temperature as the intrinsic energy of the depositing metal is sufficiently high to facilitate self-densification of the titania film on the substrate surface.

3.1.1.4 Surface cleaning

Samples were cleaned and sterilised in a reliable and repeatable manner to avoid any contamination such as particle residues and debris on the surfaces prior to each experiment.

To validate the cleaning methods, the surfaces were incubated in a solution of either fibrinogen proteins or platelet suspension prior to cleaning. An ELISA was then carried out to detect any remaining fibrinogen residues adsorbed on the surface and fluorescence microscopy was used to detect un-washed platelets using an actin stain. Results from these experiments did not detect any protein or platelets, even at trace concentrations, validating the cleaning procedure (data not shown).

3.1.1.4.1 Flat discs

The flat substrates were cleaned prior to and in-between all experiments via the following method; wiped and ultrasonically washed in degassed de-ionised water prior to Decon 90 (2% solution v/v - Sigma Aldrich), de-ionised water and ethanol (80% v/v) for 20 minutes each. The samples were then transferred to an acetone bath for 10mins followed by ultrasonic cleaning with ethanol 80% (v/v) and 100% (v/v) before being dried with N_2 gas and sterilised in an UV/Ozone chamber for 15 minutes.

3.1.1.4.2 Flat QCM-sensors

QCM sensor crystals were cleaned prior to and in-between experiments via the following method; wiped and soaked in degassed de-ionised water, Decon 90 (2% solution v/v - Sigma Aldrich), de-ionised water again and ethanol 80% (v/v) for 20 minutes each. The samples were then dried using N_2 gas and sterilised in an UV/Ozone chamber for 15minutes.

Delamination of the ta-C films were noted during the cleaning process as such only silica, TiO_2 and a-C:H crystals were used for further experimentation.

3.1.1.4.3 Nano-patterned discs

The patterned substrates were cleaned prior to experiments via the following method; soaked in degassed de-ionised water, Decon 90 (2% solution v/v - Sigma Aldrich), de-ionised water again and ethanol 80% (v/v) for 5 minutes each before gently drying with N_2 gas.

3.1.2 Surface Characterisation

Surface characterisation is essential step in the experimental process as it verifies the integrity of a substrate by allowing the detection of flaws and errors developed during the patterning and coating processes. Prior to *in-vitro* analysis, the substrates were evaluated through a series of stringent surface characterisation techniques such as; x-ray photoelectron spectroscopy (XPS), scanning electron microscopy (SEM), focused ion beam (FIB) analysis and atomic force microscopy (AFM).

3.1.2.1 X-ray Photoelectron Spectroscopy (XPS)

The surface composition of the flat substrate materials were analysed using the SAGE 150 XPS system.

3.1.2.2 Scanning Electron Microscopy (SEM)

The overall topographical characteristics of the nano-patterned and un-patterned (flat) surfaces were studied using scanning electron microscopy (SEM). Sterilised samples were stored in a desiccator before mounting on brass SEM stage holders for analysis, using carbon double-sided tape and silver paint (high purity silver paint,

SPI). Once mounted, samples were sputter coated for two minutes with platinum (15nm thick coating) using the Balzers SCD040 sputtering system before examining with SEM (Zeiss Ultra Plus, ACMM, University of Sydney, Australia). The samples were sputter coated to make their surface more conductive and therefore less susceptible to the accumulation of surface charge. Then the samples were attached to 0 degree angled SEM stages and were imaged under ultra high vacuum ($1x10^{-5}$ Pa) conditions at an accelerating voltage of 10 keV using an InLens detector.

Focused Ion Beam (FIB) microscopy

Subsections of each sample was visualised using Zeiss Auriga FIB-SEM (ACMM, University of Sydney, Australia) in ultra high vacuum with accelerating voltage of 10keV. Three sections were imaged per sample with a scan area of 2 µm x 2 µm. The FIB-SEM system uses a combination of a FIB and electron beam and secondary ion and secondary electron detectors. Gallium ions from a liquid ion source were field emitted on the sample surface at high beam currents of 50 pA, 30 KV, to mill through the surface.

3.1.2.3 Atomic Force Microscopy (AFM)

Surface topography and the overall nano-roughness of samples were analysed in air using Multimode NanoScope IIIa AFM (Dimensions 3100, Digital Instruments Inc, ANSTO) in low voltage tapping mode at 296K with a tip diameter of 10nm, scan rate of 1hz and scan area of 0.5µm x 0.5µm or 1µm x 1µm. Commercial available Si_3N_4 cantilevers were used and the force and resonant tip frequency parameters were adjusted continually to obtain the best images. 5 spots were scanned for each sample and the surface root mean square (RMS) roughness was calculated:

$$\sum(Z_i - Z_{average})/N \qquad \text{eq 2}$$

where

$Z_{average}$ is the average of the Z height values within a given area

Z_i is the individual Z-value and N is the number of pixels within the given area

Image processing and pore size analysis was performed using Nanoscope off-line software (Veeco Corp. Santa Barbara, USA).

3.2 Protein Studies

During blood contact, all biomaterial surfaces presently used in diagnostic and treatment methods exhibit some level of thrombogenic tendencies and as such can influence the delicate balance between unstopped bleeding and thrombosis in the haemostatic system. The artificial surface activates both, the blood cells (red blood cells, white blood cells and platelets) as well as the enzyme mediated coagulation cascade by exhibiting a similar surface to that found at the site of vascular injury. This involves the rapid adsorption of blood plasma proteins on the biomaterial surfaces to generate a biologically active monolayer which subsequently mediates the adhesion and activation of platelets.

Apart from surface hydrophobicity, conformational changes in the protein structure, caused by the isoelectric charge (pI) difference between the surface and specific plasma proteins, have also been implicated as a potential driving mechanism which dictates protein adsorption.

As such, plasma protein adsorption and the conformation of adsorbed proteins along with the kinetics behind protein adsorption was studied. Specifically, fibrinogen protein (Fg), well known for its intricate role in platelet adhesion and aggregation, was extensively studied and the results were compared against that of albumin (BSA), the most abundant plasma proteins that is often used to passivate biomaterial surfaces. SDS-PAGE, Western Blotting and Coomassie Stain were used to

characterise fibrinogen. Protein studies were carried out using a combination of ELISA, fluorescence microscopy, AFM and QCM-D.

Further, the ability of a material's chemistry to enhance fibrinogen's activity and prolong clotting times were analysed via a series of clotting cascade experiments.

3.2.1 Protein Preparation and Characterisation

Fibrinogen (Fg, from human plasma, >95% clottable protein, lyophilised, AbCam, Australia) was identified Western blotting and its molecular weight characterised using SDS-PAGE. Both fibrinogen and albumin (BSA - >96% purity, lyophilised, Sigma Aldrich, Australia) were diluted in Dulbecco's Phosphate buffered Saline (DPBS), pH 7.4, unless stated otherwise. These proteins were biotinylated for single and competitive protein adsorption studies on silicon, a-C:H, TiO_2 and ta-C coated surfaces. Where applicable, the TCPS well plates were pre-coated with either 0.1% (w/v) albumin (BSA) or 0.1%(w/v) casein proteins.

The efficiency of the biotinylation technique was analysed using ELISA and the concentration of each biotinylated protein was quantified using Coomassie Blue protein assay. Coomassie Blue protein assay was also used to quantify stock concentrations of non-biotinylated fibrinogen and albumin solutions used in the following experiments.

3.2.1.1 Sodium Dodecyl Sulphate Polyacrelamide Gel Electrophoresis (SDS-PAGE)

The molecular weight of fibrinogen was determined using SDS-PAGE, where proteins were separated by their molecular weight using electrophoresis. Fibrinogen was prepared at a concentration of 50µg/ml in Dulbecco's phosphate buffered saline

(DPBS) (Sigma-Aldrich, Australia), pH 7.4. Unfractionated fibrinogen samples (250µg/ml) were loaded onto the gel in a reduced and non-reduced form. In the non-reduced sample, the protein solution was mixed with sample buffer (0.5M Tris HCl, 10% (w/v) SDS, 50% (v/v) glycerol and 0.05% (w/v) Bromophenol Blue, pH 6.8), at a ratio of 7:2, in MilliQ water and stored at room temperature for 20 minutes. The reduced samples were heated in 10mM of dithiothreitol (DTT), a reducing agent, for 5 minutes in a 95 ºC waterbath before diluting in sample buffer (SB). 10 µl of samples were loaded along with a standard and electrophoresed on 3-8% Tris-acetate SDS-PAGE gels (Invitrogen, Sydney, Australia) using aTris-acetate SDS running buffer (50mM Tricine, 50mM Tris Base, 0.1% (w/v) SDS, pH 8.24) at 160 V for 60 minutes. The gels were transferred into the fixing solution (40% v/v methanol : 10% v/v acetic acid : 50% v/v MilliQ water) for 10 minutes prior to being stained in diluted solution of Simply Safe Coomassie Blue G250 dye over night.

Electrophoretic patterns under non-reducing conditions by Coomassie Blue staining showed one broad band at 340 kDa, and under reducing conditions shows its three subunits Aα-, Bβ- and γ-chains at 65, 55 and 47 kDa respectively (data not shown). Molecular weight standard used was within the range of 10-250 kDa.

3.2.1.2 Western blotting

After electrophoresis, the samples were transferred to a polyvinylidene difluoride (PVDF) membrane (Millipore, Sydney, Australia) using NuPage Transfer buffer with 10% (v/v) methanol, pH 7.2 for 60 minutes in a semi dry blotter at 300 mA and 20 V. The membranes were removed and blocked for 1 hour using 1% (w/v) BSA in Tris-buffered saline (20mM Tris Base, 136mM NaCl, pH 7.6) with 0.1% (v/v) Tween 20 (TBST) solution at room temperature. This was followed by incubation with 2 µg/ml primary antibody, monoclonal anti-human fibrinogen antibody (clone 2C2-G7, AbCam, Australia) diluted in 1% (w/v) BSA/TBST for 2 hours at room temperature. Later the membranes were rinsed with TBST and incubated with horseradish peroxidise-conjugated secondary antibodies for 60 minutes at room temperature.

After rinsing thrice in TBST and twice using TBS the membranes were placed in the chemiluminescence reagent for 2 minutes (Quantum Scientific, Cat# 34095) before being placed between two transparent overhead sheets and developed onto X-ray film. Western blot and SDS-PAGE gel electrophoresis results together identified the proteins as fibrinogen and of high purity (data not shown).

3.2.1.3 Biotin labelling of fibrinogen and albumin

Protein adsorption onto biomaterial surfaces were analysed using biotin-labelled fibrinogen and albumin in both, single and multi-protein solutions. EZ-link NHS-Biotin (Pierce Biotechnology) was diluted in dimethylsulfoxide (DMSO), resulting in a final concentration of 10mM biotin, which was added to each protein solution, 5mg/ml albumin (BSA) and 5mg/ml fibrinogen in DPBS. The solutions were incubated in the dark for 2 hours before separating the biotinylated proteins from excess biotin. Biotinylated fibrinogen was separated using centrifuging while biotinylated albumin (BSA) was separated using dialysis.

The fibrinogen solution was transferred to 10 kDa microcon (BD Diagnostics) and centrifuged for 15 minutes at 13000 rpm. Following a washing step with DPBS, the solution was centrifuged for 15 minutes and washed again. The previous step was repeated over six times before aliquoting the solution in vials.

Albumin (BSA) solution on the other hand was dialysed. After incubating in the dark for 2 hours, the solution was transferred into dialysis tubes before completely immersing the tubes in excess DPBS buffer at 4ºC for 2 hours with constant stirring. The previous step was repeated again before removing the tubes from buffer and storing it inside a bed of dry sucrose at 4 ºC. The solution was dialysed overnight before relieving the contents of the tubes into aliquots.

The relative intensity of labelled proteins were analysed using ELISA where streptavidin horse-radish peroxidase (SA-HRP, GE Healthcare Life Sciences, 1:500

dilution in DPBS containing 0.1% casein) was used as the primary antibody. 2,2'-Azino-bis(3-ethylbenzothiazoline-6-sulfonic acid) diammonium salt (ABTS, Sigma) containing hydrogen peroxide, a colorimetric substrate, was added to the wells and incubated for 30 minutes at room temperature. The absorbance was measured using a plate reader at a wavelength of 405 nm.

The concentration of the aliquoted proteins was measured using Coomassie Blue protein assay while the number of biotin molecules bound to each protein was measured using the Avidin-HABA assay, in a manner described elsewhere [449-451].

3.2.1.4 Coomassie blue protein assay

Exact concentrations of proteins in solution were quantified using a colourimetric Coomassie blue protein assay. Triplicates of 10 µl of each biotinylated and non-biotinylated fibrinogen and albumin stock solution in DPBS were pipetted into 96well plates along with the pre-calibrated albumin (BSA, Sigma Aldrich, Australia) standard solution in dilutions of 0, 0.1, 0.25, 0.75 and 1 mg/ml. 300 µl of Coomassie Plus reagent was added to each well. The well plate was mixed on a shaker for 5 mins before measuring the absorbance at 595 nm wavelength using a plate reader. The concentration values were used to titrate the protein solutions 500 µg/ml stock solutions and 50 µg/ml albumin or fibrinogen working solutions.

3.2.2 Protein Adsorption

The adsorption of proteins and the relative conformation on the flat surfaces were evaluated using a combination of ELISA, fluorescence microscopy, AFM and QCM while the concentration and conformation of fibrinogen and plasma proteins after

adhering to nano-patterned surfaces were evaluated using fluorescence microscopy and AFM.

Investigations were carried on sterilised flat (non-patterned, smooth) and nano-patterned a-C:H, Ta-C and TiO_2 coated –silicon wafers. Since the composition of adsorbed proteins change over time by a phenomenon known as the Vroman's effect, samples were incubated in protein solutions for a period of 60 minutes to allow stabilisation of the adsorbed proteins as well as to ensure its complete coverage on the biomaterial surfaces. All experiments were carried out on 12 well plates, unless stated otherwise and all solutions used were degassed and filtered using Millipore 0.2 µm Millipore filter.

3.2.2.1 Enzyme Linked Immuno-Sorbent Assay (ELISA)

3.2.2.1.1 Simple and complex studies

The adsorption of fibrinogen (Fg) and albumin (BSA) in single and complex solutions onto flat silicon, TiO_2, a-C:H and ta-C coated silicon wafers were analysed using biotinylated proteins (preparatory method detailed in Section 0). Samples, in triplicate, were placed in 0.1% (w/v) casein (diluted in DPBS) pre-coated well plates (60 minutes at 37 ºC). These samples were incubated for 60 minutes at 37 ºC in one of four conditions:

- a simple solution containing 50 µg/ml biotin labelled albumin (BSA);
- a simple solution containing 50 µg/ml biotin labelled fibrinogen (Fg);
- a complex solution composed of 500nµg/ml biotinylated albumin (BSA) and 50nµg/ml non-biotinylated fibrinogen; or,
- a complex solution composed of 500nµg/ml non biotinylated albumin (BSA) and 50 µg/ml biotinylated fibrinogen (Fg)

The physiological ratio of albumin (BSA) and fibrinogen (Fg) proteins found in blood serum is approximately 10:1 for healthy blood [452, 453] and as such albumin and fibrinogen in the complex solution were mixed in the ratio 10:1. Bovine albumin was used instead of human albumin as BSA is homologous in structure to human albumin and serve the same function in the two species. TCPS well plates pre-coated with 0.1% (w/v) casein proteins were used as negative controls while non-casein pre-coated well plates were used as positive controls. After an hour of incubation, the flat substrates were washed thrice in DPBS, incubated with 0.1% (w/v) casein block for 60 minutes at 37ºC, washed twice in DPBS-T (DPBS with 0.01% (v/v) Tween) before incubating in biotin-binding SA-HRP (dilution 1:500 in 0.1% (w/v) casein) for 30 minutes at room temperature. The samples were washed four times in DPBS-T before loading each well with excess ABTS in hydrogen peroxide and incubating in room temperature for 30minutes. 100µl duplicates from each well were transferred into a 96 high binding well plate before measuring the concentration of fibrinogen and albumin was measured as arbitrary absorbance values using a plate reader at 405nm wavelength.

The average number of biotin attached to each fibrinogen and albumin molecule, as calculated from HABA avidin assay, was used to quantify the number proteins attached to each surface.

3.2.2.1.2 Conformation of adsorbed fibrinogen measured using ELISA

The orientation of adsorbed fibrinogen in simple and complex solution was evaluated by measuring the availability of platelet binding region, fibrinogen A alpha chain, and gamma chain for antibody binding. Flat silicon, TiO_2, a-C:H and ta-C substrates, in triplicate, were placed in 0.1% (w/v) albumin (BSA) pre-coated well plates and incubated for 60 minutes at 37ºC in two different fibrinogen containing solutions: a simple solution containing only 50µg/ml fibrinogen (Fg); and a multi protein solution containing 500µg/ml albumin (BSA) and 50µg/ml fibrinogen (Fg).

The albumin and fibrinogen from the complex solution were mixed in the ratio 10:1. Albumin (BSA) pre-coated polystyrene well plates were used as negative controls while non-albumin (BSA) coated well plates were used as positive controls. After an hour of incubation, the samples were washed in DPBS, incubated with 0.1% (w/v) albumin(BSA) block for 60 minutes at 37ºC, washed twice in DPBS-T (DPBS with 0.01% v/v Tween) before incubating in primary antibodies. The antibodies used were mouse monoclonal anti-human fibrinogen antibody (2C2-G7 -Bioscientific, Australia for Cederlane) ,mouse monoclonal anti-human fibrinogen A alpha chain antibody (alpha chain binding FgA antibody – 1/1000 dilution in 0.1% w/v BSA, AbCam, Australia), and rabbit monoclonal anti-fibrinogen gamma chain antibody (gamma chain binding antibody– 3/1000 dilution in 0.1% w/v BSA, AbCam, Australia). The wells were washed twice in DPBS and incubated at room temperature with secondary antibodies; biotinylated anti-mouse IGg antibody (binds to FgA and 2C2-G7 primary antibodies) and biotinylated anti-rabbit antibody IGg (binds to Fg-gamma antibody.

The secondary antibodies were diluted in the ratio of 1:1000 in 0.1% w/v BSA and were purchased from GE Healthcare (Buckinghamshire, U.K.). After an hour of incubation, the samples were washed twice in DPBS-T and loaded with SA-HRP (dilution 1:500 in 0.1% w/v casein) for 30 minutes at room temperature. Wells were then washed four times in DPBS-T before the colour substrate ABTS with hydrogen peroxide was incubated for 30minutes in room temperature. 100µl duplicates from each well were transferred into a 96 high binding well plate and the absorbance were read using a plate reader at 405nm wavelength.

3.2.2.2 Fluorescence Microscopy

In this experiment, the concentration and conformation of adsorbed fibrinogen on flat and nano-patterned substrates from solutions of only fibrinogen proteins and plasma was determined using fluorescence microscopy.

Flat silicon, TiO_2, a-C:H and ta-C substrates, in triplicate, were placed in 0.1% (w/v) albumin (BSA) pre-coated well plates and incubated for 60 minutes at 37ºC with either 50µg/ml fibrinogen (Fg) solution or diluted plasma (ratio 1:10, in DPBS), while nano-patterned TiO_2, a-C:H and ta-C substrates, in triplicate, were incubated with only 50µg/ml fibrinogen (Fg) solution. After an hour of incubation, the samples were washed in DPBS, incubated with 0.1% (w/v) albumin (BSA) block for 60 minutes at 37ºC, washed twice in DPBS-T (DPBS with 0.01% v/v Tween) before incubating in mouse monoclonal anti-human fibrinogen primary antibody (2C2-G7 - Bioscientific, Australia for Cederlane).

After an hour of incubation the wells were washed twice in DPBS and incubated at room temperature with Alexa Fluor 488 tagged anti-mouse IGg secondary antibody for 60 minutes at 37ºC. Following a quick washing step with DPBS with 0.5% (v/v) Tween 20, the test samples were stored in DPBS prior to visualising at 500x magnification with fluorescence microscope (Zeiss Axioskop Mot Mat 2, Australia). The distribution of the protein across the surface and the total intensity from each image, measured as total number of positive pixels was estimated using ImageJ.

3.2.2.3 AFM

The conformation of adsorbed fibrinogen and serum proteins on flat and nano-patterned surfaces were visualised using AFM. In short, flat and nano-patterned silicon, TiO_2, a-C:H and ta-C substrates, in triplicate, were placed in 0.1% (w/v) albumin (BSA) pre-coated well plates and incubated for 60 minutes at 37ºC, with 50µg/ml fibrinogen (Fg) solution and diluted plasma (ratio 1:10, in DPBS). After an hour of incubation, the samples were washed in DPBS and samples were measured in liquid mode using Catalyst AFM (Bruker Bioscope Catalyst, BMIF, UNSW) in low voltage tapping mode at 296K with a tip diameter of 2nm, scan rate of 0.3Hz and scan area of 1µm x 1µm. Commercially available Si_3N_4 cantilevers were used and the force and resonant tip frequency parameters were adjusted continually to obtain

the best images. Image processing and surface topography analysis was performed using Nanoscope off-line software (Bruker, SA Australia).

3.2.2.4 Quartz Crystal Microbalance with Dissipation monitoring (QCM-D)

In this experiment, QCM-D (Q-sense AB, Sweden) was used to measure the amount of albumin (BSA), fibrinogen (Fg) and plasma proteins (diluted plasma in ratio 1:10, in DPBS) adsorbed onto TiO_2 and a-C:H coated silica resonator substrates by measuring the frequency (f) and dissipation (D) at the fundamental frequency, 5MHz, and successive overtones of 15, 25 and 35MHz. A stable overtone was selected, which in this case was 15Hz and the corresponding f and D values were compared with control silica sensors.

Typically the QCM-D crystals were calibrated in air at 37ºC ± 0.1ºC and loaded with DPBS until a stable f and D baseline was established. After washing, the sensors were exposed to 50ug/ml fibrinogen and 50ug/ml BSA, or diluted plasma (ratio 1:10, in DPBS) for 60 minutes followed by a washing step with DPBS until a stable baseline was obtained (approximately three rinses). Silica QCM-D sensors were used as negative controls. A minimum of three repeats were recorded for each material surface with each protein solution. The Voigt based viscoelastic model assumes that the adsorbed layer is of uniform thickness, conserves its shape, and does not flow and as such the time-dependent frequency shifts (f) and dissipation values (D) obtained for the 3rd (15Hz, n=3), 5th (25Hz, n=5), and 7th (35Hz, n=7) overtone were modelled using Voigt models along with their respective dissipation values to obtain the mass and the rate change of mass of adsorbed layers.

3.2.3 Clotting Cascade Experiments

Coagulation of blood plasma induced by smooth contacting surfaces was measured using clot based assays. Citrated plasma was used in all three coagulation assays to induce fibrin-dependant clot formation. The time taken to induce clot formation via the extrinsic and intrinsic coagulation pathway was measured using the prothrombin assay (PT) and activated partial thromboplastin assay (aPTT), respectively. The ability of the contacting surfaces to denature fibrinogen, preventing it from forming fibrin monomers and consequently delaying fibrin clot formation was measured using the thombin time assay (TT). Contacting surfaces include; a-C:H, TiO_2 and Ta-C coated Si-surfaces where bare Si-wafer discs and polystyrene tissue culture well plates were used as negative and positive control, respectively. Furthermore, a heparin dose response standard curve was established to assess the degree of anticoagulant activity of each material surface.

3.2.3.1 Plasma Purification for Clotting Cascade Experiments

Human blood was collected from healthy donors, under ethics approval from the University of New South Wales. Blood was collected into polypropylene tubes containing 3.2% trisodium citrate solution, where the ratio of whole blood to sodium citrate was 9:1. The whole blood was transferred into 15ml centrifuge tubes and centrifuged at 2500 x g for 15minutes. Following centrifugation, the plasma was immediately separated from the red blood cells into new polypropylene tubes and stored at 4ºC until use. The assays were performed with two hours of collecting blood plasma before the plasma was rendered unviable.

3.2.3.2 Prothrombin Time (PT)

Blood was collected and prepared according to the directions described in section 4.2.2.1. Phosphoplastin RL reagent (R2 Diagnostics, Indiana, USA), from rabbit brain particles, was pre-warmed at 37ºC for 10 minutes and inverted to form a homogenous suspension. Well plates containing triplicate of each surface was incubated with 200µl of plasma at 37ºC for 60 seconds followed by 400µl of Phosphoplastin RL reagent.

Tissue-culture polystyrene (TCPS) wells were used as positive control and plasma clotting times as a function of heparin concentration were used as negative control. Heparin (diluted in DPBS) was dissolved in blood plasma in the ratio of 1:9, totalling final heparin concentration of 0, 1, 2.5 and 5µg/ml. 200µl duplicates of each heparin-plasma sample was loaded on TCPS well plates, incubated at 37ºC for 60 seconds before loading with reagent. Clotting times were recorded when the first form of fibrin formation was observed.

3.2.3.3 Activated Partial Thromboplastin Time (aPTT)

Samples were placed in TCPS well plates, as described in Section 0. 200µl of citrated plasma was loaded onto each sample and incubated at 37ºC for 60 seconds before incubating in 200µl of resuspended Phospholin ES (R2 Diagnostics, Indiana, USA), an ellagic acid based reagent from soyabean phospholipids, for 3minutes. 200µl of 0.025M pre-warmed calcium chloride solution was pippetted to initiate clotting. Non-BSA coated polystyrene tissue-culture wells were used as positive control. Plasma clotting times as a function of heparin concentration were used as negative control in a manner described above. Time taken for clot formation was recorded.

3.2.3.4 Thrombin Time (TT)

The required concentration of lyophilised human thrombin (Sigma Aldrich, Australia) was evaluated by ensuring clot formation falls within the laboratory normal range of 16-18 seconds. Thrombin was diluted in 1% (w/v) albumin (BSA) solution to form a reagent with final concentration of 10NIH units/ml. 300µl of pre-warmed citrated plasma, collected in an eppendorf tube, was incubated with equal parts of thrombin solution and the time taken for fibrin to coagulate was recorded. The thrombin reagent was further diluted until fibrin formation was established within the reference range stated above.

Once the necessary dilution was identified, fresh thrombin solution was prepared. Triplicate of samples, placed in TCPS well plates, were loaded with 300µl of citrated plasma for 60 seconds at 37ºC before incubating in 300µl of resuspended thrombin solution for 2 minutes. TCPS wells with normal plasma were used as positive controls and TCPS well plates with plasma diluted in heparin at various concentrations were used as negative controls, as described previously in Section 0. The clotting times were measured using a stop watch.

3.2.4 Platelet Studies

Adsorbed plasma proteins, such as fibrinogen, on artificial surfaces recognise platelet adhesion receptors, potentially leading to the subsequent adhesion, spreading, aggregation and activation of platelets. In fact, prolonged exposure of biomaterials to blood, *in vivo*, have been known to cause platelet numbers in blood to decrease with surface exposure time, all the while increasing the probability of platelet-dependant, blood clot formation. Surfaces inert to platelet adhesion and activation can be achieved through surface modifications, such as surface coatings and nano-patterning, however, it is necessary to understand the influence of such surface modifications and their selective adsorption of plasma proteins on platelet interactions.

In this study, platelet responses to flat and nano-patterned silicon, TiO_2, a-C:H and ta-C substrates were examined. The volume of platelets, their morphology, spreading and aggregation, once adsorbed onto bare surfaces and protein-pre coated surfaces were analysed using a combination of fluorescence microscopy, SEM and AFM and QCM-D.

Platelets preferentially bind to fibrinogen via platelet integrin $\alpha_{IIb}\beta_3$ and as a consequence have been known to promote platelet adhesion and activation. The extent of other integrins involved in the adhesion process during platelet-biomaterial interactions still remains unknown. As such platelet interactions on biomaterial surfaces pre-exposed to fibrinogen and plasma proteins in the absence of $\alpha_{IIb}\beta_3$ integrins (using anti-integrin $\alpha_{IIb}\beta_3$ antibody) were investigated by fluorescence microscopy, AFM and QCM-D. The activation of platelets, by the activation of $\alpha_2\beta_1$ and $\alpha_{IIb}\beta_3$ integrins, and the expression of P-selectin (CD62P) on platelet plasma membranes were detected using a combination of ELISA, fluorescent microscopy and flow cytometry.

3.2.4.1 Platelet and surface preparation for platelet studies

3.2.4.1.1 Platelet isolation from human blood

Platelet adhesion assays were conducted using human blood from anonymous healthy adult donors, whose details are not provided. Platelets were isolated from blood collected from healthy donors in polypropylene tubes containing 3.2% tri-sodium citrate anticoagulant. Following the transfer of blood into centrifuge tubes, red blood cells were separated from platelet rich plasma (PRP) by centrifuging for 20 minutes at 1000rpm. The PRP supernatant was carefully transferred into fresh centrifuge tubes in which it is centrifuged for a further 10 minutes at 1000rpm to

remove any remaining red blood cells. Again, the PRP was transferred to clean centrifuge tubes and centrifuged for 10 minutes only this time at a speed of 1600rpm causing the platelets pellet in a pool of platelet poor plasma (PPP). The PPP was aliquoted and stored at -20ºC for later use. The platelets were resuspended in pre-warmed Tyrodes buffer (Sigma, supplemented with 10U apyrase, filter sterilised, 37ºC). The suspension was centrifuged at 1600rpm for a further 10 minutes to re-pellet the platelets. The supernatant, containing Tyrodes buffer and remaining plasma proteins, was discarded.

Platelets were counted in a haemocytometer and diluted in pre-warmed Tyrodes buffer to a final concentration of $1x10^7$ platelets/ml. The platelet suspension was incubated in a waterbath for 30minutes to settle at a temperature of 37ºC before use in proceeding experimentation.

Due to the inviability of the platelets within the Tyrodes solution, it is possible only to store the suspension formed by this procedure for up to 5 hours after the blood was first collected from the donor before biological interactions (from further experimentations) become null.

3.2.4.1.2 Pre-incubating platelet solutions with integrin $\alpha_{IIb}\beta_3$ antibody

For experiments analysing the influence of integrin $\alpha_{IIb}\beta_3$ in promoting platelet adhesion, platelets (prepared as described in Section 3.2.4.1.1) were pre-exposed to anti-$\alpha_{IIb}\beta_3$ F(ab) fragment antibody (1 μg/ml, ReoPro, Abciximab, Eli Lily, Sydney, Australia) for 60 minutes at 37ºC, 5% CO_2 before being loaded into wells.

3.2.4.1.3 Pre-coating surfaces with protein solutions

Typically, tissue culture polystyrene (TCPS) well plates, pre-incubated with 0.1% (w/v) BSA for 60 minutes at 37ºC, were seeded with sterilised surfaces (detailed in Section 3.1.1.4), in triplicate, before loading with one of three solutions; 50µg/ml albumin (BSA), 50µg/ml fibrinogen (Fg) and pre-warmed plasma (diluted in DPBS, ratio 1:10) for 60 minutes at 37ºC. The well plates were washed twice in DPBS and incubated with block protein, 0.1% (w/v) BSA, for 30 minutes at 37ºC. The block step is performed to reduce background staining of the substrates. Again, the wells were washed twice in DPBS before commencing the incubation of platelets. Bare substrates, without any protein coat, were compared with the protein-precoated substrates to analyse the combinatorial effect of surface chemistry and the adsorption of specific plasma proteins in modulating platelet interactions.

3.2.4.2 Platelet adhesion studies

3.2.4.2.1 Fluorescence Microscopy

Fluorescence microscopy was used to visualise platelet adhesion on nano-patterned and flat silicon, TiO_2, a-C:H and ta-C surfaces by staining the actin monomers found in the adhered platelet cytoplasm using Rhodamine-Phallodin.

Bare and protein pre-coated surfaces were prepared in a manner detailed in Section 3.2.4.1.3. Platelets (1×10^7 platelets/ml in Tyrodes buffer containing Apyrase, Section 3.2.4.1.1) were incubated for 1 h at 37°C, either alone or in combination with anti-human glycoprotein GPIIb-IIIa receptor (integrin $\alpha_{IIb}\beta_3$) F(ab) fragment antibody (1 µg/ml, Abciximab, Eli Lily, Sydney, Australia), in a manner described in Section 3.2.4.1.2. Bare and protein pre-coated nano-patterned surfaces, on the other hand, were incubated only with platelets in Tyrodes solution for 60 minutes at 37ºC. Any unbound platelets from the well plates were removed from washing with DPBS following the removal of platelet suspension from wells. The platelets were fixed with fixing solution (4% v/v Paraformaldehyde and 1% w/v sucrose) for 15 minutes at room temperature and washed with DPBS buffer. The surfaces were permeabilised

at 4ºC for 5minutes using permeabilising solution and blocked with 1% (w/v) albumin (BSA)/TBS solution for 5 minutes at 37ºC. Rhodamine-Phallodin (1/100 dilution in 1% w/v BSA/TBS, Invitrogen Corporation), a staining solution, was used to stain the actin filaments of the permeabilised platelets over 60 minutes at 37ºC.

Following a quick washing step with DPBS with 0.5% (v/v) Tween 20 (PBST), the test samples were stored in DPBS prior to visualising at 500x magnification with fluorescence microscope (Zeiss Axioskop Mot Mat 2, Australia). Microscope images were analysed for cell number and circularity by using the automated detection of cell outline feature in ImageJ (version 1.44p, NIH). TCPS well plates were used as controls.

3.2.4.2.2 SEM

Platelet morphology on flat and nano-patterned protein pre-coated substrates was also visualised using SEM. Bare and protein pre-coated flat and nano-patterned surfaces, prepared according to Section 3.2.4.1.3, were incubated with platelet solution (1×10^7 platelets/ml in Tyrodes buffer containing Apyrase, Section 3.2.4.1.1) for 1 h at 37°C. The well plates were washed twice with DPBS and soaked in a diluted glutaraldehyde fixative (2.5% (v/v) in DPBS) for 60 minutes at room temperature before another washing step. Once the adhered platelets were fixed, the well plates were dehydrated in a series of graded ethanol washes (50%, 60% and 70% v/v ethanol diluted in MilliQ water) for 10 minutes each. The well plates were then incubated overnight at 4ºC, in fresh 70% ethanol solution before dehydrating in 90% (v/v) and 95% (v/v) ethanol for 10 minutes each followed by two rises in 100% ethanol for 10 minutes, changing solution in between. Any remaining moisture and ethanol residues in the biological specimens were removed by drying the test samples in a critical point drier (CPD). The samples were mounted on stubs, before being sputter coated and imaged using SEM (described in Section 3.1.2.2).

3.2.4.2.3 AFM

AFM allows for precise high resolution imaging of platelets at the nanometer scale by probing the surface nano-topology with a mechanical cantilever. In this experiment, AFM was used to show topographical images of platelets exposed to flat and nano-patterned fibrinogen coated a-C:H substrates.

Typically, sterilised flat and nano-patterned a-C:H surfaces (from Section 3.1.1.4) loaded in albumin (BSA) pre-coated TCPS well platelets, were incubated with 50µg/ml fibrinogen (Fg) for 60 minutes at 37ºC. The well plates were washed and incubated with block protein, 0.1% (w/v) BSA, for 30 minutes at 37ºC before being washed again (detailed in Section 3.2.4.1.3). The fibrinogen pre-coated flat a-C:H substrates were then seeded with platelets (1 × 107 platelets/ml in Tyrodes buffer containing Apyrase, Section 3.2.4.1.1) for 1 h at 37°C, either alone or in combination with anti-human glycoprotein GPIIb-IIIa receptor (integrin $\alpha_{IIb}\beta_3$) F(ab) fragment antibody (1 µg/ml, Abciximab, Eli Lily, Sydney, Australia, Section3.2.4.1.2), while fibrinogen pre-coated nano-patterned surfaces were incubated only with platelets in Tyrodes solution for 60 minutes at 37ºC. Any unbound platelets from the well plates were removed from washing with DPBS following the removal of platelet suspension from wells. The platelets were fixed with 1:1 ratio Methanol : Ethanol solution for 5minutes at 4ºC before storing in DPBS for AFM imaging.

3.2.4.2.4 QCM-D

Real-time analysis of platelet interactions on bare and protein pre-coated flat surfaces was carried out using a single cell, open chamber QCM-D at 5% CO_2 and 37 ± 0.1 ºC. Silica, TiO_2 and a-C:H coated QCM sensors were exposed to DPBS until a stable *f* and D measurements were established. The QCM crystals were then incubated with one of four solutions; DPBS, 50µg/ml albumin (BSA), 50µg/ml fibrinogen (Fg) and

diluted plasma (ration 1:10, in DPBS) for 60 minutes and then rinsed with DPBS, again until a consistent *f* and D values were attained (approximately 3 rinses). The surfaces were blocked with 0.1% (w/v) BSA (this step was omitted in sensors incubated in DPBS so that platelet interactions on bare surfaces can be analysed) for 30 minutes and washed again with DPBS before incubating with platelet solution. Platelets (1×10^7 platelets/ml in Tyrodes buffer containing Apyrase, Section 3.2.4.1.1) were incubated for 1 h, either alone or in combination with anti-human glycoprotein GPIIb-IIIa receptor (integrin $\alpha_{IIb}\beta_3$) F(ab) fragment antibody (1 µg/ml, Abciximab, Eli Lily, Sydney, Australia). After incubation, the samples were again washed with DPBS and any changes in *f* and D measurements during platelet incubation were recorded.

3.2.4.3 Platelet activation studies

3.2.4.3.1 ELISA

ELISA was used to measure the presence of activated plasma membrane integrins on platelets adsorbed on bare and protein pre-coated flat surfaces by probing for $\alpha_2\beta_1$ and $\alpha_{IIb}\beta_3$ integrins using specific anti-integrin antibodies. Bare and protein pre-coated flat, prepared according to Section 3.2.4.1.3, were incubated with platelet solution (1×10^7 platelets/ml in Tyrodes buffer containing Apyrase, Section 3.2.4.1.1) for 1 h at 37°C, 5% CO_2. Again the wells were washed in DPBS twice and fixed with 1:1 ratio methanol : ethanol solution for 5 minutes at 4ºC. Upon fixing, the platelets were incubated with either:

- mouse monoclonal anti-$\alpha_2\beta_1$ (3 µg/ml, clone BHA2.1, Millipore, Sydney, Australia) primary antibody; or,
- mouse monoclonal anti-human glycoprotein GPIIb–IIIa receptor (integrin $\alpha_{IIb}\beta_3$) F(ab) fragment antibody (Abciximab – Reopro, 3µg/ml, Eli Lily, Australia)

for 2 hours at room temperature without agitation. Following a washing step with PBS-T, secondary antibodies, biotinylated anti-mouse antibody (1:1000 in 0.1% w/v BSA, GE Healthcare Buckinghamshire, U.K.) and polyclonal goat anti-human Ig F(ab) fragment peroxidase conjugated secondary antibody (1:2000, Thermo Fisher Scientific, Australia), respectively, were added to each well and incubated for 1 hour at 37ºC. The samples were washed once more in PBS-T before incubating for 30minutes at room temperature with SA-HRP colorimetric agent (1:500 dilution in 0.1% w/v BSA). After subsequent washing step, ABTS (with hydrogen peroxide) colorimetric substrate was added and incubated over night at room temperature. Duplicates of 100µl from each well plate was transferred into a 96 high binding ELISA well plates before measuring absorbance at 405nm wavelength using a plate reader. Results from each test sample were compared against polystyrene well platelets, as control. 50µg/ml collagen precoated on TCPS well plates were used as positive control when measuring integrin $\alpha_2\beta_1$ activation on platelet membrane.

3.2.4.3.2 Fluorescence microscopy

Fluorescence microscopy was used to visualise the localisation of activated $\alpha_{IIb}\beta_3$ integrins and the expression of P-selectin (CD62P) receptors on surface adsorbed platelets. Bare and protein pre-coated flat and nano-patterned surfaces, prepared according to Section 3.2.4.1.3, were incubated with platelet solution (1×10^7 platelets/ml in Tyrodes buffer containing Apyrase, Section 3.2.4.1.1) for 1 h at 37°C. Unbound platelets remaining in suspension after incubating on bare and protein-pre-coated surfaces were collected into flow cytometry glass vials for following experiments using flow cytometer.

The surface bound platelets washed in TBS and fixed, with fixing solution (4% v/v Paraformaldehyde and 1% w/v sucrose) for 15 minutes at room temperature. The samples were washed again in TBS before permeabilising the platelet membrane at 4ºC for 5minutes using permeabilising solution. The samples were then blocked with

1% (w/v) albumin (BSA)/TBS solution for 5 minutes at 37ºC before being integrin and actin staining.

Nano-patterned surfaces were dual labelled with either green staining anti-integrin $\alpha_{IIb}\beta_3$ and red staining Rhodamine-Phallodin, or, green staining anti-integrin $\alpha_{IIb}\beta_3$ and red staining anti-CD62P antibodies. The methods are described below in detail:

- For anti-integrin $\alpha_{IIb}\beta_3$ and actin staining - samples were incubated with mouse monoclonal anti-human glycoprotein GPIIb–IIIa receptor (integrin $\alpha_{IIb}\beta_3$) F(ab) fragment antibody (Abciximab – Reopro, 3µg/ml diluted in 1% (w/v) BSA/TBST, Eli Lily, Australia) for 60 minutes at 37ºC followed by quick wash in TBST. Then the samples incubated with goat polyclonal FITC conjugated F(ab) specific secondary Anti-Human IgG (1:16 dilution, Sigma Aldrich, MO, USA) antibody for 60 minutes at 37ºC. Following a quick washing step using TBST the surface adsorbed platelets were stained with Rhodamine-Phallodin for 60 minutes at 37ºC.
- For anti-integrin $\alpha_{IIb}\beta_3$ and CD62P staining – surface adsorbed platelets were incubated for for 60 minutes at 37ºC with mouse monoclonal anti-human glycoprotein GPIIb–IIIa receptor (integrin $\alpha_{IIb}\beta_3$) F(ab) fragment antibody followed by quick wash in TBST. Then a cocktail containing goat polyclonal FITC conjugated F(ab) specific Anti-Human IgG (1:16 dilution, Sigma Aldrich, MO, USA) secondary antibody and mouse monoclonal RPE conjugated anti-human CD62P (P-selectin) antibody (1:100 dilution, eBiosciences, San Diego, CA, USA) were loaded onto the platelet adsorbed surfaces for 60 minutes at 37ºC.

Flat surfaces were dual labelled with green staining anti-integrin $\alpha_{IIb}\beta_3$ and red staining anti-CD62P antibodies using the method below:

- Surfaces were incubated with mouse monoclonal anti-human glycoprotein GPIIb–IIIa receptor (integrin $\alpha_{IIb}\beta_3$) F(ab) fragment antibody for for 60 minutes at 37ºC. Following a quick wash with TBST the samples were incubated with both; goat polyclonal FITC conjugated F(ab) specific Anti-Human IgG and mouse monoclonal RPE conjugated anti-human CD62P (P-

selectin) antibody for 60 minutes at 37ºC using the dilutions mentioned above.

After dual labelling the samples were washed with 0.5% PBST, before storing the samples in DPBS for visualisation under fluorescent microscopy at 500x magnification. Microscope images were analysed for localisation of activated integrins and cytoskeletal arrangements.

3.2.4.3.3 Flow-cytometry

Activation $\alpha_{IIb}\beta_3$ and P-selectin integrins on un-bound platelets in the presence varying surface chemistries and pre-coated proteins were analysed using flow cytometry. Platelet suspension retrieved from each flat and nano-patterned test surfaces, either; bare or protein pre-coated, from fluorescence microscopy experimentation (as described in Section 3.2.4.3.2) was collected and 100µl from each test surface was pipetted into 2 glass Flow Cytometer Vials.

The vials were either:

- Incubated with 1/100 dilution of Fluorescein isothiocyanate (FITC) conjugated anti-CD62P (clone 9E1, Bio-Scientific Pty. Ltd., Australia), vortexed and incubated for 20 minutes at 37ºC; or,
- Incubated with 1/32 dilution of mouse monoclonal anti-human glycoprotein GPIIb–IIIa receptor (integrin $\alpha_{IIb}\beta_3$) F(ab) fragment antibody, vortexed and incubated for 60 minutes at 37ºC. The platelets in the vials were pelleted by centrifuging at 1000rpm for 3 minutes, the supernatant containing un-bound, excess antibodies were discarded. The vials were washed in PBST and pelleted again by centrifuging at 1000rpm for 3 minutes to remove any remaining free antibodies. After the washing step the samples were incubated with goat polyclonal FITC conjugated F(ab) specific Anti-Human IgG for 60 minutes at 37ºC before following another round of centrifuging, washing and centrifuging.

The supernatant from the vials were discarded and pellets were resuspended in 1% (w/v) Paraformaldehyde in Tyrodes Buffer for 20minutes at 4ºC. The samples were re-centrifuged for 3 minutes at 1000rpm, before being resuspended in pre-warmed (37ºC) DPBS. The FITC fluorescence intensity of 10,000 platelets was analysed using the FL-1 channel in Flow Cytometer.

4 MATERIAL CHARACTERISATION AND PROTEIN ADSORPTION

4.1 Introduction

The characterisation of a material plays a crucial role in validating its structure and integrity, and consequently aids in accurately analysing the results of its biological interactions. In this study a-C:H, TiO_2, Ta-C coated flat and nano-patterned substrates were characterised based on their surface chemistry and topography using a combination of x-ray photo electron spectroscopy (XPS), scanning electron microscopy (SEM), focused ion beam (FIB) and atomic force microscopy (AFM). The sample substrates were then subjected to a rigorous sterilisation procedure, prior to being introduced into 12-well TCPS plates for serum protein adsorption. The concentration and conformation of the adsorbed fibrinogen were examined using a combination of ELISA, QCM-D, fluorescence microscopy and AFM.

4.2 Material characterisation

4.2.1 XPS

XPS was used to characterise the surface chemistry of the thin films. Figure 4.1 (a) and (b) shows a high resolution image of the valence band XPS signals on TiO_2 coatings. XPS analysis of the TiO_2 films presented with characteristic, dominating peaks at 458eV and 463.9eV corresponding to the presence of Ti2p (titanium), with no evidence of contamination from the coating process. Trace amounts of carbon (C1) and oxygen (O1) were also recorded at 285eV and 530eV respectively, primarily due to the spontaneous oxide layer formation and the surface adsorption of organic (carbon based) molecules from exposure of the oxide layer to the atmospheric air.

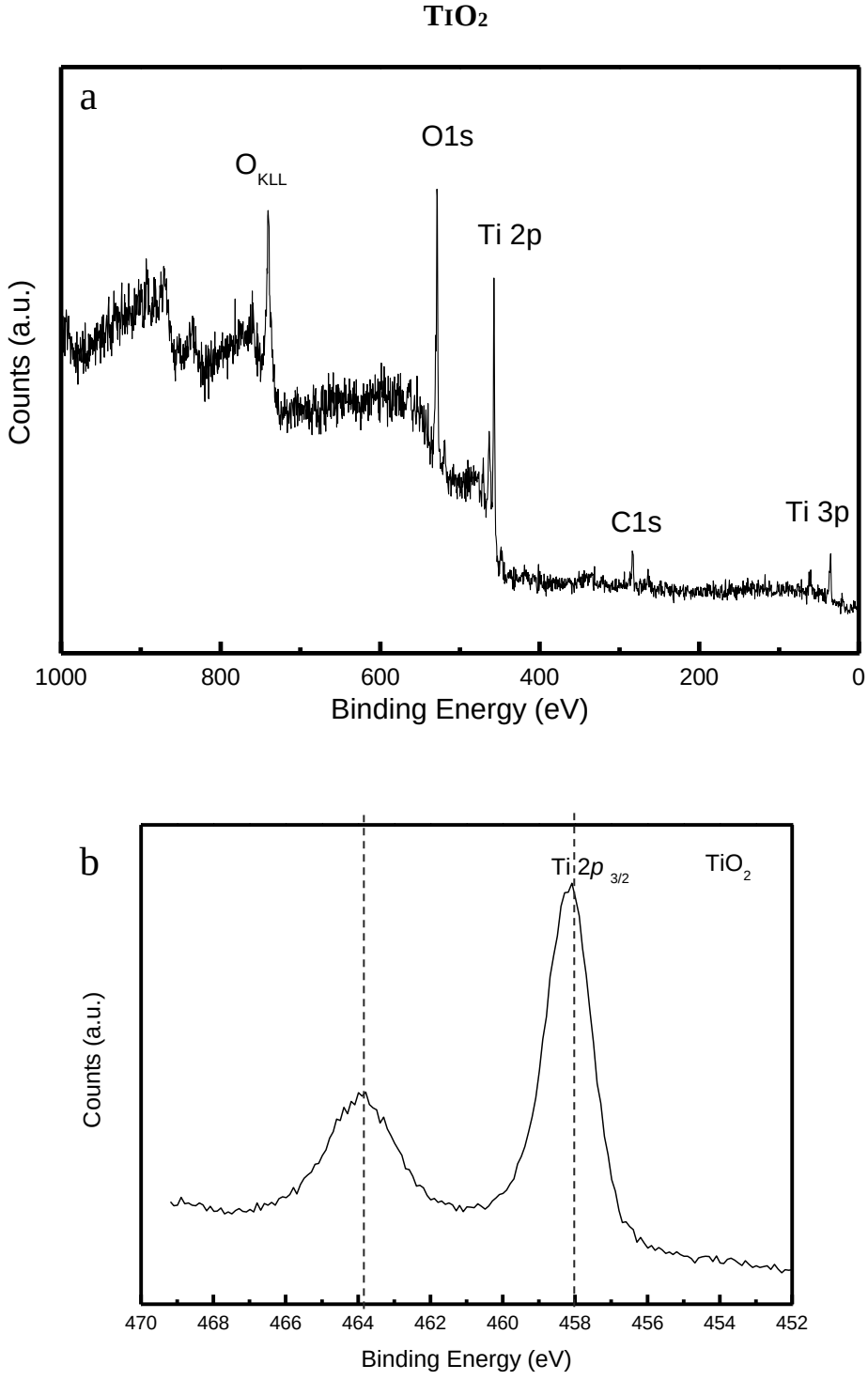

Figure 4.1 X-ray photoelectron spectroscopy graph showing a) full spectrum scan and, b) magnified view of Ti2p peaks on TiO_2 surface.

Figure 4.2 (a) and (b) shows the C1 core level XPS spectra of a-C:H films. The dominating C1 (carbon) peaks were noted at 284.6eV. Although XPS does not take

into consideration the concentration of hydrogen atoms or the presence of C-H bonds, trace amounts of oxygen atoms (O1 peaks) were noted at 532eV. Again, no other contaminants were evident from the coating process.

To identify the state of the carbon, the C1 spectrum of the adlayer was compared against that of graphite (C with sp^2 hybridisation, as indicated by the red curve) and microcrystalline diamond particles (C with sp^3 hybridisation, as indicated by the green curve) with main peaks at 284.4eV and 287.8eV, respectively. Characteristic of a-C:H coatings, the C1s value on the thin film is slightly higher than that of graphite and significantly lower than that measured for diamond, indicating the film contains a mixture of sp^2 (graphite-like) and sp^3 (diamond-like) bonded matrix. This could possibly be due to the electron system of the underlying silicon substrate and the coating parameters.

A shallow slope at the high binding energy side (between 285eV and 288eV) of the C1 curve is primarily due to the superimposition of the C-O bonds and sp3 bonds illustrating the presence of oxygen bound carbon atoms (C-O bonds, as indicated by the blue curve) in combination with sp^3 fractions. The C-O bonds demonstrate the spontaneously absorbed oxide film on the carbon adlayer under atmospheric conditions.

Similarly, the C1 peak on Ta-C films, as shown in Figure 4.3 (a) and (b) was again indicative of the saturated carbon adlayer on the silicon substrate. Trace oxygen levels are attributed to oxide layer formation on the film surface. Furthermore, the state of the carbon atoms is akin to that of sp^2 clusters, however this could possibly be due to a structurally different sp^2 overlayer formed during a high voltage bias [454].

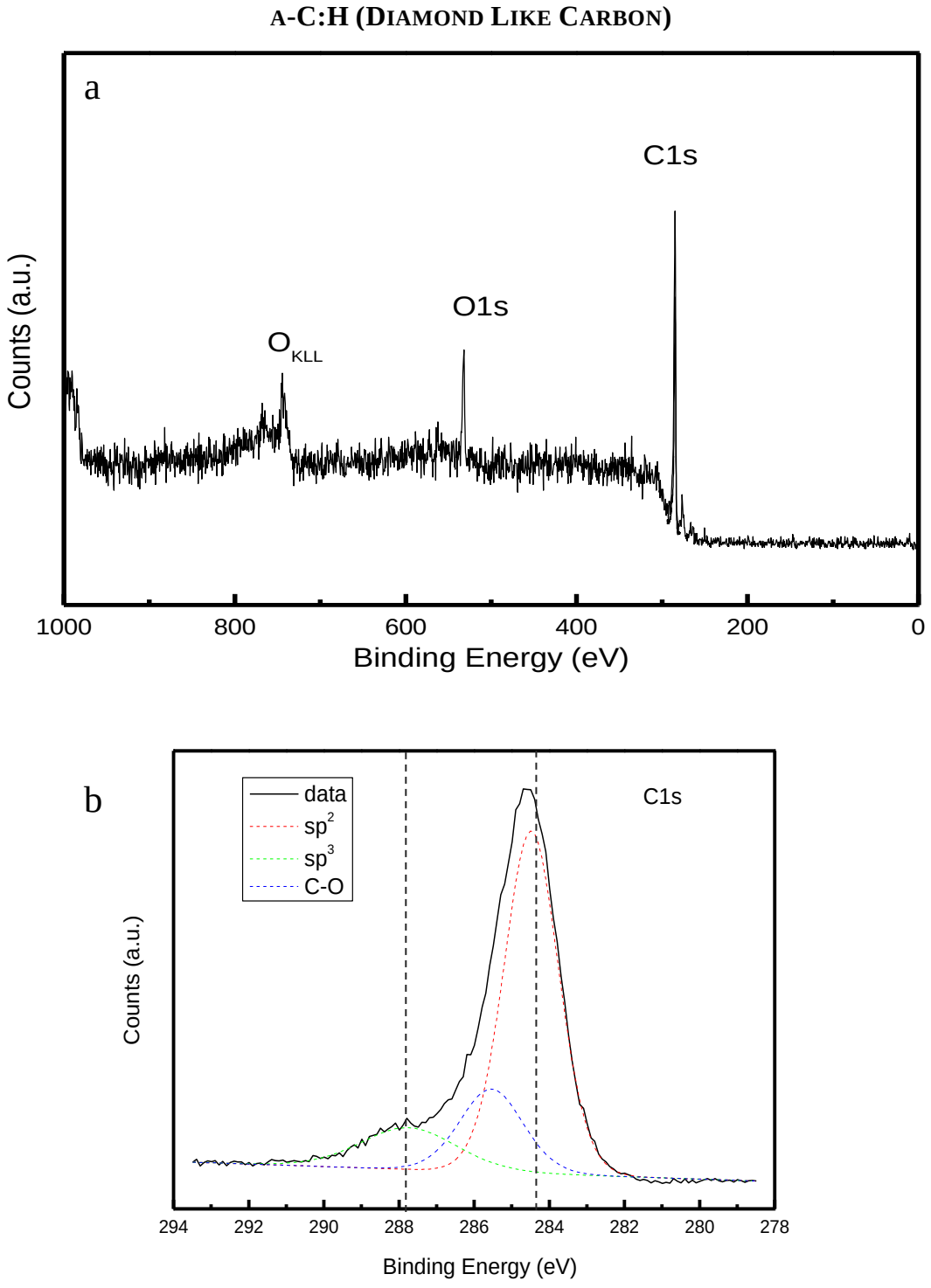

Figure 4.2 XPS graph displaying a) full spectrum scan and, b) magnified view of C1 peak on amorphous, hydrogenated diamond like carbon (a-C:H) films.

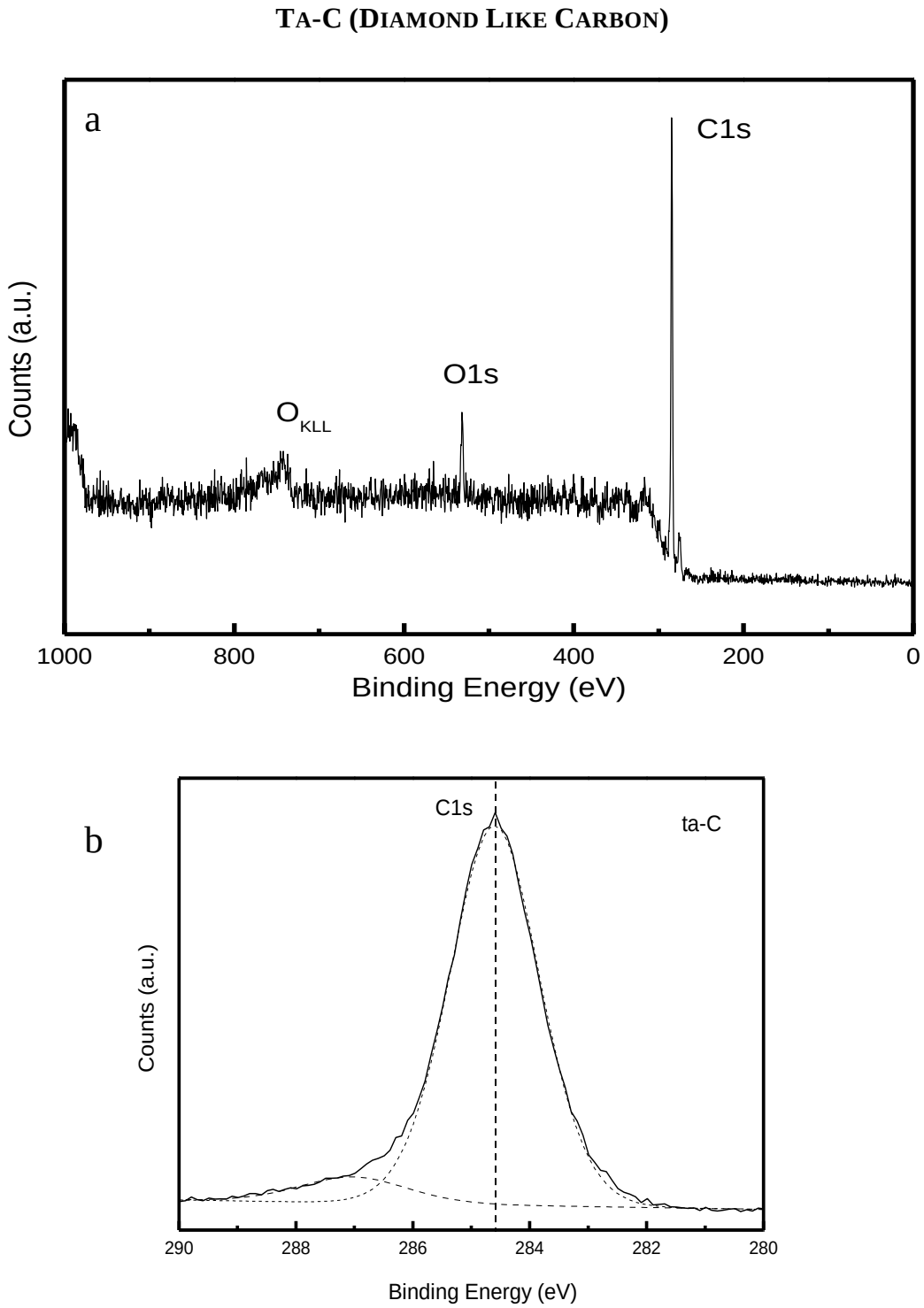

Figure 4.3 XPS image showing a) full spectrum scan and, b) magnified view of C1s spectra on Ta-C films.

4.2.2 SEM and FIB

SEM and FIB were used to determine the uniformity and the degree of penetration of the deposited layer. A thin layer of a-C:H, ta-C and TiO_2 film was deposited on ultra flat silicon substrates and silica QCM sensors; as such, it was necessary to determine the homogeneity, thickness of the coated layer and any morphological features, if present. Furthermore, silicon, TiO_2, a-C:H and ta-C nano-patterned silicon wafers, using gold nano-particles, were also characterised before being analysed for their ability to influence protein and platelet interactions.

The morphology of the silicon surfaces, before and after thin film coating, were analysed via SEM in Figure 4.4. The images show a 10 µm x 10 µm scan of topography on each surface, where SEM confirmed the smooth appearance of the four flat surfaces with no distinctive or characteristic features in the micron scale. Some pitting due to delamination was evident on the Ta-C surfaces at higher magnification (data not shown).

Figure 4.5 shows 10 µm x 10 µm SEM scans of TiO_2, a-C:H and Ta-C coated flat silica quart crystal microbalance sensors and bare silica QCM sensors. Coated QCM sensors also displayed flat and featureless, smooth topography with surface morphology influenced by the underlying control test substrate. These images also show a complete coverage by the deposited layer with no erroneous regions without coating.

The nano-patterned TiO_2, a-C:H and ta-C surfaces was also analysed by SEM, as shown in Figure 4.6. Their topographies on 10 µm x 10 µm SEM scans were compared against their respective control flat surfaces to establish if the level of surface roughness was altered through the coating process.

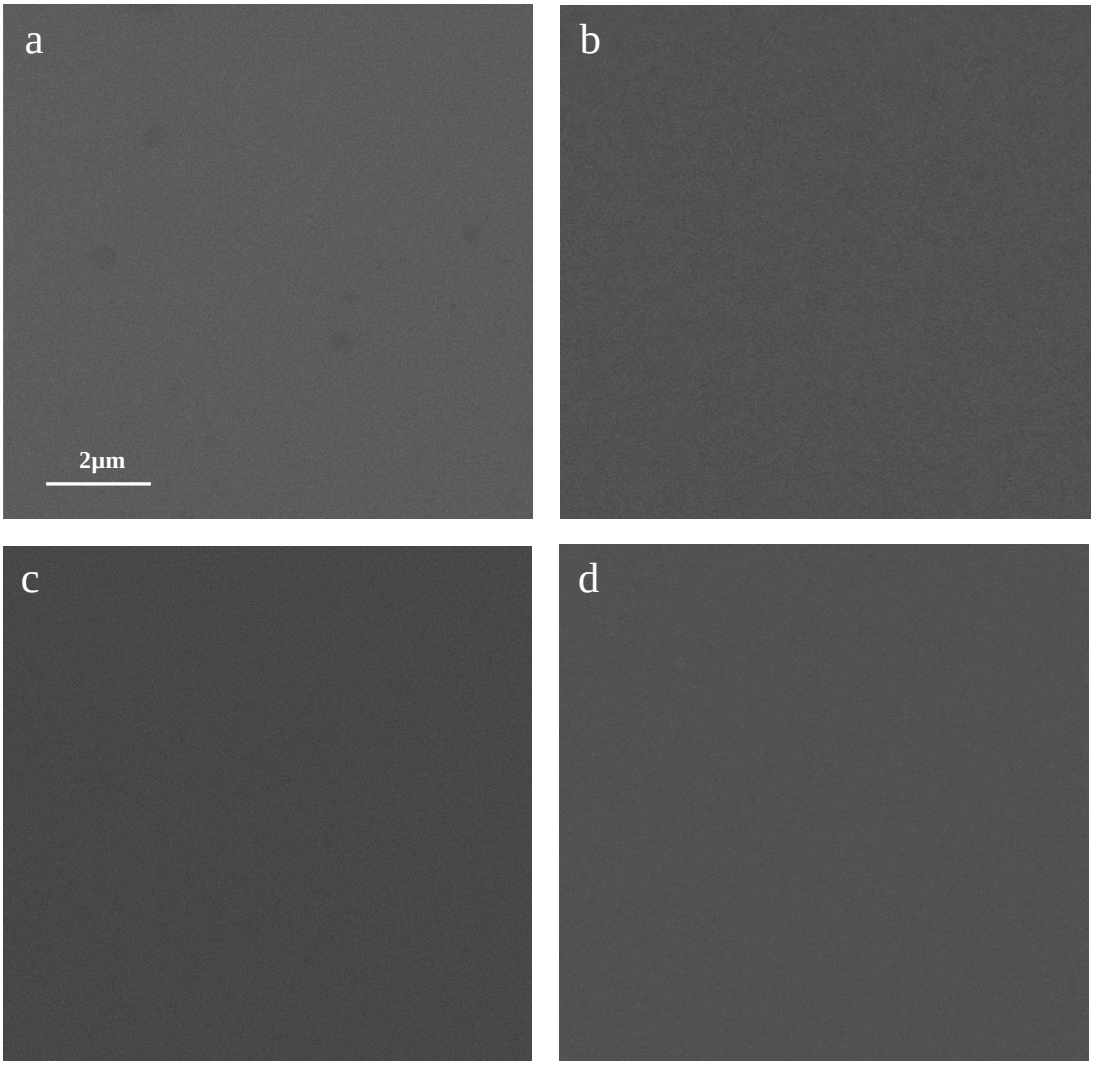

Figure 4.4 Surface topography of a. smooth silicon wafer test substrates and silicon discs coated with b. TiO_2, c. a-C:H and d. Ta-C, as visualised using SEM. Scan size of 10µm x 10µm^2 was imaged using an InLens detector (10kV).

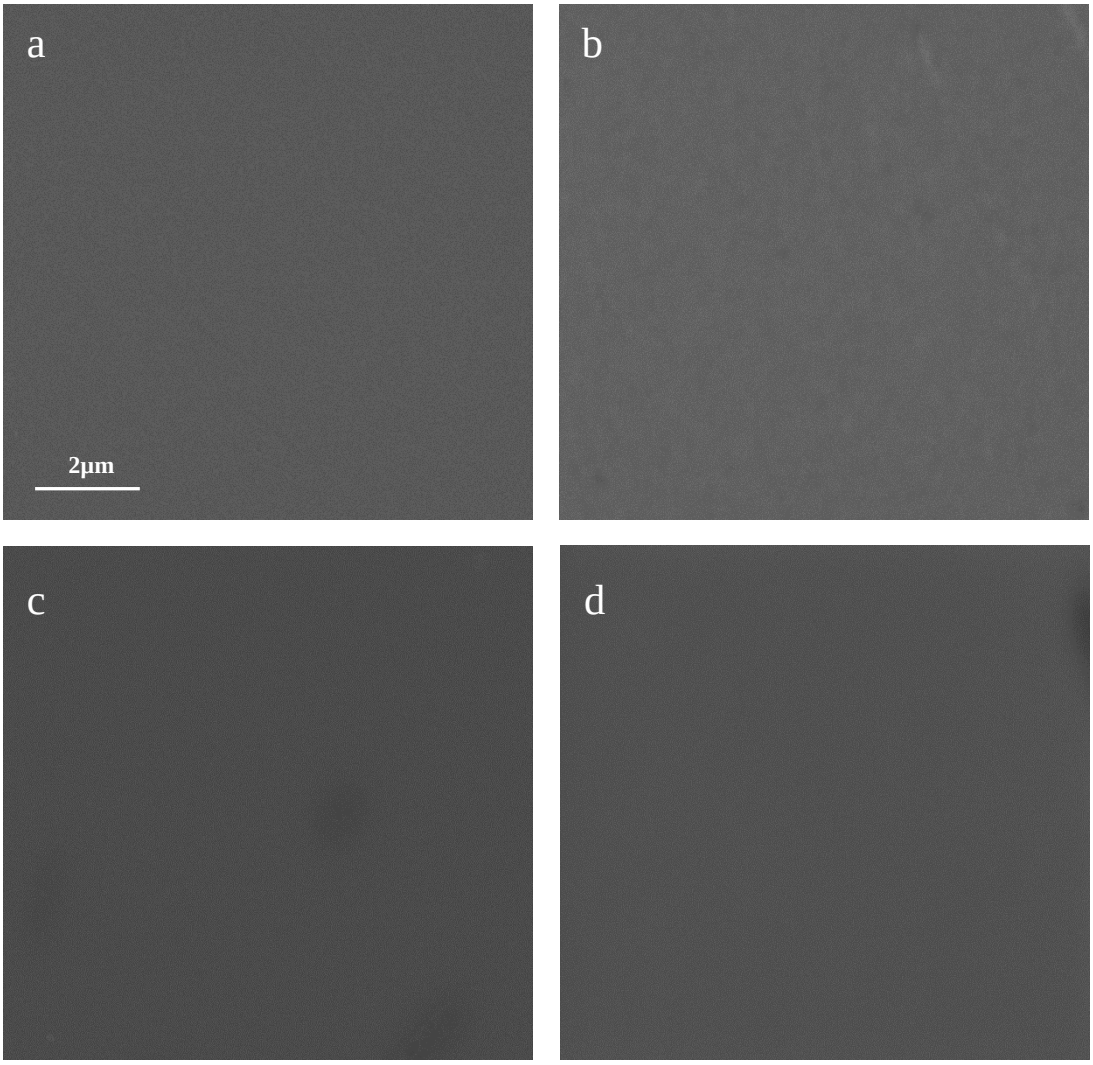

Figure 4.5 Surface topography of a. silica QCM crystal, b. TiO_2, c. a-C:H and d. Ta-C coated sensors, as visualised using SEM. Scan size of 10µm x 10µm^2 were imaged using an InLens detector (10kV).

Block co-polymer technology, using polystyrene (PS) and polyvinylpyridine (PVP) polymers, was employed to carefully create nano-patterns from gold particles on the ultra-flat silicon wafers. Figure 4.6(a) and (b) shows the flat surface and its morphology before and after nano-patterning. The particles appear as pseudo-regular islands with a pseudo-regular pitch. The TiO_2, a-C:H and ta-C coated patterned silicon wafers present similar morphological features to the patterned silicon substrate, as shown in Figure 4.6(d), 4.6(f), 4.6(h) respectively. The nano-patterns appear to vary in their dimension, although less than 100nm in diameter each and the coated films follow the morphology of the underlying patterned substrates.

Furthermore, individual nano-islands appear to vary in their dimension, although keeping within the 40nm diameter threshold.

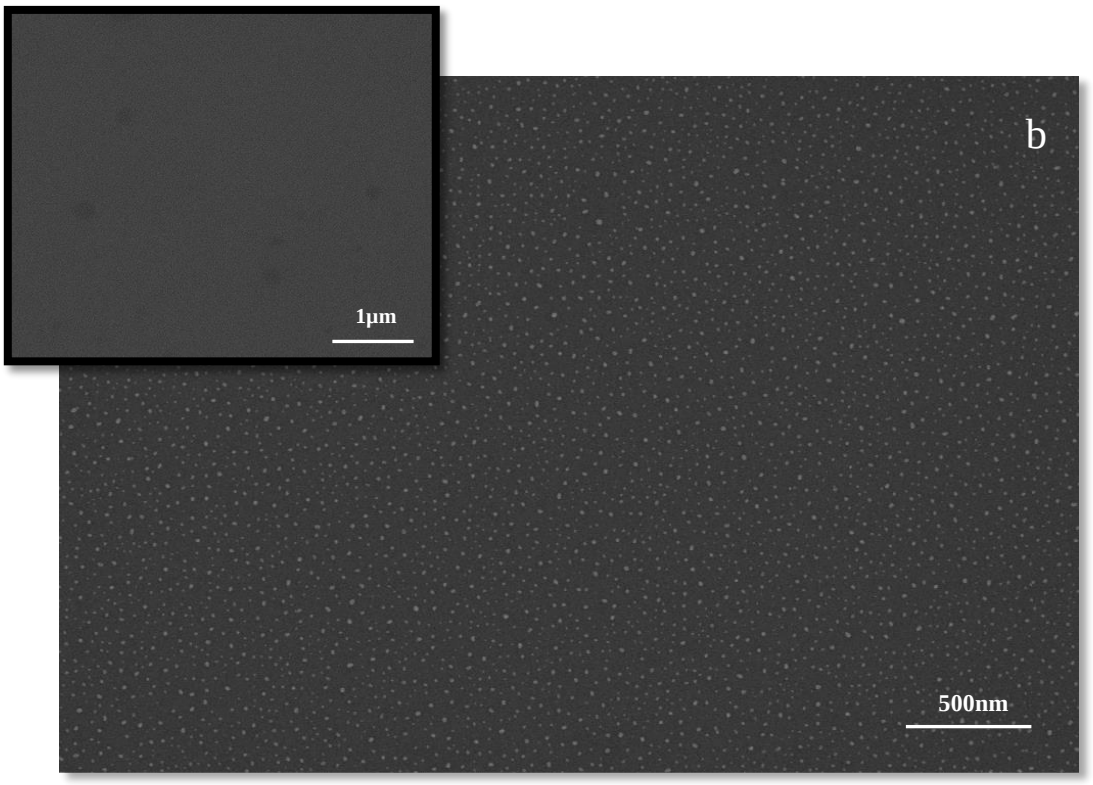

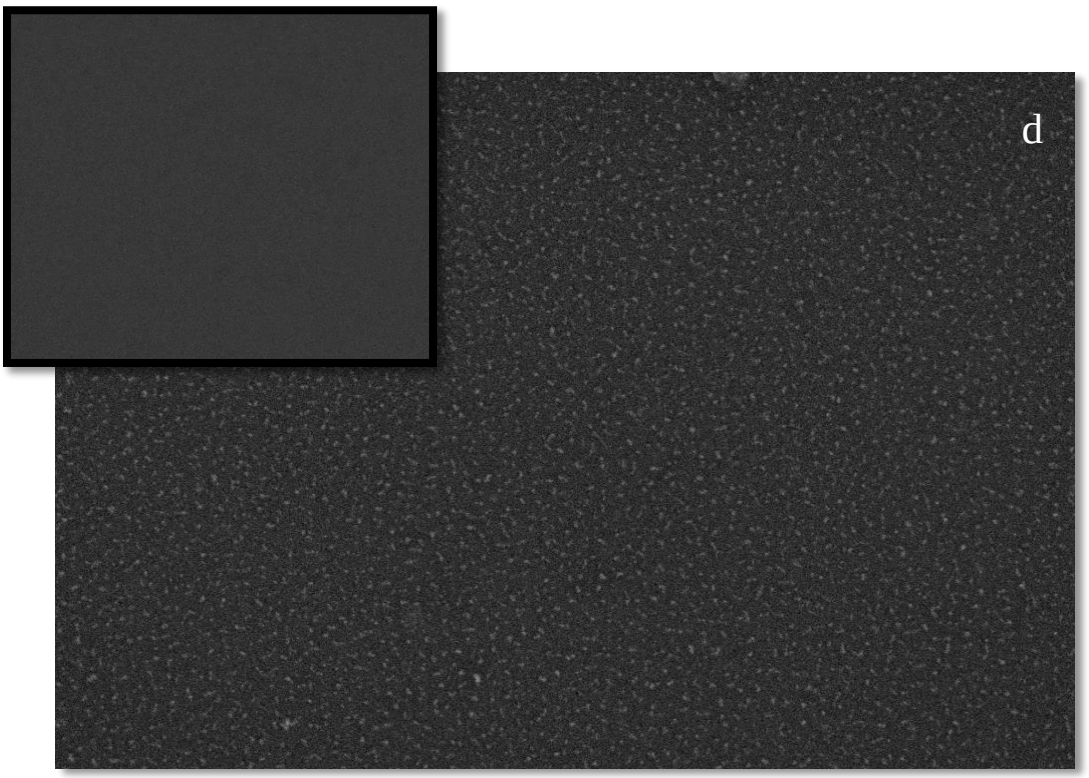

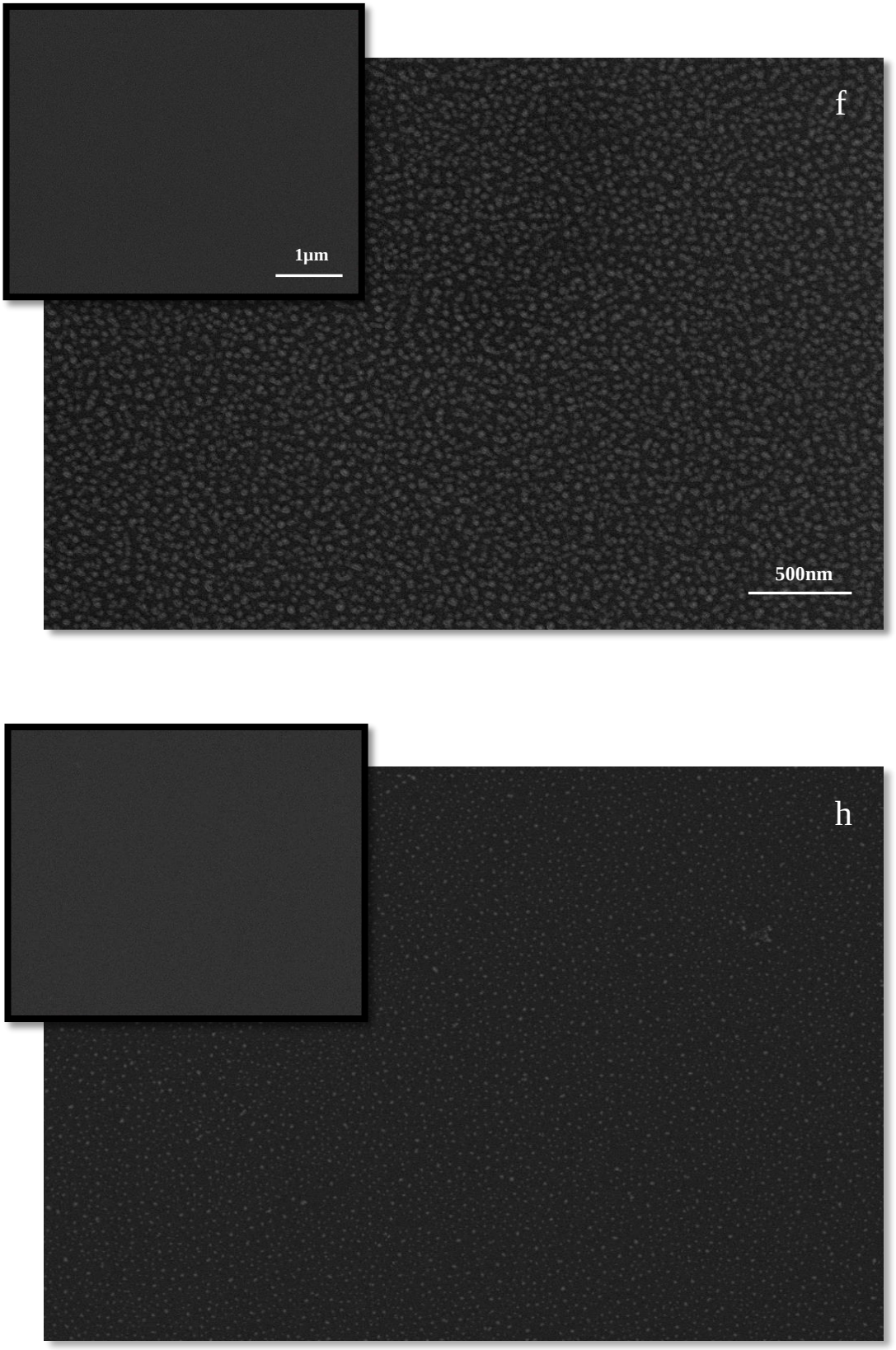

Figure 4.6 Surface topography of nano-patterned silicon substrates b. without any coating and that coated with d. TiO_2, f. a-C:H and h. Ta-C, as visualised using SEM. Topography was created by gold particle arrays in a pseudo-regular fashion using the block co-polymer method. Corresponding images of non-patterned test substrates

are given in a, c, e, and g, respectively. Scan size of 5µm x 5µm^2 were imaged using an InLens detector (10kV).

A higher magnification of the deposited a-C:H film by SEM on the nano-patterned surface is shown in Figure 4.7. It appears that the coated film envelopes the gold nano-particles, encapsulating it to form dome-like coverage. Furthermore, the islands tend to coalesce to form small clusters of two or three nano-domes thus increasing its overall geometry and decreasing the pitch between adjacent islands. Due to cluster formation, the globular islands tend to form irregular shapes, some mimicking the general cylindrical conformation of proteins. Such morphological patterns were also noted on ta-C and TiO_2 surfaces, characteristic of their respective thin film-coating process.

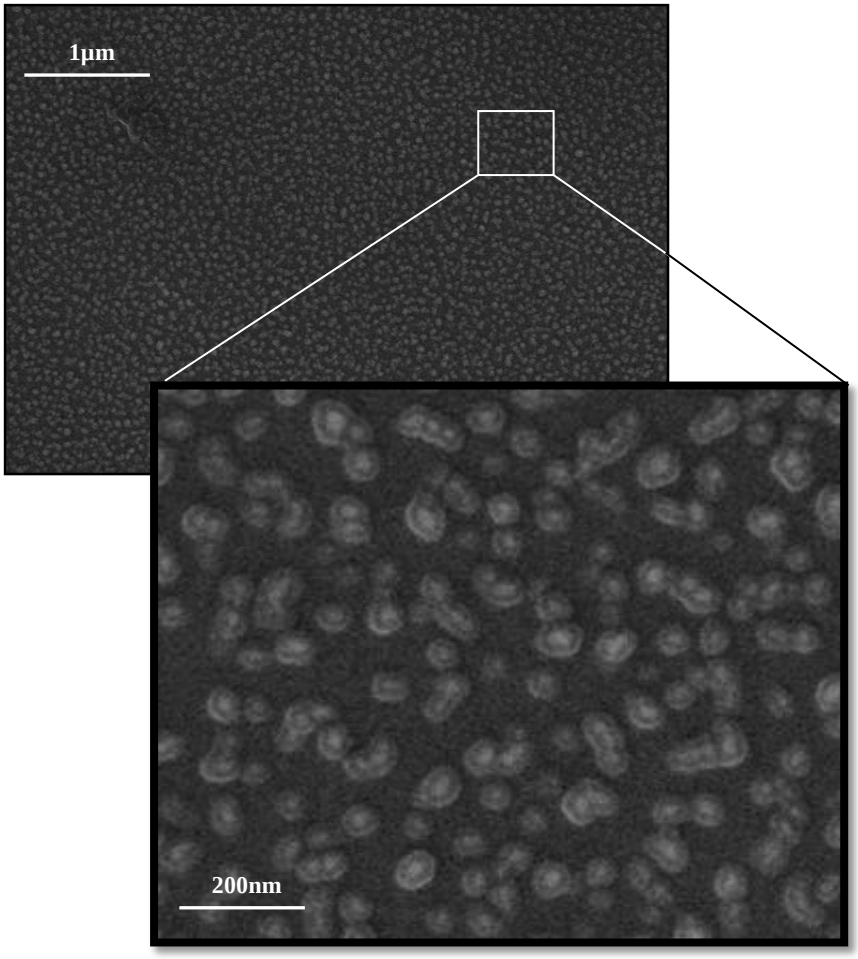

Figure 4.7 A magnified view of nano-patterned a-C:H surface from SEM. Samples were imaged using an InLens detector (10kV) at 30K X magnification (above) and 150K X magnification (below).

The thickness of the deposited film on silicon wafer was determined using FIB. High density positively charged gallium ions were bombarded onto the substrate etching away to form a cross section of the surface. The etching rate and current were chosen to minimise re-deposition of ions. Transmission signals in the form of reflected secondary ions from each point were collated to generate the images in Figure 4.8 and Figure 4.9.

The depth of deposited a-C:H, as measured by FIB, is shown in Figure 4.8. The thickness of the coated layer is indicated between the red arrows. The thick base layer below the arrows is primarily silicon with a thin native oxide layer. The thin, bright adlayer above silicon is an intermediate layer of silicon and carbon (SiC) formed rapidly during the coating process when carbon atoms were bombarded onto the silicon surface. The slightly thicker layer above SiC is the deposited a-C:H followed by a superficial layer of organic compounds adsorbed on the a-C:H surface from interacting with the atmosphere.

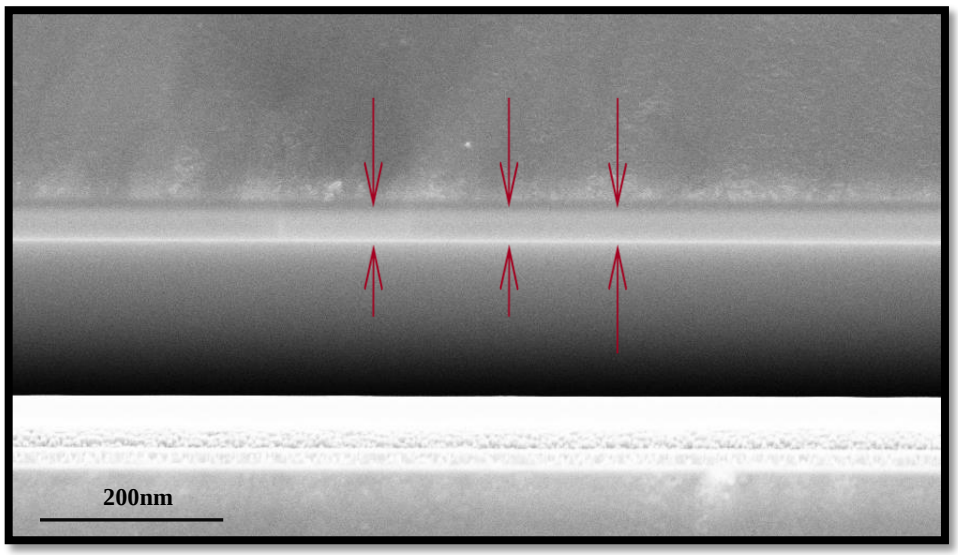

Figure 4.8 Cross-sectional view of a-C:H coated flat silicon substrate, as determined by SEM-FIB. Sample was milled using FIB image probe (30KV, 5pA) and scanned using InLens detector (10kV) at 53.8º stage tilt. Depth of the deposited layer is indicated between the red arrows. Layers between the arrows bottom to top include; native oxide on the silicon surface, a-C:H coating and organic layer formed from atmospheric conditions, respectively.

Since the samples were imaged at 53.8 degrees the images were corrected for the tilt before calibrating for thickness. The deposited a-C:H film formed a uniform deposition layer and its depth was homogenous throughout the sample. TiO_2 and ta-C films were also cross sectioned to show that TiO_2 formed the thickest layer followed by Ta-C and a-C:H. Table 4.1 summarises the thickness values of the thin films on the flat and patterned surfaces.

Table 4.1 Thickness of the thin film coating was calibrated using ImageJ from FIB measurements (1.44p, NIH).

	THICKNESS (nm)	
	Flat Surface	**Nano-patterned Surface**
TiO_2	130-140nm	30-35nm
a-C:H	75-85nm	35-40nm
Ta-C	90-100nm	30-35nm

The coating thickness of TiO_2, a-C:H and Ta-C on nano-patterned silicon substrates are shown in Figure 4.9. The gold particles appear embedded deep within the adlayer, adjacent to the silicon base and yet appear more intense than the deposited coating. This is indicative of the intrinsic conductive nature of gold. The marginally conductive deposited film, on the other hand, is marginally conductive and appeared less intense due to its relatively inert properties. Furthermore, it is evident across all three coated films that the deposited layer had formed a blanket, completely encapsulating the gold particles. It can be inferred that the film penetrated between the grooves created between the particles and the surface thus reduced the likelihood of sharp edges, and the relative roughness profile created by the gold particles.

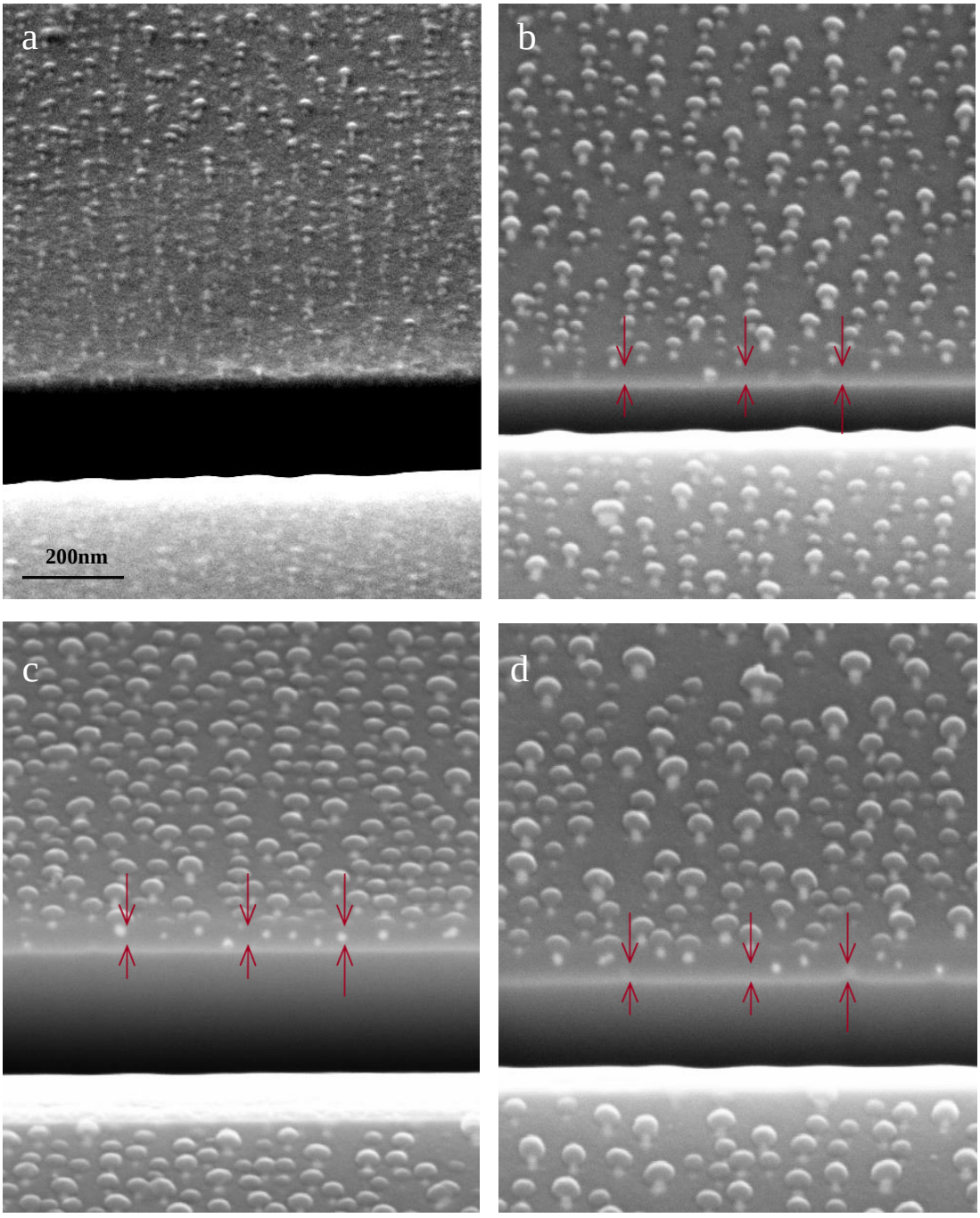

Figure 4.9 Cross-sectional view of nano-patterned si wafer substrates (a) non-coated and coated with (b) TiO_2, (c) a-C:H and (d) Ta-C, as determined by SEM-FIB. Topography was created by gold particle arrays in a pseudo-regular fashion using block co-polymer method. Samples were milled using FIB image probe (30KV, 5pA). Images were scanned InLens detector (10kV) at 53.8º stage tilt. Depth of the deposited layer, indicated between the red arrows.

4.2.3 AFM

Differences in surface nano-topography between the flat, QCM crystals and nano-patterned substrates were further analysed in air by AFM, in low voltage tapping mode. Scan rate of 1Hz and scan area of 0.5µm x 0.5µm or 1µm x 1µm were used. Surface nano-topography as well as their respective roughness scale were established using AFM. Results are shown in Figure 4.10 to 4.12 for flat, QCM sensors and nano-patterned substrates, respectively.

Ultra flat silicon wafers exhibited a stochastic roughness of 0.20nm with a maximum z-range of 2.57nm. Ta-c and a-C:H films followed this profile with RMS values of 0.36nm and 0.20nm respectively, as shown in Figure 4.10. These values were similar to that of the ultra-flat silicon wafer substrate. Furthermore, comparing the three surfaces, it is evident that both; a-C:H and ta-C films exhibit morphological features influenced by the silicon substrate indicating a uniform deposition of the thin film. TiO_2, however, presented a much higher roughness of 1.55nm. TiO_2 substrates displayed some peaks (convex summits), distributed randomly with irregular pitch. The dome like peaks range between 40-100 nm in diameter with an average height of 10.45nm, as deduced from the roughness profile on the right.

Silica QCM crystals displayed a roughness of 1.09nm and like the si-wafers, the a-C:H coatings on QCM crystals appeared homogenous with morphological features similar to the substrate. Ta-C however displayed several regions of sharp peaks increasing the overall the RMS value. This may partially be due to some level of delamination caused by the weak bonds between the silica and the carbon adlayer. TiO_2 films presented several peaks localised throughout the surface defined with a rounded geometry.

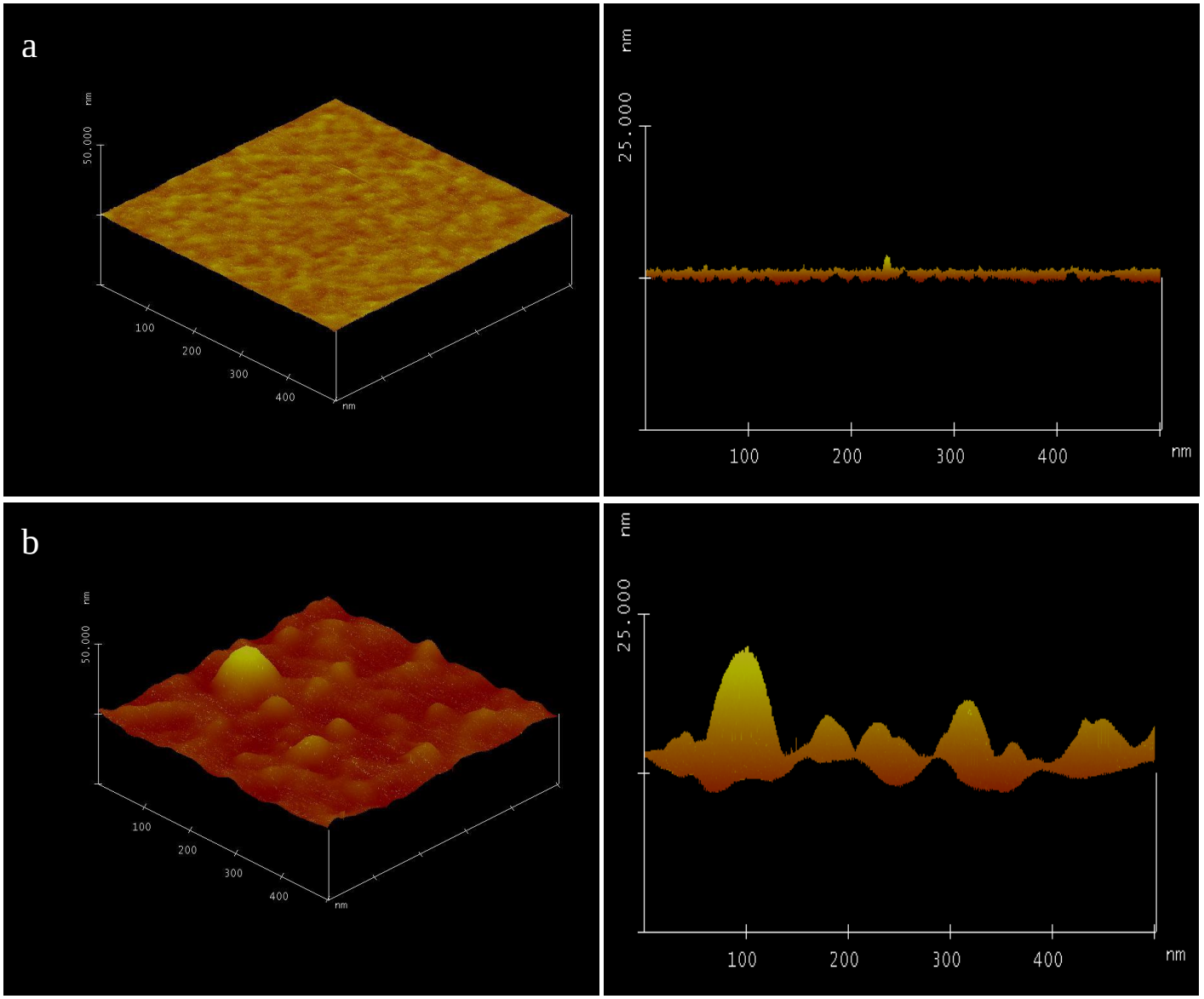
a
50.000
nm
100
200
300
400
nm
nm
25.000
100
200
300
400
nm
b
50.000
nm
100
200
300
400
nm
nm
25.000
100
200
300
400
nm

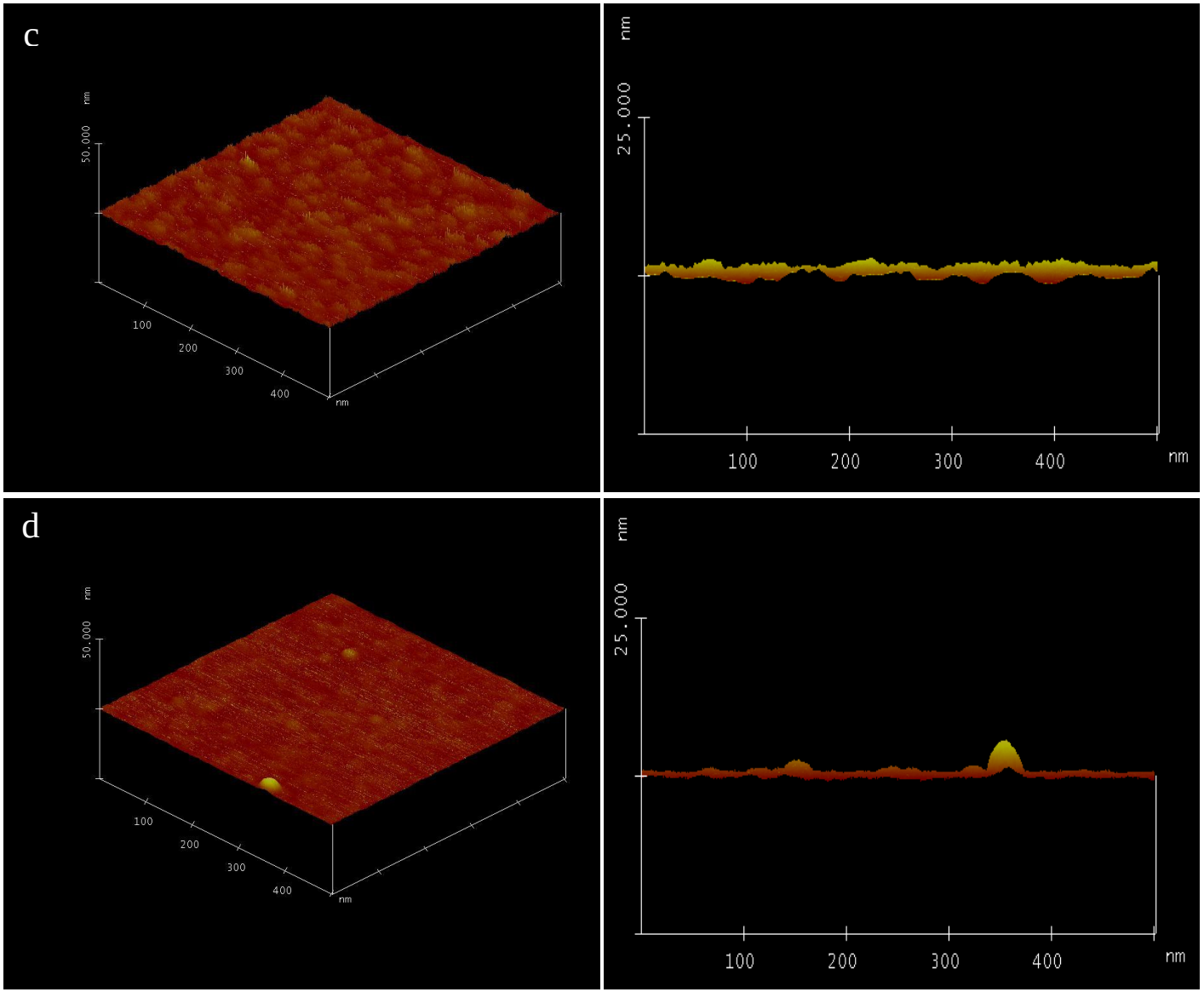
c
50.000
nm
100
200
300
400
nm
25.000
nm
100
200
300
400
nm
d
50.000
nm
100
200
300
400
nm
25.000
nm
100
200
300
400
nm

Figure 4.10 AFM topographical image (left; scan size 500 x 500nm^2) and line scans (right) of a. silicon, and, b. TiO_2, c. a-C:H and d. ta-C deposited on ultra flat silicon wafers. The lighter regions are height variations observed from the coating procedure. The vertical scale range is 50nm.

The islands appear flattened (maximum z-height of 13.7nm), some adjoining with neighbouring domains thereby reducing its overall undulations and causing a roughness value similar to the silica sensor. A comparison of the surface roughness (RMS) is shown in Table 4.2 for flat surfaces and QCM sensors.

Table 4.2 Comparison of root mean square (RMS) roughness value (measured in nm) of both flat substrates and flat QCM crystals.

	Smooth Surface	QCM Sensor
Silicon/Silica	0.203 ± 0.027	1.085 ± 0.14
TiO_2	1.554 ± 0.062	1.514 ± 0.063
a-C:H	0.36 ± 0.031	1.166 ± 0.114
Ta-C	0.204 ± 0.031	2.254 ± 0.545

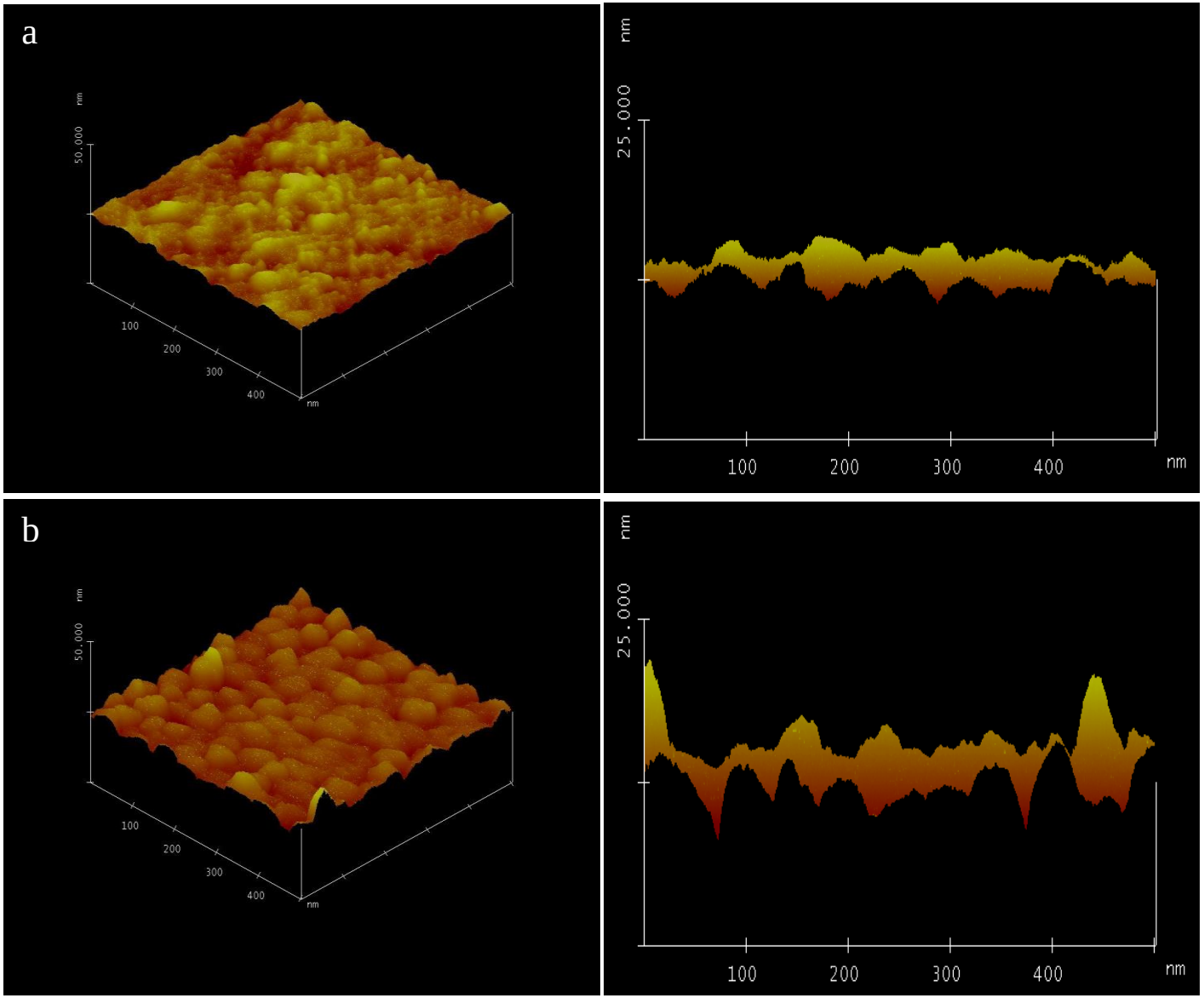
a
50.000
nm
100
200
300
400
nm
25.000
nm
100
200
300
400
nm
b
50.000
nm
100
200
300
400
nm
25.000
nm
100
200
300
400
nm

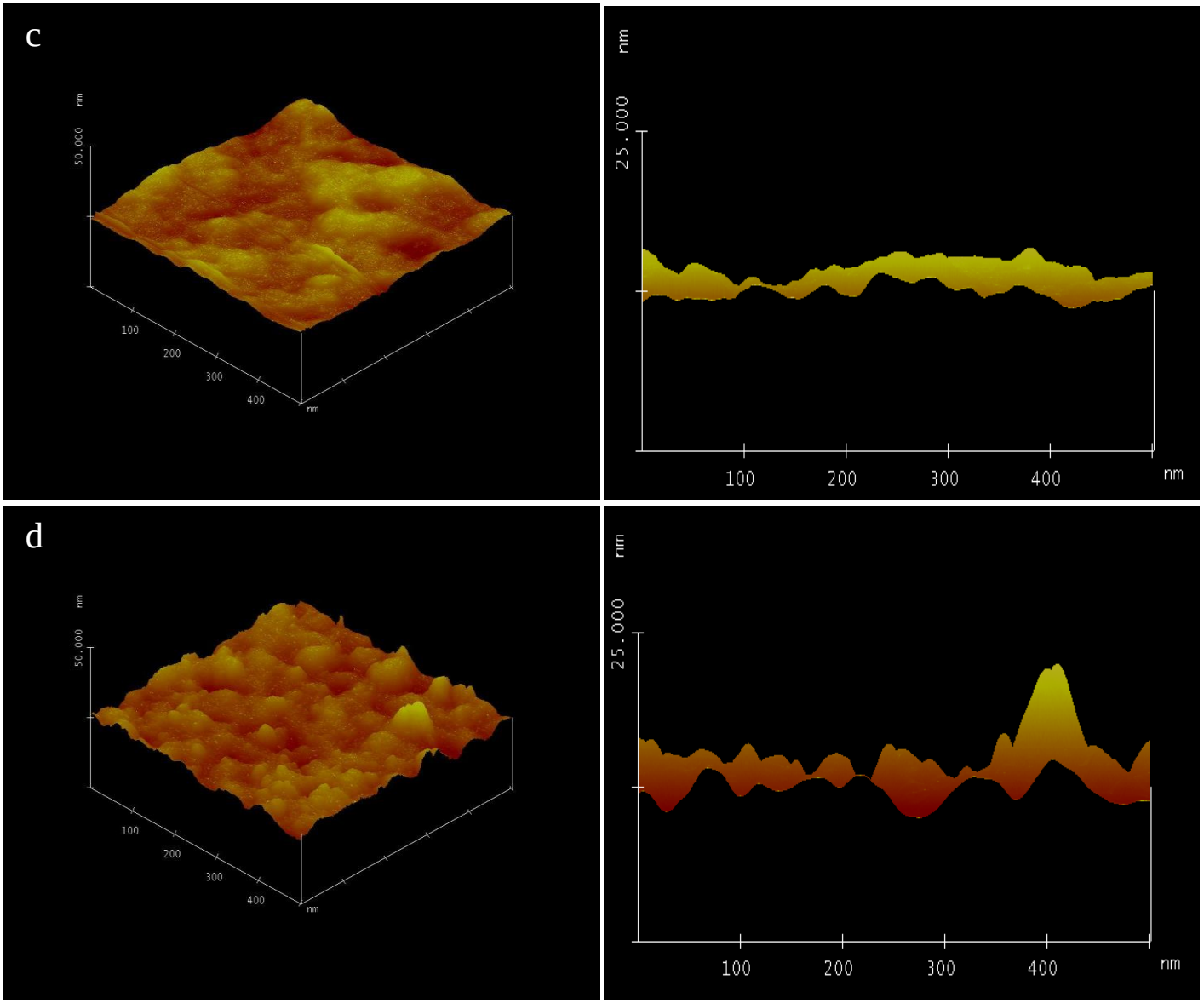
c
50.000
nm
100
200
300
400
nm
25.000
nm
100
200
300
400
nm
d
50.000
nm
100
200
300
400
nm
25.000
nm
100
200
300
400
nm

Figure 4.11 AFM topographical image (scan size 500 x 500nm^2; scale range 50nm) and corresponding line scans of a. silica b. TiO_2, c. a-C:H and d. ta-C deposited on QCM crystals.

A clear difference between the patterned and flat substrates was exhibited when the average nano-roughness was raised from 1nm to 5-10nm range. The nano-patterned surfaces, as shown in Figure 4.12, presented with an increased number of peaks with greater height differences (z-range) thereby increasing the overall RMS value of the silicon wafer to 5.25nm, as shown in Table 4.3. From Figure 4.12, it was evident the z-range between nano-particles varied significantly, with some gold particles aggregating leading to large height differences. For this reason some sporadic peaks that formed because of the fabrication process were disregarded during the roughness calculation.

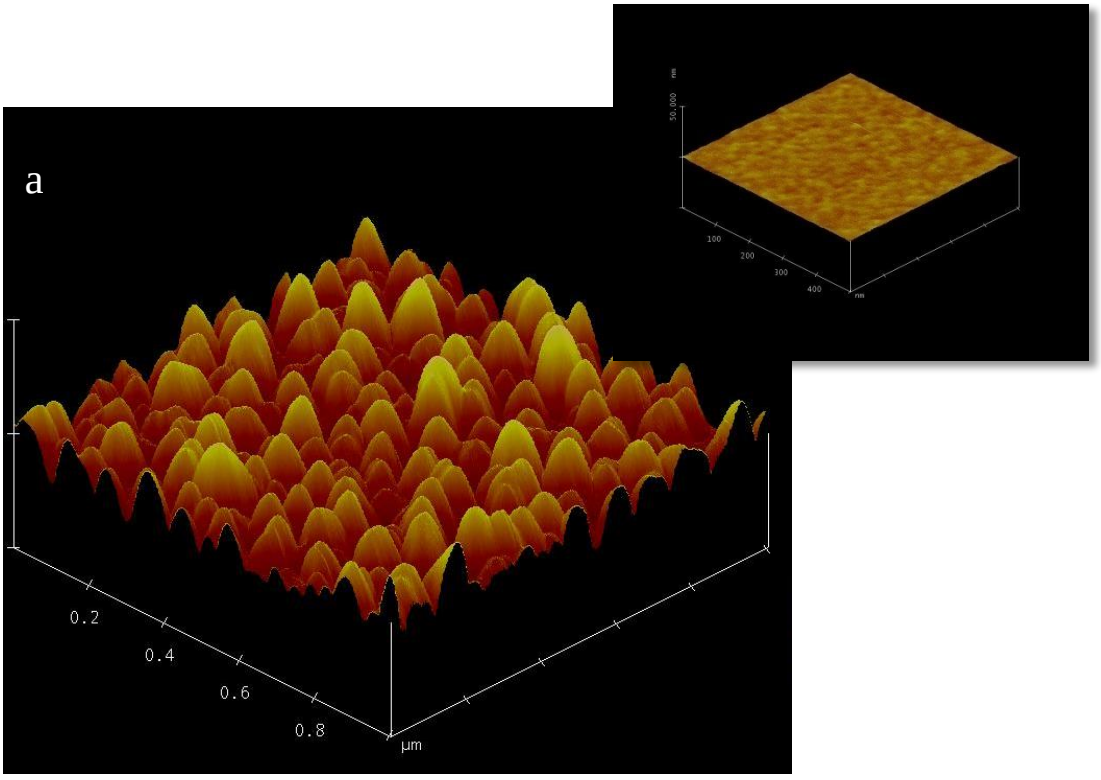

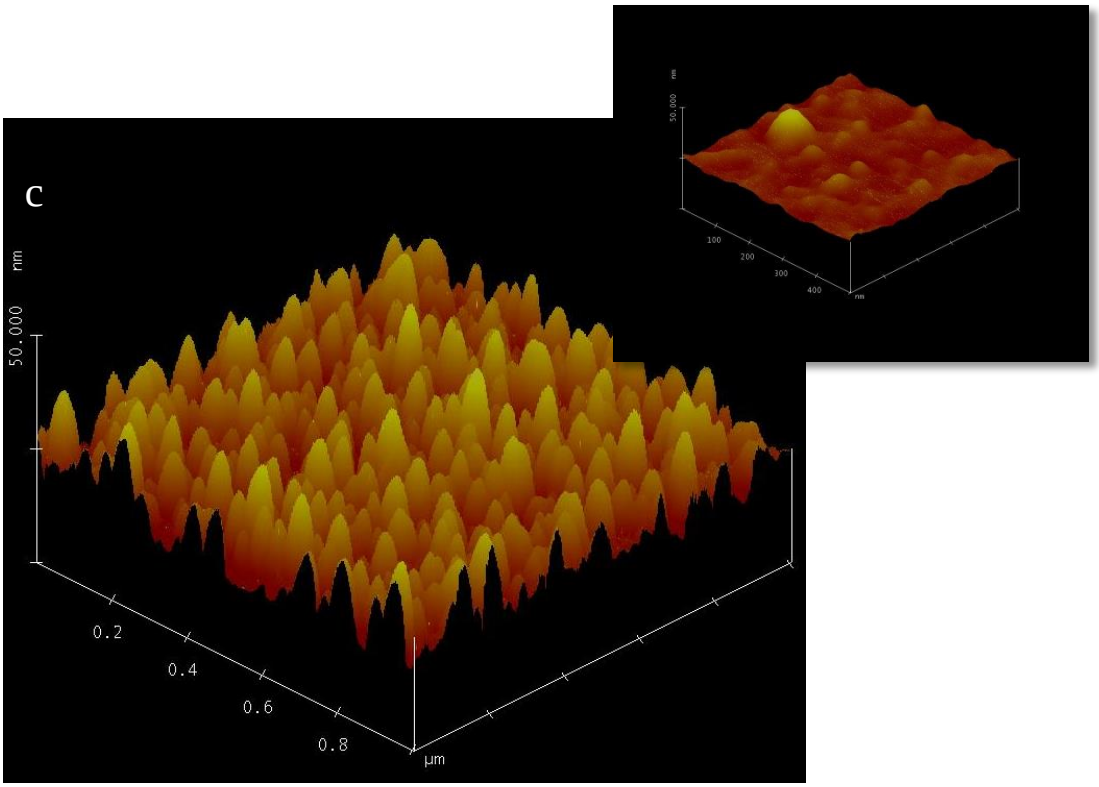
c
nm
50.000
0.2
0.4
0.6
0.8
µm
50.000 nm
100
200
300
400
nm

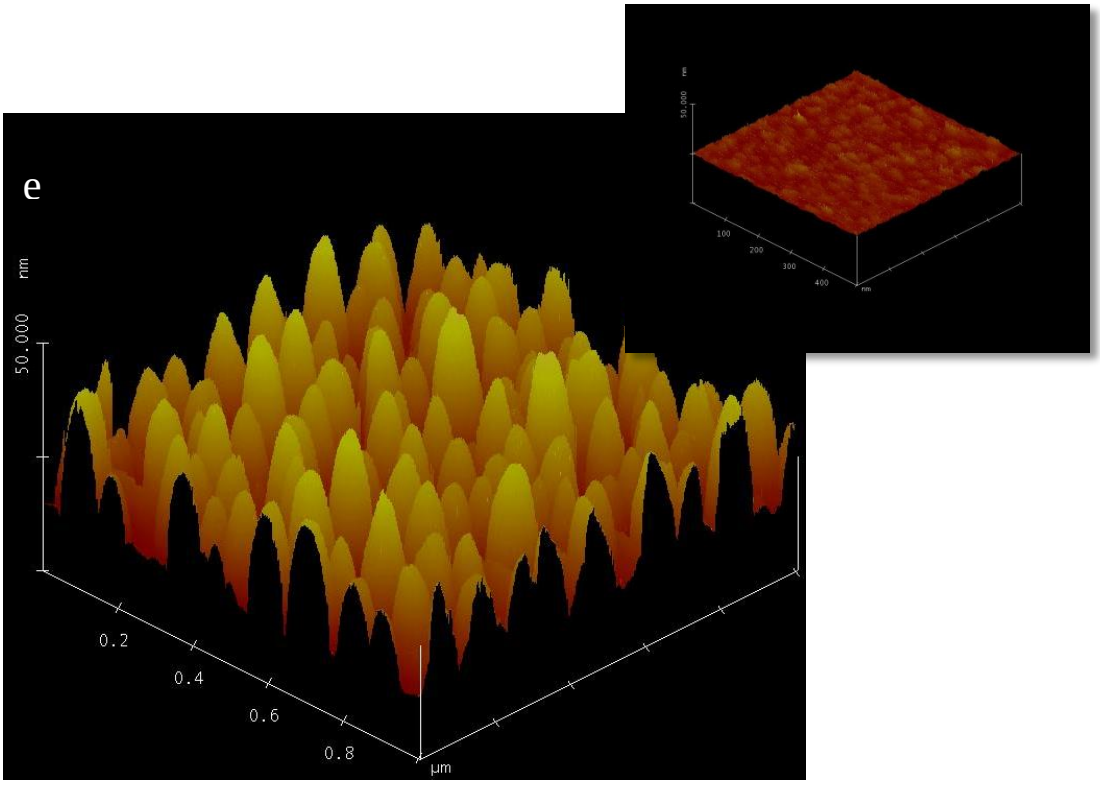
e
nm
50.000
0.2
0.4
0.6
0.8
µm
50.000 nm
100
200
300
400
nm

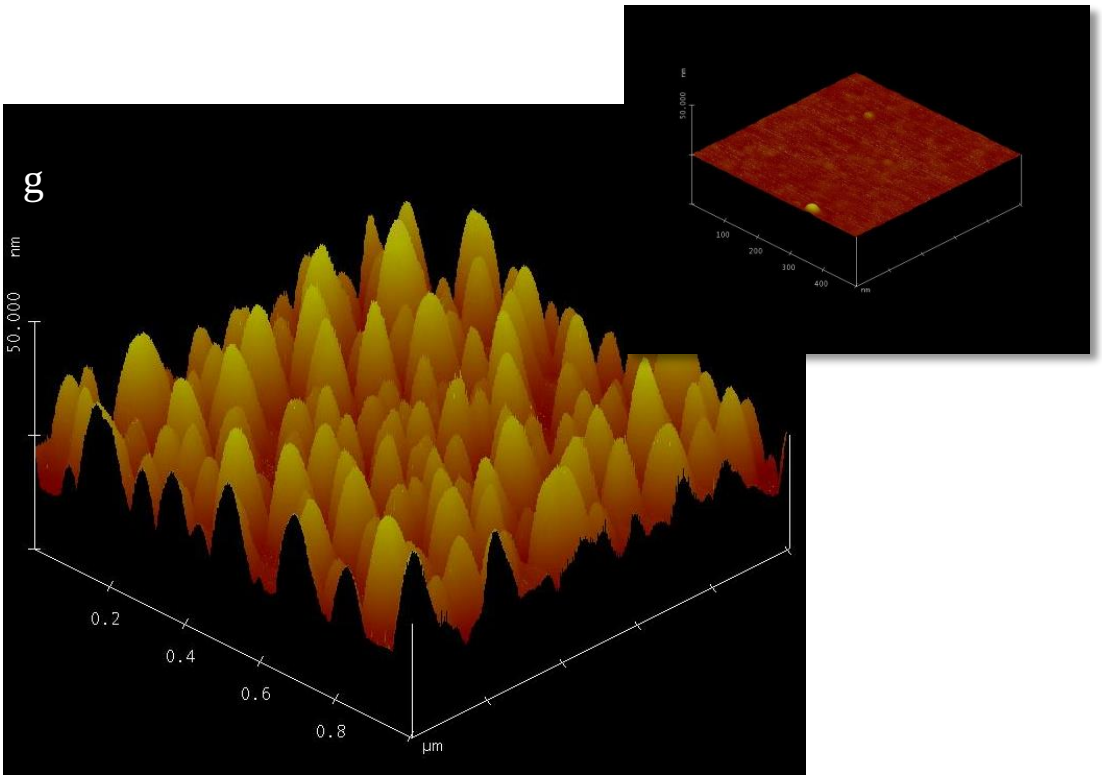

Figure 4.12 AFM topographical image (scan size 1µm x 1µm2) of a. uncoated SiO2, and, c. TiO2, e. a-C:H and g. Ta-C deposited nano-patterned surfaces. Corresponding topographies of their flat surfaces are compared in images b, d, f, and h, respectively. The vertical scale range is 50nm.

A comparison of the four surfaces showed TiO_2 followed a similar morphology to the silicon surface while ta-C and a-C:H displayed a greater roughness value. Ta-C surfaces showed minor levels of delamination creating large height differences between peaks. The average peak depth (z-range) calculated between the silicon, TiO_2, a-C:H and ta-C surfaces were 26, 27.55, 37.90 and 32.02nm, respectively, consequently increasing the overall surface area by 9.43, 10.98, 14.6 and 11.12%, respectively. These results are tabulated in Table 4.3.

Table 4.3 Comparison of root mean square (RMS) roughness value (measured in nm) of nano-patterned surfaces.

Nano-patterned Surfaces	RMS (nm)	Increase in Surface Area (%) (3s.f.)
Si	5.247 ± 0.342	9.43
TiO2	5.458 ± 0.238	10.9
a-C:H	6.943 ± 0.289	14.6
Ta-C	5.031 ± 0.723	11.2

Roughness profile images deduced from the line scans in Figure 4.13 were used to estimate the pitch between neighbouring peaks and the diameter of nano-particles. TiO_2, a-C:H and Ta-C displayed pitch of 50-150, 70-160= and 50-200nm, respectively and diameter between 21-60, 28-55 and 33-60nm, respectively. While TiO_2 surfaces show similar number of peaks as the silicon surface, a-C:H and ta-C films caused aggregation between adjacent gold nano-particles raising the overall island diameter from 25-30nm to significantly higher values. This in combination with the thicker layer of a-C:H formed on the gold particles may explain their elevated roughness values when compared to the nano-patterned control.

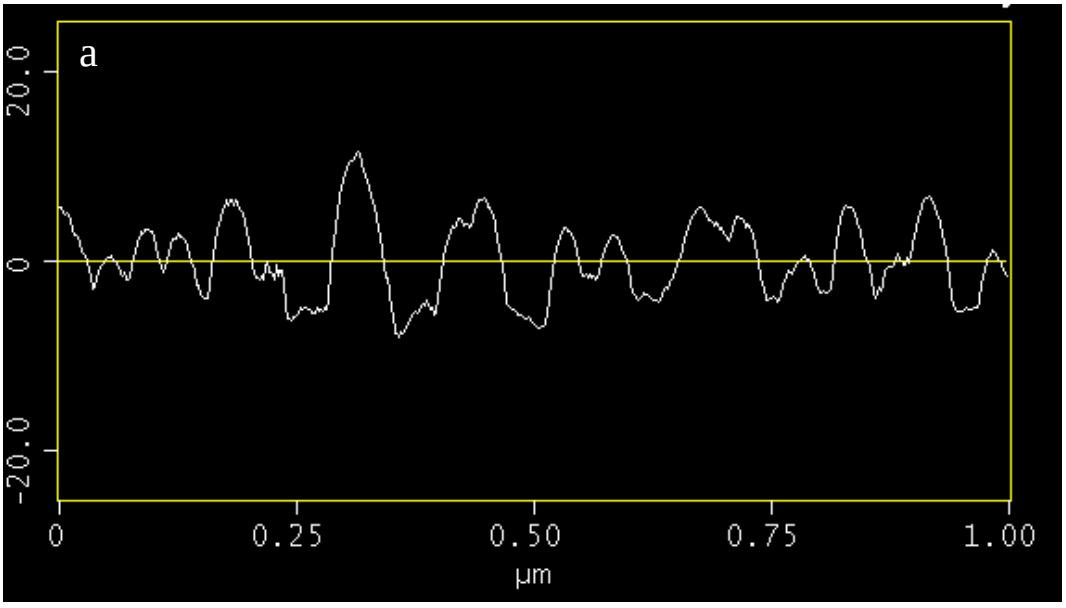

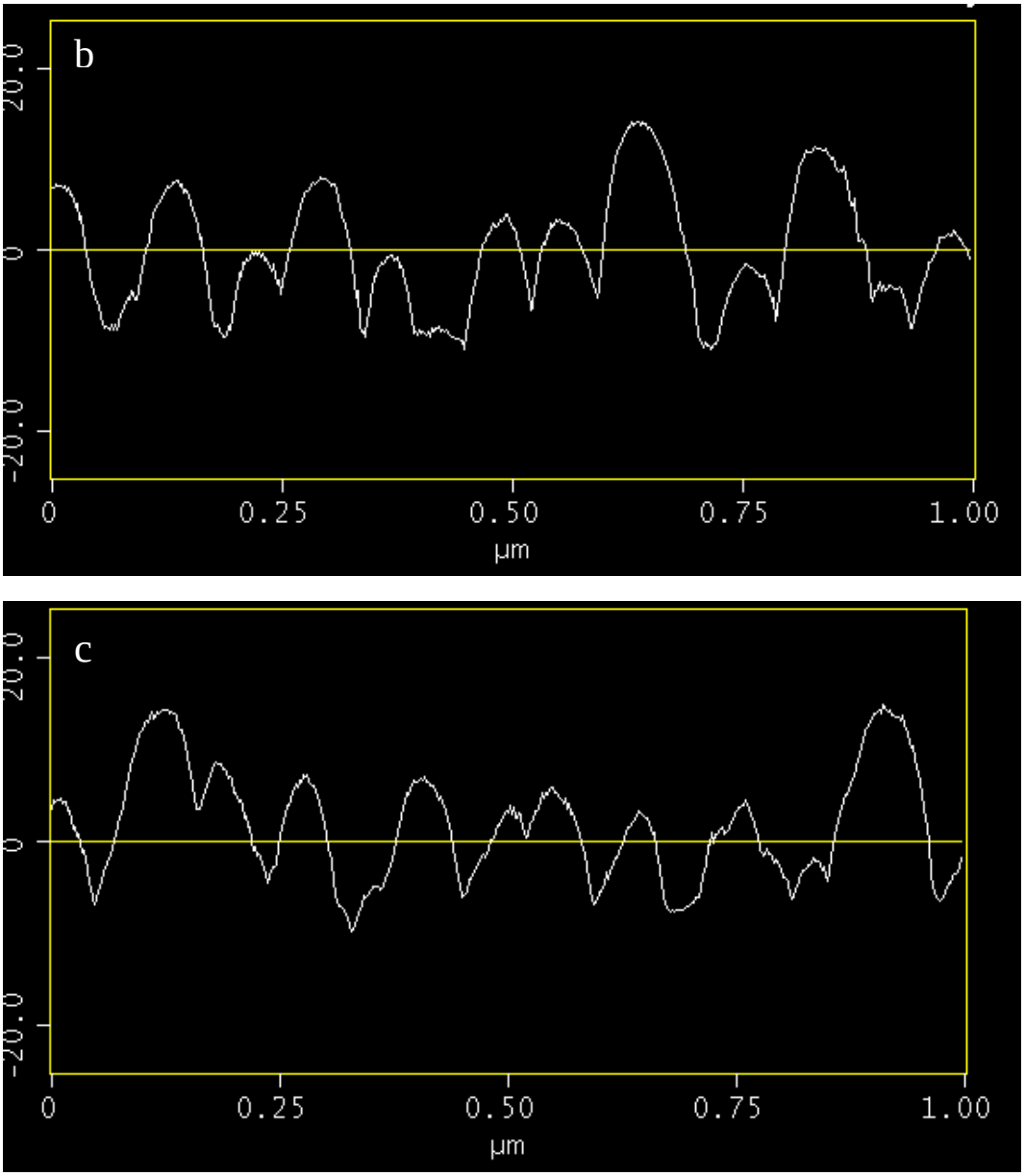

Figure 4.13 Line plot of a. TiO_2, b. a-C:H and c. Ta-C deposited nano-patterned surfaces. The vertical scale range is 50nm.

4.3 Protein adsorption studies on flat surfaces

Most implantable biomaterial surfaces come in contact with blood causing a sequence of interactions initiated by the rapid adsorption of plasma proteins that change in conformation to form a proteinacious adlayer that mediates the adhesion and activation of platelets and the clotting cascade. This may consequently lead to

the formation of blood clots (thrombus). As such, it is important to understand the adsorption of specific proteins, their exact interaction, and the mechanisms of unfolding at the solid-liquid interface. Fibrinogen, due to its abundance in blood plasma and its major role in platelet attachment, was chosen as the serum protein. Furthermore, the effect of nano-features on fibrinogen attachment was analysed.

In this study, flat surfaces, examined in section 4.1, were investigated using a combination of ELISA, AFM in liquid mode, fluorescence microscopy and QCM-D measurements for their adsorbed concentration and conformation. Fibrinogen attachment on nano-patterned surfaces was examined using fluorescence microscopy and AFM. QCM-D was used to further analyse the kinetics of protein attachment. The results obtained were compared to bare surfaces, from Section 4.2, as well as surfaces pre-coated with albumin (BSA) and/or diluted plasma proteins (ratio 1:10, in DPBS buffer).

4.3.1 ELISA

Fibrinogen is an abundant soluble extracellular matrix protein available in blood at concentration of 3mg/ml and shows a high affinity to adsorb onto most surfaces. Fibrinogen along with other serum proteins, such as fibronectin and von Willebrand factor, mediate platelet adhesion and aggregation via direct interaction with platelet receptors. Surface bound fibrinogen molecules have been known to change in conformation to perform its implicated role in mediating adhesion of platelets to synthetic surface by binding its RGDS site on the Aα chain and a non-RGD dodecapeptide sequence in the γ-chain on fibrinogen to αIIbβ3 integrin on platelets. Albumin on the other hand, is a negatively charged protein that readily adsorbs onto most materials and has been known to reduce platelet adhesion to the surface. Consequently, a higher albumin to fibrinogen ratio has often been correlated to good haemocompatibility of biomaterials by reducing the likelihood of thrombus generation. As such, adsorption of fibrinogen in a simple solution and in solution

with excess albumin was analysed using ELISA along with its adsorbed conformation.

4.3.1.1 Adsorption studies

A comparison of albumin and fibrinogen (Fg) protein adsorption on flat silicon, TiO_2, a-C:H and ta-C surfaces in a simple solution of the individual protein were studied. These results were compared against complex solutions containing both proteins: either biotinylated fibrinogen (Fg); or, biotinylated albumin (BSA), in a ratio of 1:10 (Fg:BSA, fibrinogen to albumin), as found in physiological conditions. The bound biotinylated proteins were exposed to streptavidin horseradish peroxidise (SA-HRP) label, prior to being assayed using ABTS, a colorimetric dye at 405nm wavelength.

The HABA-avidin assay was performed to determine the quantity of biotin molecules per mole of protein. It was found that 27 biotin molecules on average attach to a fibrinogen (Fg) protein and 4 biotin molecules per albumin (BSA) protein (data not shown). Accordingly, the absorbance values for fibrinogen and albumin were corrected by a factor of 27 and 4, respectively, to provide relative concentrations of attached proteins, as shown in Figure 4.14.

The general trend observed in Figure 4.14(a) is that surfaces show a higher affinity to albumin than fibrinogen, except on silicon (Si) surfaces where the adsorption ratio relatively equal. On silicon (Si) and TiO_2, the relative concentration of albumin adsorption varied marginally.

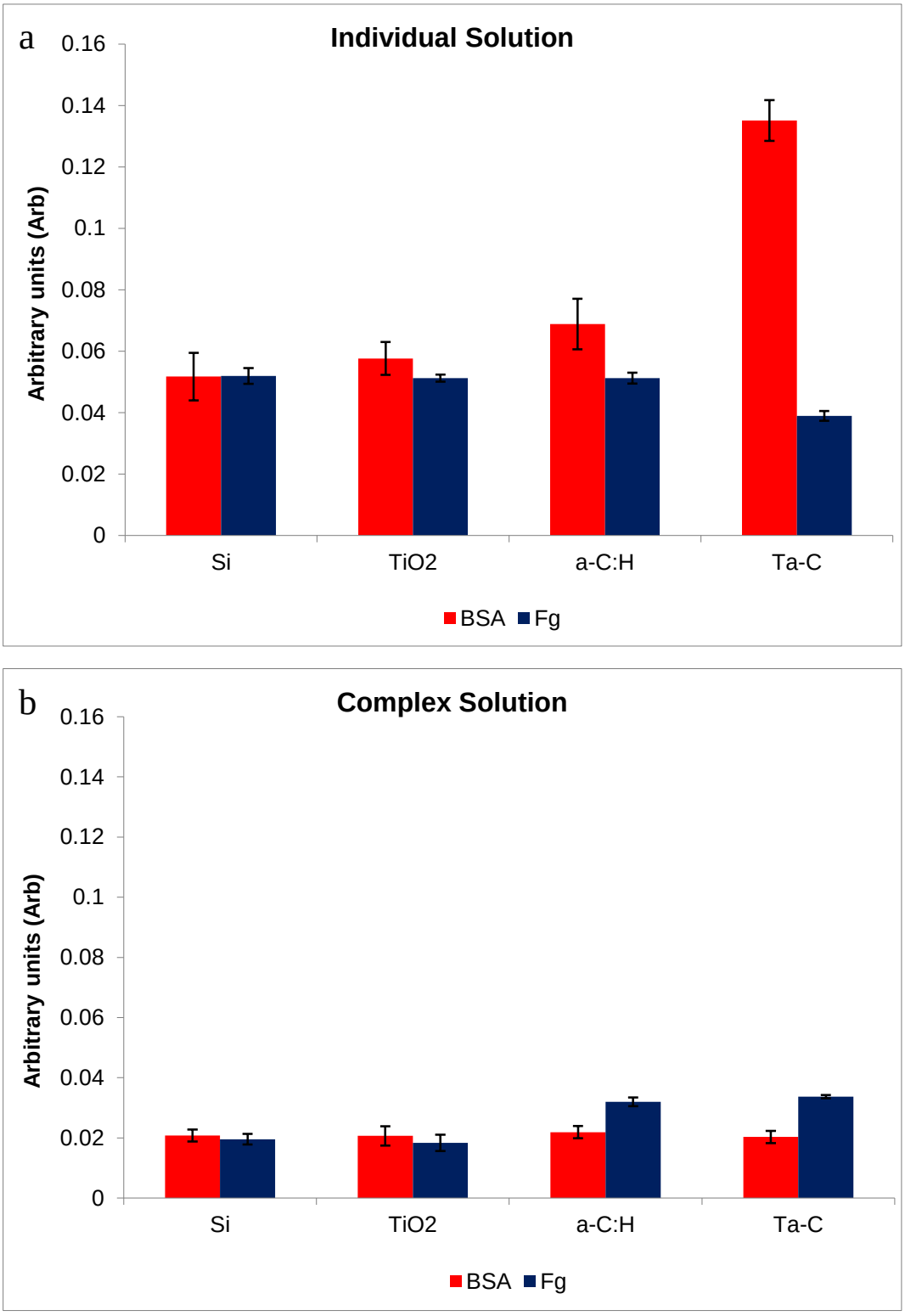

Figure 4.14 Absorbance detected for biotinylated fibrinogen (Fg) and albumin (BSA) binding to flat substrates as determined by ELISA. The results show a comparison between biotinylated fibrinogen (Fg) and albumin (BSA) adsorption from a. an individual and b. competitive solution (10:1 ratio of BSA:Fg). Error bars SD (n=3)

Both surfaces exhibited less albumin adsorption than ta-C and when compared to a-C:H, ta-C films facilitated twice as many proteins. The difference in adsorbed fibrinogen on silicon (Si), TiO_2 and a-C:H was minimal and was proven as statistically insignificant ($P<0.05$), while ta-C surfaces supported less fibrinogen than the other substrates. Furthermore, albumin is a small globular molecule, of molecular weight 67ka, than the long cylindrical shaped fibrinogen (340kDa) and so should ideally accommodate a higher quantity of protein on the substrate than fibrinogen. However, this was not the case. Similar amounts of both proteins were adsorbed indicating a conformational change within fibrinogen facilitating more protein attachment. Similarly a conformational change within albumin may also have occurred to facilitate a two-fold difference in adhesion on ta-C surfaces.

When compared to single protein solutions, the amount of protein attachment was significantly lower in a competitive solution for both albumin and fibrinogen (Figure 4.14 (b)). Increased adsorption of fibrinogen over albumin was a trend noticed on both; a-C”H and ta-C surfaces. In general, albumin’s affinity for the surface considerably decreased, in the presence of fibrinogen even though its concentration is 10 fold greater than fibrinogen. In terms of albumin adsorption; no statistically significant difference is noticed between the four substrates, while, fibrinogen facilitated a marked difference. Ta-C and a-C:H exhibited higher levels of bound-fibrinogen with ta-C facilitating the highest amount of protein. Silicon and TiO_2 both adsorbed comparable amounts of fibrinogen.

Binding affinity of fibrinogen (Fg) in the presence of albumin (BSA), and vice versa, was evaluated by computing their adsorption from a solution of both proteins described earlier, as a percentage of their absorbance from a simple solution of their own molecules (single-protein). The results are shown in Figure 4.15.

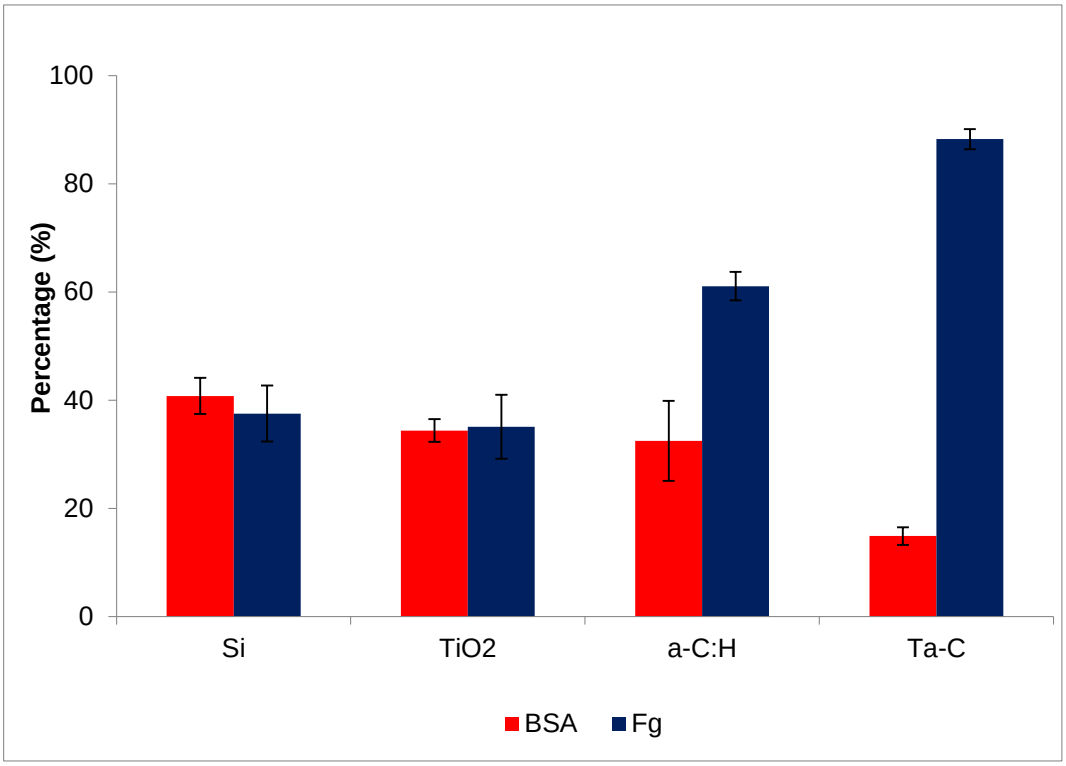

Figure 4.15 Amount of albumin (BSA) and fibrinogen (Fg) adsorbed from a complex solution containing both proteins (in ratio 10:1, respectively), as a percentage relative to their adsorption from their single solution. Error bars SD (n=3)

In the presence of fibrinogen, only 40.8% (3s.f.) of the albumin calculated from the single protein studies is shown to be adsorbed on silicon indicating a 59.2% (3s.f.) decrease in albumin adsorption. Similarly, when competitively interacting fibrinogen, TiO_2 and a-C:H showed a 65.6 and 67.5% (3s.f.) decrease in albumin binding with ta-C displaying a significant loss of 85.1% inadvertently indicating the greater influence of fibrinogen in the presence of ta-C in decreasing albumin's binding affinity. Albumin has also shown to reduce fibrinogen's binding affinity on the four samples. By competitively binding to the surface, albumin reduces fibrinogen adsorption by 62.5% (3s.f.) on silicon (Si), 65% (3s.f.) on TiO_2, 40% (3s.f.) on a-C:H and 11.5% (3s.f.) on ta-C surfaces leaving 37.5, 35, 61 and 88% (3s.f.), respectively, adsorbed.

These data indicate that the substrate-binding affinity of albumin and fibrinogen was greatly reduced in the presence of each other. Furthermore, fibrinogen has a higher binding affinity to the surface than albumin on TiO_2, a-C:H and ta-C surfaces, where

it interacts strongly with ta-C surfaces limiting albumin's influence in this dynamic process. Albumin poses a greater influence on fibrinogen in the presence of silicon, followed by TiO_2. The results not only reinforce the significant role surface chemistry plays in protein adsorption but also in the dynamic interactions between proteins.

Previous studies have often evaluated the haemocompatibility of a biomaterial surface by measuring its albumin to fibrinogen binding ratio. As such, the total amount of adsorbed albumin (BSA) was divided by the amount of adsorbed fibrinogen (Fg) from its simple solution to produce a binding ratio and this ratio was compared with the ratio of adsorbed albumin (BSA) and fibrinogen (Fg) fractions from the complex solution. The results are shown in Figure 4.16.

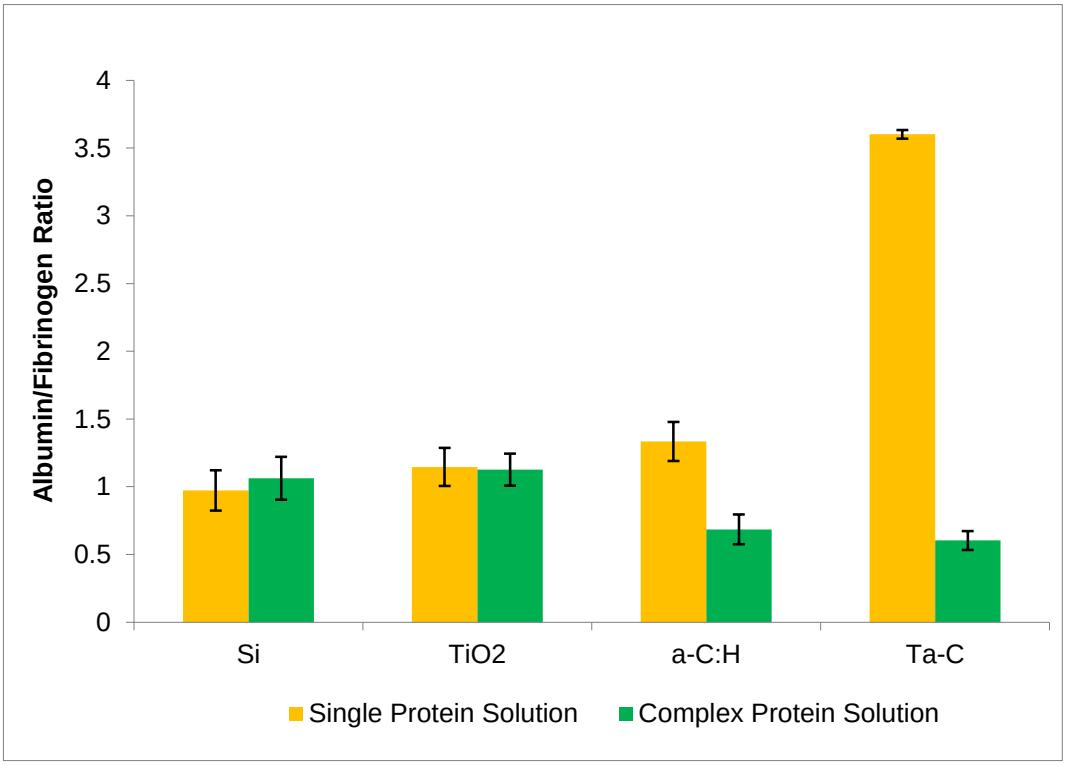

Figure 4.16 Albumin to fibrinogen binding ratio, as calculated from ELISA, for both single and complex protein solution. Error bars: SD (n=3)

Observing the ratio values from single protein solutions; Ta-C followed by a-C:H appear to be the most haemocompatible substrates, however, this is not the case when comparing the values from complex solution. The ratio was significantly

decreased, suggesting that both; a-C:H and ta-C surfaces show a high affinity for fibrinogen, thereby preferentially adsorbing fibrinogen over albumin, even when albumin was present at a 10 fold concentration. The relative adsorption ratios on silicon and TiO_2 remain unchanged between the single and complex solution, again suggesting that the binding affinity of fibrinogen remains unaltered in the presence of albumin and vice versa.

4.3.1.2 Conformation studies

Fibrinogen conformation was determined by measuring the relative concentrations of antibody binding to specific epitopes on the protein's surface in an ELISA assay. Antibodies used in this study are specific to the alpha chain (fg-alpha monoclonal antibody), gamma chain (fg-gamma mAB) and platelet binding region (2C2-G7 mAB) on fibrinogen, as shown in *Figure* 4.17. Fibrinogen coated, fibrinogen/albumin (Fg:BSA, diluted in ratio 1:10, fibrinogen to albumin) and diluted plasma (ratio 1:10, in DPBS) pre-coated flat substrates were used and the results were compared with TCPS control substrates.

The amount of mAB 2C2-G7 bound to fibrinogen adsorbed on the test substrates were evaluated in Figure 4.17(a). Despite the reduction of adsorbed fibrinogen in the presence of albumin, as mentioned in section 4.3.1.1, similar values for 2C2-G7 adsorption was evident between fibrinogen pre-coated and fibrinogen/albumin (Fg:BSA) pre-coated substrates. This reinforces the importance of conformation as well as concentration in determining the likelihood of platelet binding. Furthermore, when compared with fibrinogen and fibrinogen/albumin (Fg:BSA) coated surfaces, there is significantly less binding of 2C2-G7 on substrates pre-coated with plasma. Between the five plasma coated surfaces; TCPS exhibited the highest reading, indicating a greater exposure of its RGDS site on the Aα chain and a non-RGD dodecapeptide sequence in the γ-chain for platelet adhesion.

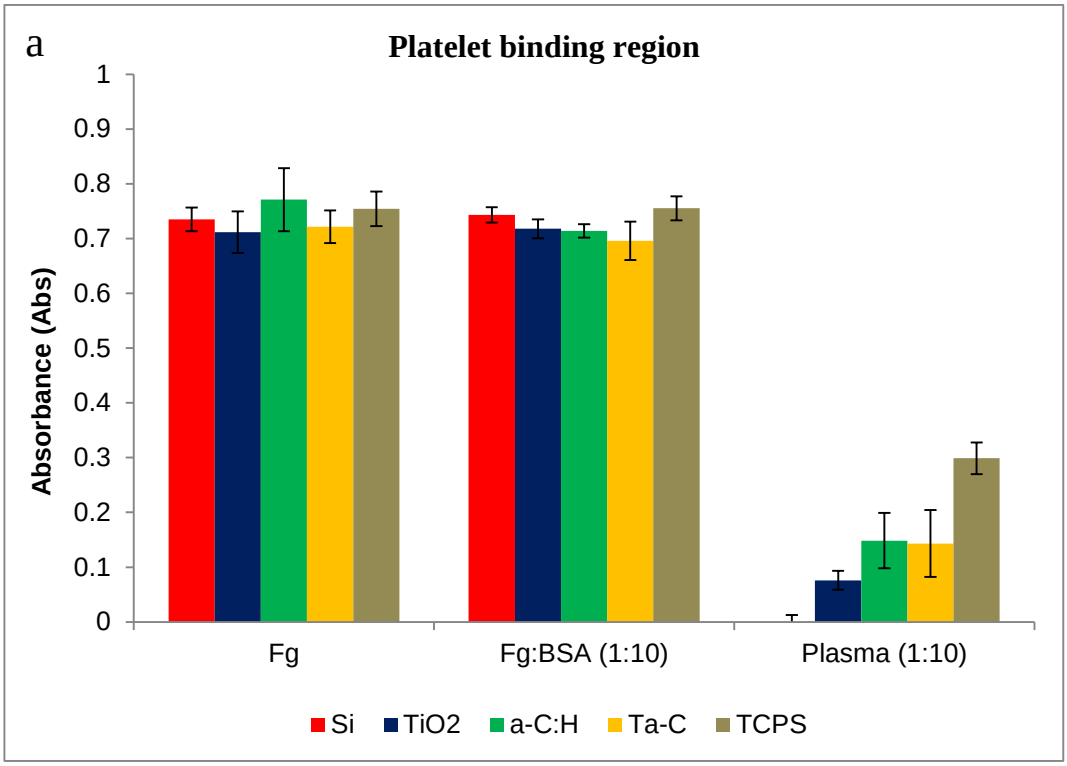
a
Platelet binding region
Absorbance (Abs)
1
0.9
0.8
0.7
0.6
0.5
0.4
0.3
0.2
0.1
0
Fg
Fg:BSA (1:10)
Plasma (1:10)
Si
TiO2
a-C:H
Ta-C
TCPS

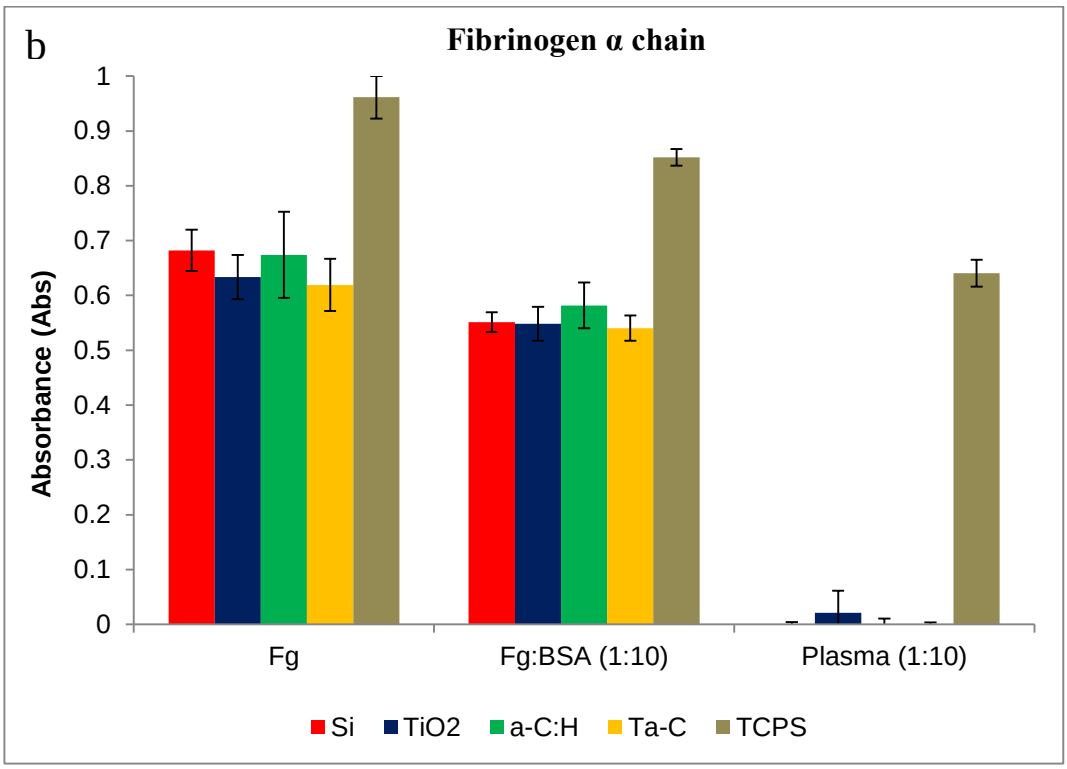
b
Fibrinogen α chain
Absorbance (Abs)
1
0.9
0.8
0.7
0.6
0.5
0.4
0.3
0.2
0.1
0
Fg
Fg:BSA (1:10)
Plasma (1:10)
Si
TiO2
a-C:H
Ta-C
TCPS

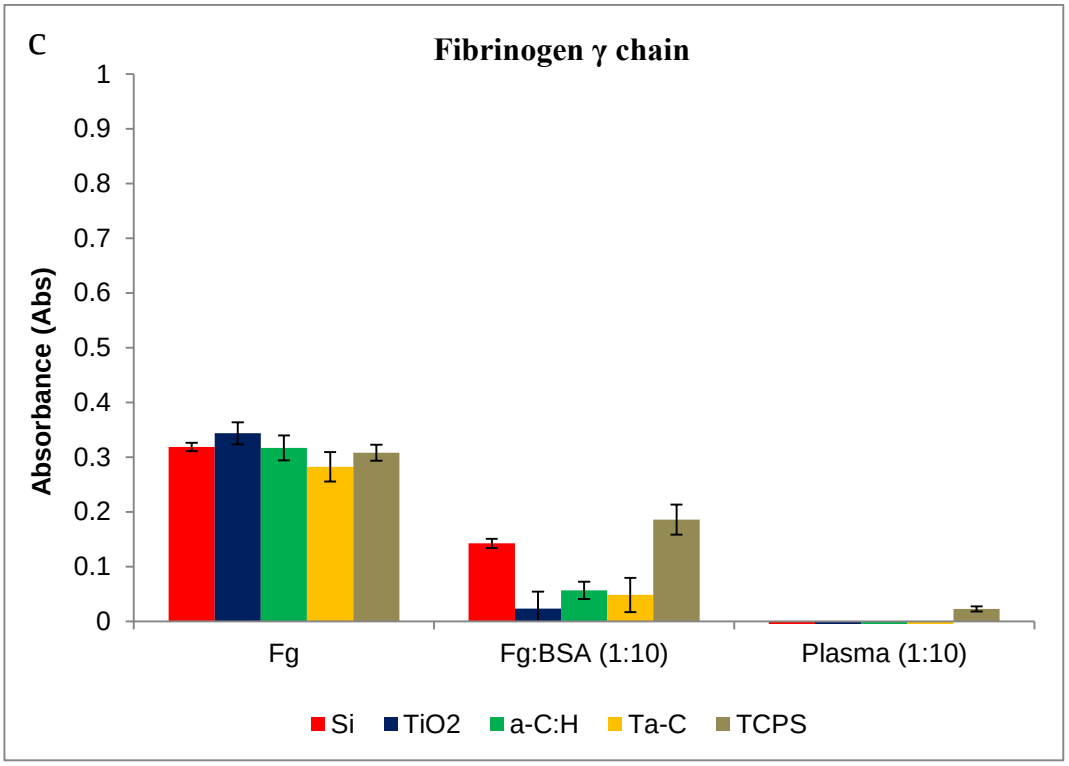

Figure 4.17 Concentration of monoclonal antibody a. 2C2-G7 b. Fg-α and c. fg-γ adhesion to fibrinogen coated test samples, as determined by ELISA. Comparison of the volume of adsorbed human fibrinogen and its relative conformation in the presence of other proteins are evaluated using single, complex (Fg:BSA) and plasma protein solution (1:10 dilution in DPBS) containing fibrinogen. Silicon (Si), TiO_2, a-C:H and ta-C surfaces were compared with control TCPS polystyrene substrates. Error bars: SD (n=3).

Also small amounts of 2C2-G7 were present on plasma coated a-C:H and ta-C surfaces. The significant difference in 2C2-G7 quantity between the three different protein coated surfaces suggest one or more of the following notions; either a limited amount of protein is absorbed from plasma due to the presence of other plasma protein of high binding affinity, or, the presence of larger molecules adjacent to the protein may sterically hinder the antibody binding site, or, a shift in protein conformation upon adsorption be the cause of protein denaturing, decreasing the exposure of its platelet binding region.

The relative absorbance from the presence of fg-alpha antibody is evaluated in Figure 4.17(b). Plasma pre-coated TCPS, like in Figure 4.17(a), presented elevated levels of antibody, while minimal absorbance is recorded for silicon (Si), TiO_2, a-C:H and ta-C surfaces, indicating that fibrinogen adhesion on TCPS surface may be

significantly greater than the other substrates or the binding region appears more pronounced in the presence of TCPS. In general, TCPS displayed elevated levels in all three protein conditions. Unlike with 2C2-G7 where the exposure of the epitope is because of the dynamic interaction between fibrinogen and other proteins, these results indicate that the exposure of fg-alpha domain is primarily dependent on TCPS surface chemistry and possibly, although not necessarily, due to fibrinogen's interaction with other proteins. It is also interesting to note that apart from the obvious TCPS, silicon (Si) and a-C:H pre-coated with fibrinogen also displayed a slightly higher level of alpha chain epitope. There is no significant difference between silicon, TiO_2, a-C:H and ta-C surfaces pre-coated with Fg:BSA ($P<0.05$) although, overall the four substrates exhibited increased adsorption on fibrinogen pre-coated surfaces when compared with pre-coated Fg:BSA, implicating the possible role of albumin in altering the orientation of fibrinogen and possibly masking its fg-alpha antibody binding epitope.

The test substrates including the control TCPS displayed no appreciable difference in fg-gamma binding. When compared with fibrinogen pre-coated, Fg:BSA coated samples showed reduced adsorption, where TiO_2, a-C:H and ta-C surfaces did not show values above background. Silicon (Si) and TCPS surfaces showed slightly higher than background values indicating a conformational change in fibrinogen protein exposing its fg-gamma epitope for antibody binding. Akin to fg-alpha, no absorbance was recorded on all plasma pre-coated surfaces, except TCPS. Comparison of the three protein coated surfaces suggest that fibrinogen underwent conformational change upon interacting with other serum proteins such as albumin, inhibiting its exposure of the fg-gamma domain.

These data establish that dynamic interactions between plasma proteins as well as fibrinogen's adsorption on biomaterial surfaces play an important role in determining the protein's conformation. While denaturing of some regions of the protein is dependent on the surface, others may be due to other biological interactions. It is a combination of both aspects that induce complete unfolding of the protein on a biomaterial surface.

4.3.2 Fluorescence microscopy

Fluorescence microscopy was used as an alternative technique to ELISA to characterise fibrinogen concentration adsorbed on test substrates using a fluorescently tagged anti-protein antibody. Fibrinogen and plasma protein pre-coated test substrates were incubated with 2C2-G7 monoclonal antibody. The antibody was fluorescently labelled using anti-mouse alexa fluorophore 488 conjugated antibody, a green fluorophore, and visualised by Zeiss Axioskop microscope at 500x magnification. The total intensity from each image, measured as total number of positive pixels, was estimated using ImageJ and distribution of the protein across the material surface was imaged. Test substrates include flat and nano-patterned silicon, TiO_2, a-C:H and ta-C. The images taken of protein coated flat substrates are shown in Figure 4.18. The surfaces generally presented homogenously distributed fluorescent tags with sporadic dots of localised high fluorophore densities. The dots may be caused by regions of highly aggregated proteins or regions where fibrinogen molecules posses a highly regulated conformation, exposing its 2C2-G7 binding region. Furthermore, control substrates (bare surfaces without any proteins) that were directly incubated with the fluorescent tag also displayed high intensity dots (data not shown). However, these dots were more rarely noticed. This may possible be from surface imperfections causing non-specific interactions between the antibody and the substrate.

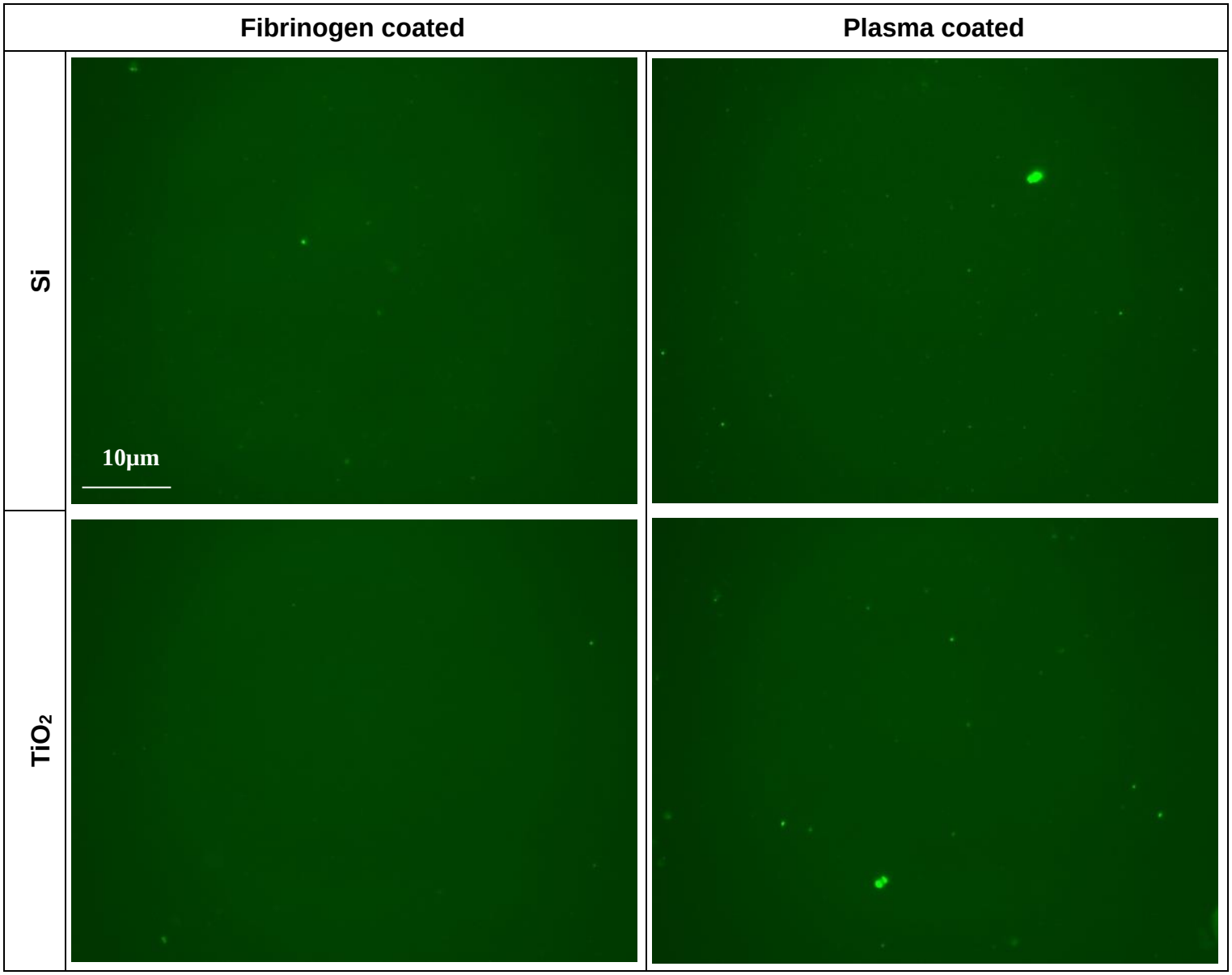
Fibrinogen coated
Plasma coated
Si
TiO2
10µm

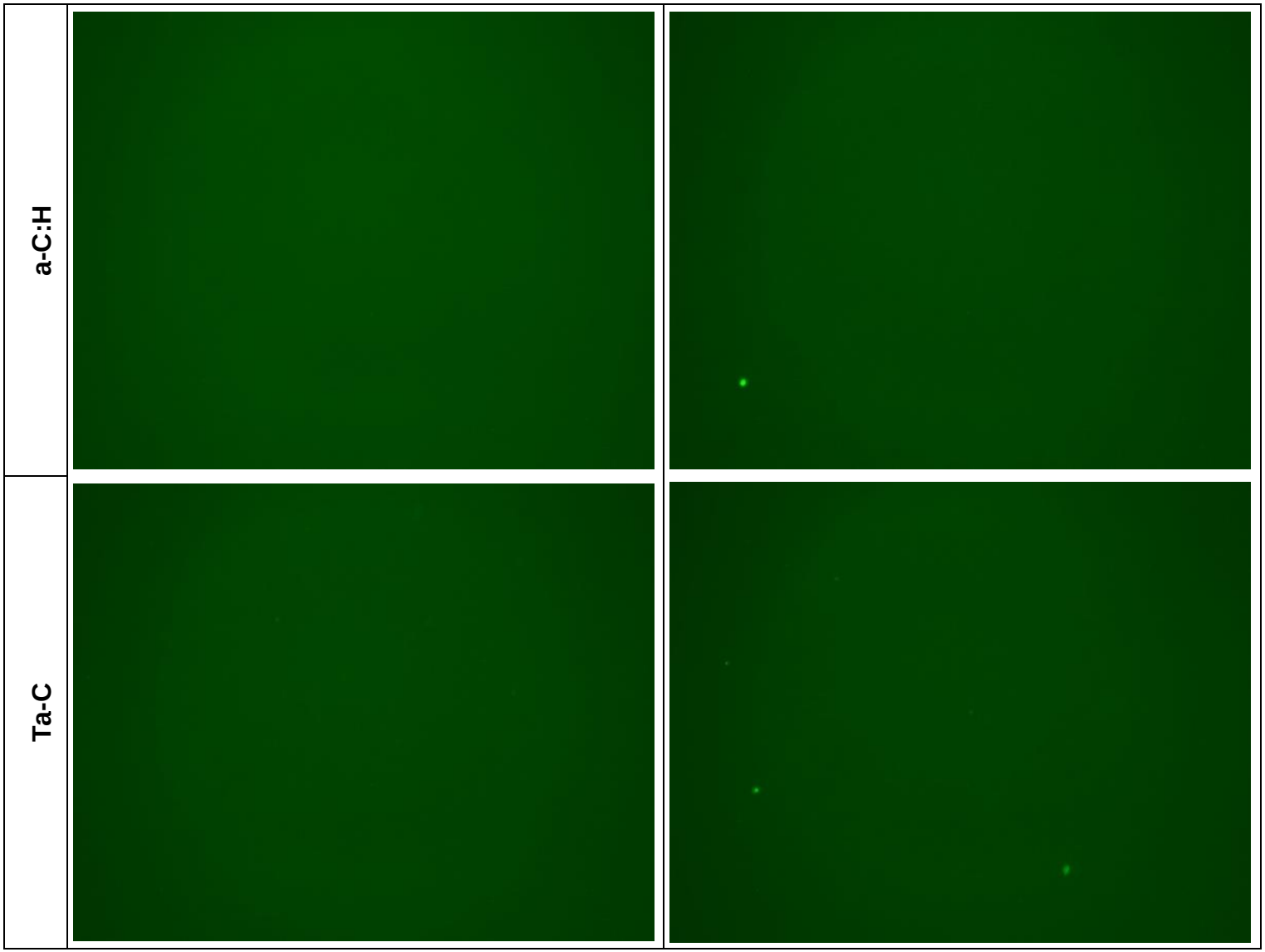
a-C:H
Ta-C

Figure 4.18 Fluorescence microscope images showing the distribution of fibrinogen on the various surfaces using alexa fluorophore 488 tagged 2C2-G7mAB antibody bound to fibrinogen proteins from fibrinogen and plasma (dilution 1:10) pre-coated flat substrates. Samples were imaged by Zeiss Axioskop (Mot Mat 2, Australia) fluorescent microscope and analysed using ImageJ (v.1.44p, NIH). Scale bar: 10µm.

Quantity and distribution of proteins across the various protein coated surfaces was difficult to discern. As such each surface was sampled for their total integrated density of positive pixels and graphed, as shown in Figure 4.19. Further, the results were corrected for false positive readings from non-specific fluorophore-surface interactions.

Results from Figure 4.19 are analogous to Figure 4.17(a) from Section 4.3.1.2, with minor variances. Similar amount of 2C2-G7 bound fibrinogen was detected on silicon (Si), TiO_2, a-C:H and ta-C fibrinogen (Fg) pre-coated surfaces, where silicon displayed the most and ta-C with the least amount of 2C2-G7 antibodies. The amount of 2C2-G7 bound fibrinogen present on plasma pre-coated surfaces were significantly less, of which differences between TiO_2, a-C:H and ta-C can be considered statistically insignificant ($P<0.05$). Plasma pre-coated silicon displayed the highest amount of 2C2-G7, contradicting data from Figure 4.17(a). Again, minor differences between the two graphs are expected due to difference in sensitivities between the two techniques.

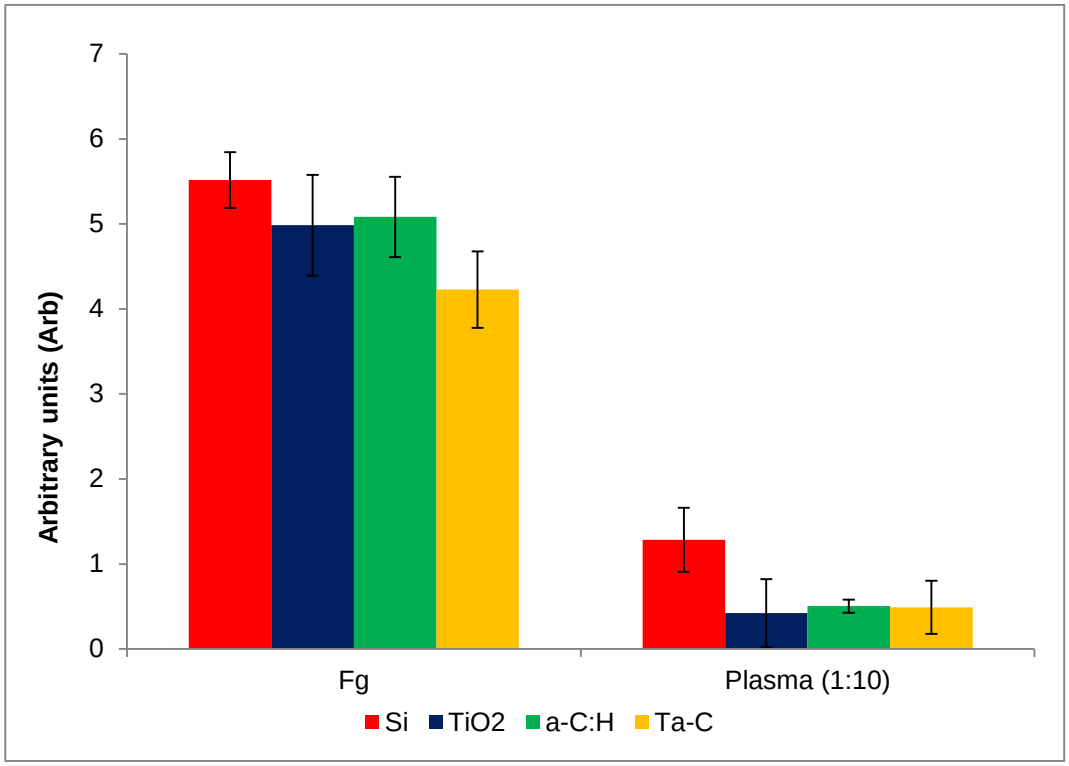

Figure 4.19 Concentration of 2C2-G7mAB on fibrinogen and plasma pre-coated flat surfaces. The amount of antibody detected was measured from the total number of positive pixels from fluorescent images and displayed as arbitrary values using ImageJ (p1.44p, NIH).

Apart from surface chemistry and competitive interactions, surface characteristics, such as nano-features, have been known to influence the quantity and conformation of protein adsorption, subsequently affect the adhesion, spreading and activation of platelets and ultimately the formation of blood clots. As such, the influence of nano-patterns on fibrinogen adsorption and its conformation was investigated in Figure 4.20 using 2C2-G7mAB on fibrinogen pre-coated flat and nano-patterned substrates.

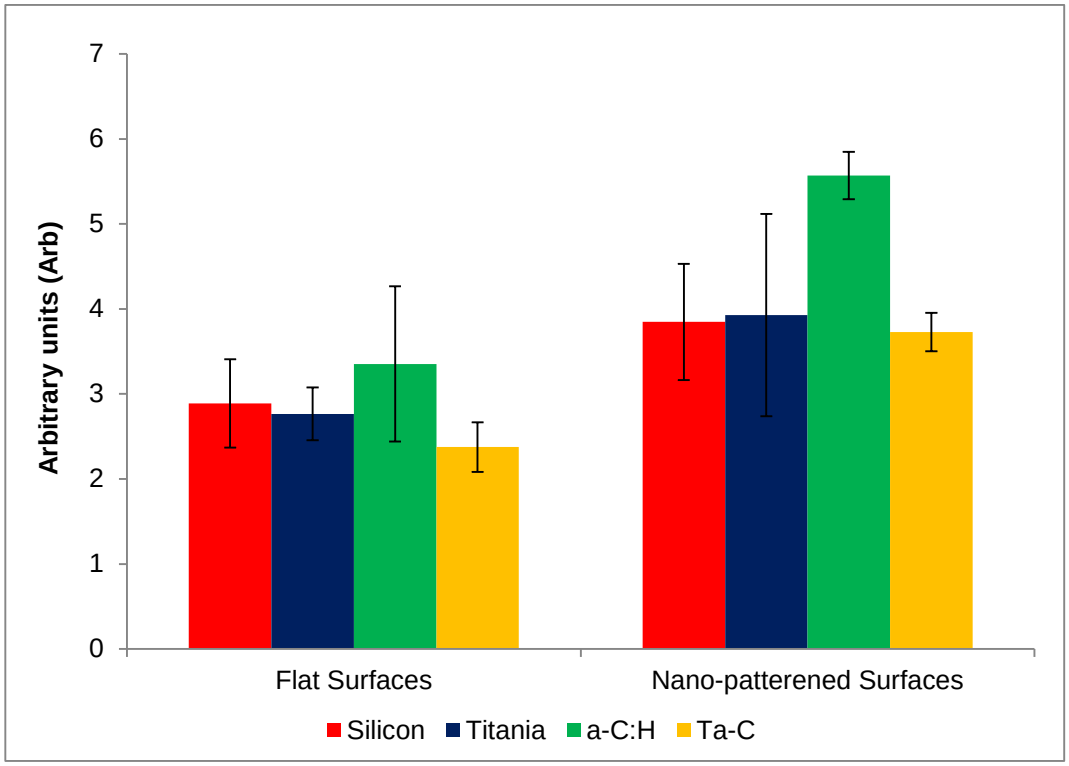

Figure 4.20 Relative level of 2C2-G7 antibody detected on flat and nano-patterned surfaces pre-coated with fibrinogen. The amount of antibody present was measured from the total number of positive pixels from fluorescent images and displayed as arbitrary values using ImageJ (p1.44p, NIH).

Protein adsorption on flat surfaces followed a trend similar to that described in Figure 4.19. When compared with flat surfaces, the nano-patterned surfaces exhibited higher level of antibody reactives and of the four patterned surfaces, a-C:H presented the highest amount of 2C2-G7 antibodies. Differences in the amount of 2C2-G7 monoclonal antibodies attached due to nano-features were tabulated as a percentage value of the flat surfaces in Table 4.4. The last column provides an estimated value independent of the increase in surface area caused by the nano-patterns.

Silicon showed the lowest increase in 2C2-G7 binding (30.4%) followed by tiania with 37.8% while a-C:H showed the highest increase by 57.7%. As mentioned earlier an increase in 2C2-G7mAB can possibly be because of an increase in protein concentration as well as an increased likelihood to conform in a particular orientation that facilitates 2C2-G7mAB binding. As such, higher 2C2-G7 levels, indicating higher levels of platelet binding region available on fibrinogen proteins, could

increase the chances of platelet binding and subsequently the haemocompatibility of a material.

Table 4.4 Percentage increase in 2C2-G7 antibody adsorbed on fibrinogen coated substrates due to presence of nano-patterns.

Nano-patterned Substrates	Increase in 2C2-G7mAB (%) (3s.f.)	Δ in Surface Area (%) - *table 4.3* (3s.f.)	Δ in 2C2-G7 mAB per unit sq (%) (3s.f.)
Silicon	33.2	9.43	30.4
TiO_2	41.9	10.9	37.8
a-C:H	66.1	14.8	57.7
Ta-C	56.9	11.1	51.2

As such, it can be hypothesised that nano-patterns with RMS values between 5-10nm may greatly alters the haemocompatibility of a material increasing its likelihood of platelet activation. When comparing the four surfaces it is evident that apart from nano-patterns, surface chemistry also plays a crucial role in protein adsorption and conformation. A-C:H supported a higher level of fibrinogen adsorption than silicon and TiO_2.

4.3.3 AFM

The conformation of serum proteins were deduced using AFM under liquid mode conditions. The purpose of the study was to analyse changes in nano-topography between the flat and nano-patterned surfaces after fibrinogen and plasma adsorption using Bioscope Catalyst, Bruker AFM, in low voltage tapping mode. Scan rate of 1Hz and scan area of 1µm x 1µm was used. Imaging was carried out on protein adsorbed silicon, TiO_2, a-C:H and ta-C surfaces incubated in DPBS at room temperature, atmospheric conditions.

The nano-topography of the bare substrates was significantly altered upon the adsorption of serum proteins. Figure 4.21 and

Figure 4.23 provides insight into fibrinogen's conformation on the four flat surfaces. On silicon (Si), fibrinogen formed a thick adlayer layer, with an over roughness value of 9.19nm. It mainly consisted of protein aggregates forming a non-uniform surface with an undulating topography. Due to high peaks formed by the protein aggregates, it is difficult to visualise individual proteins, on the silicon (Si) surface.

Though it is normal to form aggregates, other factors may have also influenced this response, such as; a change in temperature from 37 degrees to 25 degrees, causing the proteins to change in structure or protein particles adhering to the AFM tip causing affecting the characteristics of the tip, namely tip length and overall charge, which may ultimately interfere with the scanning process. Furthermore, because of the sweeping movement of the AFM tip during the scanning process proteins may have delocalised to form clusters with adjacent proteins. Protein translocation, while scanning, could have also caused the difference between trace and retrace patterns of the tip forming exaggerated peaks with shallow inclination.

Fibrinogen's conformation on TiO_2, a-C:H and ta-C, on the other hand, was clearly visualised. Fibrinogen appears to be distributed uniformly across the surfaces with fewer regions exhibiting protein clumping. When compared with the bare surface, a significant increase in roughness was noticed on the protein-adsorbed films. Side profiles along with surface 3-D plots, not only indicate the existence of proteins on the surface but also suggest that the proteins present a certain nano-topography similar to that of the patterned surfaces, mentioned previously in Section 4.2, which may behave as physical cues for cellular and platelet interactions. The roughness values of the adlayer on TiO_2, a-C:H and ta-C range between 1-3nm suggesting that the protein predominantly exists in its stable conformation, aligning flat against the surface forming a side on topography. Localised minor peaks may have been caused by other protein conformations such as end-on or bent conformation. Furthermore, larger regions of elevated peaks are indicative of protein clumping. As such, it is evident that a protein's morphology on a particular surface is not confined to a

particular conformation; while they tend to predominantly orient in a particular conformation, they may also exist in several other conformations simultaneously.

Fibrinogen's general structure on TiO_2, a-C:H and ta-C surfaces is shown in Figure 4.21(e), (h) and (k). As can be seen, the side-on oriented protein appears to form either a long fibrillar (rod-like) or bent structure. Furthermore, in some images a tri-nodular structure can be visualised. The exact size of each protein circled in red ranged between 45-55nm in length with 5-15nm thickness. The AFM tip used for scanning the proteins was approximately 5-10nm in diameter, which larger than the width of the protein. This may suggest that the peripheral regions of the tip may have inadvertently interacted with adjacent proteins on the surface, exaggerating the overall dimensions of the protein. However, the tri-nodular shape and the various conformations of the protein evident in the images corroborates with previous studies [455, 456]. In contrast to the flat surfaces, the overall RMS value of nano-patterned films after protein adsorption is less than the roughness values obtained from fibrinogen coated bare surfaces, as shown in Figure 4.22 and Figure 4.23.

.

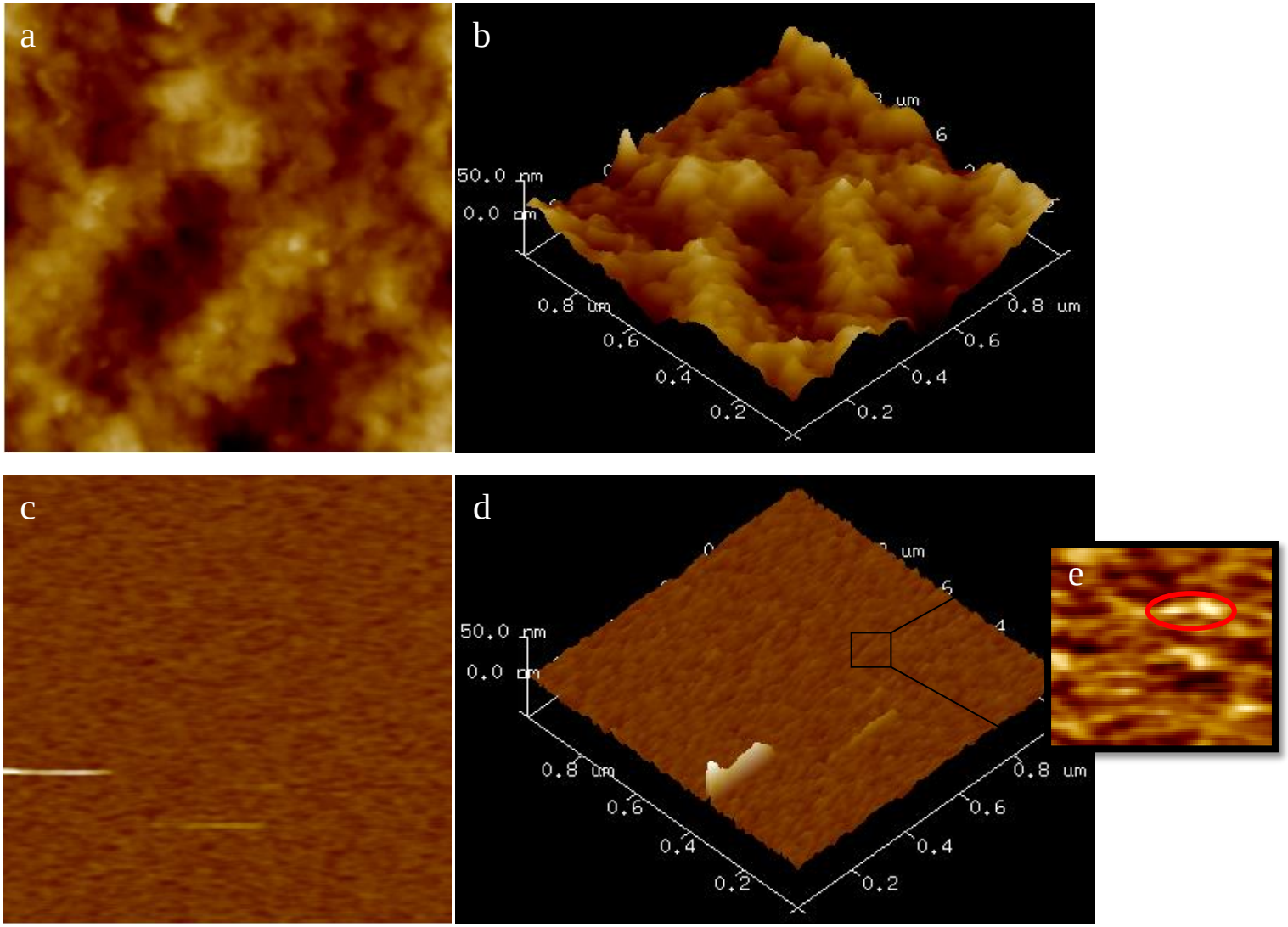
a
b
50.0 nm
0.0 nm
0.8 um
0.6
0.4
0.2
0.8 um
0.6
0.4
0.2
c
d
50.0 nm
0.0 nm
0.8 um
0.6
0.4
0.2
0.8 um
0.6
0.4
0.2
e

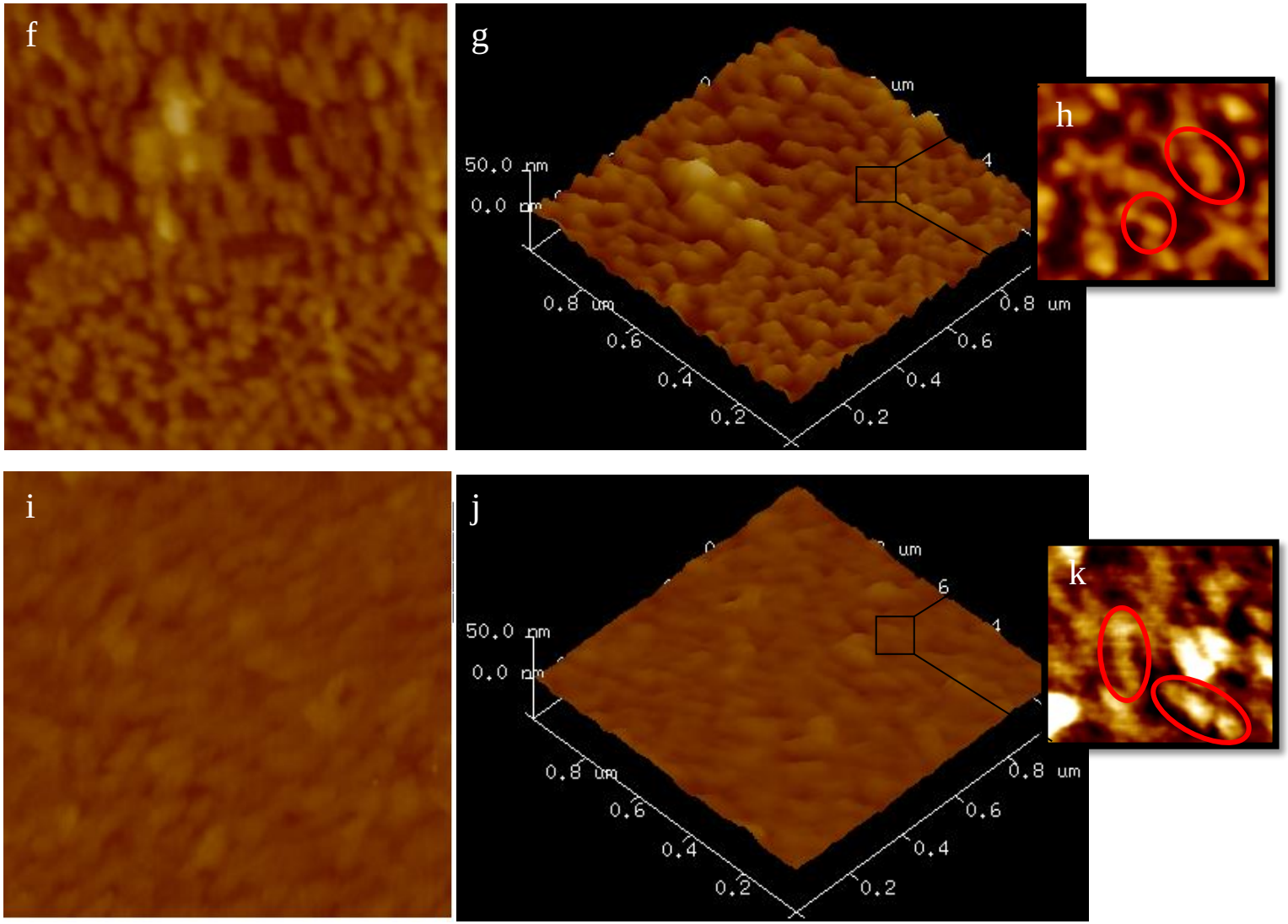

Figure 4.21 2-dimensional, 1µm^2 AFM images of flat a. silicon ; c. TiO_2; f. a-C:H; and i. ta-C surfaces incubated with 50µg/ml of fibrinogen for 1hour at 37 degrees. Image b; d; g; and j correspond to a to a 1µm^2 view of their 3-D height, respectively. A 3X high magnification of the protein layers on e. TiO_2; h. a-C:H; and k. ta-C is presented on the right with red circles indicating the conformation of fibrinogen protein.

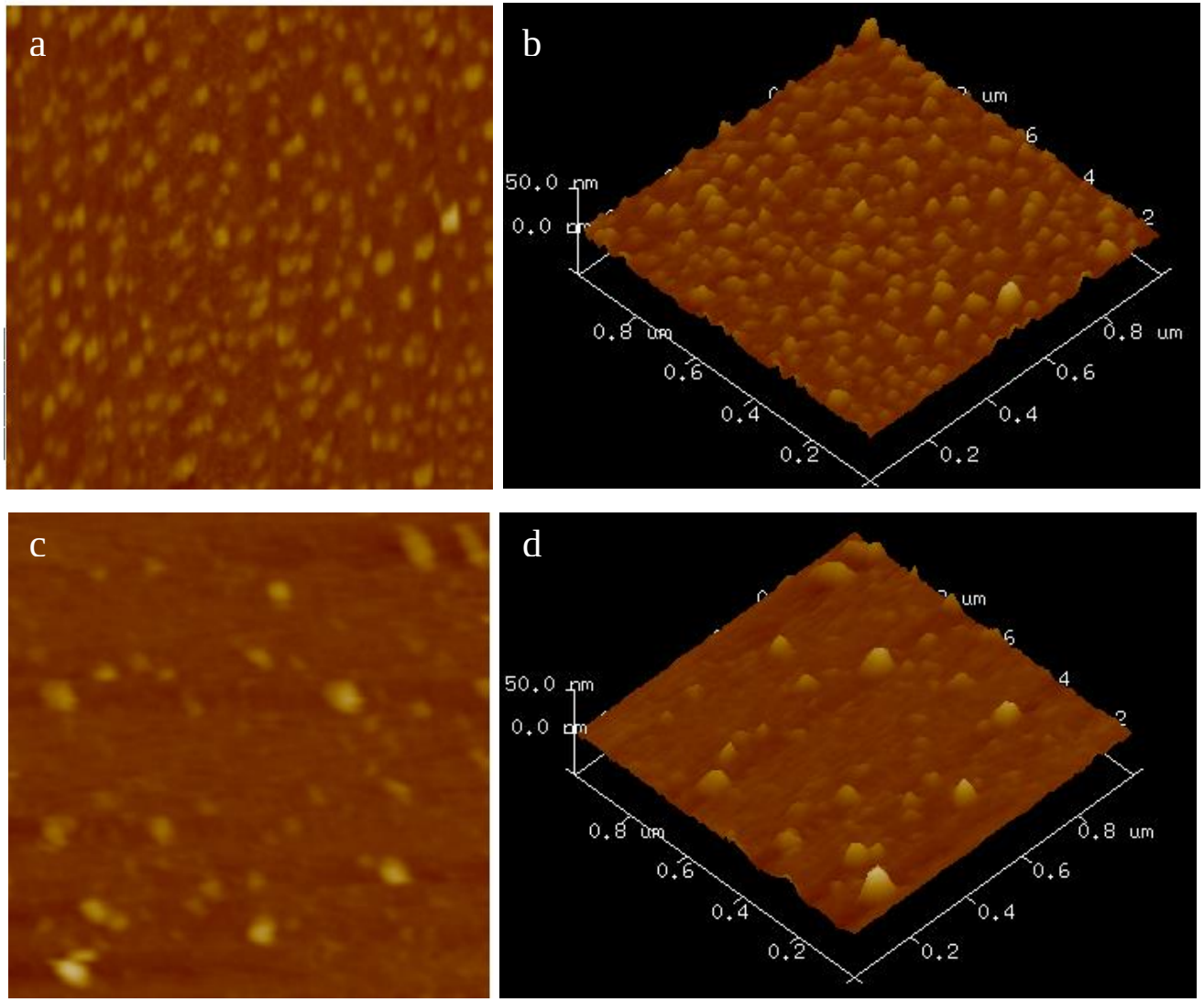
a
b
50.0 nm
0.0 nm
0.8 um
0.6
0.4
0.2
c
d

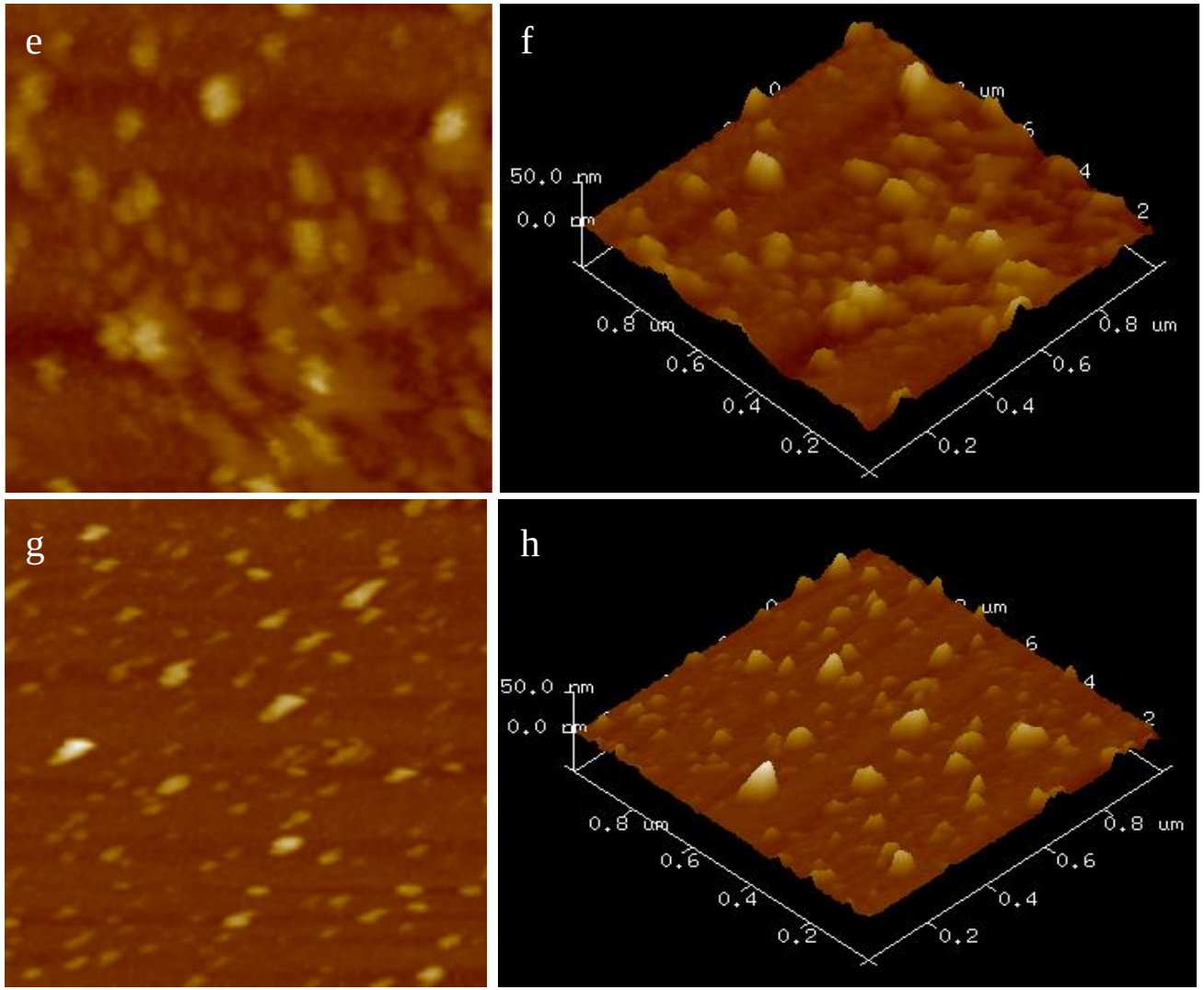

Figure 4.22 2-D images of nano-patterned a. silicon (Si), c. TiO_2, e. a-C:H and g. ta-C surfaces incubated with 50µg/ml of fibrinogen for 1hour at 37 degrees. Corresponding 1µm^2 3-D height analysis is presented on the right in b, d, f, h, respectively.

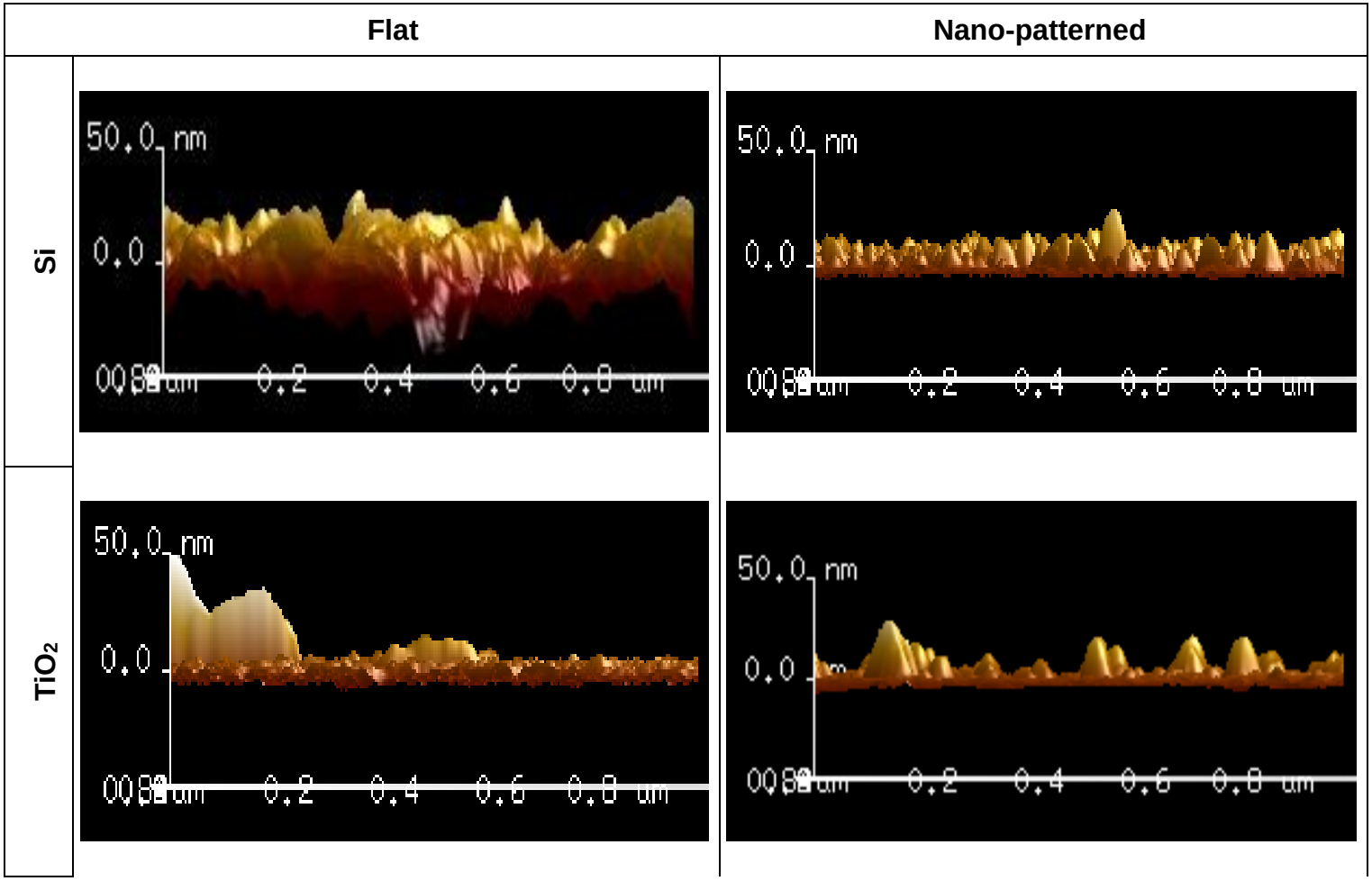
Flat
Nano-patterned
Si
TiO2
50.0 nm
0.0
0.2
0.4
0.6
0.8 um

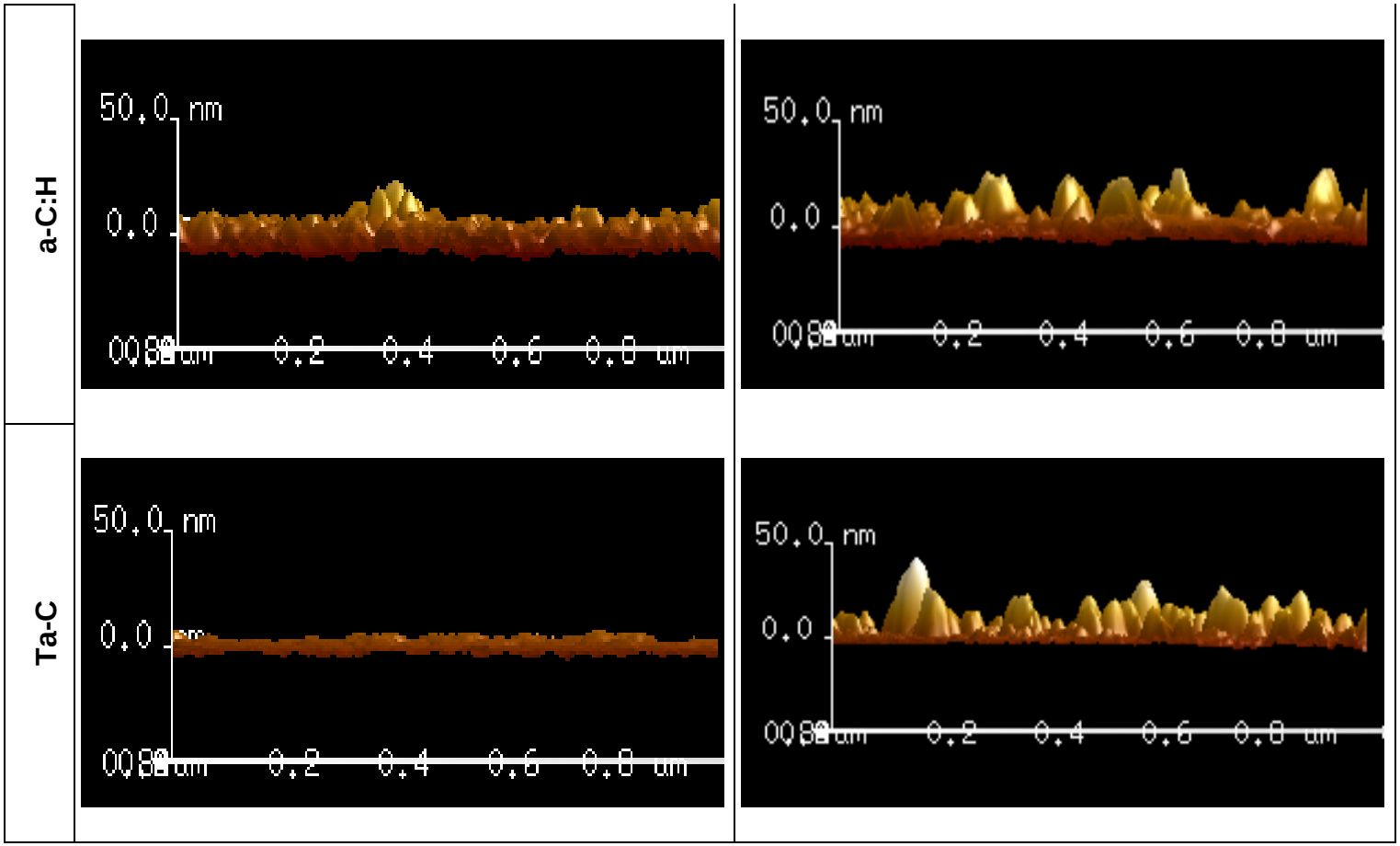

Figure 4.23 1µm² roughness profiles of flat and nano-patterned silicon (Si), TiO_2, a-C:H and ta-C surfaces pre-adsorbed with fibrinogen protein, as analysed using AFM.

The overall roughness values (RMS) on fibrinogen coated nano-patterned surfaces, shown in Figure 4.24, has been decreased to 2-4nm with a-C:H surfaces displaying the highest RMS of 3.55nm. Comparing the fibrinogen coated patterned surfaces with the bare surfaces, it is evident that the fibrinogen molecules saturate onto the concave grooves created by the nano-particles. Therefore, overall z-range of the surface nano-topology is smaller and consequently its roughness value is also decreased. It was difficult to visualise individual proteins on the nano-patterned surfaces when compared with the flat surfaces. However, judging by their 3-D plots it is evident that the proteins align themselves against the grooves and slopes following the topography of the underlying substrate. 2-D plots of the surfaces show fewer peaks than on the bare surfaces, again reinforcing the complete coverage of the surface by fibrinogen. This trend was noticed amongst all four surfaces.

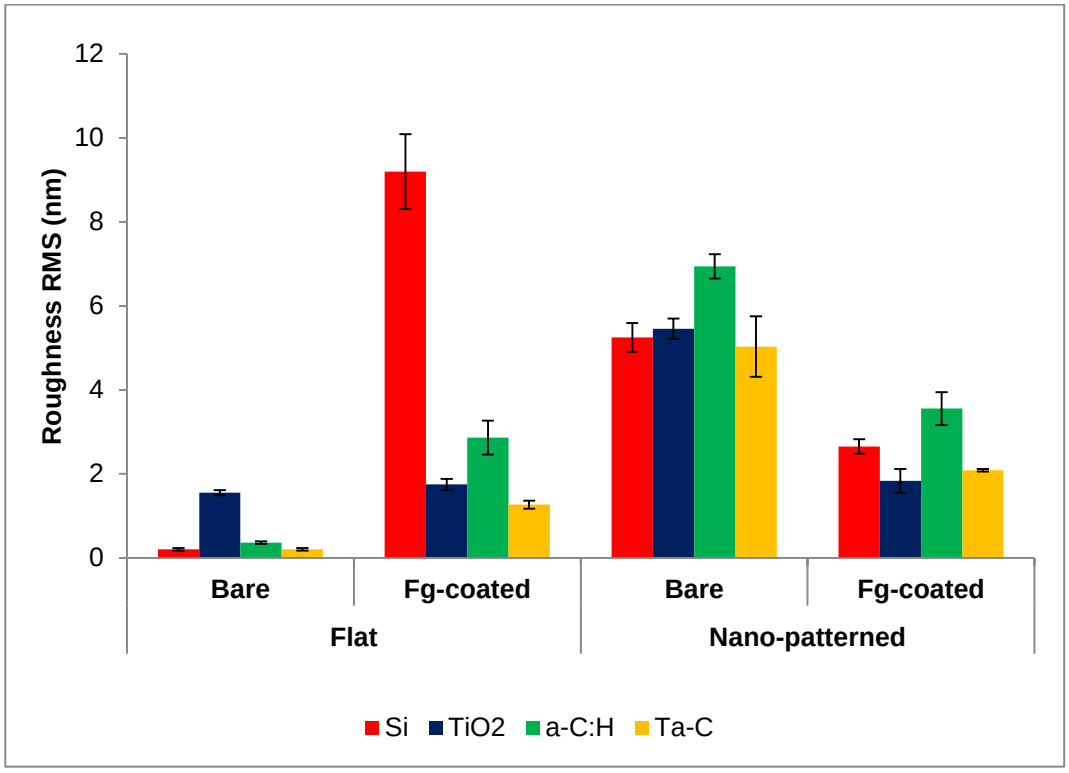

Figure 4.24 A comparison of roughness values (RMS) between flat and nano-patterned surfaces in the presence and absence of fibrinogen.

Furthermore, it was interesting to note the random fibrinogen clusters formed on the surface. The roughness profiles of the protein adsorbed nano-patterned surfaces in

Figure 4.23 showed reduced z-range when compared with the bare surfaces (Figure 4.12). A reduction in the average z-height could indicate the adhesion of multiple layers of protein. However, it is still uncertain whether these proteins are irreversibly adsorbed on the grooves or not.

Apart from fibrinogen, the general surface topography upon plasma protein adsorption (1/10 dilution in DPBS) was analysed using AFM and results are shown in Figure 4.25 and

Figure 4.27. The flat and nano-patterned plasma pre-coated surfaces were analysed for their roughness value and the results were compared with the bare surfaces in Figure 4.28.

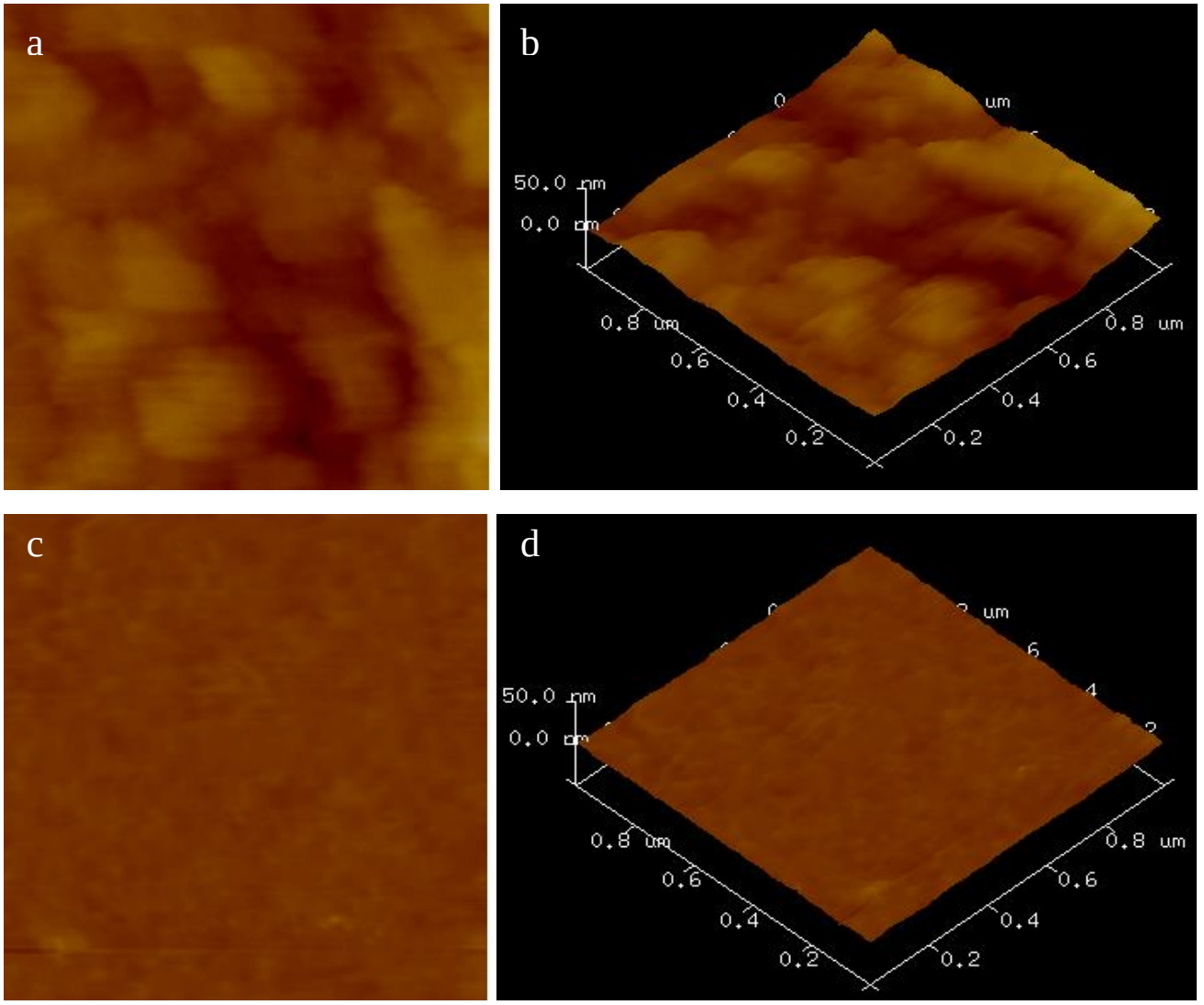
a
b
0
um
50.0 nm
0.0 nm
0.8 um
0.6
0.4
0.2
0.8 um
0.6
0.4
0.2
c
d
um
50.0 nm
0.0 nm
0.8 um
0.6
0.4
0.2
0.8 um
0.6
0.4
0.2

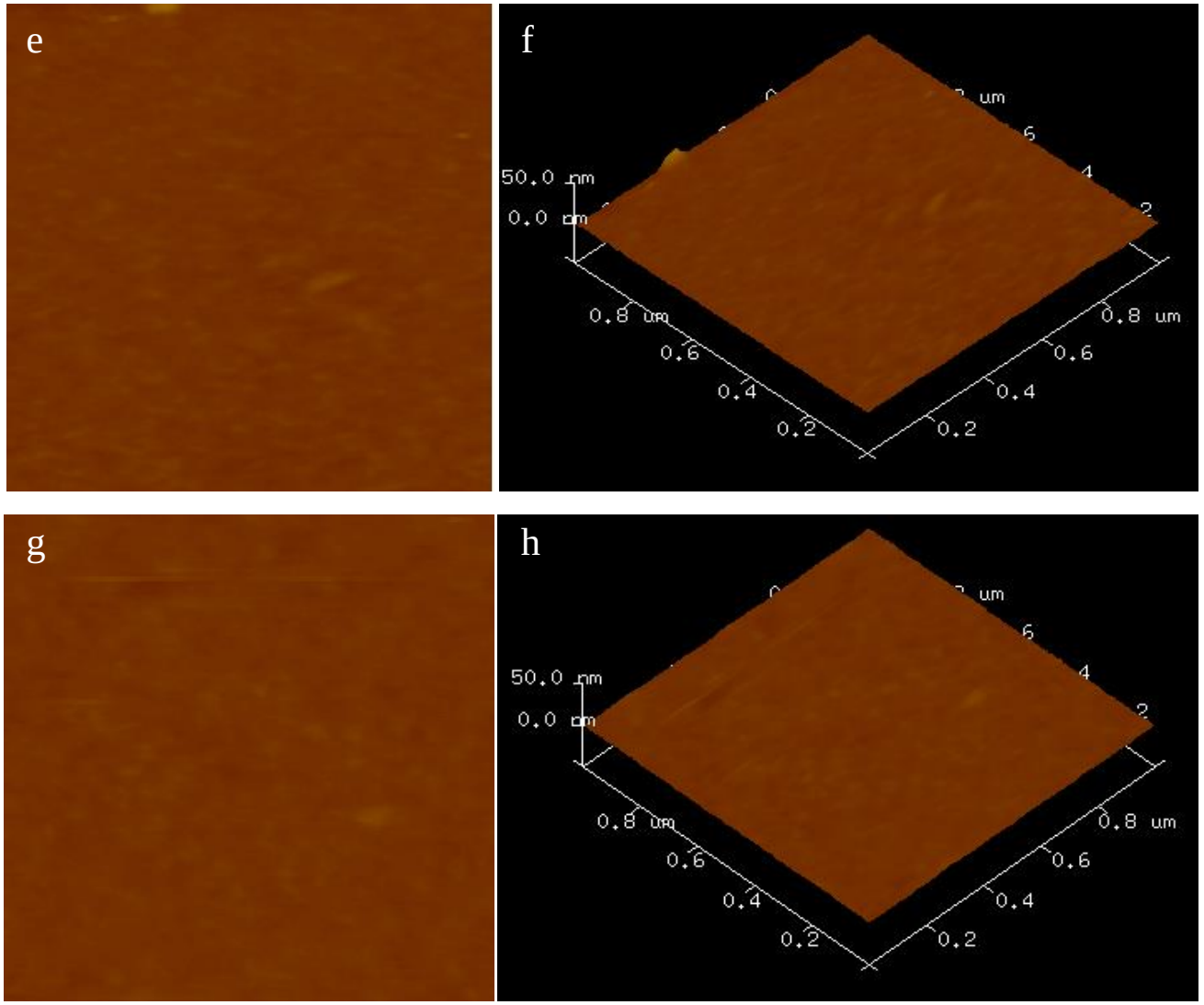

Figure 4.25 2-dimensional, 1µm^2 AFM images of flat a. silicon, c. TiO_2, f. a-C:H and i. ta-C surfaces incubated with diluted plasma (dilution factor 1:10) for 1hour at 37 degrees. Image b, d, f and h correspond to a to a 1µm^2 view of their 3-D height, respectively.

Flat silicon substrates exhibited the greatest roughness value of 4.04nm upon adsorbing plasma-proteins (Figure 4.28). The ultra smooth surface lacks physical nano-cues to act as focal adhesion points for the protein to adhere. This may have a consequent role in forming a thick protein adlayer, caused by the packing of proteins and water along the thickness of the protein coat, which may be necessary for the localisation and adhesion of the surface proteins. Furthermore, the protein film may be highly viscous affecting the overall adhesion between the tip and the surface. A viscous adlayer causes strong tip-protein interaction, increasing the force required to detach the tip from the protein adlayer upon scanning. This interferes with the trace-retrace curves of the surface nano-topography and in-turn exaggerates the z-height profile and protein conformation on the adsorbed surfaces. Consequently, the adsorbed proteins appear un-stable and delocalised. Roughness profiles on Figure 4.27 and 3-D plots in Figure 4.25 of the sample depict this notion.

While ta-C and a-C:H surfaces showed a slight increase in RMS values, TiO_2 exhibited a decrease in roughness. Flat TiO_2 surfaces originally exhibited island like features on the bare surface with peaks separated by wide grooves. The adsorbed plasma appears to have filled the void causing a decrease in the overall surface roughness. The smoothening effect of plasma proteins adsorbed on flat surfaces is evident on the surface plots shown in Figure 4.25.

While the ultra flat surfaces displayed significant rise in roughness values, the nano-patterned silicon, TiO_2 and ta-C substrates exhibited a smaller RMS value upon protein adsorption. Again, this may be due to proteins interacting with the grooves on the surface causing a decrease in z-range and consequently the roughness of the surface. A-C:h surfaces, on the other hand formed a highly featured surface with roughness of 15nm caused by the plasma protein aggregation. The plasma proteins on a-C:H surfaces localise on top of the peaks forming well connected protein clusters on the surface.

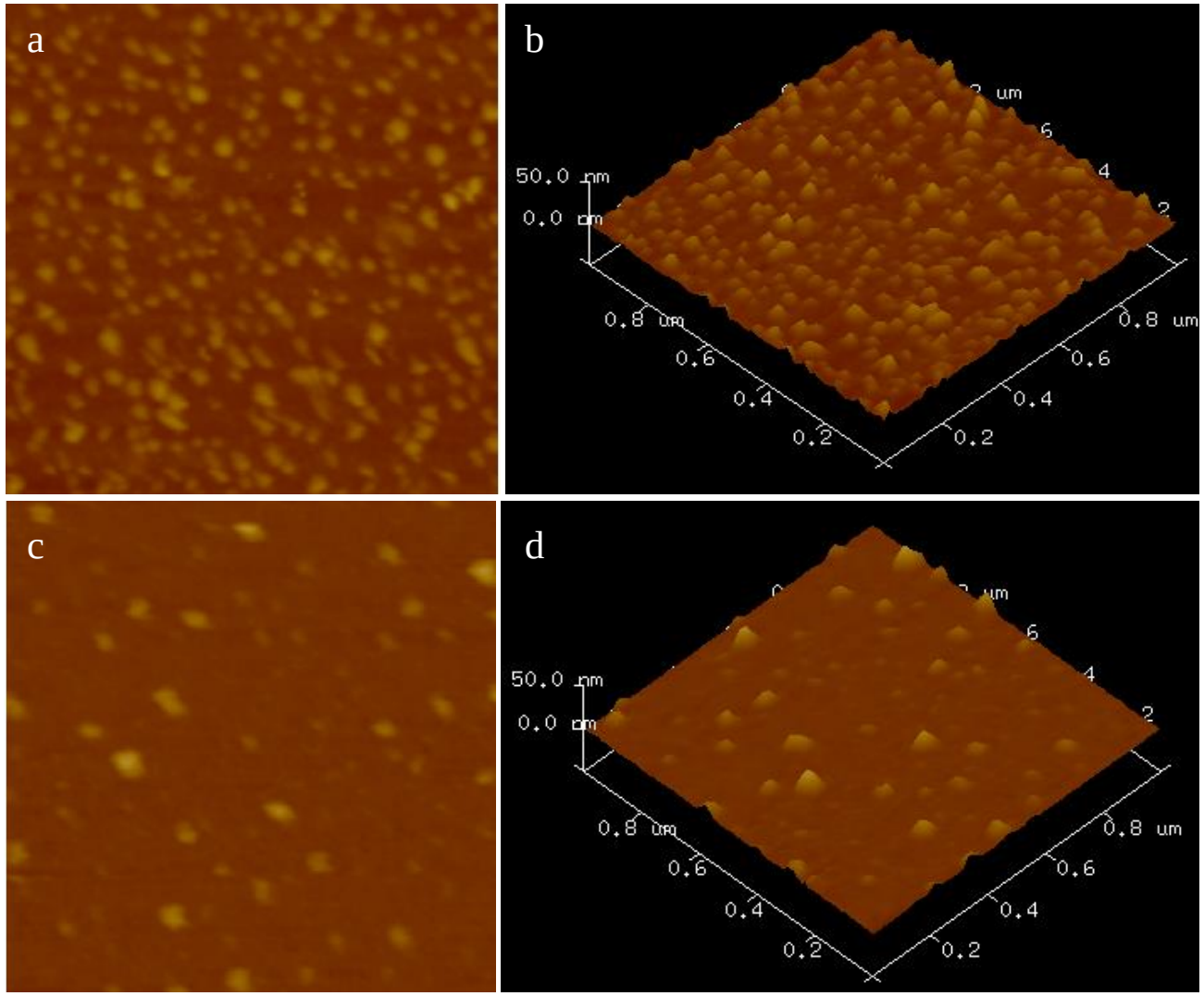
a
b
50.0 nm
0.0 nm
0.8 um
0.6
0.4
0.2
0.8 um
0.6
0.4
0.2
c
d
50.0 nm
0.0 nm
0.8 um
0.6
0.4
0.2
0.8 um
0.6
0.4
0.2

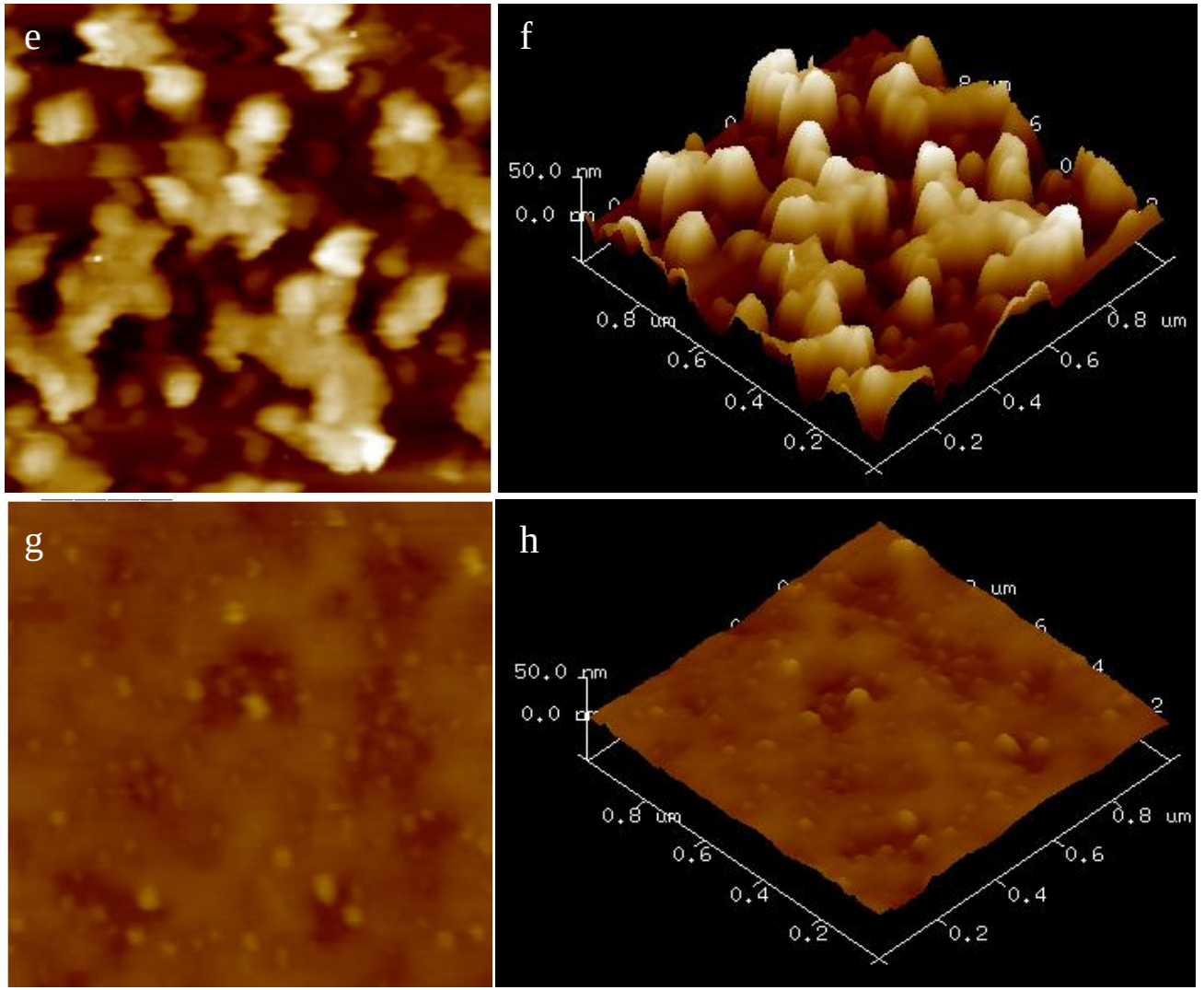

Figure 4.26 2-D images of nano-patterned a. silicon, c. TiO_2, e. a-C:H and g. ta-C surfaces incubated with diluted plasma (diluted factor 1:10) for 1hour at 37 degrees. Corresponding 1µm^2 3-D height analysis is presented on the right in b, d, f, h, respectively.

	Flat	**Nano-patterned**
Silicon	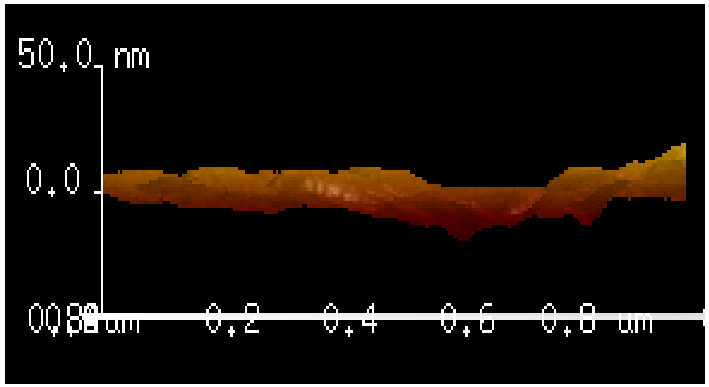	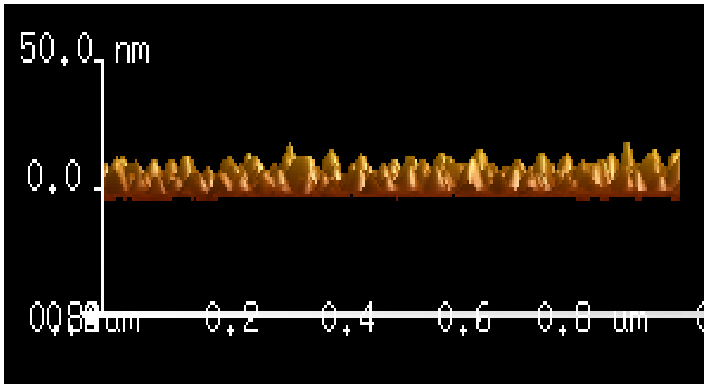
TiO_2	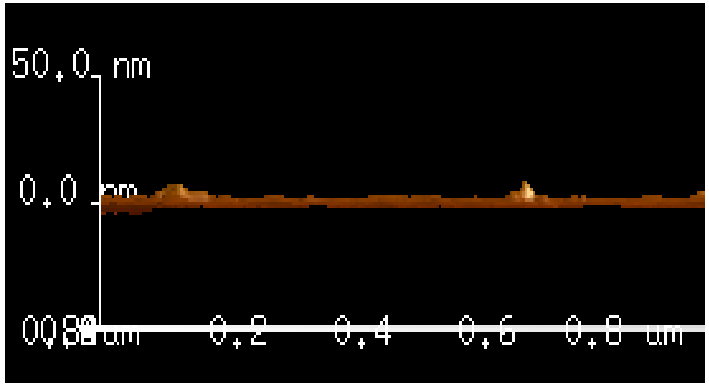	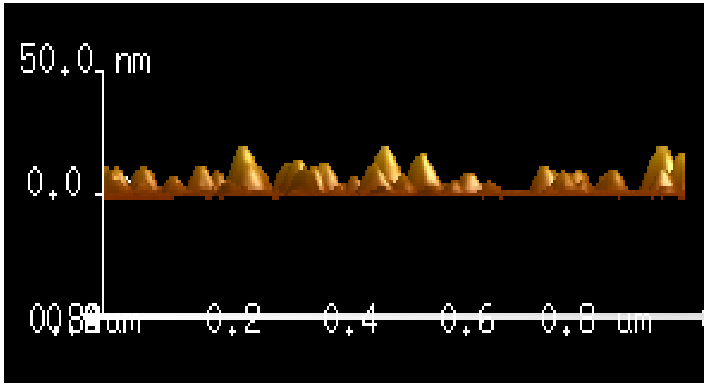

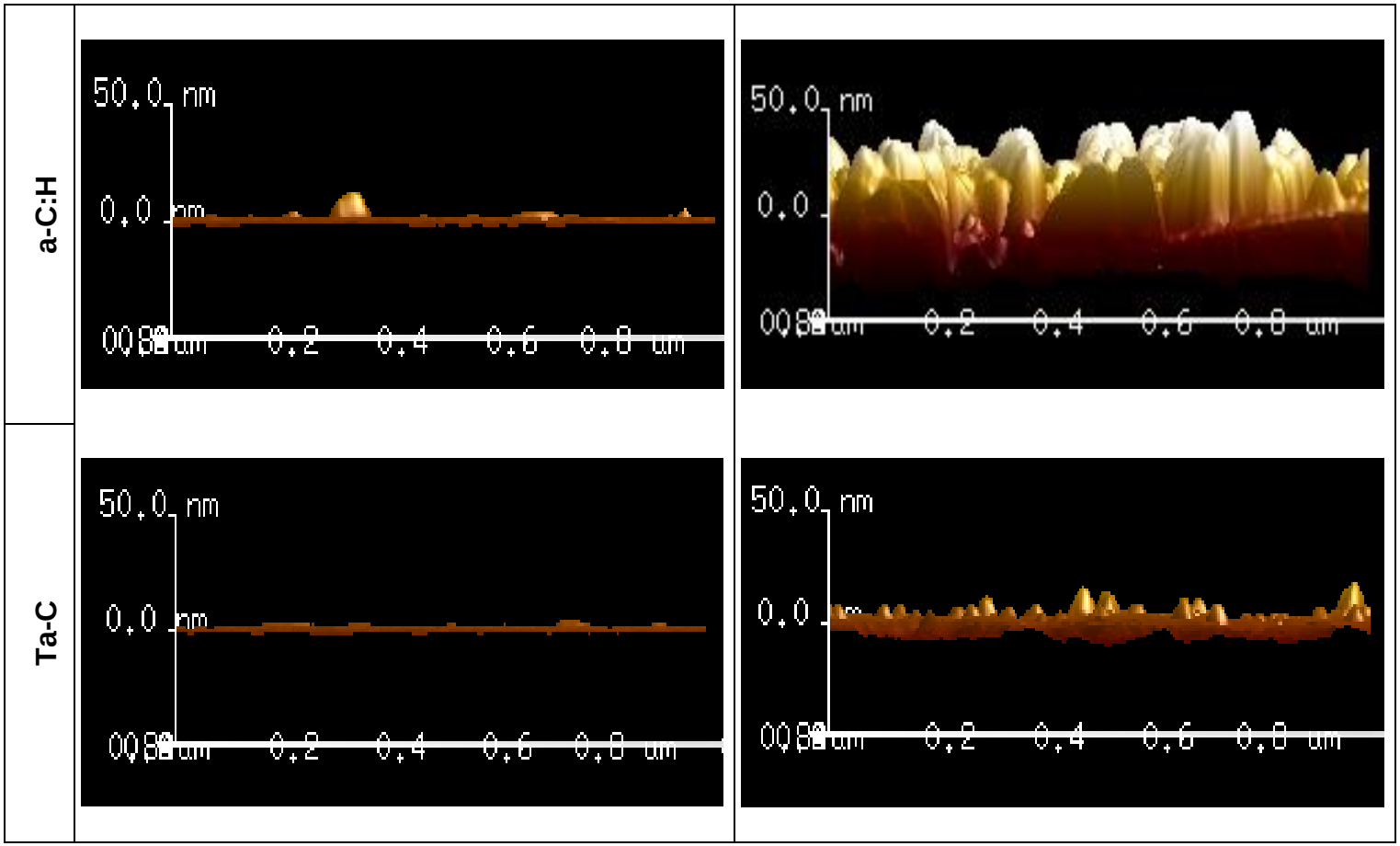

Figure 4.27 1µm^2 roughness profiles of flat and nano-patterned silicon, TiO_2, a-C:H and ta-C surfaces pre-adsorbed with diluted plasma (dilution factor 1:10), as analysed using AFM.

Though AFM graphs provide insight into overall serum protein packing on various surface chemistries and topographies, individual protein conformations of the adsorbed serum layer were not easily deductible.

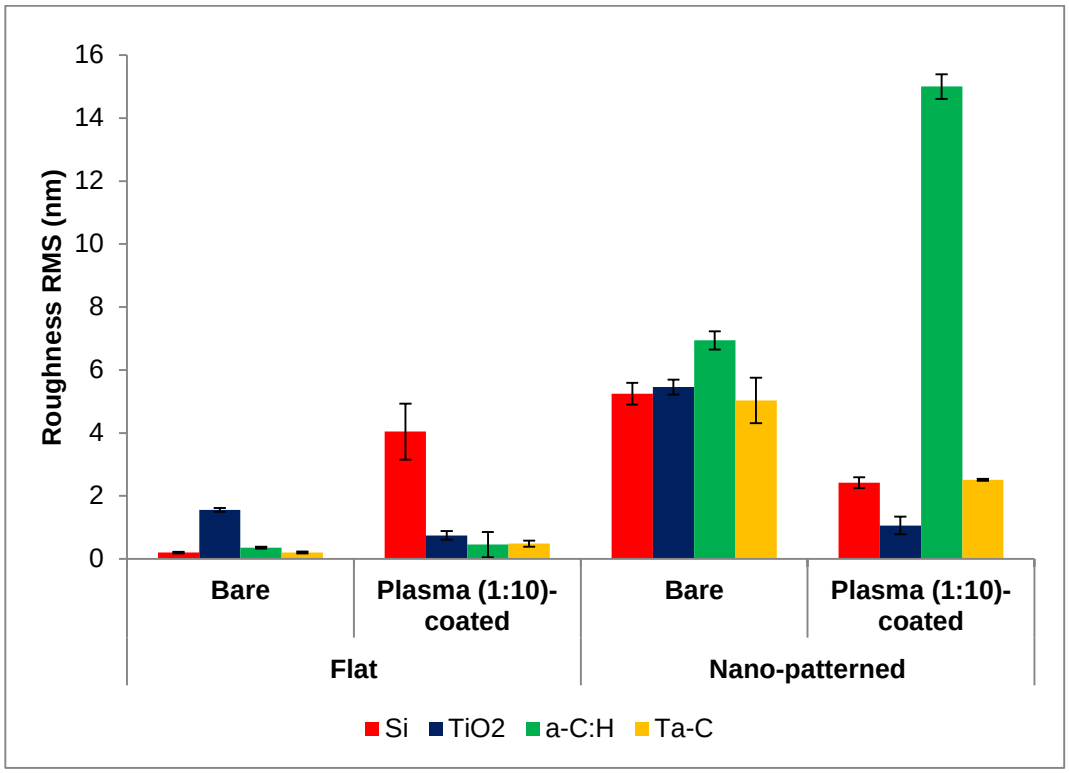

Figure 4.28 A comparison of roughness values (RMS) between flat and nano-patterned surfaces in the presence and absence of plasma proteins.

4.3.4 QCM-D

QCM-D is a quantitative tool that uses real time analyses to determine the interaction between flat QCM crystal coated with silica, TiO_2 and a-C:H, and, serum proteins such as; fibrinogen (Fg), albumin (BSA) and plasma (diluted in DPBS, 1:10 dilution factor). Ta-C surfaces sustained significant delamination of the coated film, from the weak bonding between the silica under-layer and the ta-C film, and consequently were retired from all further QCM-D experimentations. The acquired frequency (f) and dissipation (D) curves were manipulated using Voigt based models to provide insight into the conformation, concentration, viscosity and rate of adsorption of

irreversibly bound proteins on the surfaces. Each experiment was performed in triplicate, although, only one indicative replicate is shown in Figure 4.29, Figure 4.32(a) and (b), and Figure 4.33.

a. Albumin

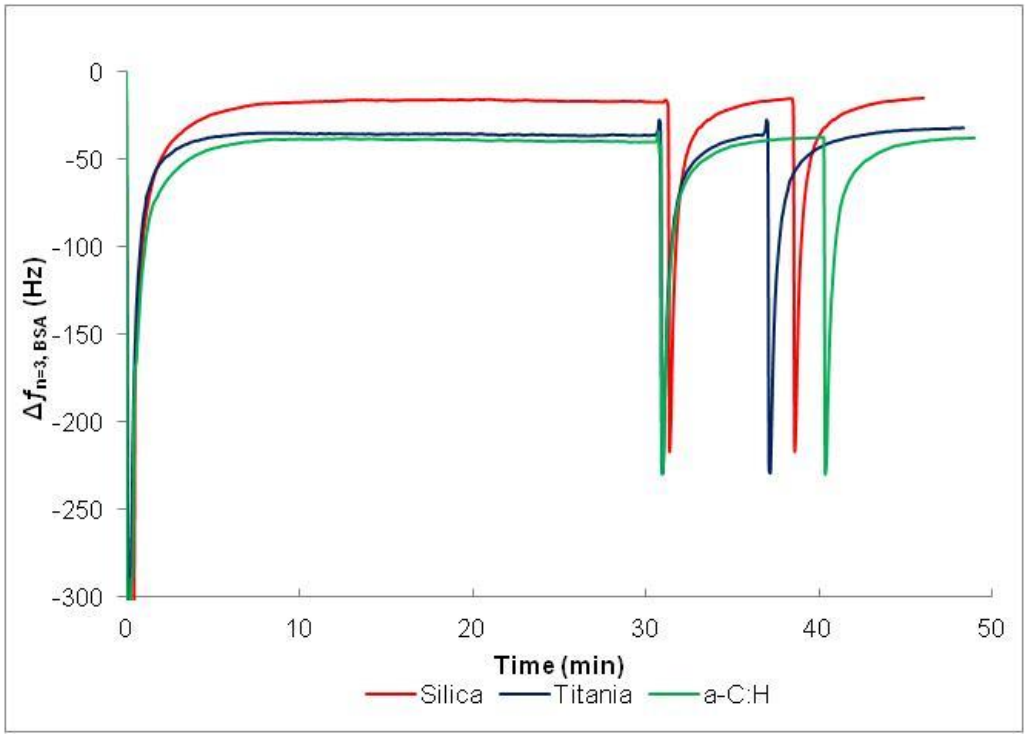

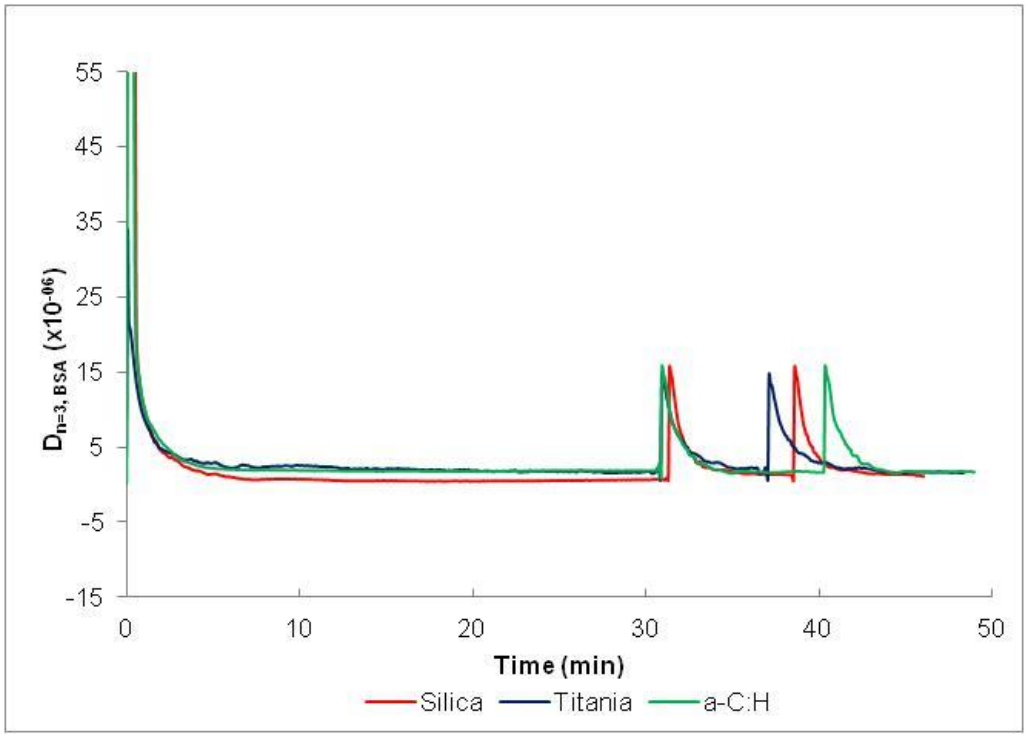

b. Fibrinogen

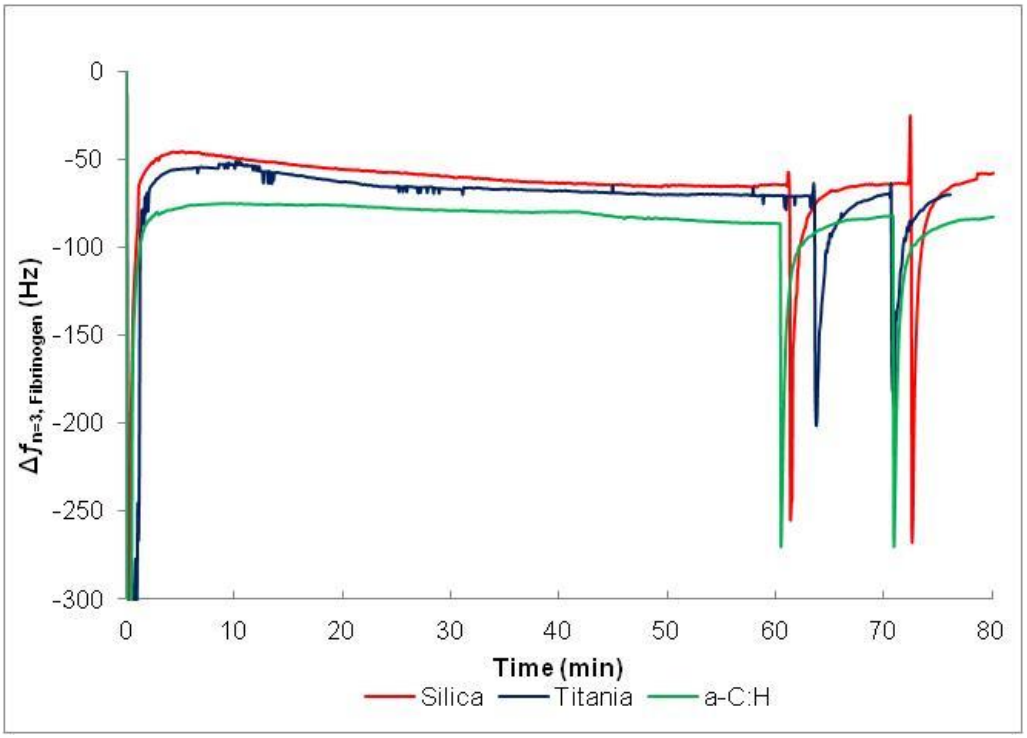

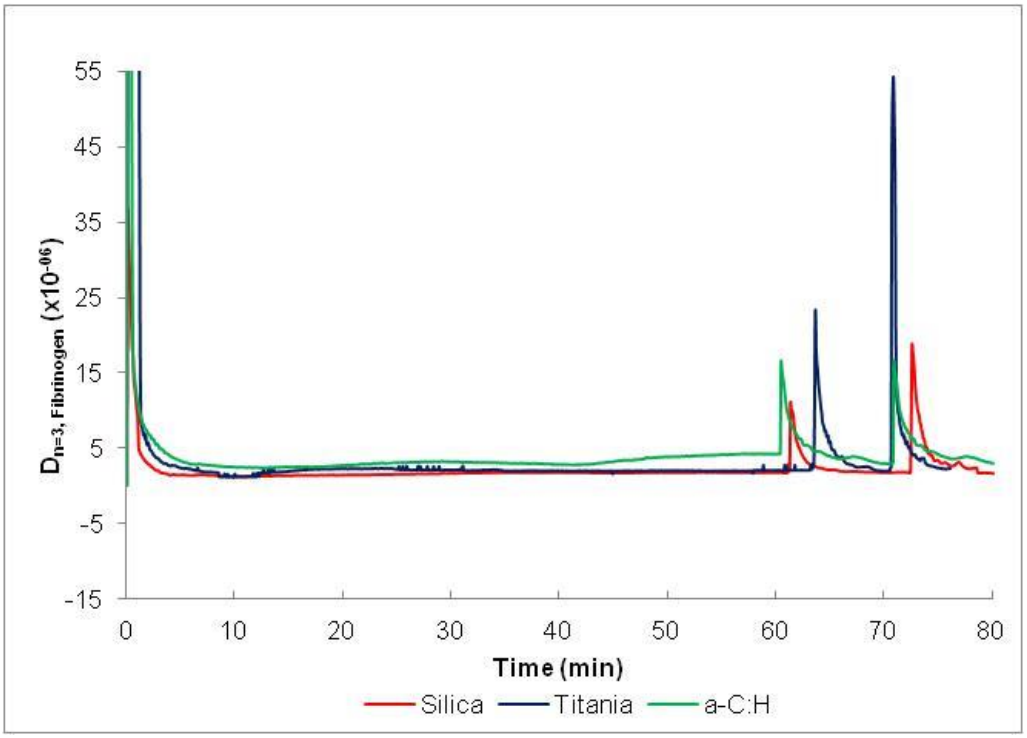

c. Plasma Proteins

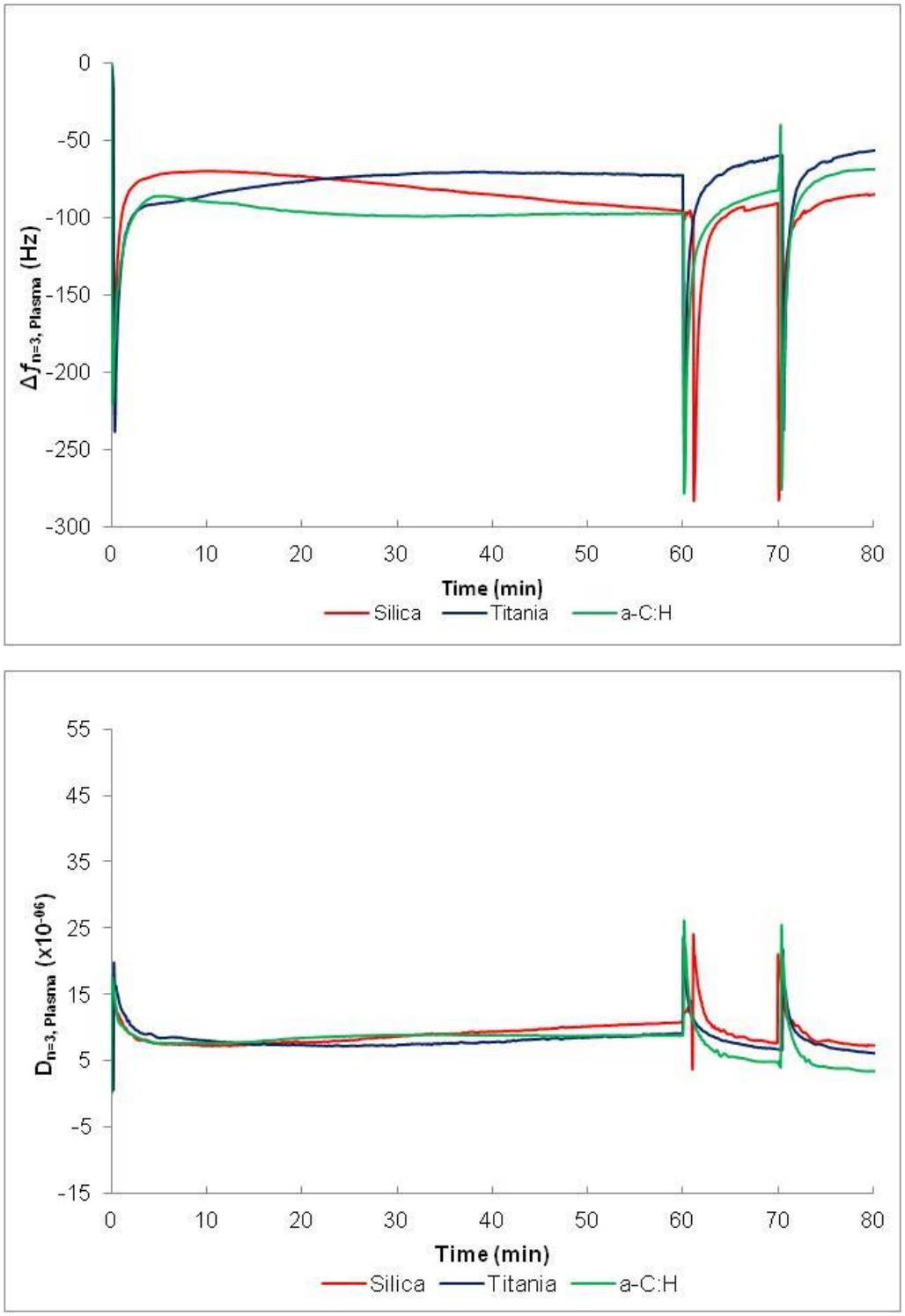

Figure 4.29 Comparison of real time a. albumin, b. fibrinogen and c. plasma (diluted 1:10 in DPBS) interaction on silica, titania (TiO_2) and a-C:H surfaces, as determined using QCM-D. The graphs display changes in frequency (Δf) and dissipation (D) as a function of time for the third overtone (15MHz).

Figure 4.29 (a), (b) and (c) shows in real time, the changes in frequency (*f*) and energy dissipation (D) obtained for the third overtone (n=15MHz) for albumin (BSA), fibrinogen (Fg) and plasma adsorption, respectively, onto silica, TiO_2 and a-C:H surfaces. A baseline was established by preconditioning the surfaces with DPBS. The crystals were incubated for either 30minutes for BSA or 1hr for fibrinogen and plasma solutions. Time t=0min denotes the onset of protein exposure. Any unbound proteins were washed away during the post-incubation DPBS rinses lasting approximately 10minutes each. The experiments were temperature controlled to at 37 ± 0.2ºC and measurements were obtained for 4 different overtones; 5, 15, 25 and 35MHz.

The protein incubated surfaces showed slight variations in *f* and D at different overtones. The differences in various overtones are caused by frequency dependence on the visco-elastic properties of the film [457] where an overtone acts as a function of penetration depth of the viscous adlayer (total distance out from the quartz crystal). A lower overtone detects properties of the furthest region of the protein layer and consequently is the least stable. The negative in the *f* is indicative of the damping effect caused by the adsorbed mass where a more negative *f* value is attributed to increased mass uptake. D values are indicative of the visco-elastic properties of the surface where a large increase in dissipative energy is indicative of a shift from a stiff, rigid, low viscoelastic surface to a highly viscoelastic surface causing the proteins to form a non-rigid bond with the crystal surface. An increase in D is also indicative of the amount of energy required to displace the proteins, where a higher D value indicates soft adlayer which requires less energy to displace the protein [458].

To allow for a direct comparison of *f* shifts between protein solutions and various surfaces, overtone n=3 (15MHz) was chosen. This overtone exhibited a good compromise between stability and sensitivity and as such consistently presents smooth curves of frequency and dissipation changes with minimal aberrations. The final D value for the third overtone is shown in Figure 4.30(b).

Within the first 5 minutes a significant drop in f was observed after which the curve plateaued over the remaining incubation period. Minor changes in frequency during the washing phases indicate that the majority of the proteins were irreversibly adsorbed onto the surfaces.

Since albumin reaches saturation levels much sooner than fibrinogen and plasma; surfaces were exposed to albumin for only 30minutes while the other two protein solutions were incubated for 60minutes. Comparing f shifts between the three proteins solutions it is evident albumin (BSA) exhibited a smaller shift in f and D when compared to fibrinogen, corroborating with previous studies [189, 218, 459-462], while plasma showed the highest change in values.

Amongst the three surfaces, it is evident a-C:H exhibited the highest f shift in the presence of all three solutions. TiO_2 surfaces showed similar frequency response curves to a-C:H and silica in the presence of albumin and fibrinogen, respectively, while exhibiting a concave like f profile during plasma protein adsorption. While adsorbing plasma, TiO_2 crystals exhibit a sudden drop followed by a slow increase in f values. The D values however, slowly increase suggesting that upon contact with the surface, the plasma proteins immediately form a densely populated rigid layer that slowly increases in viscosity. After the first few minutes, a dynamic interaction between the surface and the adlayer causes the replacement of low-affinity bound proteins with water molecules, as shown by the steady increase in D values. Frequency f curves reached maximum adsorption points sooner on silica surfaces while exhibiting the smallest shift in f and D on fibrinogen and albumin. Frequency shift associated with plasma protein adsorption did not plateau.

As mentioned above, the adsorbed mass detected by QCM-D is not only attributed to protein adsorption but also to the uptake of water coupled to protein. Ideally when the D value typically reaches above $1x10^{-6}$ the film is said to be too soft to function as a fully coupled oscillator of the crystal sensor [463], i.e. a linear relationship between f shift and mass uptake cannot be established. Since the changes in D exceed this value, it is therefore crucial to use the Voigt model in this regime to

better estimate mass adsorption by considering changes in dissipative energy. Mass estimates of irreversibly adsorbed protein hydro-dynamically coupled to water molecules are shown in Figure 4.30(a) and its corresponding D values on Figure 4.30(b).

When comparing the three protein solutions it is evident that fibrinogen and plasma exhibited saturation mass in the range of 900-1800ng/cm^2 and 1300-2800ng/cm^2, respectively, when compared with albumin (300-900ng/cm^2). Between the three surfaces, a-C:H sustained the highest mass uptake of 849ngcm^2, 1706ng/cm^2 and 2707ng/cm^2 on albumin, fibrinogen and plasma, respectively. Silica exhibited the lowest mass uptake on albumin and fibrinogen surfaces with, 306ng/cm^2 and 929ng/cm^2, respectively, while TiO_2 adsorbed the lowest amount on plasma coated surfaces with 1328ng/cm^2.

Closer analyses of these graphs indicate that on albumin and fibrinogen, the total change in dissipation is relatively proportional total increase in mass; this is not the case for plasma coated surfaces. Plasma-coated a-C:H surfaces exhibited a lower dissipation value than silica while facilitating a greater adsorbed mass which suggests a lower concentration of plasma adsorption on silica surfaces rendering the adsorbed layer highly viscous. This may be due to the initial stage of plasma clotting caused by the coagulation factors in plasma.

Concentration of the adsorbed proteins was calculated by dividing the mass of the adsorbed albumin or fibrinogen adlayer on the three surfaces by their respective molecular weights of 64.5kDa and 340kDa, respectively. The results are shown in Figure 4.31. Although, albumin exhibited a smaller mass uptake its relative protein concentration was significantly higher than fibrinogen. This is because fibrinogen is relatively larger in size than albumin, and consequently requires fewer molecules for complete coverage of the crystal surface. These results corroborate with ELISA results from Section 4.3.1.

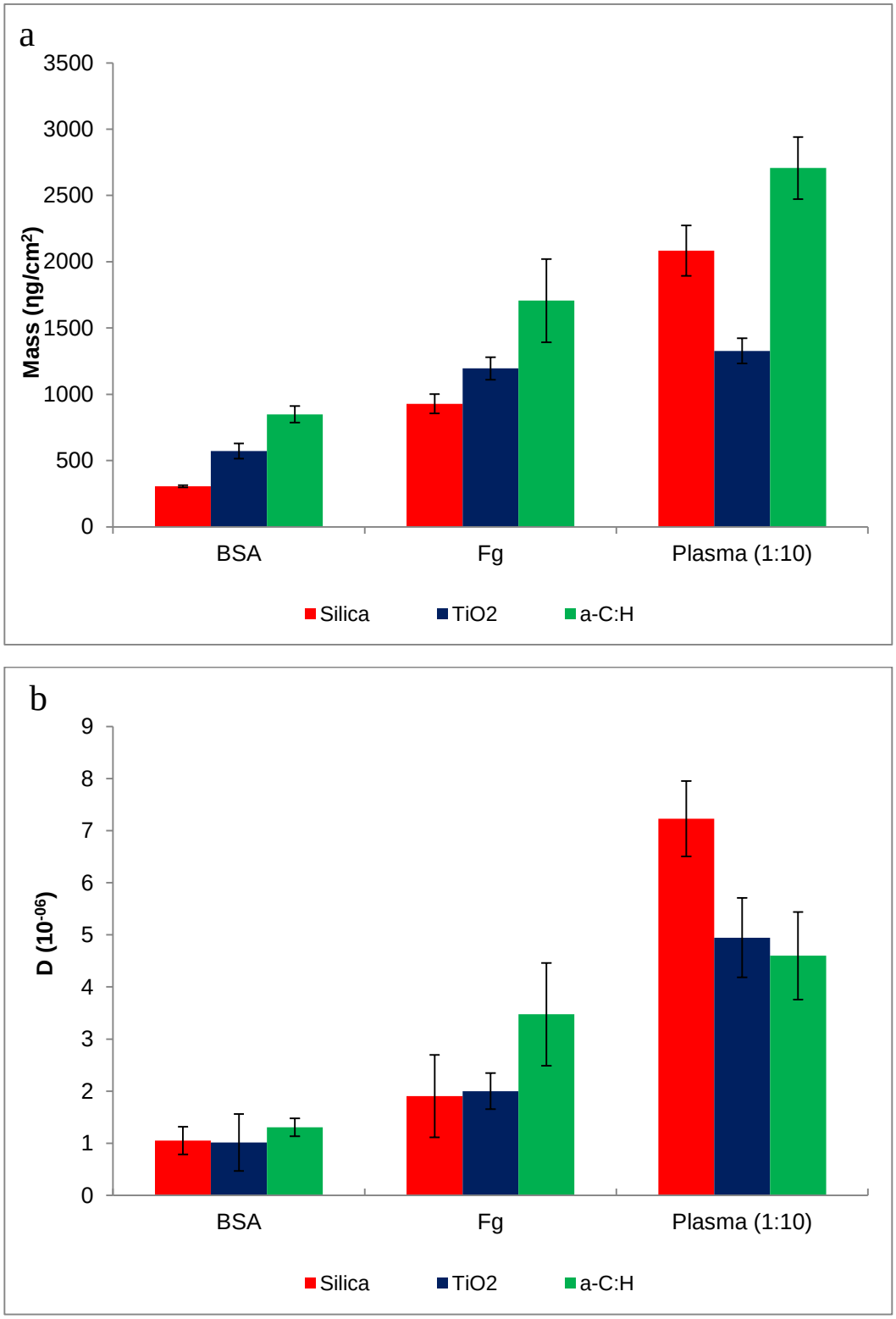

Figure 4.30 Comparison of a. adsorbed mass, as calibrated from the Voigt model and b. dissipation detected by the QCM-D of albumin, fibrinogen and diluted plasma proteins on silica, TiO_2 and a-C:H surfaces. Results were computed from raw data for the third overtone (15MHz). Error bars: SD (n=3)

Furthermore, these concentration values do not take into consideration the ratio of water molecules adsorbed along with the proteins. As the adsorbed mass encompasses both water and protein, the exact ratio of water to protein adsorption needs to be considered. A study conducted by Hook et al, in 2002 [461] comparing mass uptake values between optical waveguide lightmode spectroscopy (OWLS), ellipsometry (ELM) and quartz crystal microbalance (QCM-D) demonstrated that QCM-D over estimated the mass of albumin uptake by a factor of 1.75 and fibrinogen by a factor of 2.8-3.2. Mass values obtained for fibrinogen (Figure 4.30 (a)) fall within the theoretical monolayer mass estimates, as the theoretical side-on monolayer coverage of fibrinogen reported was approximately 140 ng/cm^2 while the close packed end-on monolayer is 1000 ng/cm^2 which can be recalculated to approximately 420 and 3000 ng/cm^2 respectively for QCM-D measurements. Subsequently, the results shown in Figure 4.31 should be corrected by these factors to provide a better estimate of the concentration of adsorbed proteins. However, while these ratios can be used as a guide to estimate the relative concentration of the adsorbed protein they cannot provide exact concentration values. The experiments conducted by Hook were primarily on TiO_2 surfaces and level of protein hydration varies between surface chemistries and consequently the overestimation of mass by QCM-D will also differ.

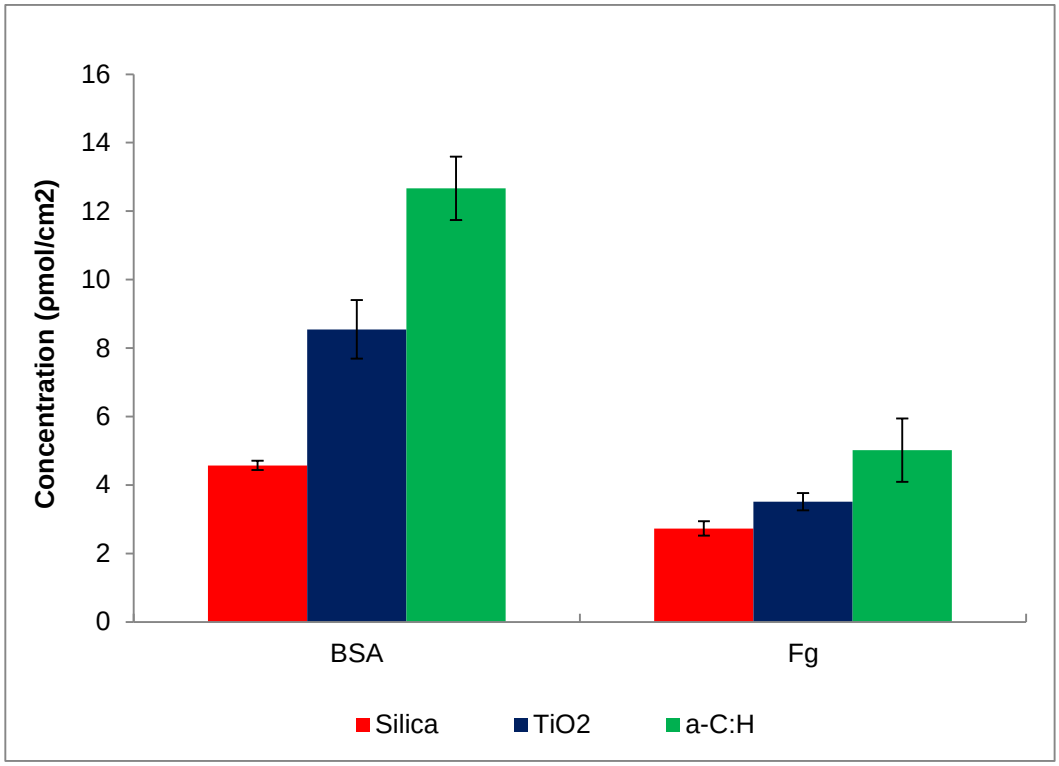

Figure 4.31 Concentration of fibrinogen and albumin adsorbed on silica, TiO_2 and a-C:H, as determined using QCM-D. Protein estimates were derived from Voigt modelling of frequency and dissipation curves for the third overtone (15MHz). Error bars: SD (n=3)

The final dissipation versus frequency ratio provides insight into the viscosity of the adsorbed layer and conformational changes in the protein. Figure 4.32(a) and (b) shows real time changes in the dissipation to frequency ratio after fibrinogen and plasma adsorption on silica, TiO_2 and a-C:H surfaces while Figure 4.32(c) shows the stable values measured after the DPBS rinses for the third overtone.

$\Delta D/\Delta f$ curves indicate the level of hydration where a higher ratio caused primarily by a high dissipation values per unit shift in frequency, is indicative of a more viscous layer. After the instantaneous adsorption of proteins upon contact with the surface, the dissipation versus frequency plots for silica and a-C:H surfaces interacting with fibrinogen and plasma protein solutions exhibited a steady decreases in frequency and while increasing in dissipation values, as shown by the black arrows. This suggests that throughout the measurement period there is a constant dynamic interaction between the adsorbed layer and the supernatant where the proteins rearrange on the surface by breaking and forming protein bonds and consequent

hydration shells to accommodate more proteins. Unlike silica and a-C:H, fibrinogen adsorption on TiO_2 appears to be initiated by a rapid adsorption of water molecules as well as protein followed by strong dispelling of water molecules from the fluidic layer causing a significant decrease in dissipation energy and a small change in frequency. The slightly more rigid layer then interacts dynamically with dissolved fibrinogen molecules continuously throughout the rest of the measurement period in a manner similar to silica and a-C:H surfaces described above. Plasma proteins on TiO_2, on the other hand, competitively bind into a rigid layer initially followed by the detachment of water molecules and weakly bound proteins, possibly due to their low affinity to the surface. The removal of weakly bound proteins is explained by the drastic increase in frequency values.

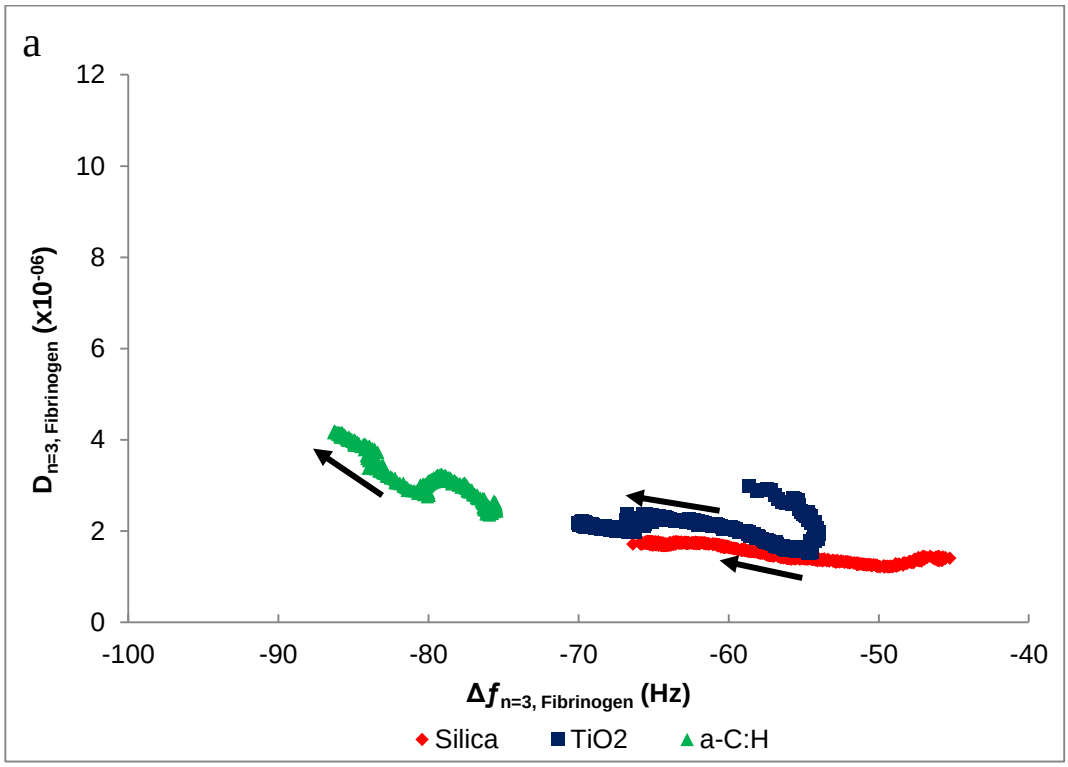

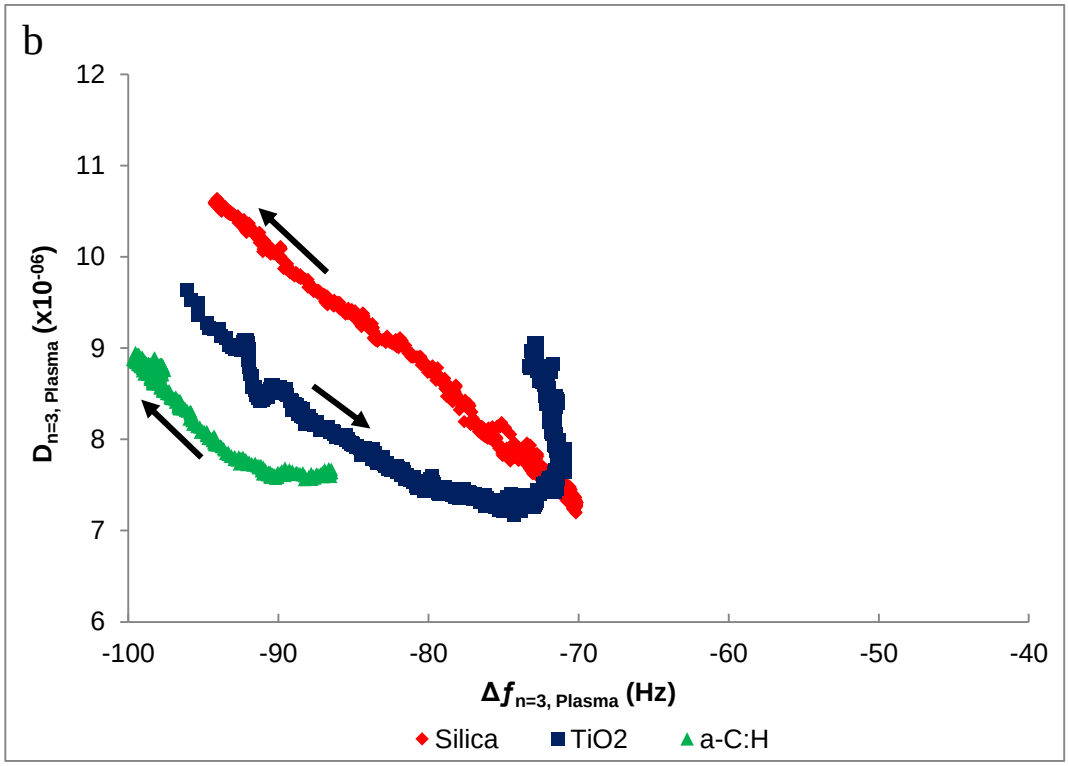

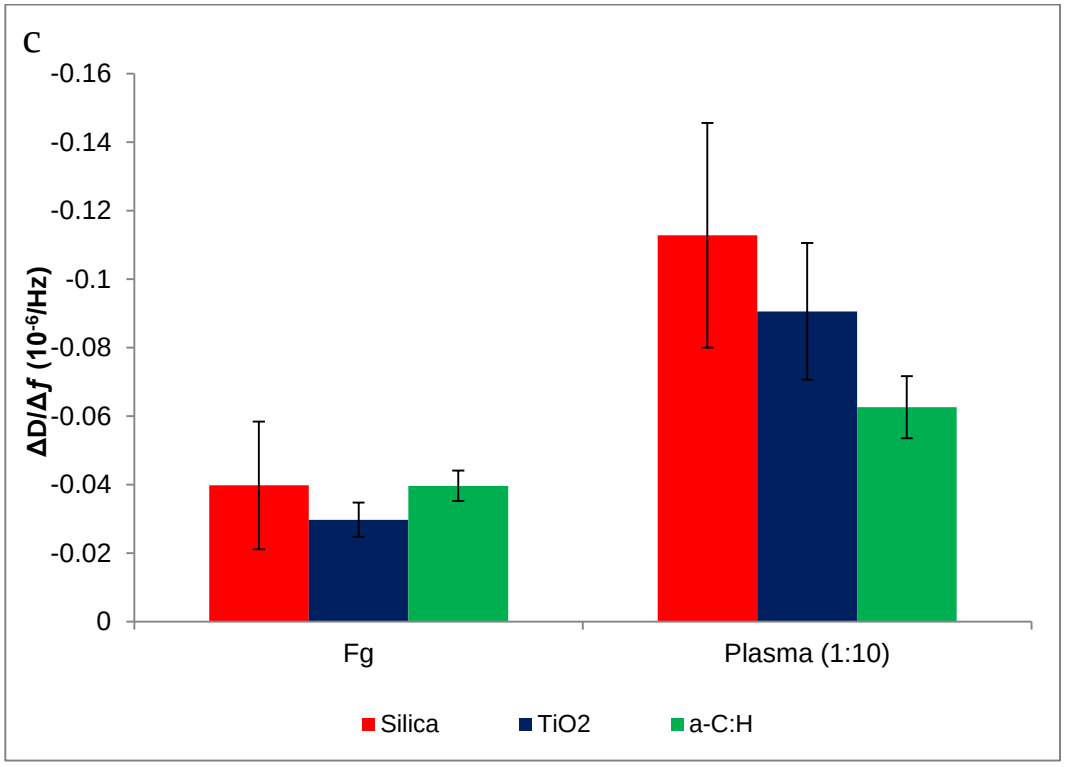

Figure 4.32 Dissipation versus frequency curves (third overtone; n=3) for a. fibrinogen, b. plasma and c. final values of dissipation vs frequency ratio for fibrinogen and plasma proteins on silica, TiO_2 and a-C:H surfaces, as determined by QCM-D. Black arrows represent the direction of increasing time.

After a few minutes an sudden influx of water molecules and some proteins is evidenced by the sharp change in curve shifting to an increase in dissipation values with small increase to frequency values. Furthermore, the results in Figure 4.32(c) indicate that when compared with plasma, fibrinogen proteins on the three surfaces formed a relatively more rigid adlayer. Between the three surfaces it is evident that plasma adsorbed on silica surfaces formed a highly viscous adlayer, while a-C:H exhibited a more rigid film. Variances in fibrinogen coated surfaces seemed minimal, of which TiO_2 exhibited a slightly more rigid film.

The kinetics of fibrinogen and plasma adsorption on silica, TiO_2 and a-C:H surfaces was further investigated by analysing the rate of mass change as a function of adsorbed mass, as shown in Figure 4.33.

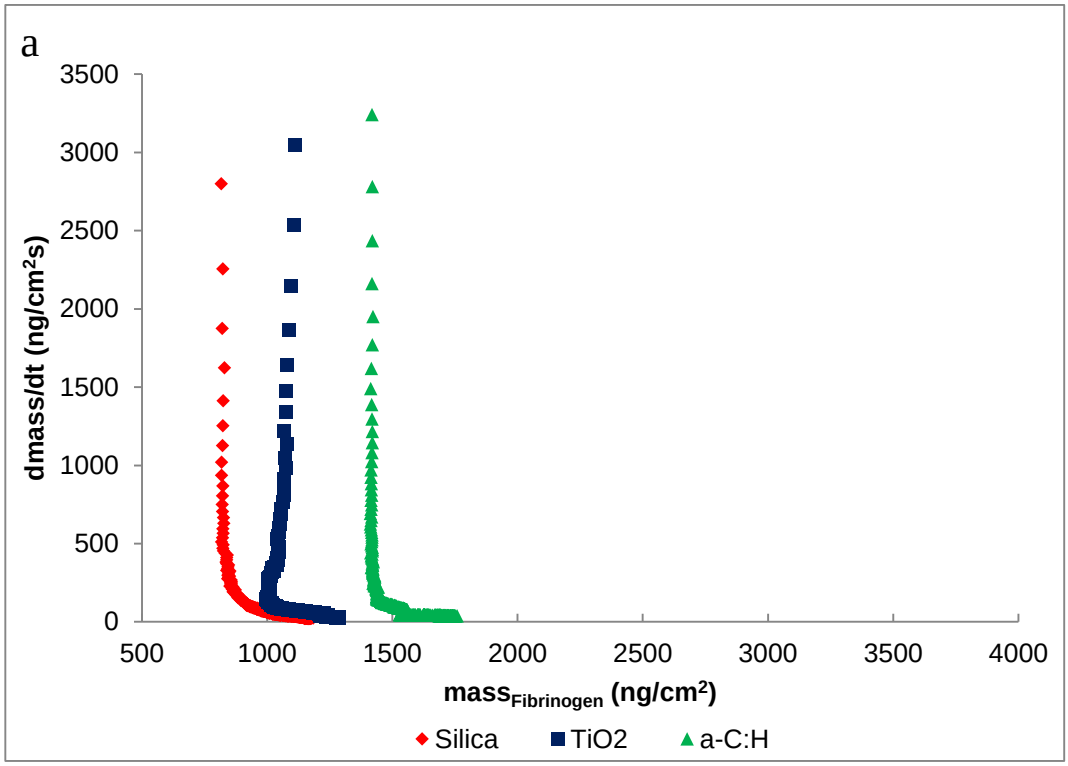

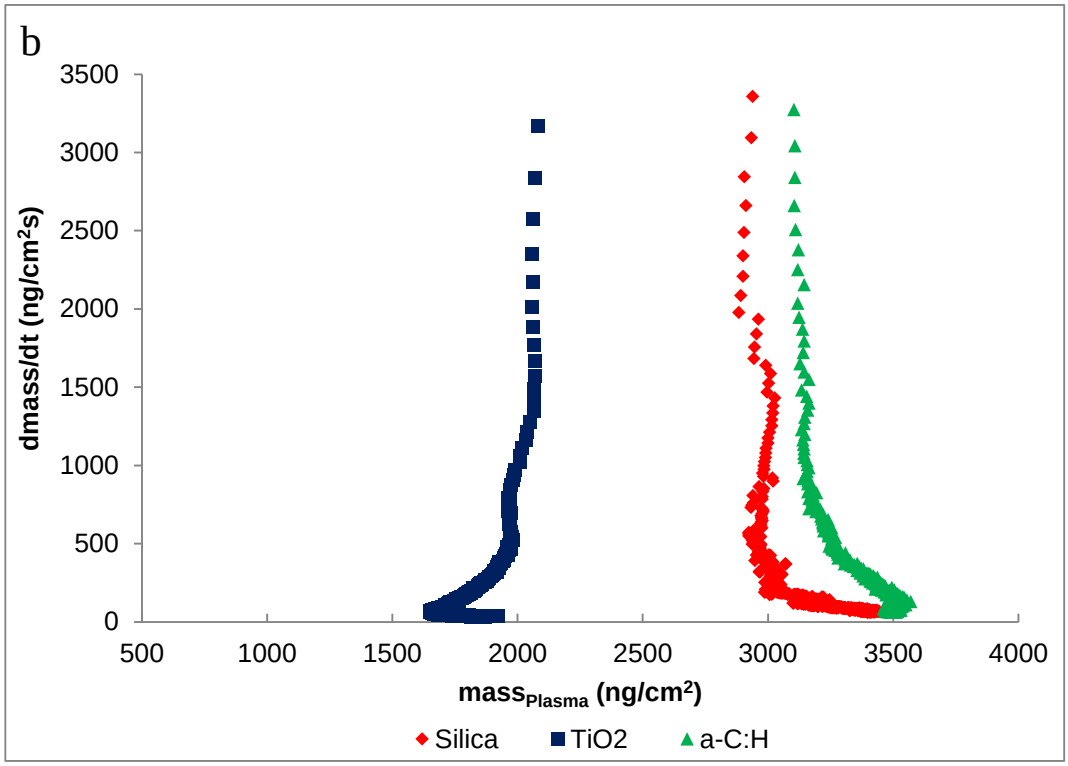

Figure 4.33 Comparison of adsorption rates of a. fibrinogen b. plasma (1:10 dilution) on silica, TiO_2 and a-C:H surfaces, as determined using QCM-D. Mass estimates were derived from Voigt modelling of frequency and dissipation curves for the third overtone (15MHz). Error bars: SD (n=3)

The gradient of curve is steeper during the initial phases of adsorption suggesting that fibrinogen upon contact with the surface is rapidly adsorbed onto all three surfaces after which the rate of adsorption decreases and saturates near zero. Rate of saturation occurs slowly on silica surfaces. A-C:H surfaces followed by TiO_2 exhibited a higher initial rate of adsorption than silica surfaces, suggesting that fibrinogen shows a higher binding affinity towards a-C:H surfaces. This may also explain the increased mass uptake on a-C:H surfaces. Further, rate of mass uptake versus mass on all three surfaces followed a concave relationship suggesting that the bound fibrinogen rearranged upon adsorption. This corroborates with results from Figure 4.32. While plasma interaction on silica and a-C:H surfaces follow similar adsorption curves to the fibrinogen bound surfaces, TiO_2 responded differently. After the initial rapid adsorption of proteins, plasma adsorbed on TiO_2 surfaces desorbed from the surfaces at a lower rate than that of the initial rate of adsorption, described by decrease in adsorbed mass. Following protein de-attachment and possible changes in protein conformation and its arrangement on the surface, the surface continues to

adsorb more proteins from solution at a lower adsorption rates subsequently saturating above zero. While the maximum rate of adsorption was similar between the plasma adsorbed and fibrinogen adsorbed surfaces, the nature of the adsorption profile supports the notion that kinetics behind protein adsorption is dependent on surface chemistry and the adsorbed proteins.

4.4 Summary

When fibrinogen and albumin were in a solution by themselves, ultra-flat test substrates, with surface roughness in the sub-nano-meter range, have been shown to exhibit a higher affinity to albumin than fibrinogen. However, when albumin was in a competitive solution with fibrinogen at physiological concentrations (ratio 10:1, albumin to fibrinogen), not only was there a decrease in adsorption of both proteins but albumin's affinity to the test surfaces became less than that of fibrinogen. This was especially evident on ta-C and a-C:H surfaces, which displayed increased concentrations of fibrinogen adsorption during competitive binding, while the ratio of albumin to fibrinogen adsorbed on TiO_2 surfaces remained unaltered. This shows that the adsorption of selective proteins is implicitly linked to the surface chemistry of the biomaterial.

The level of platelet binding region presented on fibrinogen remained unaffected even though the concentration of adsorbed fibrinogen decreased in the presence of albumin. By changing the surface nano-topography by adding nano-patterns, the overall surface roughness of the test substrates was increased to 5-10nm. This caused an increase in the adsorption of fibrinogen proteins and the proteins were found to form multiple layers, saturating in the grooves between the peaks formed by the nano-patterns. While it was evident that the morphology of adsorbed proteins were not confined to a particular conformation or orientation, it was found that the tri-nodular fibrinogen adsorbed on nano-patterned surfaces predominantly aligning themselves against the slope of the nano-patterns, decreasing the overall surface roughness, whereas, fibrinogen adsorbed on flat surfaces were shown to align flat

against the surface following side on conformation. Furthermore, fibrinogen proteins adsorbed on nano-patterned surfaces presented increased the level of platelet binding domains, where a-C:H and ta-C exhibited the highest % increase when compared with the flat surfaces.

Flat surfaces lacked the physical cues necessary to behave as focal adhesion points for plasma proteins other than albumin or fibrinogen to adhere. As such, plasma proteins formed a dense and highly viscous adlayer, when compared with the rigid albumin and fibrinogen protein coat, which was necessary for the localisation and adhesion of other surface tethering proteins. Further, when comparing the kinetics of fibrinogen and plasma protein adsorption, it was evident that fibrinogen and other plasma proteins adsorbed rapidly on a-C:H surfaces than TiO_2 during the initial stages of protein adsorption indicating a higher binding affinity between the proteins and a-C:H. However, during the latter stages of adsorption it was noticed that the rate of protein adhesion decreased to near zero while adsorbed mass continued to increase suggesting a dynamic interaction between the surface and fibrinogen and/or plasma proteins causing the rearrangement of the proteins upon adsorption.

Denaturing of fibrinogen protein on the adsorbed surfaces and its assumed conformation for platelet binding was typically dependent on a combination of surface chemistry, surface nano-topography as well as its interaction with other plasma proteins. The exposure of fibrinogen α-chain, platelet binding domain and γ-chain was affected by varying the surface chemistry of the thin film, though not to the same extent as pre-coating the substrates with plasma proteins. The presence of other plasma proteins can drastically reduce the availability of platelet binding domains exposed on fibrinogen adsorbed from plasma, implying a favourable interaction between plasma proteins and biomaterial surfaces in reducing the exposure of fibrinogen's platelet binding domain for platelet $\alpha_{IIb}\beta_3$ receptor binding.

5 PLATELET ADHESION

5.1 Introduction

Platelet adhesion on implanted biomaterial surfaces and their subsequent spreading and aggregation are known to be crucial steps in the sequence of events leading to the formation of a haemostatic plug and thrombosis. Platelet membrane receptors from the β_1 and β_3 heterodimeric integrin families such as $\alpha_2\beta_1$ and $\alpha_{IIb}\beta_3$ receptors have been known to facilitate platelet adhesion on artificial surfaces through surface adsorbed proteins. As mentioned earlier, the receptors recognise and bind to adhesive plasma proteins such as fibrinogen, fibronectin, vitronectin, immunoglobulins and von Willebrand factor von Willebrand factor, to mediate the adhesion process. While $\alpha_2\beta_1$ integrins are receptors for collagen [464], $\alpha IIb\beta_3$ receptors bind to fibrinogen. Fibrinogen plays the prominent role in the adhesion process by binding its RGD tract and γ chain of the carboxyl (C)-terminal to GPIIb/IIIa ($\alpha IIb\beta_3$) integrins on the platelet surface [121]. This is led by a change in the platelet receptor conformation where the β-integrins shift from their low affinity to their high affinity state for adhesion and subsequent platelet spreading. Adsorbed fibrinogen, due to a conformational change upon adsorption, even at small concentrations of 7ng/cm^2 has been known to mediate $\alpha_{IIb}\beta_3$ receptor adhesion in both; its low and high affinity state [116, 117]. Platelet spreading and subsequent activation which occurs as a result of tight binding of platelets to the surface occurs as multiple focal contacts form with fibrinogen and other surface adsorbed proteins [122].

The haemocompatibility of a material is evaluated by its ability to resist this adhesion process and, as such, it is necessary to determine the adhesive properties of silicon, a-C:H, TiO_2, Ta-C coated flat and nano-patterned substrates by detecting the concentration and morphological characteristics of adhered platelets as well as the kinetics behind platelet adhesion.

In this chapter test substrates, pre-coated or devoid of serum proteins, were investigated for their role in platelet adhesion and aggregation using a combination of fluorescence microscopy, scanning electron microscopy (SEM), atomic force microscopy (AFM) and quartz crystal microbalance with dissipation technology (QCM-D). Platelet adhesion was further examined to evaluate the morphology of the adhered platelets including the degree of platelet spreading, the overall surface coverage and level of platelet aggregation. The sample substrates were initially subjected to a rigorous sterilization procedure, prior to being introduced into 12-well TCPS plates for platelet adhesion studies and the results obtained were compared with that of the bare substrates.

5.2 Results and Discussion

5.2.1 Morphology and concentration of surface-adhered platelets

Morphological characteristics as well as quantitative analysis on the number of adhered platelets are used to elucidate the cells' health and how well it responds to the chemistry and topography of the underlying substrate. As such, platelet interactions on the different substrata were visualised using a combination of fluorescence microscopy, SEM and AFM. Platelets were seeded on bare and protein pre-coated, flat and nano-patterned silicon, TiO2, a-C:H and ta-C substrates, for 1 hour at 37ºC. 50µg/ml of albumin (BSA) and fibrinogen (Fg) proteins were used along with diluted plasma (diluted in ratio 1:10, in DPBS). After washing, the surface bound platelets were either fixed and permeabilised before staining the actin filaments in red with rhodamine-phalloidin fluorescent dye to reveal any cytoskeletal developments at 500x magnification using fluorescence microscopy, or, fixed with 2% glutaraldehyde (in DPBS) before progressively dehydrating in graded ethanol baths and sputter coating with platinum for SEM analysis. The influence of fixatives

in decreasing the overall nano-resolution of platelet cytoskeleton was further elucidated from AFM imaging using model flat and nano-patterned a-C:H surfaces.

The role of fibrinogen protein and $\alpha_{IIb}\beta_3$ integrin in mediating platelet attachment on the flat substrates was also evaluated using fluorescence microscopy. Platelet solution was pre-incubated with 1µg/ml anti-human integrin $\alpha_{IIb}\beta_3$ F(ab) fragment antibody prior to seeding on protein pre-coated surfaces. The images were obtained using a fluorescence microscope at 500x magnification.

5.2.1.1 Flat Surfaces

The results below quantitatively and qualitatively describe the morphology and concentration of surface bound platelets adsorbed on flat substrates. Platelet adhesion on the flat substrates was investigated to identify the effect of surface chemistry and adsorbed proteins on the adhesion process. The extent of its influence was further analysed by observing changes in platelet morphology. Figure 5.1 shows the morphology of platelets using fluorescence microscopy 60 minutes post seeding. The red regions represent the actin filaments of the platelet cytoskeleton. When comparing the various surface chemistries, it is evident that TCPS served as the positive control, exhibiting a greater concentration of platelet adhesion and spreading under all four conditions. The level of platelet attachment and subsequent spreading varied drastically between protein pre-coated surfaces rather than surface chemistry, and clear and distinct differences in the conformation of individually adsorbed platelets were observed. In general, fibrinogen pre-coated and bare test substrates supported platelet spreading, while only minor levels of spreading was evident on the albumin and plasma surfaces. Albumin coated surfaces like the bare surfaces exhibited higher levels of platelet attachment. Albumin is often used to passivate blood contacting biomaterials and does not have the necessary peptide sequences for platelet integrin binding [215] and as such, platelet interaction on albumin coated surfaces, as found on all test substrates, might be the result of non-ligand specific, surface-receptor interactions.

a. Silicon

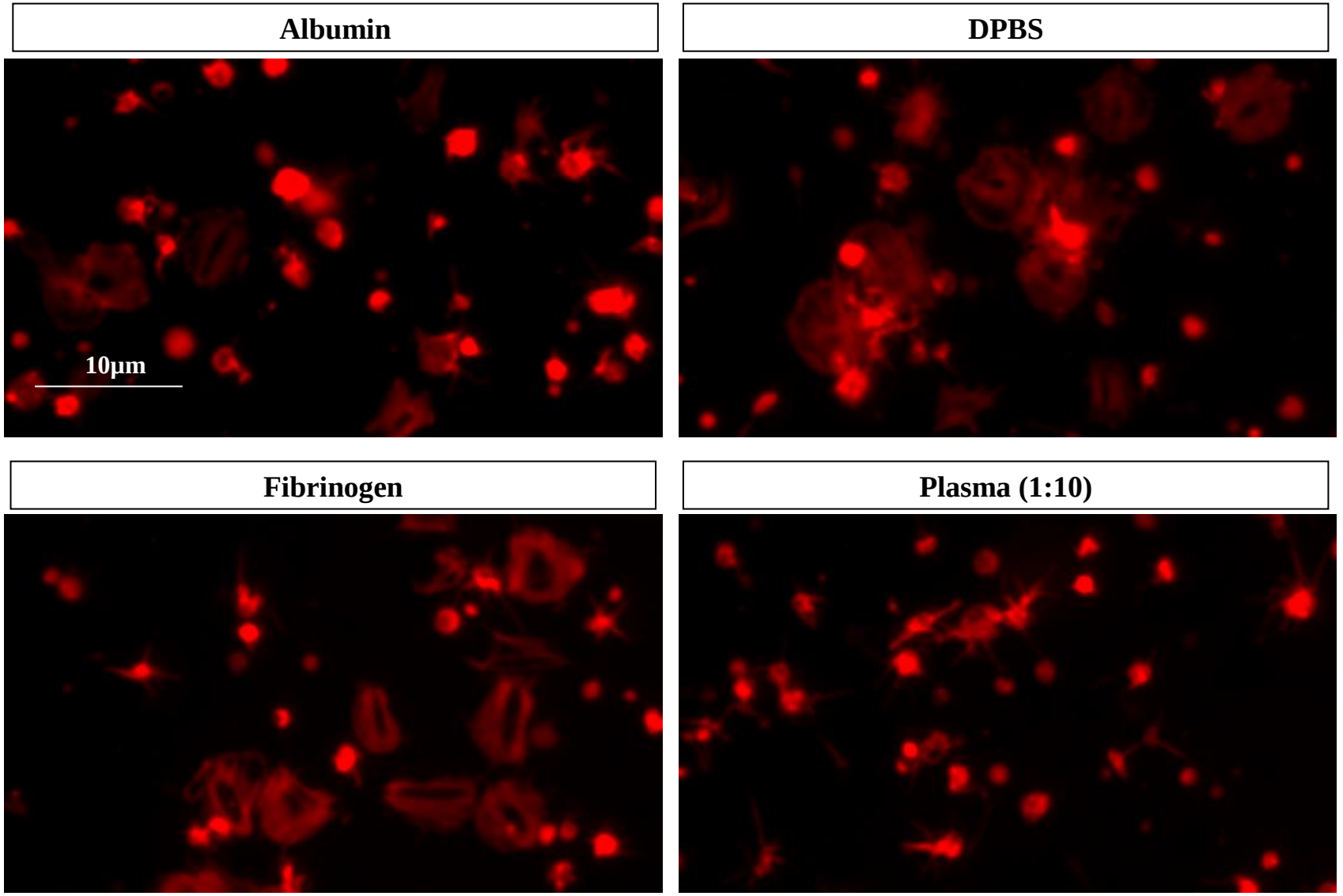

b. TiO_2

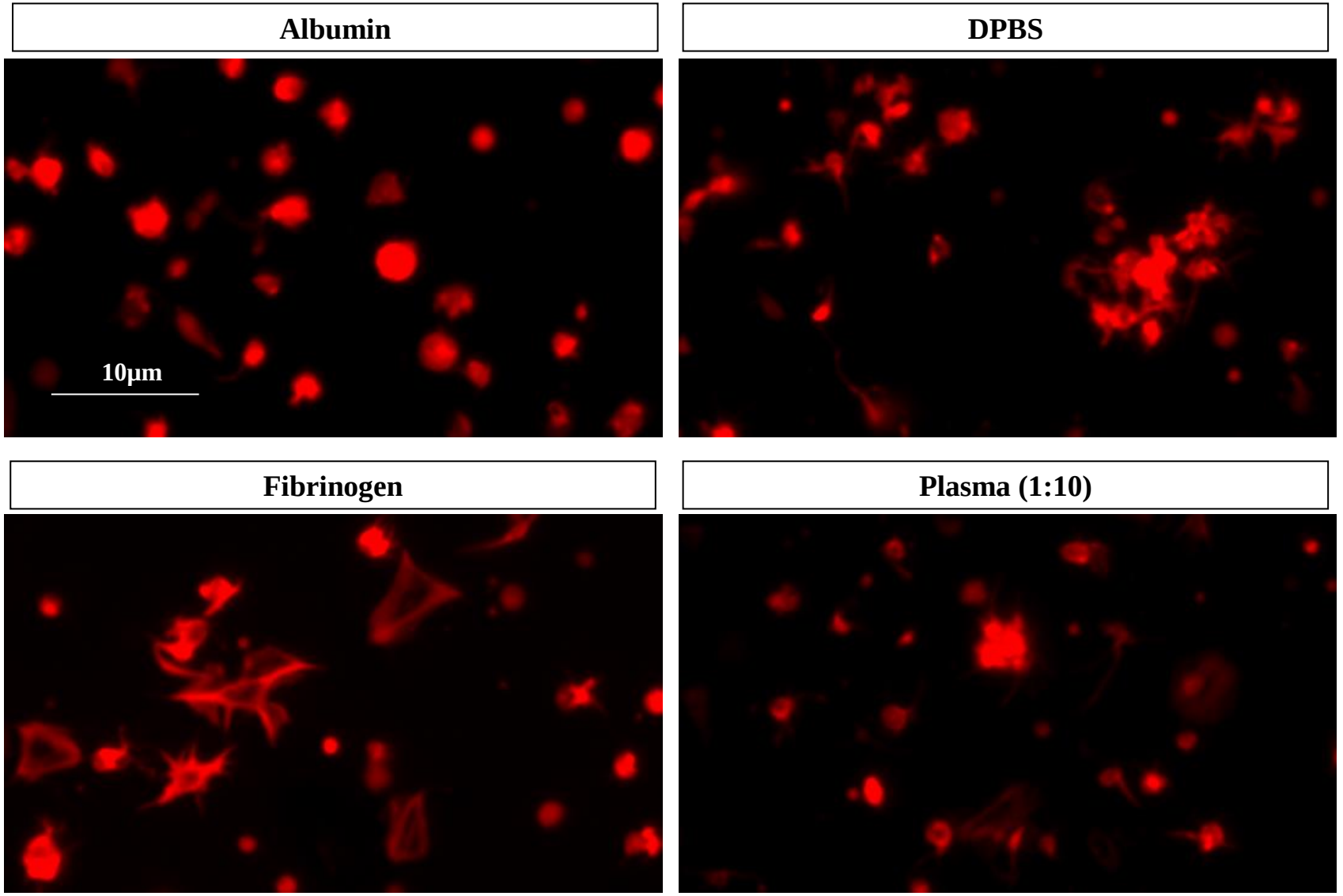

c. a-C:H

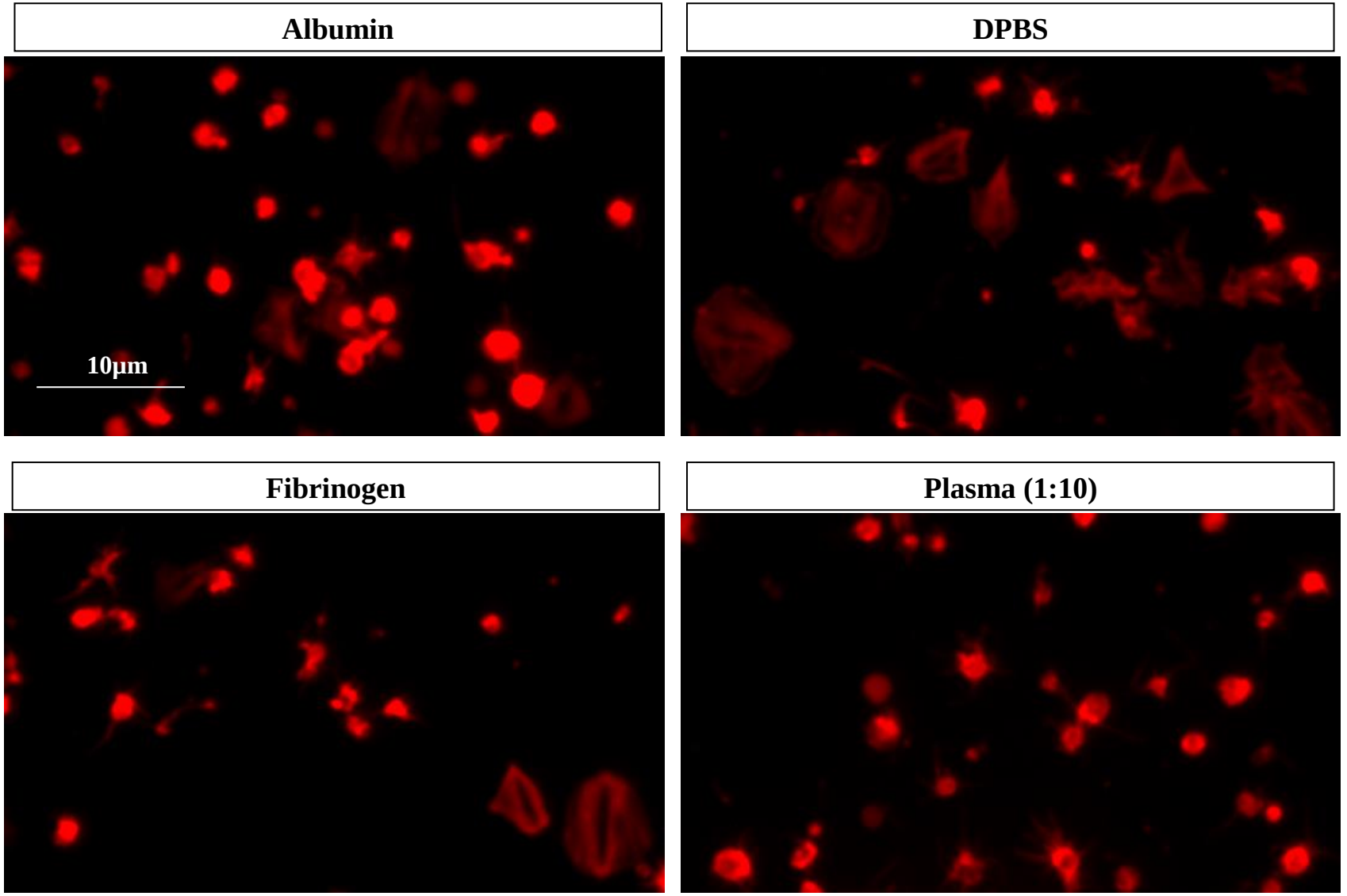

d. ta-C

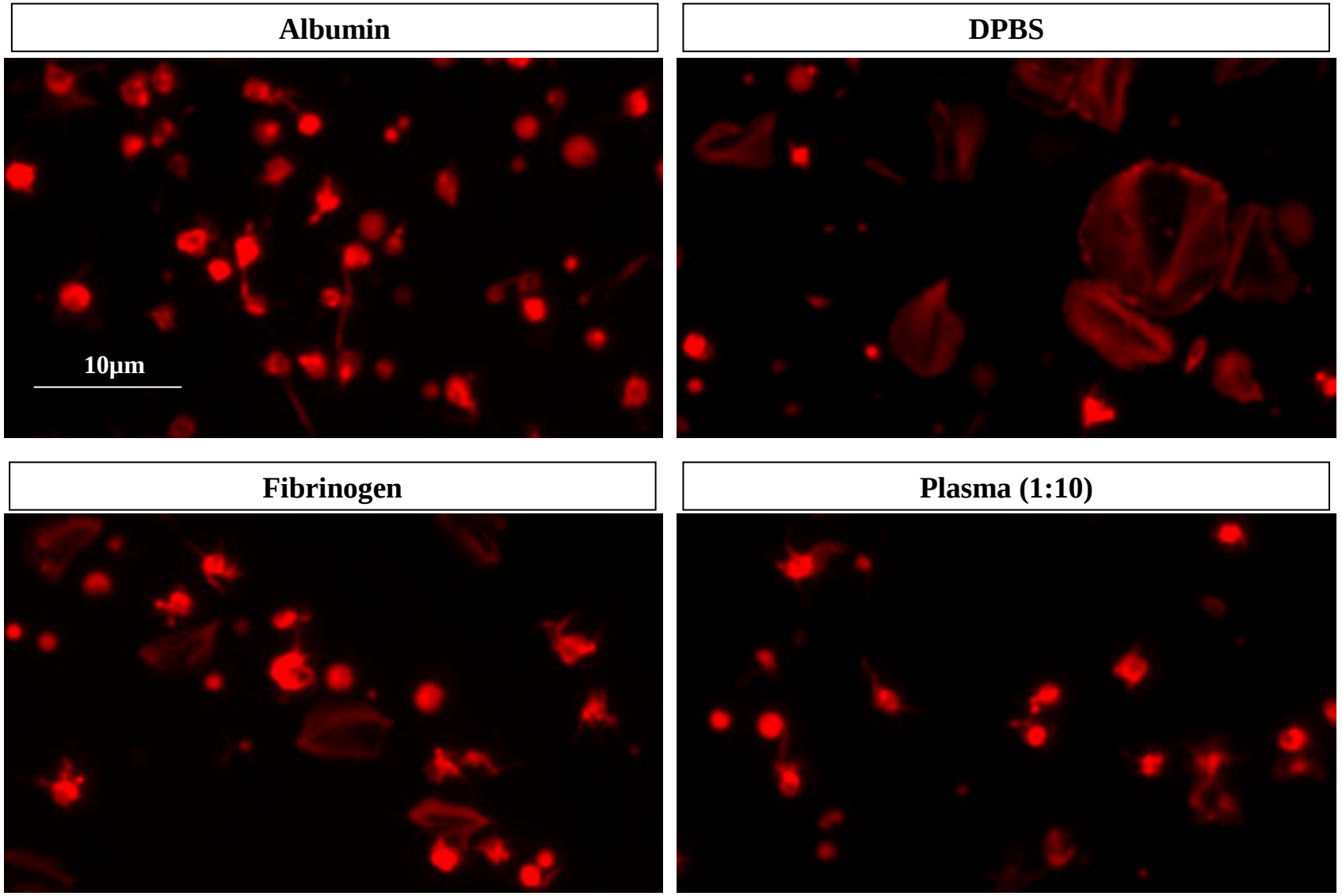

e. TCPS

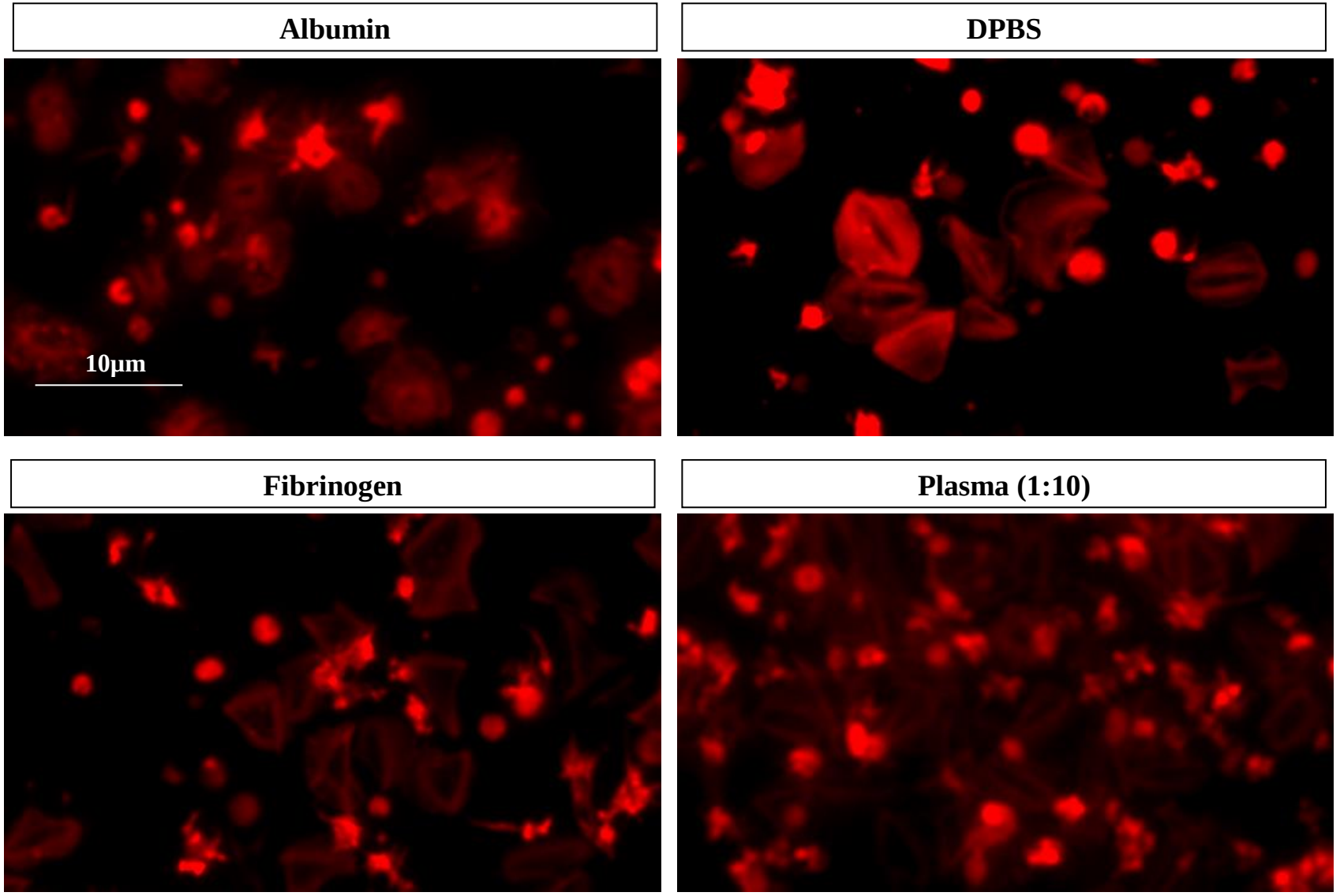

Figure 5.1 Fluorescence microscopy images showing rhodamine-phalloidin stained actin filaments of surface bound platelet cytoskeleton on bare (DPBS) and protein pre-coated a. silicon; b. TiO_2; c. a-C:H; d. ta-C; and e. TCPS flat surfaces. Protein pre-coated surfaces include 50µg/ml albumin (BSA), fibrinogen (Fg) and plasma (ratio of dilution 1:10, in DPBS). Samples were imaged at 500x magnification using Zeiss Axioskop microscope.

Various stages of platelet spreading were evident on each substrate. Platelet diameters ranged from 4-10µm. A greater degree in platelet spreading, as elucidated from increased surface coverage by individual platelets, leads to considerable thinning of the platelet as it flattens across the surface. This decreases the concentration of actin filaments, and consequently the concentration of the dye, available per unit square making the spread platelets appear fainter and more difficult to visualise. Differences in platelet conformation, once absorbed on surfaces, dictate subsequent platelet responses, and as such, techniques such as SEM was utilised to produce high resolution images of surface adsorbed platelet morphologies. Further, the degree of morphological changes appeared more pronounced in SEM images, showing exaggerated levels of platelet spreading and aggregation. As such only the most commonly found platelet conformation, as observed using fluorescence microscopy as well as SEM analysis, was imaged for each of the protein-coated conditions.

Figure 5.2 shows the most predominant conformation of platelets attached on albumin pre-coated silicon, TiO_2, a-C:H and ta-C. The adhered platelets followed a rounded morphology with no apparent actin-rich pseudopodia or displayed radial protrusions containing non-filamentous actin, except for control TCPS (Figure 5.2) which supported increased levels of platelet spreading. Filopodia act as probes as they navigate through the surfaces for potential tethering sites, and as such, round cells, predominantly found on ta-C surfaces, that present no apparent filopodia are indicative of weakly adhered cells.

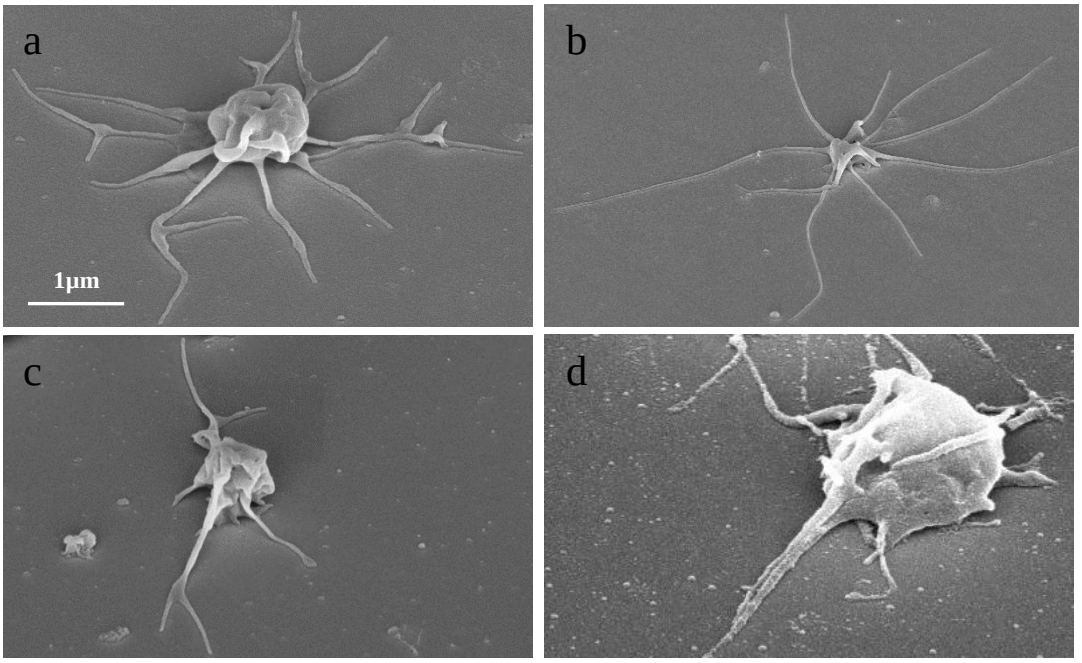

Figure 5.2 SEM images of platelets exposed to (a) silicon, (b) TiO_2, (c) a-C:H and (d) ta-C on pre-coated with albumin (BSA) at 50µg/ml concentration. Samples were imaged using an InLens detector (10KV) at 54 degrees stage tilt.

Bare surfaces displayed significant levels of platelet spreading when compared with albumin surfaces, as shown in Figure 5.3. Completely spread platelets, as found on control silicon surfaces, support increased surface adhesion points and consequently appear more strongly bound to the surface. Ta-C exhibited hemisphere shaped platelets while the platelets on a-C:H and TiO_2 surfaces exhibited spread dendritic morphologies with well-developed actin fibres at the leading edge of the cell membrane (Figure 5.1).

Similar to bare TiO_2 and a-C:H surfaces, fibrinogen coated substrates also presented spread platelets with actin rich, stellate shaped filopodia, as shown in Figure 5.4.

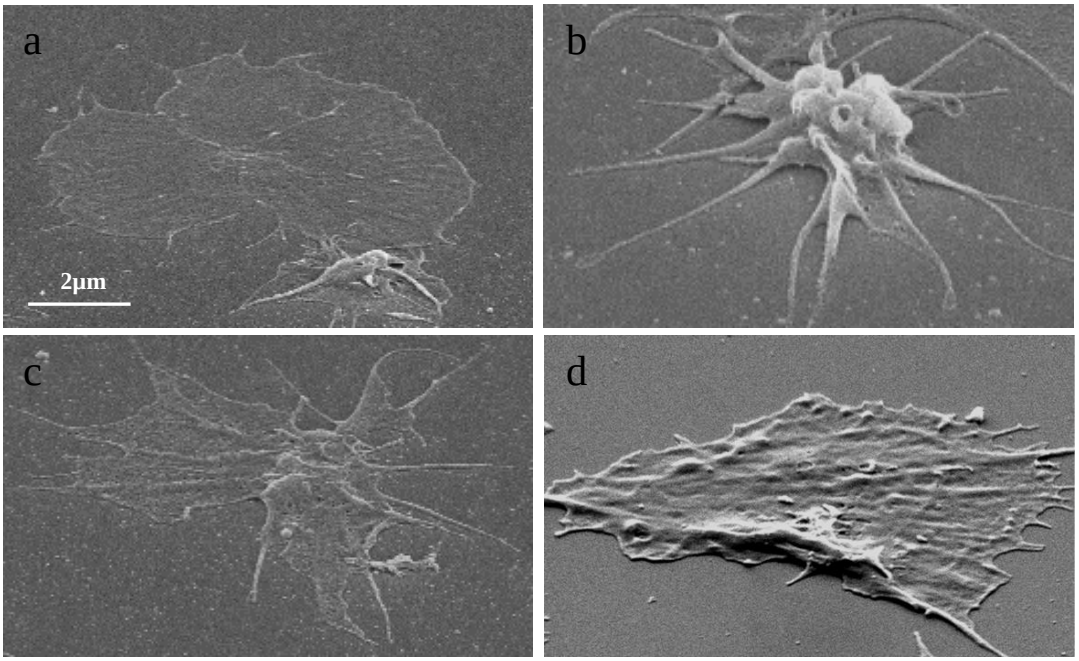

Figure 5.3 SEM images of platelets exposed to bare (a) silicon, (b) TiO_2, (c) a-C:H and (d) ta-C surfaces. Samples were imaged using an InLens detector (10KV) at 54 degrees stage tilt.

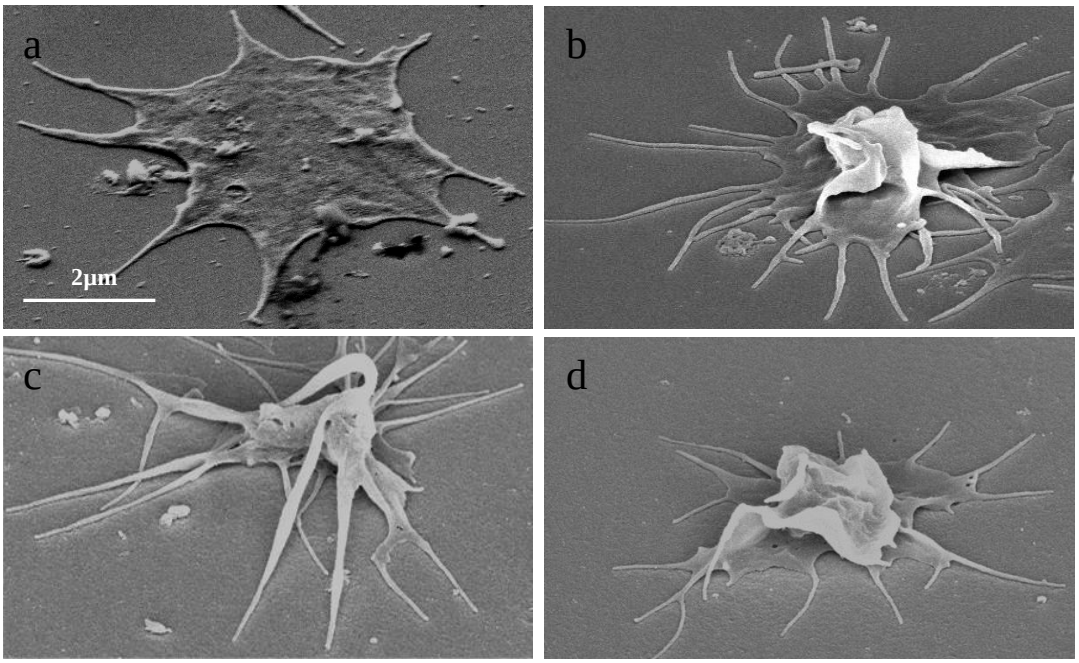

Figure 5.4 SEM images of platelets exposed to (a) silicon, (b) TiO_2, (c) a-C:H and (d) ta-C on pre-coated with fibrinogen (Fg) at 50µg/ml concentration. Samples were imaged using an InLens detector (10KV) at 54 degrees stage tilt.

Figure 5.5 shows the morphologies of exposed platelets on plasma coated substrates. Plasma surfaces exhibited lower concentrations of spread platelets when compared with pre-coated fibrinogen. Platelets in the presence of plasma proteins showed well defined filopodia and their overreaching as they communicate with adjacent platelets was also noted on all substrates. Though platelet inter-communication was evident on fibrinogen surfaces as well, it was not presented as often as seen on pre-coated plasma.

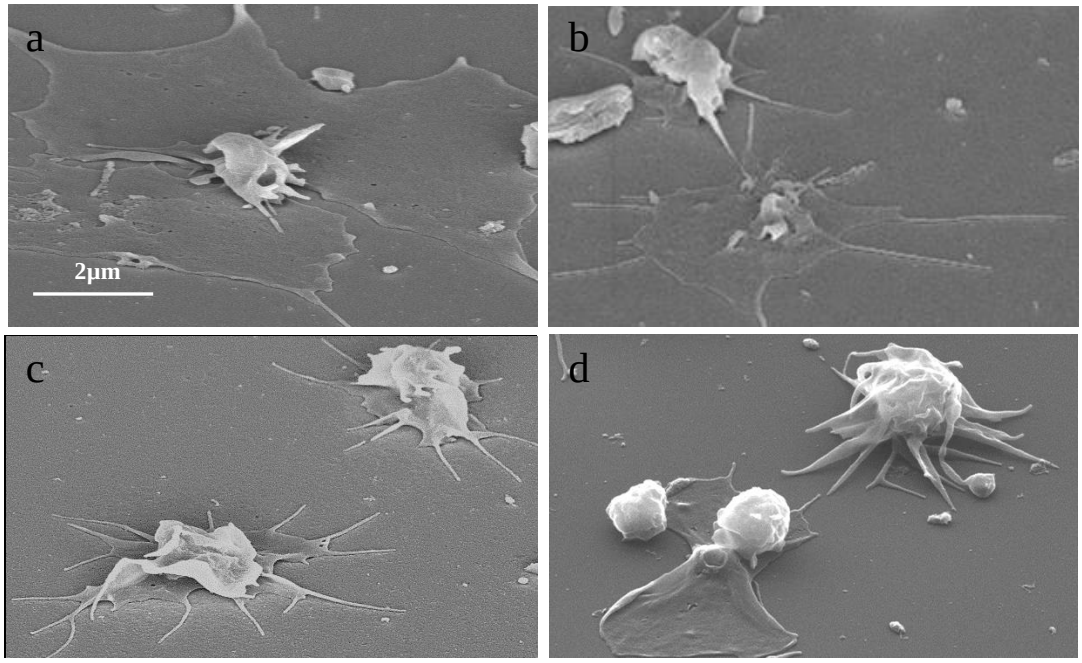

Figure 5.5 SEM images of platelets exposed to (a) silicon, (b) TiO_2, (c) a-C:H and (d) ta-C on pre-coated with diluted plasma (dilution factor 1:10, in DPBS). Samples were imaged using an InLens detector (10KV) at 54 degrees stage tilt.

Sporadic regions of platelet aggregation were evident on all surfaces, especially on control TCPS and silicon substrates. Some regions displayed multi-stacked and extensively spread platelets similar in appearance to secondary clotting as found in *in vivo*. Whilst the level of aggregation was extensive in SEM, possibly due to inadvertent platelet membrane activation caused by the gluteraldehyde fixative used during the preparation process, fluorescence microscopy also displayed inter-communication between multiple platelets and possible z-stacking. SEM images showing platelet aggregation are provided in Figure 5.6.

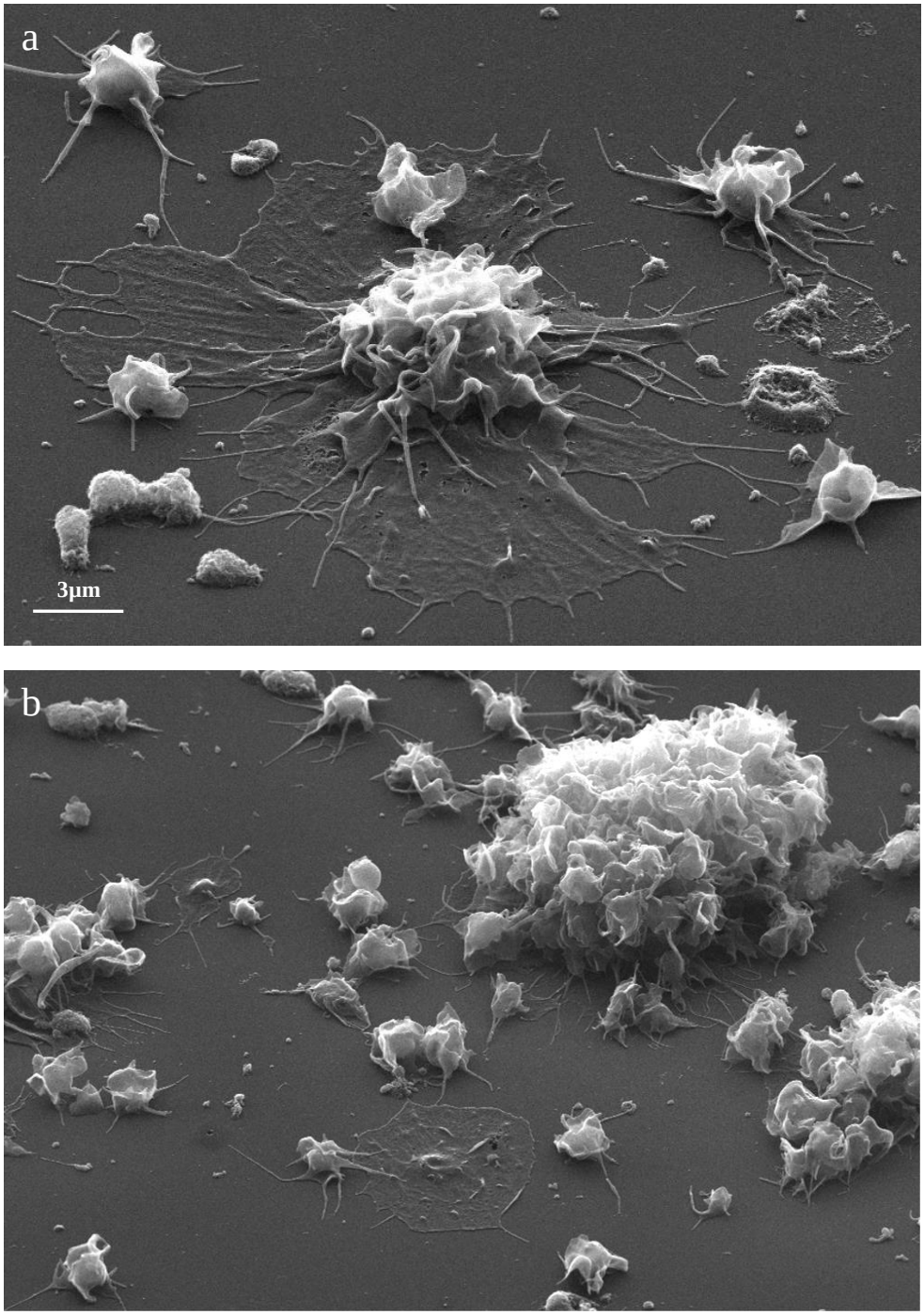

Figure 5.6 Aggregation of platelets on (a) fibrinogen pre-coated ta-C, and (b) plasma pre-coated silicon surfaces as visualised using SEM. Images were taken using an InLens detector (10KV) at 54 degrees stage tilt.

Chemical fixatives, utilised in SEM and fluorescence imaging, for platelet adhesion studies were applied to immobilise or 'fix' sub-cellular components of surface adhered platelets by halting cellular metabolism and destroying proteases and enzymes which can further affect the platelet's microstructure and integrity. Whilst

such fixatives were applied to influence the cell's preservation against harsh buffers and detergents by stabilising the actin filaments and microtubules that preserve the platelet's structure, they have also been known to dramatically reduce the nano-scale resolution of its cytoskeletal characteristics as well as initiating unwarranted membrane activation shown as increased platelet spreading and aggregation. For this reason AFM was utilised to visualise the nano-topographical features of platelets attached on model a-C:H substrates, in liquid, under tapping mode. After incubating for 60 minutes, a light fixative solution containing equal parts of pre-chilled methanol and ethanol was applied for 5mins on the surface attached platelets, prior to imaging. A-C:H surfaces were chosen as model substrates as they supported the least number of attached platelets, found through fluorescence microscopy analysis, and as such is likely to present as the most haemocompatible surface.

Figure 5.7 shows an AFM image representing the morphology of an adhered platelet on flat a-C:H substrate. AFM was employed to investigate the morphology of single platelets due to its high spatial resolution in the nano-meter scale. While fluorescence microscopy can track the localisation of single molecules, they are limited only to the visualisation of the labelled parts and electron microscopy requires the samples to be fixed and dried which significantly alters the platelet microstructure and the electron beam continually ionises the sample and burning away any topographical features [465].

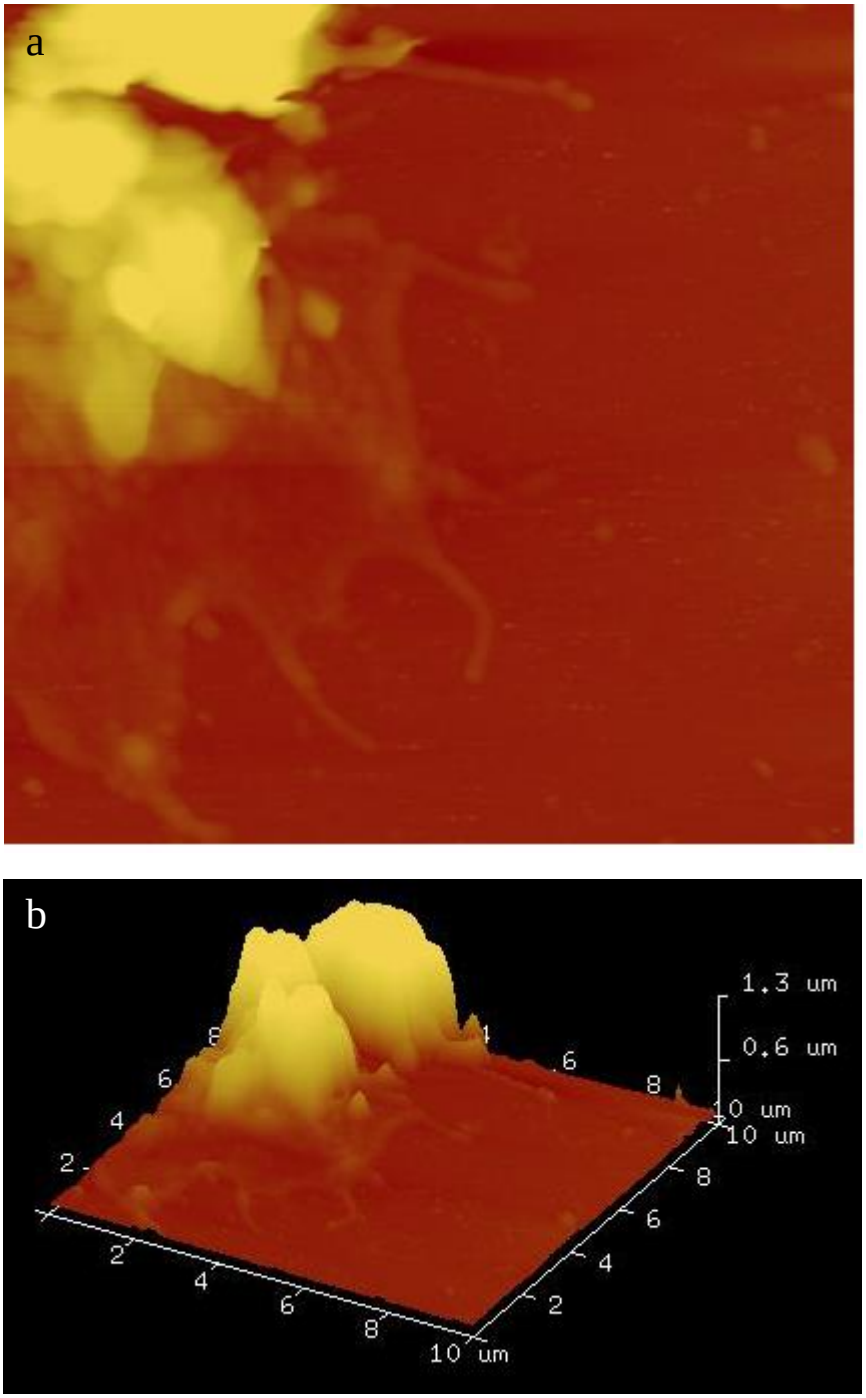

Figure 5.7 AFM topographical images showing (a) 2D and (b) 3D plots of fibrinogen pre-coated a-C:H surfaces seeded with human platelets. Surfaces were analysed in tapping mode with scan rate of 0.2Hz, vertical scale range of 1.3µm and scan size of 10µm x 10µm^2. Measurements we carried out in liquid mode and images corrected using Nanoscope analysis.

A coagulating fixative containing equal parts of ethanol and methanol was used as it rapidly changes the hydration state of the sub-cellular components without affecting the spatial structure of platelet's surface membrane and its components. The platelets

were not imaged live to avoid the risk of creating large deformations and consequently tearing of the cell membrane and dislodgement of surface features from the normal force as well as the lateral and shear forces exerted by the AFM tip [466-468]. The active compounds in glutaraldehyde and paraformaldehyde, often used as cross-linking fixatives in SEM and fluorescence microscopy, respectively, interact with and polymerise the proteins in platelets to form covalent cross groups, changing the surface nano-topography and structure of the platelet surface. Glutaraldehyde incurs a reducing step that mechanically dislodges delicate actin structures such as; filopodia and lamellipodia while paraformaldehyde fails to maintain microtubular integrity making it difficult to visualise microtubules upon fixation [465, 469].

The topographical AFM image of platelets on fibrinogen coated a-C:H thin films shows a round platelet displaying spreading around the edges as it flattens onto the cell surface. There appears to be the formation of a pseudo-nucleus due to the accumulation of dense and alpha granules and filopodia protruding from the cell periphery. The diameter of the deposited platelet ranged between 8-10µm and the height of the platelet was measured at 1.3µm, however, activated platelets have been reported to exhibits cell heights as low as 100nm [470]. Furthermore, the filopodia extended to a length of 1-2µm, although, previous studies have shown the internal actin filaments spanning up to 10µm [471]. Similar sizes of platelets were observed in fluorescence microscopy and SEM images, although, on SEM images the conformation mostly exhibited by platelets exposed to fibrinogen coated a-C:H appeared more spread that what was represented by AFM. This reinforces the need for AFM imaging and fluorescence microscopy in analysing surface-platelet interactions.

Tapping mode, when applied in liquid with a light fixative, present platelets as ‘hardened’ structures between the short time intervals due to its inherent visco-elastic properties and subsequently renders platelets less susceptible to deformation during the high resolution imaging process. This is different to contact mode, because when a constant force is applied the lateral forces are significantly larger causing local deformations followed by resealing of the cell membrane exposing the underlying

sub-membrane structures which inevitably causes platelet restructuring and consequent activation and aggregations [465, 468].

Whilst, fluorescence, SEM and AFM images qualitatively prove the level of cell adhesion, a quantitative measure better compares the different surfaces and subsequent protein coats. As such Figure 5.8 (a) and (b) describes the total concentration of platelets attached per square centimetre, and, degree of platelet spreading measured as a percentage of total surface area, respectively.

In general, the number of platelets attached on the bare and albumin pre-coated silicon, a-C:H and ta-C substrates, as shown in Figure 5.8 (a), was greater than that on fibrinogen and plasma surfaces. This was especially evident on fibrinogen surfaces which supported the lowest concentration of platelets. This suggests that platelet adhesion is not only dependent on ligand-receptor mediated adhesion but also through non-specific surface interactions as found on albumin surfaces and surfaces devoid of proteins. Further, a decreased concentration of platelets in the presence of fibrinogen and plasma proteins implies a favourable interaction between the surface and serum proteins in reducing platelet receptor activation for adhesion. While this was the case for the above mentioned surfaces, fibrinogen and plasma proteins were shown to promote platelet adhesion on TCPS surfaces, and plasma proteins alone in promoting platelet attachment on TiO_2 surfaces. A-C:H followed by ta-C facilitated the least number of platelets on plasma and fibrinogen coated surfaces. This establishes the potential role of surface chemistry in dictating specific protein adsorption from plasma, its adsorbed conformation and its consequent interactions with circulating platelets.

The difference in platelet coverage, shown in Figure 5.8 (b), on TiO_2, a-C:H and ta-C surfaces was conserved between the various pre-coated surfaces where a-C:H followed by ta-C showed the lowest level of platelet spreading.

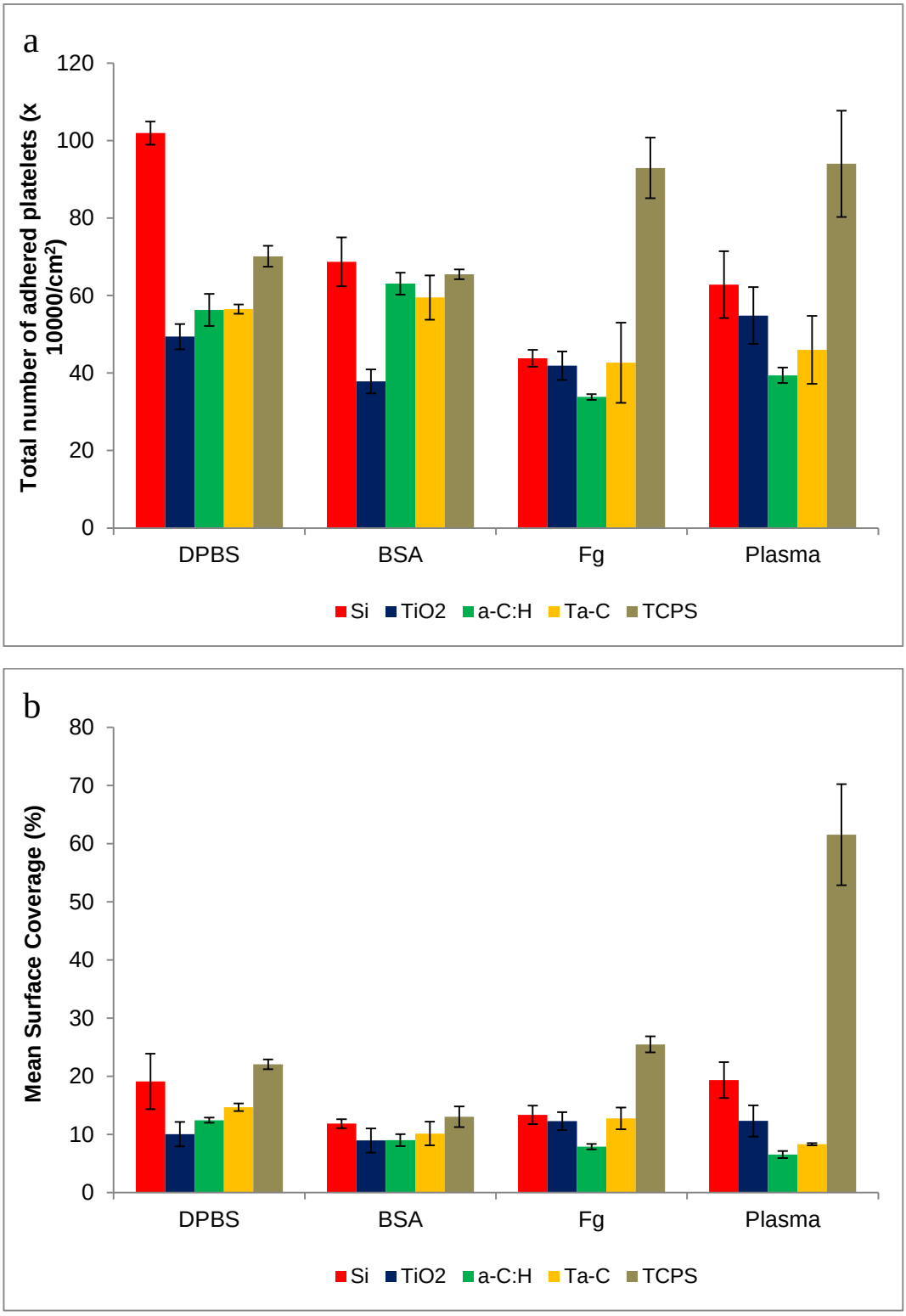

Figure 5.8 Comparison of a. surface bound platelet concentrations, per square centimetre, and b. mean surface coverage by the platelets, as percentage value, calculated from rhodamine-phalloidin stained fluorescence microscopy images. Flat silicon, TiO_2, a-C:H, ta-C and TCPS test substrates were pre-coated with albumin (BSA), fibrinogen (Fg) and diluted plasma (ratio 1:10, in DPBS) prior to platelet incubation. The results were compared with surfaces devoid of proteins (DPBS). Error bars: SD (n=3).

This was especially evident on fibrinogen and plasma surfaces. Corresponding to its increased levels of platelet attachment, TCPS followed by silicon substrates exhibited greater levels of platelet spreading on its surfaces. Control TCPS promoted significantly increased levels of platelet spreading (62% surface coverage) in the presence of plasma proteins indicating that TCPS exhibits the least haemocompatible surface chemistry for platelet interaction.

Figure 5.9 (a) and (b) shows a breakdown of adsorbed platelets in terms of their morphology where Figure 5.9 (a) shows the concentration of round cells, retaining their spherical shape with minimal radial protrusions (filopodia), and, Figure 5.9 (b) shows the concentration of spread platelets with well-developed actin fibres.

Platelet adsorption on bare surfaces indicate that silicon facilitated the greatest number of round and spread platelets when compared to control TCPS even though TCPS showed a higher percentage of surface coverage. This may suggest the spread platelets on TCPS followed a larger morphology than silicon. A-C:H and ta-C surfaces, exhibited decreased levels of platelet adhesion and its subsequent spreading on all protein-pre-coated and bare surfaces and consequently, retaining its haemocompatible properties. TiO_2 surfaces followed a similar trend to a-C:H and ta-C substrates except for on albumin coated surfaces, while, control TCPS in the presence of fibrinogen and plasma proteins have been shown to increase spreading of platelets. The percentage of surface coverage on albumin pre-coated substrates was similar between the various surface chemistries, though, only silicon, a-C:H, ta-C and TCPS surfaces presented with similar levels of adhered platelets. Lower concentrations of platelets were found on TiO_2 suggesting the degree of platelet spreading once adsorbed on TiO_2 surfaces is greater than on the other albumin surfaces. When compared with the other fibrinogen pre-coated substrates, less platelets were found to adhere on fibrinogen coated a-C:H, even though a higher concentration of adsorbed fibrinogen with higher amounts of platelet binding domains exposed were reported (Chapter 4). This can suggest that, in the presence of

fibrinogen, the other surfaces promoted more non-fibrinogen dependent (or, non-specific) adhesion of platelets to the surface.

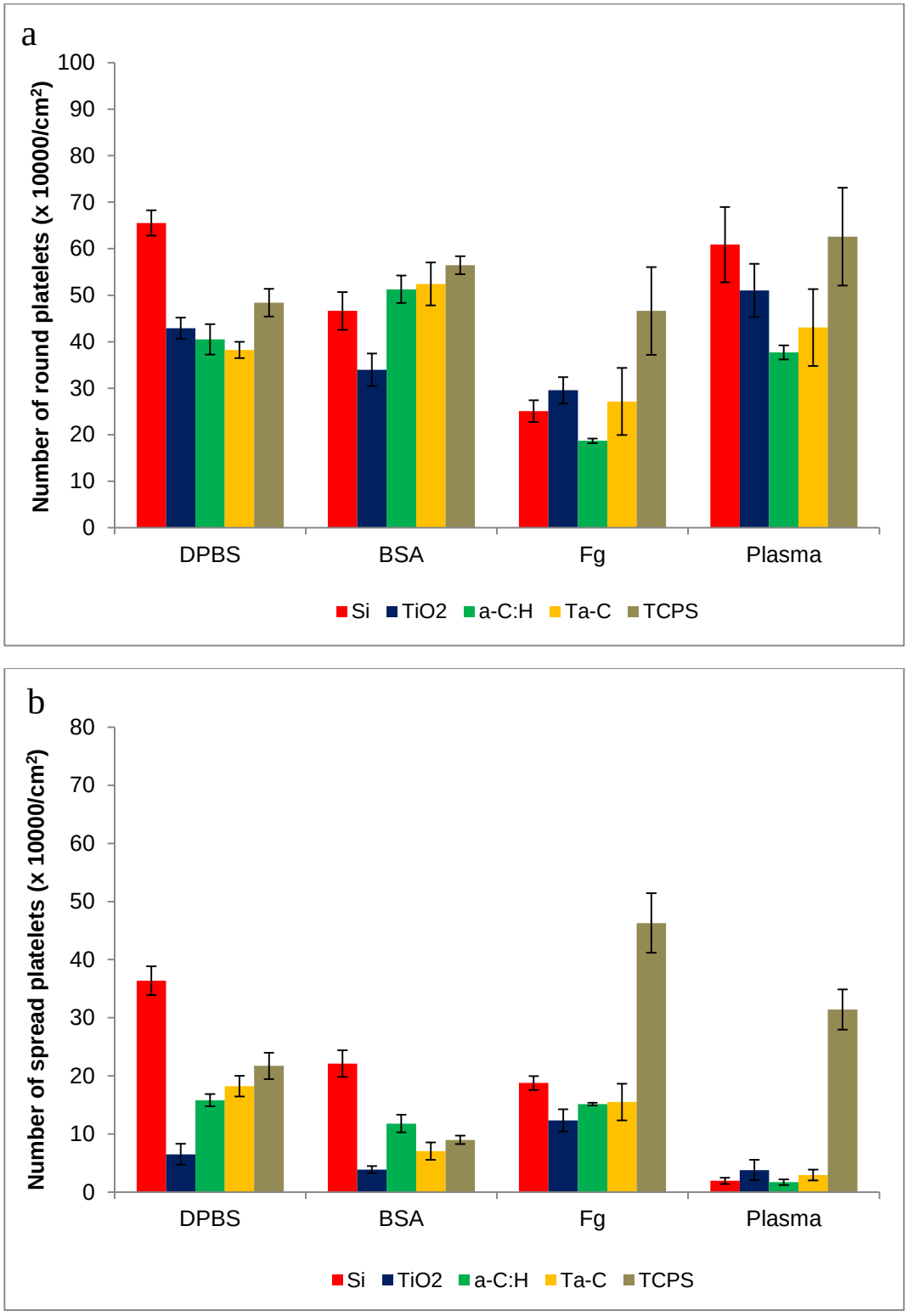

Figure 5.9 Concentration of a. round and b. spread platelets adsorbed per square centimetre of test substrates, as calculated from rhodamine-phalloidin stained

fluorescence microscopy images. Platelets were exposed to nano-patterned silicon, TiO_2, a-C:H, ta-C and TCPS flat test substrates without adsorbed proteins (DPBS) as well as albumin (BSA), fibrinogen (Fg), diluted plasma proteins (ratio 1:10, in DPBS) prior to incubation. Error bars: SD (n=3).

Figure 5.10 shows the ratio of round versus spread platelets adsorbed on the protein coated and bare surfaces. No appreciable difference in ratio of adsorbed cells was noted on bare and fibrinogen-coated silicon, a-C:H, ta-C and TCPS test substrates. Albumin surfaces displayed slightly elevated cell ratios, while a significant increase were noted on plasma adsorbed surfaces. This reinforces the favourable interaction between platelets, and, plasma proteins other than fibrinogen and to some extent albumin in limiting the level of platelet spreading but not necessarily its attachment.

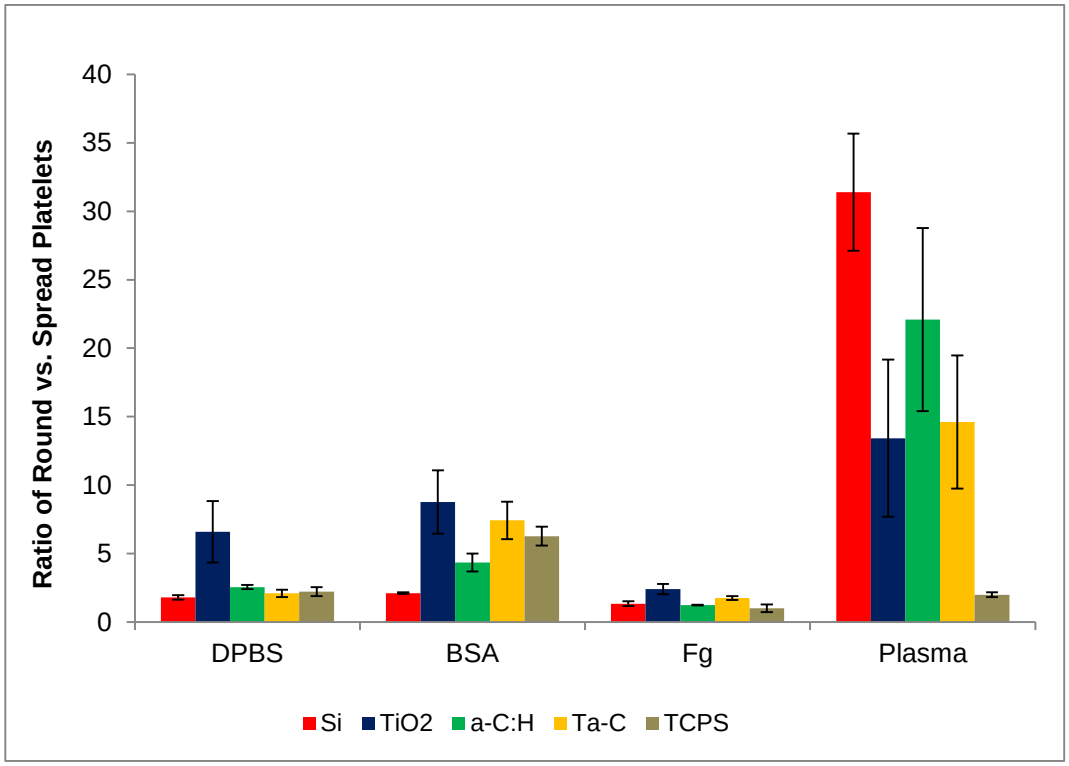

Figure 5.10 Ratios of round vs. spread platelets calculated from fluorescence microscopy images of platelets exposed to protein pre-coated and bare silicon, TiO_2, a-C:H, ta-C and TCPS flat substrates. Samples include Error bars: SD (n=3).

While, TiO_2 consistently exhibited a higher ratio of round cells on bare and surfaces coated with albumin and fibrinogen; plasma-coated silicon, followed by a-C:H and ta-C exhibited the highest ratio overall. In the presence of plasma proteins the ratio of

round cells versus spread cells on silicon increased by approximately 16-18 fold when compared with that of the bare surface. As such, the concentration of adhered cells and its breakdown, along with the cell ratio analysis indicates the marked influence plasma proteins play in decreasing the propensity of platelet adhesion and its subsequent spreading on specific surface chemistries, such as a-C:H and ta-C.

5.2.1.2 Role of $\alpha_{IIb}\beta_3$ integrins in platelet adhesion

The involvement of $\alpha_{IIb}\beta_3$ receptors in platelet-fibrinogen binding events was investigated by visualising the cytoskeletal developments of platelets attached on protein pre-coated surfaces and surfaces devoid of proteins in the presence of anti-$\alpha_{IIb}\beta_3$ antibodies. In this study, freshly prepared human platelets were incubated with an anti-human $\alpha_{IIb}\beta_3$ antibody, Abciximab (Reopro) for 1 hour before being exposed to protein pre-coated flat surfaces. Flat silicon, TiO2, a-C:H and ta-C surfaces were pre-incubated with 50µg/ml of albumin (BSA), fibrinogen (Fg) and diluted plasma (ratio 1:10, in DPBS) prior to platelet binding. After washing, the adhered platelets were fixed and stained and then imaged using fluorescence microscopy.

Figure 5.11 shows human platelet response to the protein pre-coated and bare surfaces in the presence of anti-$\alpha_{IIb}\beta_3$ antibody. The number of platelets adhered to the substrates were significantly reduced in the presence of Reopro when compared with normal platelets in absence of the anti-integrin antibody (section 5.2.1.1). The level of platelet spreading was also noticeably reduced. The densities of platelets covered across various surface chemistries appear similar, making it difficult to discern between the silicon and TCPS positive controls from a-C:H, ta-C and TiO_2 substrates. Platelets typically followed a rounded morphology, some with protruding filopodia suggesting that Reopro molecules hinder the platelet's ability to probe the surface for focal adhesion sites and consequently results in cells that are weakly adhered to the surface with a more rounded morphology and increased height. Small levels of platelet aggregation were evident on silicon and TCPS controls as well as albumin coated and bare TiO_2 surfaces. Extensive spreading of the adhered cells was

evident on bare and, fibrinogen and plasma coated silicon. Similarly, spreading was also evident on bare and fibrinogen coated TCPS substrates. A-C:H and ta-C surfaces showed reduced platelet adhesion and spreading on all four pre-coated conditions.

It was interesting to note that while Reopro suppressed the level of platelet adhesion and subsequent spreading to fibrinogen and other proteins from plasma such as, fibronectin and von Willebrand factor [472], it did not inhibit it completely. As such, it can be inferred the significant, although not exclusive, role $\alpha_{IIb}\beta_3$ receptors play in mediating the adhesion of platelets on biomaterial surfaces in the presence of serum proteins. Further, albumin and bare surfaces also showed reduced platelet adhesion which may suggest $\alpha_{IIb}\beta_3$ receptors are susceptible to non-ligand specific platelet adhesion on biomaterial surfaces, and decreased availability of $\alpha_{IIb}\beta_3$ integrins to substrate surface may reduce the likelihood of non-specific activation of $\alpha_{IIb}\beta_3$ receptors for platelet-surface binding.

a. Silicon

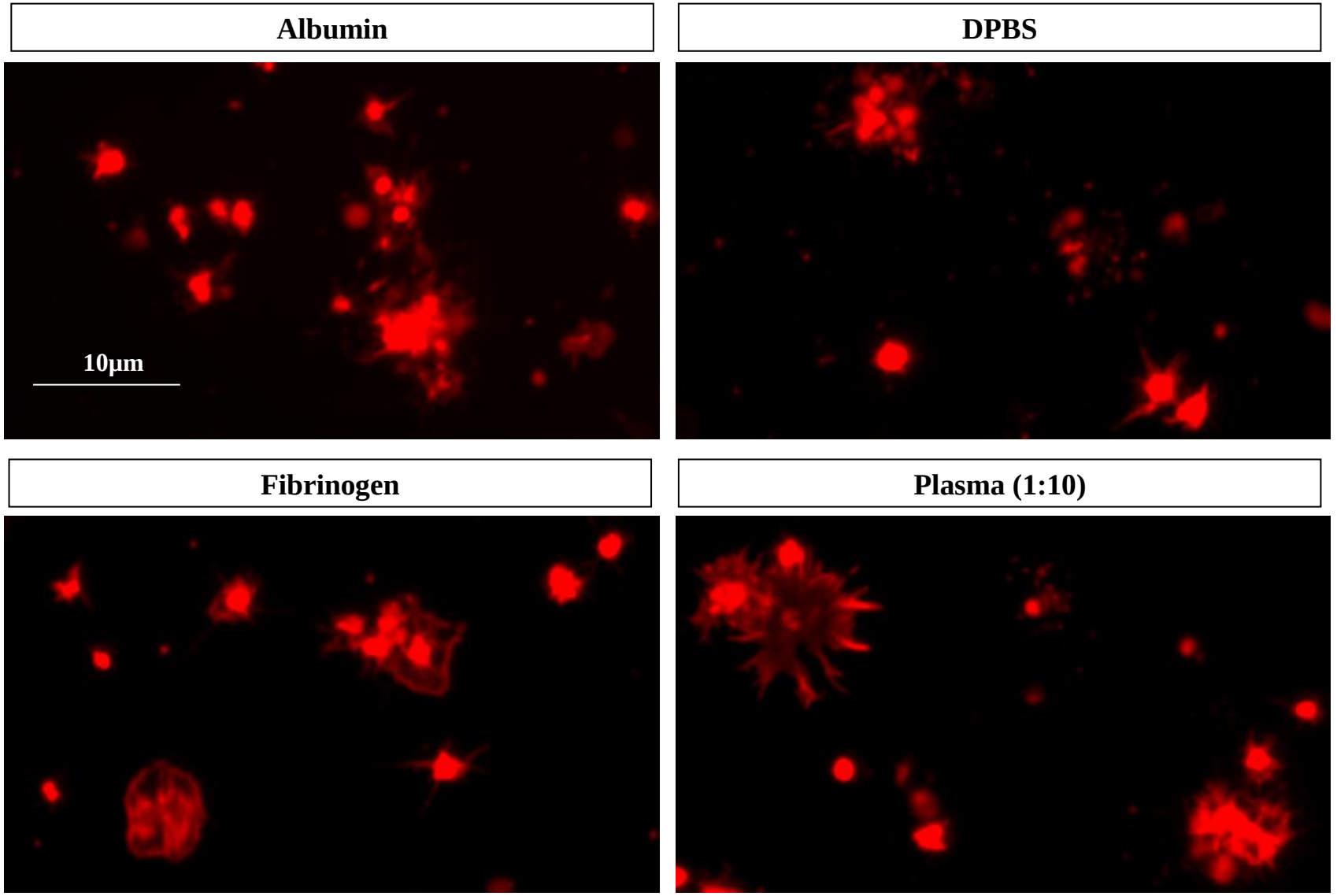

b. TiO_2

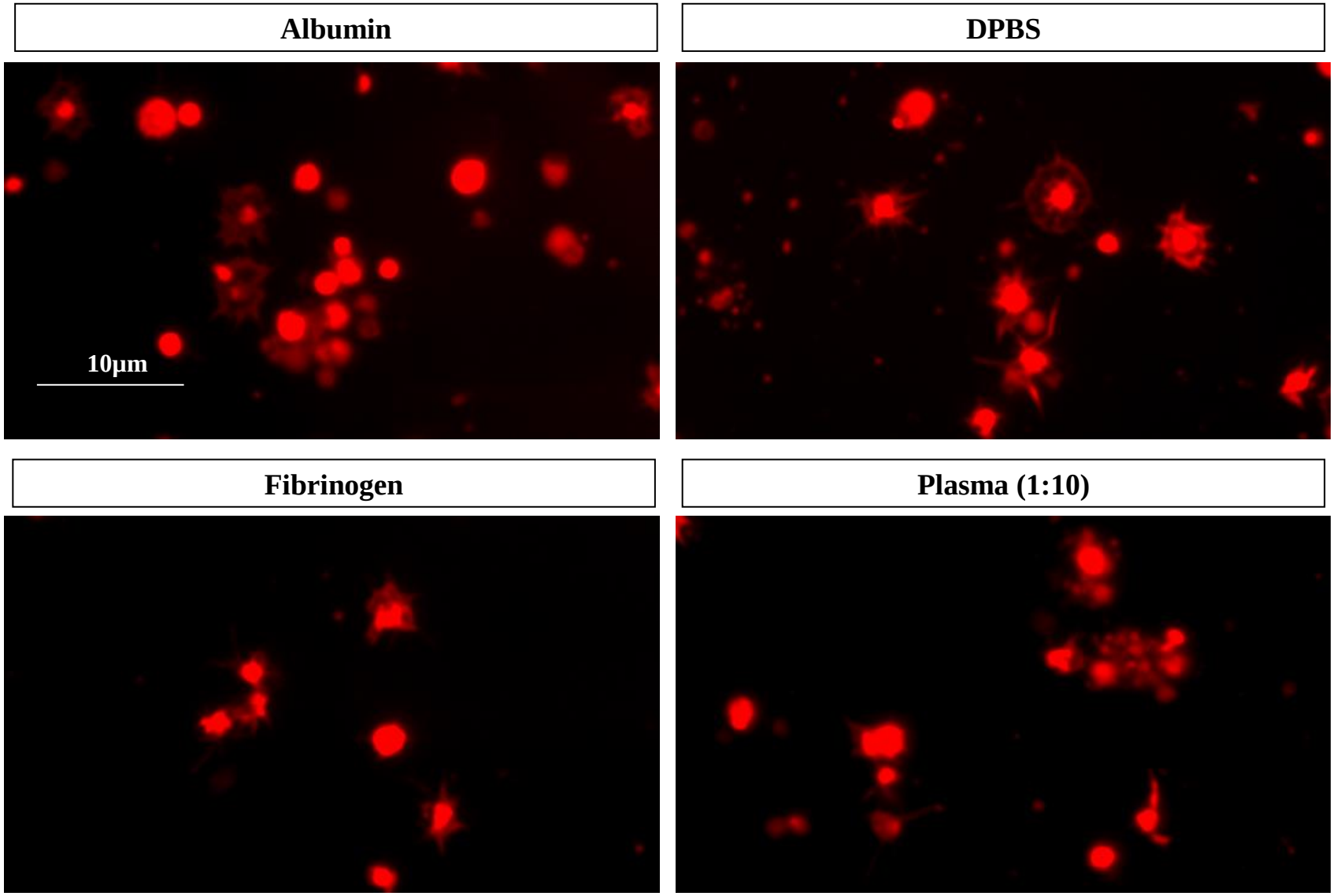

c. a-C:H

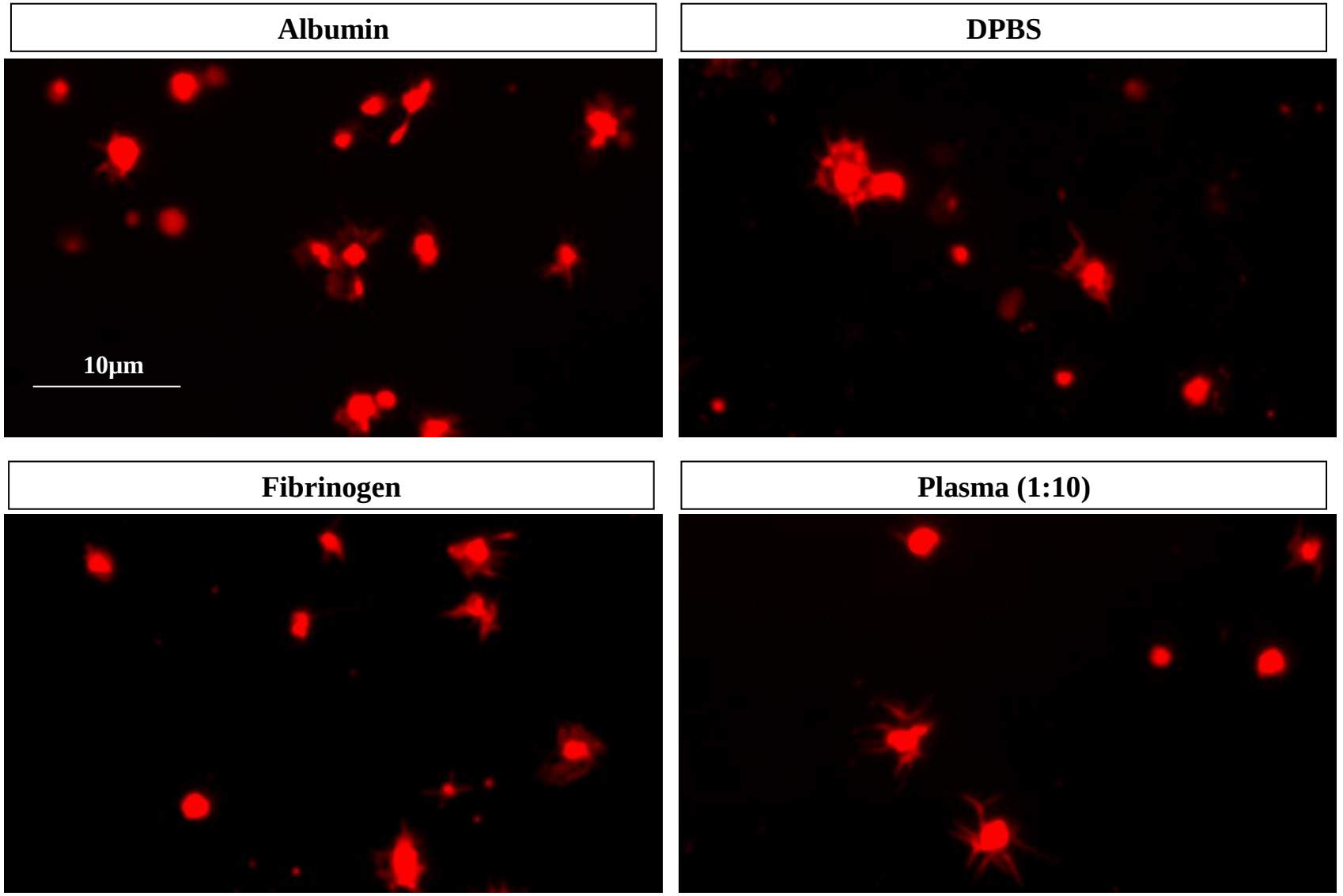

d. ta-C

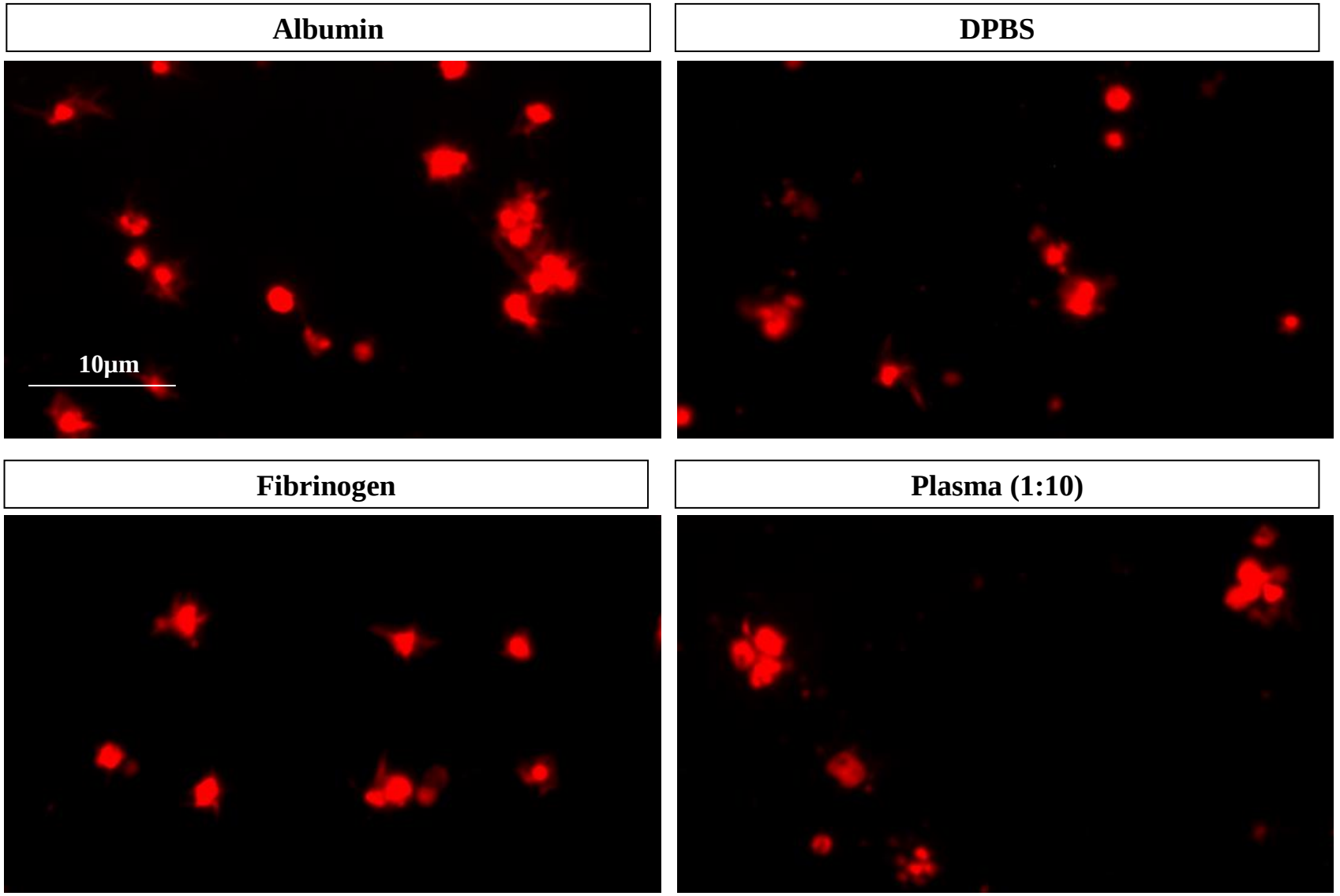

e. TCPS

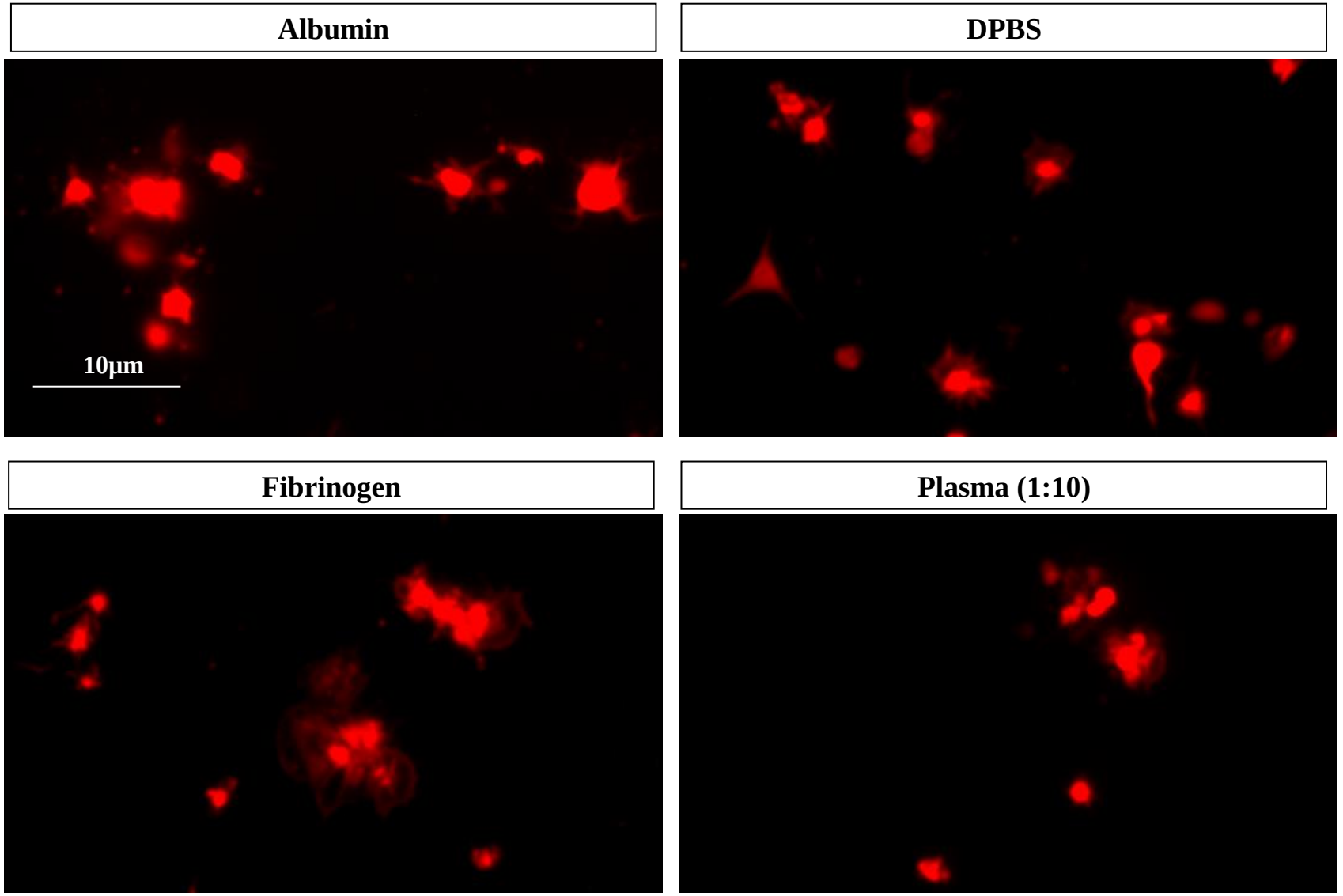

Figure 5.11 Fluorescence microscopy images of Reopro bound platelet cytoskeletons exposed to bare (DPBS) and protein pre-coated a. silicon; b. TiO_2; c. a-C:H; d. ta-C; and e. TCPS flat surfaces. Protein pre-coated surfaces include 50µg/ml albumin (BSA), fibrinogen (Fg) and plasma (diluted in ratio 1:10, in DPBS). Samples were imaged at 500x magnification.

The concentration of Reopro bound platelets attached to protein pre-coated surfaces and the mean platelet coverage after 1 hour of incubation, as calculated from fluorescence microscopy images are shown in Figure 5.12 (a) and (b), respectively. There are no significant differences ($p<0.01$) between total concentration of Reopro bound platelets adhered to substrates under the four protein pre-coated conditions when compared with platelets not exposed to Reopro (Figure 5.8 (a)). Silicon and TCPS reaffirming their role as positive controls showed increased levels of platelet attachment across all four conditions, except for plasma coated silicon, which showed lower level of attachment than plasma pre-coated TiO_2 surfaces. A-C:H and ta-C surfaces consistently supported lower concentrations of adhered platelets under each condition. This may suggest that the level of $\alpha_{IIb}\beta_3$ platelet receptor interaction with biomaterial surfaces varies on surface chemistry where adhered platelets are more likely to tether to biomaterial surfaces with specific chemistries such as a-C:H and ta-C, via its $\alpha_{IIb}\beta_3$ membrane integrins.

Fibrinogen and plasma pre-coated surfaces appeared more responsive to Reopro antibody, showing lower levels of adhesion on the substrates than its corresponding bare and albumin coated surfaces. There was no significant difference ($p<0.05$) in platelet concentrations between a-C:H and ta-C surfaces under each condition. Fibrinogen and plasma coated a-C:H and ta-C surfaces supported similar concentrations of adsorbed platelets. TiO_2 showed similar levels of platelet attachment as a-C:H surfaces except in the presence of plasma proteins where it exhibited increased platelet attachment, similar to TCPS control.

A significant decrease ($p<0.05$) in the level of surface coverage was evident with Reopro-bound platelets, Figure 5.12 (b), when compared with platelets not exposed to Reopro (Figure 5.8 (b)). A-C:H and ta-C surfaces continually showed decreased

levels of surface coverage across all conditions, except for on fibrinogen pre-coated surfaces where they showed similar levels of coverage to TiO_2 and control silicon.

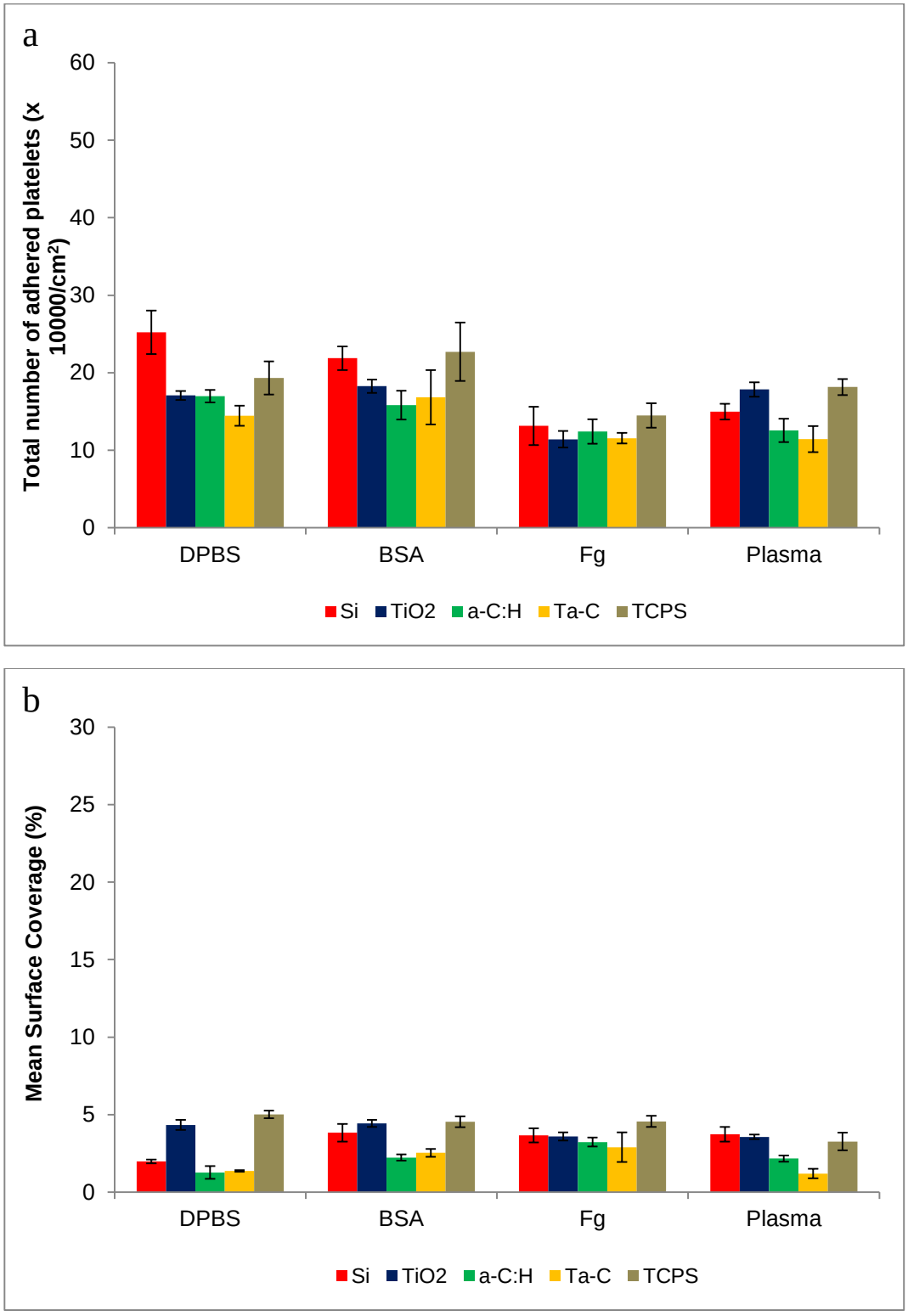

Figure 5.12 Comparison of a. Reopro bound platelet concentrations, per square centimetre, and b. mean surface coverage by the platelets, as percentage value,

calculated from rhodamine-phalloidin stained fluorescence microscopy images. Flat silicon, TiO_2, a-C:H, ta-C and TCPS test substrates were pre-coated with albumin (BSA), fibrinogen (Fg) and diluted plasma (ratio 1:10, in DPBS) prior to platelet incubation. The results were compared with surfaces devoid of proteins (DPBS). Error bars: SD (n=3).

A breakdown of the total number Reopro-bound platelets with rounded and spread morphology are shown in Figure 5.14 (a) and (b), respectively. The data was calculated from the fluorescence images in Figure 5.11.

Figure 5.14 (a) shows fibrinogen and plasma pre-coated surfaces supported lower concentrations of attached round platelets when compared with albumin pre-coated and bare substrates. This trend was also noticed in Figure 5.12 (a) but not in the concentration of adhered spread platelets (Figure 5.14 (b)). Integrin receptors on adherent cells have been known to establish tight focal contacts that link the actin filaments in the cytoskeleton to material surfaces [472]. The adhesion strength between fibrinogen and $\alpha_{IIb}\beta_3$ integrins have been reported as high as 80-100pN, while non-specific platelet interactions have shown adhesion strengths below 30pN [473], suggesting that a significant decrease in platelet $\alpha_{IIb}\beta_3$ integrins available for surface binding explains the drastic reduction in platelet attachment and its subsequent spreading. AFM images of Reopro-bound platelets attached to fibrinogen pre-coated a-C:H surfaces, shown in Figure 5.13 (a) and (b), is synonymous with this result.

The $\alpha_{IIb}\beta_3$ integrins adhere to fibrinogen and plasma coated surfaces via both the RGD and γ chain C-terminal -peptide sequence specific binding as well as from non-ligand dependent binding found on albumin and bare surfaces. Consequently, an overall reduction in the number exposed $\alpha_{IIb}\beta_3$ receptors on circulating platelets may explain the significantly lower concentrations round platelets found on fibrinogen and plasma coated surfaces when compared with the bare and albumin surfaces.

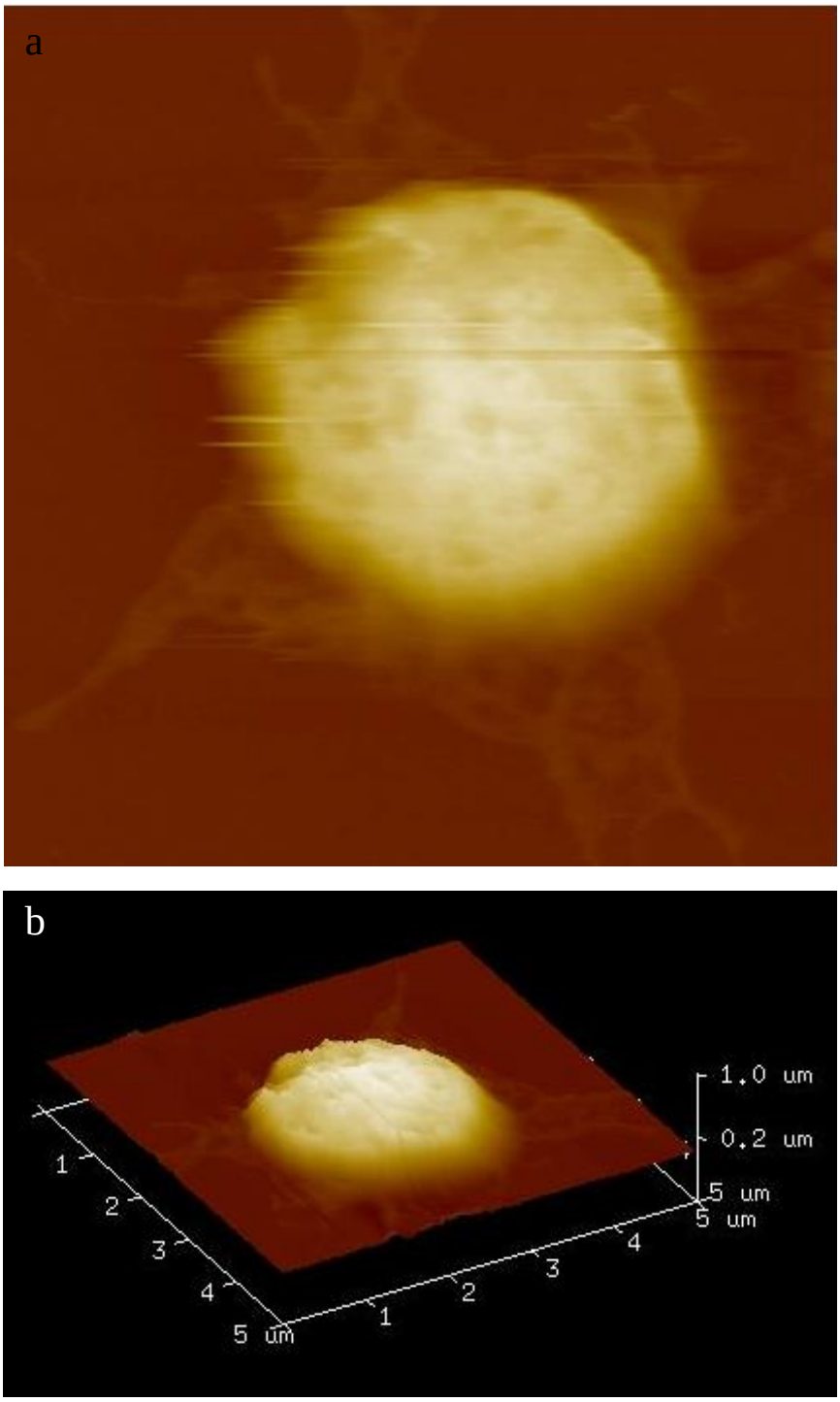

Figure 5.13 AFM topographical images showing (a) 2D and (b) 3D plots of fibrinogen pre-coated a-C:H surfaces seeded with Reopro bound human platelets. Surfaces were analysed in tapping mode with scan rate of 0.2Hz, vertical scale range of 1.0µm and scan size of 5µm x 5µm^2. Measurements we carried out in liquid mode and images corrected using Nanoscope analysis.

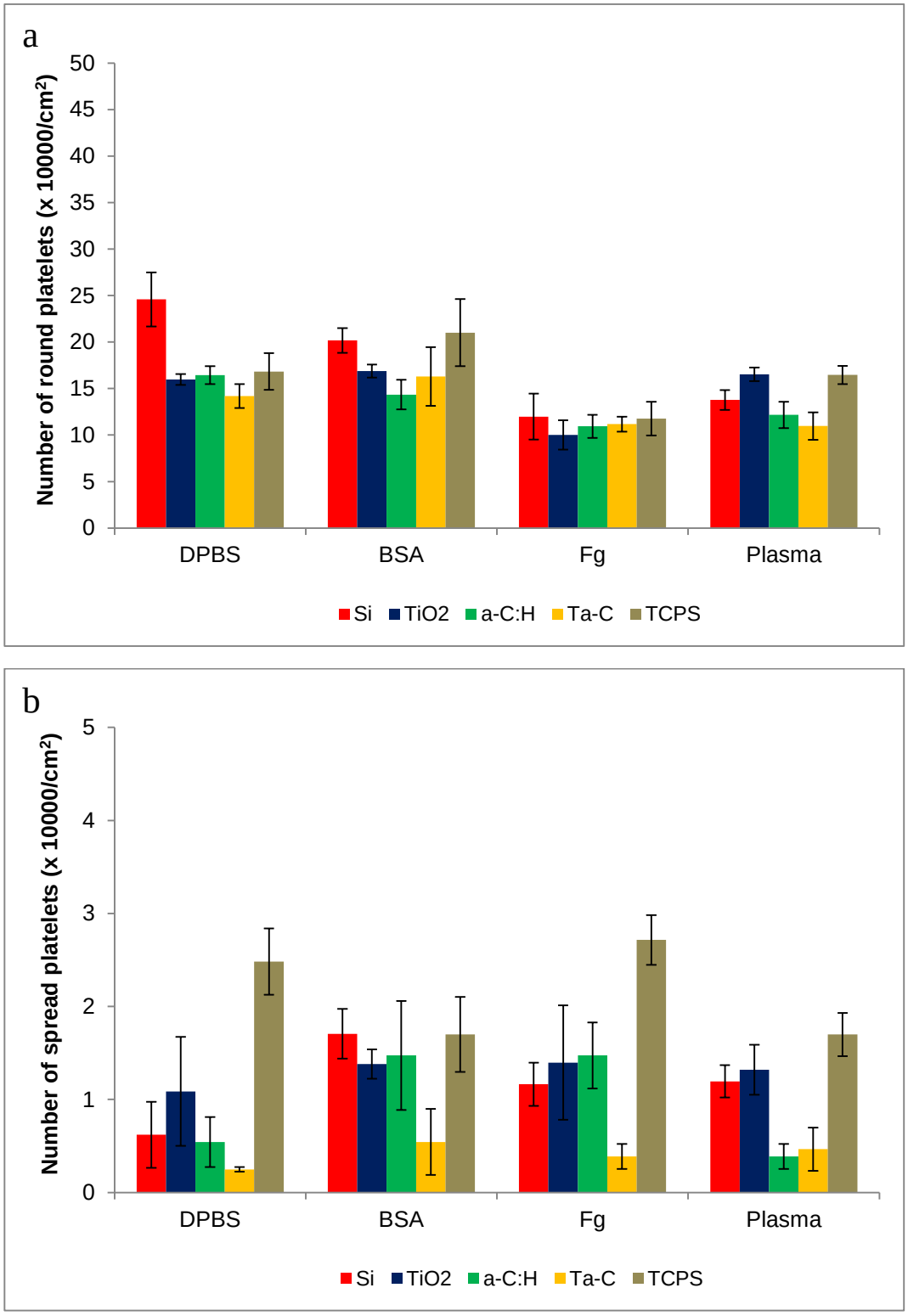

Figure 5.14 Concentration of a. round and b. spread Reopro-bound platelets adsorbed per square centimetre of test substrates, as calculated from fluorescence microscopy images. Platelets were exposed to nano-patterned silicon, TiO_2, a-C:H, ta-C and TCPS flat test substrates without adsorbed proteins (DPBS) as well as albumin (BSA), fibrinogen (Fg), diluted plasma proteins (ratio 1:10, in DPBS) prior to incubation. Error bars: SD (n=3).Statistical analysis was carried out using Student T-Tests and ANOVA.

A significant decrease ($p<0.01$) in the concentration of spread platelets across all four conditions was noticed when platelets were exposed to Reopro than platelets on albumin surfaces not exposed to Reopro (Figure 5.12 (b)). A-C:H surfaces showed decreased concentrations of spread platelets on plasma surfaces, when compared with fibrinogen and albumin pre-coated surfaces where it exhibited similar concentration of spread platelets to silicon and TiO_2 surfaces. TCPS control surfaces, in general, facilitated the higher concentrations of spread platelets, while, Ta-C surfaces supported the lowest concentrations of spread platelets. Decreased levels of platelet spreading as noticed on a-C:H and ta-C surfaces in the presence of plasma proteins may suggest the beneficial and synergistic role surface chemistry, adsorbed plasma proteins and anti- $\alpha_{IIb}\beta_3$ antibodies like Reopro play in enhancing the haemocompatibility of biomaterial surfaces by limiting platelet adhesion and its subsequent spreading.

5.2.1.3 Nano-patterned surfaces

Platelet adhesion on the nano-patterned substrates was investigated to determine the synergistic influence of nano-topography and surface chemistry on the adsorption of platelets on protein pre-coated surfaces. Nano-patterned bare silicon, TiO_2, a-C:H and ta-C surfaces as well as surfaces pre-coated with either 50µg/ml albumin, fibrinogen or diluted plasma proteins (diluted in DPBS, ratio 1:10) for 60 minutes were seeded with $1x10^7$ platelets for an incubation period of 60 minutes at 37ºC to allow sufficient adsorption and adhesion of the platelets. Surface adsorbed platelets were visualised using fluorescence microscopy, by staining the actin filaments with rhodamine-phalloidin (red) stain to reveal cytoskeletal developments, as well as imaged using SEM.

Figure 5.15 shows the conformation of platelets on the nano-patterned surfaces 60 minutes post-seeding using fluorescence microscopy. Nano-patterns on the substrate surface had a significant ($p<0.01$) influence on modulating platelet behaviour and its

subsequent response. A general trend was observed in that a greater number of platelets, as shown by the surface coverage of platelets on both; the protein pre-coated and bare test surfaces, was found on all nano-rough substrates when compared with the flat substrates from section 5.2.1.1. Some regions on each of the surfaces displayed higher concentrations, than others, indicating the formation of large platelet aggregates. Very clear and distinct differences regarding the conformation of the adsorbed platelets were also noticed between the nano-patterned and flat surfaces. Platelets on the nano-patterned surfaces appeared extensively spread out and displayed multi-layer stacking on the surface when compared with the flat surfaces. The greater degree of spreading and consequent increase in surface coverage has led to considerable thinning of the platelet's cross section. The nano-structural components seem to act as topographical cues by significantly aiding in the spreading process. The nano-structures facilitated the platelet's well defined filopodia to probe the nano-patterned surfaces for potential tethering sites and for favourable adhesion. Consequently enhanced cytoskeletal organisation as well as contact guidance was evident on the patterned surfaces where the platelets appear to be flat and well adhered to the surface with irregular morphologies.

f. Nano-patterned silicon

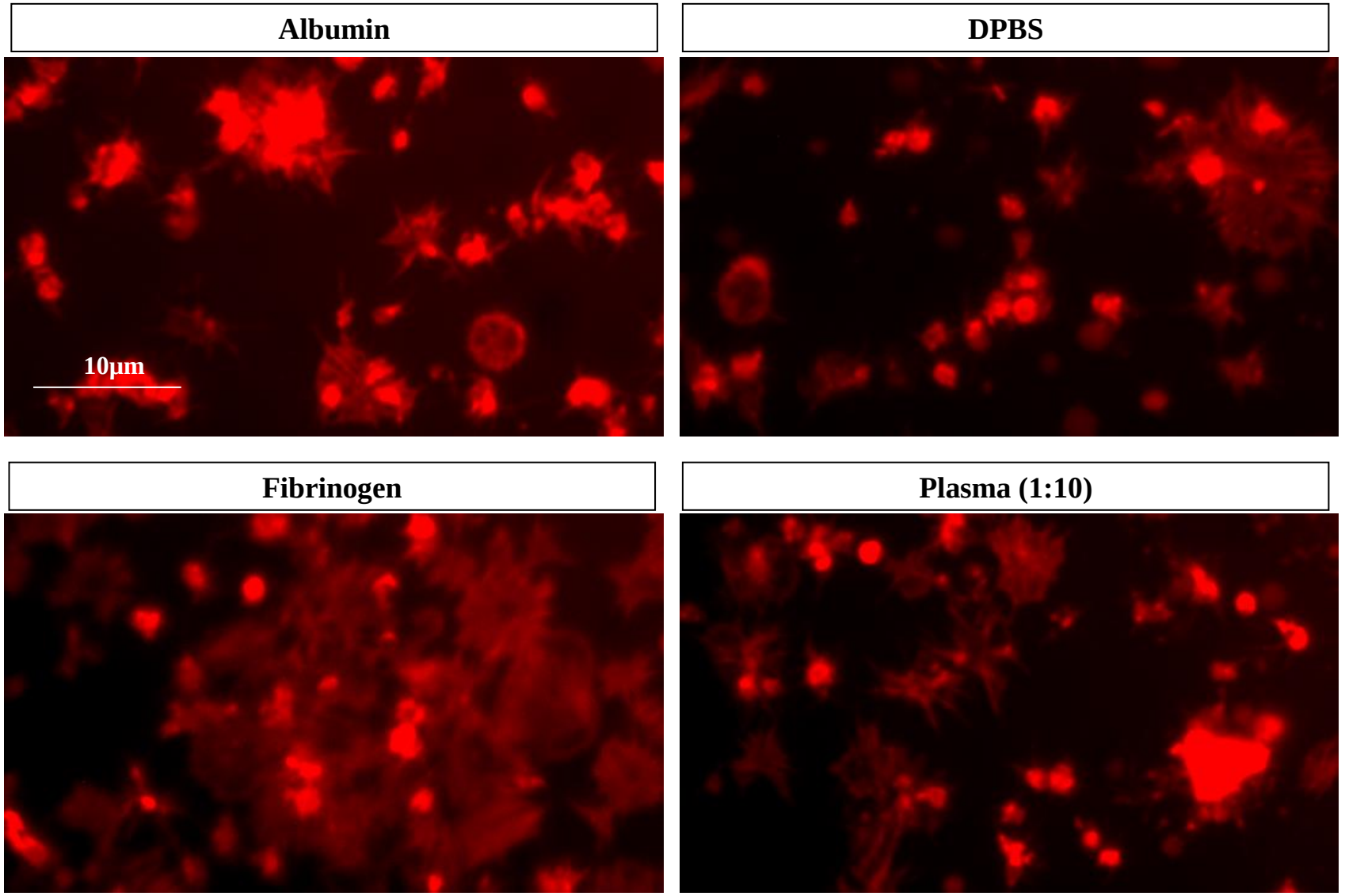

b. Nano-patterned TiO_2

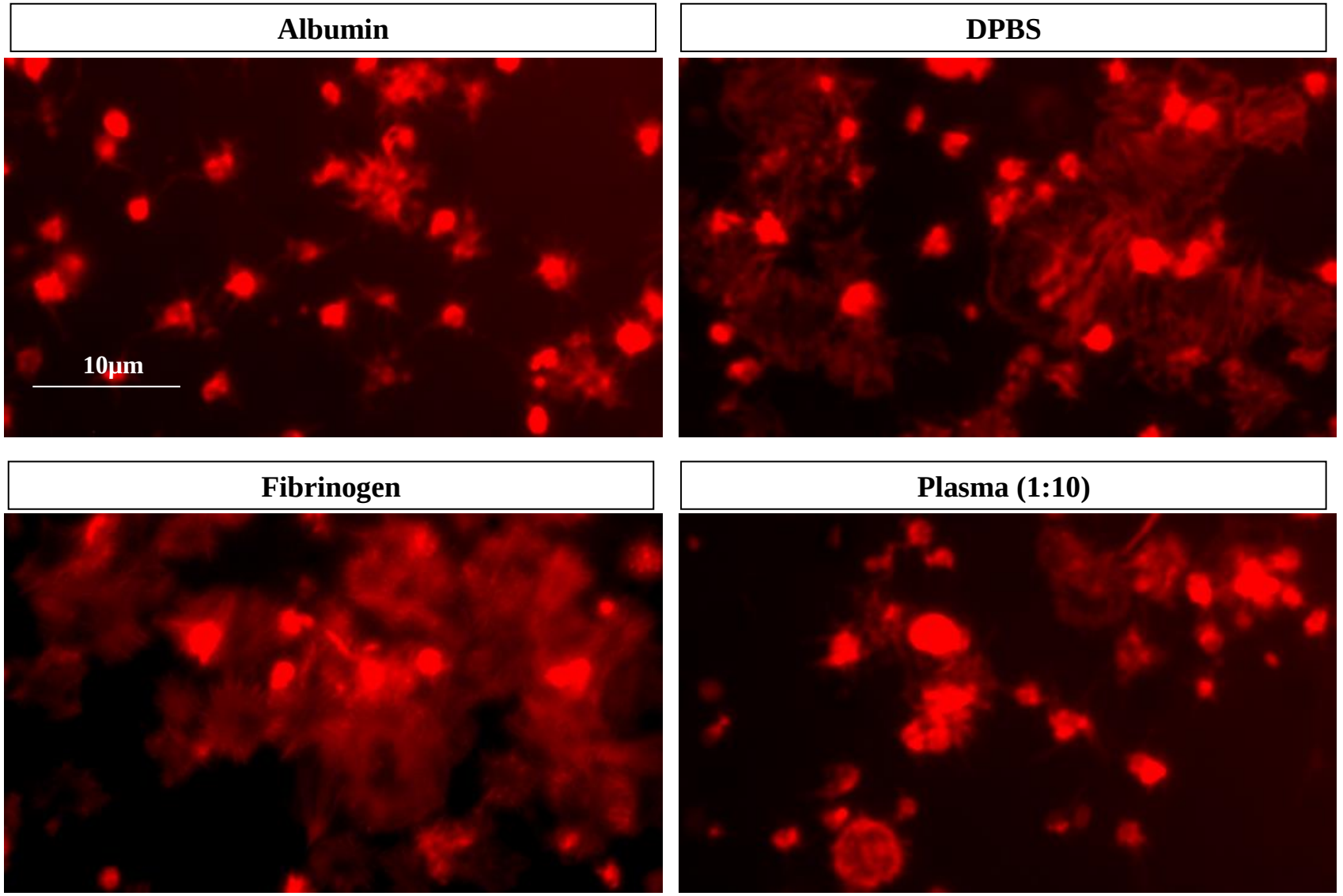

c. Nano-patterned a-C:H

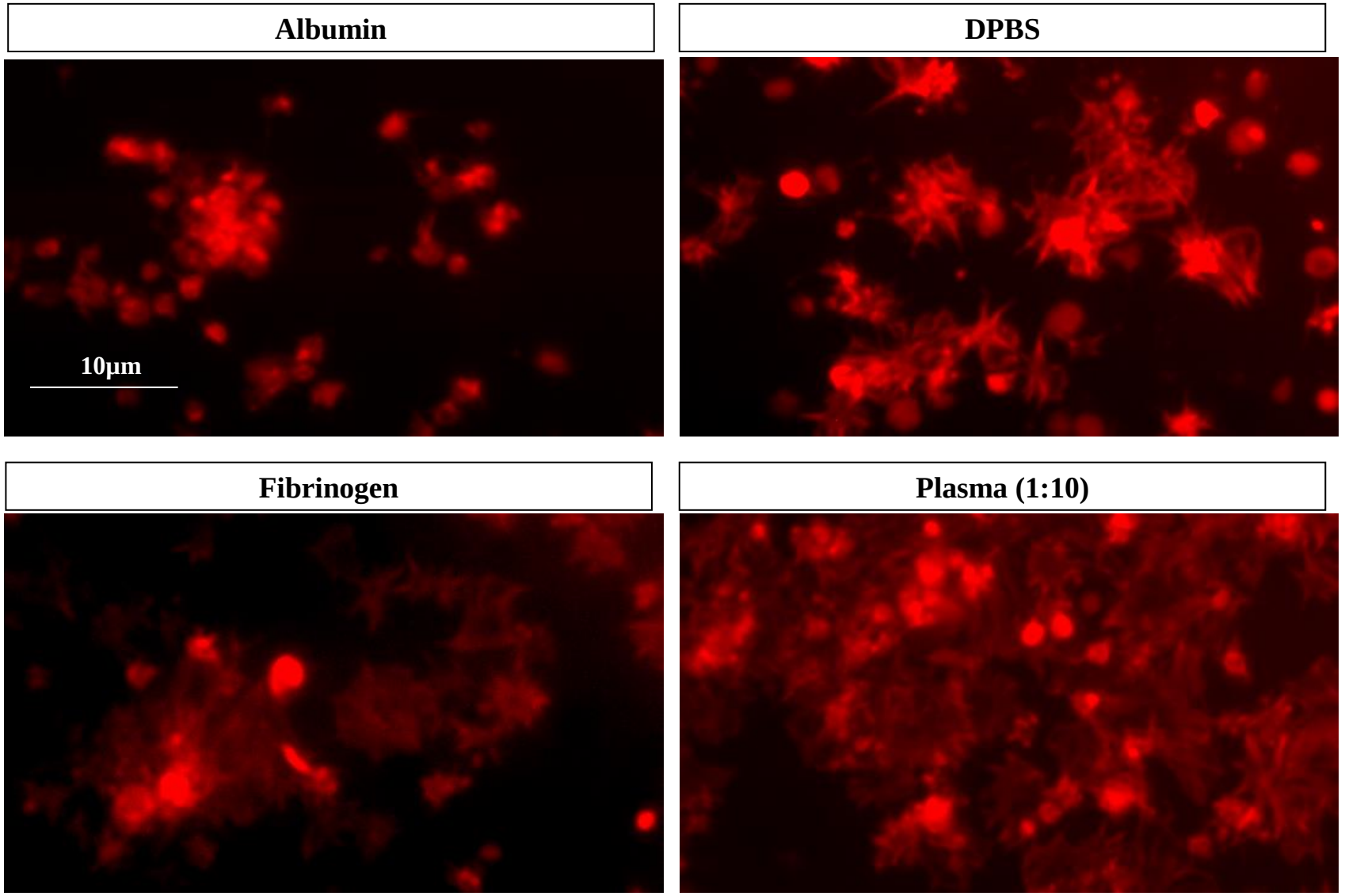

d. Nano-patterned ta-C

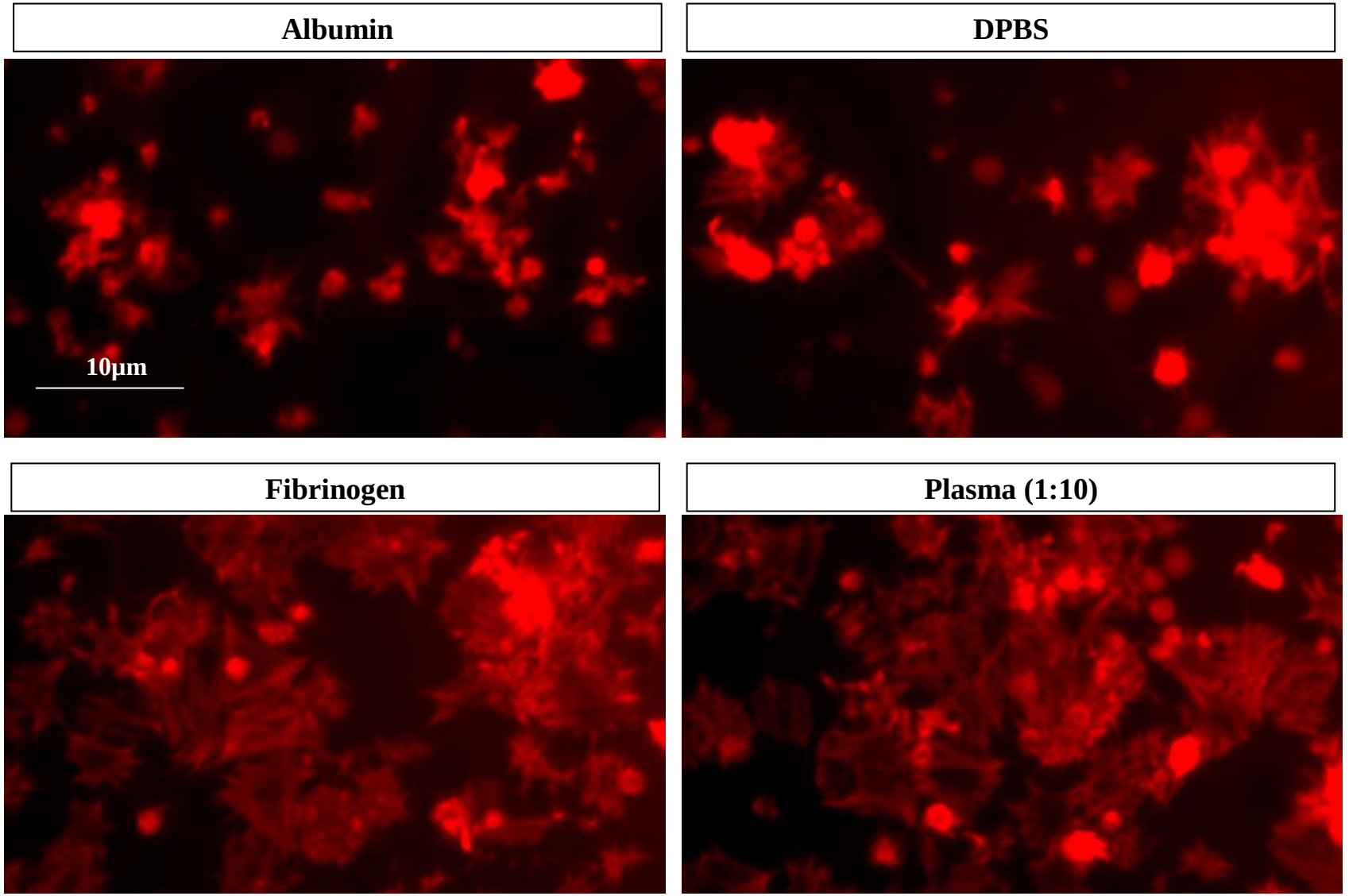

Figure 5.15 Fluorescence microscopy images showing rhodamine-phalloidin stained actin filaments of surface bound platelet cytoskeleton on bare (DPBS) and protein pre-coated a. silicon; b. TiO_2; c. a-C:H; and d. ta-C nano-patterned surfaces. Protein pre-coated surfaces include 50µg/ml albumin (BSA), fibrinogen (Fg) and plasma proteins (diluted in ratio 1:10, in DPBS). Samples were imaged at 500x magnification using Zeiss Axioskop microscope.

High resolution SEM images of platelets adsorbed on nano-patterned surfaces, as shown in Figure 5.16 to 5.19, revealed similar results to fluorescence microscopy images, from Figure 5.15. The platelets exhibited spread morphologies with well-developed actin fibres in the leading edge of the cytoplasmic cell membrane. Further, over-reaching of adjacent platelet filopodia to facilitate communication and activation of cell signalling pathways between nearby platelets was also evident on all surfaces. In some cases intermediary platelets redefine their shape into long bridges, as shown in Figure 5.16 (a) and (b), to support cross-communication between distant platelets. Significant levels of platelet aggregation were evident on all protein-precoated surfaces when compared with platelets on flat surfaces. Nano-patterns cause nano-rough surfaces with numerous peaks and troughs in a pseudo-regular fashion to provide a greater surface area and consequently an increase in potential tethering sites for platelet integrins and subsequent cytoskeletal developments. Platelets were shown to project longer filopodia and present well-developed actin fibres increasing their cohesive adherence to the surface and subsequently their overall activity.

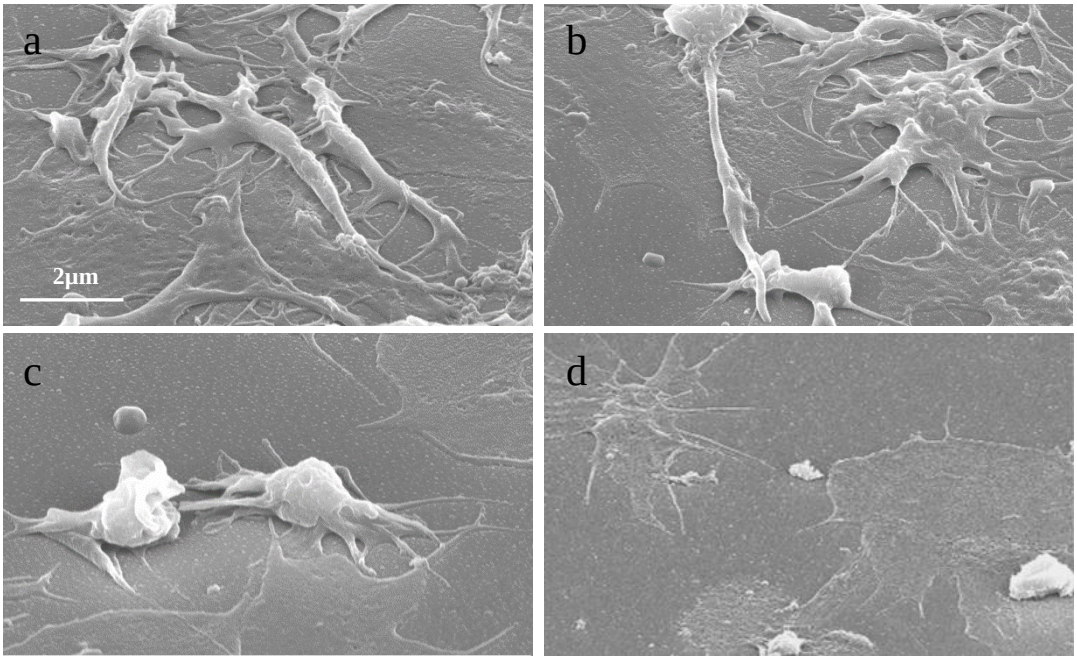

Figure 5.16 SEM images of platelets exposed to nano-patterned (a) silicon, (b) TiO_2, (c) a-C:H and (d) ta-C on pre-coated with albumin (BSA) at 50µg/ml concentration. Samples were imaged using an InLens detector (10KV) at 30K X magnification and 54 degrees stage tilt.

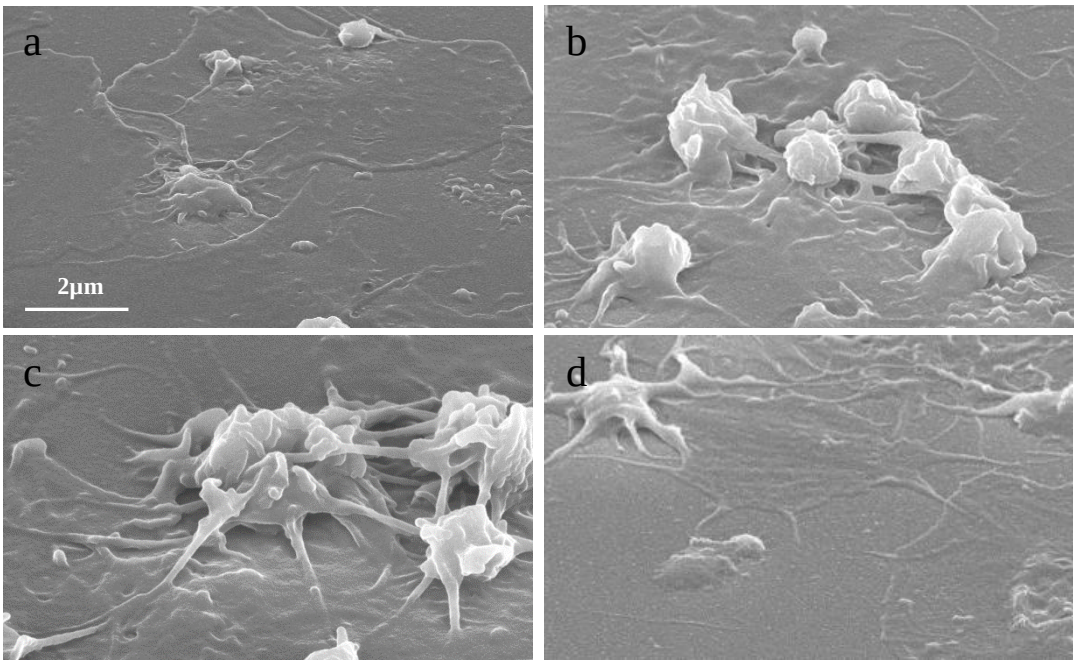

Figure 5.17 SEM images of platelets exposed to nano-patterned (a) silicon, (b) TiO_2, (c) a-C:H and (d) ta-C bare surfaces. Samples were imaged using an InLens detector (10KV) at 30K X magnification and 54 degrees stage tilt.

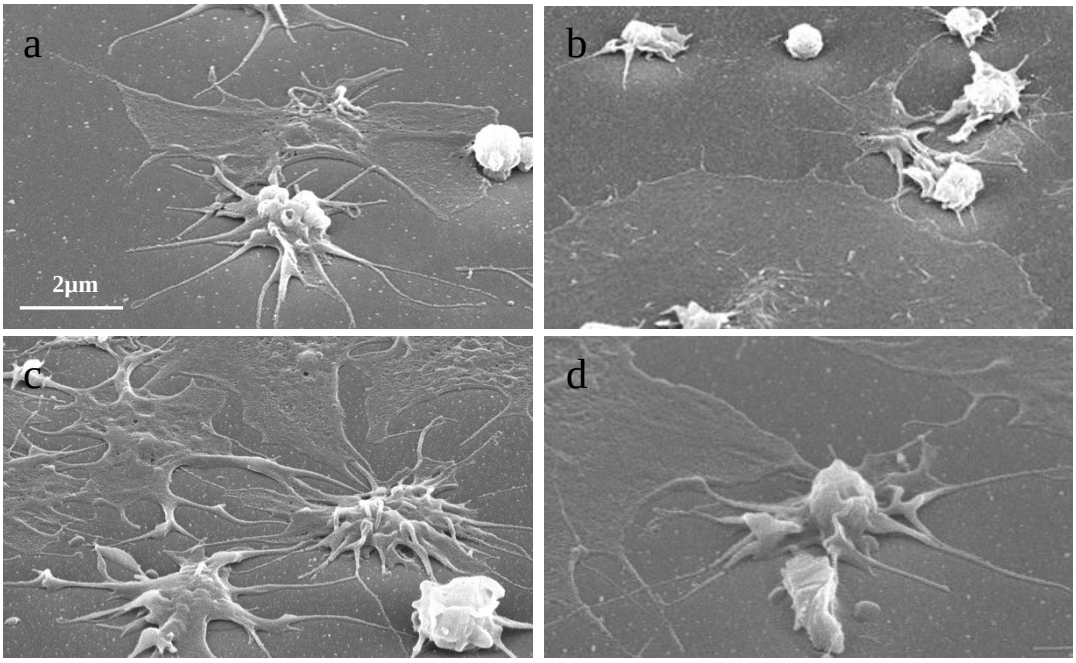

Figure 5.18 SEM images of platelets exposed to nano-patterned (a) silicon, (b) TiO_2, (c) a-C:H and (d) ta-C on pre-coated with fibrinogen (Fg) at 50µg/ml concentration. Samples were imaged using an InLens detector (10KV) at 30K X magnification and 54 degrees stage tilt.

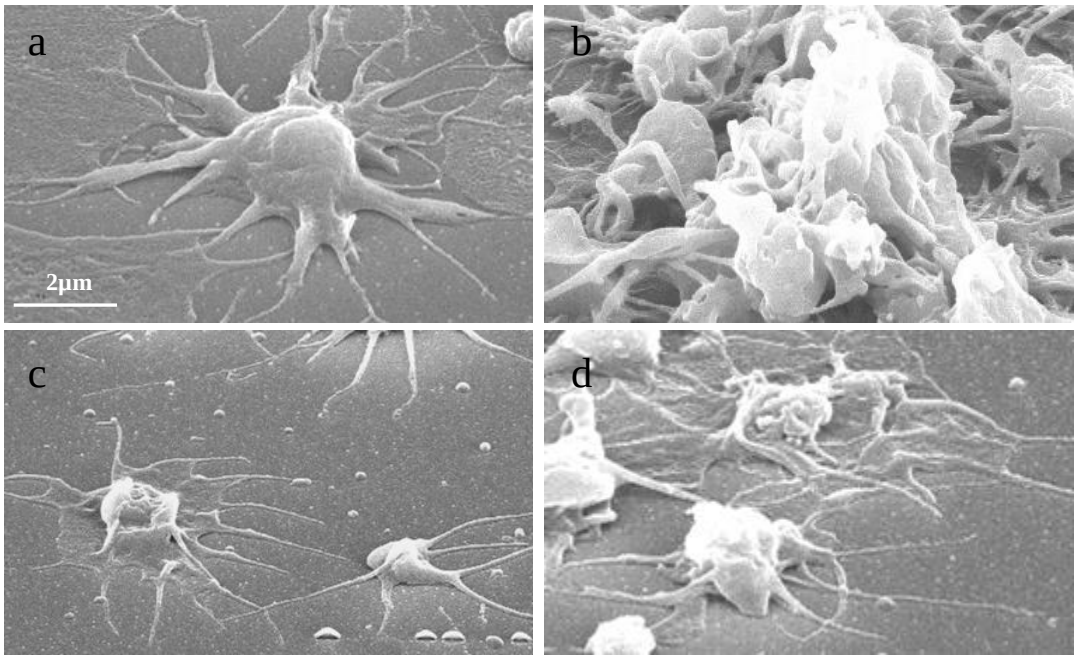

Figure 5.19 SEM images of platelets exposed to nano-patterned (a) silicon, (b) TiO_2, (c) a-C:H and (d) ta-C on pre-coated with diluted plasma (dilution factor 1:10, in DPBS). Samples were imaged using an InLens detector (10KV) at 30K X magnification and 54 degrees stage tilt.

AFM images of platelets exposed fibrinogen pre-coated a-C:H nano-patterned surfaces exposing the network of actin cytoskeleton in the platelet cytoplasm is shown in Figure 5.20 and Figure 5.21. Further, the intercommunication between adjacent platelets was visualised in high resolution in Figure 5.21. The dendritic network of platelet filopodia on the adhered platelet shown in Figure 5.20 appears more prominent than on fibrinogen coated flat surfaces (Figure 5.7) reinforcing the micro-structural and nano-structural changes in platelet's actin cytoskeleton when exposed to nano-rough surfaces. Stiffness of such protrusions have been shown to be similar to that of the active actin polymerisation sites at the edge of the cell [474] and their relative Young's modulus was determined as 46.5kPa [470].

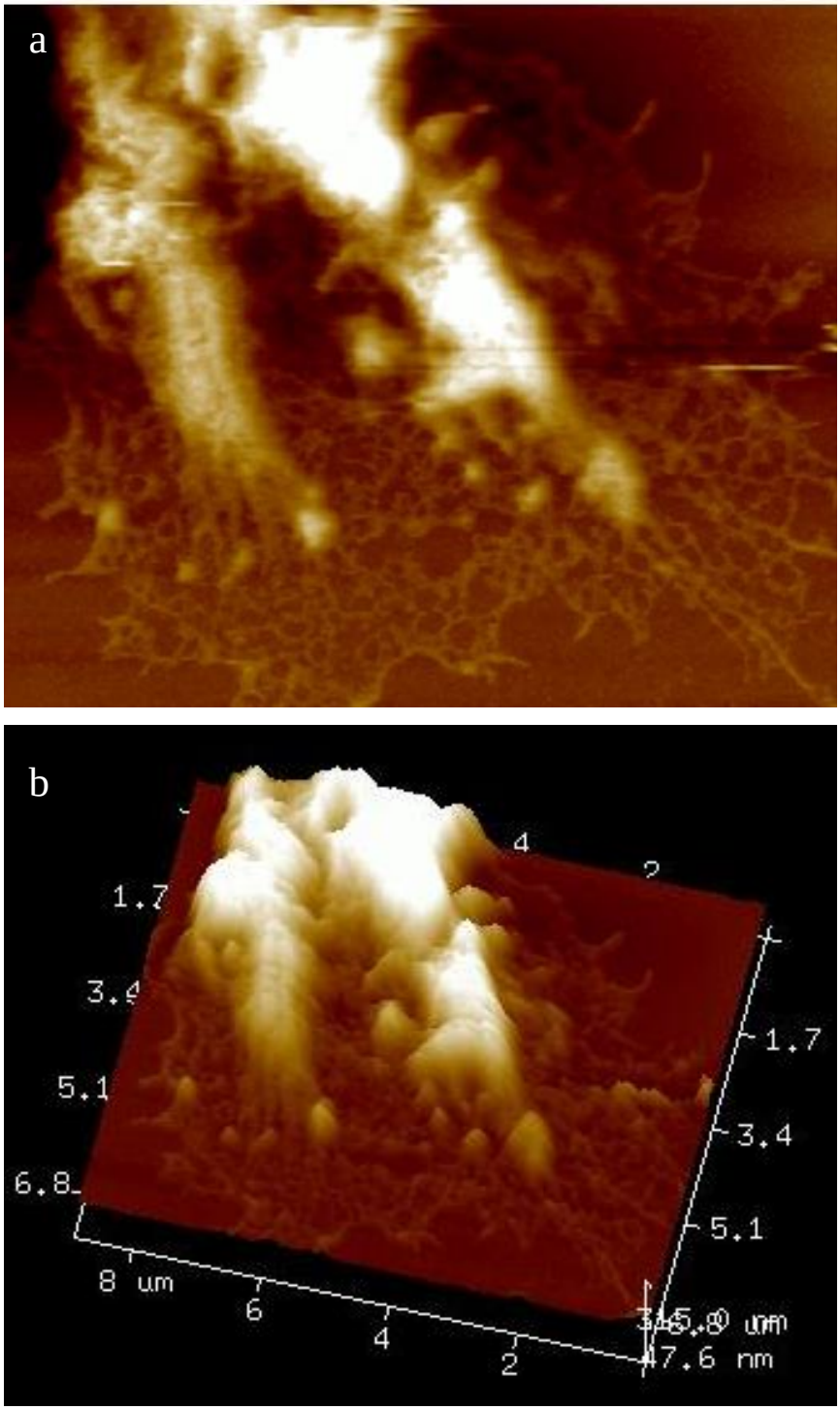

Figure 5.20 AFM topographical images showing (a) 2D and (b) 3D plots of platelets adhered to nano-patterned a-C:H surfaces pre-coated with fibrinogen. Surfaces were analysed in tapping mode with scan rate of 0.2Hz, vertical scale range of 0.4µm and scan size of 10µm x 10µm2. Measurements we carried out in liquid mode and images corrected using Nanoscope analysis.

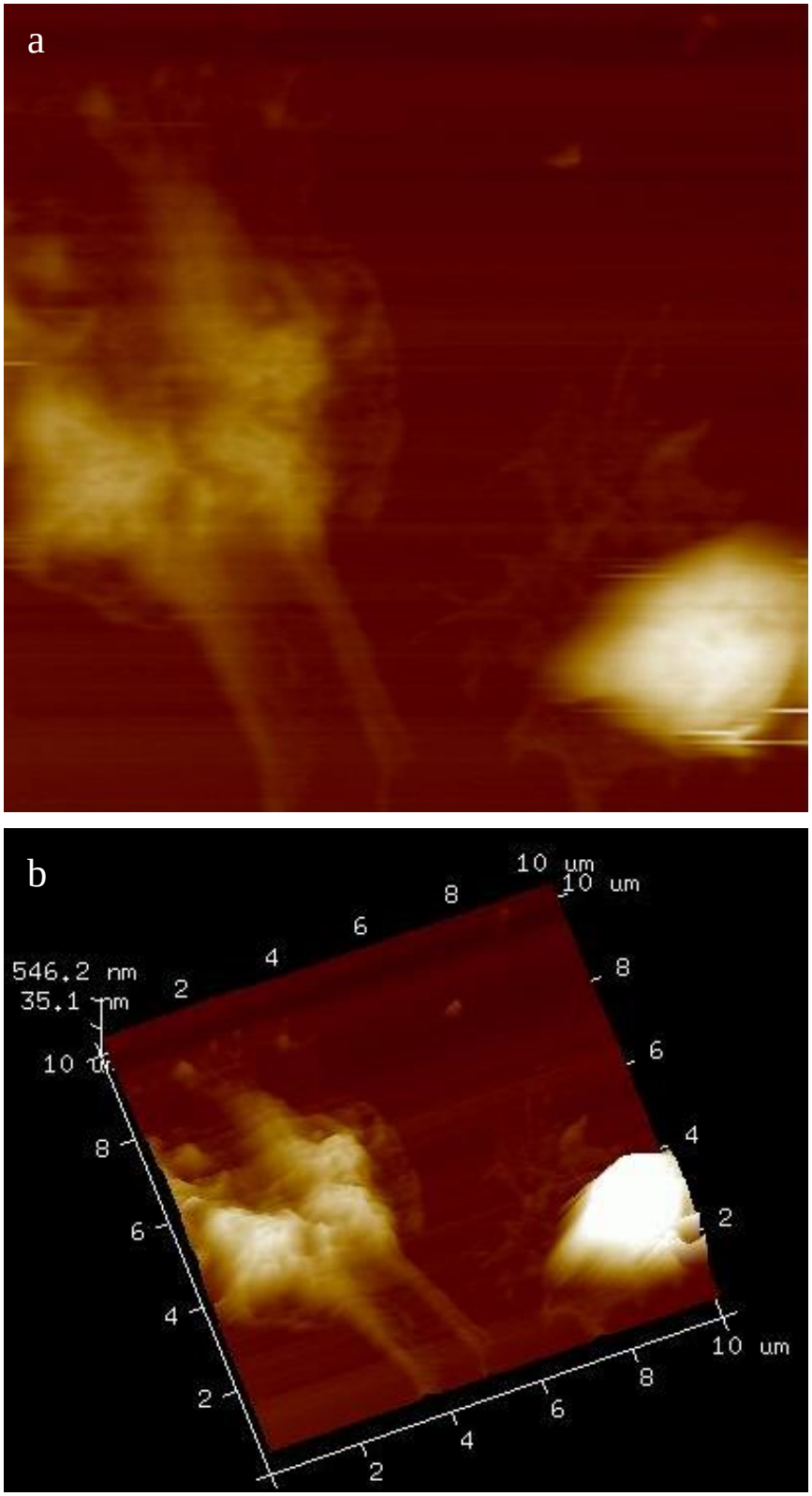

Figure 5.21 AFM topographical images showing (a) 2D and (b) 3D plots of platelet cross-communication upon adhering to nano-patterned a-C:H surfaces pre-coated with fibrinogen. Surfaces were analysed in tapping mode with scan rate of 0.2Hz, vertical scale range of 0.55µm and scan size of 10µm x 10µm^2. Measurements we carried out in liquid mode and images corrected using Nanoscope analysis.

Figure 5.22 (a) and (b) show the total concentration of adhered cells and degree of platelet spreading on the protein pre-coated nano-patterned surfaces, respectively. Enhanced cell adhesion and cytoskeletal developments (shown as mean surface coverage) was evident on the nano-patterned surfaces when compared with flat surfaces, suggesting that the specific spatial arrangement of the nano-structures formed by the block co-polymer method along with the altered surface chemistry from nano-patterning is conducive to enhanced remodelling of the actin-cytoskeleton architecture and subsequent platelet response. Fibrinogen followed by plasma coated surfaces exhibited elevated platelet concentrations and spreading when compared with albumin coated and un-coated surfaces. This reinforces that a monolayer of albumin minimises, although doesn't completely inhibit, the adhesion and spreading of platelets and consequently reducing the likelihood of thrombus formation [117, 475]. In comparison to a-C:H and ta-C surfaces, TiO_2 presented higher platelet levels and spreading on all protein conditions except plasma proteins where a-C:H and ta-C surfaces displayed significantly elevated ($p<0.01$) platelet concentrations. When compared with the bare surfaces, adsorbed albumin decreased the overall platelet adhesion on both; a-C:H and ta-C surfaces, while fibrinogen and plasma proteins enhanced platelet adhesion. Plasma proteins other than fibrinogen, have been shown to reduce platelet attachment on flat a-C:H and ta-C surfaces when compared with the bare surfaces (section 5.2.1.1), while nano-structures increase the overall adhesion and spreading of platelets by reducing the ability of plasma proteins to resist platelet attachment. Conformation of the adsorbed proteins can be evaluated using platelet adhesion studies where surfaces with increased platelet concentrations may be used as a measure to indicate the likelihood of platelets to adhere to specific binding regions on adsorbed proteins. A general increase in platelet concentrations across all four conditions suggest an altered conformation of albumin, fibrinogen and plasma proteins on the nano-patterned surfaces such that the surfaces support higher levels of ligand-dependent and non-specific platelet adhesion.

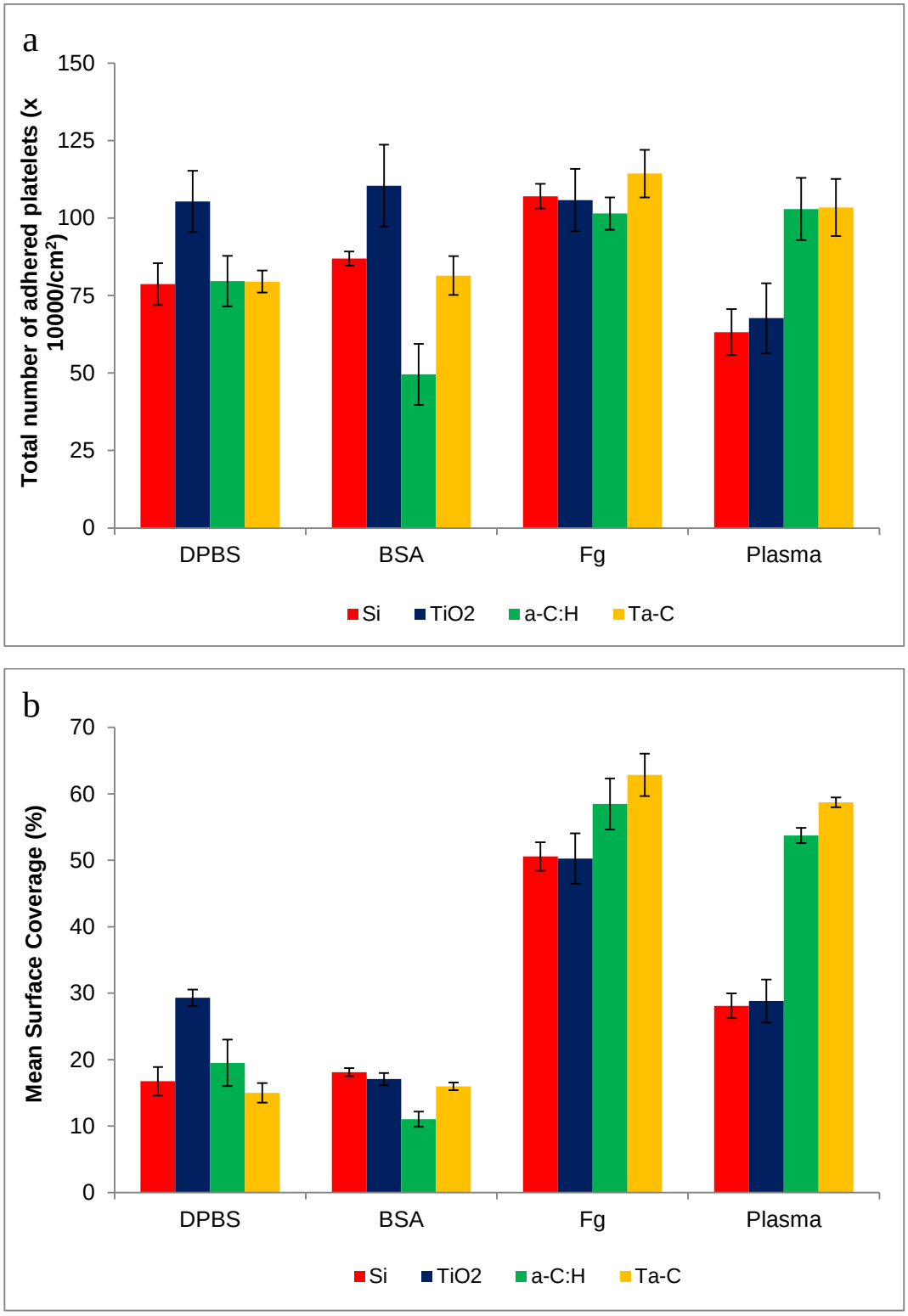

Figure 5.22 Comparison of a. surface bound platelet concentrations, per square centimetre, and b. mean surface coverage by the platelets, as percentage value, calculated from rhodamine-phalloidin stained fluorescence microscopy images. Nano-patterned silicon, TiO_2, a-C:H, ta-C and TCPS test substrates were pre-coated with albumin (BSA), fibrinogen (Fg) and diluted plasma (ratio 1:10, in DPBS) prior to platelet incubation. The results were compared with surfaces devoid of proteins (DPBS). Error bars: SD (n=3).

This may further explain why actin filaments are better tensioned on fibrinogen and plasma proteins adsorbed on nano-patterned surfaces while fewer filopodia is observed for platelets adhered on albumin coated and bare nano-patterned surfaces. As such these results further reinforce that both; surface chemistry, surface topography (as in increase in surface roughness in the nanoscale region) are important factors in influencing biological response.

A breakdown of number of round cells, retaining their spherical shape with minimal radial protrusions (filopodia), and, spread platelets with well-developed actin fibres on nano-patterned surfaces are shown in Figure 5.23(a) and (b), respectively. Fibrinogen and plasma pre-coated surfaces showed decreased adhesion of round platelets and elevated levels of spread platelets, except for plasma coated TiO_2 surfaces which showed increased concentration of round platelets. On the other hand, surfaces devoid of proteins showed elevated levels of round platelets when compared with spread platelet concentrations. In the presence of plasma proteins, nano-patterned silicon and TiO_2 presented decreased levels of spread platelets, and consequently decreased percentage of mean surface coverage (Figure 5.22 (b)) than a-C:H and ta-C. However this was not the case on flat substrates (section 5.2.1.1) where plasma and fibrinogen coated silicon and TiO_2 displayed increased adhesion round and spread platelets when compared with a-C:H and ta-C. Variances in platelet attachment between nano-patterned and un-patterned surfaces of the same material, in terms of concentrations of adsorbed cells as well as its morphology, reinforces that changes in nano-scale surface topography can markedly influence platelet-surface interactions and subsequent platelet activation to affect the overall haemocompatibility of a biomaterial surface.

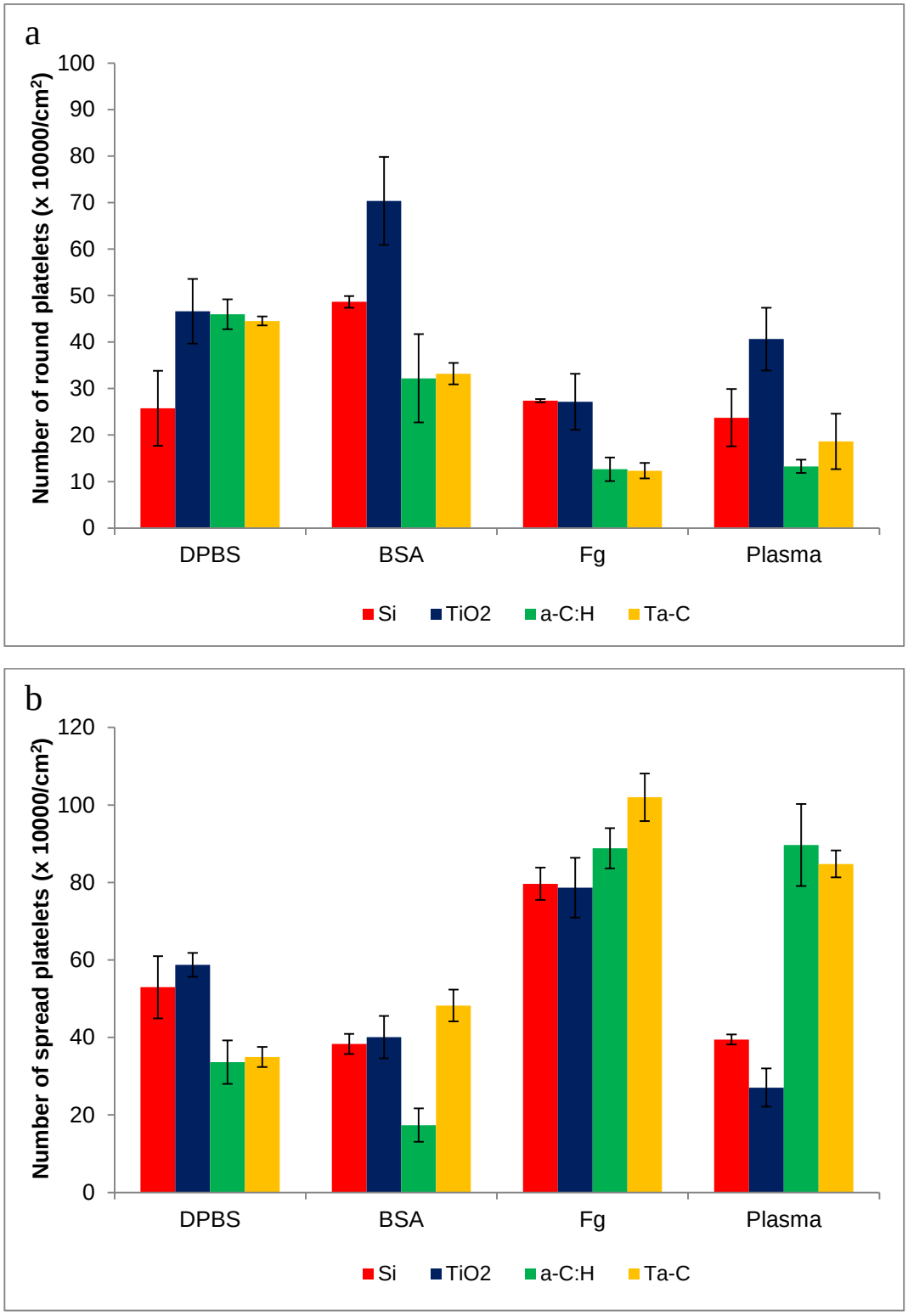

Figure 5.23 Concentration of a. round and b. spread platelets adsorbed per square centimetre of nano-patterned substrates, as calculated from rhodamine-phalloidin stained fluorescence microscopy images. Platelets were exposed to nano-patterned silicon, TiO_2, a-C:H, ta-C and TCPS nano-paterned test substrates without adsorbed proteins (DPBS) as well as albumin (BSA), fibrinogen (Fg), diluted plasma proteins (ratio 1:10, in DPBS) prior to incubation. Error bars: SD (n=3).

5.2.2 QCM-D studies

Changes in frequency and dissipation as measured via QCM-D were also used to examine platelet adhesion. Typical change in dissipation versus change in frequency ($\Delta D/\Delta f$) plots of platelet attachment on each of the bare surfaces or surfaces pre-adsorbed with proteins were constructed to provide accurate measurements of changes in coupled mass and viscoelasticity, independent of the position on the electrode [476].

QCM-D signals do not have a linear relationship with the concentration of cells attached on the resonator surface. Cells form a non-homogenous sub-monolayer, covering only a small proportion of the electrode surface, leaving a larger portion of the surface area still uncovered. Cell behaviour in situ can only be envisioned as small perturbation to the interfacial properties of the QCM crystal surface in liquid, and as such Sauerbrey equation cannot be used [477]. Further, the penetration depth of the shear wave from the surface of QCM sensors into the bulk, at 5MHz, is only 150nm [463], which is much shorter than the average platelet diameter (approximately 2-4µm). Frequency shifts and subsequent changes in dissipation energies will appear diminished as they are representative of merely a fraction of the cell mass closest to the surface of sensor electrode. An increase in the thickness of the viscoelastic layer will also affect frequency shifts further diminishing the time dependent frequency and dissipation curves.

As such Df plots were ascribed for platelet studies because the lateral sensitivity of the QCM-D sensor in measuring changes in resonant frequency (Δf) and dissipation factor (ΔD) are both proportional to the oscillating amplitude and their sensitivities vary in relation to the Gaussian functions of their distance from the middle of the electrode[476]. $\Delta D/\Delta f$ plots have also paved way for analysing the dynamic nature of the adhesion process in QCM-D, such as; the time-wise deposition of mass and the evolvement of its viscoelastic properties and the internal cytoskeletal developments as well as the overall shape of individual cells as a function of time [476, 478].

D*f* plots for platelets exposed to TiO_2, a-C:H and control silica (SiO_2) surfaces pre-incubated with either 50µg/ml of albumin, DPBS, 50µg/ml of fibrinogen or diluted plasma proteins (ratio 1:10, in DPBS) are shown in Figure 5.24 (a), Figure 5.25(a), Figure 5.26(a) and Figure 5.27 (a), respectively. And, pre-incubation of platelets with anti-$\alpha_{IIb}\beta_3$ (Reopro) antibody prior to their exposure to resonator substrates pre-coated with 50µg/ml of albumin, DPBS, 50µg/ml of fibrinogen or diluted plasma (ratio 1:10, in DPBS) are presented in Figure 5.24Figure 5.25(b), Figure 5.26(b) and Figure 5.27(b), respectively.

Silicon has a high affinity for oxygen and has been known to rapidly oxidise in air to form a native oxide layer [479], and as such silicon QCM crystals with a homogenous thin coating of SiO_2 were purchased as model control substrates to mimic similar platelet responses as on silicon surfaces from Section 5.2.1. TiO_2 and a-C:H coated as a thin layer on the these control silica crystals were analysed previously in Sections 4.2and 4.3.4. Ta-C surfaces were not studied using QCM-D as the ta-C coating repeatedly delaminated off the silica surface rendering the surfaces unusable for experimentation. The arrows (where applicable) represent the time sequence of the data for the third overtone (n = 15Hz).

Previous studies [480-482] have shown that major interactions between cells and the adhering surfaces is through integrin receptors and that frequency shifts are typically representative of specific adhesion, or integrin mediated response, between cells and surfaces of QCM sensors. Integrin receptors cluster at focal adhesions facilitating direct contact between the ventral plasma membrane and the resonator surface [483]. Direct contact is achieved through the actin cytoskeleton, as they bind the cell membrane to the end of the focal adhesion [483]. In cell studies, frequency shifts corrolate with changes in coupled mass, implying adhesion of cells to the resonator surface, while an increase in D suggest an increase in the number of cells adhered to the surface as well as the extent of their spreading [402]. However, decreases in D values with increasess in *f* are also indicative of cell spreading and cytoskeletal changes. Such changes to the D vs. *f* gradient is representative of an increase in rigidity of the cellular adlayer possibly caused by changes in the thichness of the

adlayer, increase in focal contacts on the resonator surface or their viscoelastic properties [402, 484]. Non-interacting cells, resting on the resonator surface, have not been known to show any appreciable changes in f and D [402, 485].

In Figure 5.24(a), the QCM-D response curve for platelets adhering to albumin coated TiO_2 was different to albumin coated silica and a-C:H suggesting that platelets interacted differently on TiO_2 sensors. Pure elastic mass response on a Df plot occurs when $\Delta D = 0$ while a pure liquid viscosity-density response transpires when a marked increase in the ΔD to f ratio occurs. Rise in the D and f ratio is also known as the viscosity-density effect and may suggest an absence of surface binding and only fluid above the crystal [485]. The region in-between the pure elastic and viscosity density region is known as the viscoelastic region where a proportional increase in D with decreasing f is indicative of an increase in cellular point contacts and increased platelet adhesion. The exposure of platelets to TiO_2 and a-C:H surfaces resulted in Df plots that fell well within the viscoelastic region and as such platelet interactions on these surfaces behaved as viscoelastic materials during the incubation period of 60minutes. The Df plots for platelets exposed to albumin coated silica continued to exhibit a decrease in f and an increase in D throughout the measurement period, however, control silica surfaces deviated from the viscoelastic behaviour during the last 10 minutes of the incubation period, which correlates with increased platelet surface contact and consequently increased volume of platelets being sensed during the period of measurement. Corroborating with this was the increased concentrations of spread platelets found in Figure 5.9(b). Similar platelet responses on silicon and silica surfaces with deviation from the viscoelastic behaviour during the end stages of platelet incubation in QCM-D may be attributed to the development and polymerisation of the actin monomers in the platelet cytoskeleton to form actin-rich radial protrusions or filopodia. Platelets interacting with albumin coated a-C:H surfaces exhibited a steady decrease in f with increasing D values, again suggesting an increase in focal adhesions but not necessarily cell spreading. Coupled with this was the increased numbers of round platelets than spread platelets found on a-C:H surfaces from Figure 5.9.

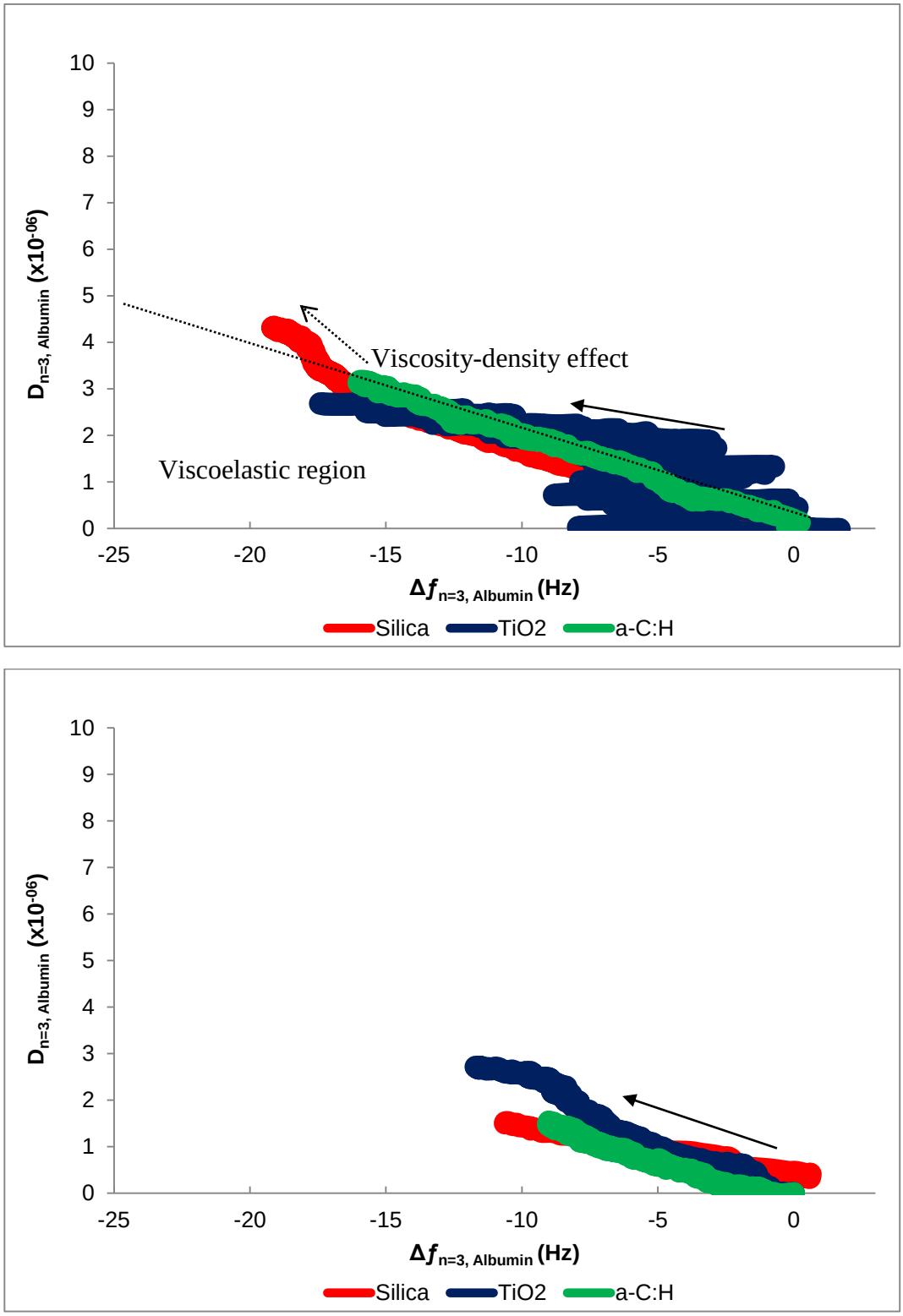

Figure 5.24 Dissipation versus frequency curves (third overtone; n=3; 15Hz) for albumin coated silica, TiO_2 and a-C:H surfaces exposed to a. normal platelets b. platelets pre-incubated with anti-$\alpha_{IIb}\beta_3$ (Reopro) antibody, as determined by QCM-D. Red, blue and green arrows represent the direction of increasing time for silica, TiO_2 and a-C:H surfaces, respectively.

Interestingly, the response of platelets on albumin coated TiO_2 surfaces, for the first 30 minutes of incubation, showed little change in measurements after the initial platelet-surface contact. This resulted in frequency shifts of approximately -5Hz during the first half of the incubation process after which platelets on albumin coated TiO_2 followed a viscoelastic behaviour, similar to that of albumin coated a-C:H substrates suggesting that even though smaller concentrations of platelets adhered on the resonator surface, their degree of spreading of the adhered platelets is greater than the platelets exposed to albumin coated a-C:H or silica surfaces. Further similar end frequency shifts could suggest that the same proportion of TiO_2 surface was covered by platelets and/or their focal contacts as on a-C:H and silica. This corroborates with the % surface coverage data obtained from fluorescence microscopy (Figure 5.8(b)) further reinforcing that although albumin reduces platelet adhesion it does not completely eliminate platelet adhesion or its subsequent spreading.

Pre-incubation of platelets with anti-$\alpha_{IIb}\beta_3$ (Reopro) antibody followed by exposure to albumin coated surfaces, as shown in Figure 5.24(b), presented time-wise decrease in frequency as dissipation increased. The resulting curve fell within the viscoelastic region of the Df plot. Furthermore, the frequency shifts caused by Reopro-bound platelets are similar in nature between the three surfaces and are smaller than the frequency shifts recorded from their corresponding normal platelet response (Figure 5.24(a)) suggesting a reduction in platelet adhesion and spreading. These results are synonymous with fluorescent microscopy analysis from Section 5.2.1.2.

In Figure 5.24(a), the QCM-D response curve for platelets exposed to bare surfaces was different to platelets exposed to albumin coated surfaces. The Df plot was significantly greater for platelets exposed to bare surfaces even though the gradient of the D f plot remained the same with maximum dissipation change were found to be 7.6×10^{-6}, 7.1×10^{-6} and 6.8×10^{-6} and frequency shifts of -38Hz, -30Hz and -31Hz for silica, TiO_2 and a-C:H surfaces, respectively. The gradient for all three surfaces were found to be relatively linear with no major fluctuations suggesting that platelets were forming attachments on the biomaterial surface and their cytoskeleton

developed over time causing spreading across the surface. Platelets exposed to bare silica surfaces exhibited a greater frequency shift than platelets exposed to a-C:H and TiO_2 suggesting that bare silica surfaces supported greater platelet adhesion than a-C:H and TiO_2 surfaces. These results are concurrent with fluorescence microscopy analysis shown in Figure 5.8 and Figure 5.9. Further, a greater frequency change for platelets exposed to bare surfaces than platelets exposed to albumin coated surfaces suggests that platelets exposed to bare surfaces present increase focal contacts, possibly due to increased cell attachment, and exhibit increased platelet spreading. These results are synonymous with fluoresce microscopy results explain in Section 5.2.1.

Pre-incubation of platelets with anti-$\alpha_{IIb}\beta_3$ (Reopro) antibody followed by exposure to bare surfaces, as shown in Figure 5.24(b), presented decreases in f and increases in D with the resulting curve falling within the viscoelastic region of the Df plot. The QCM-D responses between the three surfaces were quite different from each other, which suggest that platelets exposed on these surfaces interacted differently on each surface even though they supported the similar levels of platelet adhesion (Figure 5.12(a)). And, the change in frequency of Reopro-bound platelets on silica, TiO_2 and a-C:H surfaces were less than normal platelets exposed to these substrates suggesting lesser adhesion and subsequent spreading of cells, as found in Section 5.2.1. Reopro incubated platelets on TiO_2 sensors did not change in dissipation values as frequency decreased during the first 15minutes of the measuring period after which a steady rate of increase in dissipation was noted, proportional to changes in frequency. Cells have been known to adhere to the resonator surface within the 10 minutes after which any changes observed in f are indicative of changes cause by cell's surface contacts and/or due to protein remodelling [481].

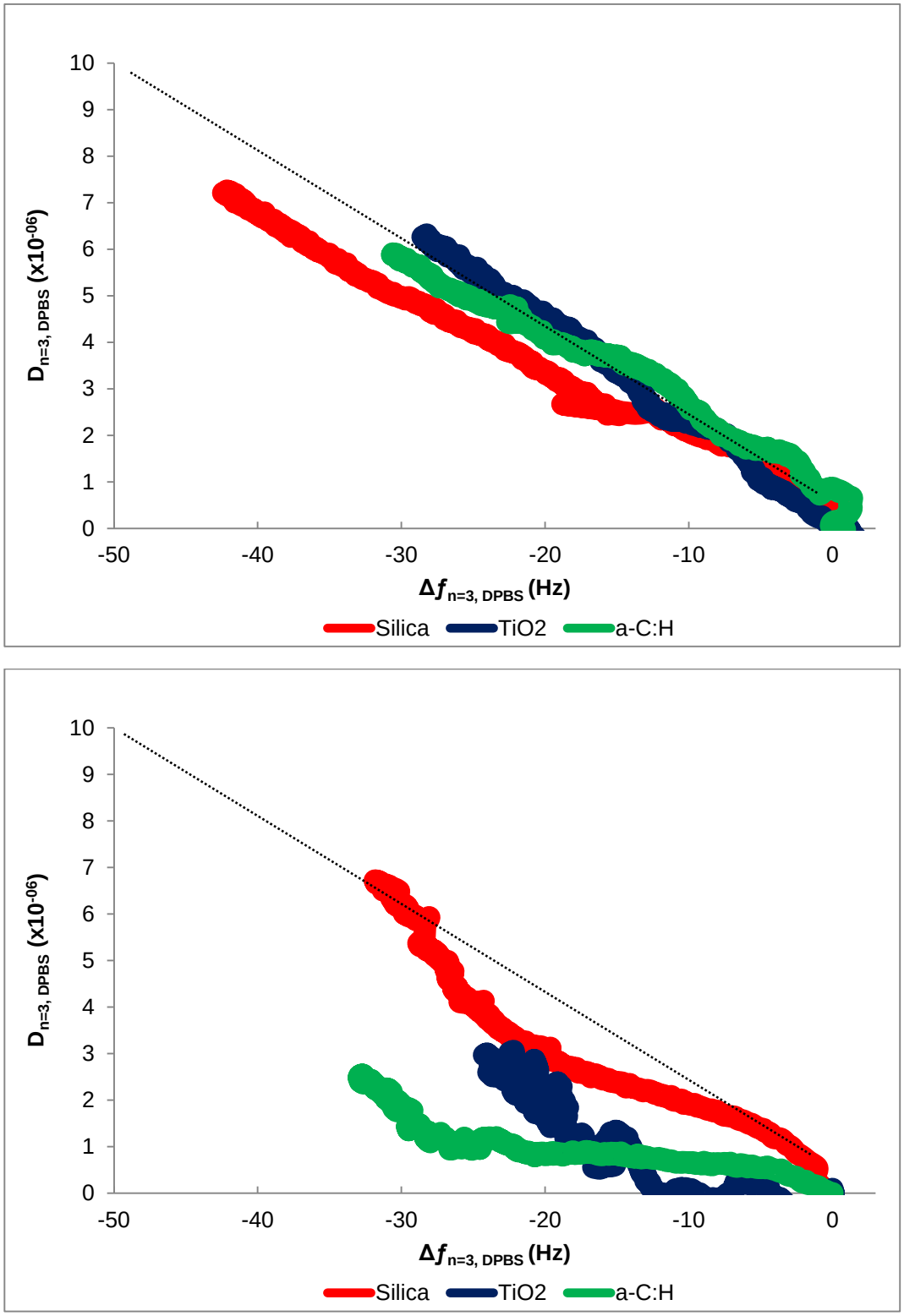

Figure 5.25 Dissipation versus frequency curves (third overtone; n=3; 15Hz) for bare silica, TiO_2 and a-C:H surfaces exposed to a. normal platelets b. platelets pre-incubated with anti-$\alpha_{IIb}\beta_3$ (Reopro) antibody, as determined by QCM-D.

This suggests reopro-bound platelets exposed on TiO_2 surfaces adhered to the surfaces within the first 15minutes of the incubation period during which they did not exhibit any remodelling of their actin cytoskeleton. Formation of tightly adhering filopods as well as changes in platelet architecture facilitating increased platelet spreading occured within the last 45 minutes of the incubation period. These results are synonymous with fluorescence microscopy images (Figure 5.12(a) and (b)) showing higher percentage of reopro-bound platelet-surface coverage and lesser concentrations of adhered reopro-bound platelets than the other substrates.

Figure 5.26(a) shows the QCM-D response curve for platelets exposed to fibrinogen pre-coated silica, TiO_2 and a-C:H surfaces. The Df plot was significantly greater for platelets exposed to fibrinogen pre-coated surfaces than platelets exposed to albumin coated surfaces. The gradient for all three surfaces were found to vary, with TiO_2 and a-C:H surfaces sustaining relatively linear gradient while platelets exposed to fibrinogen coated silica surfaces sustained an exponential increase in dissipation during the last 25 minutes of the measuring period. This indicates that platelets adhered on fibrinogen pre-coated TiO_2 and a-C:H surfaces formed focal contacts on the surface throughout the incubation period allowing its actin-cytoskeleton to polymerise forming radial protrusions on the surface, as shown in Figure 5.4. While, platelets exposed to fibrinogen pre-coated silica surfaces initially supported higher levels of focal contacts on the surface, forming a more rigid adlayer. Morphological changes within the tightly adhered platelets only occurred during the later stage of the incubation period supporting actin re-structuring and platelet spreading. Fibrinogen coated a-C:H surfaces presented lower dissipation values and frequency shift when compared with TiO_2 and silica even though same level of platelets were found to be attached on the surface (Figure 5.8(a)). This could indicate that the number of focal adhesion made by each platelet on fibrinogen coated a-C:H surfaces is lesser than platelets exposed to the other substrates suggesting that platelets form weaker attachments on fibrinogen pre-coated a-C:H surfaces.

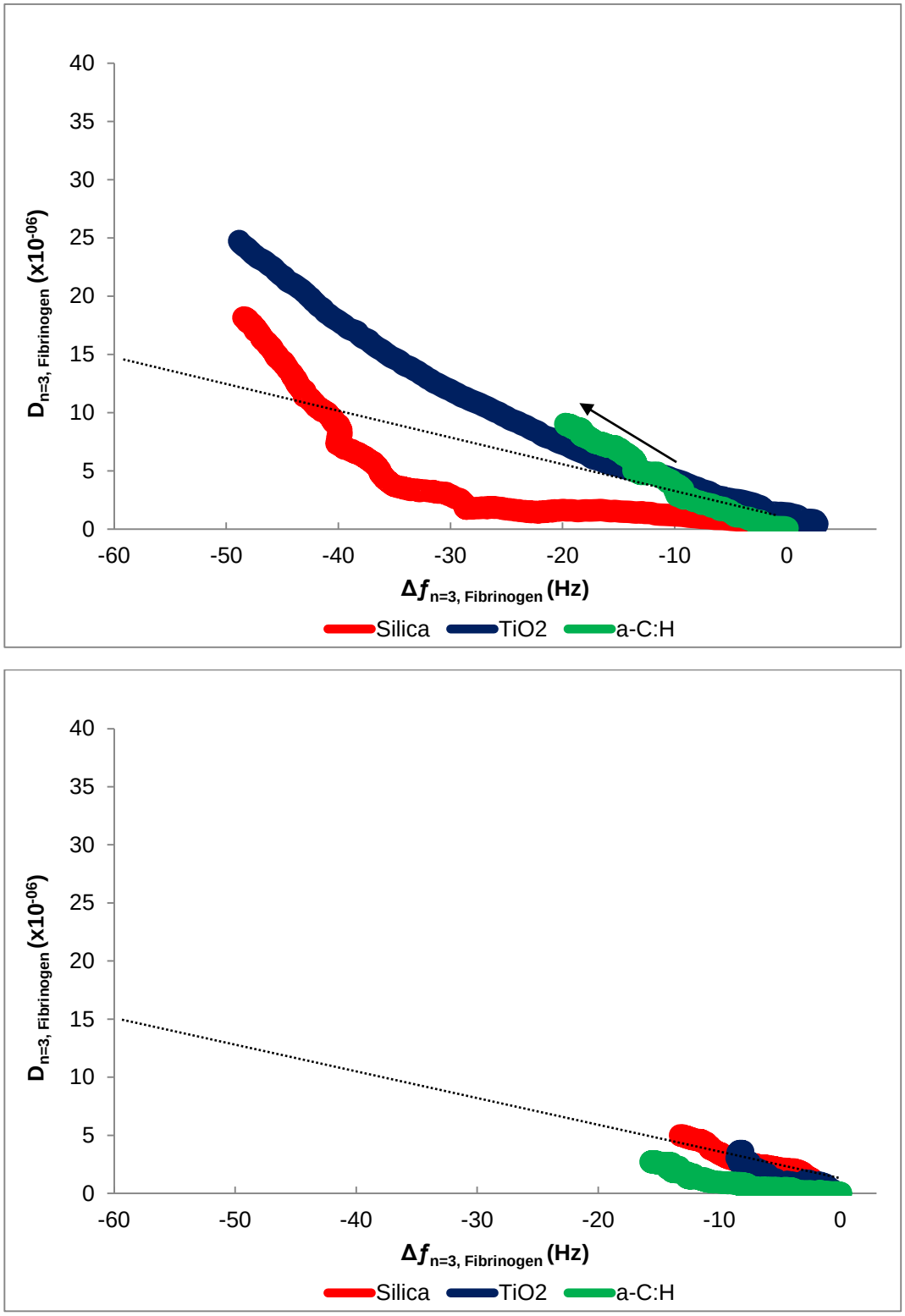

Figure 5.26 Dissipation versus frequency curves (third overtone; n=3; 15Hz) for fibrinogen coated silica, TiO_2 and a-C:H surfaces exposed to a. normal platelets b. platelets pre-incubated with anti-$\alpha_{IIb}\beta_3$ (Reopro) antibody, as determined by QCM-D.

Fluorescence studies comparing the influence of fibrinogen, when pre-coated on substrates, in eliciting a strong platelet response than bare substrates (Figure 5.8(a)) found platelets exposed to fibrinogen proteins attached at lesser concentrations. However, when compared with bare substrates, QCM-D results showed a greater shift in frequency when platelets were exposed to fibrinogen, which is typically indicative of increased mass uptake. Deviation from the viscoelastic behaviour showing significant increase in dissipation values during the later stages of platelet exposure to fibrinogen proteins, as found in Figure 5.26(a), may suggest that the obtained Df curves are indicative of a greater level of focal adhesion and cell spreading rather than an increase in platelet attachment. This may imply that fibrinogen not only plays an adhesive role in platelet-surface interactions but also an important role in potentiating restructuring of platelet cytoskeletal architecture and subsequently their spreading.

Pre-incubation of platelets with anti-$\alpha_{IIb}\beta_3$ (Reopro) antibody followed by exposure to fibrinogen surfaces is shown in Figure 5.26 (b). The Df plot presented decreases in f and increases in D with resulting curves falling within the viscoelastic region for all three surfaces. Changes in frequency of Reopro-bound platelets on fibrinogen coated silica, TiO_2 and a-C:H surfaces were less than normal platelets exposed to fibrinogen pre-coated substrates suggesting lesser adhesion and subsequent spreading of cells, as found in Section 5.2.1.

Figure 5.27(a) shows the QCM-D response curve for platelets exposed to plasma coated silica, TiO_2 and a-C:H surfaces. Plasma was diluted in DPBS, in the ratio of 1:10, to avoid time-wise clotting of the plasma proteins which could strongly influence dissipation values during the platelet incubation process. The obtained Df plots show increases in D as f decreases, however, the relationship appears non-linear. Platelets exposed to plasma coated a-C:H and silica substrates exhibited viscoelastic behaviour, while TiO_2 surfaces deviated from the viscoelastic region of the Df plot during the last 5 minutes of platelet incubation. This indicates that platelets adhered on plasma pre-coated TiO_2 facilitated greater amount of platelet spreading that a-C:H and silica substrates. Plasma coated surfaces presented lower

dissipation values and frequency shift when compared with fibrinogen pre-coated surfaces even though greater level of platelets were found to be attached on the surfaces (Figure 5.8(a)). This could indicate that platelets form less focal contacts and weaker attachments to plasma pre-coated substrates than fibrinogen pre-coated substrates. Pre-adsorbed plasma exhibit lesser concentrations of adsorbed fibrinogen, this could be a possible reason behind weaker adhesion between platelets and plasma coated surfaces. Furthermore, reduced fibrinogen adsorption from plasma during the protein incubation phase is indicative of the favourable role other plasma proteins play in reducing platelet interactions that can potentiate platelet spreading. These observations are synonymous with fluorescence studies, Figure 5.9, showing reduced platelet spreading on plasma pre-coated surfaces even though higher levels of platelet attachment was measured.

The D*f* plots showing the adhesion of platelets, pre-exposed to anti-$\alpha_{IIb}\beta_3$ (Reopro) antibody, prior to their incubation on plasma pre-coated surfaces is shown in Figure 5.27 (b). The curve presented a steady decrease in *f* with increasing D with resulting gradient falling within the viscoelastic region for all three surfaces. Frequency shifts recorded for Reopro bound platelets on plasma pre-coated silica, TiO_2 and a-C:H surfaces were less than the frequency shifts recorded for normal platelets exposed to fibrinogen pre-coated substrates. Once again, this suggests that Reopro antibodies block the $\alpha_{IIb}\beta_3$ integrins necessary for cellular adhesion and subsequent spreading, although, they do not completely inhibit platelet adhesion. These results corroborate with previous results (Section 5.2.1) and reinforce the minor, yet effective, role other platelet integrins, such as; $\alpha_2\beta_1$, $\alpha_5\beta_1$, etc [486] play during platelet adhesion.

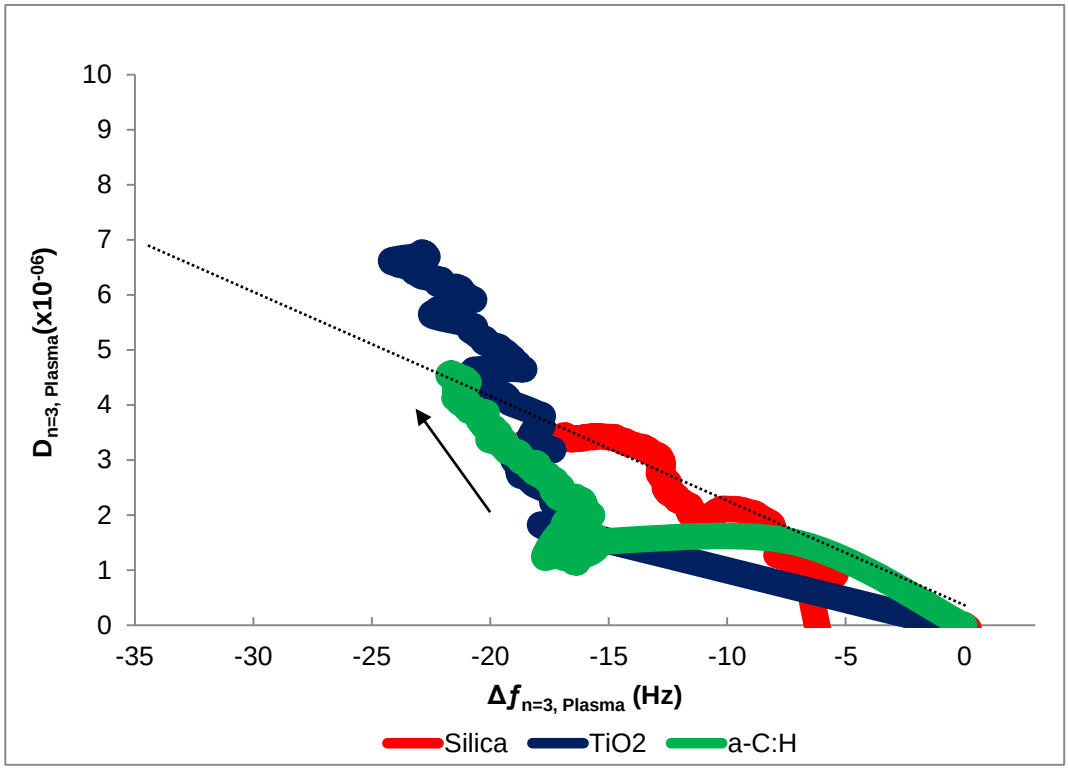

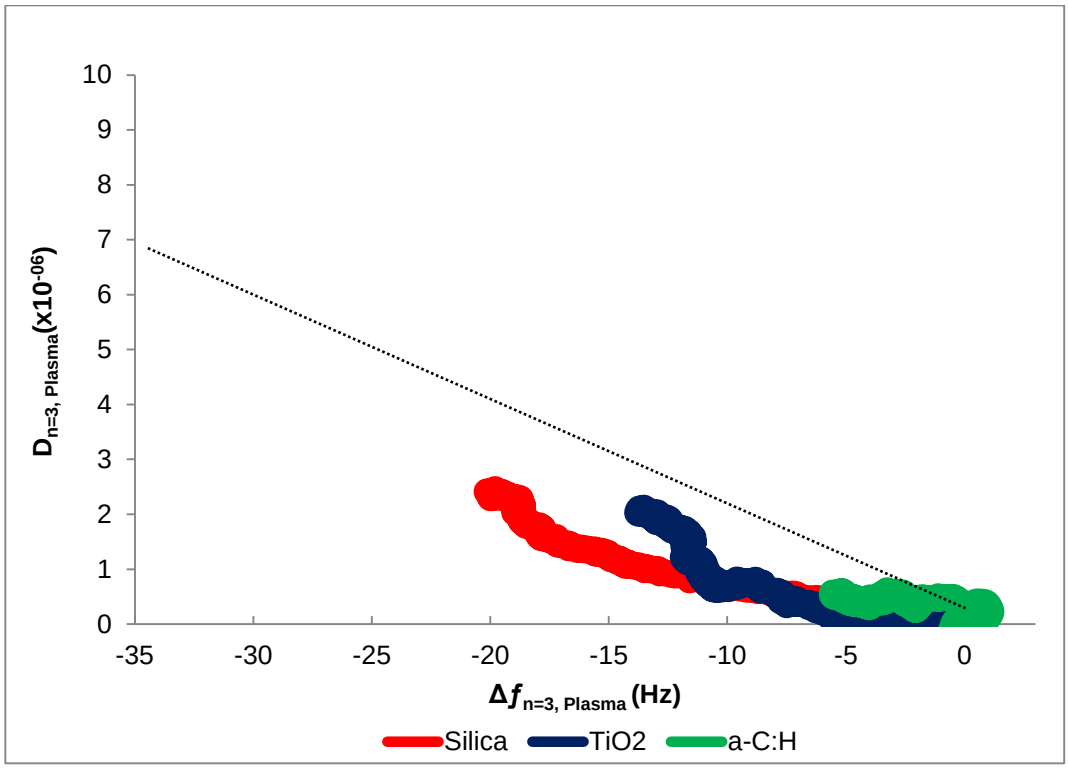

Figure 5.27 Dissipation versus frequency curves (third overtone; n=3; 15Hz) for diluted plasma (ratio 1:10, in DPBS) coated silica, TiO_2 and a-C:H surfaces exposed to a. normal platelets b. platelets pre-incubated with anti-$\alpha_{IIb}\beta_3$ (Reopro) antibody, as determined by QCM-D.

5.3 Summary

Platelet adhesion and morphological changes, such as; spreading and aggregation, on the flat test substrates varied primarily between the four protein conditions rather than the chemistry of the thin films deposited on the surfaces. Albumin coated surfaces supported high levels of platelet adhesion with little platelet spreading, while, fibrinogen pre-coated surfaces and surfaces devoid of proteins supported high levels of platelet spreading. Platelets that showed no spreading either; retained their rounded morphology without any actin-rich pseudopodia protruding radially from the platelet membrane, or, presented platelets with radial protrusions enclosing non-filamentous actin. Platelets on albumin and bare surfaces were found to change in morphology from their rounded state to a spread state during the last stages of platelet incubation; this was especially true on albumin-coated silicon-based substrates. Spread platelets have been shown to contain actin rich, stellate shaped filopodia. Further, the degree of platelet spreading on TiO_2 surfaces was reported higher than on a-C:H and silicon-based substrates. Platelets exposed to plasma surfaces showed very little spreading, when compared with albumin, bare and fibrinogen pre-coated surfaces and yet presented increased levels of platelet-platelet intercommunication (identified by the over-reaching of filopodia between adjacent platelets) than fibrinogen surfaces. High levels of platelet adhesion on bare and albumin coated surfaces suggest that platelet adhesion on biomaterial surfaces is dependent on non-specific interactions between platelet receptors and biomaterial surfaces as well as passivating proteins such as albumin. Pre-coating the surfaces with fibrinogen and plasma proteins have been shown to reduce the level of platelet adhesion when compared with platelets exposed to surfaces devoid of proteins suggesting a favourable interaction between serum proteins including fibrinogen, platelets and biomaterial surfaces in reducing platelet adhesion. Furthermore, when compared with silicon (Si), TiO_2, a-C:H and ta-C surfaces were shown to support the least number of adhered round and spread platelets on fibrinogen and plasma surfaces. Platelets were shown to form focal contacts with fibrinogen pre-coated TiO_2 and a-C:H surfaces throughout the incubation period where number of focal contacts formed on a-C:H surfaces was less than that of TiO_2 suggesting that platelets adhered on fibrinogen coated a-C:H surfaces form weaker attachments than on the

other surfaces. Again, TiO_2 surfaces exhibited greater levels of platelet spreading than a-C:H surfaces in the presence of plasma proteins, although the amount of focal contacts formed by platelets on plasma coated surfaces wereless than fibrinogen coated surfaces.

Anti-$\alpha_{IIb}\beta_3$ integrin antibody (Reopro) treated platelets decreased the overall levels of platelet adhesion and spreading on flat test substrates and substrates exposed to albumin, fibrinogen and plasma proteins suggesting the important role of $\alpha_{IIb}\beta_3$ integrins in platelet adhesion and spreading on all four conditions. Fibrinogen and plasma surfaces supported the lowest concentrations of Reopro-exposed platelets. The adhered platelets displayed rounded morphologies with limited filopodial extensions. While the concentrations of adhered platelets were lower in the presence of the anti-integrin antibody, it did not completely inhibit binding indicating that platelet adhesion is dependent on both $\alpha_{IIb}\beta_3$ ligand-dependent as well as non-specific interaction between platelet receptors and biomaterial surfaces. Albumin and bare surfaces also showed reduced platelet adhesion which implies that $\alpha_{IIb}\beta_3$ platelet integrins are susceptible to non-ligand specific activation and consequent binding of its receptors to the biomaterial surfaces and albumin proteins. A-C:H and ta-C surfaces continually supported decreased levels of anti- $\alpha_{IIb}\beta_3$ integrin treated platelets on all protein pre-coated and bare surfaces, although a-C:H surfaces showed higher levels of platelet spreading similar to TiO_2 surfaces on albumin and fibrinogen coated surfaces. This reinforces the influence of surface chemistry as well as specific plasma proteins in affecting $\alpha_{IIb}\beta_3$ ligand activation for platelet-surface binding. Normal platelets exposed on nano-patterned surfaces exhibited high concentrations of adhesion as well as extensive levels of spreading. Platelets formed multi-level stacked aggregates on the surfaces when compared with the flat surfaces suggesting that the nano-patterns behaved as topographical cues, which act as potential tethering sites for platelet integrin adhesion. The dendritic network of actin cytoskeleton in the cytoplasm of platelets adhered on nano-patterned surfaces appeared more pronounced. TiO_2 surfaces presented higher levels of platelet adhesion and spreading on all protein pre-coated and bare conditions, except on plasma pre-coated surfaces where a-C:H and ta-C surfaces supported higher platelet concentrations. On nano-patterned surfaces both fibrinogen and plasma proteins were found to enhance

platelet adhesion and it's spreading. This was especially noticeable on a-C:H and ta-C nano-patterned surfaces which showed the highest level of platelet adhesion and spreading in the presence of fibrinogen and plasma proteins.

6 CLOTTING CASCADE AND PLATELET ACTIVATION

6.1 Introduction

Blood coagulation and thrombus formation on biomaterial surfaces *in vivo* is ultimately dependent on a sequence of plasma protein reactions causing the activation of fibrinogen to form fibrin induced primary haemostasis as well as tightly controlled intracellular reactions mediating platelet activation and consequently aggregation. These two events are inextricably coupled, and along with the activated platelet surface for clotting factor assembly and thrombin binding, functions as a potent agonist for circulating platelets. While the haemocompatibility of a biomaterial is implicitly linked to its tribological properties, the extent to which it can influence these interactions remains unknown.

In this study, the influence of surface chemistry, nano-topography and serum protein adsorption on fibrin clot formation and platelet activation was analysed. Plasma clotting experiments on flat surfaces, examined in Section 4.1, were investigated by a series of coagulation assays and the ability of these surfaces to modulate the activity of heparin, was further evaluated. The degree of platelet activation on flat and nano-patterned surfaces was determined by the expression of activation markers: P-selectin (CD-62P), activated $\alpha_{IIb}\beta_3$, and $\alpha_2\beta_1$ integrins on the platelet membrane, using a combination of ELISA, flow cytometry and fluorescence. The results obtained were compared to serum pre-coated surfaces.

6.2 Results and Discussion

6.2.1 Coagulation of Plasma Proteins

The influence of various surface chemistries in modulating the coagulant properties of plasma proteins and the anti-coagulant properties of heparin was examined by comparing the time taken to induce fibrin-clot formation via the extrinsic and intrinsic coagulation pathways. This was determined by prothrombin (PT) and activated partial thromboplastin (aPTT) coagulation based assays, respectively. The ability of the contacting surfaces to denature fibrinogen, impairing its function and consequently delaying fibrin clot formation was evaluated using thombin time assay (TT). Clotting times were determined using heparinised and non-heparinised plasma on flat silicon, TiO_2, a-C:H and ta-C surfaces and the results were compared with control TCPS.

6.2.1.1 Prothrombin (PT) clotting assay

The effect of surface chemistry on the extrinsic cascade was analysed using PT coagulation test. The time taken for fibrin-dependent clot formation to form was measured upon the addition of phospholin ES rich, ellagic-acid based aPTT reagent and calcium chloride on flat surfaces pre-incubated with plasma proteins. The negatively charged ellagic acid activator initiates the extrinsic cascade by activating coagulation factors XII and XI and subsequently the activation of factors IX and X before proceeding through the common pathway. Activation of factor X is the dominant mechanism that leads to clot formation.

Figure 6.1 shows the clotting times measured by PT assay of the test substrates and control TCPS. Of the test substrates, ta-C surfaces prolonged clotting the most by 19 seconds closely followed by a-C:H, silicon and TiO_2 with 17, 16 and 15 seconds

respectively. Plasma proteins on the control TCPS surfaces clotted more readily within 14.5 seconds. This may suggest while the test surfaces prolong the activation of extrinsic clotting factors, the difference in time delay is not significant P(<0.1), with exception to ta-C, which exhibited a delay in clotting time by 31%.

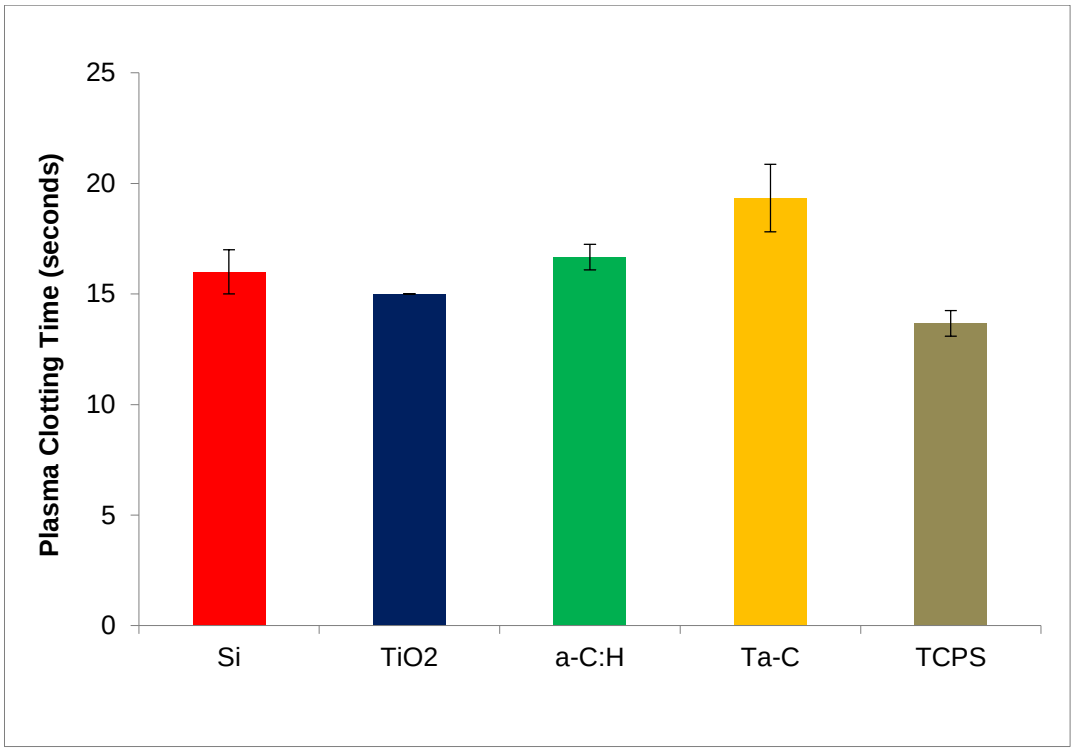

Figure 6.1 Anticoagulant activity of flat silicon, TiO_2, a-C:H, ta-C and TCPS biomaterial surfaces in prolonging plasma protein coagulation via the extrinsic pathway, as measured using an rabbit brain based thromboplastin PT clotting assay. Error bars: SD (n=3)

The anticoagulant activity of heparin via the extrinsic pathway, at increasing concentrations, on the flat surfaces, was described in Figure 6.2. Heparin is a commercially available anti-coagulant that behaves as a catalyst by reversibly binding to antithrombin III (ATIII) which increases its affinity to activated coagulation factors IX, XI, XII, X and thrombin by 1000 fold. Consequently, the ATIII-heparin complex accelerates ATIII's ability neutralise thrombin and inhibits the factors from participating in the coagulation cascade. The maximum therapeutic range for anti-factor Xa heparin concentration is 0.7U/ml where 0.1U is equivalent to 1µg, calculated from the stock concentration of heparin used (180U/mg, H3393,

Sigma) [487-491]. As such, the concentration of heparin dissolved in plasma was titrated to 1-5µg per ml of plasma, within the therapeutic range.

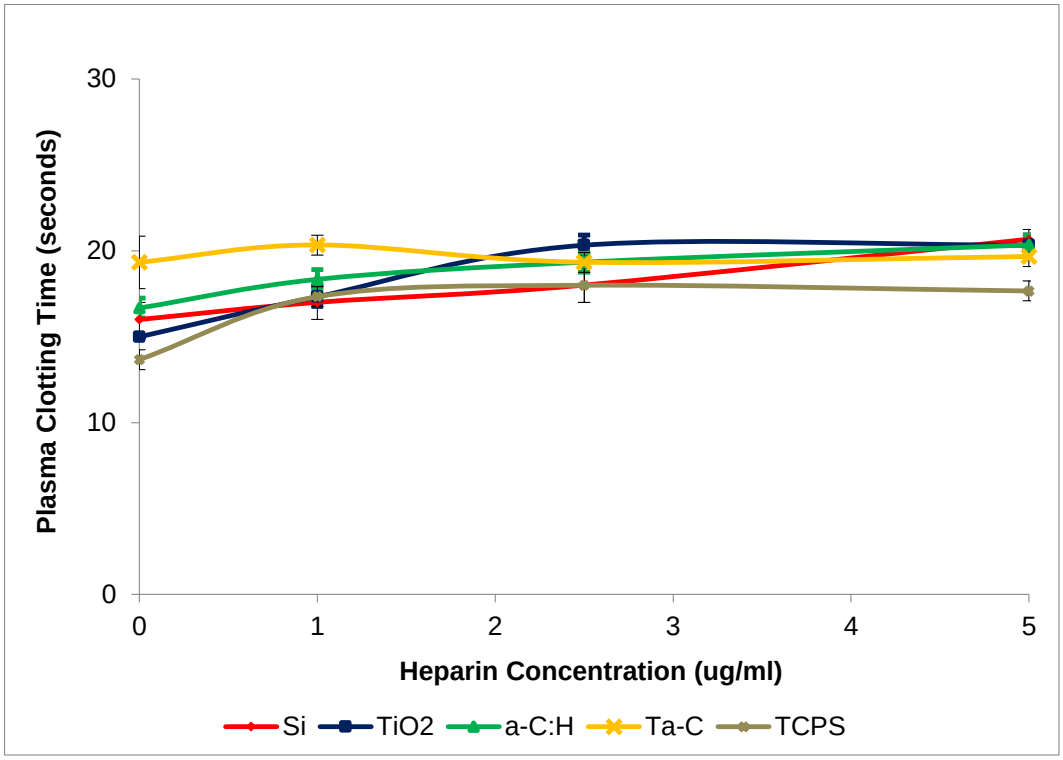

Figure 6.2 Changes in anti-coagulant activity of heparin, after incubation with plasma protein adsorbed flat silicon, TiO_2, a-C:H, ta-C and control TCPS surfaces, as measured using an PT clotting assay. Error bars: SD (n=3)

Fibrin clot formation, in the absence of heparin, occurs within 13-19seconds, while, at increased heparin concentrations, of 5µg/ml, range between 17-21 seconds. Silicon, TiO_2, a-C:H and TCPS showed an increase of 4-5seconds while clotting times of ta-C surfaces remained unchanged. Since elevated heparin concentrations did not affect the clotting times significantly it can be deduced heparin plays a limited role in inhibiting the activation of extrinsic clotting factors. Further, similar clotting periods between the substrates suggests that activation of the extrinsic pathway may not be influenced by surface chemistry, however, whether it is dependent on the presence of a synthetic biomaterial remains unknown.

6.2.1.2 Activated partial thromboplastin (aPTT) clotting assay

The effect of surface chemistry on the intrinsic cascade was experimentally analysed using aPTT clotting assay. The time taken for factor-dependent clot formation to form was measured upon the addition of phosphoplastin RL rich, rabbit brain based thromboplastin reagent on flat surfaces pre-incubated with plasma proteins. Thromboplastins are a combination of phospholipid membrane bound tissue factor (III) and calcium ions (IV). Membrane bound tissue factor activates the intrinsic cascade by coupling to coagulation factors VII and X, and subsequently activates factor IX followed by factor X before proceeding through the common pathway. The aPTT clotting assay results on the flat surfaces reinforces the role of surface chemistry in fibrin related clot formation. From Figure 6.3 it can be deduced that a-C:H and silicon surfaces prolong clotting time the most, by 63 seconds and 57 seconds, respectively, followed by TiO_2 and ta-C surface by 52 and 53 seconds, respectively.

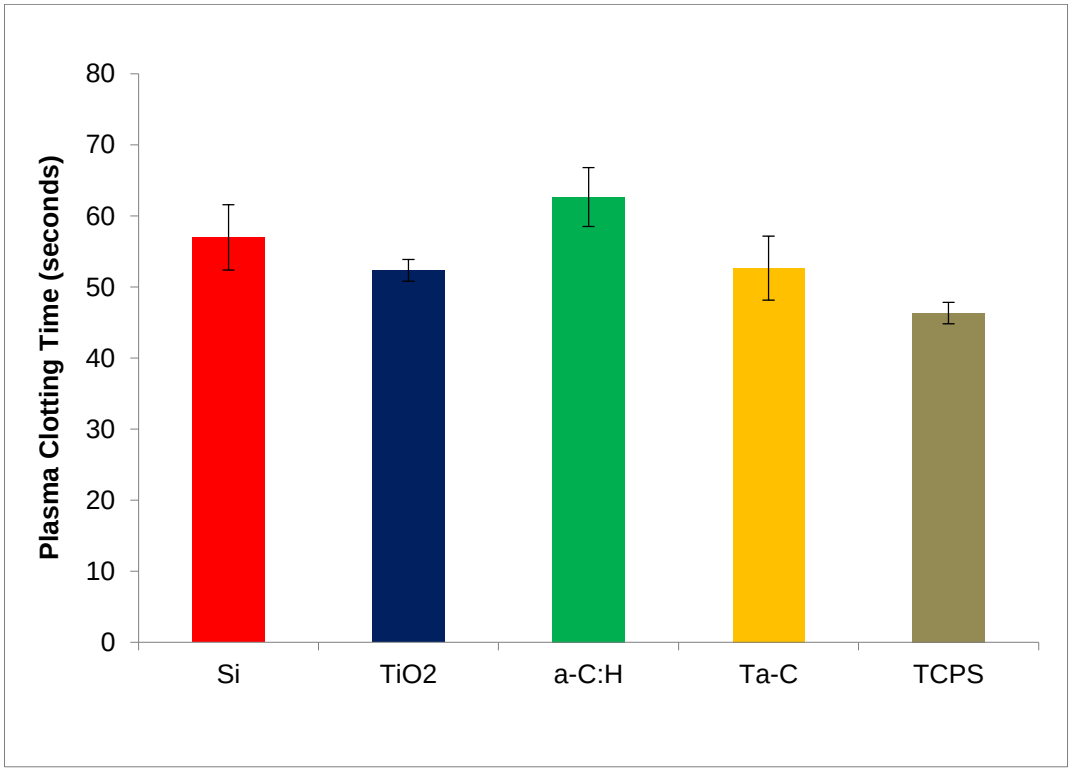

Figure 6.3 Anticoagulant activity of flat silicon, TiO_2, a-C:H, ta-C and TCPS biomaterial surfaces in prolonging plasma protein coagulation via the intrinsic

pathway, as measured using an ellagic acid based aPTT clotting assay. Error bars: SD (n=3)

The prolonged response to the ellagic activator by a-C:H and silicon, when compared to the control surface, may indicate that these materials impede the intrinsic activation pathway more readily, by behaving as an inhibitor to factors VII, IX and XI. The anticoagulant activity of heparin via the intrinsic pathway, at increasing concentrations on the flat surfaces, is shown in Figure 6.4.

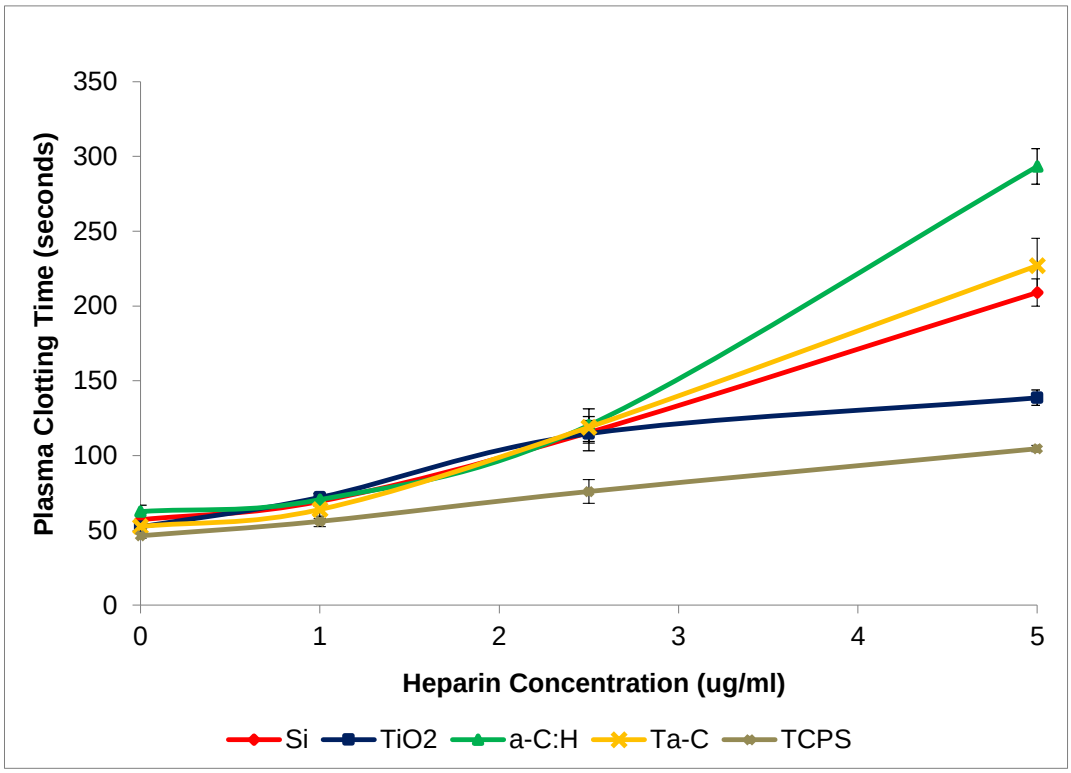

Figure 6.4 Changes in anti-coagulant activity of heparin, after incubation with plasma protein adsorbed flat silicon, TiO_2, a-C:H, ta-C and control TCPS surfaces, as measured using an aPTT clotting assay. Error bars: SD (n=3)

As mentioned earlier, without heparin, fibrin clot formation via the intrinsic pathway occurs between approximately 45-65seconds. Increasing the heparin concentration extends the aPTT clotting times significantly in an exponential manner. This is especially evident on silicon, a-C:H and ta-C surfaces. However, TiO_2 followed a plateauing trend similar to control TCPS showing minimal variances to increasing heparin concentrations. While minimal differences between silicon, a-C:H and ta-C was noticed at 1 and 2.5µg/ml, at 5µg/ml, the time taken to induce clots varied

significantly between surfaces. A-C:H (4 minutes and 53 seconds) was the most perceptive to heparin activity, followed by ta-C (3 minutes 47 seconds) and silicon (3 minutes and 29 seconds). While these surfaces inevitably exhibited plasma clot formation; the results indicate that the synergistic effect between surface chemistry and heparin can be enhanced by modulating surface chemistry of a biomaterial, especially at higher therapeutic concentrations of heparin.

6.2.1.3 Thrombin time (TT) clotting assay

Ability of the contacting surfaces to severely impair fibrinogen's structure, by denaturation, and consequently their function in forming fibrin clots was analysed using the thombin time assay (TT). The time taken for fibrin-dependent clot formation to form was measured upon the addition of excess thrombin and calcium chloride on flat surfaces pre-incubated with plasma proteins. The active thrombin enzyme acts on soluble fibrinogen to convert it to an insoluble fibrin mesh.

The thrombin times shown in Figure 6.5 are the recorded time, in seconds, to clot formation after the addition of thrombin and calcium chloride ions. Concentrated thrombin enzymes were reconstituted with calcium chloride salt in 1% (w/v) albumin solution (in DPBS buffer) to a final ratio of 1: 1: 8 of thrombin: $CaCl_2$: 1% albumin, respectively, to produce clotting times within the normal reference range. Silicon and a-C:H surfaces prolonged clotting the most by 21 seconds closely followed by TiO_2 and ta-C with 20 and 19 seconds respectively. Plasma proteins on control TCPS clotted more readily within 14 seconds.

The results above show test substrates prolong clot formation by 5-7seconds (30-50% increase), suggesting that the substrates denature fibrinogen more readily than TCPS and consequently impede its conversion to fibrin. While surface bound fibrinogen have been known to unfold upon adsorption, as shown in Section 4.3, the amount of suspended proteins, in solution, that have denatured is still uncertain.

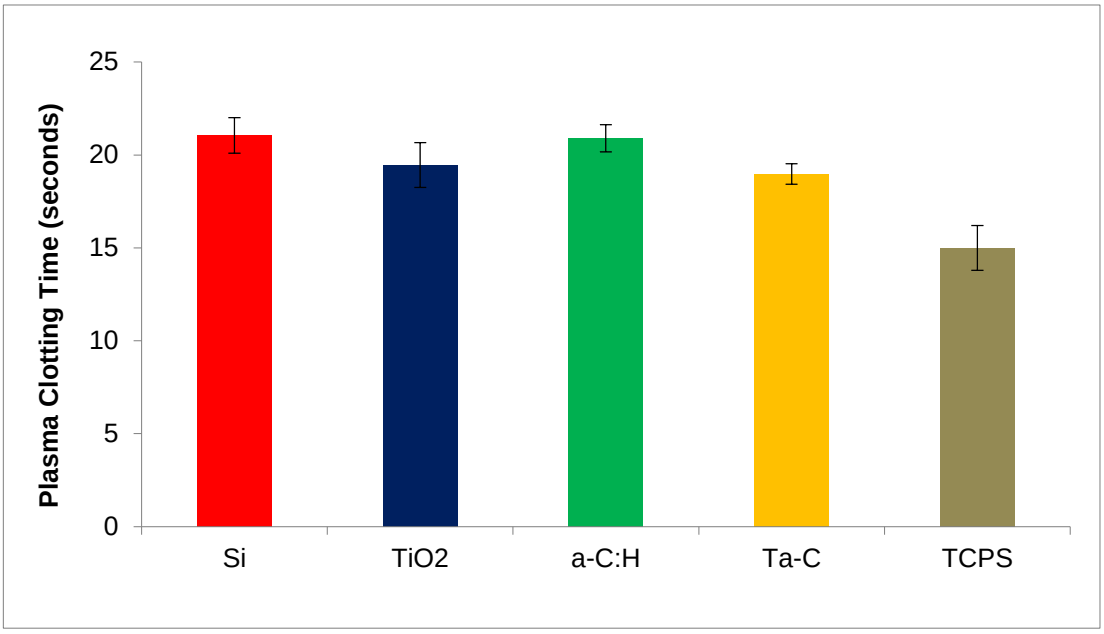

Figure 6.5 TT clotting assay measuring the anticoagulant activity of flat silicon, TiO_2, a-C:H, ta-C and TCPS biomaterial surfaces in prolonging plasma protein coagulation in the presence of excess thrombin and calcium chloride ions. Error bars: SD (n=3)

6.2.2 Platelet Activation Studies

Activation of circulating platelets upon contacting biomaterial surfaces, *in vivo*, is primarily mediated by platelet integrins, which trigger successive stages of outside-in and inside-out signalling processes. This results in the formation of a pro-coagulant platelet surface. The activated extracellular integrins increase the integrin affinity to biomaterial surfaces and extra cellular ligands which influences the strength of platelet adhesion, and ultimately, its aggregation. Activation caused from binding of extra cellular ligands, such as plasma proteins, promotes both, the translocation and expression of intracellular integrins on the extracellular surface (e.g. intracellular $\alpha_{IIb}\beta_3$ and p-selectin), and, a conformational change within extracellular integrins to their activated state (e.g. extracellular $\alpha_{IIb}\beta_3$ and $\alpha_2\beta_1$).

Ordinarily, resting platelets express un-activated $\alpha_{IIb}\beta_3$, $\alpha_2\beta_1$, $\alpha_5\beta_1$, $\alpha_6\beta_1$, $\alpha_V\beta_3$ and small amounts of P-selectin (CD62P) receptors on the plasma membrane of which

$\alpha_{IIb}\beta_3$ is the most abundant. During the initial stages of activation, $\alpha_2\beta_1$ activates in the presence of circulating and exposed collagen from the sub-endothelium, while, the $\alpha_{IIb}\beta_3$ receptor activates upon binding to surface adsorbed fibrinogen proteins. In addition, fibrinogen circulating in plasma binds to and cross-links the activated $\alpha_{IIb}\beta_3$ receptors on two different platelets which can lead to platelet aggregation. Apart from fibrinogen, other adhesive plasma proteins, such as von Willebrand factor, thrombospondin, fibronectin and vitronectin, containing RGD sequences can also bind to activated $\alpha_{IIb}\beta_3$. Therefore, activated $\alpha_{IIb}\beta_3$ and $\alpha_2\beta_1$ receptors serves as a strong biomarker for initial platelet activation. Upon activation, the α-granule docks on the platelet membrane causing the translocation of intracellular P-selectin (CD62P) to the extracellular membrane, at high concentrations. As such detection of P-selectin (CD62P) on the membranes of adsorbed platelets can pose as an indication of end stage activation. Further, when platelets spread as a result of activation, they lose their discoid shape and release granular contents of their secretory organelles, which in turn act as agonists to platelet activation, and subsequently, aggregation.

As such, the activation of attached platelets on serum-pre-coated flat substrates was evaluated, *in vitro*, for the surface expression of activated $\alpha_{IIb}\beta_3$ and $\alpha_2\beta_1$ receptors, using ELISA. The expression of P-selectin (CD62P) and $\alpha_{IIb}\beta_3$ from circulating platelets on flat and nano-patterned surfaces was evaluated using flow cytometry. Lastly, the presence of activated $\alpha_{IIb}\beta_3$ and P-selectin (CD62P) and the localisation of activation markers on the surface membrane of adsorbed platelets was analysed using fluorescence microscopy.

6.2.2.1 ELISA

Expression of activated $\alpha_{IIb}\beta_3$ integrins on surface bound platelets was analysed using ELISA, in the manner described in Section 3.2.4.3.1. In brief, flat silicon, TiO_2, a-C:H, ta-C and TCPS surfaces were pre-adsorbed with albumin (BSA), fibrinogen (Fg) and diluted plasma proteins (ratio 1:10, in DPBS buffer). The results were compared to platelet integrin expression on bare surfaces. An anti-human $\alpha_{IIb}\beta_3$

antibody, Abciximab (ReoPro), was used to screen for $\alpha_{IIb}\beta_3$ integrins. The antibody bound platelets were incubated with peroxidase conjugated secondary antibodies followed by ABTS colorimetric dye.

From Figure 6.6 it is evident the level of $\alpha_{IIb}\beta_3$ activation varied between the protein-coated surfaces. While albumin coated surfaces served as a negative control for the assay by exhibiting reduced platelet activation, it did not however prevent the activation process. The bare surfaces presented increased activation when compared with albumin pre-coated surfaces. From this it could be inferred that adsorbed albumin molecules decrease the surface exposure to circulating platelets in solution and consequently reduce the surfaces overall activation. Under static conditions, fibrinogen surfaces are known for being traditionally more responsive for $\alpha_{IIb}\beta_3$ mediated platelet activation, and consequently showed substantially high receptor activation. Plasma coated surfaces, when compared to fibrinogen pre-coated surfaces, displayed reduced overall activation. This may suggest plasma proteins interact favourably with test substrates to reduce fibrinogen adsorption, or, by steric hindrance, reduce the overall exposure of adsorbed fibrinogen to circulating platelets in order to decrease $\alpha_{IIb}\beta_3$ mediated platelet activation.

Comparing the different surface chemistries it is evident that TCPS served as the positive control by supporting the highest levels of platelet activation on bare and protein pre-coated conditions. Ta-C and TCPS coated with plasma exhibited reduced platelet activation than when coated with fibrinogen or devoid of proteins. This may suggest that adsorbed serum proteins decrease the overall surface exposure and present decreased surface-bound fibrinogen for platelet activation. Further, ta-C surfaces showed decreased activation when coated with plasma than with albumin. This may be due to greater surface coverage by non-activating serum proteins including; fibronectin, vitronectin, vonWillebrand factors, thrombospondin, laminins, etc, than by albumin. Silicon followed by TiO_2 and a-C:H presented lower levels of activated $\alpha_{IIb}\beta_3$ on bare surfaces and higher levels on plasma pre-coated surfaces, when compared with ta-C. Plasma proteins adsorbed on a-C:H surfaces did not change the activation levels of the bare surfaces. Further, platelet activation on

plasma coated silicon and TiO_2 was higher than on the bare surface, suggesting that unlike ta-C, plasma adsorbed on silicon and titania may exhibit pro-coagulant tendencies.

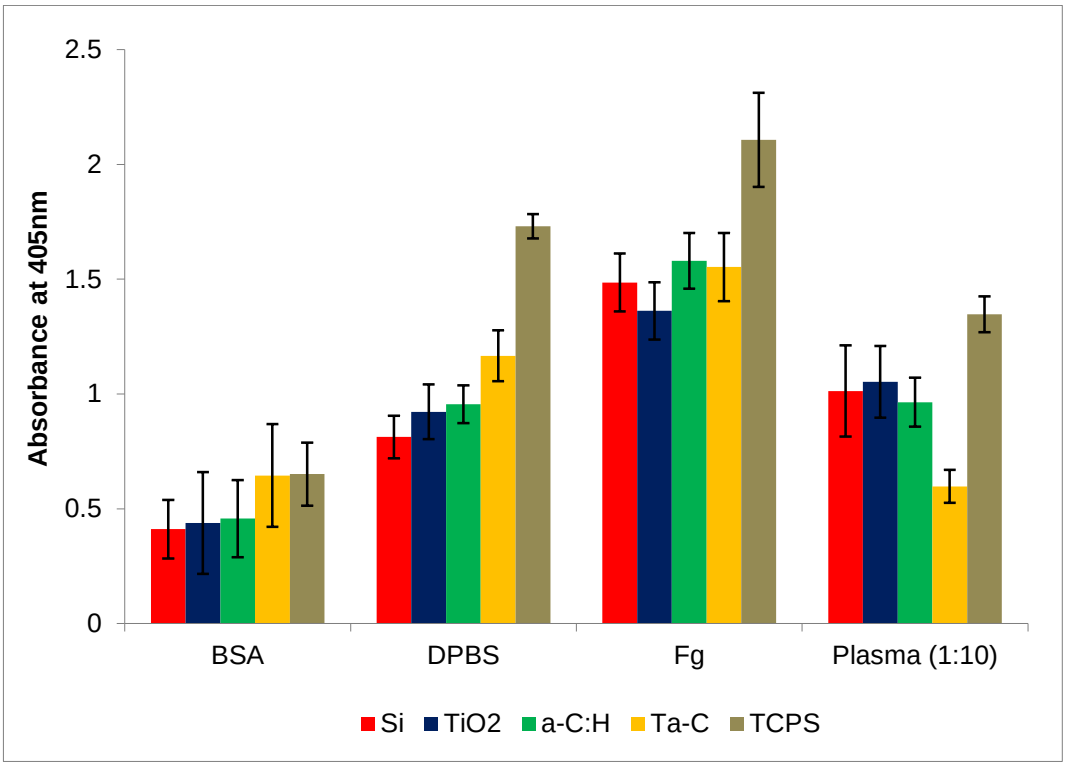

Figure 6.6 Expression of activated $\alpha_{IIb}\beta_3$ receptors measured as absorbance from the attachment of ReoPro antibody to activated $\alpha_{IIb}\beta_3$ receptors on surface bound platelets, as determined by ELISA. Silicon, TiO_2, a-C:H, ta-C and TCPS test substrates were pre-coated with 50µg/ml of albumin (BSA), 50µg/ml fibrinogen (Fg) and diluted plasma (ratio 1:10, in DPBS) before platelet incubation. The results were compared with surfaces devoid of proteins. Error bars: SD (n=3).

It was interesting to note that the fibrinogen pre-coated substrates supported similar levels of $\alpha_{IIb}\beta_3$ activation even though a higher concentration of fibrinogen, with higher levels of its platelet binding domain was exposed on fibrinogen adsorbed on a-C:H (Chapter 4). It appears that even smaller amounts of adsorbed fibrinogen with less exposure of its platelet binding domain, as found with TiO_2 and silicon, can mediate similar levels of platelet $\alpha_{IIb}\beta_3$ receptor activation. This could suggest that while the presence fibrinogen dictates $\alpha_{IIb}\beta_3$ activation, its relative concentration on the surface may not necessarily be a good indicator of the level of $\alpha_{IIb}\beta_3$ mediated activation. Other factors such as surface chemistry might be a contributing factor. Hence, the adsorption of specific plasma proteins, their interaction on the test

substrates as well as surface chemistry plays a significant role in the pro-coagulant activity of platelets via the $\alpha_{IIb}\beta_3$ mediated pathway.

Figure 6.7 describes the expression of activated $\alpha_2\beta_1$ integrins on surface adsorbed platelets using anti-$\alpha_2\beta_1$ antibody, clone BHA2.1, as determined using ELISA. The flat surfaces were pre-adsorbed with albumin (BSA), fibrinogen (Fg), diluted plasma proteins (ratio 1:10, in DPBS buffer) and collagen, and the results were compared to platelet integrin expression on bare surfaces.

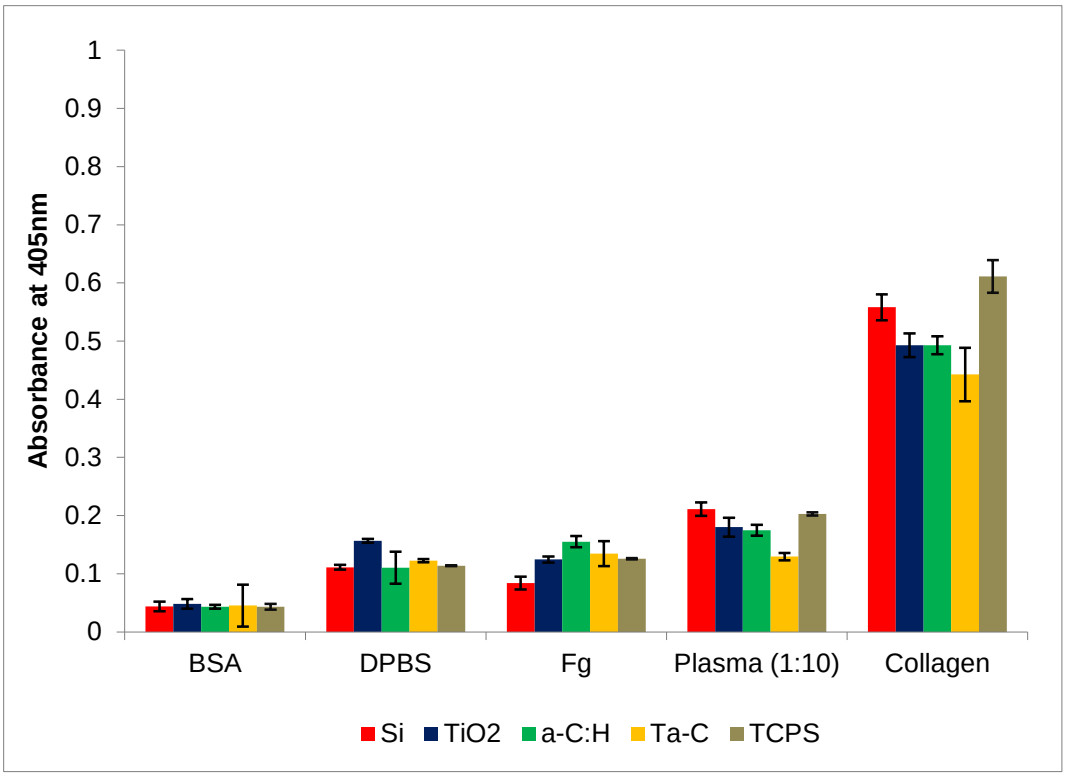

Figure 6.7 Expression of activated $\alpha_2\beta_1$ receptors measured as absorbance from the attachment of anti-$\alpha_2\beta_1$ antibody to activated $\alpha_2\beta_1$ receptors on surface bound platelets, as determined by ELISA. Silicon, TiO_2, a-C:H, ta-C and TCPS test substrates were pre-coated with 50µg/ml of albumin (BSA), fibrinogen (Fg), diluted plasma (ratio 1:10, in DPBS)and collagen before platelet incubation. The results were compared with surfaces devoid of proteins. Error bars: SD (n=3).

Absorbance values recorded for albumin coated surfaces are similar to that of the background indicating that the activation of $\alpha_2\beta_1$ was inhibited in the presence of albumin. Fibrinogen, plasma and bare surfaces exhibit similar level of activation which is slightly higher than that of albumin but significantly lower than that of the positive control, collagen. Furthermore, there was a modest, but not statistically

significant increase in platelet integrin $\alpha_2\beta_1$ activation in the presence of plasma, reinforcing that collagen behaves as a powerful agonist and supports the activation of $\alpha_2\beta_1$ integrins while the bare surfaces and serum proteins do not. As such, $\alpha_2\beta_1$ mediated activation is not dependent on the surface chemistry of the test substrates or serum proteins, while, $\alpha_{IIb}\beta_3$ mediated activation is.

6.2.2.2 Fluorescence Microscopy

Fluorescence microscopy is not only a useful technique for elucidating the interactions of platelets with different substrata, as described in Section 5.2.1, but also allows visualisation of membrane functional activity through immuno-cytochemical staining. In this study, platelets were seeded on bare and protein pre-coated, flat and nano-patterned substrates, for 1 hour at 37 degrees. After washing the attached platelets were fixed and dual-labelled with RPE conjugated anti-CD62P-selectin antibody, and, Reopro (human $\alpha_{IIb}\beta_3$ biomarker) followed by FITC conjugated secondary anti-human antibody. To observe the localisation of $\alpha_{IIb}\beta_3$ integrins on the platelet membrane, platelets were visualised by fluorescence microscopy after staining these integrins and the actin cytoskeleton. Platelets exposed to flat and nano-patterned surfaces without absorbed proteins as well as pre-coated with albumin, fibrinogen and diluted plasma (ratio 1:10, in DPBS) were imaged at 500x magnification.

6.2.2.2.1 $\alpha_{IIb}\beta_3$ Activation and Actin staining on Nano-patterned Surfaces

The localisation of platelet receptor $\alpha_{IIb}\beta_3$ on the platelet membrane was visualised by dual staining the attached platelets, on bare and protein pre-coated nano-patterned silicon, titania, a-C:H and ta-C surfaces. Rhodamine-phalloidin was used to stain for actin filaments and FITC conjugated antibody was used specifically to bind to the antibody that bound to activated αIIbβ3 platelet receptors. The results are shown in Figure 6.8 to 6.11.

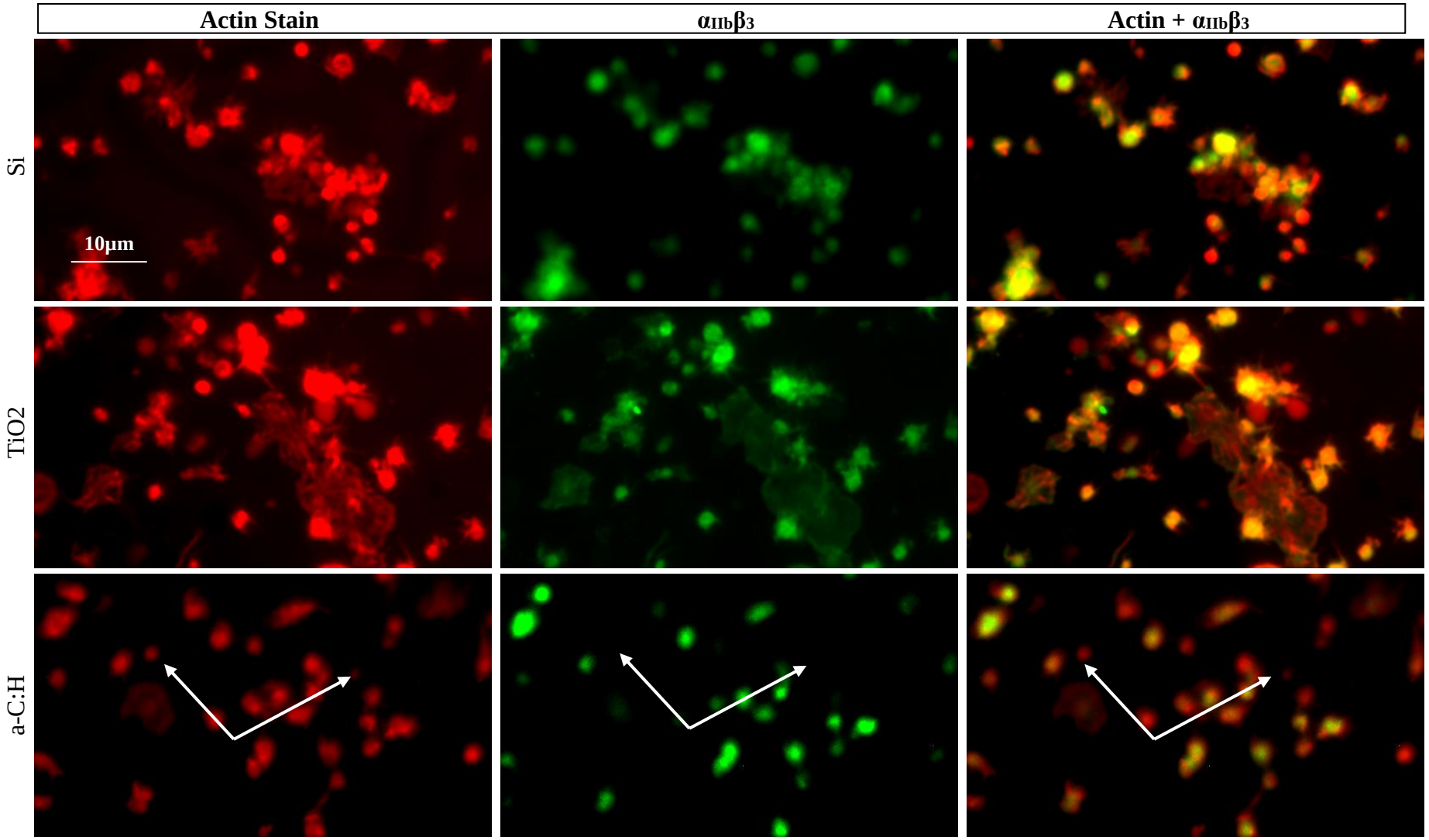
Actin Stain
αIIbβ3
Actin + αIIbβ3
Si
TiO2
a-C:H
10μm

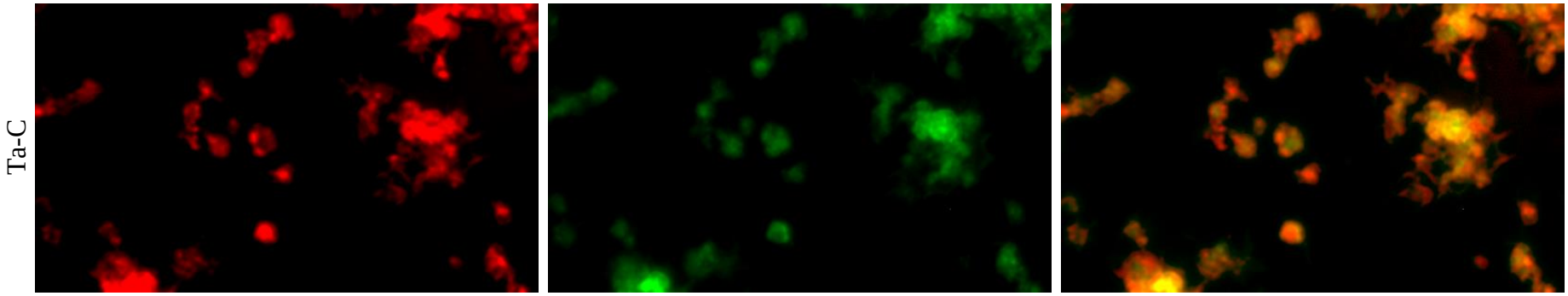

Figure 6.8 Fluorescence microscopy images of platelet cytoskeletons (left, red rhodamine-phalloidin actin stain) and the membrane distribution of activated $\alpha_{IIb}\beta_3$ integrins (middle, green-FITC conjugated antibody to Reopro bound $\alpha_{IIb}\beta_3$ receptor)on platelets attached to albumin coated silicon, TiO_2, a-C:H and ta-C nano-patterned surfaces. Samples were imaged at 500x magnification using Zeiss Axioskop.The arrows show platelets that do not present detectable levels of the activation marker.

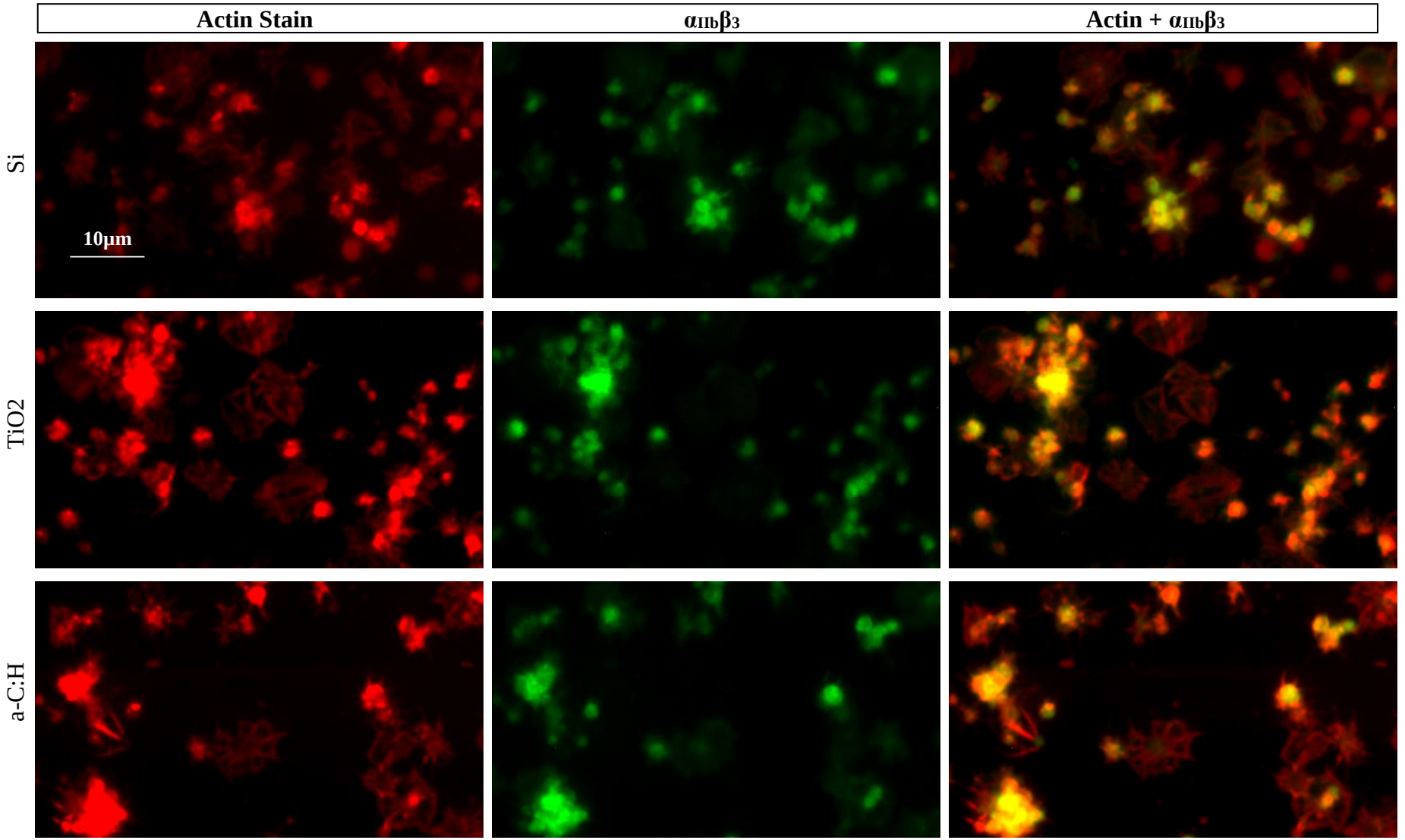
Actin Stain
αIIbβ3
Actin + αIIbβ3
Si
TiO2
a-C:H
10μm

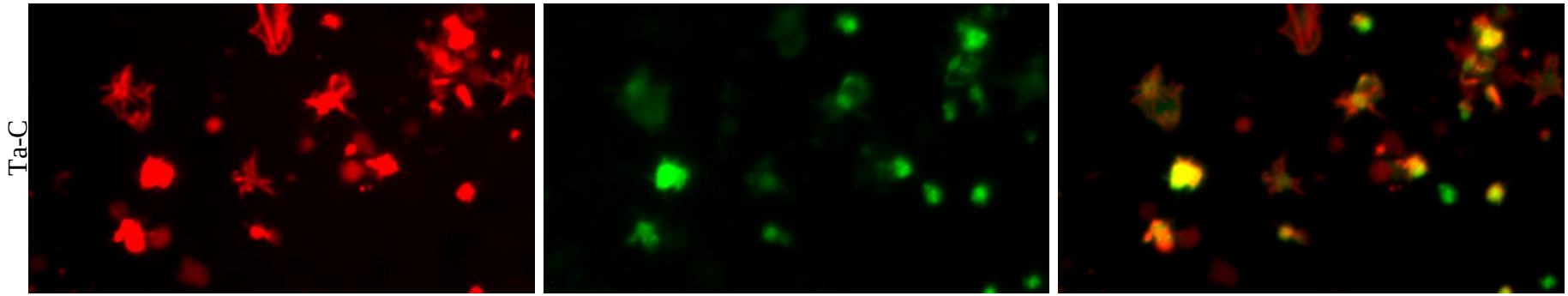

Figure 6.9 Fluorescence microscopy images of platelet cytoskeletons (left, red rhodamine-phalloidin actin stain) and the membrane distribution of activated αIIbβ3 integrins (middle, green-FITC conjugated antibody to Reopro bound αIIbβ3 receptor)on platelets attached to bare silicon, TiO2, a-C:H and ta-C nano-patterned surfaces. Samples were imaged at 500x magnification using Zeiss Axioskop microscope.

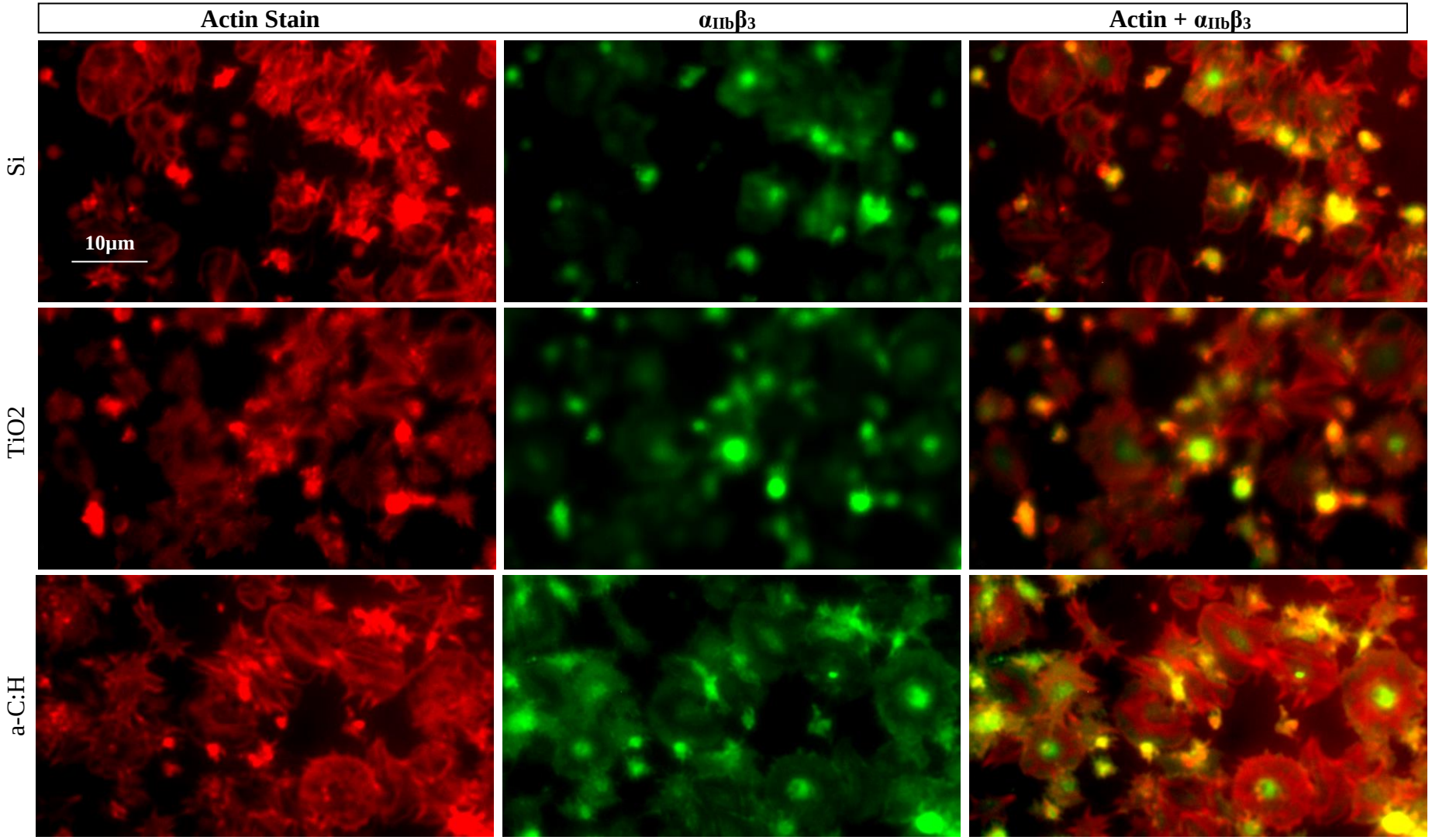
Actin Stain
αIIbβ3
Actin + αIIbβ3
Si
TiO2
a-C:H
10μm

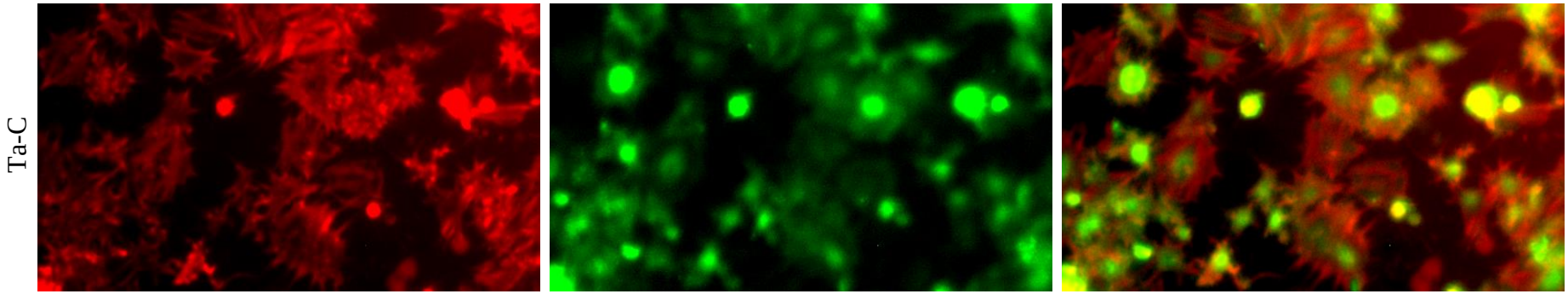

Figure 6.10 Fluorescence microscopy images of platelet cytoskeletons (left, red rhodamine-phalloidin actin stain) and the membrane distribution of activated $\alpha_{IIb}\beta_3$ integrins (middle, green-FITC conjugated antibody to Reopro bound $\alpha_{IIb}\beta_3$ receptor)on platelets attached to fibrinogen coated silicon, TiO_2, a-C:H and ta-C nano-patterned surfaces. Samples were imaged at 500x magnification Zeiss Axioskop.

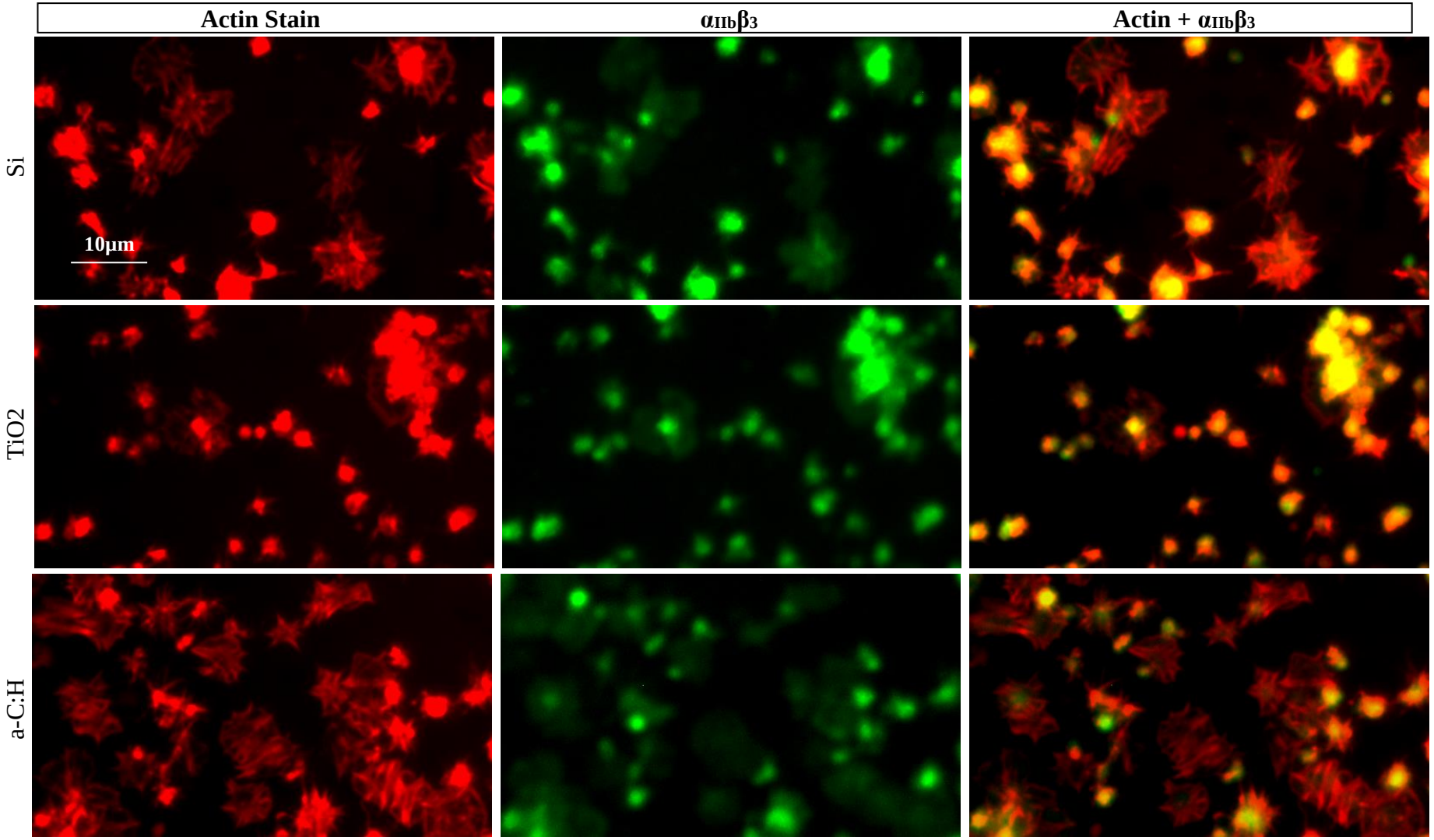
Actin Stain
αIIbβ3
Actin + αIIbβ3
Si
TiO2
a-C:H
10μm

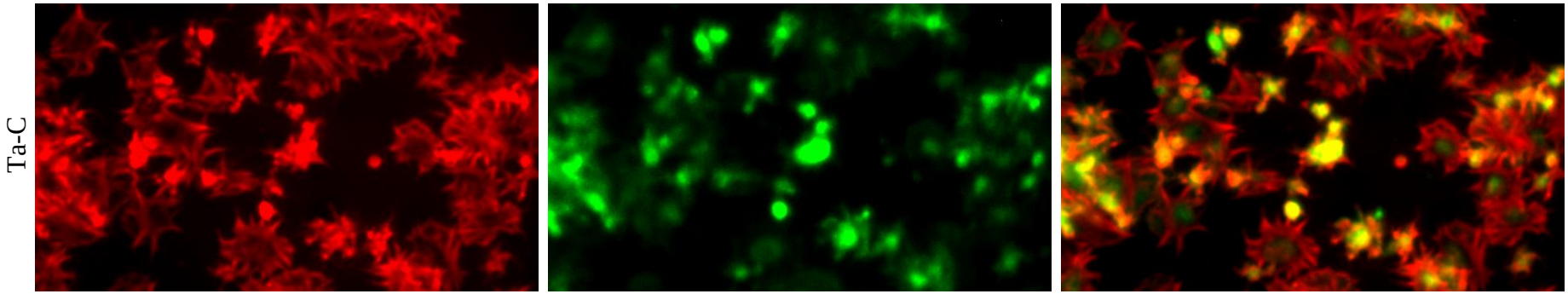

Figure 6.11 Fluorescence microscopy images of platelet cytoskeletons (left, red rhodamine-phalloidin actin stain) and activated membrane αIIbβ3 integrins (middle, green-FITC conjugated antibody to Reopro bound αIIbβ3 receptor)on platelets attached to plasma (dilution ratio 1:10, in DPBS) coated silicon, TiO2, a-C:H and ta-C nano-patterned surfaces. Samples were imaged at 500x magnification.

Platelet attachment on albumin pre-coated nano-patterned surfaces is shown in Figure 6.8, where the morphology of the bound platelets, as elucidated from the actin cytoskeleton as well as the distribution of activated $\alpha_{IIb}\beta_3$ integrins are shown. Platelets exposed to albumin coated surfaces were rounded in morphology with $\alpha_{IIb}\beta_3$ integrins present at high intensities. Especially on a-C:H surfaces, indicated by the arrows, certain platelets do not show detectable levels of the activation marker. This may suggest that the level of activation is independent of platelet morphology and that a platelet may remain in its rounded shape while exhibiting higher levels of activation. However, activation seemed ubiquitous on spread platelets, where, the degree of spreading (or, increase in a platelet's surface coverage) is inversely proportional to the intensity of $\alpha_{IIb}\beta_3$ per unit area. This may be due to expansion of the platelet's cytoplasm across the surface, which may stretch its membrane and consequently distribute the finite number of activation markers presented on the membrane.

Furthermore, the level of activation varied drastically between the albumin pre-coated nano-patterned substrates, primarily due to the number of attached platelets and their level of spreading. Platelets on TiO_2 surfaces exhibited increased spreading while platelets on ta-C surfaces presented a rounded morphology with high degree of clumping. The level of activation per unit square appeared lower on a-C:H surfaces, which presented decreased platelet attachment and limited spreading.

Activation of platelets on bare surfaces, as well as fibrinogen pre-coated and plasma pre-coated substrates are shown in Figure 6.9 to 6.11, respectively. Similar to albumin pre-coated surfaces, the level of activation observed on the various materials was dependent on platelet number and morphology of the adhered platelets. Not all round platelets displayed detectable levels of activation while spread platelets presented activated $\alpha_{IIb}\beta_3$ receptors at varying concentrations. Fibrinogen and plasma pre-coated surfaces exhibited increased platelet attachment, spreading and multi-level stacking, and consequently presented higher activation levels than albumin or bare surfaces. This was especially evident on TiO_2 and a-C:H surfaces. Furthermore, between plasma and fibrinogen surfaces, fibrinogen surfaces achieved higher levels

of activation where $\alpha_{IIb}\beta_3$ integrins appear more pronounced in the central region of the spread platelet while little or no actin was detected. This may suggest that the extracellularisation process of activated $\alpha_{IIb}\beta_3$ integrins, upon contacting the protein coated surface may occur centrally to facilitate platelet-platelet adhesion due to fibrinogen-mediated biological cues. Similar morphologies of spread platelets were evident on plasma coated surfaces, however, not to the same extent, suggesting a favourable interaction between plasma proteins and the nano-patterned surfaces.

6.2.2.2.2 P-selectin and $\alpha_{IIb}\beta_3$ Activation on Flat Surfaces

The distribution of platelet receptors; P-selectin and $\alpha_{IIb}\beta_3$, on the platelet membrane were visualised by dual labelling the attached platelets with RPE conjugated antibody specific for P-selectin (CD62P) and FITC conjugated secondary antibody specific to ReoPro bound $\alpha_{IIb}\beta_3$. Platelets were then incubated for 1 hour on bare and protein pre-coated flat silicon, Tio_2, a-C:H and ta-C surfaces and the results shown in Figure 6.12, Figure 6.14 and Figure 6.15, correspond to activation of platelets on albumin, fibrinogen and diluted plasma (ratio 1:10, in DPBS) pre-coated substrates, respectively. These results were then compared with platelet activation on substrates devoid of proteins, as shown in Figure 6.13.

Platelet activation on protein pre-coated and bare flat surfaces are shown in Figure 6.12 to 6.15. The images show P-selectin (CD62P) activation on the membranes of bound platelets, activated $\alpha_{IIb}\beta_3$ integrins, and their co-localisation.

The level of P-selectin activation varies between protein coats as well as surface substrates. In general, higher intensities of the P-selectin and greater number of activated cells were evident on fibrinogen followed by DPBS and plasma, with albumin supporting the lowest level of integrin activation. Silicon and ta-C surfaces facilitated a greater concentration of the activated cells when pre-coated with fibrinogen, where the concentration of cells activated in the presence of albumin is greater than when devoid of proteins, suggesting that P-selectin activation is not initiated by platelet interaction to the bare surfaces.

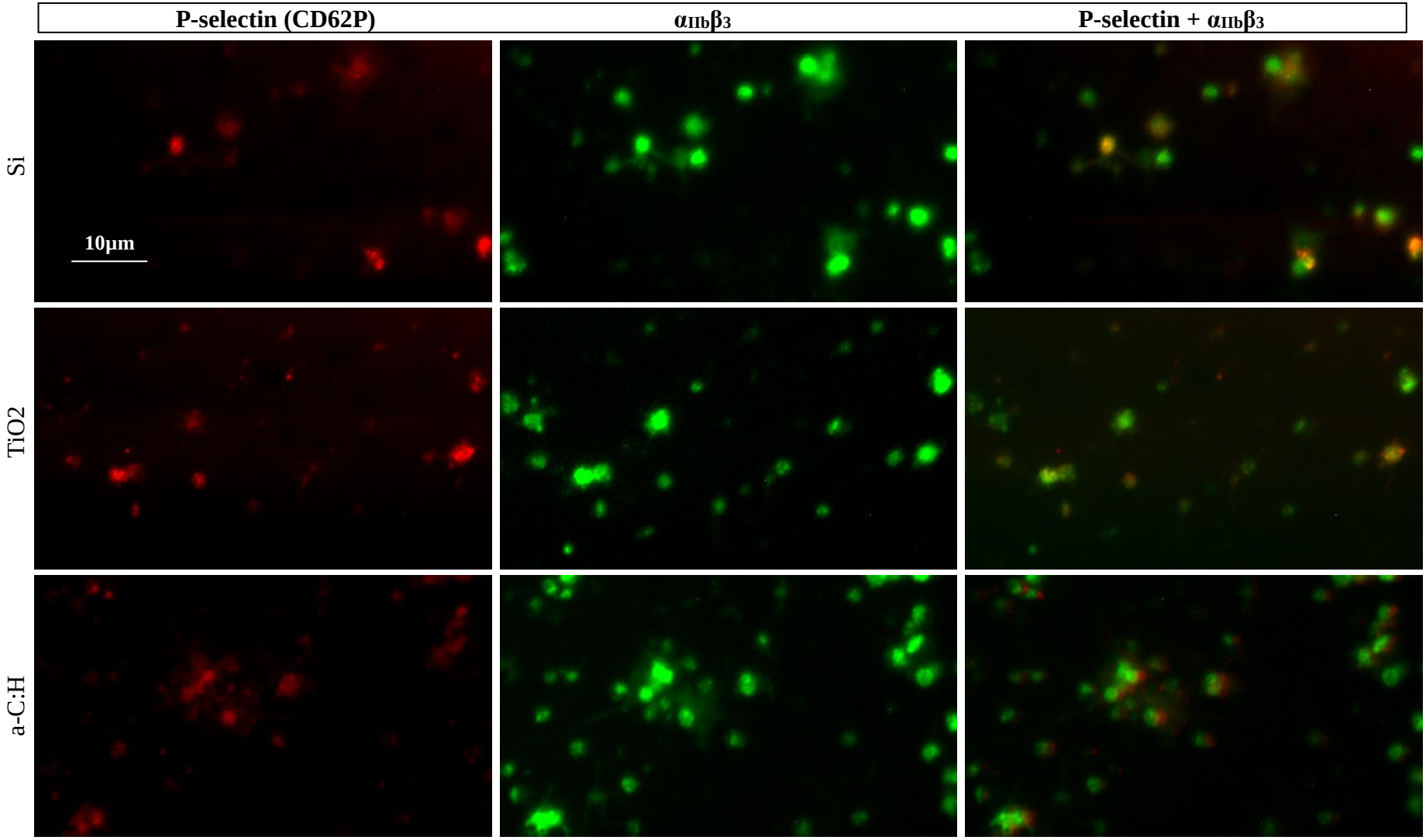
P-selectin (CD62P)
αIIbβ3
P-selectin + αIIbβ3
Si
TiO2
a-C:H
10µm

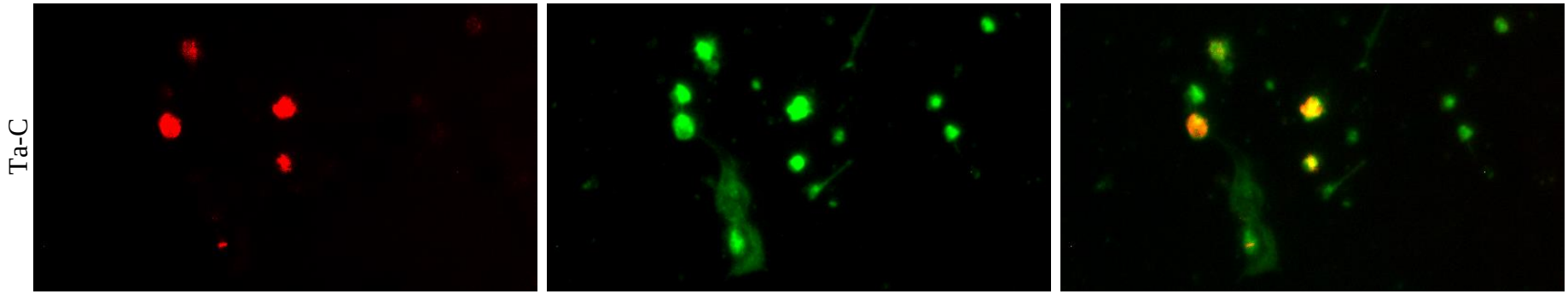

Figure 6.12 Fluorescence microscopy images showing membrane distribution of activated P-selectin (left, red-RPE conjugated anti-CD62 P-selectin) and $\alpha_{IIb}\beta_3$ integrins (middle, green-FITC conjugated antibody to Reopro bound $\alpha_{IIb}\beta_3$ receptor)on platelets attached to albumin coated silicon, TiO_2, a-C:H and ta-C flat surfaces. Samples were imaged at 500x zoom using Zeiss Axioskop microscope.

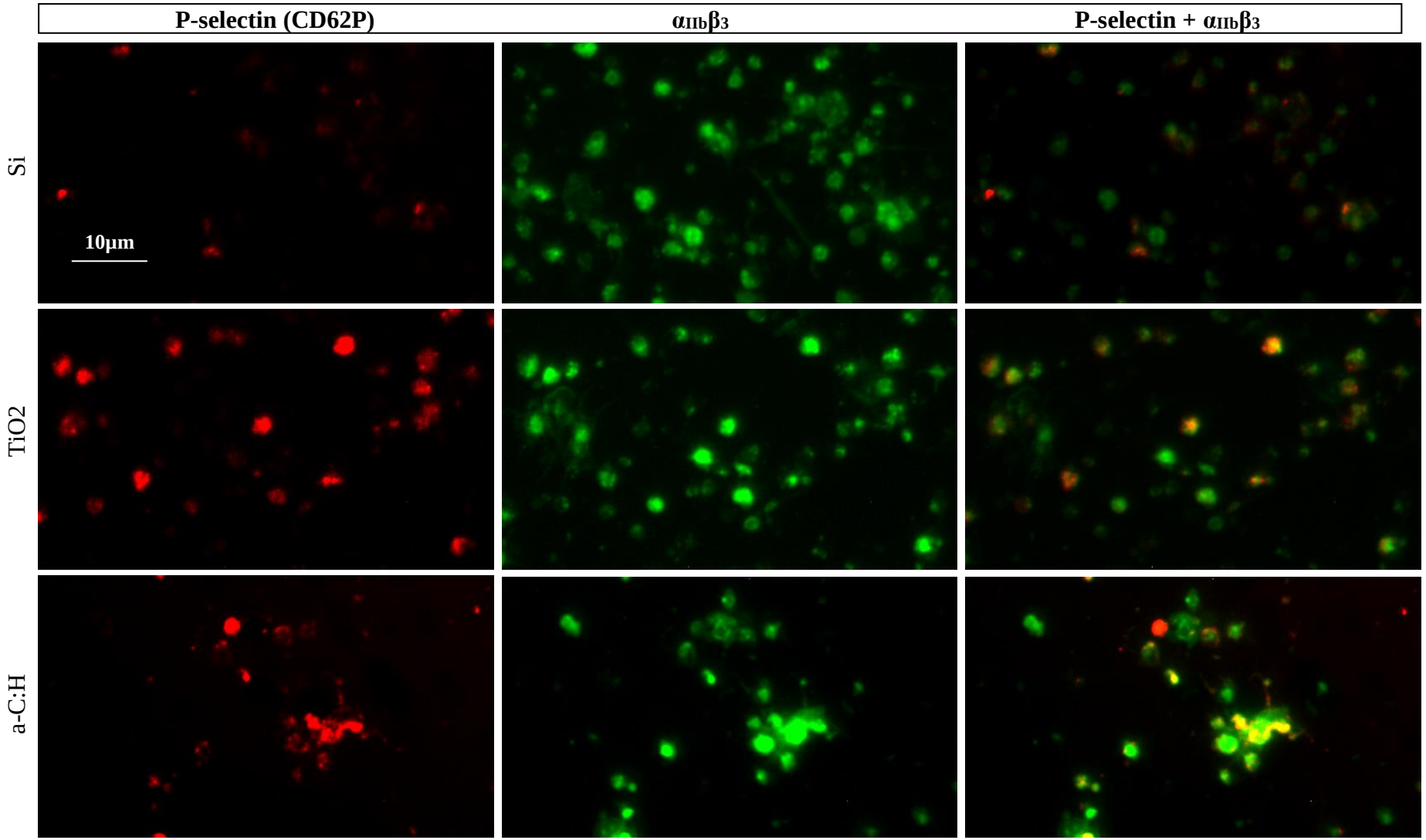
P-selectin (CD62P)
αIIbβ3
P-selectin + αIIbβ3
Si
TiO2
a-C:H
10µm

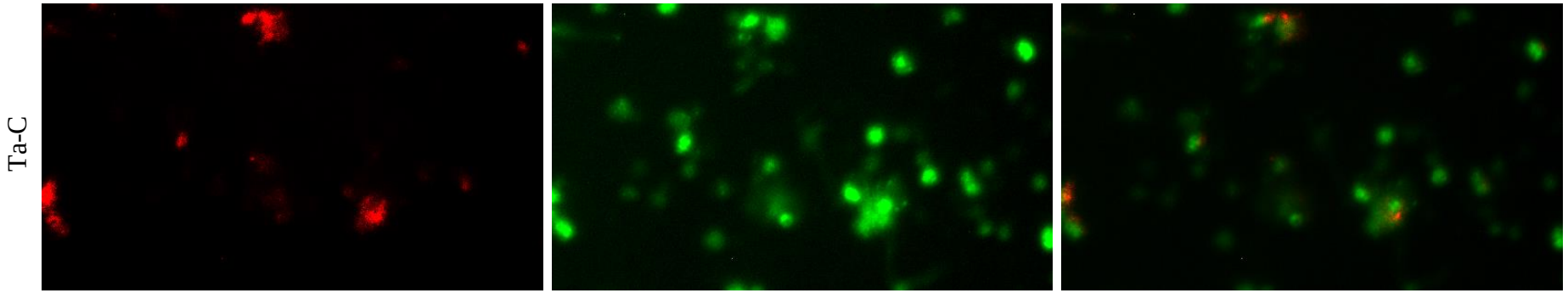

Figure 6.13 Fluorescence microscopy images showing membrane distribution of activated P-selectin (left, red-RPE conjugated anti-CD62 P-selectin) and $\alpha_{IIb}\beta_3$ integrins (middle, green-FITC conjugated antibody to Reopro bound $\alpha_{IIb}\beta_3$ receptor)on platelets attached to bare silicon, TiO_2, a-C:H and ta-C flat surfaces. Samples were imaged at 500x zoom using Zeiss Axioskop microscope.

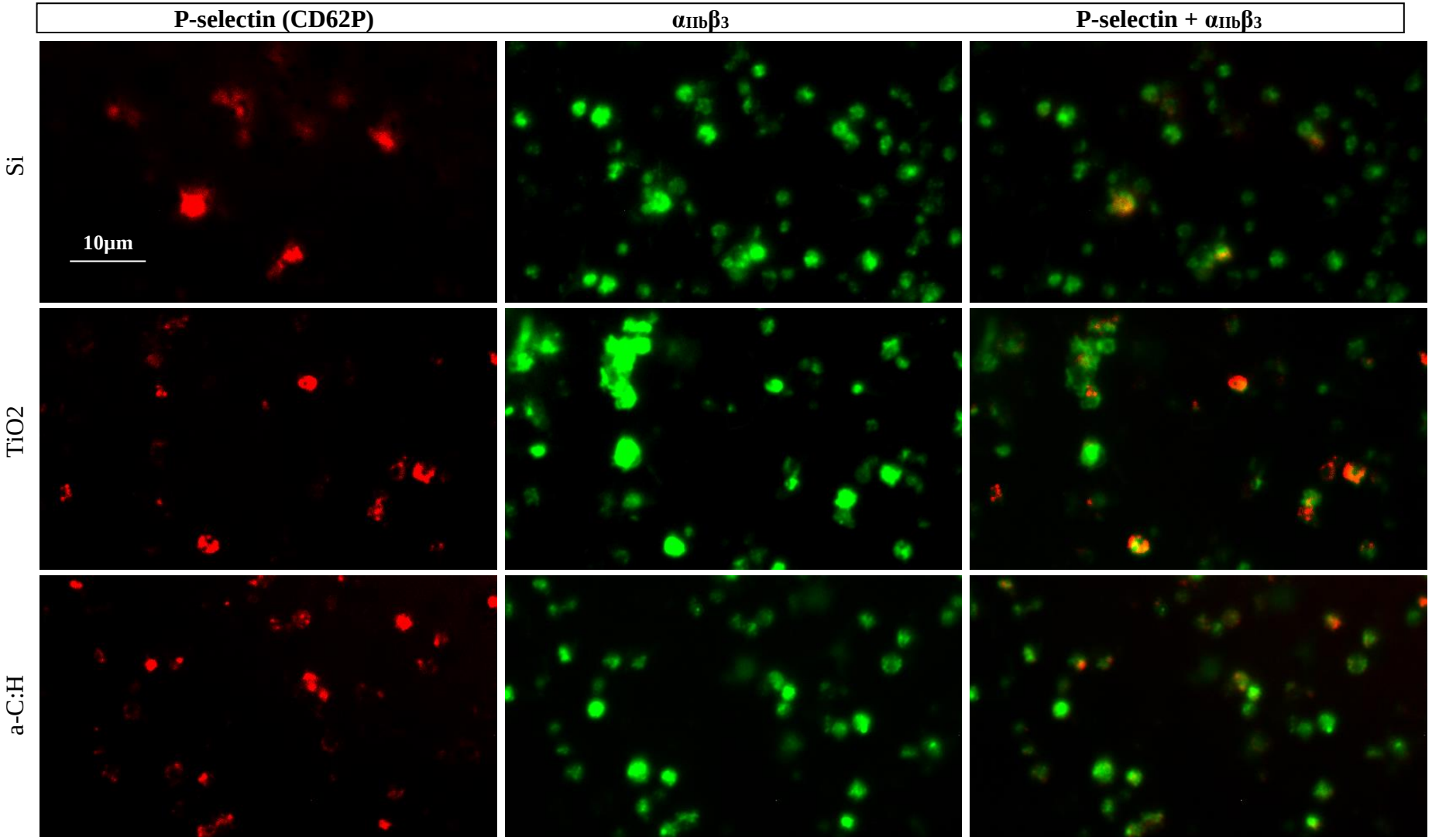
P-selectin (CD62P)
αIIbβ3
P-selectin + αIIbβ3
Si
TiO2
a-C:H
10µm

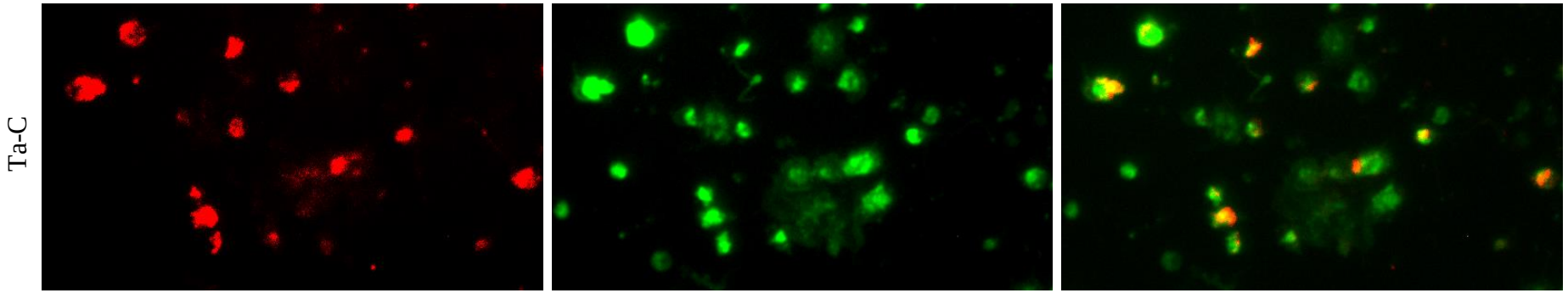

Figure 6.14 Fluorescence microscopy images showing membrane distribution of activated P-selectin (left, red-RPE conjugated anti-CD62 P-selectin) and $\alpha_{IIb}\beta_3$ integrins (middle, green-FITC conjugated antibody to Reopro bound $\alpha_{IIb}\beta_3$ receptor)on platelets attached to fibrinogen pre-coated silicon, TiO_2, a-C:H and ta-C flat surfaces. Samples were imaged at 500x zoom using Zeiss Axioskop microscope.

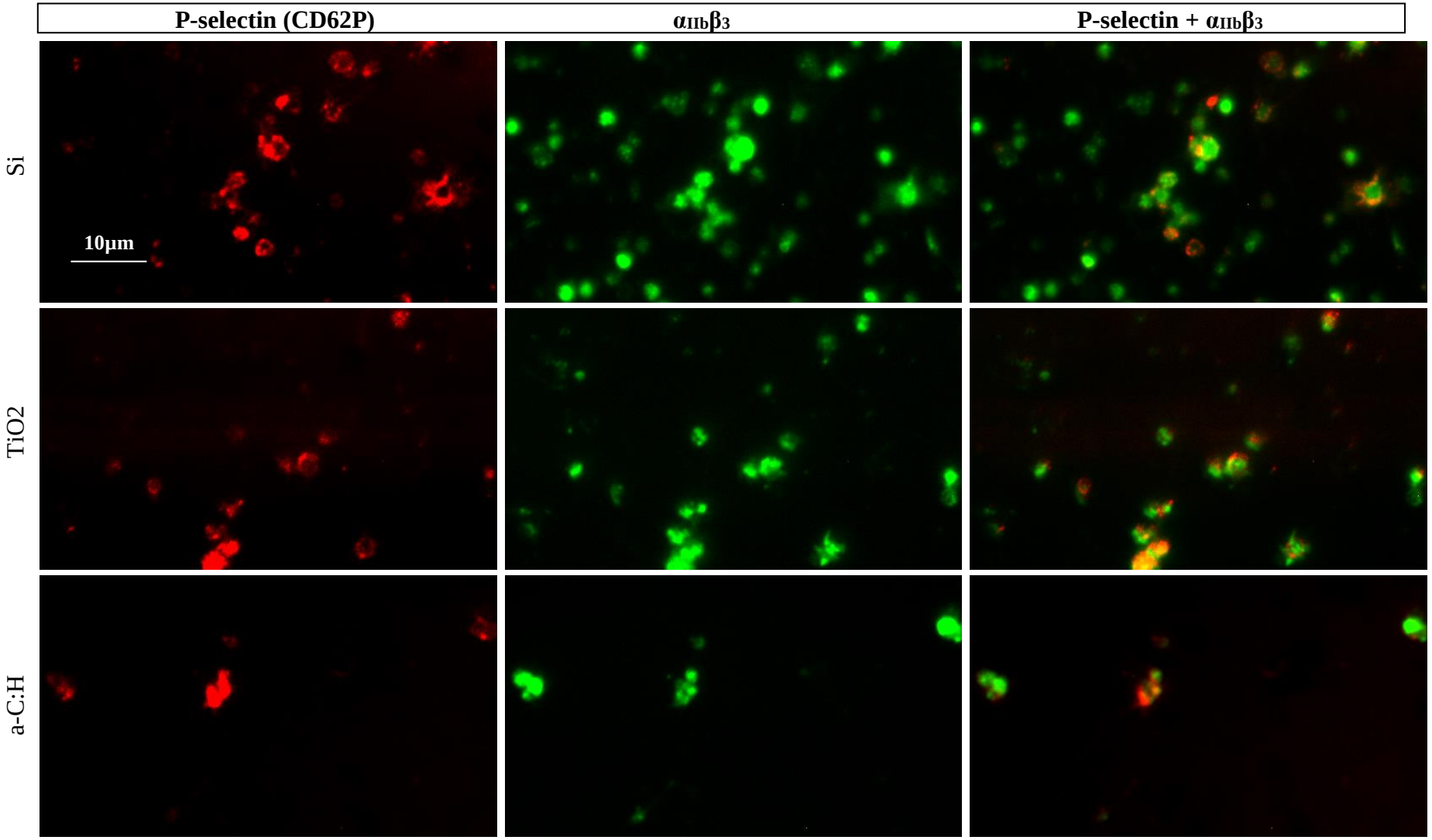
P-selectin (CD62P)
αIIbβ3
P-selectin + αIIbβ3
Si
TiO2
a-C:H
10µm

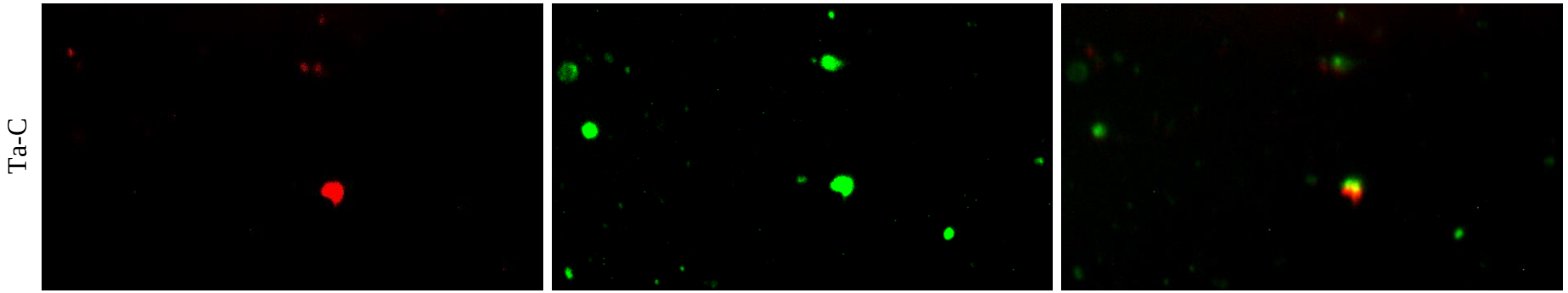

Figure 6.15 Fluorescence microscopy images showing membrane distribution of activated P-selectin (left, red-RPE conjugated anti-CD62 P-selectin) and $\alpha_{IIb}\beta_3$ integrins (middle, green-FITC conjugated antibody to Reopro bound $\alpha_{IIb}\beta_3$ receptor)on platelets attached to plasma pre-coated silicon, TiO_2, a-C:H and ta-C flat surfaces. Samples were imaged at 500x zoom using Zeiss Axioskop microscope.

Furthermore, while the level of activation on ta-C surfaces is decreased in the presence of plasma proteins than when compared with only fibrinogen, silicon responded adversely showing greater activation levels on plasma pre-coated surfaces. TiO_2 and a-C:H surfaces supported increased concentrations of activated platelets when incubated on fibrinogen pre-coated surfaces followed by bare surfaces than on albumin. Furthermore, the number of activated platelets plummeted in the presence of plasma proteins than when compared with control albumin. This may suggest a favourable interaction between plasma proteins than TiO_2 and a-C:H surfaces limiting P-selectin activation, while the surfaces alone promote non-ligand specific activation. It was interesting to note ta-C surfaces supported the least number of activated platelets on plasma-pre-coated surfaces.

The activation of $\alpha_{IIb}\beta_3$ integrins followed a similar trend to the ELISA data reported in Section 6.3.1, with fibrinogen pre-coated surfaces supporting the highest concentration of activated platelets followed by plasma pre-coated surfaces and the bare surfaces. In general, a-C:H surfaces, supported the least amount of activated platelets and a-C:H and ta-C surfaces responded more favourably in the presence of plasma proteins than silicon and TiO_2.

Comparing the images on the right hand column, it is evident that platelets attached upon 1 hour of incubation, readily exhibit $\alpha_{IIb}\beta_3$ activation than when compared with P-selectin, and P-selectin activation only occurs in platelets that present activated $\alpha_{IIb}\beta_3$ receptors. This not only proves the significance of activated $\alpha_{IIb}\beta_3$ in P-selectin activation but also reinforces the role of P-selectin as an late stage activation marker. It was also interesting to note that activation of P-selectin was not dependent on the level of $\alpha_{IIb}\beta_3$ activation or platelet spreading. The presence of P-selectin was not limited to spread platelets, but also ones that retained their rounded morphology. Further, activated P-selectin was detected on platelets exhibiting high intensities of $\alpha_{IIb}\beta_3$ as well as lower intensities, suggesting that P-selectin activation is dependent although not limited to the level of $\alpha_{IIb}\beta_3$ activation.

6.2.2.2.3 P-selectin and $\alpha_{IIb}\beta_3$ Activation on Nano-patterned Surfaces

The distribution of activated P-selectin and $\alpha_{IIb}\beta_3$ membrane receptors on surface bound platelets was visualised by dual labelling the integrins with RPE conjugated antibody specific for P-selectin (CD62P) and FITC conjugated secondary antibody specific to ReoPro bound $\alpha_{IIb}\beta_3$. Platelets were incubated on bare and protein pre-coated nano-patterned surfaces. The results shown in Figure 6.16, Figure 6.18 and Figure 6.19 correspond to activation of platelets on albumin, fibrinogen and diluted plasma (ratio 1:10, in DPBS) pre-coated substrates, respectively. These results were compared with platelet activation on silicon, TiO_2 a-C:H and ta-C substrates devoid of proteins, as shown in Figure 6.17.

A greater level of P-selectin and $\alpha_{IIb}\beta_3$ activation was exhibited on nano-patterned surfaces than on flat surfaces. This was especially evident on albumin pre-coated surfaces (Figure 6.16), where higher concentrations of $\alpha_{IIb}\beta_3$ activated platelets presented P-selectin activation. Silicon surfaces supported higher levels of p-selectin activation while TiO_2 surfaces showed increased $\alpha_{IIb}\beta_3$ activation. A-C:H surfaces presented lower levels of both markers, followed by ta-C. Further, it appears that while $\alpha_{IIb}\beta_3$ is highly aggregated in the central region of a spread platelet, P-selectin integrins are localised in such a way they not only appear as aggregates in the centre abut also form the outer pheripheral ring of a platelet, as indicated by the white arrows on silicon, a-C:H and ta-C of Figure 6.16.

Figure 6.17 to 6.19 show platelet activation on bare, fibrinogen and diluted plasma (ratio 1:10, in DPBS) pre-coated surfaces, respectively. As can be seen, the level of P-selectin activation remains relatively the same on all four substrates on fibrinogen pre-coated and bare surfaces, except for ta-C bare surfaces which present lower concentrations of activated cells. Plasma pre-coated surfaces however display significantly lower levels of P-selectin activation, similar to plasma-pre-coated flat surfaces, suggesting that while nano-patterns increase P-selectin activation, plasma proteins interact to counteract the effect and restore activation levels of the flat surfaces.

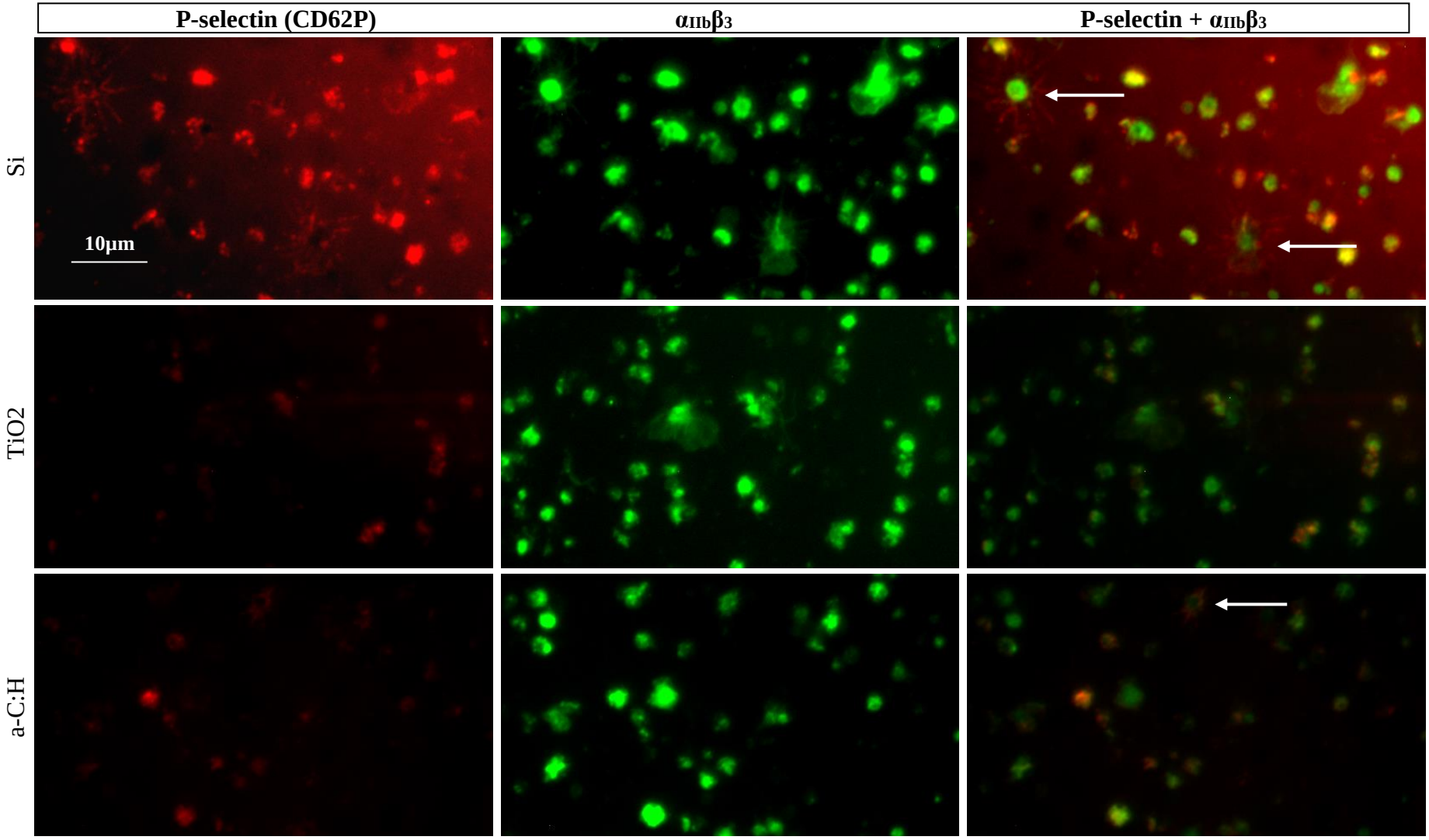
P-selectin (CD62P)
αIIbβ3
P-selectin + αIIbβ3
Si
TiO2
a-C:H
10µm

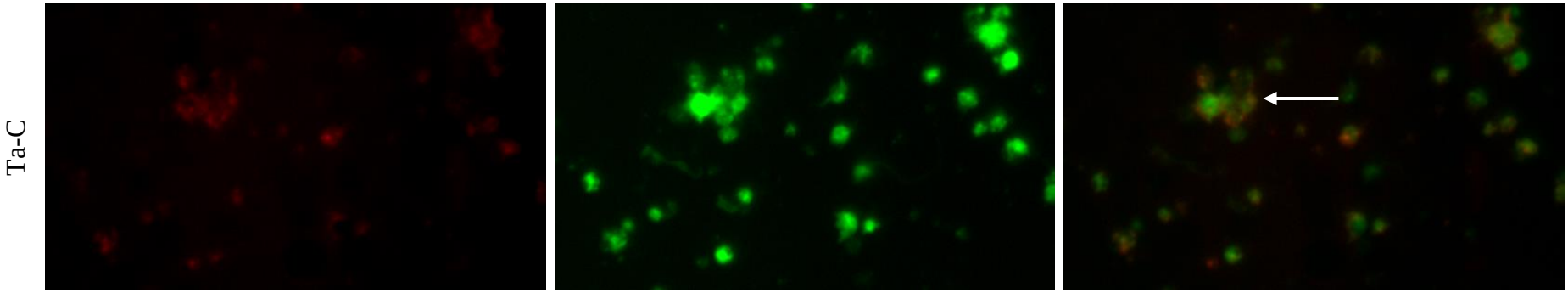

Figure 6.16 Fluorescence microscopy images showing membrane distribution of activated P-selectin (left, red-RPE conjugated anti-CD62 P-selectin) and $\alpha_{IIb}\beta_3$ integrins (middle, green-FITC conjugated antibody to Reopro bound $\alpha_{IIb}\beta_3$ receptor)on platelets attached to albumin pre-coated silicon, TiO_2, a-C:H and ta-C nano-patterned surfaces. Samples were imaged at 500x zoom using Zeiss Axioskop microscope.

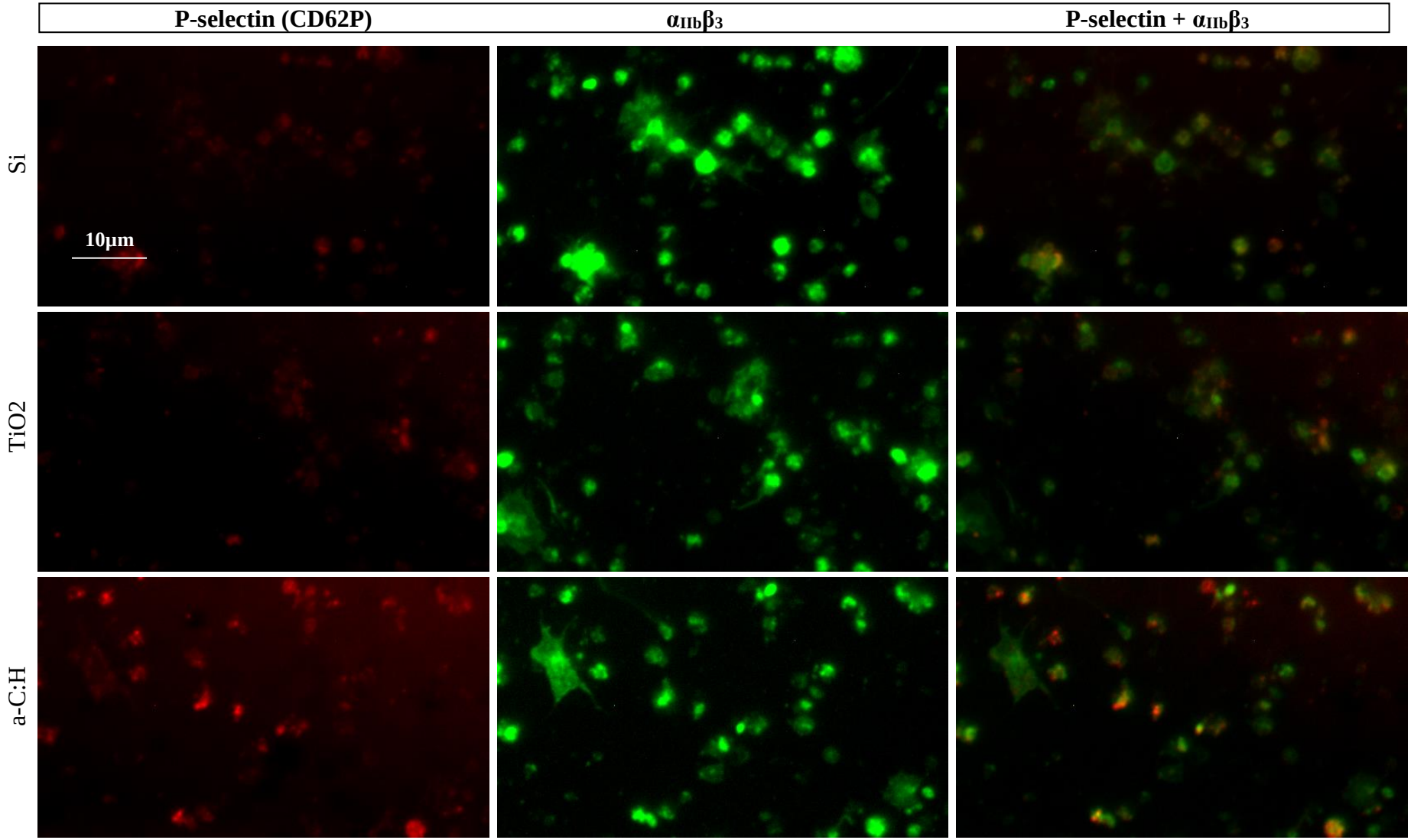
P-selectin (CD62P)
αIIbβ3
P-selectin + αIIbβ3
Si
TiO2
a-C:H
10µm

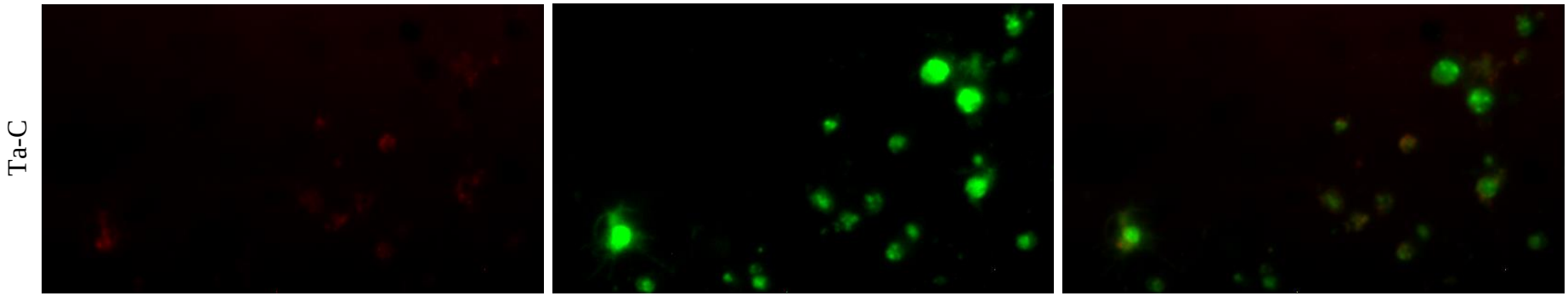

Figure 6.17 Fluorescence microscopy images showing membrane distribution of activated P-selectin (left, red-RPE conjugated anti-CD62 P-selectin) and $\alpha_{IIb}\beta_3$ integrins (middle, green-FITC conjugated antibody to Reopro bound $\alpha_{IIb}\beta_3$ receptor)on platelets attached to bare silicon, TiO_2, a-C:H and ta-C nano-patterned surfaces. Samples were imaged at 500x zoom using Zeiss Axioskop microscope.

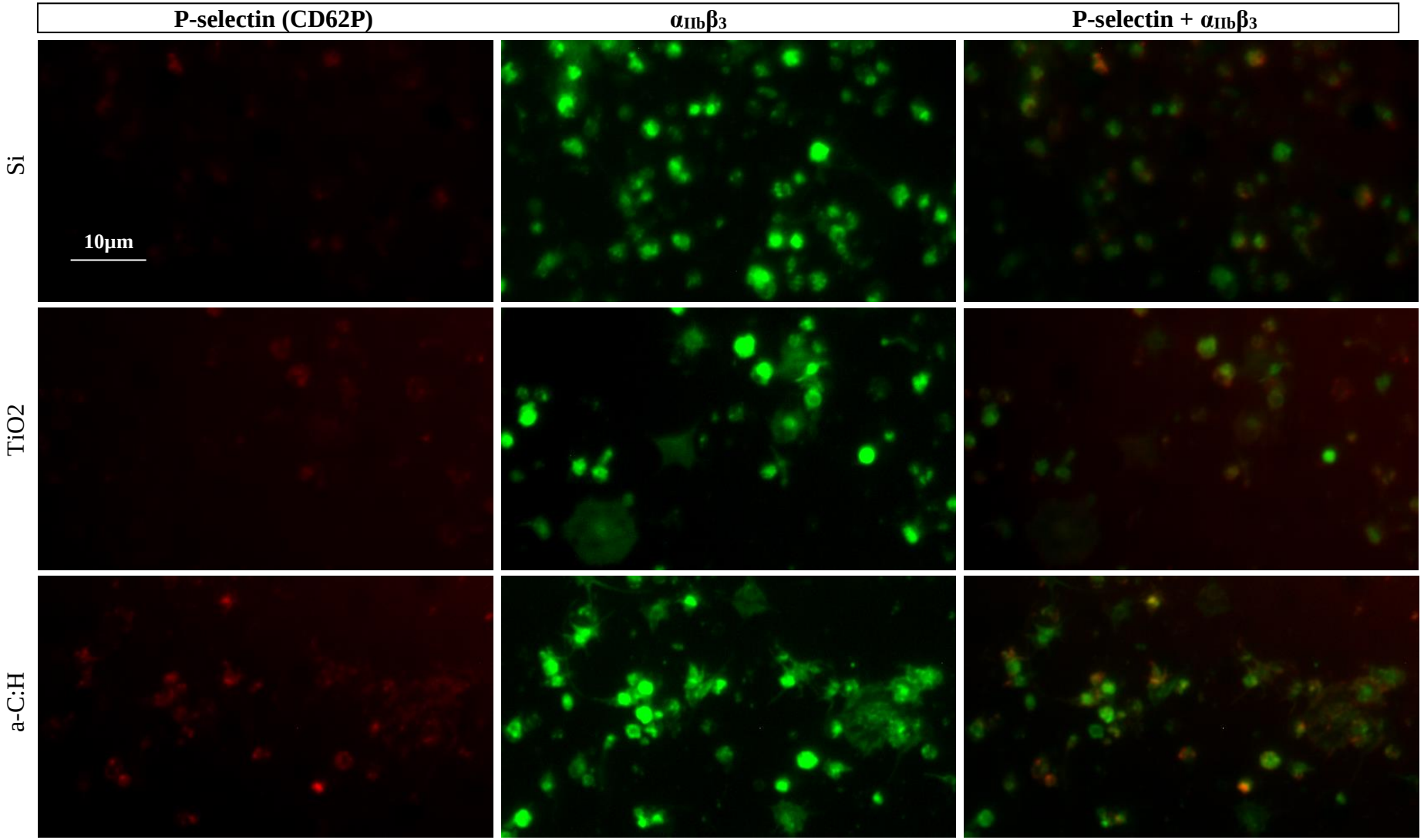
P-selectin (CD62P)
αIIbβ3
P-selectin + αIIbβ3
Si
TiO2
a-C:H
10µm

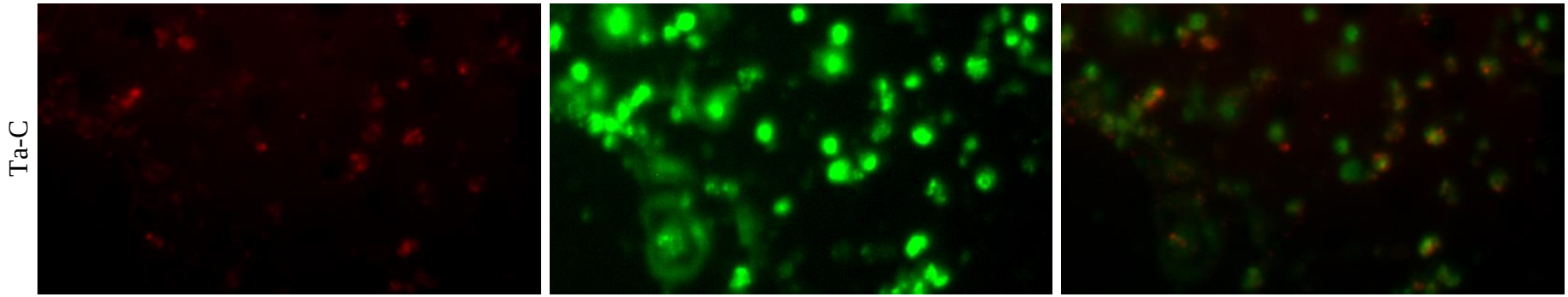

Figure 6.18 Fluorescence microscopy images showing membrane distribution of activated P-selectin (left, red-RPE conjugated anti-CD62 P-selectin) and $\alpha_{IIb}\beta_3$ integrins (middle, green-FITC conjugated antibody to Reopro bound $\alpha_{IIb}\beta_3$ receptor)on platelets attached to fibrinogen pre-coated silicon, TiO_2, a-C:H and ta-C nano-patterned surfaces. Samples were imaged at 500x zoom using Zeiss Axioskop microscope.

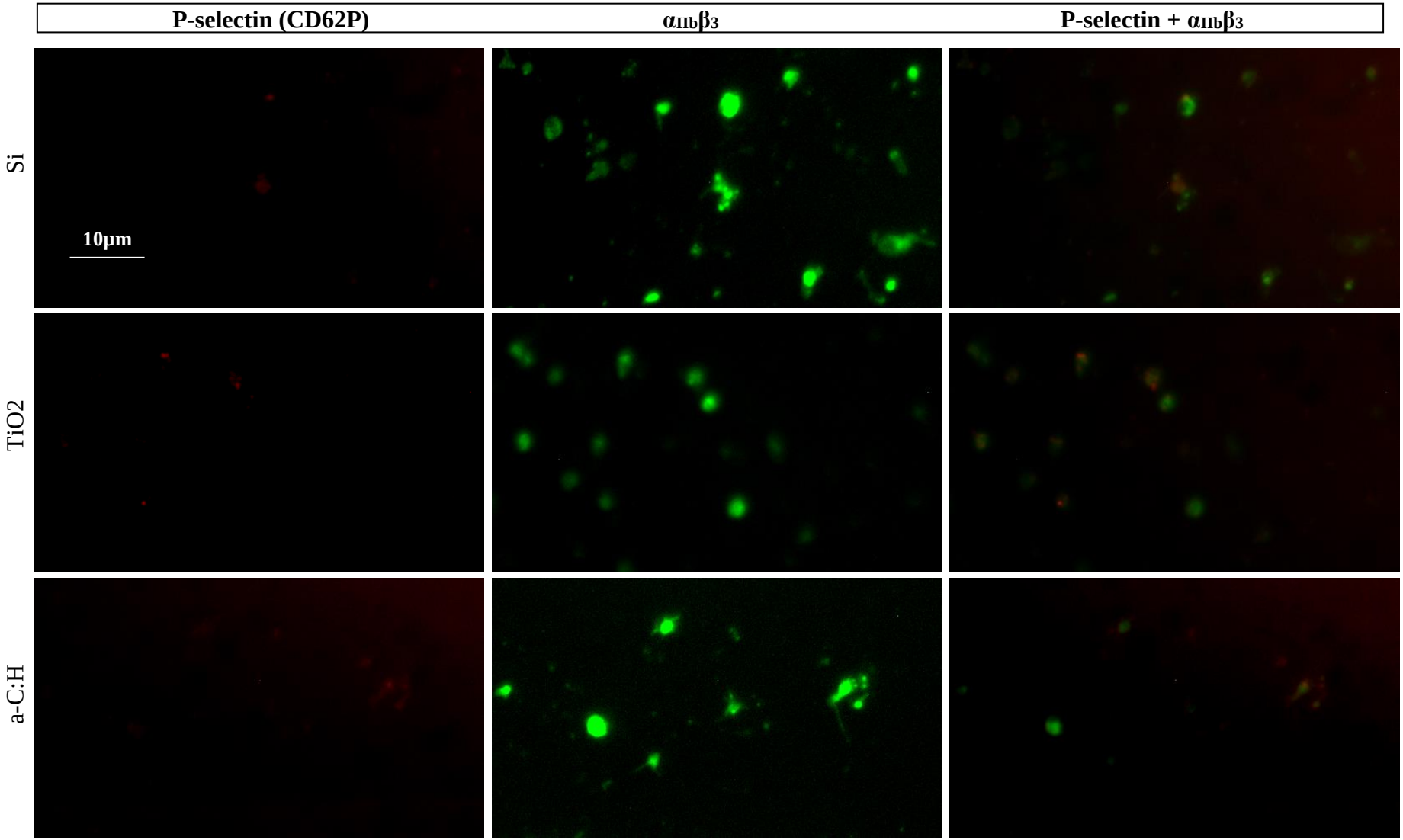
P-selectin (CD62P)
αIIbβ3
P-selectin + αIIbβ3
Si
TiO2
a-C:H
10µm

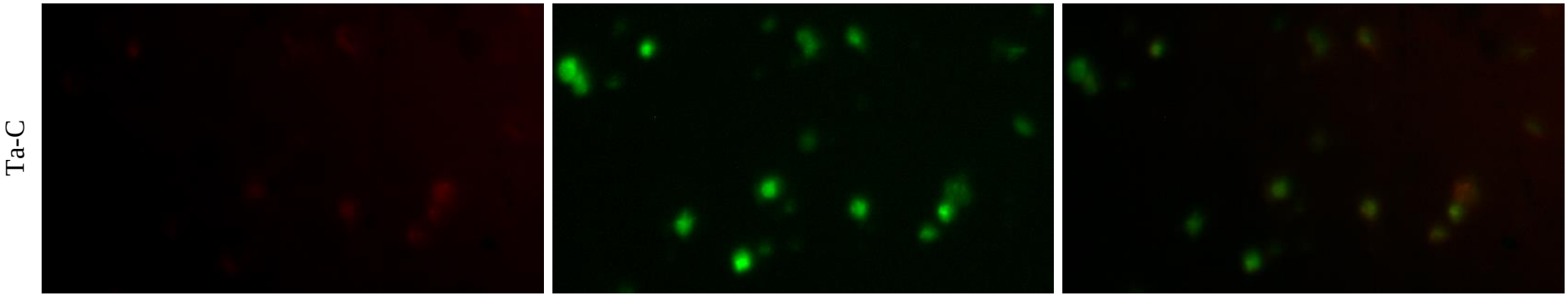

Figure 6.19 Fluorescence microscopy images showing membrane distribution of activated P-selectin (left, red-RPE conjugated anti-CD62 P-selectin) and $\alpha_{IIb}\beta_3$ integrins (middle, green-FITC conjugated antibody to Reopro bound $\alpha_{IIb}\beta_3$ receptor)on platelets attached to plasma coated silicon, TiO_2, a-C:H and ta-C nano-patterned surfaces. Samples were imaged at 500x zoom using Zeiss Axioskop microscope.

The level of $\alpha_{IIb}\beta_3$ activation on fibrinogen coated and bare nano-patterned substrates was significantly greater than the corresponding flat surfaces. This may be due to increased platelet spreading. A-C:H and ta-C bare surfaces showed decreased levels of platelet activation when compared with silicon and titania, while TiO_2 and a-C:H fibrinogen pre-coated surfaces showed decreased activation when compared with silicon and ta-C substrates. Although it was difficult to discern between the test substrates, the level of activation on plasma proteins was substantially lower, suggesting that either; these surfaces preferentially adsorb proteins not involved in activation, and/or, the conformation of proteins are altered after adsorbing on these surfaces such that they limit platelet activation. Again, this reinforces the overall favourable interaction between plasma proteins and nano-patterned surfaces limiting the overall $\alpha_{IIb}\beta_3$ activation.

6.2.2.3 Flow Cytometry

Activation of unattached platelets in response to exposure to silicon, TiO_2, a-C:H and ta-C surfaces, and, serum proteins including albumin, fibrinogen and diluted plasma, was evaluated after exposing the platelet suspension to fluorescently tagged antibodies specific to activated $\alpha_{IIb}\beta_3$ and P-selectin expression and measured using a flow cytometer.

The one parameter histograms showing cellular fluorescent intensities as fold increase using the FL-1 channel (Figure 6.20) was used to determine the presence of activated $\alpha_{IIb}\beta_3$ receptors. Reopro antibody was used to probe for activated $\alpha_{IIb}\beta_3$ integrins and detected using an anti-human antibody conjugated with FITC. Bare silicon and plasma pre-coated ta-C, showed decreased activated $\alpha_{IIb}\beta_3$ in solution. While a difference in receptor activation was observed on some bare and plasma substrates, no appreciable difference were detected between flat substrates and control TCPS pre-coated with albumin and fibrinogen. The nano-patterned surfaces showed the same level of activation between protein pre-coated surfaces as well as surface chemistry. Further, the fluorescent levels on the nano-patterned surfaces were

similar to that of the flat surfaces, suggesting that varying the underlying nano-topography of the surface had no effect on $\alpha_{IIb}\beta_3$ activation in solution for non-adherent platelets. Figure 6.21 shows P-selectin exposure on platelets from solution. Apart from plasma pre-coated ta-C, which showed a decrease in P-selectin expression, activation levels followed a similar trend to $\alpha_{IIb}\beta_3$, where they did not vary between surfaces, protein pre-coated surfaces and nano-topography.

Overall, it is evident that the above mentioned surface chemistries, nano-topography and adsorbed proteins do not markedly mediate ligand or integrin conformation in solution but rather exerts its influence upon surface contact (as shown in Section6.2.2.1 and 6.2.2.2), *in vitro*.

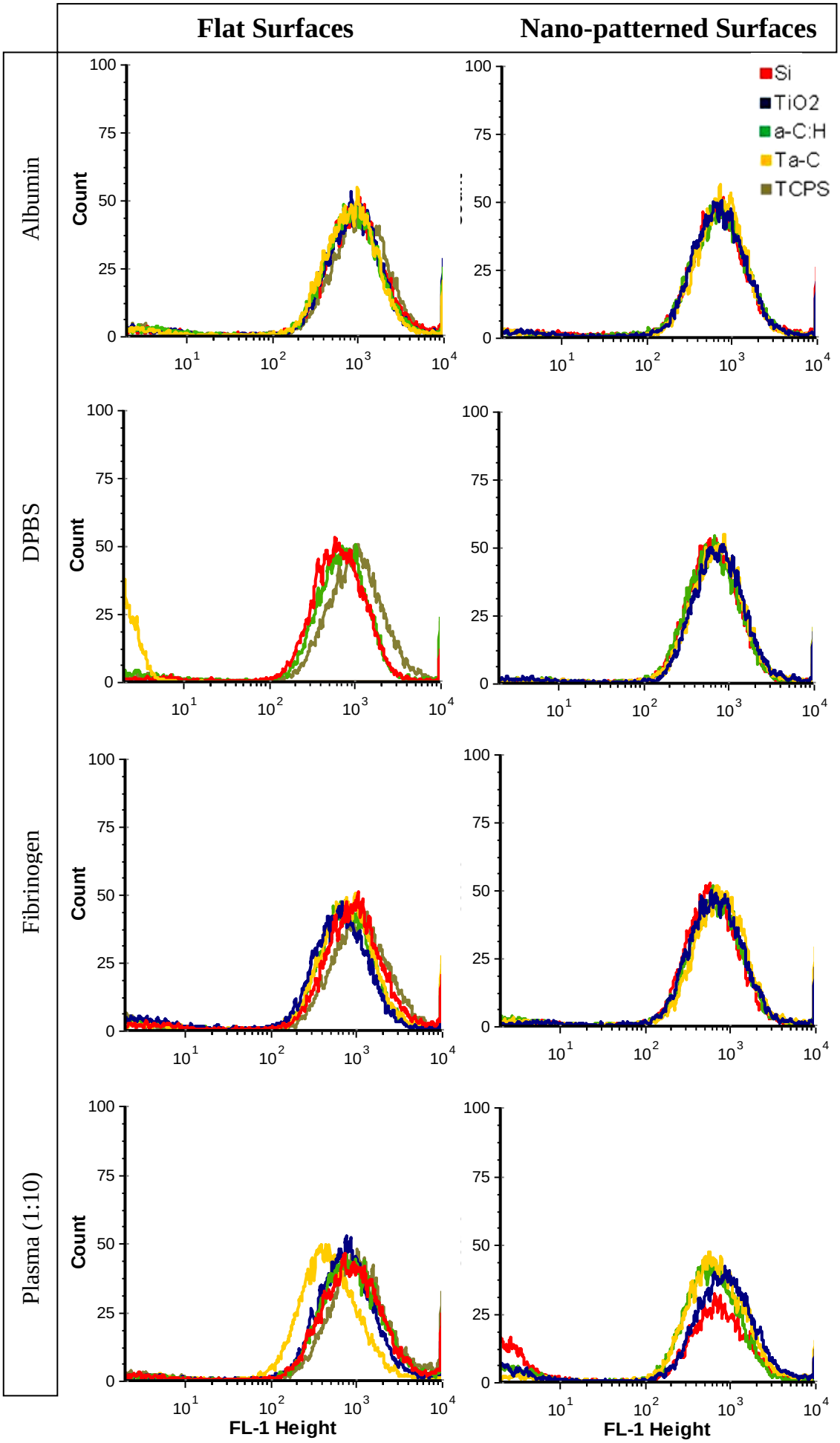
Flat Surfaces
Nano-patterned Surfaces
Albumin
DPBS
Fibrinogen
Plasma (1:10)
Count
FL-1 Height
Si
TiO2
a-C:H
Ta-C
TCPS

Figure 6.20 *Flow cytometric analysis of αIIbβ3 expression on platelet membranes on flat and nano-patterned Si, TiO_2, a-C:H and Ta-C surfaces either devoid of proteins (DPBS), or, in the presence of proteins including albumin (BSA), fibrinogen (Fg), or diluted plasma (ratio 1:10, in DPBS). The results from the flat surfaces were compared with control TCPS. The profiles are representative of three experiments for each condition.*

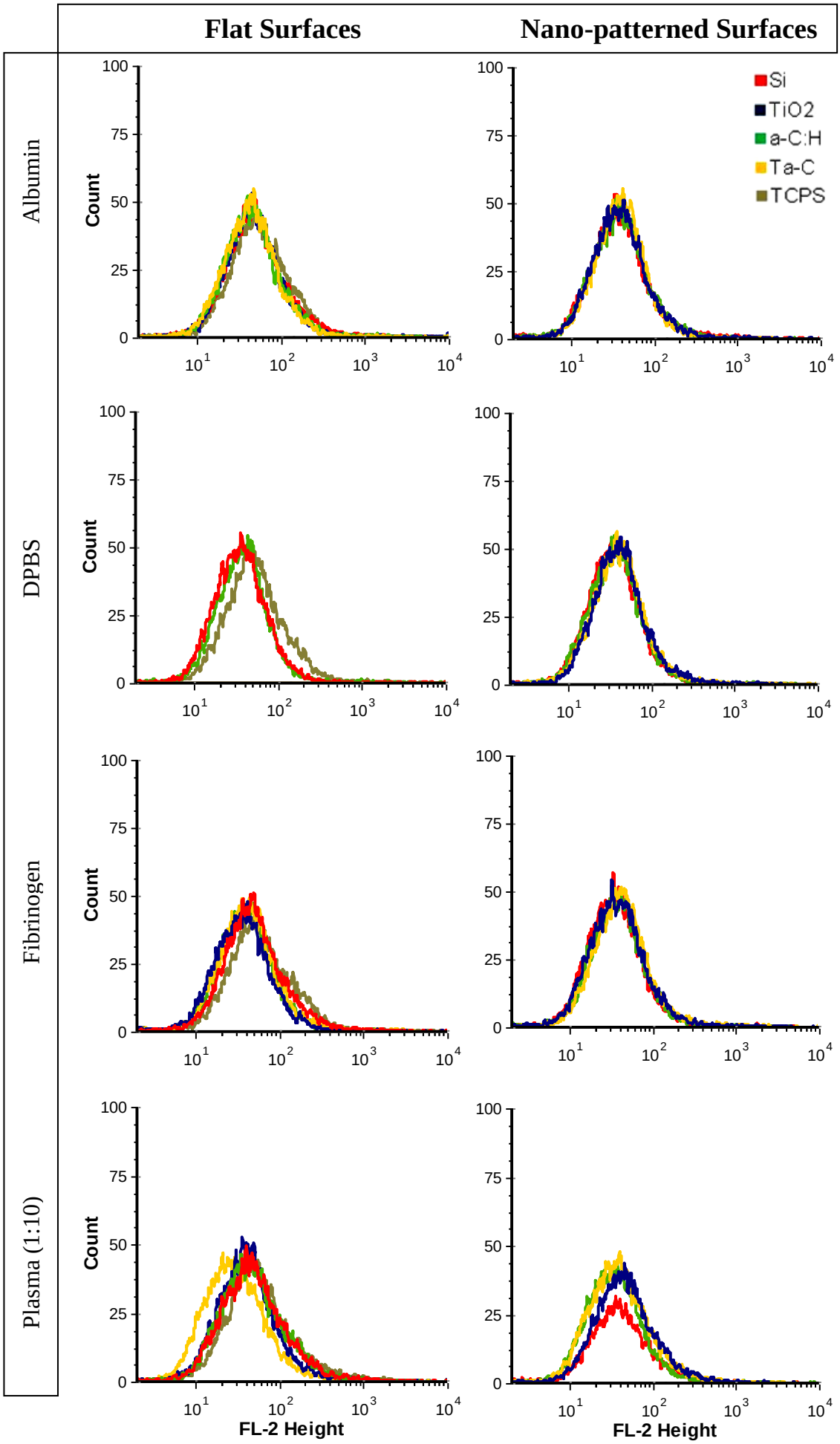
Flat Surfaces
Nano-patterned Surfaces
Albumin
DPBS
Fibrinogen
Plasma (1:10)
Count
FL-2 Height
Si
TiO2
a-C:H
Ta-C
TCPS

Figure 6.21 *Flow cytometric analysis of P-selectin (CD62P) expression on platelet membranes on flat and nano-patterned Si, TiO_2, a-C:H and Ta-C surfaces either devoid of proteins (DPBS), or, in the presence of proteins including albumin (BSA), fibrinogen (Fg), or diluted plasma (ratio 1:10, in DPBS). The results from the flat surfaces were compared with control TCPS. The profiles are representative of three experiments for each condition.*

6.3 Summary

The time taken for the polymerisation of fibrin monomers into fibrin clots on the test substrates was delayed when the test surfaces were pre-exposed to plasma proteins. A-C:H has shown the longest delay, especially when the plasma proteins were diluted with higher concentrations of heparin. The intrinsic and common pathways have been proven accountable for this response. Intrinsic factors are readily influenced by biomaterial surfaces; causing the inhibition of their function. The samples also impede the conversion of fibrinogen to fibrin, by denaturing the protein and consequently temporarily retarding the clotting process.

The level of platelet activation was reduced on plasma pre-coated surfaces. Plasma proteins, other than fibrinogen, not only reduce the overall exposure of the bare surfaces but also reduce the binding of fibrinogen to the surface either by; steric hindrance or by reducing the overall exposure of adsorbed fibrinogen to circulating platelets in order to decrease $\alpha_{IIb}\beta_3$ mediated platelet activation. This was especially evident on a-C:H and ta-C substrates. There was no activated $\alpha_2\beta_1$ receptors detected on bare and protein-pre-coated flat substrates. P-selectin activation was not dependent on the chemistry of the bare surfaces, but rather dependent on whether the platelets exhibit activated $\alpha_{IIb}\beta_3$ receptors. The level of activation between the various materials was dependent on concentration of adsorbed platelets and their respective morphology. Not all platelets with a rounded morphology displayed detectable levels of activation while spread platelets presented activated receptors at varying concentrations.

Nano-patterned surfaces exhibited increased activated P-selectin and $\alpha_{IIb}\beta_3$ integrins and again, a favourable interaction between plasma proteins and patterned surfaces reduced the overall activation levels of the bare and fibrinogen pre-coated substrates. Although it was difficult to discern between the various surface chemistries, it was clearly evident that nano-patterns decreased the overall haemocompatibility of a given biomaterial surface.

While platelet activation studies using ELISA and fluorescence microscopy show surface chemistry, nano-topography and adsorbed proteins mediate ligand or integrin conformation on surface adsorbed platelets; flow cytometry experiments indicated platelets suspended in solution remain uninfluenced by varying chemical and physical properties of a-C:H, ta-C and titania thin films.

7 OVERALL DISCUSSION

Driven by the increasing economic and social burden associated with thrombus development on blood-contacting medical devices, and despite over half a century of progress in understanding the interactions at play at the blood-biomaterial interface [5, 219, 220], the level of knowledge required to design and develop haemocompatible materials has not yet been attained. In fact, Ratner has stated that a truly blood compatible surface is still yet to be produced after 60 years of research into haemocompatibility and numerous approaches to solving the blood-biomaterial dilemma [5].

The haemocompatibility of a material is essentially the tolerance of blood to the surface of blood contacting devices and is of great importance as blood is the first bodily fluid that contacts artificial surfaces. Blood is in contact with artificial surfaces during many modern health care treatment and diagnostic procedures such as: venous catheters, stents, vena cava filters, vascular grafts, LVAD's and prosthetic heart valve implants, cardiopulmonary bypass, dialysis, and blood transfusions and even when blood is drawn for commonly run blood tests. Approaches such as surface coating and surface modification have been recently undertaken in an effort to improve blood compatibility. Modification of the biomaterial surface to minimise the overall blood-biomaterial interactions (by chemically modifying the surface of the biomaterial with anti-coagulant and anti-thrombotic drugs or seeding with endothelial cells) are still far from perfect. Such surface modifications are not economically viable; rather, they require complex experimental procedures and are likely to endure potential regulatory-approval complications downstream [439, 492]. Further, these surfaces require long term stability from delamination under shear stress. Modulating the surfaces with endothelial cells can be beneficial as it mimics the inner surface of blood vessel walls, however the adhesion and proliferation of endothelial cells on implant surfaces is a complicated task and occurs only with a long turn over time, therefore rending this option unviable during emergency situations requiring immediate implantation. Surface coatings such as inorganic coatings (carbon based) [493] or passivating the surface by forming covalently linked

oxidised surface adlayer [331] are also options, but the interaction between blood and biomaterial surfaces is multi-staged and complex - it is an interlinked process involving protein adsorption, platelet adhesion and activation, involving several factors including surface chemical composition, charge, flexibility, wettability and conditions of blood flow [494-497] – and the exact mechanism of selective adsorption of plasma proteins and the adhesion, spreading and activation of platelets at the blood-biomaterial interface still remains unknown.

Therefore, this study investigated the influence of surface chemistry, nano-roughness and adsorption of specific plasma proteins on human platelet interactions. The impact of surface chemistry was tested by changing the biomaterial thin film coating applied, while the surface nano-topography was altered by engineering pseudo-regular surface nano-patterns. Surface engineering was carried out on silicon wafers as these substrates presented an ultra-flat surface with topographical features, if any, only in the sub-nano-meter range. Further, the influence of plasma proteins was evaluated by allowing specific adsorption of albumin and fibrinogen as well as plasma on the surface engineered biomaterial surfaces. The results were then compared with surfaces devoid of proteins.

7.1 Influence of Surface Chemistry on Plasma Protein Adsorption and Coagulation Cascade Activation

Blood plasma is mainly constituted of proteins and so far over 300 different proteins have been documented. These proteins have contained plasma concentrations ranging from 35-50 mg/mL for serum albumin to only 0-5 pg/mL for interleukin 6 [179]. In the process of developing new haemocompatible materials, hundreds of surface coatings and bulk materials have been evaluated with regard to their interactions with proteins such as fibrinogen, fibronectin, von Willebrand factor, and albumin etc; although overall plasma protein compatibility has been assessed less often. Protein adsorption from plasma is far more complicated than from a single protein solution [498]. Blood plasma is a multi-protein solution, which is

concentrated with various proteins at varying concentrations. Adsorption is regarded as a selective and competitive process with adsorbed proteins not always bound indefinitely to the surface. The composition of adsorbed proteins is subject to change over time in a phenomenon known as the Vroman effect [184]. This phenomenon covers a monolayer on the surface with a thickness of 2-10 nm [185]. Surfaces resistant to protein adsorption, as found with non-fouling surfaces, have generally been evaluated from experiments involving single-protein solutions. Such surfaces may not necessarily present a similarly high efficiency in resisting protein adsorption from plasma [498]. When fibrinogen and albumin were in a solution by themselves, ultra-flat test substrates with surface roughness in the sub-nano-meter range, have been shown to exhibit a higher affinity to albumin than fibrinogen.

Biomaterial substrates used in this study include: flat (un-patterned) silicon wafers coated with either a-C:H (hydrogenated amorphous carbon) and ta-C (tetrahedral amorphous carbon) diamond like carbon or crystalline TiO_2 (titania).

Commercially used a-C:H and ta-C diamond like carbon (DLC) coatings were studied as these materials have exhibited excellent biocompatible, haemocompatible, anti-thrombogenic and non-cytotoxic properties, when compared with pyrolytic carbon, stainless steel and polyurethane [315, 499]. DLC is a hydrophobic material with reported surface energies ranging between 40-54mNm^{-1} and contact angles between 55-70º [304, 305, 500-502]. As a surface coating, DLC has been proven to be wear resistant, chemically inert and low friction, reducing the surface energy of the underlying biomaterial by reducing the number of free bonds which are known to cost energy [270].

TiO_2 coatings were studied in this project as opposed to the titanium surfaces which are commercially used in the biomedical industry because TiO_2 has shown better haemocompatibility than the bulk titanium. Titanium and its alloys are highly regarded and often used due to the excellent corrosion resistive properties of the native oxide layer formed on the bulk material [329-331]. The native oxide layer primarily consists of amorphous titanium dioxide (TiO_2) [333-336]. This protective

and highly stable, passive film is, in effect, the surface that will interact with the *in vivo* environment and is therefore of huge importance when considering cell-surface interactions. A study conducted by Sunny et al. [344] found the ratio of adsorbed albumin to fibrinogen (albumin/fibrinogen ratio) increased 7 fold when the thickness of the coated TiO_2 layer increased by 180nm. Furthermore, the adsorption of serum proteins on TiO_2 substrates were found to occur through calcium binding sites in a similar manner to the adhesion of hydroxyapatite crystals [369]. Another study conducted by Smith et al. [503] found a decrease in overall thrombogenic effects of TiO_2 nano-tube arrays when compared with biomedical grade titanium after 2 hours of contact with whole blood plasma. While the native oxide layer has increased the overall corrosion resistance of the biomaterial, the oxide layer formed is only a few nanometres thick, failing to prevent the leaching of titanium ions and allowing the diffusion of oxygen ions into adjacent tissues, *in vivo* [504, 505]. As such, there is a growing interest in the development of thicker TiO_2 coatings for biological applications. The TiO_2 coated substrates studied in this project were deposited using filtered arc deposition and the surface energy and contact angle values of the hydrophilic substrates were previously reported to be $50J/m^2$ and 70^o, respectively, by Randeniya et al. [501] and Ismail et al. [500].

So far, the haemocompatibility of a biomaterial has been dictated by the ratio of adsorbed albumin and fibrinogen. A high ratio of albumin to fibrinogen proteins adsorbed on an implant can be correlated with a low number of adhering platelets, and therefore with low tendency of thrombus formation. A study conducted by Weber et al. [197] showed that fibrinogen, even at less than physiological concentrations, can sufficiently initiate full-scale platelet activation. However, other plasma proteins such as fibronectin, at ten times the physiological concentration of albumin, cannot mediate the same response [198]. In single protein solution studies, the albumin to fibrinogen ratio was approximately 1 for TiO_2 and 1.1 for a-C:H surfaces. This can be compared to ta-C surfaces that exhibited a protein ratio greater than 3.5. The ratios obtained for both TiO_2 and a-C:H were similar to the results obtained by Jones et al. [387] and Dion et al. [255]. However, when albumin was in a competitive solution with fibrinogen at physiological concentrations (ratio 10:1, albumin to fibrinogen), not only was there a decrease in adsorption of both proteins,

but albumin's affinity to the test surfaces became less than that of fibrinogen. This was especially evident on ta-C and a-C:H surfaces, which displayed only a small decrease in fibrinogen adsorption but a significant drop in albumin adsorption, resulting in an overall decrease in albumin to fibrinogen ratio during competitive binding. Conversely, the ratio of albumin to fibrinogen adsorbed on TiO_2 surfaces remained unaltered. This shows that the adsorption of selective proteins is implicitly linked to the surface chemistry of the biomaterial.

Whilst the adsorption of albumin retards the adhesion and activation of platelets; the adsorption of fibrinogen, with a conformation that exhibits increased availability of its platelet binding domain, promotes platelet adhesion and activation. The level of platelet binding region presented on fibrinogen from single protein solutions was similar to the complex solution, notwithstanding, the concentration of adsorbed fibrinogen decreased in the presence of albumin. Fibrinogen adsorbed on flat surfaces was shown to align flat against the surface, following side on and bent conformation. The conformation of fibrinogen on TiO_2 was similar to the conformation suggested by Hemmersam and Foss [460] and Moseke et al [462] using QCM-D and ELISA. Conversely, plasma proteins formed a dense and highly viscous layer on the flat substrates when compared with the rigid albumin and fibrinogen protein coated surfaces.

When comparing the kinetics of fibrinogen and plasma protein adsorption, it was evident that fibrinogen and other plasma proteins adsorbed more rapidly on a-C:H surfaces than TiO_2 during the initial stages of protein adsorption. This indicated a higher binding affinity between the proteins and a-C:H. During the latter stages of adsorption however it was noticed that the rate of protein adhesion decreased to near zero while adsorbed mass continued to increase. This phenomenon suggested a dynamic interaction between the surface and fibrinogen and/or plasma proteins causing the rearrangement of the proteins upon adsorption. Furthermore, it was observed that the adsorbed fibrinogen may have denatured and formed a rigid dense layer on the surface with only a small fraction of incorporated water. This

assumption correlates with Moseke and Ewald's [462] analysis of fibrinogen adsorption on TiO_2 surfaces.

The adsorption of the vastly overlooked apolipoprotein A1 proteins, other high molecular weight HDL's [506, 507] and plasma proteins such as: fibronectin, von Willebrand factor, viteronectin, etc [116], may explain the drastically reduced availability of platelet binding domains exposed on fibrinogen proteins that are adsorbed from plasma. This implies a favourable interaction between plasma proteins and biomaterial surfaces in reducing the exposure of fibrinogen's platelet binding domain for platelet $\alpha_{IIb}\beta_3$ receptor binding. The exposure of fibrinogen α-chain and γ-chain was also affected by the presence of other plasma proteins as well as surface chemistry. This indicated that the denaturing of the fibrinogen protein on the adsorbed surfaces and its assumed conformation for platelet binding was typically dependent on a combination of surface chemistry, surface nano-topography and its interaction with other plasma proteins.

Furthermore, the thrombin time (TT), prothrombin time (PT), and activated partial prothrombin time (APTT) maintain the anticoagulation mechanism, as found in physiology. They also regulate the plasma coagulation defects. Specifically, the APTT test governs how the biomaterial affects coagulation time while both PT and APTT tests account for the enzymatic activities which lead to clot formation. The measured anti-coagulant activity of the surfaces show that TiO_2 and a-C:H and ta-C substrates behave favourably with plasma in delaying the time taken to form fibrin clots when compared with control TCPS. The intrinsic and common pathways have been proven accountable for this response. These factors are readily influenced by biomaterial surfaces causing the inhibition of their function. The samples also impede the conversion of fibrinogen to fibrin by denaturing the protein and temporarily retarding the clotting process.

While previous studies have conducted similar tests with results corroborating with the APTT times found on a-C:H surfaces [319, 320, 327, 508], no one study has looked at the effect of surface chemistry of DLC and TiO_2 in influencing clotting

times in the presence of anticoagulant therapies such as heparin. Heparin is an anticoagulant ('blood thinner') which works by decreasing the clotting ability of the blood through binding to anti-thrombin III. When serum plasma diluted with heparin was administered on the test substrates, as expected, their subsequent clotting times increased with increasing heparin concentrations. However, it was interesting to note that a-C:H surfaces delayed clot formation the longest when compared with TiO_2 and ta-C. This suggests that surface chemistry of blood contacting devices can influence the functionality of heparin molecules in turn affecting their interaction with plasma proteins.

7.2 Influence of Plasma Proteins on Platelet Interactions

Although the studies mentioned above are considered to be important to evaluate the entire haemocompatibility of the test substrates, platelet adhesion may be considered to be the primary issue in the blood-biomaterial dilemma as it directly influences platelet-related coagulation and thrombosis. Platelet adhesion receptors recognise and bind to surface-adsorbed key adhesive proteins such as fibrinogen, and supporting proteins such as fibronectin, vitronectin, immunoglobulins and von Willebrand factor. This leads to the adhesion of circulating platelets onto biomaterial surfaces as well as its subsequent spreading and activation. As such, it was necessary to analyse the anti-platelet effects of surface chemistry and the adsorption of specific plasma proteins in this study.

Prolonged exposure of platelets in blood to non-haemocompatible thrombogenic materials *in vivo* has showed that platelet numbers in blood decrease with surface exposure time. Lee et al. [496] showed platelets in plasma adhered in increasing numbers with decreasing wettability of surfaces. Since fibrinogen is known to preferentially adsorb on hydrophobic rather than hydrophilic surfaces, it could imply that platelet adhesion on hydrophobic surfaces is dictated by increasing concentrations of adsorbed fibrinogen.

Platelet adhesion and morphological changes, such as spreading and aggregation on the flat test substrates, varied drastically between the four protein conditions when compared with small differences found between the chemistries of the thin films deposited on the surfaces. This in understandable as TiO_2, a-C:H and ta-C exhibit similar surface energies and hydrophobic tendencies. In general, albumin coated surfaces supported high levels of platelet adhesion with little platelet spreading, while fibrinogen pre-coated surfaces and surfaces devoid of proteins supported high levels of platelet spreading. This shows that platelet adhesion and subsequent spreading is not only depend on ligand mediated platelet interactions but also because of non-specific activation of platelet adhesive receptors on biomaterial surfaces. Platelets that showed no spreading either retained their rounded morphology without any actin-rich pseudopodia protruding radially from the platelet membrane, or, presented platelets with radial protrusions enclosing non-filamentous actin.

The kinetics of platelet adhesion studied by Yayapour et al. [509] shows that platelets adsorb rapidly within the first few seconds of incubation on hydrophobic surfaces. This is in comparison to the time taken to adhere on hydrophilic surfaces (more than 30 seconds). Considering the intrinsic nature of circulating platelets in blood this is not surprising given that the main role of platelets is to rapidly adhere and aggregate at the site of blood vessel injury. In this study, platelets on bare surfaces were shown to rapidly adhere within the first few seconds of incubation followed by a slow decline in the rate of platelet adhesion before saturation. This reinforces the hydrophobic nature of the test substrates. Furthermore, the adsorbed platelets were found to change in morphology from their rounded state to a spread state during the last stages of incubation.

Spread platelets have been shown to contain actin-rich, stellate shaped filopodia. The degree of platelet spreading on plasma pre-coated TiO_2 surfaces was reported to be higher than on plasma coated a-C:H substrates, even though QCM-D data showed a-C:H surfaces supported higher concentrations than TiO_2. Nan et al [267] was able to show that TiO_2 surfaces performed better than pyrolytic carbon (a biomaterial

commonly used in heart valves) when exposed to plasma containing both plasma proteins and platelets. Platelets exposed to plasma surfaces showed very little spreading when compared with albumin, bare and fibrinogen pre-coated surfaces, yet these platelets presented increased levels of platelet-platelet intercommunication than fibrinogen surfaces (identified by the over-reaching of filopodia between adjacent platelets).

Though albumin proteins reduced the levels of platelet spreading found on bare surfaces, it did not limit platelet adhesion. Albumin is known to be the most abundantly available plasma protein and is often used to passivate biomaterials from platelet interaction due to its anti-thrombotic characteristics. This is because albumin proteins lack any known amino acid sequences necessary for binding platelet adhesive receptors. However, once adsorbed on artificial surfaces, albumin has been proven to undergo conformational change and unfold at the surface interface. When the degree of unfolding of albumin proteins exceeded a 34% loss in its α-helical structure, surface adsorbed albumin proteins were found to adhere to Arg-Gly-Asp (RGD) specific platelet receptors ($\alpha_{IIb}\beta_3$ integrins) [510, 511]. Furthermore, platelet adhesion response was shown to increase with further unfolding of albumin just as strongly as that which was observed for adsorbed fibrinogen. Sivaraman and colleagues [510, 511] further found that it is the exposed Arg residue in the unfolded protein that plays a prominent role in mediating platelet adhesion to albumin proteins. Therefore, high levels of platelet adhesion on bare and albumin coated surfaces found in this study, suggest that platelet adhesion on biomaterial surfaces is not only dependent on non-specific interactions between platelet receptors and bare and albumin coated biomaterial surfaces, but may also be influenced by RGD specific platelet receptor-albumin interactions.

Pre-coating the surfaces with fibrinogen and plasma proteins have been shown to reduce the level of platelet adhesion as compared to platelets exposed to surfaces devoid of proteins. This suggests a favourable interaction between serum proteins including fibrinogen, platelets and biomaterial surfaces in reducing platelet adhesion. Furthermore, TiO_2, a-C:H and ta-C surfaces were shown to support the least number

of adhered round and spread platelets when compared with control silicon substrates, on fibrinogen and plasma coated surfaces. Platelets formed focal contacts with fibrinogen pre-coated TiO_2 and a-C:H surfaces throughout the incubation period where the number of focal contacts formed on a-C:H surfaces was less than that of TiO_2. This suggests that platelets adhered on fibrinogen coated a-C:H surfaces form weaker attachments than on the other surfaces.

TiO_2 surfaces exhibited greater levels of platelet spreading than a-C:H surfaces in the presence of plasma proteins, although the amount of focal contacts formed by platelets on plasma coated surfaces were less than fibrinogen coated surfaces. When an *in vivo* investigation involving the implantation of pyrolytic carbon and TiO_2 coated pyrolytic carbon into the ventral aorta of a dog (for the duration of two weeks) was conducted by Zhang et al. [512], the results showed that the amount of thrombus on TiO_2 coated valve was only 1/8 compared to that of pyrolytic carbon. This suggests that though spreading was evident on all plasma coated substrates, the level of adhesion and spreading is significantly lower than what is available commercially. Furthermore, when compared with TiO_2, a-C:H and ta-C surfaces, exhibited higher levels of platelet binding region exposure from fibrinogen adsorbed from plasma. However, both plasma coated a-C:H and ta-C displayed reduced levels of platelet binding and spreading than plasma coated TiO_2. This suggests a higher level of adsorption of denatured albumin and von Willebrand factor, fibronectin, and other plasma proteins on TiO_2 substrates mitigating platelet adhesion. Therefore, it is sufficient to conclude that a-C:H and ta-C surfaces are more haemocompatible than TiO_2 substrates, although the delamination of ta-C coating over time can be a limiting factor on using ta-C coated substrates in cardiovascular implantation. A-C:H's excellent haemocompatibility when exposed to plasma proteins and platelets was also exhibited in studies conducted by Jones et al. [387].

Platelet activation studies conducted in this project show that plasma proteins interact favourably with test substrates, especially a-C:H and ta-C when compared with TiO_2. This was shown to reduce the overall bare surface exposure and reduce fibrinogen adsorption either by steric hindrance or by reducing the overall exposure of adsorbed

fibrinogen to circulating platelets in order to decrease $\alpha_{IIb}\beta_3$ mediated platelet activation. There were no activated $\alpha_2\beta_1$ receptors detected on bare and protein-pre-coated flat substrates. Leistikow et al [513] revealed that the $\alpha_{IIb}\beta_3$ integrin moves from the platelet membrane surface towards the outer cytoplasm in the activation process using cross-sectional images of platelets that adhered to formvar-coated grids. The $\alpha_{IIb}\beta_3$ integrin found on the protein pre-coated and bare substrates appeared more pronounced in the central region of the spread platelets where little actin filaments were detected. This suggests that the expression of activated $\alpha_{IIb}\beta_3$ integrins upon contacting the protein coated surface may occur more centrally before distributing to the periphery. P-selectin activation was not dependent on the chemistry of the bare surfaces, but rather dependent on whether the platelets exhibit activated $\alpha_{IIb}\beta_3$ receptors.

The level of activation between the various materials was dependent on concentration of adsorbed platelets and their respective morphology. Not all platelets with a rounded morphology displayed detectable levels of activation while spread platelets presented activated receptors at varying concentrations. A study conducted by Gutensohn et al [383] (using platelet-rich-plasma in a dynamic flow condition) revealed that the fluorescence intensity of the activation-dependent antigens P-selectin (CD62P) showed higher levels in non-coated 316L stainless steel than DLC-coated stents. Since 316L stainless steel is a commonly used cardiovascular material, a lower level of platelet activation detected on a-CH is indicative of a more haemocompatible material. Though a similar level of activation was detected on plasma pre-coated TiO_2, a-C:H and ta-C surfaces, it can be concluded that all three substrates possess good haemocompatibility. Furthermore, while it is evident that under static conditions surface chemistry and adsorbed proteins mediate ligand or integrin conformation on surface adsorbed platelets, they do not exhibit any influence on platelets suspended in solution.

Anti-$\alpha_{IIb}\beta_3$ integrin antibody (Reopro) treated platelets decreased the overall levels of platelet adhesion and spreading on flat test substrates and substrates exposed to albumin, fibrinogen and plasma proteins. This suggests the important role of $\alpha_{IIb}\beta_3$

integrins in platelet adhesion and spreading on all four conditions. Fibrinogen and plasma surfaces supported the lowest concentrations of Reopro-exposed platelets. The adhered platelets displayed rounded morphologies with limited filopodial extensions. While the concentrations of adhered platelets were lower in the presence of the anti-integrin antibody it did not completely inhibit binding. This indicated that platelet adhesion is dependent on both $\alpha_{IIb}\beta_3$ ligand-dependent as well as non-specific interaction between platelet receptors and biomaterial surfaces. Albumin and bare surfaces also showed reduced platelet adhesion which implies that $\alpha_{IIb}\beta_3$ platelet integrins are susceptible to non-ligand specific activation and consequent binding of its receptors to the biomaterial surfaces and albumin proteins. A-C:H and ta-C surfaces continually supported decreased levels of anti- $\alpha_{IIb}\beta_3$ integrin treated platelets on all protein pre-coated and bare surfaces. However, a-C:H surfaces showed higher levels of platelet spreading similar to TiO_2 surfaces on albumin and fibrinogen coated surfaces. Further, it was interesting to note that the fibrinogen pre-coated substrates supported similar levels of $\alpha_{IIb}\beta_3$ activation even though a higher concentration of fibrinogen with increased exposure of its platelet binding domain was evident on fibrinogen adsorbed on a-C:H. It appears that even smaller amounts of adsorbed fibrinogen with less exposure of its platelet binding domain, as found on fibrinogen pre-coated TiO_2 and silicon, can mediate similar levels of platelet $\alpha_{IIb}\beta_3$ receptor activation. This could suggest that while the presence fibrinogen dictates $\alpha_{IIb}\beta_3$ activation, its relative concentration on the surface may not necessarily be a an indicator of $\alpha_{IIb}\beta_3$ mediated platelet activation levels. Other factors such as surface chemistry might be a contributing factor. This reinforces the influence of surface chemistry as well as specific plasma proteins in affecting $\alpha_{IIb}\beta_3$ ligand activation for platelet-surface binding.

7.3 Influence of Surface Nano-topography on Protein Adsorption and Platelet Interactions

One of the goals of this study was to substantiate, with experimental evidence, the case for introducing nano-scale topographical changes to commercially used DLC

and TiO_2 surface coatings in an effort to improve the haemocompatibility of currently used biomaterials. Many studies have assessed the biocompatibility and haemocompatibility of DLC and TiO_2 surfaces however there is limited knowledge and study on presenting the effects of defined nano-topography of such surface coatings and their effect on protein adsorption and platelet interactions. As such it was necessary to investigate the influence of surface nano-topography on protein adsorption and platelet interactions.

Nano-structures are fabricated on the silicon substrates with two or more polymers using the block co-polymer method. Through phase separation the polymers tend to organise themselves into laterally ordered, periodic arrays of self-assembled features in the order of 3-50nm [514-516]. The original block co-polymers are etched away after the films are exposed to metal salts, resulting in a pattern of metal nano-structures on the surface replicating the pattern of the phase-separated block co-polymer features. The size of the particles, its relative pitch, and regularity of the organised nano-arrays, are determined by block lengths within the block co-polymer as well as a suitable energy source. Under the right conditions this can cause the block co-polymer film to heat and arrange themselves into organised domains [435, 436]. By varying the polymers, many different arrangements involving changes in nano-particle size, shape and pitch between adjacent particles can be achieved on the substrate surface. The directed self-assembly (DSA) of block co-copolymers offer several advantages over the commercially used nano-lithographic techniques. These advantages include precision of nano-scale patterning, ultrafine line edge roughness (LER), dense area of packing of nano-domains, low cost of processing, and large area scalable nano-patterning [517]. Furthermore, block co-polymer is a reproducible method for producing high quantities of pseudo-identical substrates of larger surface areas.

In this study, nano-patterns were formed on ultra-flat silicon wafers using gold (Au) nano-particles on polystyrene and polyvinylpyridine (PVP) block co-polymer film. The flat substrates were then coated with either a-C:H (hydrogenated amorphous carbon) and ta-C (tetrahedral amorphous carbon) diamond like carbon or crystalline

TiO_2 (titania). The nano-roughness (RMS) of the block co-polymer modified flat substrates were measured to be in the 5-10nm scale.

The hydrophilic or hydrophobic nature of a surface, also known as surface wettability, is identified by the static contact angle formed between a water droplet and the substrate surface. A hydrophilic surface is one that embodies a contact angle value less than 65ºand a hydrophobic surface exhibits a contact angle greater than 65º. Surfaces with contact angle between 65-90º are considered to be intermediate hydrophobic surfaces [518-520]. Increasing the surface roughness of the surface has been shown to enhance the hydrophobic nature of the surface and decrease its surface energy [521-524].

Curtis et al. [443] suggested an increase in the van der Waals interaction caused by the closely packed nano-structures prevents the wetting of surfaces and consequently increases the overall hydrophobic characteristics of nano-patterned surfaces. Higher adsorption of fibrinogen protein is thought to have been influenced by hydrophobic surfaces [387]. However, an increase in surface hydrophillicity has been known to elevate albumin adsorption. As such, changing surface nano-roughness has been shown to increase fibrinogen and other plasma protein adsorption, consequently increasing human platelet adhesion. This is synonymous to the results found in this study, where changing the surface nano-topography by adding nano-patterns that increased the overall surface roughness of the test substrates to 5-10nm caused an increase in the adsorption of fibrinogen and plasma proteins.

Previous studies [525-527] have shown that although highly hydrophobic surfaces initially promote the adsorption of large amounts of proteins due to hydrophobic interaction, they nevertheless become easily desorbed because of low surface energy. This was not found to be the case on nano-patterned surfaces. The proteins were found to form multiple layers, saturating in the grooves between the peaks formed by the nano-patterns. While it was evident that the morphology of adsorbed proteins were not confined to a particular conformation, the tri-nodular structure of fibrinogen was retained. Once adsorbed on nano-patterned surfaces, fibrinogen predominantly

aligned itself against the slope of the nano-patterns decreasing the overall surface roughness. Even after several washes the majority of the proteins did not desorb off the surface suggesting that nano-patterns act as topographical cues for protein adsorption. Furthermore, fibrinogen proteins adsorbed on nano-patterned surfaces presented increased levels of platelet binding domains, where a-C:H and ta-C exhibited the highest % increase when compared with TiO_2.

The two ideal responses from platelets upon interacting with biomaterial surfaces are either, the formation of a passivating film of platelets or total non-adherence of platelets (such that platelets remain in their non-activated state) [528, 529]. Ratner et al. [529] have shown platelets to initially adhere and activate when forming a passivating layer, and only spread to form a thin stable layer on the biomaterial surface afterwards. However, the continual adherence of platelets tend to form an unstable covering which over time breaks off into emboli. This leads to tissue and organ failure and ultimately death [528, 529]. As such, quantification of adhered platelet numbers, their morphology and the degree of surface coverage by platelets on the biomaterial was necessary. Normal platelets exposed on nano-patterned surfaces exhibited high concentrations of adhesion as well as extensive levels of spreading. Platelets formed multi-level stacked aggregates on the surfaces when compared with the flat surfaces suggesting that the nano-patterns behaved as topographical cues acting as potential tethering sites for platelet integrin adhesion. The dendritic network of actin cytoskeleton in the cytoplasm of platelets adhered on nano-patterned surfaces appeared more pronounced. TiO_2 surfaces presented higher levels of platelet adhesion and spreading on all protein pre-coated and bare conditions. The exception to this was on plasma pre-coated surfaces where a-C:H and ta-C surfaces supported higher platelet concentrations. On nano-patterned surfaces, both fibrinogen and plasma proteins were found to enhance platelet adhesion and its spreading, while this was not the case on flat substrates. However, Smith et al. [503] was able to show improved blood-compatibility of TiO_2 due to nano-tube array surface patterning after incubating the samples in blood plasma for over two hours. He identified that the nano-architecture of the nano-tube arrays was the key in potentiating an optimal interface for promoting non-thrombogenic response. From the multi-layering of platelets, as found in the *in-vitro* experiments

performed in this study, it can be inferred that within the time scale examined platelets do form an unstable covering on the block co-polymer modified substrates.

With respect to platelet activation, platelets attached on nano-patterned surfaces exhibited increased levels of activated P-selectin and $\alpha_{IIb}\beta_3$ integrins, while platelets suspended in solution did not exhibit changes in P-selectin and $\alpha_{IIb}\beta_3$ integrin activation when compared with flat substrates. The level of platelet activation was lower on plasma coated nano-patterned surfaces than fibrinogen pre-coated and bare nano-patterned surfaces. This suggested a favourable interaction between plasma proteins and nano-patterned surfaces in reducing the overall activation levels of the bare and fibrinogen pre-coated substrates. While surface chemistry played a dominant role on platelet adhesion and activation on the flat surfaces, it was difficult to discern the levels of platelet activation between the various surface chemistries of the nano-patterned surfaces. This suggested that nano-features are able to overcome chemical influence. A similar notion was reported by Koh et al. [530] where the level of platelet interaction was severely altered in the presence nano-pillars when compared with their unstructured substrates, even though the difference in platelet response between the nano-patterned substrates did not vary. Hence, tailoring substrate surfaces with suitable nano-topographical features in addition to specific surface chemistry can remarkably influence the overall platelet response. As with changing the surface nano-roughness by 5-10nm and pitch between 50-150nm, it was evident that nano-patterns decreased the overall haemocompatibility of a given biomaterial surface by increasing the availability of platelet binding domain on fibrinogen adsorbed on the surface, and enhancing the adhesion, spreading and overall surface activation of platelets. Though previous studies have been able to demonstrate a decrease in platelet adhesion and its subsequent activation by introducing nano-patterns on the surfaces, it has become more evident over the last few years that structures of 200-800nm height/depth, 100-200nm width and interspacing less than 200nm [530, 531] have been shown to reduce platelet adhesion and subsequent activation *in vitro*. This is despite its ability under shear flow that still remains unknown. Further, the nano-topography presented in this study may show increased levels of platelet adhesion under static mode, however, in the presence of shear flow the blood platelets might respond differently.

Therefore, to deepen the overall understanding of the haemocompatibility of a biomaterial, in an effort to be able to design and develop biomaterials with improved haemocompatibilities, this study was able to show the significance of surface chemistry, surface nano-topography and adsorption of specific plasma proteins in modulating platelet response on biomaterial surfaces. Modifying one aspect alone is insufficient, as each factor is dependent on another and it is the dynamic interplay between topographical, chemical and biological cues that can aid in the minimisation of the adhesion and activation of platelets for thrombus clot development.

8 CONCLUSIONS

The future success of fabricating a truly haemocompatible biomaterial implicitly depends on understanding the mechanisms involved within the dynamic interactions between platelets, plasma proteins and biomaterial surfaces. In this study, the influence of different surfaces chemistries and nano-topographies on protein adsorption and conformation as well as the resulting platelet responses was investigated *in vitro*. From each of these studies the hypothesis that surfaces modulate protein-surface, platelet-surface and platelet-protein-surface interactions has been demonstrated through numerous conclusions, which have been listed below:

- Surfaces only exhibit a high affinity for albumin, when albumin is in a solution by itself. At physiological ratio's, surfaces present a higher binding affinity for fibrinogen when compared with albumin. When binding competitively, DLC (a-C:H and ta-C) surfaces presented severely reduced albumin/fibrinogen binding ratio which was primarily owed to a significant drop in adsorbed albumin.
- A-C:H surfaces support higher concentrations of fibrinogen and plasma protein adsorption when compared with TiO_2
- Fibrinogen binding on DLC occurs over a constant dynamic interaction, while fibrinogen on TiO_2 initially forms a proteinacious layer that is highly viscous after which is followed by dispelling of water molecules to form a rigid protein layer. Fibrinogen adsorbed on ta-C surfaces exhibited a side on conformation to align flat against the surface, while, fibrinogen on TiO_2 surfaces followed a bent conformation.
- Surface chemistry was not the only deciding factor on the conformation of adsorbed fibrinogen. The conformation of adsorbed fibrinogen was severely altered when exposed to albumin even though DLC and TiO_2 surfaces presented similar levels of platelet binding region on fibrinogen from single protein solutions and complex solutions.
- DLC and TiO_2 surfaces presented reduced platelet binding domains exposed on fibrinogen proteins adsorbed from plasma. Plasma proteins were found to

reduce the overall bare surface exposure and reduce fibrinogen adsorption either by steric hindrance or by reducing the overall exposure of adsorbed fibrinogen to circulating platelets.

- TiO_2 and a-C:H and ta-C substrates behaved favourably with plasma in delaying the time taken to form fibrin clots. When compared with ta-C and TiO_2, a-C:H surfaces exhibited enhanced anti-coagulant properties with increasing heparin concentrations.
- Platelet adhesion on biomaterial surfaces is primarily dependent on integrin $\alpha_{IIb}\beta_3$-ligand mediated binding, although, non-specific binding to the surface, through covalent interactions between platelets and localised sites on the biomaterial surface devoid of proteins, is also evident.
- Platelets were found to adhere rapidly on hydrophobic surfaces; and integrin $\alpha_{IIb}\beta_3$ was identified in mediating platelet adhesion as well as platelet spreading on biomaterial surfaces.
- Platelet adhesion and spreading was reduced but not inhibited on albumin coated biomaterials. Generally, platelets on albumin coated biomaterials presented a rounded morphology, however, platelets on albumin coated TiO_2 surfaces presented increased spreading when compared with a-C:H and ta-C.
- TiO_2 surfaces exposed to fibrinogen supported increased concentrations of adhered platelets when compared with a-C:H and ta-C surfaces primarily because of elevated non-specific platelet interactions between platelets and TiO_2 surfaces. When compared with fibrinogen, other plasma proteins interact favourably with DLC and TiO_2 surfaces in reducing the material's inherent thrombogenic response by reducing platelet attachment and their subsequent spreading.
- While fibrinogen is necessary for $\alpha_{IIb}\beta_3$ activation, its relative concentration does not play a ubiquitous role in its activation levels. Even small concentrations of fibrinogen can elicit high levels of $\alpha_{IIb}\beta_3$ activation.
- Not all platelets with a rounded morphology displayed detectable levels of activation while spread platelets presented activated receptors at varying concentrations. Integrin $\alpha_{IIb}\beta_3$ were found to occur more centrally before distributing to the periphery receptors.

- The surface chemistry of DLC and TiO_2 was found to elicit a stronger activation of $\alpha_{IIb}\beta_3$ receptors than plasma proteins. P-selectin activation was not dependent on the chemistry of the bare surfaces, but rather dependent on whether the platelets exhibit activated $\alpha_{IIb}\beta_3$ receptors.
- DLC and TiO_2 surfaces did not induce activation of collagen receptor $\alpha_2\beta_1$.
- Block co-polymer fabrication method along with well established coating deposition techniques were an effective means of assessing protein adsorption and their respective conformation, as well as platelet interactions.
- Nano-topography in the roughness scale of 5-10nm was found to promote the adsorption of large amount of proteins. The nano-patterns behaved as topographical cues to enhance protein adsorption. The proteins formed multiple layers, saturating in the grooves of the nano-patterns.
- When compared with TiO_2, nano-patterns increased the overall thrombogenic response of a-C:H and ta-C surfaces. When compared with flat surfaces, adsorbed fibrinogen on nano-patterned surfaces presented increased platelet binding domains for platelet binding. Platelets adhered at high concentrations, developed a stiff structure and displayed extensive levels of spreading and aggregation. The level of thrombogenic was further aggravated by fibrinogen and plasma protein adsorption.
- It was difficult to discern the levels of platelet activation between the various surface chemistries of the nano-patterned surfaces. Nano-patterns exacerbated the activated P-selectin and $\alpha_{IIb}\beta_3$ integrins such that nano-features were able to overcome chemical influence.

Overall this study illustrated that *in vitro* plasma protein and platelet responses can be modulated by altering topographical and chemical parameters of a biomaterial, and the specific adsorption of serum proteins. The ongoing challenge lies in completely understanding the mechanisms involved in platelet-protein-surface interactions which will allow development of materials that will elicit desired haemocompatible responses.

Recommendations

Present research has introduced the effect of specific plasma proteins, surface chemistry and nano-features in eliciting thrombogenic response, *in vitro*. An almost natural next step in this field would be to transition into developing and optimising various nano-patterning techniques that can produce a range of nano-topographies to study the influence of nano-topographies on plasma protein and platelet interactions.

Engineering biomaterial surfaces with well-defined nanoscale topographies and roughness has become a significant step towards modulating biological responses on bio-surfaces. The adsorption of nano-sized proteins, their binding affinity, conformation and spatial distribution is a result of complex processes influenced by surface wettability, surface chemistry, and surface topography. Altering the nano-topography of surfaces changes the surface properties such as surface wettability and surface contact, and as such can greatly influence the way in which proteins interact with the bio-surface without compromising on surface chemistry or mechanical properties of the bulk material. Further, modulating nano-topographies have been shown to influence platelet adhesion, where the nano-features mimic the conformation of proteins and consequently behave as physical cues which dictate platelet adhesion, their spreading, activation and aggregation. Therefore it would be of great interest to optimise physical features, such as size, shape and pitch, on an implant surface such that it can greatly reduce haemostatic responses. Present nano-patterning techniques are limited by their inability to produce homogenous, regular features with well-defined pitch and size within the 1-10nm range over large surface areas, required for commercial applications. The shape of nano-structures produced also need to be optimised to design hetero-structures that mimic the nano-sized conformation of platelet-repelling proteins that line the endothelial cells of the vascular wall, or the conformational state of circulating proteins when they illicit an -thrombotic responses.

9 REFERENCES

1. (WHO), W.H.O. [cited 2014 9 May]; Available from: http://www.who.int/healthinfo/global_burden_disease/GlobalHealthRisks_report_full.pdf.
2. Hench, L., *(ii) The challenge of orthopaedic materials.* Current orthopaedics, 2000. **14**(1): p. 7-15.
3. (AIHW), A.I.H.W. [cited 2014 4 Mar]; Available from: http://www.aihw.gov.au/WorkArea/DownloadAsset.aspx?id=10737418530.
4. National Heart Foundation, A. [cited 2014 9 May]; Available from: http://www.heartfoundation.org.au/information-for-professionals/data-and-statistics/Pages/default.aspx.
5. Ratner, B.D., *The catastrophe revisited: blood compatibility in the 21st century.* Biomaterials, 2007. **28**(34): p. 5144-5147.
6. PressWIRE, M. *Cardiac Bio Implant Devices Market to Grow US$ 27 Billion by 2017*. 2014 [cited 2014 9 May]; Available from: http://www.equities.com/index.php?option=com_k2&view=newsdetail&id=18543#sthash.VXRXCX64.dpuf
7. Sherwood, L., *Human physiology: from cells to systems* 2007: Thomson, Brooks & Cole.
8. World, R. [cited 2013 28 Aug]; Available from: http://www.revisionworld.com/a2-level-level-revision/biology/physiology-transport/human-circulatory-system.
9. Collin-Osdoby, P., *Role of vascular endothelial cells in bone biology.* Journal of Cellular Biochemistry, 1994. **55**(3): p. 304-309.
10. Venkatraman, S., F. Boey, and L.L. Lao, *Implanted cardiovascular polymers: Natural, synthetic and bio-inspired.* Progress in Polymer Science, 2008. **33**(9): p. 853-874.
11. Biobook. [cited 2012 17 Nov]; Available from: https://adapaproject.org/bbk/tiki-index.php?page=Leaf%3A+What+are+the+major+cell+types+in+human+blood%3F.
12. Hoffman, M. and D. Monroe, *A cell-based model of hemostasis.* Thrombosis and haemostasis, 2001. **85**(6): p. 958-965.
13. Horne, M., *Overview of hemostasis and thrombosis; current status of antithrombotic therapies.* Thrombosis research, 2005. **117**(1): p. 15-17.
14. Hürlimann, D., F. Ruschitzka, and T. Lüscher, *The relationship between the endothelium and the vessel wall.* European heart journal supplements, 2002. **4**(A): p. A1-A7.
15. Wagner, D.D. and P.S. Frenette, *The vessel wall and its interactions.* Blood, 2008. **111**(11): p. 5271-5281.
16. Liu, X., et al., *Blood compatible materials: state of the art.* Journal of Materials Chemistry B, 2014. **2**(35): p. 5718-5738.
17. University, B. [cited 2013 30 Aug]; Available from: http://biomed.brown.edu/Courses/BI108/2006-108websites/group01Heparin-coatedOxygenators/pages/Background.htm.

18. Dubay, D.A. and M.G. Franz, *Acute wound healing: the biology of acute wound failure.* Surgical Clinics of North America, 2003. **83**(3): p. 463-481.
19. Diegelmann, R.F. and M.C. Evans, *Wound healing: an overview of acute, fibrotic and delayed healing.* Front Biosci, 2004. **9**(1): p. 283-289.
20. Velnar, T., T. Bailey, and V. Smrkolj, *The wound healing process: an overview of the cellular and molecular mechanisms.* Journal of International Medical Research, 2009. **37**(5): p. 1528-1542.
21. Anderson, J.M., *Mechanisms of inflammation and infection with implanted devices.* Cardiovascular Pathology, 1993. **2**(3): p. 33-41.
22. Gorbet, M.B. and M.V. Sefton, *Biomaterial-associated thrombosis: roles of coagulation factors, complement, platelets and leukocytes.* Biomaterials, 2004. **25**(26): p. 5681-5703.
23. Cassatella, M.A., *The production of cytokines by polymorphonuclear neutrophils.* Immunology today, 1995. **16**(1): p. 21-26.
24. Del Maschio, A., E. Dejana, and G. Bazzoni, *Bidirectional modulation of platelet and polymorphonuclear leukocyte activities.* Annals of hematology, 1993. **67**(1): p. 23-31.
25. Bazzoni, G., E. Dejana, and A. Del Maschio, *Platelet-dependent modulation of neutrophil function.* Pharmacological research, 1992. **26**(3): p. 269-272.
26. Maschio, A., et al., *Platelet-dependent induction and amplification of polymorphonuclear leucocyte lysosomal enzyme release.* British journal of haematology, 1989. **72**(3): p. 329-335.
27. Kuijpers, T., et al., *Distinct adhesive properties of granulocytes and monocytes to endothelial cells under static and stirred conditions.* The Journal of Immunology, 1990. **145**(8): p. 2588-2594.
28. Rousseau, Y., et al., *Dissociation between complement activation, integrin expression and neutropenia during hemodialysis.* Biomaterials, 1999. **20**(20): p. 1959-1967.
29. Videm, V., et al., *Heparin-coated cardiopulmonary bypass equipment. I. Biocompatibility markers and development of complications in a high-risk population.* The Journal of thoracic and cardiovascular surgery, 1999. **117**(4): p. 794-802.
30. Camerer, E., A.-B. Kolstø, and H. Prydz, *Cell biology of tissue factor, the principal initiator of blood coagulation.* Thrombosis research, 1996. **81**(1): p. 1-41.
31. Smith, J.A., *Neutrophils, host defense, and inflammation: a double-edged sword.* Journal of Leukocyte Biology, 1994. **56**(6): p. 672-686.
32. Gemmell, C.H., *Flow cytometric evaluation of material-induced platelet and complement activation.* Journal of Biomaterials Science, Polymer Edition, 2000. **11**(11): p. 1197-1210.
33. Eriksson, C. and H. Nygren, *Polymorphonuclear leukocytes in coagulating whole blood recognize hydrophilic and hydrophobic titanium surfaces by different adhesion receptors and show different patterns of receptor expression.* Journal of Laboratory and Clinical Medicine, 2001. **137**(4): p. 296-302.
34. Kuwahara, T., M. Markert, and J. Wauters, *Proteins adsorbed on hemodialysis membranes modulate neutrophil activation.* Artificial organs, 1989. **13**(5): p. 427-431.

35. Gorbet, M., E. Yeo, and M. Sefton, *Flow cytometric study of in vitro neutrophil activation by biomaterials.* Journal of Biomedical Materials Research, 1999. **44**(3): p. 289-297.
36. Grooteman, M., et al., *Mechanisms of intra-dialyser granulocyte activation: a sequential dialyser elution study.* Nephrology Dialysis Transplantation, 1997. **12**(3): p. 492-499.
37. Bull, B., et al., *Heparin therapy during extracorporeal circulation. II. The use of a dose-response curve to individualize heparin and protamine dosage.* The Journal of thoracic and cardiovascular surgery, 1975. **69**(5): p. 685-689.
38. van Beusekom, H.M., et al., *Histology after stenting of human saphenous vein bypass grafts: observations from surgically excised grafts 3 to 320 days after stent implantation.* Journal of the American College of Cardiology, 1993. **21**(1): p. 45-54.
39. Willoughby, S., A. Holmes, and J. Loscalzo, *Platelets and cardiovascular disease.* European Journal of Cardiovascular Nursing, 2002. **1**(4): p. 273-288.
40. Battinelli, E., et al., *Induction of platelet formation from megakaryocytoid cells by nitric oxide.* Proceedings of the National Academy of Sciences, 2001. **98**(25): p. 14458-14463.
41. Semple, J.W., J.E. Italiano, and J. Freedman, *Platelets and the immune continuum.* Nat Rev Immunol, 2011. **11**(4): p. 264-274.
42. Blockmans, D., H. Deckmyn, and J. Vermylen, *Platelet actuation.* Blood Reviews, 1995. **9**(3): p. 143-156.
43. Brass, l.f., Stalker, T.J., Zhu, L.,, *Signal transduction during platelet plug formation*. 2007: Elsevier. 319-346.
44. McRedmond, J.P., et al., *Integration of Proteomics and Genomics in Platelets: A profile of platelet proteins and platelet specific genes.* Molecular & cellular proteomics, 2004. **3**(2): p. 133-144.
45. Gregg, D. and P.J. Goldschmidt-Clermont, *Platelets and cardiovascular disease.* Circulation, 2003. **108**(13): p. e88-e90.
46. Andrews, R.K. and M.C. Berndt, *Platelet physiology and thrombosis.* Thrombosis research, 2004. **114**(5): p. 447-453.
47. Booyse, F.M., T.P. Hoveke, and M.E. Rafelson, *Human Platelet Actin ISOLATION AND PROPERTIES.* Journal of Biological Chemistry, 1973. **248**(11): p. 4083-4091.
48. Landon, F., et al., *Human platelet actin.* European Journal of Biochemistry, 1977. **81**(3): p. 571-577.
49. White, J.G., *Platelet microtubules and microfilaments: effects of cytochalasin B on structure and function* Platelet aggregation ed. J. Caen. 1971, Paris: Masson. 15-52.
50. Fox, J., *The Platelet Skeleton* Thrombosis and Haemostasis, ed. M. Verstraete, Vermylen, J., Lynen, R., Arnout, J. . 1987: Leuven University Press.
51. Fox, J. and D. Phillips, *Role of phosphorylation in mediating the association of myosin with the cytoskeletal structures of human platelets.* Journal of Biological Chemistry, 1982. **257**(8): p. 4120-4126.
52. Plow, E.F., Collen, D., *The presence and release of alpha 2-antiplasmin from human platelets.* Blood, 1981. **58**(6): p. 1069-1074.
53. Blair, P. and R. Flaumenhaft, *Platelet α-granules: basic biology and clinical correlates.* Blood Reviews, 2009. **23**(4): p. 177-189.

54. Italiano, J.E., et al., *Angiogenesis is regulated by a novel mechanism: pro-and antiangiogenic proteins are organized into separate platelet α granules and differentially released.* Blood, 2008. **111**(3): p. 1227-1233.
55. Rendu, F. and B. Brohard-Bohn, *The platelet release reaction: granules' constituents, secretion and functions.* Platelets, 2001. **12**(5): p. 261-273.
56. Legrand, Y., G. Pignaud, and J. Caen, *Human blood platelet elastase and proelastase.* Pathophysiology of Haemostasis and Thrombosis, 1977. **6**(3): p. 180-189.
57. Chesney, C.M., E. Harper, and R.W. Colman, *Human platelet collagenase.* Journal of Clinical Investigation, 1974. **53**(6): p. 1647.
58. Vreys, V. and G. David, *Mammalian heparanase: what is the message?* Journal of cellular and molecular medicine, 2007. **11**(3): p. 427-452.
59. King, S.M. and G.L. Reed. *Development of platelet secretory granules*. in *Seminars in cell & developmental biology*. 2002. Elsevier.
60. Hynes, R.O., *Integrins: a family of cell surface receptors.* Cell, 1987. **48**(4): p. 549-554.
61. Kunicki, T.J., et al., *The human fibroblast class II extracellular matrix receptor mediates platelet adhesion to collagen and is identical to the platelet glycoprotein Ia-IIa complex.* Journal of Biological Chemistry, 1988. **263**(10): p. 4516-4519.
62. Sonnenberg, A., P.W. Modderman, and F. Hogervorst, *Laminin receptor on platelets is the integrin VLA-6.* Nature, 1988.
63. Wayner, E.A., et al., *The function of multiple extracellular matrix receptors in mediating cell adhesion to extracellular matrix: preparation of monoclonal antibodies to the fibronectin receptor that specifically inhibit cell adhesion to fibronectin and react with platelet glycoproteins Ic-IIa.* The Journal of Cell Biology, 1988. **107**(5): p. 1881-1891.
64. Byron, A., et al., *Anti-integrin monoclonal antibodies.* Journal of cell science, 2009. **122**(22): p. 4009-4011.
65. Banno, A. and M.H. Ginsberg, *Integrin activation.* Biochemical Society Transactions, 2008. **36**(Pt 2): p. 229.
66. Giancotti, F.G. and E. Ruoslahti, *Integrin signaling.* Science, 1999. **285**(5430): p. 1028-1033.
67. Plow, E.F. and Y.-Q. Ma, *Inside-out, outside-in: what's the difference?* Blood, 2007. **109**(8): p. 3128-3129.
68. Shattil, S.J., C. Kim, and M.H. Ginsberg, *The final steps of integrin activation: the end game.* Nature reviews Molecular cell biology, 2010. **11**(4): p. 288-300.
69. Shattil, S.J., H. Kashiwagi, and N. Pampori, *Integrin signaling: the platelet paradigm.* Blood, 1998. **91**(8): p. 2645-2657.
70. Ware, J.A. and B. Coller, *Platelet morphology, biochemistry, and function.* Williams hematology, 1995. **5**: p. 1161-1201.
71. Marcus, A., et al., *Platelet activation.* Atherosclerosis and coronary artery disease, 1996. **1**: p. 607-637.
72. Savage, B., F. Almus-Jacobs, and Z.M. Ruggeri, *Specific Synergy of Multiple Substrate Receptor Interactions in Platelet Thrombus Formation under Flow.* Cell, 1998. **94**(5): p. 657-666.

73. Coller, B.S., *Interaction of normal, thrombasthenic, and Bernard-Soulier platelets with immobilized fibrinogen: defective platelet-fibrinogen interaction in thrombasthenia.* Blood, 1980. **55**(2): p. 169-178.
74. Hourani, S. and N. Cusack, *Pharmacological receptors on blood platelets.* Pharmacological reviews, 1991. **43**(3): p. 243-298.
75. Kasirer-Friede, A., M.L. Kahn, and S.J. Shattil, *Platelet integrins and immunoreceptors.* Immunological Reviews, 2007. **218**(1): p. 247-264.
76. Barczyk, M., S. Carracedo, and D. Gullberg, *Integrins.* Cell and tissue research, 2010. **339**(1): p. 269-280.
77. Bennett, J., B. Berger, and P. Billings, *The structure and function of platelet integrins.* Journal of Thrombosis and Haemostasis, 2009. **7**(s1): p. 200-205.
78. Plow, E.F., et al., *Related binding mechanisms for fibrinogen, fibronectin, von Willebrand factor, and thrombospondin on thrombin-stimulated human platelets.* Blood, 1985. **66**(3): p. 724-727.
79. Calvete, J., *Clues for understanding the structure and function of a prototypic human integrin: the platelet glycoprotein IIb/IIIa complex.* Thrombosis and haemostasis, 1994. **72**(1): p. 1-15.
80. Estavillo, D., et al., *Functional Analysis of a Recombinant Glycoprotein Ia/IIa (Integrin α2β1) I Domain That Inhibits Platelet Adhesion to Collagen and Endothelial Matrix under Flow Conditions.* Journal of Biological Chemistry, 1999. **274**(50): p. 35921-35926.
81. Santoro, S. and M. Zutter, *The alpha 2 beta 1 integrin: a collagen receptor on platelets and other cells.* Thrombosis and haemostasis, 1995. **74**(3): p. 813-821.
82. Nieswandt, B., et al., *Glycoprotein VI but not α2β1 integrin is essential for platelet interaction with collagen.* The EMBO journal, 2001. **20**(9): p. 2120-2130.
83. Santoro, S.A., *Identification of a 160,000 dalton platelet membrane protein that mediates the initial divalent cation-dependent adhesion of platelets to collagen.* Cell, 1986. **46**(6): p. 913-920.
84. Moroi, M. and S. Jung, *Platelet receptors for collagen.* Thrombosis and haemostasis, 1997. **78**(1): p. 439-444.
85. Siljander, P., et al., *Platelet receptor interplay regulates collagen-induced thrombus formation in flowing human blood*. Vol. 103. 2004. 1333-1341.
86. Nakamura, T., et al., *Platelet Adhesion to Native Type I Collagen Fibrils: Role of GPVI in divalent cation-dependent and -independent adhesion and thromboxane A2 generation.* Journal of Biological Chemistry, 1998. **273**(8): p. 4338-4344.
87. Tandon, N.N., U. Kralisz, and G.A. Jamieson, *Identification of glycoprotein IV (CD36) as a primary receptor for platelet-collagen adhesion.* Journal of Biological Chemistry, 1989. **264**(13): p. 7576-7583.
88. Diaz-Ricart, M., et al., *Platelets lacking functional CD36 (glycoprotein IV) show reduced adhesion to collagen in flowing whole blood*. Vol. 82. 1993. 491-496.
89. McKeown, L., et al., *Platelet adhesion to collagen in individuals lacking glycoprotein IV.* Blood, 1994. **83**(10): p. 2866-2871.
90. Yamamoto, N., et al., *Normal aggregations of glycoprotein IV (CD36)-deficient platelets from seven healthy Japanese donors.* British journal of haematology, 1992. **81**(1): p. 86-92.

91. Kehrel, B., et al., *Platelets deficient in glycoprotein IIIb aggregate normally to collagens type I and III but not to collagen type V.* Vol. 82. 1993. 3364-3370.
92. Ferrell, J.E. and G.S. Martin, *Tyrosine-specific protein phosphorylation is regulated by glycoprotein IIb-IIIa in platelets.* Proceedings of the National Academy of Sciences, 1989. **86**(7): p. 2234-2238.
93. Nakamura, T., et al., *Activation of the GP IIb-IIIa complex induced by platelet adhesion to collagen is mediated by both α2β1 integrin and GP VI.* Journal of Biological Chemistry, 1999. **274**(17): p. 11897-11903.
94. Bergelson, J., et al., *Identification of the integrin VLA-2 as a receptor for echovirus 1.* Science, 1992. **255**(5052): p. 1718-1720.
95. Lee, J.-O., et al., *Crystal structure of the A domain from the a subunit of integrin CR3 (CD11 b/CD18).* Cell, 1995. **80**(4): p. 631-638.
96. Emsley, J., et al., *Structural basis of collagen recognition by integrin α2β1.* Cell, 2000. **101**(1): p. 47-56.
97. McEver, R.P., *GMP-140: A receptor for neutrophils and monocytes on activated platelets and endothelium.* Journal of Cellular Biochemistry, 1991. **45**(2): p. 156-161.
98. Bevilacqua, M.P. and R.M. Nelson, *Selectins.* Journal of Clinical Investigation, 1993. **91**(2): p. 379.
99. Blann, A.D. and G.Y.H. Lip, *Hypothesis: is soluble P-selectin a new marker of platelet activation?* Atherosclerosis, 1997. **128**(2): p. 135-138.
100. Wu, K.K., *Platelet activation mechanisms and markers in arterial thrombosis.* Journal of internal medicine, 1996. **239**(1): p. 17-34.
101. Hamburger, S.A. and R.P. McEver, *GMP-140 mediates adhesion of stimulated platelets to neutrophils.* Blood, 1990. **75**(3): p. 550-554.
102. Wagner, D., *The Weibel-Palade body: the storage granule for von Willebrand factor and P-selectin.* Thrombosis and haemostasis, 1993. **70**(1): p. 105-110.
103. Gibbins, J.M., *Platelet adhesion signalling and the regulation of thrombus formation.* Journal of cell science, 2004. **117**(16): p. 3415-3425.
104. Chow, T.W., et al., *Shear stress-induced von Willebrand factor binding to platelet glycoprotein Ib initiates calcium influx associated with aggregation.* Blood, 1992. **80**(1): p. 113-120.
105. Savage, B. and Z.M. Ruggeri, *Platelet thrombus formation in flowing blood.* Platelets, 2007: p. 359-367.
106. Kroll, M., et al., *Platelets and shear stress.* American Society of Hematology, 1996. **88**(5).
107. Verkleij, M.W., et al., *Simple Collagen-Like Peptides Support Platelet Adhesion Under Static But Not Under Flow Conditions: Interaction Via α2β1 and von Willebrand Factor With Specific Sequences in Native Collagen Is a Requirement to Resist Shear Forces.* Blood, 1998. **91**(10): p. 3808-3816.
108. Poole, A., et al., *The Fc receptor [gamma]-chain and the tyrosine kinase Syk are essential for activation of mouse platelets by collagen.* EMBO J, 1997. **16**(9): p. 2333-2341.
109. Varga-Szabo, D., A. Braun, and B. Nieswandt, *Calcium signaling in platelets.* Journal of Thrombosis and Haemostasis, 2009. **7**(7): p. 1057-1066.
110. Bennett, J. and G. Vilaire, *Exposure of platelet fibrinogen receptors by ADP and epinephrine.* Journal of Clinical Investigation, 1979. **64**(5): p. 1393.

111. Ginsberg, M.H., et al., *Reduced surface expression and binding of fibronectin by thrombin-stimulated thrombasthenic platelets.* Journal of Clinical Investigation, 1983. **71**(3): p. 619.
112. Hantgan, R.R., *Fibrin protofibril and fibrinogen binding to ADP-stimulated platelets: evidence for a common mechanism.* Biochimica et Biophysica Acta (BBA)-Molecular Cell Research, 1988. **968**(1): p. 24-35.
113. Karczewski, J., et al., *The interaction of thrombospondin with platelet glycoprotein GPIIb-IIIa.* Journal of Biological Chemistry, 1989. **264**(35): p. 21322-21326.
114. Ruggeri, Z.M., R. Bader, and L. De Marco, *Glanzmann thrombasthenia: deficient binding of von Willebrand factor to thrombin-stimulated platelets.* Proceedings of the National Academy of Sciences, 1982. **79**(19): p. 6038-6041.
115. Thiagarajan, P. and K.L. Kelly, *Exposure of binding sites for vitronectin on platelets following stimulation.* Journal of Biological Chemistry, 1988. **263**(6): p. 3035-3038.
116. Tsai, W.-B., et al., *Platelet adhesion to polystyrene-based surfaces preadsorbed with plasmas selectively depleted in fibrinogen, fibronectin, vitronectin, or von Willebrand's factor.* Journal of Biomedical Materials Research, 2002. **60**(3): p. 348-359.
117. Tsai, W.-B., J.M. Grunkemeier, and T.A. Horbett, *Human plasma fibrinogen adsorption and platelet adhesion to polystyrene.* Journal of Biomedical Materials Research, 1999. **44**(2): p. 130-139.
118. Wetterö, J., P. Tengvall, and T. Bengtsson, *Platelets stimulated by IgG-coated surfaces bind and activate neutrophils through a selectin-dependent pathway*. Biomaterials, 2003. **24**(9): p. 1559-1573.
119. Grunkemeier, J., et al., *The effect of adsorbed fibrinogen, fibronectin, von Willebrand factor and vitronectin on the procoagulant state of adherent platelets.* Biomaterials, 2000. **21**(22): p. 2243-2252.
120. Savage, B. and Z. Ruggeri, *Selective recognition of adhesive sites in surface-bound fibrinogen by glycoprotein IIb-IIIa on nonactivated platelets.* Journal of Biological Chemistry, 1991. **266**(17): p. 11227-11233.
121. Gresele, P., *Platelets in thrombotic and non-thrombotic disorders: Pathophysiology, pharmacology and therapeutics*. 2002: Cambridge University Press.
122. Ratner, B.D.H., Allan S.; Schoen, Frederick J.; Lemons, Jack E., *Biomaterials Science : An Introduction to Materials in Medicine*. 3 ed. 2012: Elsevier Science. 1597.
123. Osdoit, S. and J.-P. Rosa, *Fibrin Clot Retraction by Human Platelets Correlates with αIIbβ3Integrin-dependent Protein Tyrosine Dephosphorylation.* Journal of Biological Chemistry, 2001. **276**(9): p. 6703-6710.
124. Hillery, C.A., Smyth, S.S., Parise, L.V., *Phosphorylation of human platelet glycoprotein IIIa (GPIIIa). Dissociation from fibrinogen receptor activation and phosphorylation of GPIIIa in vitro.* The Journal of Biological Chemistry, 1991. **266**(22): p. 14663-14669.
125. Shattil, S.J. and L.F. Brass, *Induction of the fibrinogen receptor on human platelets by intracellular mediators.* Journal of Biological Chemistry, 1987. **262**(3): p. 992-1000.

126. Harper, M. and A. Poole, *Isoform-specific functions of protein kinase C: the platelet paradigm.* Biochem Soc Trans., 2007. **35**(5): p. 1005-1009.
127. University, L. [cited 2013 30 Aug]; Available from: http://platelets.se/biomaterial/#content.
128. Haslam, R.J., Dickinson, N.T., Jang, E.K.,, *Cyclic Nucleotides and Phosphodiesterases in Platelets.* Thrombosis and Haemostasis, 1999. **82**(2): p. 412-423.
129. Yang, J., et al., *Signaling through Gi family members in platelets. Redundancy and specificity in the regulation of adenylyl cyclase and other effectors.* J Biol Chem., 2002. **277**(48): p. 46035-46042.
130. Guan, j., J. Trevithick, and R. Hynes, *Fibronectin/integrin interaction induces tyrosine phosphorylation of a 120-kDa protein.* Cell Regulation, 1991. **2**(11): p. 951-964.
131. Shattil, S.J. and J.S. Brugge, *Protein tyrosine phosphorylation and the adhesive functions of platelets.* Current Opinion in Cell Biology, 1991. **3**(5): p. 869-879.
132. Dhar, A. and S.D. Shukla, *Tyrosine kinases in platelet signalling.* British Journal of Haematology, 1993. **84**(1): p. 1-7.
133. M., C., *Platelet P2 receptors: old and new targets for antithrombotic drugs.* Expert Rev Cardiovasc Ther., 2007. **5**(1): p. 45-55.
134. Savi P, N.P., Nurden AT, Levy-Toledano S, Herbert JM., *Clopidogrel: a review of its mechanism of action.* Platelets., 1998. **9**(3/4): p. 251-255.
135. Sun, B., et al., *P2X1 purinoceptor in human platelets. Molecular cloning and functional characterization after heterologous expression.* Journal of Biological Chemistry, 1998. **273**: p. 11544-11547.
136. Woulfe, D., et al., *Defects in secretion, aggregation, and thrombus formation in platelets from mice lacking Akt2.* The Journal of Clinical Investigation, 2004. **113**(3): p. 441-450.
137. Crittenden, J.R., et al., *CalDAG-GEFI integrates signaling for platelet aggregation and thrombus formation.* Nat Med, 2004. **10**(9): p. 982-986.
138. Leung, L. and R. Nachman, *Molecular Mechanisms of Platelet Aggregation.* Annual Review of Medicine, 1986. **37**(1): p. 179-186.
139. Offermanns, S., *Activation of Platelet Function Through G Protein–Coupled Receptors.* Circulation Research, 2006. **99**(12): p. 1293-1304.
140. Kuwahara, M., et al., *Platelet Shape Changes and Adhesion Under High Shear Flow.* Arteriosclerosis, Thrombosis, and Vascular Biology, 2002. **22**(2): p. 329-334.
141. Huang, M., et al., *Adhesive ligand binding to integrin alpha IIb beta 3 stimulates tyrosine phosphorylation of novel protein substrates before phosphorylation of pp125FAK.* The Journal of Cell Biology, 1993. **122**(2): p. 473-483.
142. Prévost, N., et al., *Eph kinases and ephrins support thrombus growth and stability by regulating integrin outside-in signaling in platelets.* National Academy of Sciences, 2005. **102**(28): p. 9820-9825.
143. Ruggeri, Z.M., *Mechanisms of shear-induced platelet adhesion and aggregation.* Thromb Haemost., 1993. **70**(1): p. 119-123.
144. Ostermann, G., et al., *JAM-1 is a ligand of the [beta]2 integrin LFA-1 involved in transendothelial migration of leukocytes.* Nat Immunol, 2002. **3**(2): p. 151-158.

145. Santoso, S., et al., *The Junctional Adhesion Molecule 3 (JAM-3) on Human Platelets is a Counterreceptor for the Leukocyte Integrin Mac-1.* The Journal of Experimental Medicine, 2002. **196**(5): p. 679-691.
146. Stalker, T., et al., *Endothelial cell specific adhesion molecule (ESAM) localizes to platelet-platelet contacts and regulates thrombus formation in vivo.* Journal of Thrombosis and Haemostasis, 2009. **7**(11): p. 1886-1896.
147. Kojima, H., et al., *CD226 Mediates Platelet and Megakaryocytic Cell Adhesion to Vascular Endothelial Cells.* Journal of Biological Chemistry, 2003. **278**(38): p. 36748-36753.
148. Nanda, N., et al., *Platelet aggregation induces platelet aggregate stability via SLAM family receptor signaling.* Blood, 2005. **106**(9): p. 3028-3034.
149. Martin, M., et al., *CD84 Functions as a Homophilic Adhesion Molecule and Enhances IFN-γ Secretion: Adhesion Is Mediated by Ig-Like Domain 1.* The Journal of Immunology, 2001. **167**(7): p. 3668-3676.
150. Furman, M.I., Gardner, T M., Goldschmidt-Clermont, P J., *Mechanisms of cytoskeletal reorganization during platelet activation.* Thromb Haemost., 1993. **70**(1): p. 229-232.
151. Ridley, A.J. and A. Hall, *The small GTP-binding protein rho regulates the assembly of focal adhesions and actin stress fibers in response to growth factors.* Cell, 1992. **70**(3): p. 389-399.
152. Moers, A., et al., *G13 is an essential mediator of platelet activation in hemostasis and thrombosis.* Nat Med, 2003. **9**(11): p. 1418-1422.
153. Pandey, D., et al., *Regulation of LIM-kinase 1 and cofilin in thrombin-stimulated platelets.* Blood, 2006. **107**(2): p. 575-583.
154. Fukuhara, S., H. Chikumi, and J. Gutkind, *RGS-containing RhoGEFs: the missing link between transforming G proteins and Rho?* Oncogene, 2001. **20**: p. 1661-8.
155. Klages B, B.U., Simon MI, Schultz G, Offermanns S., *Activation of G12/G13 results in shape change and Rho/Rho-kinase-mediated myosin light chain phosphorylation in mouse platelets.* J Cell Biol., 1999. **144**(4): p. 745-754.
156. Covic, L., A.L. Gresser, and A. Kuliopulos, *Biphasic Kinetics of Activation and Signaling for PAR1 and PAR4 Thrombin Receptors in Platelets†.* Biochemistry, 2000. **39**(18): p. 5458-5467.
157. Shapiro, M.J., et al., *Protease-activated Receptors 1 and 4 Are Shut Off with Distinct Kinetics after Activation by Thrombin.* Journal of Biological Chemistry, 2000. **275**(33): p. 25216-25221.
158. Dörmann, D., K.J. Clemetson, and B.E. Kehrel, *The GPIb thrombin-binding site is essential for thrombin-induced platelet procoagulant activity.* Blood, 2000. **96**(7): p. 2469-2478.
159. De Candia, E., et al., *Binding of Thrombin to Glycoprotein Ib Accelerates the Hydrolysis of Par-1 on Intact Platelets.* Journal of Biological Chemistry, 2001. **276**(7): p. 4692-4698.
160. Offermanns, S., et al., *Defective platelet activation in G[alpha]q-deficient mice.* Nature, 1997. **389**(6647): p. 183-186.
161. Grosser, T., Fries, S., Fitzgrald, G.A.,, *Thromboxane Generation*. Platelets, ed. M. A.D. 2007: Elsevier. 565-574.
162. Kikkawa, U. and Y. Nishizuka, *The Role of Protein Kinase C in Transmembrane Signalling.* Annual Review of Cell Biology, 1986. **2**(1): p. 149-178.

163. Hanson, S.R. and L. Harker, *Blood coagulation and blood-materials interactions.* Biomaterials Science, Academic Press, San Diego, 1996: p. 193-199.
164. Colman, R.W., et al.,, *Overview of Hemostasis*. Hemostasis and Thrombosis: Basic Principles and Clinical Practice. 2001, Philadelphia: Lippincott Williams and Wilkins.
165. Osterud, B. and E. Bjorklid, *Sources of tissue factor.* Semin Thromb Hemost., 2006. **32**(1): p. 11-23.
166. Chung, J.H., et al., *Pericardial blood activates the extrinsic coagulation pathway during clinical cardiopulmonary bypass.* Circulation, 1996. **93**(11): p. 2014-2018.
167. Wilhelm, C., et al., *Monocyte tissue factor expression and ongoing complement generation in ventricular assist device patients.* The Annals of thoracic surgery, 1998. **65**(4): p. 1071-1076.
168. Ernofsson, M., S. Thelin, and A. Siegbahn, *Monocyte tissue factor expression, cell activation, and thrombin formation during cardiopulmonary bypass: a clinical study.* The Journal of thoracic and cardiovascular surgery, 1997. **113**(3): p. 576-584.
169. Hong, J., et al., *A new in vitro model to study interaction between whole blood and biomaterials. Studies of platelet and coagulation activation and the effect of aspirin.* Biomaterials, 1999. **20**(7): p. 603-611.
170. Morrissey JH, M.B., Neuenschwander PF, Comp PC., *Quantitation of activated factor VII levels in plasma using a tissue factor mutant selectively deficient in promoting factor VII activation.* Blood., 1993. **81**(3): p. 734-744.
171. Radcliffe, R., Nemerson, Y.,, *Activation and control of factor VII by activated factor X and thrombin. Isolation and characterization of a single chain form of factor VII.* Journal of Biological Chemistry, 1975. **250**(2): p. 388-395.
172. Seligsohn, U., et al.,, *Activation of human factor VII in plasma and in purified systems- Roles of activated factor IX, Kallikrein and activate activated factor XII.* Journal of Clinical Investigation, 1979. **64**(4): p. 1056-1065.
173. Mackman, N., R.E. Tilley, and N.S. Key, *Role of the Extrinsic Pathway of Blood Coagulation in Hemostasis and Thrombosis.* Arteriosclerosis, Thrombosis, and Vascular Biology, 2007. **27**(8): p. 1687-1693.
174. Morrissey, J., *Tissue Factor and Factor VII Initiation of Coagulation*. Hemostasis and Thrombosis: Basic Principles and Clinical Practice. 2001, Philadelphia: Lippincott Williams and Wilkins.
175. Furie, B. and B.C. Furie, *The molecular basis of blood coagulation.* Cell, 1988. **53**(4): p. 505-518.
176. Schmaier, A., *Contact activation: a revision.* Thrombosis and haemostasis, 1997. **78**(1): p. 101-107.
177. Hanson, S.R., *Device thrombosis and thromboembolism.* Cardiovascular Pathology, 1993. **2**(3): p. 157-165.
178. Blajchman, M. and A. Ozge-Anwar, *The role of the complement system in hemostasis.* Progress in hematology, 1985. **14**: p. 149-182.
179. Anderson, N.L. and N.G. Anderson, *The human plasma proteome history, character, and diagnostic prospects.* Molecular & cellular proteomics, 2002. **1**(11): p. 845-867.

180. Nygren, H., P. Tengvall, and I. Lundstroem, *The initial reactions of TiO2 with blood.* Journal of Biomedical Materials Research, 1997. **34**(4): p. 487-492.
181. Nygren, H., *Initial reactions of whole blood with hydrophilic and hydrophobic titanium surfaces.* Colloids and Surfaces B: Biointerfaces, 1996. **6**(4): p. 329-333.
182. Anderson, J., T. Bonfield, and N. Ziats, *Protein adsorption and cellular adhesion and activation on biomedical polymers.* The International journal of artificial organs, 1990. **13**(6): p. 375-382.
183. Vroman, L. and A.L. Adams, *Findings with the recording ellipsometer suggesting rapid exchange of specific plasma proteins at liquid/solid interfaces.* Surface Science, 1969. **16**: p. 438-446.
184. Vroman, L. and A. Adams, *Peculiar behavior of blood at solid interfaces.* Journal Polymer Science Part C, 1971. **34**: p. 159-165.
185. Tengvall, P., I. Lundström, and B. Liedberg, *Protein adsorption studies on model organic surfaces: an ellipsometric and infrared spectroscopic approach.* Biomaterials, 1998. **19**(4-5): p. 407-422.
186. Ortega-Vinuesa, J., et al., *Stagnant versus dynamic conditions: a comparative adsorption study of blood proteins.* Biomaterials, 1998. **19**(1-3): p. 251-262.
187. Haynes, C.A. and W. Norde, *Globular proteins at solid/liquid interfaces.* Colloids and Surfaces B: Biointerfaces, 1994. **2**(6): p. 517-566.
188. Wilson, C.J., et al., *Mediation of biomaterial-cell interactions by adsorbed proteins: a review.* Tissue engineering, 2005. **11**(1-2): p. 1-18.
189. Cacciafesta, P., et al., *Human Plasma Fibrinogen Adsorption on Ultraflat Titanium Oxide Surfaces Studied with Atomic Force Microscopy.* Langmuir, 2000. **16**(21): p. 8167-8175.
190. Cacciafesta, P., et al., *Characterization of Ultraflat Titanium Oxide Surfaces.* Chemistry of Materials, 2002. **14**(2): p. 777-789.
191. Jung, S.-Y., et al., *The Vroman Effect: A Molecular Level Description of Fibrinogen Displacement.* Journal of the American Chemical Society, 2003. **125**(42): p. 12782-12786.
192. Veklich, Y.I., et al., *Carboxyl-terminal portions of the alpha chains of fibrinogen and fibrin. Localization by electron microscopy and the effects of isolated alpha C fragments on polymerization.* Journal of Biological Chemistry, 1993. **268**(18): p. 13577-13585.
193. Stanford, M., P. Munoz, and L. Vroman, *Platelets adhere where flow has left fibrinogen on glass.* Annals of the New York Academy of Sciences, 1983. **416**(1 Surface Phenomena in Hemorheology: Their Theoretical, Experimental, and Clinical Aspects): p. 504-512.
194. Sapsford, K.E. and F.S. Ligler, *Real-time analysis of protein adsorption to a variety of thin films.* Biosensors and Bioelectronics, 2004. **19**(9): p. 1045-1055.
195. Salzman, E.W., et al., *Role of fibrinogen in activation of platelets by artificial surfaces.* Annals of the New York Academy of Sciences, 1987. **516**(1): p. 184-195.
196. Balasubramanian, V., et al., *Residence-time dependent changes in fibrinogen adsorbed to polymeric biomaterials.* Journal of Biomedical Materials Research, 1999. **44**(3): p. 253-260.

197. Weber, N., et al., *Viscoelastic Properties of Fibrinogen Adsorbed to the Surface of Biomaterials Used in Blood-Contacting Medical Devices.* Langmuir, 2007. **23**(6): p. 3298-3304.
198. Weber, N., et al., *Small changes in the polymer structure influence the adsorption behavior of fibrinogen on polymer surfaces: Validation of a new rapid screening technique.* Journal of Biomedical Materials Research, 2004(3).
199. Sims, P.J., et al., *Effect of platelet activation on the conformation of the plasma membrane glycoprotein IIb-IIIa complex.* Journal of Biological Chemistry, 1991. **266**(12): p. 7345-7352.
200. Chiumiento, A., S. Lamponi, and R. Barbucci, *Role of fibrinogen conformation in platelet activation.* Biomacromolecules, 2007. **8**(2): p. 523-531.
201. Bennett, J.S., *Platelet-Fibrinogen Interactions.* Annals of the New York Academy of Sciences, 2001. **936**(1): p. 340-354.
202. Tsai, W.B., J.M. Grunkemeier, and T.A. Horbett, *Variations in the ability of adsorbed fibrinogen to mediate platelet adhesion to polystyrene-based materials: A multivariate statistical analysis of antibody binding to the platelet binding sites of fibrinogen.* Journal of Biomedical Materials Research, 2003(4).
203. Tao, L., et al., *Recent advances in the understanding of the molecular mechanisms regulating platelet integrin αIIbβ3 activation.* Protein & Cell, 2010. **1**(7): p. 627-637.
204. Kamata, T. and Y. Takada, *Platelet Integrin αIIbβ3-Ligand Interactions: What Can We Learn From the Structure?* International Journal of Hematology, 2001. **74**(4): p. 382-389.
205. Tang, L., A.H. Lucas, and J.W. Eaton, *Inflammatory responses to implanted polymeric biomaterials: role of surface-adsorbed immunoglobulin G.* Journal of Laboratory and Clinical Medicine, 1993. **122**(3): p. 292-300.
206. Herve, F., et al., *Drug binding in plasma. A summary of recent trends in the study of drug and hormone binding.* Clinical pharmacokinetics, 1994. **26**(1): p. 44.
207. Carter, D. and J. Ho, *Structure of serum albumin.* Advances in protein chemistry, 1994. **45**: p. 153.
208. Sack, R., et al., *Specificity and biological activity of the protein deposited on the hydrogel surface. Relationship of polymer structure to biofilm formation.* Investigative ophthalmology & visual science, 1987. **28**(5): p. 842-849.
209. Salzman, E.W., et al., *Protein-platelet interaction on heparinized surfaces.* Journal of Biomedical Materials Research, 1969. **3**(1): p. 69-81.
210. Salzman, E.W., *Nonthrombogenic surfaces: critical review.* Blood, 1971. **38**(4): p. 509-523.
211. Amiji, M., H. Park, and K. Park, *Study on the prevention of surface-induced platelet activation by albumin coating.* Journal of Biomaterials Science, Polymer Edition, 1992. **3**(5): p. 375-388.
212. Tang, L. and J.W. Eaton, *Inflammatory responses to biomaterials.* American journal of clinical pathology, 1995. **103**(4): p. 466-471.
213. Tang, L., et al., *Molecular determinants of acute inflammatory responses to biomaterials.* Journal of Clinical Investigation, 1996. **97**(5): p. 1329.

214. Brunette, D., et al. *Update on improving the bio-implant interface by controlling cell behaviour using surface topography*. in *International Congress Series*. 2005. Elsevier.
215. Brunette, D.M., et al., *Improving the bio-implant interface by controlling cell behaviour using surface topography.* Bio-Implant Interface, CRC Press, Boca Raton, 2003: p. 103-122.
216. Nimeri, G., et al., *Neutrophil interaction with protein-coated surfaces studied by an extended quartz crystal microbalance technique.* Colloids and Surfaces B: Biointerfaces, 1998. **11**(5): p. 255-264.
217. Renner, L., et al., *Fibronectin Displacement at Polymer Surfaces.* Langmuir, 2005. **21**(10): p. 4571-4577.
218. Wertz, C. and M. Santore, *Adsorption and relaxation kinetics of albumin and fibrinogen on hydrophobic surfaces: Single-species and competitive behavior.* Langmuir, 1999. **15**(26): p. 8884-8894.
219. Heyligers, J., et al., *Improving small-diameter vascular grafts: from the application of an endothelial cell lining to the construction of a tissue-engineered blood vessel.* Annals of vascular surgery, 2005. **19**(3): p. 448-456.
220. Kakisis, J.D., et al., *Artificial blood vessel: the Holy Grail of peripheral vascular surgery.* Journal of vascular surgery, 2005. **41**(2): p. 349-354.
221. Werner, C., M.F. Maitz, and C. Sperling, *Current strategies towards hemocompatible coatings.* Journal of materials chemistry, 2007. **17**(32): p. 3376-3384.
222. Ratner, B.D., et al., *An introduction to materials in medicine.* Biomaterials Science, 1996. **484**.
223. Lee, J.H., et al., *The effect of fluid shear stress on endothelial cell adhesiveness to polymer surfaces with wettability gradient.* Journal of colloid and interface science, 2000. **230**(1): p. 84-90.
224. Gage, K.L. and W.R. Wagner, *Cardiovascular devices.* Standard handbook of biomedical engineering and design, 2004.
225. Khang, G., et al., *Method of manufacturing a vascular graft impregnated with polysaccharide derivatives*. 1995, Google Patents.
226. Helmus, M., et al., *Sterility and pyrogenicity issues of synthetic vascular grafts.* American Society for Testing and Materials, 1986. **898**: p. 236-249.
227. Cao, L., et al., *Plasma-deposited tetraglyme surfaces greatly reduce total blood protein adsorption, contact activation, platelet adhesion, platelet procoagulant activity, and in vitro thrombus deposition.* Journal of Biomedical Materials Research Part A, 2007. **81**(4): p. 827-837.
228. Hansson, K.M., et al., *Whole blood coagulation on protein adsorption-resistant PEG and peptide functionalised PEG-coated titanium surfaces.* Biomaterials, 2005. **26**(8): p. 861-872.
229. Fushimi, F., et al., *Platelet Adhesion, Contact Phase Coagulation Activation, and C5a Generation of Polyethylene Glycol Acid-Grafted High Flux Cellulosic Membrane with Varieties of Grafting Amounts.* Artificial organs, 1998. **22**(10): p. 821-826.
230. Chen, H., et al., *Protein repellant silicone surfaces by covalent immobilization of poly (ethylene oxide).* Biomaterials, 2005. **26**(15): p. 2391-2399.

231. Shen, M., et al., *PEO-like plasma polymerized tetraglyme surface interactions with leukocytes and proteins: in vitro and in vivo studies.* Journal of Biomaterials Science, Polymer Edition, 2002. **13**(4): p. 367-390.
232. Sheu, M.-S., et al., *A new gas discharge process for preparation of non-fouling surfaces on biomaterials.* Clinical materials, 1993. **13**(1): p. 41-45.
233. Borgdorff, P., et al., *Pump-induced platelet aggregation in albumin-coated extracorporeal systems.* The Journal of thoracic and cardiovascular surgery, 1999. **118**(5): p. 946-952.
234. Adrian, K., et al., *The effect of albumin priming solution on platelet activation during experimental long-term perfusion.* Perfusion, 1998. **13**(3): p. 187-191.
235. Videm, V., et al., *Heparin-coated cardiopulmonary bypass equipment. I. Biocompatibility markers and development of complications in a high-risk population.* The Journal of thoracic and cardiovascular surgery, 1999. **117**(4): p. 794-802.
236. Lavaud, S., et al., *Optimal anticoagulation strategy in haemodialysis with heparin-coated polyacrylonitrile membrane.* Nephrology Dialysis Transplantation, 2003. **18**(10): p. 2097-2104.
237. Øvrum, E., et al., *Complement and granulocyte activation in two different types of heparinized extracorporeal circuits.* The Journal of thoracic and cardiovascular surgery, 1995. **110**(6): p. 1623-1632.
238. von Segesser, L.K., *Heparin-bonded surfaces in extracorporeal membrane oxygenation for cardiac support.* The Annals of thoracic surgery, 1996. **61**(1): p. 330-335.
239. Weitz, J.I., et al., *Clot-bound thrombin is protected from inhibition by heparin-antithrombin III but is susceptible to inactivation by antithrombin III-independent inhibitors.* The Journal of Clinical Investigation, 1990. **86**(2): p. 385-391.
240. Liaw, P.C.Y., et al., *Molecular Basis for the Susceptibility of Fibrin-bound Thrombin to Inactivation by Heparin Cofactor II in the Presence of Dermatan Sulfate but Not Heparin.* Journal of Biological Chemistry, 2001. **276**(24): p. 20959-20965.
241. Olsson, P., et al., *On the blood compatibility of end-point immobilized heparin.* Journal of Biomaterials Science, Polymer Edition, 2000. **11**(11): p. 1261-1273.
242. Kidane, A.G., et al., *Anticoagulant and Antiplatelet Agents: Their Clinical and Device Application(s) Together with Usages to Engineer Surfaces.* Biomacromolecules, 2004. **5**(3): p. 798-813.
243. Grombe, R., et al., *Sulfated Glycopolymer Thin Films—Preparation, Characterization, and Biological Activity.* Macromolecular Bioscience, 2007. **7**(2): p. 195-200.
244. Phaneuf, M.D., et al., *Covalent linkage of recombinant hirudin to poly(ethylene terephthalate) (Dacron): creation of a novel antithrombin surface.* Biomaterials, 1997. **18**(10): p. 755-765.
245. Wyers, M.C., et al., *In Vivo Assessment of a Novel Dacron Surface with Covalently Bound Recombinant Hirudin.* Cardiovascular Pathology, 1999. **8**(3): p. 153-159.

246. Gouzy, M.-F., et al., *Benzamidine-based coatings: Implication of inhibitor structure on the inhibition of coagulation enzymes in solution and in vitro hemocompatibility assessment.* Biointerphases, 2006. **1**(4): p. 146-155.
247. Åsberg, A.E. and V. Videm, *Concentration-dependent effect of abciximab on platelets and neutrophils in a model of cardiopulmonary bypass.* Perfusion, 2006. **21**(6): p. 343-352.
248. Gouzy, M.F., et al., *In vitro blood compatibility of polymeric biomaterials through covalent immobilization of an amidine derivative.* Biomaterials, 2004. **25**(17): p. 3493-3501.
249. Nablo, B.J. and M.H. Schoenfisch, *In vitro cytotoxicity of nitric oxide-releasing sol–gel derived materials.* Biomaterials, 2005. **26**(21): p. 4405-4415.
250. Kidd, K.R., V.B. Patula, and S.K. Williams, *Accelerated endothelialization of interpositional 1-mm vascular grafts.* Journal of Surgical Research, 2003. **113**(2): p. 234-242.
251. Lu, A. and R. Sipehia, *Antithrombotic and fibrinolytic system of human endothelial cells seeded on PTFE: the effects of surface modification of PTFE by ammonia plasma treatment and ECM protein coatings.* Biomaterials, 2001. **22**(11): p. 1439-1446.
252. Aoki, J., et al., *Endothelial Progenitor Cell Capture by Stents Coated With Antibody Against CD34: The HEALING-FIM (Healthy Endothelial Accelerated Lining Inhibits Neointimal Growth-First In Man) Registry.* Journal of the American College of Cardiology, 2005. **45**(10): p. 1574-1579.
253. Van Belle, E., et al., *Accelerated Endothelialization by Local Delivery of Recombinant Human Vascular Endothelial Growth Factor Reduces In-Stent Intimal Formation.* Biochemical and Biophysical Research Communications, 1997. **235**(2): p. 311-316.
254. Dion, I., et al., *Blood haemolysis by ceramics.* Biomaterials, 1993. **14**(2): p. 107-110.
255. Dion, I., et al., *Hemocompatibility of diamond-like carbon coating.* Biomedical materials and engineering, 1993. **3**(1): p. 51-55.
256. Aris, A., et al., *The spanish monostrut study group: A ten-year experience with 8,599 implants.* The Annals of thoracic surgery, 1996. **62**(1): p. 40-47.
257. Barragan, P., et al., *The BioDiamond and BioDiamond F stents.* Handbook of Coronary Stents, 2000: p. 29.
258. Hong, J., et al., *Titanium is a highly thrombogenic biomaterial: possible implications for osteogenesis.* Thrombosis and haemostasis, 1999. **82**: p. 58-64.
259. Bendavid, A., et al., *Structural and optical properties of titanium oxide thin films deposited by filtered arc deposition.* Thin Solid Films, 1999. **355**: p. 6-11.
260. McAlarney, M.E., et al., *TEM immunogold staining of C3 from plasma onto titanium oxides.* Journal of Biomedical Materials Research, 1991. **25**(7): p. 845-864.
261. Armitage, D.A. and D.M. Grant, *Characterisation of surface-modified nickel titanium alloys.* Materials Science and Engineering: A, 2003. **349**(1–2): p. 89-97.

262. Nan, H., et al., *Blood compatibility of amorphous titanium oxide films synthesized by ion beam enhanced deposition.* Biomaterials, 1998. **19**(7–9): p. 771-776.
263. Jones, M.I., et al., *Haemocompatibility of DLC and TiC–TiN interlayers on titanium.* Diamond and Related Materials, 1999. **8**(2–5): p. 457-462.
264. Huang Nan, et al., *In vitro Investigation of Blood Compatibility of Ti with Oxide Layers of Rutile Structure.* Journal of biomaterials applications, 1994. **8**(4): p. 404-412.
265. Huang, N., et al., *Surface modification of biomaterials by plasma immersion ion implantation.* Surface and Coatings Technology, 2004. **186**(1–2): p. 218-226.
266. Windecker, S., et al., *Stent Coating With Titanium-Nitride-Oxide for Reduction of Neointimal Hyperplasia.* Circulation, 2001. **104**(8): p. 928-933.
267. Nan, H., et al., *Blood compatibility of amorphous titanium oxide films synthesized by ion beam enhanced deposition.* Biomaterials, 1998. **19**(7-9): p. 771-776.
268. Bolz, A. and M. Schaldach, *Artificial Heart Valves: Improved Blood Compatibility by PECVD a-SiC:H Coating.* Artificial organs, 1990. **14**(4): p. 260-269.
269. Harder, C., A. Rzany, and M. Schaldach, *Coating of vascular stents with antithrombogenic amorphous silicon carbide.* Prog Biomed Res, 1999. **4**: p. 71-77.
270. Robertson, J., *Diamond-like amorphous carbon.* Materials Science and Engineering: R: Reports, 2002. **37**(4): p. 129-281.
271. Ma, W.J., et al., *DLC coatings: Effects of physical and chemical properties on biological response.* Biomaterials, 2007. **28**(9): p. 1620-1628.
272. Vetter, J., *60 Years of DLC coatings: Historical highlights and technical review of cathodic arc processes to synthesize various DLC types, and their evolution for industrial applications.* Surface and Coatings Technology, 2014(0).
273. Robertson, J., *Properties of diamond-like carbon.* Surface and Coatings Technology, 1992. **50**(3): p. 185-203.
274. McKenzie, D., *Tetrahedral bonding in amorphous carbon.* Reports on Progress in Physics, 1996. **59**(12): p. 1611.
275. Balakrisnan, B., B. Tomcik, and D. Blackwood, *Influence of carbon sputtering conditions on corrosion protection of magnetic layer by an electrochemical technique.* Journal of The Electrochemical Society, 2002. **149**(3): p. B84-B88.
276. Koidl, P., et al. *Plasma deposition, properties and structure of amorphous hydrogenated carbon films*. in *Materials Science Forum*. 1991. Trans Tech Publ.
277. Robertson, J., *Amorphous carbon.* Advances in Physics, 1986. **35**(4): p. 317-374.
278. Robertson, J., *Hard amorphous (diamond-like) carbons.* Progress in Solid State Chemistry, 1991. **21**(4): p. 199-333.
279. Pandey, M., et al., *Structural and optical properties of diamond like carbon films.* Journal of alloys and compounds, 2005. **386**(1): p. 296-302.

280. Kim, H.-G., et al., *Corrosion performance of diamond-like carbon (DLC)-coated Ti alloy in the simulated body fluid environment.* Diamond and Related Materials, 2005. **14**(1): p. 35-41.
281. Anne Thomson, L., et al., *Biocompatibility of diamond-like carbon coating.* Biomaterials, 1991. **12**(1): p. 37-40.
282. Maguire, P., et al., *Mechanical stability, corrosion performance and bioresponse of amorphous diamond-like carbon for medical stents and guidewires.* Diamond and Related Materials, 2005. **14**(8): p. 1277-1288.
283. Franks, J., T. Ng, and A. Wright, *Preparation and characteristics of diamond-like carbon films.* Vacuum, 1988. **38**(8): p. 749-751.
284. Matthews, A. and S. Eskildsen, *Engineering applications for diamond-like carbon.* Diamond and Related Materials, 1994. **3**(4): p. 902-911.
285. Grill, A., *Diamond-like carbon: state of the art.* Diamond and Related Materials, 1999. **8**(2): p. 428-434.
286. Hauert, R., *A review of modified DLC coatings for biological applications.* Diamond and Related Materials, 2003. **12**(3): p. 583-589.
287. Fyta, M.G., et al., *Structure, stability, and stress properties of amorphous and nanostructured carbon films.* Thin Solid Films, 2005. **482**(1): p. 56-62.
288. HEF. [cited 2014 22 May]; Available from: http://www.hefusa.net/pvd_coating/DLC-coatings.html.
289. Hofsäss, H., et al., *Doping and growth of diamond-like carbon films by ion beam deposition.* Diamond and Related Materials, 1994. **3**(1): p. 137-142.
290. Shim, K.-S., et al., *Fabrication and characterization of diamond-like carbon thin films by pulsed laser deposition.* Applied Surface Science, 2000. **154**: p. 482-484.
291. He, X., W. Li, and H. Li, *Bonding structure and tribological properties of DLC films synthesized by dual ion beam sputtering.* Vacuum, 1994. **45**(9): p. 977-980.
292. Sanchez, N., et al., *Characterization of diamond-like carbon (DLC) thin films prepared by rf magnetron sputtering.* Thin Solid Films, 2000. **373**(1): p. 247-250.
293. Thorwarth, G., et al., *Investigation of DLC synthesized by plasma immersion ion implantation and deposition.* Surface and Coatings Technology, 2005. **193**(1): p. 206-212.
294. Zou, Y., et al., *Influence of the gas atmosphere on the microstructure and mechanical properties of diamond-like carbon films by arc ion plating.* Materials Letters, 2004. **58**(26): p. 3271-3275.
295. Seung Lee, C., et al., *Structure and properties of Si incorporated tetrahedral amorphous carbon films prepared by hybrid filtered vacuum arc process.* Diamond and Related Materials, 2002. **11**(2): p. 198-203.
296. Sanchez-Lopez, J., et al., *Diamond-like carbon prepared by high density plasma.* Diamond and Related Materials, 2000. **9**(3): p. 638-642.
297. Li, D., F. Cui, and H. Gu, *Studies of diamond-like carbon films coated on PMMA by ion beam assisted deposition.* Applied Surface Science, 1999. **137**(1): p. 30-37.
298. Angus, J.C., et al., *Plasma deposited thin films.* CRC, 1986. **1564**.
299. Marton, D., et al., *Semiquantitative subplantation model for low energy ion interactions with surfaces. II. Ion beam deposition of carbon and carbon*

nitride. Journal of Vacuum Science & Technology A, 1998. **16**(2): p. 455-462.
300. Moseler, M., et al., *The ultrasmoothness of diamond-like carbon surfaces.* Science, 2005. **309**(5740): p. 1545-1548.
301. Bhushan, B., *Chemical, mechanical and tribological characterization of ultra-thin and hard amorphous carbon coatings as thin as 3.5 nm: recent developments.* Diamond and Related Materials, 1999. **8**(11): p. 1985-2015.
302. Erdemir, A., et al., *Effect of source gas chemistry on tribological performance of diamond-like carbon films.* Diamond and Related Materials, 2000. **9**(3): p. 632-637.
303. Voevodin, A.A., et al., *Friction induced phase transformation of pulsed laser deposited diamond-like carbon.* Diamond and Related Materials, 1996. **5**(11): p. 1264-1269.
304. Grischke, M., et al., *Variation of the wettability of DLC-coatings by network modification using silicon and oxygen.* Diamond and Related Materials, 1998. **7**(2–5): p. 454-458.
305. Butter, R.S., et al., *Production and wetting properties of fluorinated diamond-like carbon coatings.* Thin Solid Films, 1997. **311**(1–2): p. 107-113.
306. Erdemir, A., *The role of hydrogen in tribological properties of diamond-like carbon films.* Surface and Coatings Technology, 2001. **146**: p. 292-297.
307. Sullivan, J., T. Friedmann, and K. Hjort, *Diamond and amorphous carbon MEMS.* MRS bulletin, 2001. **26**(04): p. 309-311.
308. Monaghan, D., et al., *Deposition of wear resistant coatings based on diamond like carbon by unbalanced magnetron sputtering.* Surface and Coatings Technology, 1993. **60**(1): p. 525-530.
309. Dowling, D., et al., *Evaluation of diamond-like carbon-coated orthopaedic implants.* Diamond and Related Materials, 1997. **6**(2): p. 390-393.
310. Allen, M., B. Myer, and N. Rushton, *In vitro and in vivo investigations into the biocompatibility of diamond-like carbon (DLC) coatings for orthopedic applications.* Journal of Biomedical Materials Research, 2001. **58**(3): p. 319-328.
311. Mielke, N.A., et al., *In vitro evaluation of a new resilient, hard-carbon, thin-film coating as a bearing material for ventricular assist devices——In Vitro Bearing Evaluation of BioMedFlex.* Journal of Biomedical Science and Engineering, 2010. **3**: p. 525.
312. Ratner, B.D., *The biocompatibility manifesto: biocompatibility for the twenty-first century.* Journal of cardiovascular translational research, 2011. **4**(5): p. 523-527.
313. Mitura, E., et al., *Diamond-like carbon coatings for biomedical applications.* Diamond and Related Materials, 1994. **3**(4–6): p. 896-898.
314. Evans, A.C., J. Franks, and P.J. Revell, *Diamond-like carbon applied to bioengineering materials.* Surface and Coatings Technology, 1991. **47**(1–3): p. 662-667.
315. Ball, M., et al., *Macrophage responses to vascular stent coatings.* Journal of Biomedical Materials Research Part A, 2004. **70**(3): p. 380-390.
316. Du, C., et al., *Morphological behaviour of osteoblasts on diamond-like carbon coating and amorphous C–N film in organ culture.* Biomaterials, 1998. **19**(7–9): p. 651-658.

317. Butter, R., et al., *In vitro studies of DLC coatings with silicon intermediate layer.* Diamond and Related Materials, 1995. **4**(5–6): p. 857-861.
318. Mohanty, M., et al., *Long term tissue response to titanium coated with diamond like carbon.* Biomolecular Engineering, 2002. **19**(2–6): p. 125-128.
319. Nurdin, N., et al., *Hemocompatible diamond-like carbon (DLC) surfaces.* Eur Cells Mater, 2003. **5**: p. 17-28.
320. Yang, P., et al., *Haemocompatibility of hydrogenated amorphous carbon (a-C:H) films synthesized by plasma immersion ion implantation-deposition.* Nuclear Instruments and Methods in Physics Research, 2003. **206**(0): p. 721-725.
321. Yu, L.J., et al., *Haemocompatibility of tetrahedral amorphous carbon films.* Surface and Coatings Technology, 2000. **128–129**(0): p. 484-488.
322. Hinüber, C., et al., *Biocompatibility and mechanical properties of diamond-like coatings on cobalt-chromium-molybdenum steel and titanium-aluminum-vanadium biomedical alloys.* Journal of Biomedical Materials Research Part A, 2010. **95**(2): p. 388-400.
323. Hauert, R., et al., *Surface analysis and bioreactions of F and Si containing aC: H.* Thin Solid Films, 1997. **308**: p. 191-194.
324. Kim, H.-G., et al., *Electrochemical behavior of diamond-like carbon films for biomedical applications.* Thin Solid Films, 2005. **475**(1–2): p. 291-297.
325. Dorner-Reisel, A., et al., *Diamond-like carbon: alteration of the biological acceptance due to Ca–O incorporation.* Thin Solid Films, 2002. **420–421**(0): p. 263-268.
326. Singh, A., et al., *Glial cell and fibroblast cytotoxicity study on plasma-deposited diamond-like carbon coatings.* Biomaterials, 2003. **24**(28): p. 5083-5089.
327. Roy, R.K., et al., *Hemocompatibility of Surface Modified Si Incorporated Diamond-like Carbon Films.* Thin Solid Films, 2005. **482**: p. 299-304.
328. Oh, H.-J., et al., *Microstructural characterization of biomedical titanium oxide film fabricated by electrochemical method.* Surface and Coatings Technology, 2005. **198**(1–3): p. 247-252.
329. Lausmaa, J., *Surface spectroscopic characterization of titanium implant materials.* Journal of Electron Spectroscopy and Related Phenomena, 1996. **81**(3): p. 343-361.
330. Lausmaa, J., B. Kasemo, and H. Mattsson, *Surface spectroscopic characterization of titanium implant materials.* Applied Surface Science, 1990. **44**(2): p. 133-146.
331. Schutz, R. and D. Thomas, *Metals Handbook.* Metals Handbook, 1987. **13**.
332. Davies, J. and B.E. Workshop, *Bone engineering*. 2000: em squared.
333. Hanawa, T. and M. Ota, *Calcium phosphate naturally formed on titanium in electrolyte solution.* Biomaterials, 1991. **12**(8): p. 767-774.
334. Hanawa, T. and M. Ota, *Characterization of surface film formed on titanium in electrolyte using XPS.* Applied Surface Science, 1992. **55**(4): p. 269-276.
335. Williams, D., *Biocompatibility of clinical implant materials*. Vol. 1. 1981: CRC press Boca Raton, Florida.
336. Williams, D.F., *On the mechanisms of biocompatibility.* Biomaterials, 2008. **29**(20): p. 2941-2953.

337. Fraker, A., et al., *Surface preparation and corrosion behavior of titanium alloys for surgical implants.* Titanium Alloys in Surgical Implants, 1983: p. 206-219.
338. Liu, X., P.K. Chu, and C. Ding, *Surface modification of titanium, titanium alloys, and related materials for biomedical applications.* Materials Science and Engineering: R: Reports, 2004. **47**(3): p. 49-121.
339. Steinemann, S.G., *Titanium—the material of choice?* Periodontology 2000, 1998. **17**(1): p. 7-21.
340. Placko, H.E., et al., *Surface characterization of titanium-based implant materials.* The International journal of oral & maxillofacial implants, 1999. **15**(3): p. 355-363.
341. Brunette, D.M., *Titanium in medicine: material science, surface science, engineering, biological responses, and medical applications*. 2001: Springer.
342. Hong, J., et al., *Titanium is a highly thrombogenic biomaterial: possible implications for osteogenesis.* Thrombsis and Haemostasis, 1999. **82**: p. 58-64.
343. Valles, G., et al., *Differential inflammatory macrophage response to rutile and titanium particles.* Biomaterials, 2006. **27**(30): p. 5199-5211.
344. Sunny, M. and C.P. Sharma, *Titanium-protein interaction: changes with oxide layer thickness.* Journal of biomaterials applications, 1991. **6**(1): p. 89-98.
345. Kubacka, A., M. Fernández-García, and G. Colón, *Advanced Nanoarchitectures for Solar Photocatalytic Applications.* Chemical Reviews, 2011. **112**(3): p. 1555-1614.
346. Hagfeldt, A. and M. Graetzel, *Light-Induced Redox Reactions in Nanocrystalline Systems.* Chemical Reviews, 1995. **95**(1): p. 49-68.
347. Fujishima, A., X. Zhang, and D.A. Tryk, *TiO2 photocatalysis and related surface phenomena.* Surface Science Reports, 2008. **63**(12): p. 515-582.
348. Thompson, T.L. and J.T. Yates, *Surface Science Studies of the Photoactivation of TiO2New Photochemical Processes.* Chemical Reviews, 2006. **106**(10): p. 4428-4453.
349. Sabate, J., et al., *Nature and properties of pure and nb-doped Ti02 ceramic membranes affecting the photocatalytic degradation of 3-chlorosalicylic acid as a model of halogenated organic compounds.* Journal of catalysis, 1992. **134**(1): p. 36-46.
350. Williams, L. and D. Hess, *Structural properties of titanium dioxide films deposited in an rf glow discharge.* Journal of Vacuum Science & Technology A, 1983. **1**(4): p. 1810-1819.
351. Fujii, T., et al., *Characteristics of titanium oxide films deposited by an activated reactive evaporation method.* Journal of materials research, 1994. **9**(06): p. 1468-1473.
352. Ben Amor, S., et al., *Elaboration and characterization of titania coatings.* Thin Solid Films, 1997. **293**(1): p. 163-169.
353. Okimura, K., et al., *Preparation of rutile TiO 2 films by RF magnetron sputtering.* Japanese journal of applied physics, 1995. **34**(9R): p. 4950.
354. Gilo, M. and N. Croitoru, *Study of HfO2 films prepared by ion-assisted deposition using a gridless end-hall ion source.* Thin Solid Films, 1999. **350**(1): p. 203-208.

355. Aarik, J., et al., *Effect of crystal structure on optical properties of TiO2 films grown by atomic layer deposition.* Thin Solid Films, 1997. **305**(1): p. 270-273.
356. Yoon, H.-S. and H. Im, *Structural Properties of TiO2 Films Grown by Pulsed Laser Deposition.* Korean Chemical Society, 1997. **18**: p. 640-643.
357. Bendavid, A., P.J. Martin, and H. Takikawa, *Deposition and modification of titanium dioxide thin films by filtered arc deposition.* Thin Solid Films, 2000. **360**(1–2): p. 241-249.
358. Schmidt, M. and S.G. Steinemann, *XPS studies of amino acids adsorbed on titanium dioxide surfaces.* Fresenius' journal of analytical chemistry, 1991. **341**(5-6): p. 412-415.
359. Gold, J., M. Schmidt, and S. Steinemann, *XPS study of amino-acid adsorption to titanium surfaces.* Helvetica Physica Acta, 1989. **62**(2-3): p. 246-249.
360. Parks, G.A., *The isoelectric points of solid oxides, solid hydroxides, and aqueous hydroxo complex systems.* Chemical Reviews, 1965. **65**(2): p. 177-198.
361. Cornell, R., A. Posner, and J. Quirk, *A titrimetric and electrophoretic investigation of the pzc and the iep of pigment rutile.* Journal of colloid and interface science, 1975. **53**(1): p. 6-13.
362. Parsegian, V.A., *Molecular forces governing tight contact between cellular surfaces and substrates.* The Journal of prosthetic dentistry, 1983. **49**(6): p. 838-842.
363. Bischoff, B.L. and M.A. Anderson, *Peptization process in the sol-gel preparation of porous anatase (TiO2).* Chemistry of Materials, 1995. **7**(10): p. 1772-1778.
364. Mukherjee, B., C. Karthik, and N. Ravishankar, *Hybrid Sol− Gel Combustion Synthesis of Nanoporous Anatase.* The Journal of Physical Chemistry C, 2009. **113**(42): p. 18204-18211.
365. Hossain, M., et al., *Investigation of sputter-deposited TiO< sub> 2</sub> thin film for the fabrication of dye-sensitized solar cells.* Thin Solid Films, 2008. **516**(20): p. 7149-7154.
366. Meacock, G., et al., *The improved whitening of minced cod flesh using dispersed titanium dioxide.* Journal of the Science of Food and Agriculture, 1997. **73**(2): p. 221-225.
367. Li, P., et al., *Bonelike Hydroxyapatite Induction by a Gel-Derived Titania on a Titanium Substrate.* Journal of the American Ceramic Society, 1994. **77**(5): p. 1307-1312.
368. Wu, J.-M., et al., *Low-temperature deposition of rutile film on biomaterials substrates and its ability to induce apatite deposition in vitro.* Journal of Materials Science: Materials in Medicine, 2007. **18**(8): p. 1529-1536.
369. Ellingsen, J.E., *A study on the mechanism of protein adsorption to TiO2.* Biomaterials, 1991. **12**(6): p. 593-596.
370. Rivera-Chacon, D., et al., *Fibronectin and vitronectin promote human fetal osteoblast cell attachment and proliferation on nanoporous titanium surfaces.* Journal of Biomedical Nanotechnology, 2013. **9**(6): p. 1092.
371. Yang, J.-S., et al., *Response of fetal rat calvarial cells to nanotubular titanium oxide surface.* Journal of nanoscience and nanotechnology, 2011. **11**(2): p. 1807-1810.

372. Yao, C., et al., *Anodized Ti and Ti 6 Al 4 V possessing nanometer surface features enhances osteoblast adhesion.* Journal of Biomedical Nanotechnology, 2005. **1**(1): p. 68-73.
373. Brammer, K.S., et al., *Enhanced Cellular Mobility Guided by TiO2 Nanotube Surfaces.* Nano Letters, 2008. **8**(3): p. 786-793.
374. Peng, L., et al., *The effect of TiO2 nanotubes on endothelial function and smooth muscle proliferation.* Biomaterials, 2009. **30**(7): p. 1268-1272.
375. Choudhary, S., K. Haberstroh, and T. Webster, *Enhanced functions of vascular cells on nanostructured Ti for improved stent applications.* Tissue engineering, 2007. **13**(7): p. 1421-1430.
376. Kurashina, Y., et al. *Proliferation and Adhesion of L929 Fibroblasts on Surface with Different Microtopography*. in *MRS Proceedings*. 2014. Cambridge Univ Press.
377. Kwok, S.C.H., J. Wang, and P.K. Chu, *Surface energy, wettability, and blood compatibility phosphorus doped diamond-like carbon films.* Diamond and Related Materials, 2005. **14**(1): p. 78-85.
378. Okpalugo, T., et al., *Platelet adhesion on silicon modified hydrogenated amorphous carbon films.* Biomaterials, 2004. **25**(2): p. 239-245.
379. Saito, T., et al., *Antithrombogenicity of fluorinated diamond-like carbon films.* Diamond and Related Materials, 2005. **14**(3): p. 1116-1119.
380. Logothetidis, S., et al., *Haemocompatibility studies on carbon-based thin films by ellipsometry.* Thin Solid Films, 2005. **482**(1): p. 126-132.
381. Leng, Y., et al., *Mechanical properties and platelet adhesion behavior of diamond-like carbon films synthesized by pulsed vacuum arc plasma deposition.* Surface Science, 2003. **531**(2): p. 177-184.
382. Chen, J., et al., *Blood compatibility and sp 3/sp 2 contents of diamond-like carbon (DLC) synthesized by plasma immersion ion implantation-deposition.* Surface and Coatings Technology, 2002. **156**(1): p. 289-294.
383. Gutensohn, K., et al., *In vitro analyses of diamond-like carbon coated stents: reduction of metal ion release, platelet activation, and thrombogenicity.* Thrombosis research, 2000. **99**(6): p. 577-585.
384. Alanazi, A., et al., *Engineering Analysis of Diamond-Like Carbon Coated Polymeric Materials for Biomedical Applications.* Artificial organs, 2000. **24**(8): p. 624-627.
385. Alanazi, A., et al., *Improved blood compatibility of DLC coated polymeric material.* Asaio Journal, 2000. **46**(4): p. 440-443.
386. Leach, K., et al., *Thrombogenicity of hydrophilically coated guide wires and catheters.* Radiology, 1990. **175**(3): p. 675-677.
387. Jones, M.I., et al., *Protein adsorption and platelet attachment and activation, on TiN, TiC, and DLC coatings on titanium for cardiovascular applications.* Journal of Biomedical Materials Research, 2000. **52**(2): p. 413-421.
388. FergusonJr, A.B., P.G. Laing, and E.S. Hodge, *The ionization of metal implants in living tissues.* The Journal of Bone & Joint Surgery, 1960. **42**(1): p. 77-90.
389. Bartorelli, A.L., et al., *Aspirin alone antiplatelet regimen after intracoronary placement of the Carbostent™: The Antares study.* Catheterization and cardiovascular interventions, 2002. **55**(2): p. 150-156.

390. Antoniucci, D., et al., *Clinical and angiographic outcome after coronary arterial stenting with the carbostent.* The American journal of cardiology, 2000. **85**(7): p. 821-825.
391. Schaefer, O., et al., *Endovascular treatment of superficial femoral artery occlusive disease with stents coated with diamond-like carbon.* Clinical radiology, 2004. **59**(12): p. 1128-1131.
392. Haase, J., et al., *Comparison of stainless steel stents coated with turbostratic carbon and uncoated stents for percutaneous coronary interventions.* Journal of Invasive cardiology, 2003. **15**(10): p. 562-565.
393. Airoldi, F., et al., *Comparison of diamond-like carbon-coated stents versus uncoated stainless steel stents in coronary artery disease.* The American journal of cardiology, 2004. **93**(4): p. 474-477.
394. Maitz, M.F., et al., *Blood compatibility of titanium oxides with various crystal structure and element doping.* Journal of biomaterials applications, 2003. **17**(4): p. 303-319.
395. McAlarney, M.E., M.A. Oshiro, and C.V. McAlarney, *Effects of titanium dioxide passive film crystal structure, thickness, and crystallinity on C3 adsorption.* The International journal of oral & maxillofacial implants, 1995. **11**(1): p. 73-80.
396. Chen, J., et al., *Antithrombogenic investigation of surface energy and optical bandgap and hemocompatibility mechanism of TiO2 thin films.* Biomaterials, 2002. **23**(12): p. 2545-2552.
397. Baurschmidt, P. and M. Schaldach, *Electrochemical aspects of thrombogenicity of a material.* Journal of Bioengineering, 1977. **1**(4): p. 261-278.
398. Browne, M., P. Gregson, and R. West, *Characterization of titanium alloy implant surfaces with improved dissolution resistance.* Journal of Materials Science: Materials in Medicine, 1996. **7**(6): p. 323-329.
399. Bakir, M., *Haemocompatibility of titanium and its alloys.* Journal of biomaterials applications, 2012. **27**(1): p. 3-15.
400. Leng, Y., et al., *The microstructure and properties of titanium dioxide films synthesized by unbalanced magnetron sputtering.* Nuclear Instruments and Methods in Physics Research, 2007. **257**(1): p. 451-454.
401. Kasemo, B., *Biological surface science.* Surface Science, 2002. **500**(1): p. 656-677.
402. Lord, M.S., et al., *Monitoring cell adhesion on tantalum and oxidised polystyrene using a quartz crystal microbalance with dissipation.* Biomaterials, 2006. **27**(26): p. 4529-4537.
403. Rechendorff, K., et al., *Enhancement of protein adsorption induced by surface roughness.* Langmuir, 2006. **22**(26): p. 10885-10888.
404. Teixeira, A.I., et al., *Epithelial contact guidance on well-defined micro-and nanostructured substrates.* Journal of cell science, 2003. **116**(10): p. 1881-1892.
405. Wójciak-Stothard, B., et al., *Guidance and activation of murine macrophages by nanometric scale topography.* Experimental cell research, 1996. **223**(2): p. 426-435.
406. Dalby, M., et al., *In vitro reaction of endothelial cells to polymer demixed nanotopography*. Biomaterials, 2002. **23**(14): p. 2945-2954.

407. Dalby, M.J., et al., *The control of human mesenchymal cell differentiation using nanoscale symmetry and disorder.* Nature materials, 2007. **6**(12): p. 997-1003.
408. Sutherland, D.S., et al., *Influence of nanoscale surface topography and chemistry on the functional behaviour of an adsorbed model macromolecule.* Macromolecular Bioscience, 2001. **1**(6): p. 270-273.
409. Tsai, W.-B., et al., *Fibronectin modulates the morphology of osteoblast-like cells (MG-63) on nano-grooved substrates.* Journal of Materials Science: Materials in Medicine, 2009. **20**(6): p. 1367-1378.
410. Vertegel, A.A., R.W. Siegel, and J.S. Dordick, *Silica nanoparticle size influences the structure and enzymatic activity of adsorbed lysozyme.* Langmuir, 2004. **20**(16): p. 6800-6807.
411. Webster, T.J., et al., *Enhanced osteoclast-like cell functions on nanophase ceramics.* Biomaterials, 2001. **22**(11): p. 1327-1333.
412. Webster, T.J., et al., *Mechanisms of enhanced osteoblast adhesion on nanophase alumina involve vitronectin.* Tissue engineering, 2001. **7**(3): p. 291-301.
413. Lord, M.S., M. Foss, and F. Besenbacher, *Influence of nanoscale surface topography on protein adsorption and cellular response.* Nano Today, 2010. **5**(1): p. 66-78.
414. Guo, L.J., *Nanoimprint lithography: methods and material requirements.* Advanced Materials, 2007. **19**(4): p. 495-513.
415. Grigorescu, A. and C. Hagen, *Resists for sub-20-nm electron beam lithography with a focus on HSQ: state of the art.* Nanotechnology, 2009. **20**(29): p. 292001.
416. Chou, S.Y., et al., *Sub-10 nm imprint lithography and applications.* Journal of Vacuum Science & Technology B, 1997. **15**(6): p. 2897-2904.
417. Yi, J.-H., et al., *Characterization of a bioactive nanotextured surface created by controlled chemical oxidation of titanium.* Surface Science, 2006. **600**(19): p. 4613-4621.
418. Variola, F., et al., *Improving biocompatibility of implantable metals by nanoscale modification of surfaces: an overview of strategies, fabrication methods, and challenges.* Small, 2009. **5**(9): p. 996-1006.
419. Turner, S., et al., *Cell attachment on silicon nanostructures.* Journal of Vacuum Science & Technology B, 1997. **15**(6): p. 2848-2854.
420. Variola, F., et al., *Tailoring the surface properties of Ti6Al4V by controlled chemical oxidation.* Biomaterials, 2008. **29**(10): p. 1285-1298.
421. Kokubo, T., H.-M. Kim, and M. Kawashita, *Novel bioactive materials with different mechanical properties.* Biomaterials, 2003. **24**(13): p. 2161-2175.
422. Miyazaki, T., et al., *Bioactive tantalum metal prepared by NaOH treatment.* Journal of Biomedical Materials Research, 2000. **50**(1): p. 35-42.
423. Dolatshahi-Pirouz, A., et al., *Bovine serum albumin adsorption on nano-rough platinum surfaces studied by QCM-D.* Colloids and Surfaces B: Biointerfaces, 2008. **66**(1): p. 53-59.
424. Buzea, C., et al., *Control of power law scaling in the growth of silicon nanocolumn pseudo-regular arrays deposited by glancing angle deposition.* Nanotechnology, 2005. **16**(10): p. 1986.

425. Robbie, K. and M. Brett, *Sculptured thin films and glancing angle deposition: Growth mechanics and applications.* Journal of Vacuum Science & Technology A, 1997. **15**(3): p. 1460-1465.
426. Wood, M., M. Riehle, and C. Wilkinson, *Patterning colloidal nanotopographies.* Nanotechnology, 2002. **13**(5): p. 605.
427. Affrossman, S., S.A. O'Neill, and M. Stamm, *Topography and surface composition of thin films of blends of polystyrene with brominated polystyrenes: effects of varying the degree of bromination and annealing.* Macromolecules, 1998. **31**(18): p. 6280-6288.
428. Müller-Buschbaum, P., et al., *Phase separation and dewetting of weakly incompatible polymer blend films.* Macromolecules, 1998. **31**(15): p. 5003-5009.
429. Dalby, M.J., et al., *Interactions of human blood and tissue cell types with 95-nm-high nanotopography.* NanoBioscience, IEEE Transactions on, 2002. **1**(1): p. 18-23.
430. Dalby, M., et al., *Rapid fibroblast adhesion to 27nm high polymer demixed nano-topography.* Biomaterials, 2004. **25**(1): p. 77-83.
431. Dalby, M., et al., *Fibroblast reaction to island topography: changes in cytoskeleton and morphology with time.* Biomaterials, 2003. **24**(6): p. 927-935.
432. Hamley, I.W., *Introduction to soft matter: synthetic and biological self-assembling materials*. 2008: John Wiley & Sons.
433. Khandpur, A.K., et al., *Polyisoprene-polystyrene diblock copolymer phase diagram near the order-disorder transition.* Macromolecules, 1995. **28**(26): p. 8796-8806.
434. Hamley, I., *Nanostructure fabrication using block copolymers.* Nanotechnology, 2003. **14**(10): p. R39.
435. Buriak, J., X. Zhang, and K. Harris, *Method for organising a block co-polymer*. 2011, WO Patent 2,011,094,857.
436. Buriak, J., et al., *Method for forming a block co-polymer pattern*. 2011.
437. Park, S.-M., et al., *Patterning sub-10 nm line patterns from a block copolymer hybrid.* Nanotechnology, 2008. **19**(45): p. 455304.
438. Sun, T., et al., *No platelet can adhere—largely improved blood compatibility on nanostructured superhydrophobic surfaces.* Small, 2005. **1**(10): p. 959-963.
439. Chen, L., D. Han, and L. Jiang, *On improving blood compatibility: From bioinspired to synthetic design and fabrication of biointerfacial topography at micro/nano scales.* Colloids and Surfaces B: Biointerfaces, 2011. **85**(1): p. 2-7.
440. Milner, K.R., A.J. Snyder, and C.A. Siedlecki, *Sub-micron texturing for reducing platelet adhesion to polyurethane biomaterials.* Journal of Biomedical Materials Research Part A, 2006. **76**(3): p. 561-570.
441. Minelli, C., A. Kikuta, and A. Yamamoto. *Blood interaction with nano-topography*. in *Nanoscience and Nanotechnology*. 2006. IEEE.
442. Kubo, K., et al., *Cellular behavior on TiO< sub> 2</sub> nanonodular structures in a micro-to-nanoscale hierarchy model.* Biomaterials, 2009. **30**(29): p. 5319-5329.

443. Curtis, A., et al., *Substratum nanotopography and the adhesion of biological cells. Are symmetry or regularity of nanotopography important?* Biophysical chemistry, 2001. **94**(3): p. 275-283.
444. Koh, L.B., I. Rodriguez, and J. Zhou, *Platelet adhesion studies on nanostructured poly (lactic-co-glycolic-acid)–carbon nanotube composite.* Journal of Biomedical Materials Research Part A, 2008. **86**(2): p. 394-401.
445. Stadler, H., M. Mondon, and C. Ziegler, *Protein adsorption on surfaces: dynamic contact-angle (DCA) and quartz-crystal microbalance (QCM) measurements.* Analytical and Bioanalytical Chemistry, 2003. **375**(1): p. 53-61.
446. Kern, W. and D. Puotinen, *The RCA-clean.* RCA Review, 1970. **31**: p. 197.
447. Bendavid, A., et al., *The properties of fluorine containing diamond-like carbon films prepared by plasma-enhanced chemical vapour deposition.* Diamond and Related Materials, 2009. **18**(1): p. 66-71.
448. Bendavid, A., P.J. Martin, and H. Takikawa, *The properties of nanocomposite aluminium–silicon based thin films deposited by filtered arc deposition.* Thin Solid Films, 2002. **420–421**(0): p. 83-88.
449. Janolino, V.G., J. Fontecha, and H.E. Swaisgood, *A spectrophotometric assay for biotinbinding sites of immobilized avidin.* Applied Biochemistry and Biotechnology, 1996. **56**(1): p. 1-7.
450. Green, N., *[74] Spectrophotometric determination of avidin and biotin.* Methods in enzymology, 1970. **18**: p. 418-424.
451. Green, N., *A spectrophotometric assay for avidin and biotin based on binding of dyes by avidin.* The Biochemical Journal, 1965. **94**: p. 23C.
452. Greenblatt, D., *Reduced serum albumin concentration in the elderly: a report from the Boston Collaborative Drug Surveillance Program.* Journal of the American Geriatrics Society, 1979. **27**(1): p. 20-22.
453. Oswald, M., H. Hunt, and J. Lazarchick, *Normal range of plasma fibrinogen.* The American journal of medical technology, 1983. **49**(1): p. 57-59.
454. Reinke, P., M.G. Garnier, and P. Oelhafen, *In situ photoelectron spectroscopy analysis of tetrahedral amorphous carbon films.* Journal of Electron Spectroscopy and Related Phenomena, 2004. **136**(3): p. 239-245.
455. Tunc, S., et al., *In situ conformational analysis of fibrinogen adsorbed on Si surfaces.* Colloids and Surfaces B: Biointerfaces, 2005. **42**(3–4): p. 219-225.
456. Sit, P.S. and R.E. Marchant, *Surface-dependent conformations of human fibrinogen observed by atomic force microscopy under aqueous conditions.* Thrombosis and haemostasis, 1999. **82**: p. 1053-1060.
457. Rodahl, M. and B. Kasemo, *On the measurement of thin liquid overlayers with the quartz-crystal microbalance.* Sensors and Actuators A: Physical, 1996. **54**(1-3): p. 448-456.
458. Kasemo, B., *Biological surface science.* Current Opinion in Solid State and Materials Science, 1998. **3**(5): p. 451-459.
459. Choi, K.H., et al., *Simultaneous atomic force microscope and quartz crystal microbalance measurements: Investigation of human plasma fibrinogen adsorption.* Applied Physics Letters, 2002. **81**(7): p. 1335-1337.
460. Hemmersam, A.G., et al., *Adsorption of fibrinogen on tantalum oxide, titanium oxide and gold studied by the QCM-D technique.* Colloids and Surfaces B: Biointerfaces, 2005. **43**(3-4): p. 208-215.

461. Höök, F., et al., *A comparative study of protein adsorption on titanium oxide surfaces using in situ ellipsometry, optical waveguide lightmode spectroscopy, and quartz crystal microbalance/dissipation.* Colloids and Surfaces B: Biointerfaces, 2002. **24**(2): p. 155-170.
462. Moseke, C. and A. Ewald, *Cell and protein adsorption studies using . quartz crystal microgravimetry with dissipation monitoring.* Materialwissenschaft und Werkstofftechnik, 2009. **40**(1-2): p. 36-42.
463. Voinova, M.V., et al., *Viscoelastic Acoustic Response of Layered Polymer Films at Fluid-Solid Interfaces: Continuum Mechanics Approach.* Physica Scripta, 1999. **59**(5): p. 391.
464. Kasirer-Friede, A., M.L. Kahn, and S.J. Shattil, *Platelet integrins and immunoreceptors.* Immunological Reviews, 2007. **218**(1): p. 247-264.
465. Li, M., et al., *Progress of AFM single-cell and single-molecule morphology imaging.* Chinese Science Bulletin, 2013. **58**(26): p. 3177-3182.
466. Henderson, E., P. Haydon, and D. Sakaguchi, *Actin filament dynamics in living glial cells imaged by atomic force microscopy.* Science, 1992. **257**(5078): p. 1944-1946.
467. Weisenhorn, A.L., et al., *Deformation and height anomaly of soft surfaces studied with an AFM.* Nanotechnology, 1993. **4**(2): p. 106.
468. Putman, C.A., et al., *Viscoelasticity of living cells allows high resolution imaging by tapping mode atomic force microscopy.* Biophysical Journal, 1994. **67**(4): p. 1749-1753.
469. Pawley, J.B., *Handbook of Biological Confocal Microscopy*. 1995: Springer Dordrecht.
470. Lee, I. and R.E. Marchant, *Force measurements on platelet surfaces with high spatial resolution under physiological conditions.* Colloids and Surfaces B: Biointerfaces, 2000. **19**(4): p. 357-365.
471. Risca, V.I., et al., *Actin filament curvature biases branching direction.* Proceedings of the National Academy of Sciences, 2012. **109**(8): p. 2913-2918.
472. Phillips, D.R., I.F. Charo, and R.M. Scarborough, *GPIIb-IIIa: The responsive integrin.* Cell, 1991. **65**(3): p. 359-362.
473. Litvinov, R.I., et al., *Binding strength and activation state of single fibrinogen-integrin pairs on living cells.* Proceedings of the National Academy of Sciences, 2002. **99**(11): p. 7426-7431.
474. Rotsch, C., K. Jacobson, and M. Radmacher, *Dimensional and mechanical dynamics of active and stable edges in motile fibroblasts investigated by using atomic force microscopy.* Proceedings of the National Academy of Sciences, 1999. **96**(3): p. 921-926.
475. Kottke-Marchant, K., et al., *Effect of albumin coating on the in vitro blood compatibility of Dacron® arterial prostheses.* Biomaterials, 1989. **10**(3): p. 147-155.
476. Fredriksson, C., et al., *The Piezoelectric Quartz Crystal Mass and Dissipation Sensor: A Means of Studying Cell Adhesion.* Langmuir, 1998. **14**(2): p. 248-251.
477. Sauerbrey, G., *The use of quartz oscillators for weighing thin layers and for microweighing.* Journal of Physics, 1959. **155**: p. 206–222.

478. Lord, M.S., et al., *Protein adsorption on derivatives of hyaluronic acid and subsequent cellular response.* Journal of Biomedical Materials Research Part A, 2009. **91A**(3): p. 635-646.
479. Raider, S., et al., *Surface oxidation of silicon nitride films.* Journal of The Electrochemical Society, 1976. **123**(4): p. 560-565.
480. Wegener, J., et al., *Analysis of the Composite Response of Shear Wave Resonators to the Attachment of Mammalian Cells.* Biophysical Journal, 2000. **78**(6): p. 2821-2833.
481. Wegener, J., A. Janshoff, and H.J. Galla, *Cell adhesion monitoring using a quartz crystal microbalance: comparative analysis of different mammalian cell lines.* European Biophysics Journal, 1998. **28**(1): p. 26-37.
482. Keselowsky, B.G., D.M. Collard, and A.J. García, *Integrin binding specificity regulates biomaterial surface chemistry effects on cell differentiation.* Proceedings of the National Academy of Sciences, 2005. **102**(17): p. 5953-5957.
483. Hirata, H., C.T. Lim, and H. Miyata, *3D Coupling of Fibronectin Fibril Arrangement with Topology of Ventral Plasma Membrane.* Cell Communication and Adhesion, 2012. **19**(2): p. 17-23.
484. Galli Marxer, C., et al., *Cell spreading on quartz crystal microbalance elicits positive frequency shifts indicative of viscosity changes.* Analytical and Bioanalytical Chemistry, 2003. **377**(3): p. 578-586.
485. Lord, M.S., et al., *Extracellular matrix remodelling during cell adhesion monitored by the quartz crystal microbalance.* Biomaterials, 2008. **29**(17): p. 2581-2587.
486. Shattil, S.J., M.H. Ginsberg, and J.S. Brugge, *Adhesive signaling in platelets.* Current Opinion in Cell Biology, 1994. **6**(5): p. 695-704.
487. Hull, R.D., et al., *Continuous intravenous heparin compared with intermittent subcutaneous heparin in the initial treatment of proximal-vein thrombosis.* The New England journal of medicine, 1986. **315**(18): p. 1109-1114.
488. Hull, R.D., et al., *Heparin for 5 Days as Compared with 10 Days in the Initial Treatment of Proximal Venous Thrombosis.* New England Journal of Medicine, 1990. **322**(18): p. 1260-1264.
489. Turpie, A.G., et al., *Comparison of high-dose with low-dose subcutaneous heparin to prevent left ventricular mural thrombosis in patients with acute transmural anterior myocardial infarction.* The New England journal of medicine, 1989. **320**(6): p. 352-357.
490. Chiu, H., et al., *Relationship between the anticoagulant and antithrombotic effects of heparin in experimental venous thrombosis.* Blood, 1977. **49**(2): p. 171-184.
491. Kitchen, S. and F.E. Preston, *The therapeutic range for heparin therapy: relationship between six activated partial thromboplastin time reagents and two heparin assays.* Thrombosis and haemostasis, 1996. **75**(5): p. 734-739.
492. Klee, D. and H. Höcker, *Polymers for biomedical applications: improvement of the interface compatibility*, in *Biomedical Applications Polymer Blends*. 1999, Springer. p. 1-57.
493. Cui, F. and D. Li, *A review of investigations on biocompatibility of diamond-like carbon and carbon nitride films.* Surface and Coatings Technology, 2000. **131**(1): p. 481-487.

494. Wegner, G., *Mehrphasige polymere.* Polymere Werkstoffe. Thieme Verlag, Stuttgart, 1985. **679**.
495. Shalaby, S.W., *Polymers of biological and biomedical significance.* American Chemical Society, 1994.
496. Lee, J.H. and H.B. Lee, *Platelet adhesion onto wettability gradient surfaces in the absence and presence of plasma proteins.* Journal of Biomedical Materials Research, 1998. **41**(2): p. 304-311.
497. Cazenave, J.-P., *Blood-surface interactions: biological principles underlying haemocompatibility with artificial materials*. 1986: Elsevier Publishing Company.
498. Zhang, Z., et al., *Blood compatibility of surfaces with superlow protein adsorption.* Biomaterials, 2008. **29**(32): p. 4285-4291.
499. Kwok, S.C.H., et al., *Hemocompatibility of nitrogen-doped, hydrogen-free diamond-like carbon prepared by nitrogen plasma immersion ion implantation–deposition.* Journal of Biomedical Materials Research Part A, 2004. **70A**(1): p. 107-114.
500. Ismail, F.S.M., et al., *The influence of surface chemistry and topography on the contact guidance of MG63 osteoblast cells.* Journal of Materials Science: Materials in Medicine, 2007. **18**(5): p. 705-714.
501. Randeniya, L.K., et al., *Thin-film nanocomposites of diamond-like carbon and titanium oxide; Osteoblast adhesion and surface properties.* Diamond and Related Materials, 2010. **19**(4): p. 329-335.
502. Bendavid, A., et al., *The mechanical and biocompatibility properties of DLC-Si films prepared by pulsed DC plasma activated chemical vapor deposition.* Diamond and Related Materials, 2007. **16**(8): p. 1616-1622.
503. Smith, B.S. and K.C. Popat, *Titania Nanotube Arrays as Interfaces for Blood-Contacting Implantable Devices: A Study Evaluating the Nanotopography-Associated Activation and Expression of Blood Plasma Components.* Journal of Biomedical Nanotechnology, 2012. **8**(4): p. 642-658.
504. Ducheyne, P., et al., *In vivo metal-ion release from porous titanium-fiber material.* Journal of Biomedical Materials Research, 1984. **18**(3): p. 293-308.
505. Woodman, J.L., et al., *Metal ion release from titanium-based prosthetic segmental replacements of long bones in baboons: A long-term study.* Journal of Orthopaedic Research, 1983. **1**(4): p. 421-430.
506. Cedervall, T., et al., *Detailed Identification of Plasma Proteins Adsorbed on Copolymer Nanoparticles.* Angewandte Chemie International Edition, 2007. **46**(30): p. 5754-5756.
507. Cornelius, R.M., J. Macri, and J.L. Brash, *Interfacial interactions of apolipoprotein AI and high density lipoprotein: Overlooked phenomena in blood-material contact.* Journal of Biomedical Materials Research Part A, 2011. **99**(1): p. 109-115.
508. Roy, R.K., et al., *Hemocompatibility of surface-modified, silicon-incorporated, diamond-like carbon films.* Acta Biomaterialia, 2009. **5**(1): p. 249-256.
509. Yayapour, N. and H. Nygren, *Interactions between whole blood and hydrophilic or hydrophobic glass surfaces: kinetics of cell adhesion.* Colloids and Surfaces B: Biointerfaces, 1999. **15**(2): p. 127-138.

510. Sivaraman, B. and R.A. Latour, *The adherence of platelets to adsorbed albumin by receptor-mediated recognition of binding sites exposed by adsorption-induced unfolding*. Vol. 31. 2010. 1036-44.
511. Sivaraman, B. and R.A. Latour, *Time-Dependent Conformational Changes in Adsorbed Albumin and Its Effect on Platelet Adhesion.* Langmuir, 2011. **28**(5): p. 2745-2752.
512. Zhang, F., et al., *Artificial heart valves:: improved hemocompatibility by titanium oxide coatings prepared by ion beam assisted deposition.* Surface and Coatings Technology, 1998. **103**: p. 146-150.
513. Leistikow, E.A., et al., *Receptor–ligand complexes are cleared to the open canalicular system of surface-activated platelets.* British journal of haematology, 1990. **74**(1): p. 93-100.
514. Kim, J.K., et al., *Functional nanomaterials based on block copolymer self-assembly.* Progress in Polymer Science, 2010. **35**(11): p. 1325-1349.
515. Fredrickson, G.H. and F.S. Bates, *Dynamics of block copolymers: theory and experiment.* Annual Review of Materials Science, 1996. **26**(1): p. 501-550.
516. Bates, F.S. and G.H. Fredrickson, *Block copolymer thermodynamics: theory and experiment.* Annual Review of Physical Chemistry, 1990. **41**(1): p. 525-557.
517. Jeong, S.-J., et al., *Directed self-assembly of block copolymers for next generation nanolithography.* Materials Today, 2013. **16**(12): p. 468-476.
518. Yong Chae, J. and B. Bharat, *Contact angle, adhesion and friction properties of micro-and nanopatterned polymers for superhydrophobicity.* Nanotechnology, 2006. **17**(19): p. 4970.
519. Johansson, G. and R.J. Pugh, *The influence of particle size and hydrophobicity on the stability of mineralized froths.* International Journal of Mineral Processing, 1992. **34**(1–2): p. 1-21.
520. Vogler, E.A., *Structure and reactivity of water at biomaterial surfaces.* Advances in Colloid and Interface Science, 1998. **74**(1-3): p. 69-117.
521. Bico, J., U. Thiele, and D. Quéré, *Wetting of textured surfaces.* Colloids and Surfaces A: Physicochemical and Engineering Aspects, 2002. **206**(1–3): p. 41-46.
522. Hazlett, R.D., *Fractal applications: Wettability and contact angle.* Journal of colloid and interface science, 1990. **137**(2): p. 527-533.
523. Onda, T., et al., *Super-Water-Repellent Fractal Surfaces.* Langmuir, 1996. **12**(9): p. 2125-2127.
524. Öner, D. and T.J. McCarthy, *Ultrahydrophobic Surfaces. Effects of Topography Length Scales on Wettability.* Langmuir, 2000. **16**(20): p. 7777-7782.
525. Müller, R., et al., *Chemiluminescence-based detection and comparison of protein amounts adsorbed on differently modified silica surfaces.* Analytical biochemistry, 2006. **359**(2): p. 194-202.
526. Kumar, V., et al., *Amphiphilic Copolymer Coatings via Plasma Polymerisation Process: Switching and Anti-Biofouling Characteristics.* Plasma Processes and Polymers, 2011. **8**(5): p. 373-385.
527. Kumar, V., et al., *Fluorocarbon Coatings Via Plasma Enhanced Chemical Vapor Deposition of 1H, 1H, 2H, 2H-perfluorodecyl Acrylate-2, Morphology, Wettability and Antifouling Characterization.* Plasma Processes and Polymers, 2010. **7**(11): p. 926-938.

528. Ratner, B.D., *Blood compatibility—a perspective.* Journal of Biomaterials Science, Polymer Edition, 2000. **11**(11): p. 1107-1119.
529. Haycox, C.L. and B.D. Ratner, *In vitro platelet interactions in whole human blood exposed to biomaterial surfaces: Insights on blood compatibility.* Journal of Biomedical Materials Research, 1993. **27**(9): p. 1181-1193.
530. Koh, L.B., I. Rodriguez, and S.S. Venkatraman, *The effect of topography of polymer surfaces on platelet adhesion.* Biomaterials, 2010. **31**(7): p. 1533-1545.
531. Ferraz, N., et al., *Influence of nanoporesize on platelet adhesion and activation.* Journal of Materials Science: Materials in Medicine, 2008. **19**(9): p. 3115-3121.
532. Briggs, D., *Handbook of X-ray Photoelectron Spectroscopy C. D. Wanger, W. M. Riggs, L. E. Davis, J. F. Moulder and G. E.Muilenberg Perkin-Elmer Corp., Physical Electronics Division, Eden Prairie, Minnesota, USA, 1979. 190 pp. $195.* Surface and Interface Analysis, 1981. **3**(4): p. v-v.
533. Attard, G. and C. Barnes, *Oxford Chemistry Primer*. Surfaces, ed. R.G. Compton. 1998, Oxford: Oxford Science Publications.
534. Texas, U.o. *X-ray photoelectron spectroscopy*. 1999 [cited 2014 26 May]; Available from: http://wiki.utep.edu/download/attachments/51217390/XPS.pdf?version=1.
535. Goodhew, P.J., *Electron microscopy and analysis*. Wykeham science series. 1975.
536. Illinois, U.o. *Scanning electron microscopy*. 2012 [cited 2013 3 Mar]; Available from: http://mrl.illinois.edu/sites/default/files/AMC/downloads/AMC-Workshop-2012_Tutorial-7_SEM.pdf.
537. Laboratory, L.P.I.P. *Experimental and numerical techniques: Atomic force microscopy*. 2007 [cited 2013 27 Mar]; Available from: http://www-liphy.ujf-grenoble.fr/Microscopie-a-force-atomique-AFM?lang=en.
538. Merritt, K., C.R. Edwards, and S.A. Brown, *Use of an enzyme linked immunosorbent assay (ELISA) for quantification of proteins on the surface of materials.* Journal of Biomedical Materials Research, 1988. **22**(2): p. 99-109.
539. Bradbury, S. and P.J. Evennett, *Contrast techniques in light microscopy*. 1996: Bios Scientific Publishers.
540. Sumner, J.P. and R. Kopelman, *Alexa Fluor 488 as an iron sensing molecule and its application in PEBBLE nanosensors.* Analyst, 2005. **130**(4): p. 528-533.
541. Maheshwari, G., et al., *Cell adhesion and motility depend on nanoscale RGD clustering.* Journal of cell science, 2000. **113**(10): p. 1677-1686.
542. Rajnicek, A. and C. McCaig, *Guidance of CNS growth cones by substratum grooves and ridges: effects of inhibitors of the cytoskeleton, calcium channels and signal transduction pathways.* Journal of cell science, 1997. **110**(23): p. 2915-2924.
543. Rodahl, M., et al., *Quartz crystal microbalance setup for frequency and Q-factor measurements in gaseous and liquid environments.* Review of Scientific Instruments, 1995. **66**(7): p. 3924-3930.
544. Nomura, T. and M. Okuhara, *Frequency shifts of piezoelectric quartz crystals immersed in organic liquids.* Analytica Chimica Acta, 1982. **142281**.

545. Kasemo, B. and J. Gold, *Implant surfaces and interface processes.* Advances in Dental Research, 1999. **13**(1): p. 8-20.
546. Dixon, M., *Quartz Crystal Microbalance with Dissipation Monitoring: Enabling Real-Time Characterization of Biological Materials and Their Interactions.* Journal of Biomolecular Techniques: JBT, 2008. **19**(3): p. 151.
547. Jordan, J.L. and E.J. Fernandez, *QCM-D sensitivity to protein adsorption reversibility.* Biotechnology and Bioengineering, 2008. **101**(4): p. 837-842.
548. Rodahl, M. and B. Kasemo, *Frequency and dissipation-factor responses to localized liquid deposits on a QCM electrode.* Sensors and Actuators B: Chemical, 1996. **37**(1): p. 111-116.
549. Steinem, C., et al., *Impedance and shear wave resonance analysis of ligand-receptor interactions at functionalized surfaces and of cell monolayers.* Biosensors and Bioelectronics, 1997. **12**(8): p. 787-808.
550. Johannsmann, D., *Feature Article Viscoelastic analysis of organic thin films on quartz resonators.* Macromol. Chem. Phys, 1999. **200**: p. 501-516.
551. Lucklum, R., C. Behling, and P. Hauptmann, *Role of mass accumulation and viscoelastic film properties for the response of acoustic-wave-based chemical sensors.* Analytical Chemistry, 1999. **71**(13): p. 2488-2496.
552. Janshoff, A., et al., *Double-mode impedance analysis of epithelial cell monolayers cultured on shear wave resonators.* European Biophysics Journal, 1996. **25**(2): p. 93-103.
553. Shapiro, H.M., *Practical flow cytometry*. 2005: John Wiley & Sons.
554. Givan, A.L., *Flow cytometry: first principles*. 2004: John Wiley & Sons.
555. Biosciences, B. *Introduction to Flow Cytometry: A Learning Guide*. 2000 [cited 2012 19 Nov]; Available from: http://www.d.umn.edu/~biomed/flowcytometry/introflowcytometry.pdf.

10 APPENDIX A

10.1 Experimental Techniques

Theoretical aspects behind the various experimental techniques used in this study are detailed below.

10.1.1 X-ray Photoelectron Spectroscopy (XPS)

XPS is an essential tool used to identify the chemistry and physics of the material surface, which aids greatly in understanding the interactions that occur on the top layer of the material as it interfaces with biology. It uses Einstein's principle of the Photoelectric Effect to identify the elemental components on a material surface. Beams of x-rays are bombarded at the solid surface, as a result of the photoemission process, irradiates a small surface area to liberate electrons from the core and valence bands of the interfacial atoms. Even though the x-ray photons, emitted from an Al-K_α or Mg-K_α primary source, penetrate up to 10µm within the solid material, the X-ray spectrometer only detects electrons emitted within the top 10-15 nm, as shown in

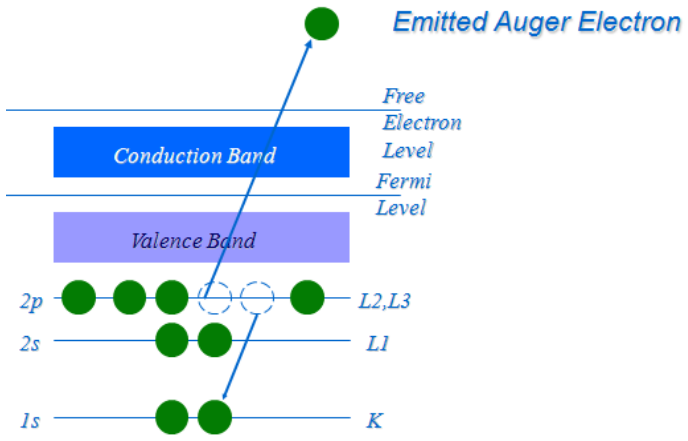

Figure 10.1Figure 10.1. This is because the deeper photo-emitted 'Auger' electrons are either recaptured or trapped at various excited states within the substrate material [532].

The kinetic energy of the emitted photoelectrons can be estimated by;

$$E_{KIN} = h\upsilon - E_B + \phi \qquad \text{eq 3}$$

where

$h\upsilon$ is the energy of the photon

E_B is the binding energy of the core level electrons in an atom respective to their highest occupied electron level in the solid

ϕ is the spectrometer work function

While $h\upsilon$ and ϕ are known constants dependent on the primary x-ray source, E_B, which is characteristic of the electronic structure of each element at a particular oxidation state, can be deduced from measuring the kinetic energy of the photons [533].

This process occurs in vacuum to avoid cross contamination and erroneous detection of elements found in air. Each element with respect to its oxidation state produces a unique sequence of peaks at specific E_B values in the XPS spectrum, which is used to identify the individual elements present as well as to the species to which it is bonded on the material surface. Further, the concentration of detected electrons in each characteristic E_B peaks can be used to determine the elemental composition within the irradiated area [532].

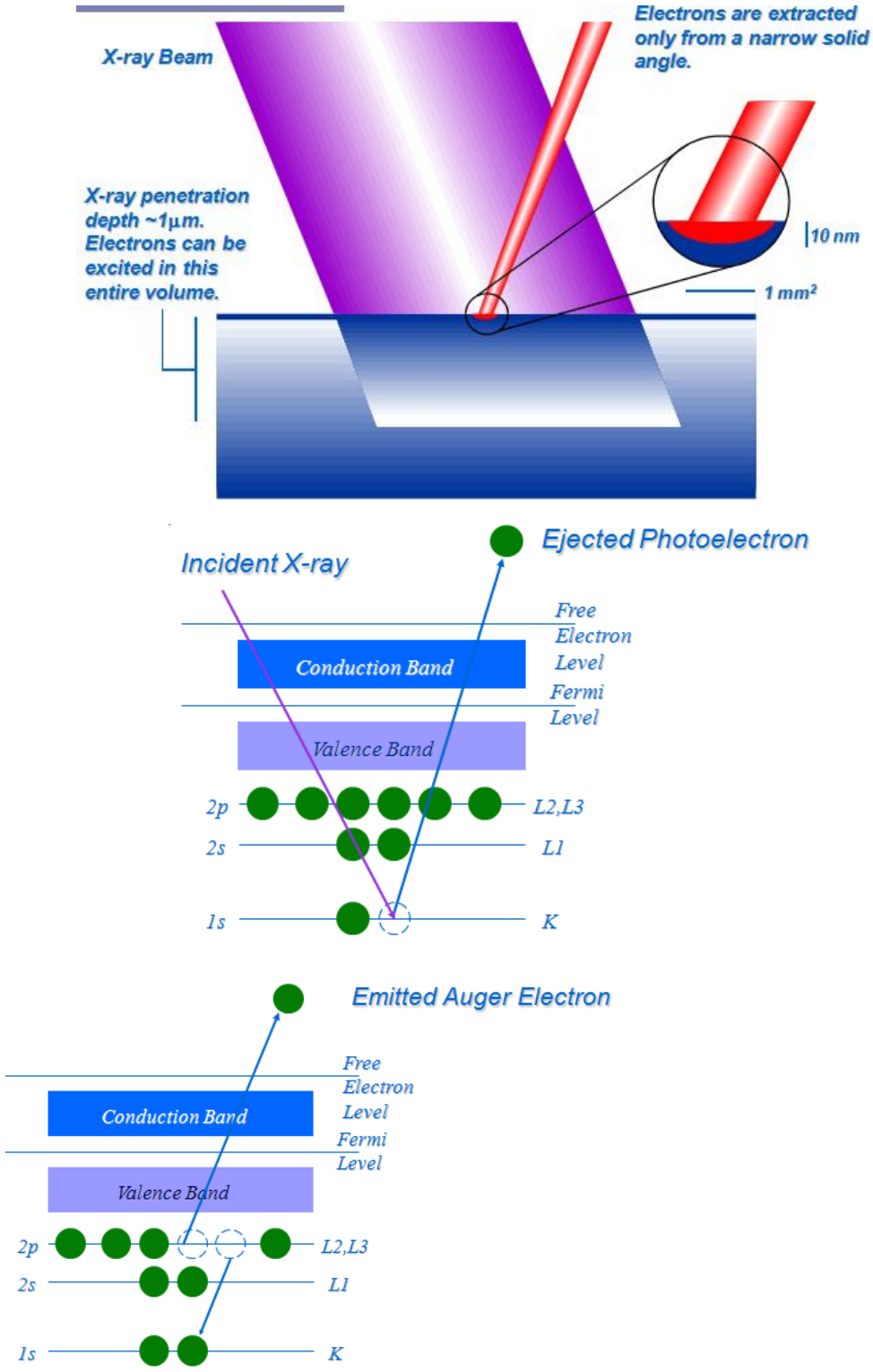

Figure 10.1 Schematic diagram of the X-ray photoelectron spectroscopy and principle behind the photoemission process[534].

10.1.2 Scanning Electron Microscopy (SEM)

SEM's are microscopes that uses focused beam of high energy electrons to generate images representing morphological features and compositional analyses of inorganic and organic specimens on solid surfaces. The SEM produces high resolution, stable and noise-free images using beam of electrons projected from an electron gun, which follows a vertical pathway within a highly vacuumised environment of the microscope. The electron gun either uses heated tungsten or LaB_6 filament for thermionic emission [535]. Electromagnetic fields assist in the deflection for electrons and the lenses allow the direction of the electrons to remain parallel to the magnetic field to optimise the position of the electron beam and to focus the beam directly towards a small rectangular scanning region on the sample [535]. Once the beam is in contact with the sample, the beam interacts with the material such that light, electrons and X-rays from the atoms of the interfacial layers of the surface are ejected, as shown in Figure 10.2.

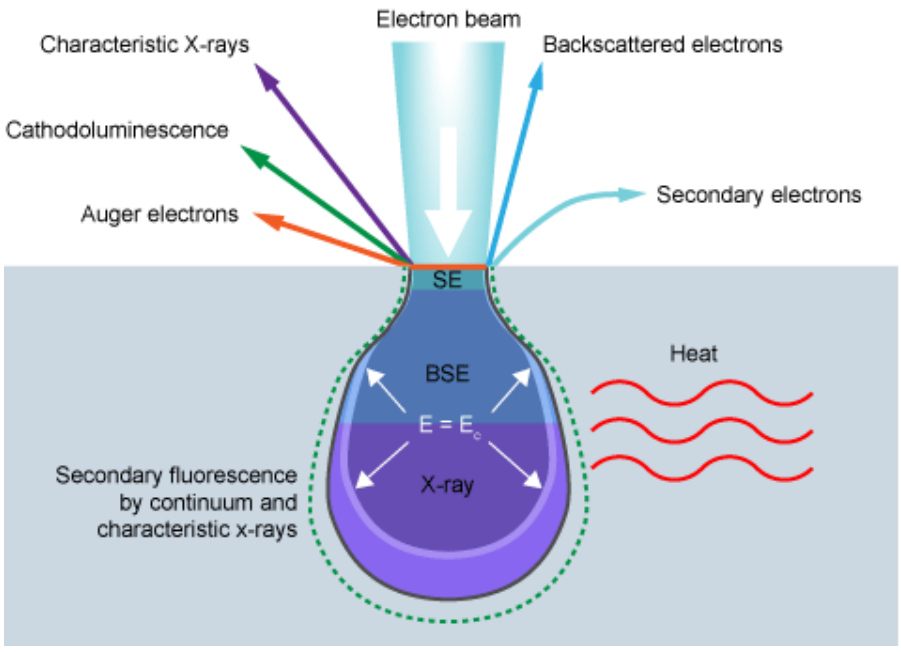

Figure 10.2 Complex interactions between the beam electrons of an SEM with material surfaces [536]

Electrons travel in air only for short distances and therefore require a vacuum environment to operate successfully. X-ray, secondary electron (SE) and electron

backscattered (EsB) detectors capture the X-rays, backscattered electrons and secondary electrons, respectively, from the range of signals collected and are modulated to produce topographical images and elemental analyses (EsB detectors only) of the surface.

10.1.3 Focused Ion Beam (FIB) Microscopy

FIB microscope was used to sequester a slice of the surface's cross section to determine the overall coverage of the deposited layer and the thickness of each coating. FIB functions along the same principle as the SEM, however, instead of electrons the charged particle beam projected within the column consists of positively charged ions, Figure 10.3.

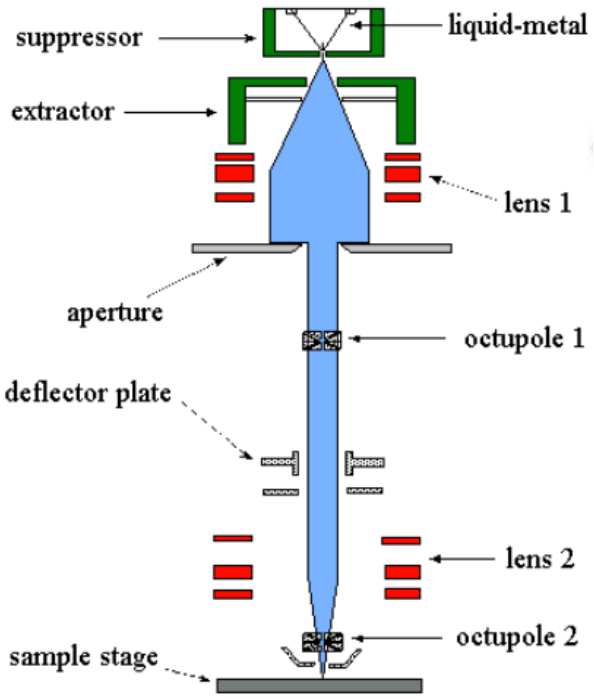

Figure 10.3 Schematic diagram of the FIB column [536]

Essentially a beam of charged particles rasters across a specified rectangular area and the captured signals from each raster position is plotted to form an image. The FIB produces high-current density beams from high-brightness ion sources for in-situ sectioning. Signals from the secondary sputtered electrons were detected by the InLens detector of the SEM to image the cross-section. The SEM system is operated with column pressures in the range of 10^{-5} Pa with pressures between 10^{-4} and 10^{-3} Pa in the working chamber with the stage tilted at an angle of 53.8 degrees from the horizontal. A schematic diagram of the etching process is shown in Figure 10.4.

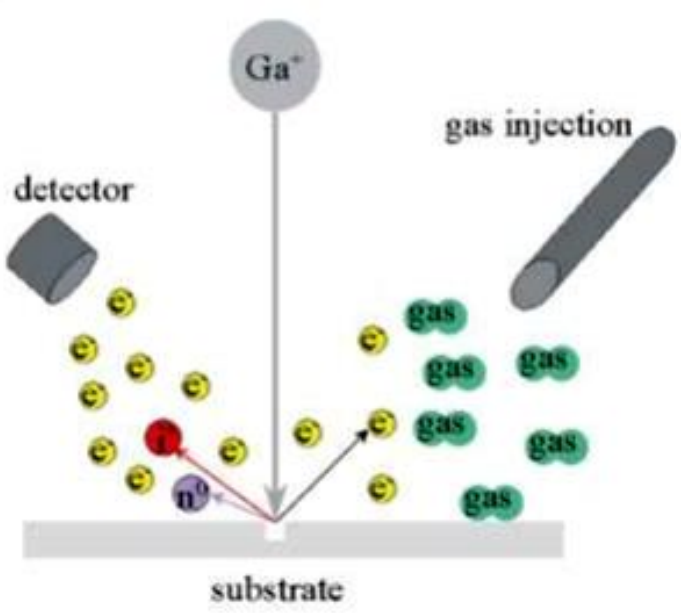

Figure 10.4 Focused ion beam induced milling [536]

10.1.4 Atomic Force Microscopy (AFM)

The AFM is a three dimensional imaging tool often used to measure the micro and nano-topography of any solid surfaces. Apart from surface imaging, it can also be used to measure interfacial material properties and colloidal scale interactions forces in air and liquid medium.

The AFM is essentially composed of a stage where samples are mounted using a nano-positioning system, and a thin metallic tip, attached to a cantilever, that scans across the surface at a pre-set scan rate. The cantilever is mounted on a piezoelectric

scanner which allows for 3-D positioning of the pyramid shaped nano-tip at high resolution, as shown in Figure 10.5. In tapping mode, a laser beam is reflected onto the point where the tip is mounted on the cantilever and the cantilever acts as a spring as it taps across the material surface. The force of attraction between the tip and the surface as the tip approaches the surface causes the cantilever beam to deflect in the x-y-z plane. The angular deflection of the reflected laser beam, caused by the angular deflection of the cantilever, is focused onto two side-by-side position-sensitive photodiodes of a photo detector. The estimated difference in signals between the two photodiodes dictates the positioning of the laser spot on the detector and consequently, the angular deflection of the cantilever. The measurements across a specified scan area are recorded as 3-D images.

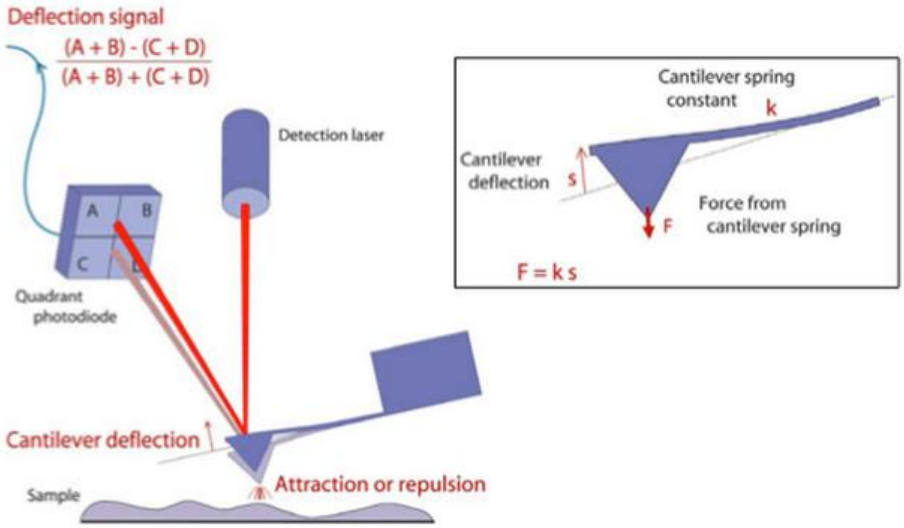

Figure 10.5 Principle of AFM operation [537]

10.1.5 Enzyme-Linked Immunosorbant Assay (ELISA)

ELISA is a technique that is commonly used in *in-vitro* studies to indirectly quantify the adsorption of proteins or the adhesion of cells/platelets on biomaterial surfaces as well as the conformation of surface adsorbed proteins, or, expression of specific cell-receptor proteins localised on the plasma membrane. This is done using antibodies specific to the antigen. Both monoclonal and polyclonal antibodies, specific for various epitopes on proteins can be used for quantification purposes.

Essentially, several molecular complexes are adhered onto the adsorbed protein in a sequential manner followed by an end-stage enzymatic reaction before enabling their detection using a colorimetric, fluorescent or luminescent dye [538]. The enzyme label, Horseradish peroxidase (HRP), is often used in combination with 2,2'-azino-di(3-ethylbenthiazoline) sulfonate (ABTS) colorimetric substrate. Proteins can also be probed after their extraction from the surface; however, the sensitivity of the technique is limited by the efficiency of the extraction process. Direct ELISA's can usually be executed on tissue culture plates, which have been incubated with test proteins or cells/platelets in the presence or absence of a biomaterial surface. However, the surface area of the sample biomaterial must comply with the linear relation between optical density and surface area for optimum measurements [538].

10.1.6 Fluorescence Microscopy

A fluorescence microscope is an optical microscope that uses fluorescence and phosphorescence in addition to reflection and absorption to allow visualisation of cells on non-transparent, opaque surfaces during cell-surface interactions. Typically the sample of interest is labelled with a fluorochrome (also termed fluorophore), which are excited by specific wavelengths of irradiating light. Fluorophores are stains that bind to visible and sub-cellular structures, such as proteins and actin filaments on platelet cytoskeleton, and are often highly specific for their target. They have a significant quantum yield (the ratio of photon absorption to emission) and as such can emit light of defined and useful intensity [539]. Common fluorophore labels include FITC (green), Alexa Fluor 488 (green) [540] and rhodamine (red). Phalloidin molecules bind to actin filaments and usually conjugated with rhodamine to enable direct labelling and visualisation of sub-cellular structures of cells, however this requires the cells to be fixed prior to staining [541, 542].

10.1.7 Quartz Crystal Microbalance with Dissipation monitoring (QCM-D)

Quartz Crystal Microbalance (QCM) is an ultra-sensitive weighing balance often used to measure the mass of deposited films. Until the 1980's QCM was exclusively used in vacuum or gaseous environments [543]. It was used in the monitoring of metal plating in vacuum deposition systems, in measuring dry etch rates and oxidation rates of metal surfaces, and in measuring the degree of gas adsorption and desorption for various applications.

It was not until 1982 however when Nomura and Okuhara [544] proved that a quartz crystal when immersed in solution can also oscillate in a stable mode, that the liquid application of QCM technology expanded. Nomura and Okuhara established that a change in frequency of the dry and wet crystal is dependent on density and the viscosity of the highly damped liquid media, not its dielectric constant [544]. Since then the use of QCM in liquid environments has been increasing rapidly, especially in the characterisation of bio-interfaces. The inclusion of dissipation monitoring provides information about visco-elastic properties of biofilms adsorbed to the metal coated quartz crystal. The implementation of the QCM-D setup as a liquid flow system provides the possibility of time-resolved observation of multi-stage adsorption processes from peptides to proteins to cell attachments. The versatility of QCM has enabled several biochemically oriented studies [545].

The QCM-D technique, described in detail by Rodahl [543], is an highly-sensitive (< 1ng/cm^2) microgravimetric device that uses AT-cut quartz crystals that oscillates in thickness shear mode. In liquid mode resonant frequency drift is approximately zero at 'near ambient' temperatures, and consequently any small shift in resonant frequency is associated with induced mass change per area from adsorbed particles, such as proteins in solution. Change in frequency (Δf) can be quantitatively represented as change in mass using the Sauerbrey relation [477];

$$\Delta m = (C/n)\,\Delta f \qquad \text{eq 4}$$

where

n is the frequency overtone number (n= 1,2,3,…), and

C is the mass sensitivity constant

$$C = (t_q \rho_q)/f_o \qquad \text{eq 5}$$

where

t_q is the thickness of quartz, and

ρ_q , the density of the quartz

For a 5-MHz crystal the mass sensitivity constant is ~ -17.7 Hz ng/cm^2. This relationship however will only hold true if the adsorbed mass is evenly distributed over an active region of the crystal surface and is a small fraction compared to the mass of the quartz crystal, the adsorbed layer is thin and is rigidly attached to the crystal surface in such a way that no slip or deformation occurs during oscillation [477, 546, 547].

Frequency measurements at several overtones are a good indication of the viscosity of the adsorbed layer. If the upper most region of the adsorbed layer is soft, this layer furthest away from the quartz crystal surface, would not couple to the oscillation of the crystal sensor. In such cases Sauerbrey's relation will underestimate the mass of the adsorbed layer. However, by measuring energy dissipated by this soft adlayer at several harmonics one can estimate visco-elastic properties and even film thickness and film density in the case of soft films such as protein adnd cell layers. The QCM-D (QCM with dissipation monitoring) achieves this. It provides information on energy dissipated during the pulsed, forced oscillation of the QCM crystal [547]. The rate of dissipation is related to the properties of the crystal and the adsorbed layer. A viscous layer is intrinsically soft and will not oscillate along with the sensor exactly. Friction consequently arises within the adlayer causing dissipation and formation of a rigid film on the crystal therefore indicates little viscoelastic coupling and longer

decay time, while a non-rigid surface demonstrates increased viscoelastic coupling and a significant decrease in decay time [546, 547]. In the case of proteins, changes in dissipation upon adsorption have been predominantly attributed to increased inter-layer density due to water adsorption, with minimal contributions from changes in surface roughness. Dissipation curves can be used to measure properties related to the viscoelastic properties of the protein layer. The dissipation rate for a system is related to the crystal's electrical parameters and the ratio of dissipated and stored energy:

$$D = \frac{R}{2\pi f L} = \frac{E_{\text{dissipated}}}{2\pi E_{\text{stored}}} \qquad \text{eq 6}$$

where

R and L are the resistance and inductance value of the crystal, respectively, and $E_{dissipated}$ and E_{stored} are the dissipated and stored energy during each period of oscillation

By measuring and analysing the frequency spectrum it is possible to measure the degree and rate of the protein mass attached to the surface, as well as any changes in the attached mass. However, the estimates of adsorbed mass measurements are based on the assumption that the system maintains uniform density throughout the process [548]. In reality, this is not true. The adhesion and adsorption of biomolecules tend to form an incomplete coverage on the surface or cause changes in material density limiting the application of the linear Sauerbrey relationship [546]. In such circumstances, the raw data obtained for multiple harmonics (n = 1, 3, 5, 7, 9, 11 and 13) can be modelled into Voigt-based visco-elastic solid; or, Maxwell-based viscoelastic liquid models for meaningful parameters such as shear viscosity (η), thickness (h) and mass (m) [549]. Protein surface interactions are best described by the Voigt model, which assume that the adhered film is of uniform thickness and density. The fitted f and D values, as well as mass m, calculated using Voigt based models [549-551] is shown below:

$$\Delta f \approx -\frac{1}{2\pi m_q}\left(\frac{\eta_2}{\delta_2}+h_1\rho_1\omega-2\left(\frac{\eta_2}{\delta_2}\right)^2\frac{h_1\omega^2\eta_1}{\mu_1^2+\omega^2\eta_1^2}\right) \quad \text{eq 7}$$

$$\Delta D \approx \frac{1}{\pi f m_q}\left(\frac{\eta_2}{\delta_2}+2\left(\frac{\eta_2}{\rho_2}\right)^2\frac{h_1\omega\mu_1}{\mu_1^2+\omega^2\eta_1^2}\right) \quad \text{eq 8}$$

$$m \approx m_q\left(1-\frac{\eta_2\rho_2\omega\eta_1}{\rho_1\left(\mu_1^2+\omega^2\eta_1^2\right)}\right) \quad \text{eq 9}$$

where: m is the mass, ρ is the density, η is the viscosity, μ is the shear elastic modulus, ω is the angular frequency, h is the thickness, and, δ is the penetration depth of the acoustic shear wave into the bulk of the adsorbed layer. Furthermore, subscripts 1, 2 and q represent layer 1, layer 2 and the quartz crystal, respectively.

The homogenous distribution of the protein layer is identified by solving for 4 unknown parameters: ρ, h, μand η [548]. A unique solution can only be obtained by using two or more harmonics, as *f* and D values for one overtone is insufficient to solve for four parameters.

Furthermore, cell adhesion also cannot be analysed using Sauerbrey relation, as cells do not behave as rigid masses on the sensor surface and the entire cell cannot be sensed as their sizes are significantly larger than the penetration depth of the shear wave [551, 552]. The penetration depth of a shear wave from the crystal surface into the bulk is determined by the oscillation frequency as well as density and viscosity of the contacting liquid [549]:

$$\delta = \sqrt{\frac{\eta}{\pi\rho f}} \quad \text{eq 10}$$

where: δ is the penetration depth, η, ρ and *f* are the viscosity, density and frequency of the fluid.

To investigate mechanical properties of adhered cells on QCM sensors, it is crucial to analyse cell adhesion using an appropriate model with adjustable parameters

dependent on the physical properties of the cell. For this, it is necessary to understand the specific parts of the cellular body that contribute to the measured QCM-D response [549]. The lateral sensitivity of the QCM-D for changes in both f and D are proportional to the oscillating amplitude and vary according to Gaussian functions of the same width, centred at the middle of the active electrode. Hence, the ratio between ΔD and Δf can be used to characterise the cell adhesion, independent of position on the electrode [549]. The time dependant changes to $\Delta D/\Delta f$ will depend on the mass that is deposited on the surface; the adlayer's viscoelastic properties; physical properties of the cell such as: its internal structure and shape; and, how these features evolve over time during interactions with a surface [549, 552]. QCM-D can be used as a high sensitivity technique to monitor and analyse the region where actual adhesion occur and the possibility to dynamically probe effects involving the adsorbing surface, surface adhesion proteins, the membrane and changes in cytoskeleton as cells spread from their rounded shape [552].

10.1.8 Flow-cytometry

A flow cytometer is a laser based biophysical technique that utilises an optical to electronic coupling system to measure and analyse multiple physical characteristics of single cell suspensions as they flow in a fluidic stream. Ideally cells are tagged with a fluorophore specifically targeted to the cell or sub-cellular components, such as integrins, and the solution is passed through a fluidic system called the 'sample core'. Lenses and detectors in the flow cytometer's electronic system collect and measure the fluorescent light emitted as well as the scattered incident rays caused by the cells as they are taken up into the system to provide information such as the relative size and granularity of the cell and relative fluorescent intensity [553, 554]. This is shown in Figure 10.6.

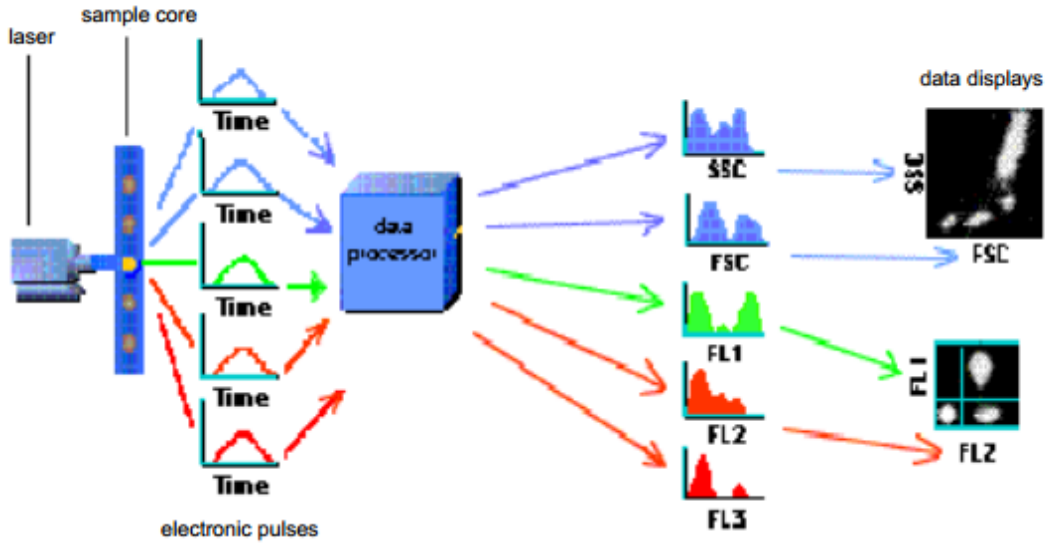

Figure 10.6 Basic principles behind flow cytometry[555]